LEABHARLANN CHOLÁISTE NA TRÍONÓIDE, BAILE ÁTHA CLIATH | TRINITY COLLEGE LIBRARY DUBLIN
Ollscoil Átha Cliath | The University of Dublin

Terms and Conditions of Use of Digitised Theses from Trinity College Library Dublin

Copyright statement

All material supplied by Trinity College Library is protected by copyright (under the Copyright and Related Rights Act, 2000 as amended) and other relevant Intellectual Property Rights. By accessing and using a Digitised Thesis from Trinity College Library you acknowledge that all Intellectual Property Rights in any Works supplied are the sole and exclusive property of the copyright and/or other IPR holder. Specific copyright holders may not be explicitly identified. Use of materials from other sources within a thesis should not be construed as a claim over them.

A non-exclusive, non-transferable licence is hereby granted to those using or reproducing, in whole or in part, the material for valid purposes, providing the copyright owners are acknowledged using the normal conventions. Where specific permission to use material is required, this is identified and such permission must be sought from the copyright holder or agency cited.

Liability statement

By using a Digitised Thesis, I accept that Trinity College Dublin bears no legal responsibility for the accuracy, legality or comprehensiveness of materials contained within the thesis, and that Trinity College Dublin accepts no liability for indirect, consequential, or incidental, damages or losses arising from use of the thesis for whatever reason. Information located in a thesis may be subject to specific use constraints, details of which may not be explicitly described. It is the responsibility of potential and actual users to be aware of such constraints and to abide by them. By making use of material from a digitised thesis, you accept these copyright and disclaimer provisions. Where it is brought to the attention of Trinity College Library that there may be a breach of copyright or other restraint, it is the policy to withdraw or take down access to a thesis while the issue is being resolved.

Access Agreement

By using a Digitised Thesis from Trinity College Library you are bound by the following Terms & Conditions. Please read them carefully.

I have read and I understand the following statement: All material supplied via a Digitised Thesis from Trinity College Library is protected by copyright and other intellectual property rights, and duplication or sale of all or part of any of a thesis is not permitted, except that material may be duplicated by you for your research use or for educational purposes in electronic or print form providing the copyright owners are acknowledged using the normal conventions. You must obtain permission for any other use. Electronic or print copies may not be offered, whether for sale or otherwise to anyone. This copy has been supplied on the understanding that it is copyright material and that no quotation from the thesis may be published without proper acknowledgement.

Investigations into the Development, Diagnosis and Treatment of Oral Cancer

A dissertation submitted to the University of Dublin,

for the degree of Doctor of Philosophy

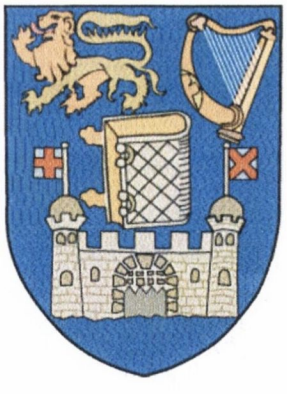
by

Katharine O'Callaghan

Supervisor - Dr. Jeff O'Sullivan

School of Dental Science,

Trinity College Dublin





May 2015

TRINITY COLLEGE
2 9 JUL 2015
LIBRARY DUBLIN

Thesis 10630

Declaration

I declare that this theis is entirely my own work and has not been submitted for any degree at this or at any other University. I agree that the library may lend or copy this thesis upon request.

Katharine O'Callaghan

Acknowledgements

First and foremost, I would like to sincerely thank my supervisor, Dr. Jeff O'Sullivan for his constant support, understanding and patience throughout my project and for all of the advice and help he has given me along the way. I would like to thank you for giving me this opportunity to grow as a scientist and researcher under your guidance and the many invaluable experiences I have gained I will carry with me throughout my career. I would also like to express my gratitude to Dr. Gavin Davey for being so generous with lab space and equipment. A special thank you must go to the staff of the Dublin Dental School and Hospital, in particular Prof. June Nunn and Prof. Stephen Flint. I must also thank Dr. Mary Clarke and the patients who provided me with samples. I would also like to thank the staff of the Focus Institute in DIT for helping me with my Raman spectroscopy work, especially Felipe who's help was invaluable throughout and for his patience in putting up with my endless amounts of questions! I must also thank Eleonora Palagano for all her help with the PBOX study.

My time in the lab wouldn't have been the same if I didn't have two best friends to experience it with. Níal, my partner in crime, so many laughs (and moans!) were had, I am not sure how we got all this work done! To Kim, a huge thank you, I will miss the endless chats and gossip over coffee and teaching Níal all about the female essentials (hair and shellac!).

I have met some incredible people and made some amazing friends during my time in Lab 1 and the 5th floor. Sandra, thank you so much for all the help, the proofreading, chats over lunch and for the general craic. A special thank you to Stephen (Super Steve!) the lab has never been the same since you left, especially when there's dry ice to be played with! To Laura Brady, I thank you for your encouragement, chats and gossip through the days of the dreaded western blots and wish you the best of luck in the coming weeks. I would also like to express my gratitude to Dr. Jer Hayes, for his knowledge and advise in the past year. To the original crew from 'the old building'- Trev, Dan & Chris and the newer 5th floor 'barn' members- Nicoletta, Darren, Andy, Laura, Natalie, Ryan, YounJing, Nick, Paul, Jenni, Rob, Niki, Simon, Ray, Roisin and Lois Lee- thank you so much for everything. A big thank you also to Dr. Glynis Robinson and the prep room team for all the help during my demonstrating hours. I would also like to acknowledge Mary Pat for keeping this place running day to day and

the water cooler chats, big thank you to Gavin for all your help with the confocal and to Barry for introducing me to the wonders of flow cytometry.

I have to thank all my friends outside the lab especially Karen and Bryony. You ladies are always there for the chats (&overeating!) and gave me huge support of which I can't thank you enough. Karen, we have experienced the highs and lows of a PhD together and I wish you all the luck in the world in your last few months! A massive thank you also to my hockey family, you all kept me sane, especially in the last few weeks.

The support of my family has been instrumental in allowing me to carry out this work. I can't possible express in words my gratitude to my parents in giving me constant support, both edible and emotional, throughout the four years. Thank you for taking me back in! To my brothers, Stephen, Philip and Kevin, thank you for your encouragement! I couldn't mention my family without mentioning Holly, who is no longer with us, but provided countless hugs and entertainment.

Finally, to my biggest support of all, Stephen, I cant thank you enough for the endless support, encouragement and positivity. Words cannot express just how important it was to me to have you there. I couldn't have done this without you.

I gratefully acknowledge the financial support of the Dublin Dental Hospital and Trinity College Dublin.

Abstract

Oral cancer is the sixth most common cancer in the world and has one of the highest mortality rates primarily due to the disease being largely asymptomatic until the latter stages. It is among one of the major worldwide public health problems with the incidence and mortality rates rising in several regions of the world, including Europe, South Central Asia and Australia. Smoking poses the highest risk for oral cancer followed closely by the consumption of alcohol. Furthermore diagnosis and treatment of oral cancer can prove to be challenging which seems surprising since the site of malignancy is so easily accessible.

Ethanol (EtOH), the active component of alcoholic beverages, has previously been implicated in cancer of the liver and is a known risk factor in oral cancer. Its role in oral tissue transformation is yet to be determined but it is known to modulate reactive oxygen species (ROS) in other cell types. The antioxidant response in cells controls ROS and is essential for cell maintenance. Alterations in these enzymes have been shown to be drivers of transformation. Two oral cell lines, a dysplastic cell type and isolated primary oral epithelial cells were used as representative models of the oral mucosa at defined stages of oral dysplasia/cancer. EtOH concentrations from 0.1- 3% showed no detrimental effect on cell survival over the given time course (n=8). The presence of EtOH was found to reduce the release of H_2O_2 in a dose dependent manner ($p< 0.5$-0.001) in relation to control, n=3). Antioxidant enzyme expression was modified with EtOH treatment however expression levels were dependent on cell types examined. Further analysis showed p53-dependant signalling in the case of certain antioxidant enzymes suggesting p53 has a regulatory role in the response to H_2O_2 deprivation. Cell cycle analysis, using flow cytometry, revealed EtOH also caused a modulation of cell cycle phases in addition to alteration of cyclin expression, as determined by immunoblotting. Lack of induction of apoptosis with EtOH treatment may allow for both the low levels of ROS and antioxidant enzyme alteration to cause progressive damage to cell regulation, which may potentiate carcinogenic transformation.

Raman spectroscopy can provide a molecular-level fingerprint of the biochemical composition and structure of cells with excellent spatial resolution and has been shown to be useful in discriminating between normal and cancer cells in other forms of malignancies. In this study, Raman spectra of nucleoli, nuclei and cytoplasm were

collected from oral cancer cell lines, dysplastic cells and normal primary epithelial cells *in vitro*. Principal component analysis was utilised as a multivariate statistical method to discriminate the spectra. Results show significant discrimination between cancer and normal cell lines based on contribution of nucleic acids and proteins for nucleolar and nuclear sites and lipids for cytoplasmic area. This technique many provide a rapid screening method and have potential use in the diagnosis of dysplasia and early, non-invasive oral cancer, the treatment of which involves much less extensive and complex surgery and a reduction in co-morbidity for the patient. In addition, Raman spectroscopy was utilised to monitor changes in the cells molecular fingerprints due to EtOH treatment to attempt to identify regions of cellular change. Findings indicate that EtOH is directly affecting the function of the nucleoli, a cell structure modified in malignancies to support increasing cellular proliferation.

Oral squamous cell carcinoma (OSCC) cells, being tumorigenic, are non-apoptotic in nature and recently a number of OSSCs have displayed resistance to a variety of current commonly used chemotherapeutic drugs. The novel microtubule-targeting pyrrolo-1,5-benzoxazepine (PBOX) compounds have demonstrated an ability to induce apoptosis in a number of chemotherapy resistant cell lines. In this study preliminary investigations into the efficacy of PBOX compounds in inducing apoptosis in OSCC cell lines were also undertaken. Initial viability studies have shown that the two PBOX test compounds, (PBOX-6 & PBOX-15) have a therapeutic potential in the treatment of OSCC. IC-50 values were 35μM and 470nM in TR146 cells and 2.6μM and 83nM in Ca9.22 cells for PBOX-6 and-15, respectively, over a 72h period. Using flow cytometric analysis of propidium iodide stained cells it was revealed that the PBOXs decreased cellular viability through induction of G2/M arrest. Through fluorescent microscopy analysis and immunoblotting techniques we determined that apoptosis was induced via tubulin depolymerisation. These results demonstrate the potential of PBOX-6 and PBOX-15 in inducing apoptosis in OSCC and further studies are warranted to access the potential of these drugs in treating OSCC.

Collectively, these results help to elucidate the mechanism through which alcohol promotes OSCC development, identifies a potential novel technique for early detection of OSCC and suggests the use of novel compounds for the treatment of OSCC. This body of work enhances the current knowledge in the field of oral cancer research and establishes a number of new and exciting avenues of research.

Abbreviations

ADH	Alcohol dehydrogenase
ALDH	Acetaldehyde dehydrogenase
APAF	Apoptotic protease activating factor
BCL	B-cell lymphoma
BCP	1-Bromo-3-chloropropane
BER	Base excision repair
$CaCl_2$	Calcium chloride
CAT	Catalase
CDK	Cyclin dependant kinase
CIN	Cervical intraepithelial neoplasia
CKI	Cyclin dependant kinase inhibitor
CML	Chronic myeloid leukaemia
DAPI	4',6-Diamidino-2-phenylindole, dihydrochloride
DCF	dichloroflourescin
DCFH-DA	2',7'-dichlorfluorescein-diacetate
DISC	Death inducing signalling complex
DNA	Deoxyribonucleic acid
DSB	Double strand breaks
EMT	Epithelial to mesenchymal transition
FADD	Fas-associated death domain
FBS	Fetal bovine serum
FTIR	Fourier transform infrared spectroscopy
G0	Quiescence
G1	Gap 1
G2	Gap 2
GOF	Gain of function

GPx	Glutathione peroxidise
GSSG	Glutathione disulfide
H&E	Hematoxylin and eosin
H_2O_2	Hydrogen peroxide
HIF	Hypoxia inducible factor
HIV	Human immunodeficiency virus
HPV	Human papillomavirus
HR	Homologous recombination
HRE	Hypoxic response elements
HRP	Horse radish peroxidase
IAP	Inhibitors of apoptosis
IMM	Inner mitochondrial membrane
LOF	Loss of function
M	Mitosis
MAPK	Mitogen-activated protein kinase
$MgSO_4$	Magnesium sulphate
MnSOD	Manganese superoxide dismutase
MPTP	Mitochondrial permeability transition pore
mRNA	Messenger ribonucleic acid
MTA	Microtubule targeting agents
mTOR	Mammalian target of rapamycin
NaCl	Sodium chloride
NAD	Nicotinamide adenine dinucleotide
NER	Nucleotide excision repair
NHEJ	Non-homologous end joining
NK	Natural killer
O_2	Molecular oxygen
O_2^-	Superoxide radical

OC	Oral cancer
$OH^{\cdot}$	Hydroxyl radical
OMM	Outer mitochondrial membrane
OSCC	Oral squamous cell carcinoma
p53	Tumour suppressor protein 53
PBOX	Pyrrolo-1,5-benzoxazepine
PBS	Phosphate buffered saline
PCA	Principal component analysis
PI	Propidium iodide
qRT-PCR	Quantitative reverse transcription PCR
RAPTOR	Regulatory-associated protein of mTOR
Rb	Retinoblastoma
RNA	Ribonucleic acid
ROS	Reactive oxygen species
S	Synthesis
SAC	Spindle assembly checkpoint
SDS	Sodium dodecyl sulfate
siRNA	Small interfering RNA
Smac	Second mitochondrial-derived activator of caspases
SOD	Superoxide dismutase
SSB	Single strand breaks
TBST	Tris buffered saline tween
TNF	Tumour necrosis factor
TRAIL	Tumour necrosis factor related apoptosis inducing ligand
UV	Ultraviolet
VEGF	Vascular endothelial growth factor
VEGF-R	Vascular endothelial growth factor receptor

Table of Contents

1 GENERAL INTRODUCTION 1

1.1 INTRODUCTION 2

1.2 PREMALIGNANT LESIONS 5

1.2.1 LEUKOPLAKIA 5

1.2.2 ERYTHROPLAKIA 5

1.3 CARCINOGENS 6

1.4 OC RISK FACTORS 8

1.4.1 SMOKING 8

1.4.2 HUMAN PAPILLOMAVIRUS 8

1.4.3 ETOH 9

1.5 DEVELOPMENT OF OSCC 9

1.6 SCREENING AND DIAGNOSIS OF OC 11

1.7 THERAPEUTIC STRATEGY IN OC 13

1.7.1 SURGERY 14

1.7.2 RADIATION THERAPY 14

1.7.3 CHEMOTHERAPY 14

1.7.4 GENE THERAPY 15

1.7.5 ANGIOGENESIS INHIBITORS 16

1.7.6 PYRROLO-1,5-BENZOXAZEPINE (PBOX) 17

1.8 MOLECULAR BIOLOGY OF CANCER 17

1.8.1 APOPTOSIS 19

1.8.2 INTERPHASE AND MITOSIS 21

1.8.3 DNA DAMAGE REPAIR 24

1.9 MALIGNANT TRANSFORMATION 25

1.10 TUMOUR ENVIRONMENT 26

1.11 ROS AND ANTIOXIDANTS 27

1.12 AIM OF THESIS 31

2 MATERIALS AND METHODS 33

2.1 GENERAL METHODOLOGY 34

2.1.1 PREPARATION OF SOLUTIONS 34

2.1.2 PIPETTING 34

2.1.3 CENTRIFUGATION 34

2.1.4 SPECTROPHOTOMETRY 34

2.1.5 Reagents 34
2.1.6 Cell culture 34
2.2 Cell culture 35
2.2.1 Culture of Ca9.22 oral carcinoma cell line 35
2.2.2 Culture of TR146 oral carcinoma cell line 35
2.2.3 Culture of DOK dysplastic oral cell line 36
2.2.4 Culture of SCC-4 oral carcinoma cell line 36
2.2.5 Culture of primary oral epithelial cells 36
2.2.6 Determination of cell density and viability-trypan blue exclusion 37
2.3 Analysis of cell proliferation and cytotoxicity 38
2.4 ADH activity assay. 38
2.5 Determination of extracellular ROS 39
2.6 Determination of intracellular ROS 39
2.7 Cell Cycle Analysis 41
2.8 Transfection with p53 siRNA 41
2.9 Western Blotting 42
2.9.1 Preparation of cell lysates 42
2.9.2 Determination of protein content 42
2.9.3 Sodium Dodecylsulphate-polyacrylamide Gel Electrophoresis 43
2.9.4 Western blotting 43
2.10 RNA extraction 44
2.11 Quantitative Reverse Transcription PCR 45
2.12 Raman Spectroscopy 46
2.12.1 Sample preparation 46
2.12.2 Raman Instrumentation 46
2.12.3 Data preprocessing 46
2.13 Analysis of tubulin polymerisation by Western Blot 48
2.14 Fluorescence microscopy 48
2.14.1 Analysis of tubulin morphology 48
2.14.2 Analysis of nucleolar morphology 49
2.15 PBOX synthesis 49

3 ETOH MODULATION OF HYPOXIC RESPONSE PROTEINS IN ORAL EPITHELIAL CELLS 51

3.1 Introduction 52
3.1.1 Alcohol and OC 52
3.1.2 EtOH 53

3.1.3 EtOH and oxidative stress in OC 54
3.1.4 ROS and p53 56
3.2 Aims of this chapter 58
3.3 Results 60
3.3.1 EtOH does not affect the viability of cell lines 60
3.3.2 ADH is absent from OSCC cell lines 62
3.3.3 The effect of EtOH on H_2O_2 production in OSCC cell lines 64
3.3.4 The effect of EtOH on HIF1-a in OSCC cell lines. 73
3.3.5 Modulation of antioxidant enzymes in OSCC cells in response to EtOH exposure. 76
3.3.6 The influence of EtOH on the cell cycle in OSCC cell lines 88
3.3.7 The effect of EtOH on dysplastic cell viability. 95
3.3.8 ADH is absent from a dysplastic oral cell line. 97
3.3.9 The effect of EtOH on H_2O_2 production in a dysplastic oral cell carcinoma cell line. 99
3.3.10 The effect of EtOH on HIF1-a in a dysplastic oral cell line. 101
3.3.11 Modulation of antioxidant enzymes in oral dysplastic cells in response to EtOH exposure. 103
3.3.12 The influence of EtOH on the cell cycle in a dysplastic oral cell line. 109
3.3.13 The effect of p53 on antioxidant response in the TR146 cell line. 111
3.3.14 The effect of p53 knockdown on HIF-1a activity in the presence and absence of EtOH in TR146 cells. 113
3.3.15 The effect of p53 knockdown on antioxidant enzyme activity in the presence and absence of EtOH in TR146 cells 115
3.3.16 Determining the effect of EtOH on redox status in isolated human primary oral epithelial cells 121
3.3.17 The effect of EtOH on HIF-1a activity in isolated human primary oral epithelial cells 123
3.3.18 Analysis of antioxidant enzyme expression in human primary epithelial cells 125
3.4 Discussion 131

4 DISCRIMINATION OF OSCC CELLS USING RAMAN SPECTROSCOPY 143

4.1 Introduction 144
4.1.1 OC diagnosis 144
4.1.2 Vibrational spectroscopy 145
4.1.3 Theoretical basis of Raman spectroscopy 147
4.1.4 Identification of biochemical and molecular changes using Raman Spectroscopy 149

4.1.5 Raman spectroscopy in cervical cancer 151
4.1.6 Principal components analysis 152
4.2 Aims of the chapter 154
4.3 Results 155
4.3.1 Raman analysis of the subcellular regions within human primary oral epithelial cells. 155
4.3.2 Determination and analysis of the variation between Raman spectra of human OC cell lines and human primary oral mucosal cells. 161
4.3.3 Raman spectroscopy has potential in differentiation of dysplastic lesions from OSCC 176
4.4 Discussion 189

5 ANALYSIS OF ETOH INDUCED CHANGES IN THE BIOCHEMICAL PROFILE OF ORAL EPITHELIAL CELLS USING RAMAN SPECTROSCOPY. 197

5.1 Introduction 198
5.2 Aims of the chapter 200
5.3 Results 201
5.3.1 Raman analysis of OSCC cellular components after exposure to EtOH 201
5.3.2 Analysing the effect of EtOH on the DOK dysplastic cell line using Raman spectroscopy and principal component analysis 224
5.3.3 Raman spectroscopy and principal component analysis of isolated human primary cells after exposure to EtOH 236
5.4 Confirmation of the effect of EtOH on the nucleoli Raman spectra of TR146 and Ca9.22 cells using fluorescent microscopy 248
5.5 Discussion 256

6 INDUCTION OF APOPTOSIS IN OSCC CELL LINES BY PYRROLO-1,5-BENZOXAZEPINES 261

6.1 Introduction 262
6.1.1 Microtubules 262
6.1.2 Microtubule targeting agents 264
6.1.3 Pyrrolo-1,5-Benzoxazepine (PBOX) 267
6.2 Aims of the chapter 270
6.3 Results 271
6.3.1 PBOX compounds reduced OC cell proliferation 271
6.3.2 PBOX compounds destabilised the microtubule network in OC cells 273
6.3.3 PBOX compounds induce G2/M arrest and apoptosis in OC cell lines 280

6.3.4 PBOX COMPOUNDS INDUCE DEGRADATION OF PARP IN OC CELL LINES 282
6.3.5 THE EFFECT OF P53 KNOCKDOWN ON THE VIABILITY OF TR146 CELLS IN THE PRESENCE OF PBOX COMPOUNDS 284
6.4 DISCUSSION 286

7 GENERAL DISCUSSION 289

7.1 GENERAL DISCUSSION 290
7.2 FUTURE WORK 294
7.2.1 EXAMINATION OF THE ROLE OF ALCOHOL IN OC DEVELOPMENT 294
7.2.2 INVESTIGATION OF THE USE OF RAMAN SPECTROSCOPY AS A DIAGNOSTIC AID IN OC 295
7.2.3 EXPLORE THE THERAPEUTIC EFFICACY OF PBOX COMPOUNDS IN OC TREATMENT 296
7.3 CONCLUSIONS OF THE THESIS 296

8 REFERENCES 297

9 PUBLICATIONS 317

10 APPENDIX 1 319

10.1 ETHICS APPROVAL 320
10.2 PATIENT CONSENT FORM 321
10.3 PATIENT INFORMATION SHEET 322

11 APPENDIX 2 325

11.1 DIT MATLAB SCRIPT 326

1 GENERAL INTRODUCTION

1.1 Introduction

Oral cancer (OC) is the sixth most common cancer globally and has one of the highest mortality rates, due to it being largely asymptomatic until the latter stages of the disease. Oral squamous cell carcinomas (OSCC) account for 90% of all cancers that occur in the oral cavity and 2-3% of all malignancies. Cancers of the oral cavity include malignancies found in the tongue, floor of the mouth, buccal mucosa, retromolar trigone, gingiva, hard palate and lips (Zhang *et al.*, 2012, Arosarena *et al.*, 2006, Iype *et al.*, 2004, Conley, 1954, Genden *et al.*, 2003, Srivastava and Sharma, 1968, Reddy *et al.*, 1975, Moretti *et al.*, 2011).

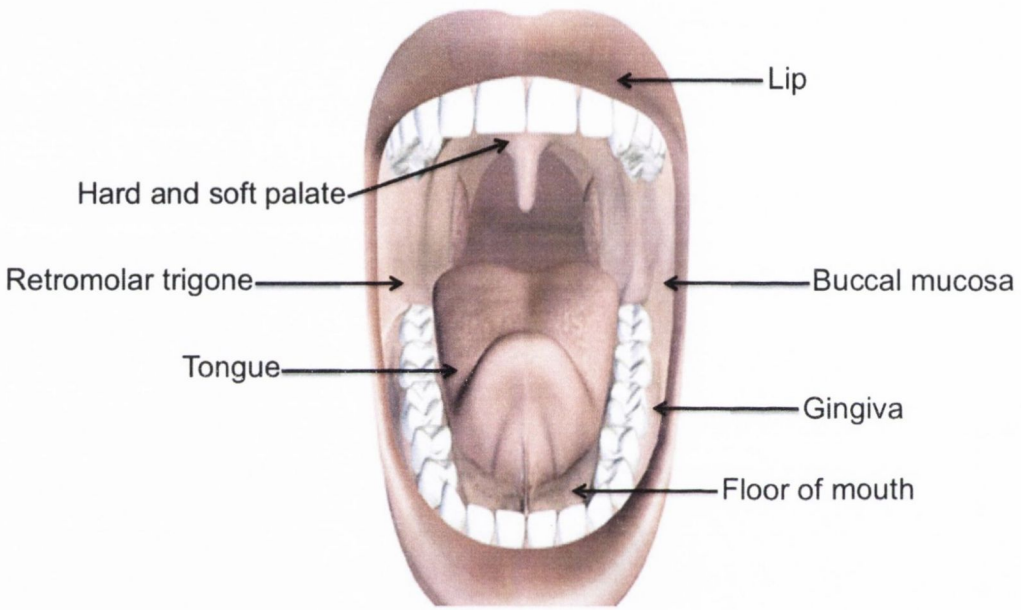


Figure 1-1 Diagrammatic representation of the most common sites of cancer in the oral cavity.

Cancer of the oral cavity can develop on the lip, the floor of the mouth, the buccal mucosa, both hard and soft palates and the retromolar trigone.

OC is a major worldwide public health problem (Franceschi *et al.*, 2000) with incidence and mortality rates rising in several regions of the world, including Europe, South Central Asia and Australia (Parkin *et al.*, 2005). Around 40% of the total diagnosed cases of OC occur in some of the poorest countries in the world including India, Pakistan, Bangladesh and Sri Lanka (Ahluwalia *et al.*, 2005). India has one of the highest rates in the world, accounting for one-third of OC cases and this trend is continuing to rise (Pal and Mittal, 2004). In Ireland over 300 cases are reported every

year with the incidence being more common in men than women. However the rate of mouth cancer in women has increased significantly at a rate of 3% per year since 1994 (NCRI). In Britain the incidence of mouth cancer has increased faster than any other cancer in the past 25 years (Cancer Research UK).

Ireland	Years	No of cases	% of total*	Crude rate**
Female	1994-2009	1312	0.7%	4.14
Male	1994-2009	3304	1.8%	10.52
Both genders	1994-2009	4616	1.2%	

Table 1-1 Incidence rates of cancers of the oral cavity and pharnyx for the Irish population for 1994-2009.

This figure is a percentage of total cancers in Ireland for the same years. * percentage of the total population. ** The crude rate is the number of cases or deaths divided by the population at risk, expressed per 100,000 persons per year (Irish Cancer Society, 2009).

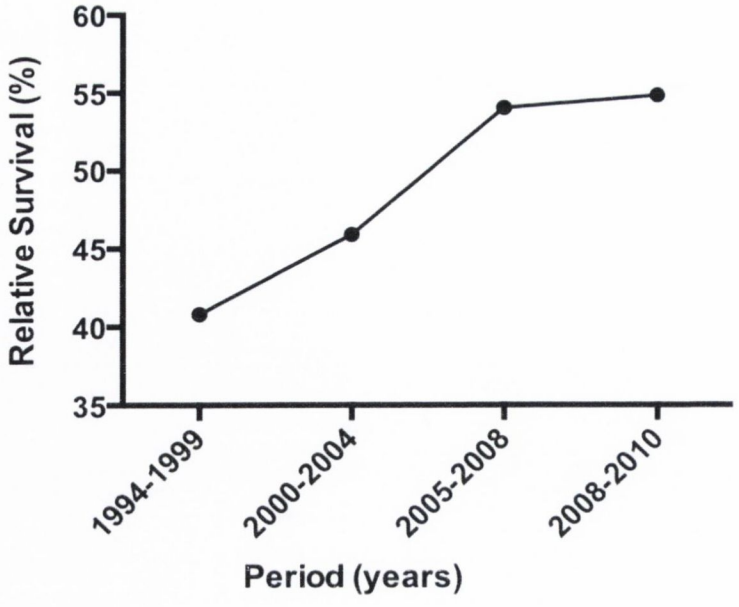


Figure 1-2 The increase in the 5 year relative survival of OC cases in Ireland.

Shown are the 5-year survival rates for OC from the period of 1994 until 2010. The number of people surviving more than 5 years with OC has continued to rise during this period (National Cancer Registry Ireland, 2011).

Known risk factors include both lifestyle and biological factors. Smoking poses the highest risk for OC followed closely by the consumption of alcohol (Blot, 1992). The human papillomavirus (HPV) is most commonly known for being a major cause of cervical cancer however in more recent times it has been implicated in a large number of OCs and in particular cancers of the oropharynx which accounts for ~30% of these cancers (D'Souza and Dempsey, 2011). The majority of OSCC progress from premalignant lesions, which can result from one of the many risk factors associated with the disease. Premalignant lesions, termed plakias are plaques or patches located usually on a mucous membrane and include erythroplakia (red spots) and more commonly leukoplakia (white spots) or a combination of both (Figure 1-3) and are described in detail in the following section.

1.2 Premalignant lesions

1.2.1 Leukoplakia

Leukoplakia, as defined by the World Health Organisation (WHO), is a "white patch or plaque that cannot be characterised clinically or pathologically as any other disease". It occurs more frequently in older men with an increasing prevalence associated with an increase in age (over 80% of men over the age of 70 have leukoplakia (Bouquot and Gorlin, 1986, Shafer and Waldron, 1961). The frequency of dysplastic or malignant alterations in oral leukoplakia ranges from 15.6% to 39.2% depending on the study (Shafer and Waldron, 1961, Waldron and Shafer, 1975, Pindborg *et al.*, 1963, Banoczy and Csiba, 1976, Feller *et al.*, 1991). The location of oral leukoplakia has a significant correlation with the frequency of finding dysplastic or malignant changes in biopsies. In the study by Waldron and Shafer, 1975, the floor of the mouth was the highest risk site with 42.9% of leukoplakias showing some degree of epithelial dysplasia, carcinoma *in situ*, or unsuspected invasive squamous cell carcinoma. The tongue and lip were also identified as high-risk sites with dysplasia or carcinoma present in 24.2% and 24% of these cases, respectively. The clinical appearance of the lesion may also indicate some correlation with the probability that the lesion will show dysplastic or malignant features. In general the thicker the plaque the greater the chance of finding dysplastic changes. Thicker more verrucous leukoplakia is more likely to show dysplasia in comparison to thick homogenous leukoplakia. Additionally, a thick homogenous leukoplakia is more likely to show dysplasia than a thin leukoplakia. Furthermore leukoplakias with mixed red (erythroplakia)/white components are at the greatest risk for presenting with dysplasia or carcinoma. Pindborg found that 14% of speckled leukoplakias exhibit carcinoma whereas another 52% showed epithelial dysplasia (Pindborg *et al.*, 1963).

1.2.2 Erythroplakia

Similar to the definition of leukoplakia, erythroplakia is a clinical term that refers to a red patch that cannot be defined clinically or pathologically as any other condition. The floor of the mouth, lateral tongue, retromolar pad and soft palate are the most frequent sites of involvement. It does not occur as frequently as leukoplakia but it is much more likely to show dysplasia or carcinoma. In combination with their studies on leukoplakia,

Shafer and Waldron, 1961, also analysed 65 cases of erythroplakia. All cases showed some degree of epithelial dysplasia; 51% were invasive cell carcinoma, 40% were carcinoma *in situ* or severe dysplasia and the remaining 9% demonstrated mild-moderate dysplasia (Shafer and Waldron, 1961).

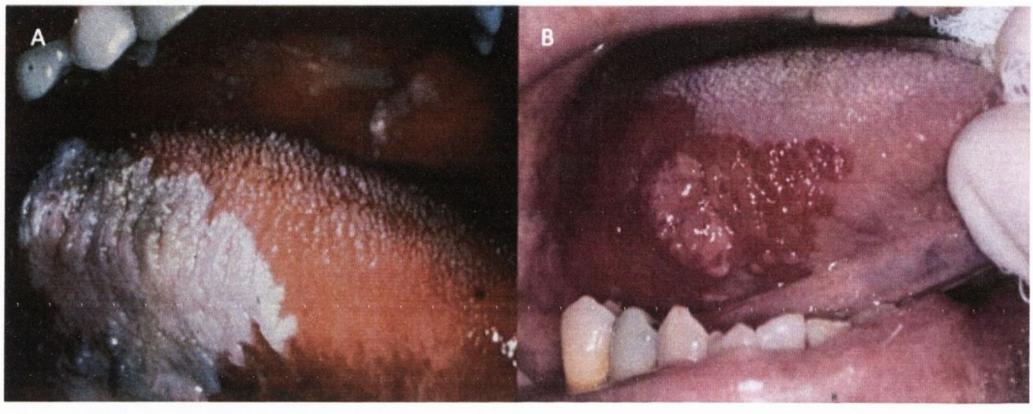


Figure 1-3 Common lesions of the oral mucosa

Leukoplakia (A) and erythroplakia (B) located on the lateral border of the tongue, a common site of malignancies in the oral cavity.

1.3 Carcinogens

A carcinogen is any substance, radio nucleotide or radiation that is directly involved in causing cancer. They directly target deoxyribonucleic acid (DNA) or interfere with cellular metabolic processes eventually causing different types of mutations in the DNA. Carcinogens can be physical, chemical, or biological and can have various sources. There are two different types of mutations that can occur in cells as a result of exposure to a carcinogen. A somatic or acquired mutation is an alteration in DNA that occurs after conception. These types of mutations occur in cells excluding germ cells, usually surface epithelial cells that are generally more exposed. These mutations are therefore not passed on to further generations. A germline mutation differs to a somatic mutation as it occurs in the DNA of the egg or sperm and affects the next generations. The chance of offspring having the mutation depends on if genetic material has been passed on at crossing over point in meiosis where chromatids exchange genetic material. Examples of germline mutations include cystic fibrosis (X-linked) (Devaney *et al.*, 2003) and amelogenesis imperfecta, causing abnormal formation of the enamel, which occurs due

to mutations in several different genes (Gadhia *et al.*, 2012). Common cancer causing mutations are mutations in the BRCA1 or BRCA2 genes, which can lead to a higher rate of breast cancer (Paul and Paul, 2014). This type of mutation is also called a hereditary mutation and can only be passed on if the carcinogen has irreparably damaged a germ cell through exposure.

Numerous carcinogens are found throughout the environment. A multitude of different chemicals are believed to have carcinogenic properties but insufficient evidence is yet to be found to support these. Natural chemicals such as asbestos and formaldehyde are listed on the International Agency for Research on Cancer (IARC) Group 1 carcinogens listing. Group 1 carcinogens are agents that have been confirmed as causing cancer in humans. Compounds in Groups 2A and 2B are probably and possibly carcinogenic, respectively. Groups 3 and 4 contain agents that are unconfirmed or probably not carcinogenic to humans. Asbestos is a group of naturally occurring silicate minerals, which are used commercially in household cleaning products, cigarettes and in building materials (Goswami *et al.*, 2013). Inhalation of these micro fibres can be seriously damaging to an individual's health and can even cause mesothelioma (malignant lung cancer) (Liu *et al.*, 2010b). The EU has banned all use of asbestos including the extraction, manufacture and processing of asbestos products (Commission, 2009). These fibres are believed to damage lung cells after inhalation by becoming tangled in the cellular chromosomes (Liu *et al.*, 2010b).

Several agents are found in food or occur through the preparation of food, for example acrylamide in foods heated above 120°C, are also found on the IARC's list of group 1 carcinogens (Dearfield *et al.*, 1988). Also included are some artificial sweeteners (aspartame), fluoride and ethanol (EtOH), which is present in alcoholic beverages. Other carcinogenic factors include inherited genes (for example, BRCA1, BRCA2), hormones, infectious agents, radiation, sunlight, tobacco and obesity. Carcinogens can be classified as being genotoxic or non-genotoxic. Genotoxins have a direct deleterious effect on DNA in the cell affecting its integrity. Carcinogens that are non-genotoxic affect growth within a cell by interfering with proteins and biochemical secondary messengers. They can be chemical or non-chemical agents.

Physical	Chemical	Biological
Ultraviolet (UV) light	Asbestos	Viruses-HIV, HPV
Ionizing radiation	Tobacco smoke	Inherited genes
Electromagnetic fields	Acrylamide	Hormones

Table 1-2 - Examples of carcinogens from the group 1 list of carcinogens as classified by the IARC.

1.4 OC risk factors

1.4.1 Smoking

The single greatest risk factor for OC is tobacco, although people who do not smoke or have no known risk factors can still develop the disease. All forms of tobacco products have been implicated in OC including cigars, cigarettes and chewing tobacco. Snuff, a type of smokeless tobacco, gives people who use this product a 50% chance of developing cancer of the cheek and gums (Society, 2011). Tobacco smoke contains almost 250 known harmful chemicals and at least 69 of these are recognised carcinogens (Hecht, 1999) including arsenic, benzene and nickel among many others. In India tobacco related deaths are high, due to the type and quantities of tobacco used. There are about 700,000 new cases of cancer every year and almost half of them are tobacco related and it has been shown that 1 in 4 of all cancers there are OCs. This may also be due to the age at which young people start using tobacco related products. Gutka, a mixture of betel nut and chewing tobacco, is extremely addictive and is targeted at the younger population (WHO, 2010).

1.4.2 Human Papillomavirus

The human papillomavirus (HPV) has been well documented in various types of cancer and infection. In addition HPV is a known risk factor for OCs and in particular oropharynx and throat cancer (Jayaprakash *et al.*, 2011). There are over 120 types of HPV but HPV type 16 has been predominantly associated with OCs and is also implicated in a vast majority of cervical cancers (Elango *et al.*, 2011). HPV- induced cancers often have viral sequences integrated into their DNA. Some of these sequences

of genes have the ability to act as oncogenes that promote tumour growth and malignant transformation (Madkan *et al.*, 2007).

1.4.3 EtOH

EtOH, more commonly known as alcohol (or ethyl alcohol), has been implicated in a number of cancers, particularly malignancies of the liver. It is a psychoactive compound and one of the oldest recreational drugs in use. It results in more than 2.5 million deaths per annum (WHO, 2010). Approximately 9% of deaths in the 15-29 age category are attributed to alcohol consumption globally through liver failure and alcohol poisoning. EtOH has been documented as the second most common risk factor in OC behind smoking however individuals who smoke and consume alcoholic beverages have been seen to have a five times greater risk of developing OC (Blot *et al.*, 1988). The exact mechanisms underlying the associations between alcohol and OC are yet to be elucidated. There are several mechanisms by which alcohol is proposed to cause an increased risk of OC development, including both local and systemic effects. Local effects include increased penetrability of carcinogens into the oral mucosa both by improved solubility due to EtOH and increased permeability. Long term alcohol consumption has also been shown to cause a reduction in epithelial thickness in human tongues (Valentine *et al.*, 1985). Possible systemic effects of EtOH include the altering of the hepatic metabolism, which results in the liver being unable to deal with toxic substances at a normal rate. This causes a build-up of toxins in the system, which could potentially lead to carcinogenesis. EtOH has also been shown to cause immunosuppression by impairing both the innate and adaptive immune systems. Both of which are essential in tumour cell surveillance (Poschl and Seitz, 2004). In particular, natural killer (NK) cells induction is supressed by EtOH consumption in livers of mice (Pan *et al.*, 2006).

1.5 Development of OSCC

OSCCs progress through stages of hyperplasia to dysplasia of varying degrees to carcinoma *in situ* before developing into an invasive metastatic tumour. In the beginning a stem cell must undergo a genetic alteration, which a number of factors could be a cause of. This stem cell is located in the basal layer of the oral mucosa. As this stem cell

divides its daughter cells inherit all the genetic alterations from the parent cell (White *et al.*, 2013). The majority of genetic alterations that occur in cells throughout the body are either repaired or the cell will undergo apoptosis (Section 1.8.1). This is due to specific biochemical mechanisms in response to cellular maintenance. However in some cases these alterations are not detected by the regulatory checkpoints that exist within the cell so ultimately the cell continues to divide and can go on to develop into a malignant tumour. Once established the genetically altered group of cells continually divide and form a tumour in the basal layer of the mucosa, which can then break through the overlying epithelial cells and present as a visible patch in the mouth.

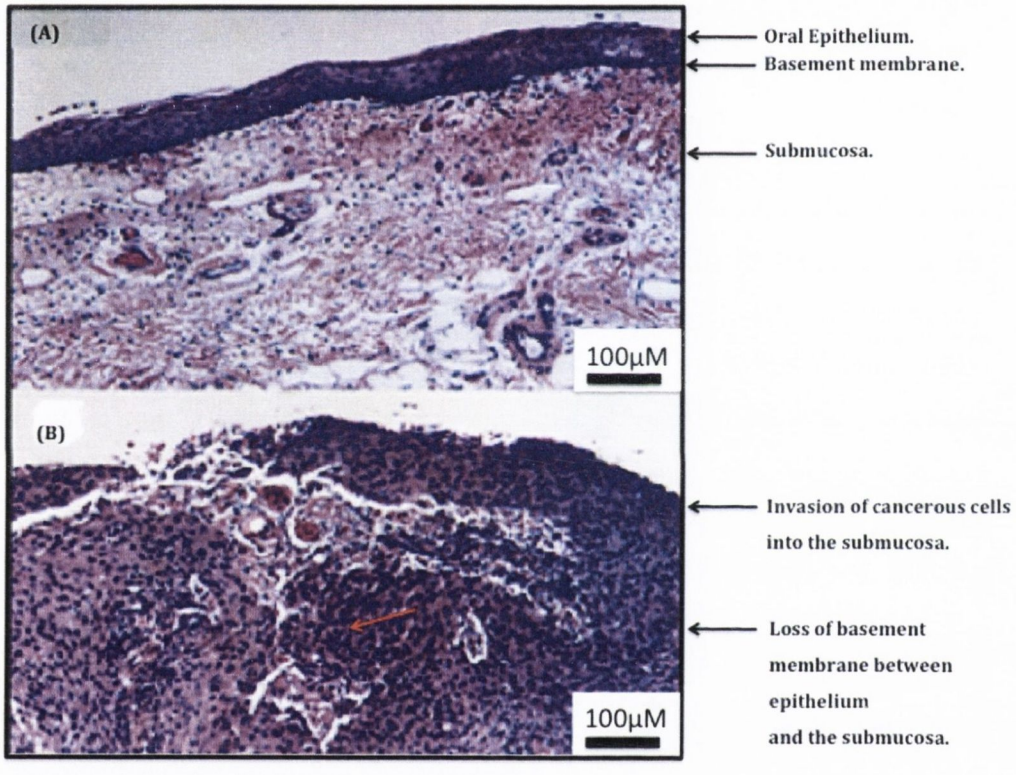


Figure 1-4 Sections of healthy oral mucosa and OC.

In the healthy mucosa (A) a clear boundary can be seen between the epithelium and the oral mucosal layers beneath. OC cells (B) invade from the epithelium into the deeper mucosa beneath with no distinct boundary and cells are irregularly shaped with enlarged nuclei (red arrow). Sections are stained with hematoxylin and eosin stain (H&E). Nuclei are stained dark purple/blue and cytoplasm is stained light pink (Dublin Dental Hospital, Dr S.Flint).

The biochemical mechanisms of OC remain unclear but all to date appear evolve through a multistep process of genetic changes resulting from exposure to carcinogens, the most commonly known to be derived via smoking and alcohol intake. Many studies describe the importance of oncogenes and tumour suppressor genes during the development of OC. One of the most commonly seen mutations in OC is a mutation in the tumour suppressor protein 53 (p53) gene. p53 is an extremely important regulator of the cell cycle. P53 is activated in response to DNA damage, oncogene activation and hypoxia in which is subsequently coordinates biological outputs such as apoptosis cell-cycle arrest, senescence and modulation of autophagy (Yee and Vousden, 2005, Riley *et al.*, 2008, Green and Kroemer, 2009). Alteration or inactivation of p53 by mutation or by its interactions with oncogene products of DNA tumour viruses can lead to cancer. p53 mutations are categorised as loss-of-function mutations or gain-of-function mutations depending on the resulting function of the protein. The resulting function depends on where in the gene p53 is mutated. For example the mutation R248W, which has a point mutation at codon 248, is a gain-of-function mutation. Gain-of-function p53 mutations lose their normal tumour suppressor functions but gain new activities, in comparison to loss-of-function mutations, which do not gain any new functions. For example, wildtype p53 upregulated c-myc *in vitro* whereas mutated gain-of-function mutation repressed c-myc (Frazier *et al.*, 1998). Mutations in the p53 gene are one of the most common mutations in all cancers and occur in 30%-70% of all OSCC. Tumours with mutations in this gene grow faster and have a worse prognosis with an overall reduced survival rate (Acha-Sagredo *et al.*, 2009).

1.6 Screening and Diagnosis of OC

Screening is extremely important in OC. Effective screening can detect disease at the asymptomatic stage when it can be readily interrupted providing an improved prognosis for the patient. Well-known examples of screening programmes for other forms of cancer include the Pap smear for cervical cancer and mammography for breast cancer (Irish Cancer Society). To date there is no official screening process for OC. Current clinical diagnostics include visual examination for potentially malignant lesions including leukoplakia and erythroplakia (Section 1.2) Depending on the size, shape and texture of the lesion further tests may be carried out in the clinic to investigate the risk for these pieces of tissue. Which lesions are selected for analysis can be subjective and is

very much the decision of the clinician leading to the fundamental reason for misdiagnosis, which is inconsistent differentiation between pre-malignant and benign lesions of the mouth (Abbey *et al.*, 1995). Effective tests and screening programmes are urgently needed for early stage detection of OC.

Current diagnostic aids for suspicious lesions in the mouth include brush biopsy, toluidine blue stains and light based detection systems. These tests are not 100% definitive and all abnormal results from tested lesions must undergo subsequent scalpel biopsy and pathological examination, which is the gold standard for OC diagnosis. Brush biopsies were introduced in 1999 as a potential OC diagnostic device. In recent years results from brush biopsy studies have shown encouraging results such as those observed in a multicentre study from the United States which consisted of 945 patients that underwent a brush biopsy (OralCDx) procedure to class oral lesions. Suspicious lesions underwent both brush biopsy and scalpel biopsy. Innocuous lesions just underwent brush biopsy. The results showed that just using the suspicious lesions cohort there was greater than 90% specificity. However, a major weakness in the study was the lack of surgical biopsies in the innocuous lesions cohort; this caused a loss in critical information from the brush technique. Without that information the true sensitivity and specificity in the innocuous lesions were lost and cannot be compared to the suspicious lesions. An effective test would have the diagnostic capability to detect cancer in an otherwise non-suspicious lesion. Other studies showed similar results but with similar weaknesses (Sciubba, 1999).

Toluidine blue stain, known as an exclusion dye, has been used for decades as an aid to identify mucosal abnormalities and to identify margins or abnormal tissue before excision. Toluidine blue is an acidophilic metachromatic dye containing a heterocyclic thiazine group that selectively stains acidic tissue components, therefore it can stain both DNA and ribonucleic acid (RNA). It has been shown to be a potentially useful tool as a screening technique in the detection of OC (Epstein *et al.*, 1997) and although it is not as proficient a screening tool for OC when compared with a brush biopsy, it may be effective it may be effective in detecting satellite lesions of patients with abnormal mucosa (Epstein *et al.*, 1997).

The most commonly used light based detection system is the commercially available Vizilite which works by disrupting the glycoproteins on the surface epithelium, desiccating the mucosa and allowing light to penetrate into the cells. Abnormal oral cells

are more fluorescent due to their changes in refractive properties from the increasing amount of DNA. Recent studies suggest that Vizilite is more useful as an adjunctive tool to identify asymptomatic and clinically non-evident lesions and for follow up treatment in OC cases (Vashisht *et al.*, 2014). All of the non-invasive diagnostic tools are effective to a certain extent in cancer diagnosis, but none are selective or specific enough to confidently confirm the presence or absence of dysplasia or cancer without the need for an invasive surgical biopsy. Continued advances in screening tools are needed to aid oral health care professionals in the detection of relevant potentially malignant lesions.

A recent development in optical diagnostics is the use of Raman spectroscopy. The power of this method is primarily related to the molecular and biochemical signature it provides of the biological sample when the fingerprint region is analysed. The Raman effect is a result of inelastic scattering of monochromatic electromagnetic radiation due to interaction with molecular vibrations, such that the frequency of the scattered radiation is different from the incident radiation (Raman, 1928). Raman has been explored for routine biopsy screening in cases of cervical cancer and has proven to be highly selective and specific (Lyng *et al.*, 2007). Using Raman for OC screening could prove very beneficial, as it would cause little or no discomfort to the patient and samples can be screened rapidly.

1.7 Therapeutic strategy in OC

Treatment in OC is typically a multidisciplinary approach since in a large amount of cases the disease is caught at the latter stages. Treatment choice is specific for each patient and is decided on by a team of health care professionals including pathologists, radiologists, surgeons and oncologists. Early stage OSCC is typically treated with surgery, chemotherapy or radiation. The decision as to which treatment is used is usually based on site, size and histological findings. Unfortunately, as mentioned previously, the majority of cancers present at an advanced stage where therapeutic strategies are more complex. There are several treatment regimes available for the management of OC. No one type of treatment is effective in all cases and the success of treatment usually comes down to an individual basis. Complete removal of the tumour without harming other tissues in the body is the goal of the treatment however some therapy options can damage adjacent healthy tissue.

1.7.1 Surgery

In the treatment of cancer, surgery can be used under several different conditions. It can be a primary form of treatment in small-localized tumours and but is not commonly used as a form of treatment cancers which have undergone metastasis as it is not possible to locate and remove all of the metastatic cells. Tumours that have a more precise boundary are easier to remove and have a higher successful outcome. Surgery in OC can be used to remove the tumour and to help restore appearance and function in areas affected by the treatment. In more advanced cases of OC, parts of the jaw (mandibulectomy) and neck must also be removed. Glossectomy, removal of the tongue, can be necessary in more developed cases of OC (Shah and Gil, 2009).

1.7.2 Radiation Therapy

Radiation is energy that is carried by waves or a stream of particles. Ionizing radiation is a type of cancer therapy that is used to kill cancerous cells by inducing damage with the cells DNA and utilising the cells normal response to this damage to induce apoptosis (programmed cell death). This form of treatment has been used in cancer therapy for over 100 years and targets cells that are dividing rapidly therefore damaging a lot more cancer cells than normal cells (Grubbe, 1902). However it can cause significant side effects by damaging normal cells that are undergoing division. Radiation of the mouth can cause xerostomia (dry mouth) but recent advances in radiation therapy have demonstrated that reducing parotid gland exposure can significantly reduce subsequent xerostomia and improve quality of life (Anand *et al.*, 2006). Additionally, the use of a cytoprotective adjuvant such as Amifostine in radiation therapy can significantly reduce xerostomia in patients with OC undergoing treatment (Gu *et al.*, 2014).

1.7.3 Chemotherapy

Chemotherapy is based on the same principle as radiation therapy and also targets cells that are actively and rapidly dividing. Chemotherapy is the general term for a group of drugs called antineoplastic agents that interfere with the cell cycle (Donehower *et al.*, 1979). All chemotherapeutic drugs affect cell division and causes damaged cells to undergo apoptosis. These drugs can be used alone or in combination with one other agent to treat malignant cells. The use of chemotherapy alone in OC treatment has

shown no evidence of increased survival rates and is usually used in combination with radiation therapy (Burri and Lee, 2009). The most common chemotherapeutic drugs used for OC treatment include cisplatin, carboplatin, 5-fluorouracil and the taxanes, which are all radiation sensitisers. Combination chemoradiation therapy is used after surgery for patients with poor-prognosis late stage cancer. Additionally neo adjuvant (pre surgery) chemotherapy has not been shown to improve survival rates (Licitra and Vermorken, 2004).

1.7.4 Gene Therapy

Gene therapy is a form of cancer therapy that is used to correct defective genes responsible for disease development. There are several different types of gene therapy that can involve the insertion, alteration, and removal of genes within individual cells and biological tissues. It is commonly known that cancer cells have the ability to grow without detection by the immune system. One type of gene therapy aims to overcome this problem by harvesting cancer cells from patients and making them more recognizable to the immune system by the addition of one or more genes. The cells are then cultured *in vitro*, destroyed and their cellular contents are incorporated into a vaccine (Kowalczyk *et al.*, 2003). Other types of gene therapy include direct delivery of cytokines into a tumour (Nawrocki *et al.*, 2001) or removal and alteration of immune cells which are primed outside the body and reinserted back into the individual (Kikuchi, 2006). Although gene therapy is not currently used to treat OC, recent advances in gene therapy trials in other cancers look promising and could offer increased effectiveness in comparison to other therapeutic strategies. In 2010 alone, 84 clinical trials were approved worldwide for gene therapy. One of the more recent trials for gene therapy was a study involving the local direct injection of rAD-p53 monotherapy with either concurrent radiotherapy or chemotherapy in advanced stage head and neck carcinoma (Clinicaltrials.gov-NCT00902083). Results are as yet unpublished however the increase in clinical trials for this type of therapy worldwide could signify that the treatment looks promising. There is currently no form of gene therapy approved by the FDA.

1.7.5 Angiogenesis Inhibitors

Angiogenesis, the formation of new bloods vessels, has been an area of interest in recent years for targeting tumour growth. As a tumour grows the blood vessels surrounding it are not able to provide the site with the nutrients and oxygen (O_2) it requires (Jones and Thompson, 2009). As a consequence of this the centre of the tumour mass becomes hypoxic and this drop in O_2 levels within the tumour causes O_2 sensors in the cells like hypoxia inducible factor (HIF)-1α to activate factors that stimulate angiogenesis (Harris, 2002). These factors include vascular endothelial growth factor (VEGF), which can also stimulate healthy cells surrounding the tumour to promote angiogenesis. Not only do the new blood vessels provide nutrients and O_2 to the tumour, they also provide an exit for cancerous cells to metastasize and spread to other tissues in the body (Bacac and Stamenkovic, 2008).

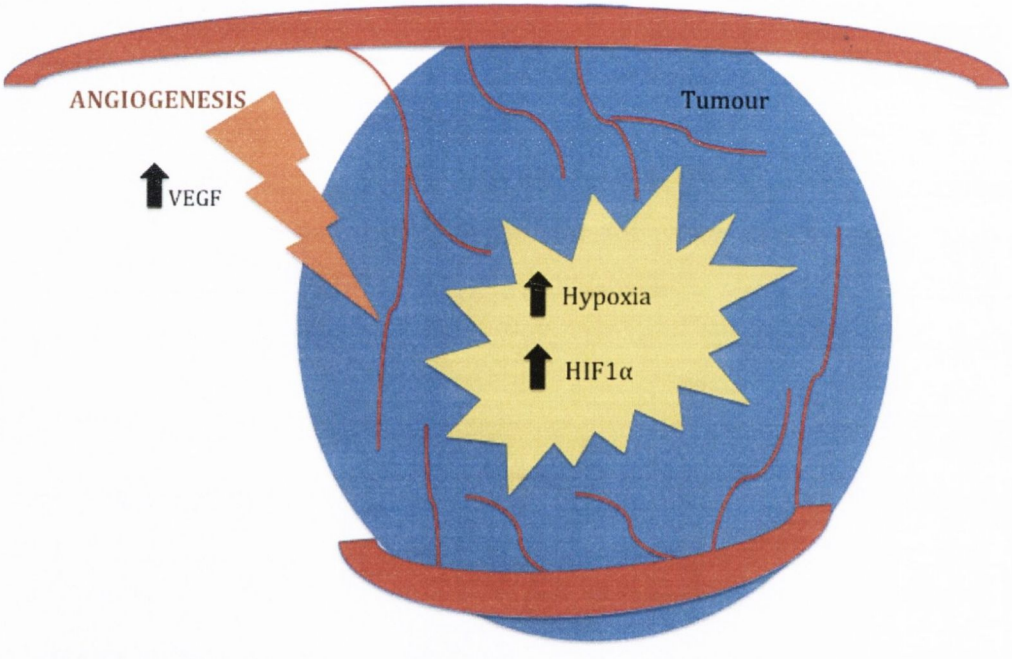


Figure 1-5-Angiogenesis in a tumour due to hypoxic areas.

Lack of blood supply and O_2 to the centre of the tumour as the tumour grows causes induction of HIF-1α, which switches on hypoxia genes including VEGF. VEGF causes the growth of new blood vessels to the hypoxic areas of the tumour.

The importance of angiogenesis to tumour growth has given rise to the formation of new types of treatment. Tumours can only grow to a certain size without new blood vessels so inhibiting tumour growth through reducing the angiogenic capacity of the tumour limits the cancerous activity. Angiogenesis inhibitors work by targeting the factors release from cells, for example VEGF or the receptors they bind to, subsequently blocking their effect. Examples of angiogenesis inhibitors include bevacizumab, a monoclonal antibody that binds to and inhibits the activity of VEGF (Modest *et al.*, 2012, Boulaamane *et al.*, 2012, Morotti *et al.*, 2012). Therefore it cannot bind to its receptor (VEGF-R) and activate signals that stimulate angiogenesis. Other inhibitors like sorafenib and sunitinub bind to receptors on endothelial cells or proteins in the angiogenic signalling pathway blocking their activities (Furuse, 2008, Liu *et al.*, 2009).

1.7.6 Pyrrolo-1,5-Benzoxazepine (PBOX)

PBOXs are novel tubulin depolymerising agents that have been shown to exhibit proapoptotic activity in a variety of human tumour cell types which are resistant to chemotherapy. PBOXs have also been shown to specifically target tumour cells and are non-toxic to normal cells (McElligott *et al.*, 2009). The anticancer activity of drugs that interfere with tubulin dynamics are collectively known as microtubule targeting agents (MTA) and these drugs show a promising future as anti cancer drugs. These drugs are yet to be evaluated in the treatment of OSCC.

1.8 Molecular biology of cancer

On a basic level cancer is a disease that arises when cells lose the ability to control their rates of proliferation, resulting in the production of masses of cells all programmed to continuously divide. Originally, all cancers were thought to develop the same six 'classic' hallmark capabilities. In more recent times these hallmarks have had additions made and we now see as much as ten true hallmarks of cancer (Figure 1-6) (Hanahan and Weinberg, 2011). Of these 10 hallmarks, of particular interest is the abnormal cell proliferation in which a cancer cell can bypass protective mechanisms in the cell cycle. This allows for continual growth of cancer cells where normal cells would have the ability to trigger cell death.

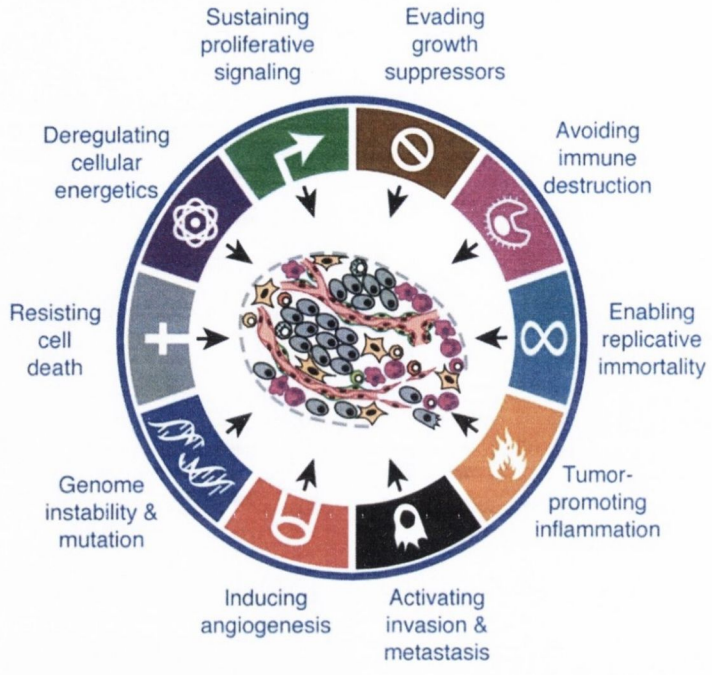


Figure 1-6 The hallmarks of cancer.

This figure highlights the six 'classic' hallmarks of cancer that include apoptotic evasion, angiogenesis, sustained proliferation and growth, and the ability to invade neighbouring cells and organs. In addition new hallmarks of cancer have also been added which include avoiding immune detection, promoting inflammation, genome instability/mutations, and deregulating cellular energetics (Adapted from Hanahan and Weinberg, 2011).

The cell cycle is a series of events occurring within the cell, which ultimately leads to the process of cellular division and multiplication. The majority of somatic cells divide by a process known as mitosis which was first discovered and named by Walther Flemming in the late 19th Century (Flemming, 1878). In order for tissues to function normally all cells must grow and replicate their genetic material. For this to occur, large amounts of nutrients and proteins must be synthesized within the cell. The cell cycle is tightly controlled and can be divided into three stages with some of these stages containing sub stages.

The first stage of the cell cycle is the quiescent or senescent stage (G0). This is the resting phase of the cell cycle and it is during this phase where it is decided if the cell will go on to divide or induce apoptosis, which is important in cancer prevention and is discussed in detail in the next section. Cells emerge from the cell cycle in response to mitogenic stimuli and cell proteins called cyclins are induced (Evans *et al.*, 1983).

1.8.1 Apoptosis

Apoptosis, the process of controlled cell death, can be activated by external or internal stimuli. Both the external and the internal pathways both eventually converge on the same pathway and have the same outcome- cell death without the release of toxic cell debris into the surrounding area. The other form of cell death is necrosis, a pathway that results in unregulated digestion of cell components and can damage surrounding cells and tissue (Kanduc *et al.*, 2002).

The extrinsic apoptotic pathway is initially activated by death signals that cause the activation of proapoptotic receptors on the surface of the cell. Extracellular signals include Apo2 ligand/tumour necrosis factor (TNF) related apoptosis inducing ligand (TRAIL) and CD95 ligand /FAS ligand which bind to DR4/DR5 and CD95/FAS respectively, on the cells surface (Elmore, 2007).

Ligand binding induced receptor clustering on the plasma membrane and the recruitment of the adaptor protein Fas-associated death domain (FADD) and the initiator caspases 8/10 as pro-caspases forming a death inducing signalling complex (DISC). Caspases are a family of proteases that play a central role in both apoptotic pathways. As a result of DISC formation, caspase molecules cluster together and activate pro-caspases that are released into the cytoplasm. The resulting pro-caspases activate another family of caspases known as the effector caspases (3,6 and/or 7) thereby converging on the internal apoptotic pathway (McIlwain *et al.*, 2013).

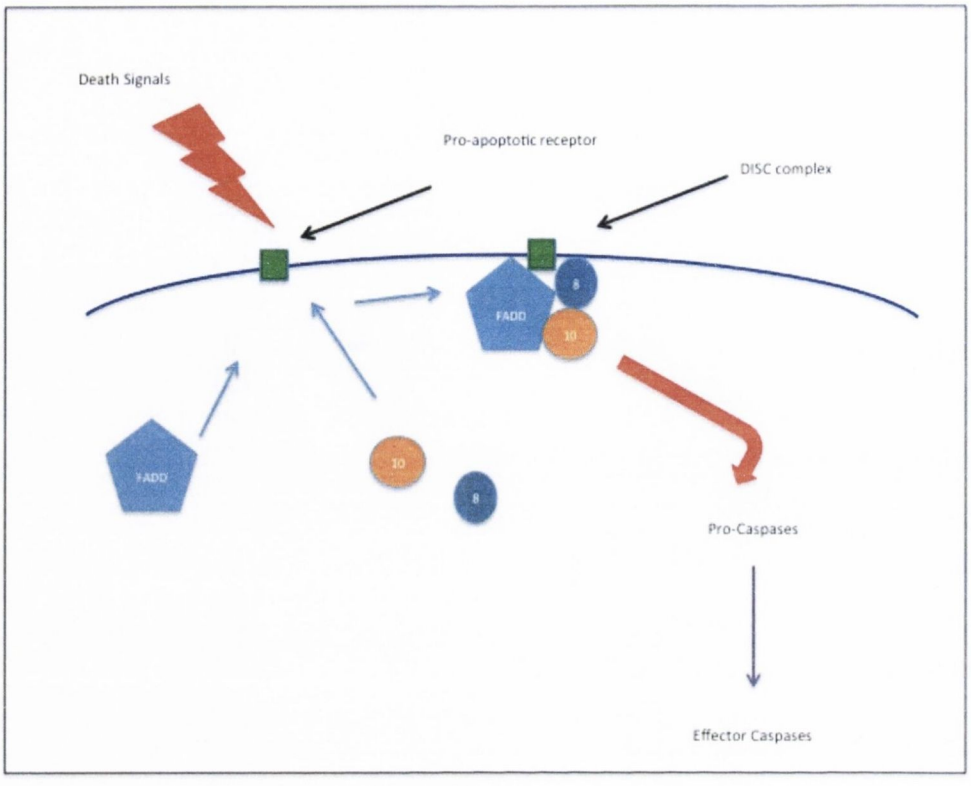


Figure 1-7 The external apoptotic pathway.

Death signals cause the formation of the DISC complex on the plasma membrane. The DISC complex causes the upregulation and activation of pro-caspases, which subsequently activate effector caspases. Effector caspases proteolitically cleave structural and enzymatic targets thus destroying and killing the cell. 10= caspase 10, 8= caspase 8, FADD =Fas-associated death domain.

The internal apoptotic pathway is initiated by death signals within the cell itself. The most common cause of activation of the internal pathway is DNA damage. Pro-apoptotic proteins in the internal pathway activate caspase enzymes in the mitochondria. The B cell lymphoma 2 (BCL-2) family of proteins regulate apoptosis. They coordinate the permeability of the mitochondrial membrane via the mitochondrial permeability transition pore (MPTP).

Upon membrane permeabilisation cytochrome *c* and second mitochondrial-derived activator of caspases (Smac/DIABLO) have the ability to translocate from the

mitochondria to the cytosol. Smac/DIABLO promote apoptosis by directly interfering with inhibitors of apoptosis (IAPs) and disrupting their ability to inactivate the caspase enzymes (Zhou *et al.*, 2005). Cytochrome *c* binds to the adaptor apoptotic protease activating factor (APAF) -1 forming the apoptosome. The apoptosome activates and regulates caspase 9. Activation of caspase 9 causes a downstream activation of effector caspases 3,6 and 7 (also activated by the external pathway). These caspases translate upstream death signals into the physical manifestations of apoptosis by proteolitically cleaving structural and enzymatic targets thus destroying the cell.

1.8.2 Interphase and Mitosis

Assuming the cell is committed to division the next phase is interphase. During this phase the cell grows and accumulates the nutrients and proteins that are needed for mitosis or cell division. Interphase is broken up into three distinct phases; Gap1 (G1), synthesis (S), and Gap2 (G2) (Figure 1-8). During the G1 phase the cell begins to grow in size. This stage also contains a checkpoint, called the G1 checkpoint, to ensure there is no DNA damage within the cell. This G1 checkpoint will also inhibit the cell from dividing if the external conditions, for example pH and temperature, are not at optimum levels. If the cell is not ready to divide then division may be delayed or the cell may enter a state of quiescence known as the G0 stage. This results in the duration of the G1 phase varying greatly between individual cells (Bertoli *et al.*, 2013).

The G1 checkpoint is primarily controlled by the protein cyclin dependant kinase (CDK) inhibitor (CKI) -p16, an inhibitor of the CDK 4/6 protein (Serrano *et al.*, 1993). CDK 4/6 protein binding to cyclin D1 is a key mediator in cell cycle progression through the G1 checkpoint. Cyclin D1 has been implicated in several forms of cancer. High levels of cyclin D1 can cause a damaged cell to overcome the G1 phase checkpoint (Kim and Diehl, 2009, Nelson *et al.*, 2002).

The synthesis of DNA within the cell is referred to as the S phase. The S phase is completed when all of the cellular chromosomes have been duplicated. It has been noted that protein synthesis in the cell during the S phase is very low with the exception of histones (Nelson *et al.*, 2002). Histones are essential for packaging the newly made DNA into nucleosomes (Lowary and Widom, 1997).

The length of time between DNA synthesis completion and mitosis is called the G2 phase. Protein production in the cell is at a high level in preparation for cell division, an example of this would be the synthesis of microtubules (Inoue and Sato, 1967, Zhai *et al.*, 1996). Microtubules are an essential protein structure in mitosis. The second checkpoint of the cell cycle is during the G2 phase. The checkpoint known as the G2/M checkpoint functions to ensure the cell is healthy before mitosis begins. During DNA replication in the S phase it is common for the cell to contain some damaged DNA. This checkpoint ensures the cell is ready for the final stage of division.

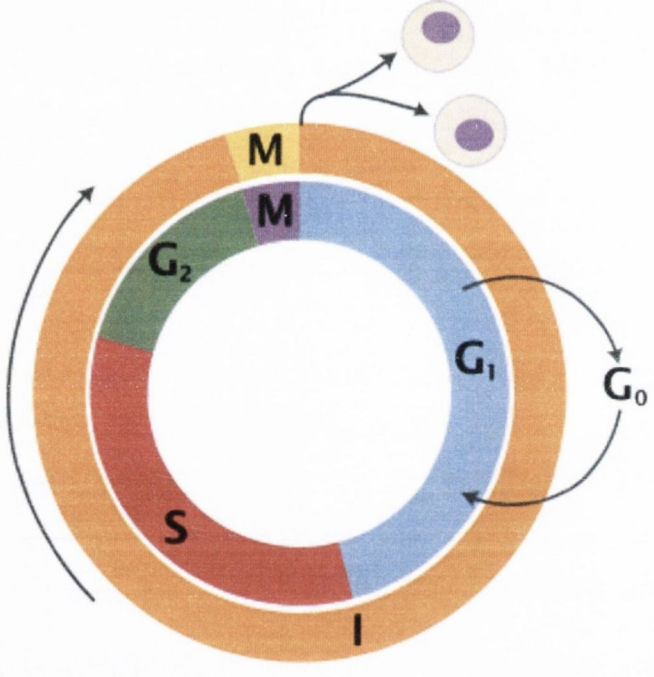


Figure 1-8 The stages of the cell cycle

Cells enter the cell cycle from the resting phase (G0) into interphase to start the process of cell division. Interphase (I), Mitosis (M), G1 (Gap 1), G2 (Gap 2), S (Synthesis). Adapted from (Wheeler, 2006).

Mitosis (M phase) is the process by which a eukaryotic cell divides its chromosomes, nuclei and cytoplasm into two identical sets at either end of the cell so it is ready to divide (cytokinesis) (Paweletz, 2001). It begins when the cell is preparing to divide. In comparison to interphase, the M phase is relatively short. The M phase is broken down into several distinct phases known as; prophase, metaphase, anaphase, and telophase.

The cell cycle is controlled by a group of proteins known as CDKs and cyclins and without the both functionally correctly the cell cycle cannot proceed (Figure 1-9). CDKs exert their control on the cell cycle through phosphorylating target proteins while cyclins function to guide CDKs to the appropriate targets. The levels of CDKs stay constant throughout the cell cycle while cyclins levels fluctuate depending on the stage of the cycle. As cells emerge from G0 in response to stimuli D type cyclins are induced and their levels remain detectable throughout the rest of the cell cycle. D-type cyclins associate with CDK4 and CDK6. The first cell cycle checkpoint is located at this point and is controlled by the inhibitor CKI-p16. This protein inhibits CDK4/6 causing these kinases to dissociate from cyclin D1 and progression through the cell cycle cannot occur. In some forms of cancer cyclin D1 is overexpressed, thus circumventing this inhibition. This can allow damaged cells to continue into the next phase of the cell cycle.

Just before the onset of the S phase, cyclin E is induced and associates with CDK2. Cyclin A is expressed as DNA synthesis begins to occur and its association with CDK2 and later with cdc2 will continue until late into the G2 phase until B-type cyclins are triggered and mitosis begins to occur (Hochegger *et al.*, 2008).

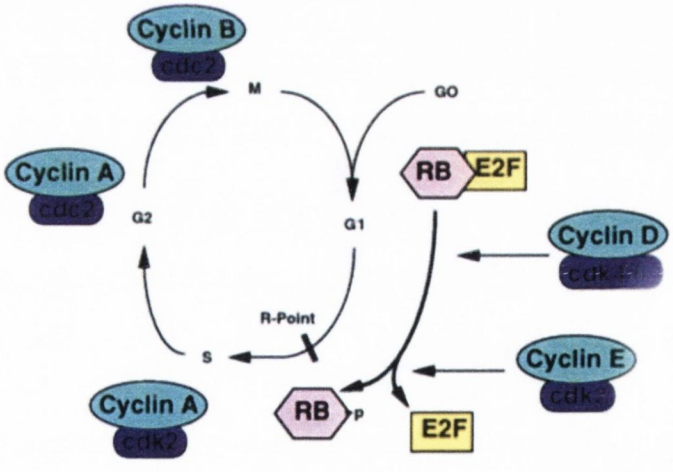


Figure 1-9- Proteins that control the progressions thought the different stages of the cell cycle.

Retinoblastoma (Rb) protein prevents cells dividing damaged DNA. The Rb protein binds to and inhibits transcription factors of the family E2F. Adapted from (Lundberg and Weinberg, 1999).

1.8.3 DNA damage repair

The majority of cells in the human body at any one time are undergoing replication and passing through the cell cycle. Due to the large amount of replication in the S phase there are frequently mismatch errors and replication fork collapses. Proteins involved in the checkpoints of the cell cycle can identify the resulting DNA errors, which present as mutations. The checkpoints activate the appropriate response whether it is apoptosis or DNA repair. If a cell goes unchecked with a mutation in the newly synthesised DNA this can cause the development of tumourigenesis or abnormalities in the subsequent daughter cells (Sancar *et al.*, 2004).

Cells in the G1 phase of the cell cycle need to repair any damage resulting from external forces such as UV light, reactive oxygen species (ROS), or chemical agents. This damage must be repaired before the onset of replication to prevent perpetuation of the error into any daughter cells. As the cell progresses into the S phase of the cell cycle there is constant surveillance of new DNA as base pair mismatches can occur regularly. When the chromatin begins to condense in the G2/M phase it can be very difficult for the cell to discover any damage in the DNA. There are several different methods of repairing damage within the cell depending on what phase and the type of damage (Friedberg, 1995).

Cells in the G1 phase need to repair accidental damage before the start of cell division. UV, ROS and chemical agents are the main causes of damage in this phase of the cell cycle however the process of replication of DNA causes the majority of the damage in the cell cycle. This can include double stranded breaks (DSB), single strand breaks (SSB) and mismatches of base pairs. The nucleotide excision repair (NER) pathway functions to repair damage caused by UV and also to repair bulky lesions of transcribed genes (Marteijn *et al.*, 2014). The base excision repair (BER) repairs damage to single bases (Krokan and Bjoras, 2013). DSBs, the most harmful type of DNA damage, can be repaired by either the homologous recombination (HR) pathway using the sister strand as a template or the non-homologous end joining (NHEJ) pathway (Mladenov and Iliakis, 2011, Moynahan and Jasin, 2010). Cells that bypass these protective mechanisms are usually the first step to malignant transformation and tumorigenesis.

1.9 Malignant transformation

The progression from a single cancerous cell to a malignant carcinoma requires specific interactions between the cancer cells and their microenvironment. Although there are multiple potential causes of cancer, there are several characteristics specific to all malignancies. One essential characteristic is the loss of regulation of the cell cycle, as previously mentioned this is one of the hallmarks of cancer (Section 1.8). Cancers have a heightened rate of cell proliferation, which goes unnoticed through the checkpoints in the cell cycle. As a result, aberrant cells, which would usually apoptose, are unregulated and continue to divide (King, 2000).

The extracellular matrix is made up of various cell types and secreted proteins that help maintain the organization of the higher-order cellular structures. Remodelling of this matrix is required for a cancerous cell to become motile. The metastatic cancer cell modifies its adhesion properties and implements a program of non-adhesion through multiple modifications. One of the main proteins involved in a cancerous cell becoming motile is E-cadherin, a transmembrane protein involved in cell-cell interactions. Down regulation or mutation of this protein is seen in all motile tumour cells. The change in E-cadherin is essential but not sufficient in cancer cell motility (Yang *et al.*, 2008). The epithelial to mesenchymal transition (EMT) is a switch of E-cadherin to N-cadherin phenotype which signals downstream pathways including phospholipase C-γ, phosphatidylinositol 3 kinase and mitogen-activated protein kinase (MAPK). These signalling pathways promote cell survival, migration and invasion (Cavallaro and Christofori, 2004).

Rapid tumour growth will ultimately result in an inability of blood vessels surrounding the aberrant cell mass to provide nutrients and O_2 to all parts of the tumour. Consequently hypoxic regions form within the tumour. Hypoxia is toxic to both normal cells and cancer cells however cancer cells can undergo genetic and adaptive switches from aerobic to anaerobic glycolysis this ability is known as the Warburg Effect (Hirschhaeuser *et al.*, 2011). Hypoxia is the state within the cell when the demand for O_2 exceeds the availability. This occurs in all locally advanced solid tumours and begins in early tumour development. Hypoxia is believed to play an important role in tumour progression with regards to metastatic spread and aggressive phenotypes of cells through modulation of the surrounding microenvironment (Zhou *et al.*, 2006).

1.10 Tumour Environment

O_2 levels in the cell are tightly controlled in all healthy tissues. In tumours the supply and demand for O_2 changes as the tumour grows and biochemical changes occur within the cells. Both acute and chronic hypoxic regions are believed to be heterogeneously distributed within the tumour mass (Helmlinger *et al.*, 1997). Acute hypoxia occurs when there is a transient reduction in the level of O_2 delivered to the cells. Hypoxia in tumours can be caused by an increase in diffusion distances (>70μm away) so cells further away from the blood vessel receive fewer nutrients and O_2 which results in chronic hypoxia (Thomlinson and Gray, 1955, Alqawi *et al.*, 2007). There is evidence that both types of hypoxic states influence tumour development and response to treatment (Bristow and Hill, 2008). Intratumoral hypoxic regions are associated with decreased disease free survival for cancers involving the cervix, prostate, breast, head and neck (Vaupel and Mayer, 2007).

As the tumour grows the demand for O_2 becomes too great for the irregular microvasculature network surrounding the cancerous growth. As O_2 levels drop below 10-15mmHg in the cells, genes within the hypoxic cells are switched on to cope with the decreased O_2 levels. HIF is the O_2 sensing transcription factor in the cell and can modulate hundreds of genes to compensate for hypoxia. Genes involved in angiogenesis, metabolism, pH regulation, proliferation, metastasis formation and a range of other cellular and molecular processes are all activated by HIF (Semenza, 2010). The HIF protein consists of an O_2 regulated HIF-1α subunit and a constitutively expressed HIF-1β subunit. In well-oxygenated cells HIF-1α is hydroxylated on a proline residue. The hydroxylated α subunit, which is bound by a protein called the Von Hippel-Lindow tumour suppressor protein (VHL), recruits an E3 ubiquitin ligase that targets HIF-1α for proteosomal degradation (Tanimoto *et al.*, 2000, Cockman *et al.*, 2000). Reduced O_2 availability results in the proline residue not being hydroxylated therefore inducing HIF-1α in the cells (Jaakkola *et al.*, 2001, Ivan *et al.*, 2001).

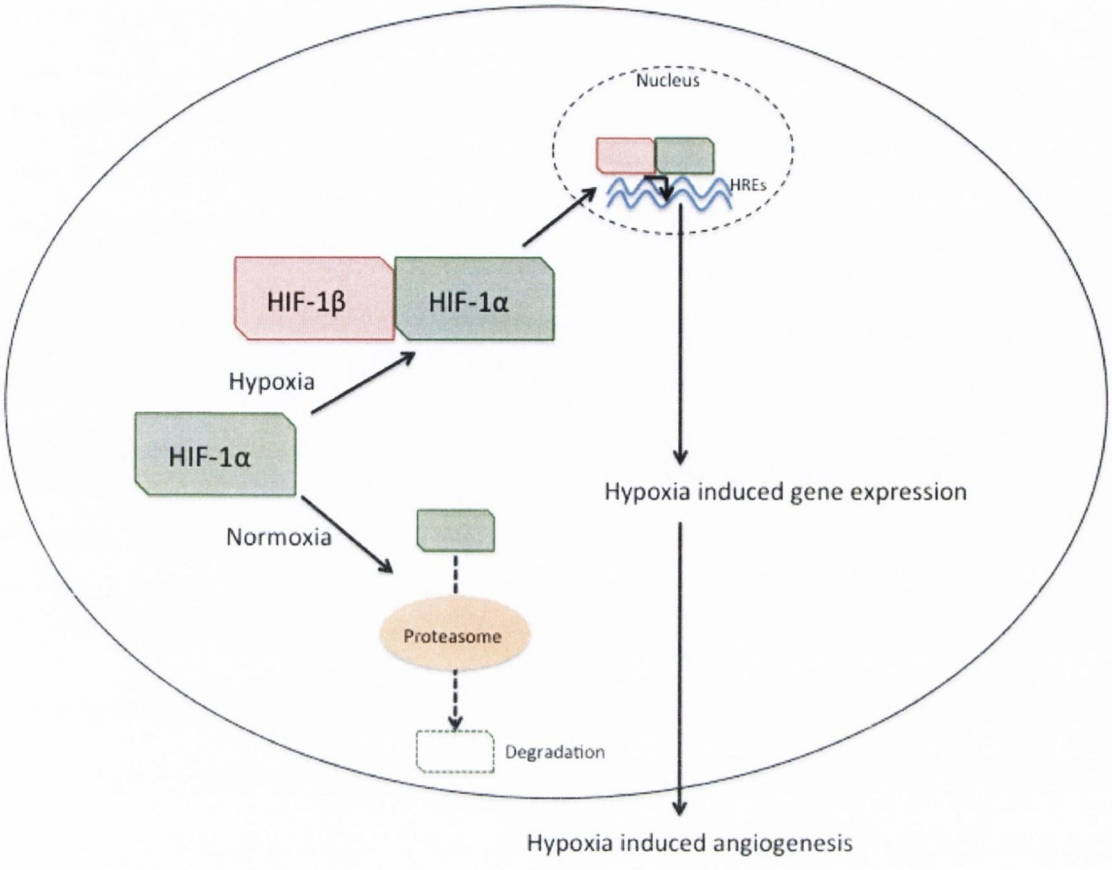


Figure 1.9 – The cellular hypoxic switch.

In the case of low O_2 levels HIF-1α is not degraded by the proteasome and binds to HIF-1β. When bound these subunits act as transcription factors and switch on hundreds of genes to cope with hypoxia in the cell.

1.11 ROS and antioxidants

ROS are free radicals that contain the O_2 atom. ROS radicals contain unpaired valence shell electrons which make them highly reactive (Turrens, 2003). ROS are predominantly formed under normal conditions as a by-product of the metabolism of O_2 in the electron transport chain located on the inner mitochondrial membrane in mitochondria and they have important intracellular roles in cell signalling (Figure 1-10). ROS can also arise from several enzymatic sources such as NADPH oxidases (E.C 1.6.3.1), cyclooxygenases (E.C 1.14.99.1) and lipoxygenases among others. Types of ROS include the superoxide radical (O_2^-), hydrogen peroxide (H_2O_2) and hydroxyl

radical (OH^-), which are all known to be cytotoxic at high levels and have been implicated in the etiology of number of human diseases including cancer (Waris and Ahsan, 2006). The normal production of ROS does not induce cellular problems due to the action of antioxidant enzymes, such as superoxide dismutase (SOD) (E.C 1.15.1.1), glutathione peroxidise (GPx) (E.C 1.11.1.9) and catalase (CAT) (E.C 1.11.1.6), which all convert ROS to less reactive species that are easily broken down in the cell. CAT catalyses the conversion of H_2O_2 to water and O_2, and GPx converts H_2O_2 to glutathione disulfide (GSSG) (E.C 1.8.4.2) and water. Heme oxygenase (HO), another antioxidant enzyme, catalyses the degradation of heme into biliverdin, iron and carbon monoxide. Free heme can catalyse the production of cytotoxic hydroxyl radical from H_2O_2 (Figure 1-11). During occasions of environmental stress ROS levels can increase significantly which can cause a lot of damage to cell structures. This is known as oxidative stress. The severity of the damage produced is determined by the ROS species involved. O_2^- and H_2O_2 are less reactive, while OH^- is extremely damaging to cellular structures.

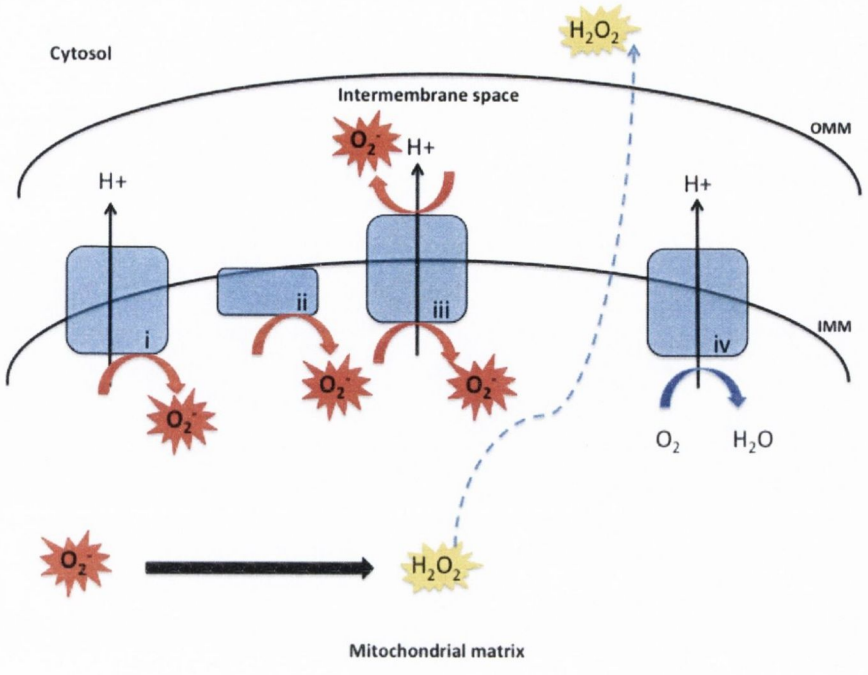


Figure 1-10 The production of O_2^- from the electron transport chain on the inner mitochondrial membrane.

The electron transport chain complexes, located on the inner mitochondrial membrane (IMM) produce O_2^-, which is rapidly broken down to H_2O_2 and diffuses out of the mitochondria into the cytosol.

According to the "canonical" view, ROS contribute greatly to carcinogenesis and aid in driving malignant progression of tumour cells. OH^- can react with pyrimidines, purines and chromatin protein resulting in base modifications in DNA causing genomic alterations and instability. ROS can be formed as a result of chronic inflammation secondary to infections and chronic chemical irritants such as tobacco smoke and asbestos. Tyrosine receptors, which play an important role in cell cycle progression, have been shown to signal via ROS dependant mechanisms and thus have been implicated in carcinogenesis (Sundaresan *et al.*, 1995, Bae *et al.*, 1997). The more modern view of ROS is that at high levels they are very damaging to cell structures while at lower levels they can function as a signalling molecule. It was not until the 1970s that it was discovered that ROS had a signalling function in cells. Low levels of H_2O_2 can mimic the signalling activity of insulin (Czech *et al.*, 1974) and more recently

it has been discovered that H_2O_2 can stimulate cell proliferation in epithelial cells (Sigaud *et al.*, 2005).

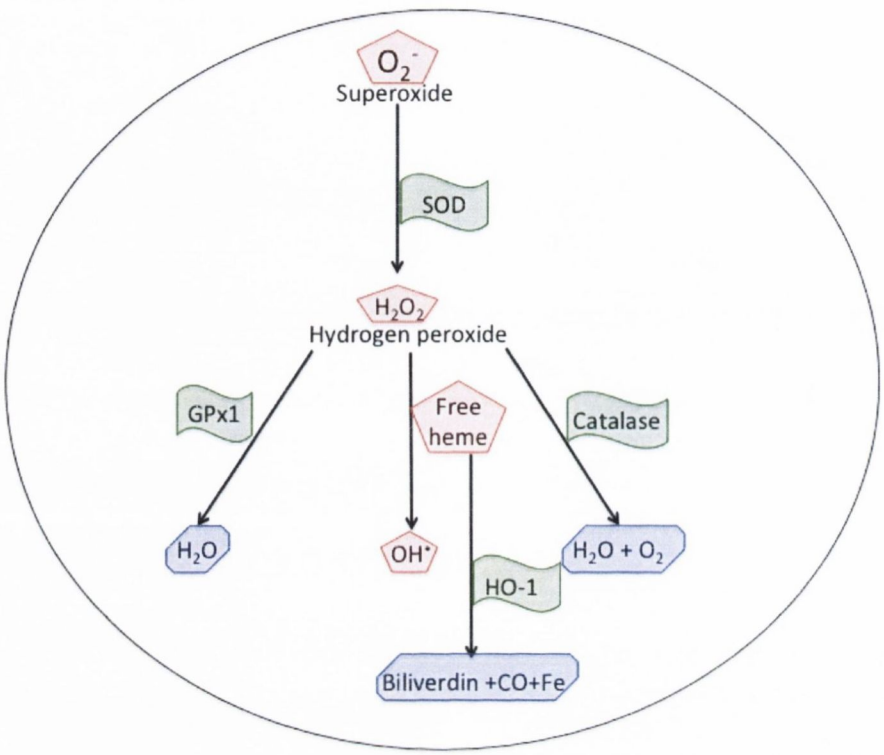


Figure 1-11 The breakdown of ROS by antioxidant enzymes present in the cell.

Antioxidant enzymes defend the cell from increased levels of ROS by breaking them down into less toxic end products, which do not harm the cell.

1.12 Aim of Thesis

The mortality rates for OC are extremely high and the incidence rate has increased significantly in women and the younger population. The mechanisms underlying OC are complex and it is difficult to diagnose at early stages thus treatment options can be limited. The aims of this project are to investigate the role of alcohol in the pathogenesis of OC, examine Raman spectroscopy as a new method of early detection, and assess the efficacy of novel PBOX compounds as alternatives to common chemotherapeutic agents. This will be achieved through the following objectives:

1. Optimisation of an *in-vitro* model of alcohol exposure followed by determination of a number of metabolic and molecular events including but not limited to; cell viability, cell cycle flux and protein expression analysis.

2. The culture of a number of different geno/phenotypical cell types representing a number of defined stages from primary epithelial cells to OSCC followed by the analysis described previously.

3. The novel application of Raman spectroscopy in the differentiation of defined stages oral cancer, from primary epithelial cells to OSCC. Optimisation of the mounting technique along with cell density and wavelength prioritisation will be required.

4. Utilisation of Raman Spectroscopy to follow molecular events/disruption in defined regions of the cell over time in response to exposure to alcohol in order to determine possible location of early molecular changes.

5. Determination of the efficacy and mechanism of action of novel microtubulin targeting agents will be evaluated as potential alternatives to the current prescribed chemotherapeutic drugs.

2 Materials and Methods

2.1 General Methodology

2.1.1 Preparation of solutions

Chemicals were weighed using a Mettler College analytical balance (for substances <5g) and a Mettler Top-Loading balance (Model K7T) for larger weights. Aqueous solutions were prepared using ultra-pure water from a Millipore Direct-Q3 Water Purification System. Solutions were adjusted to the required pH using a Corning pH meter, model 240, and calibrated daily using standard buffers of pH4.0, 7.0 and 10.0.

2.1.2 Pipetting

Solutions ranging from 0.2µl to 5ml were pipetted using a set of standard Eppendorf automatic pipettes, which were calibrated regularly in accordance with the manufacturer's instructions.

2.1.3 Centrifugation

Substances were centrifuged in a bench top Eppendorf Centrifuge 5415 and temperature controlled when required.

2.1.4 Spectrophotometry

For spectrophotometric analysis, a SPECTRAmax PLUS Microplate spectrophotometer FV 200µl/well was used for absorbance readings. For kinetic and fluorescent analysis a SPECTRAmax microplate Gemini XS was used and for larger volumes (~2ml) a Shimadzu UV-vis spectrophotometer was used.

2.1.5 Reagents

All chemicals were acquired from Sigma Aldrich and all consumables were acquired from Cruinn, unless stated otherwise.

2.1.6 Cell culture

All cell culture work was carried out under sterile conditions in a NUAIRE laminar flow hood. All cells were maintained at 37°C, in 95% humidity and 5% CO_2. Cell growth and viability was monitored visually using a Nikon Eclipse TS100 light microscope with 10X and 40X dry objectives.

2.2 Cell culture

2.2.1 Culture of Ca9.22 oral carcinoma cell line

The Ca9.22 cell line (Health Science Research Resources Bank, Osaka, Japan) is a squamous cell carcinoma derived from the gingiva of a male subject. This cell line contains a p53 point mutation at codon 248 (R248W), which is known as a p53 gain of function mutation.

The Ca9.22 cell line was maintained in Minimum Essential Medium (MEM) supplemented with 10% (v/v) Fetal Bovine Serum (FBS), penicillin/streptomycin (100U/100ug) and L-glutamine (2mM). The media was pre-warmed at 37°C before incubation with the Ca9.22 cells. Cells were cultured until 90-100% confluent in a humidified environment at 95% O_2 and 5% CO_2, before being passaged. When confluent, the cells were washed in pre-warmed phosphate buffered saline (PBS) (0.01M phosphate buffer, 0.154 M sodium chloride) and incubated with trypsin-EDTA (0.5% trypsin, 0.02% EDTA) for 5 min at 37°C. Fresh pre-warmed medium was added to deactivate trypsin, and the suspended cells were centrifuged (1200 rpm/5 min). The supernatant was discarded and the cell pellet resuspended in a sufficient volume of fresh pre-warmed medium, counted and passaged at a ratio of 1:3 as described in Section 2.2.6.

2.2.2 Culture of TR146 oral carcinoma cell line

The TR146 (HPA cultures, UK) is a squamous cell carcinoma derived from the neck node of a 67 year-old female (primary tumour was sited in the nuccal mucosa) and does not contain a p53 mutation.

The TR146 cell line was cultured in Dulbecco Modified Eagle's Medium (DMEM) supplemented with 10% (v/v) FBS, penicillin/streptomycin (100U/100µg) and L-glutamine (2mM). The cells were cultured as described in Section 2.2.1.

2.2.3 Culture of DOK dysplastic oral cell line

The DOK cell line (HPA cultures, UK) is a dysplastic (mild-moderate) cell line and was derived from the dorsal tongue of a 57 year old male subject. Expression of p53 is increased with a 12 base pair in-frame deletion from codon 188-191 of the p53 gene.

The DOK cell line was cultured in Dulbecco Modified Eagle's Medium supplemented with 10% (v/v) FBS, penicillin/streptomycin (100U/100µg), L-glutamine (2mM) and hydrocortisone (5µg/ml). The cells were cultured as described in Section 2.2.1.

2.2.4 Culture of SCC-4 oral carcinoma cell line

The SCC-4 is a squamous cell carcinoma derived from the tongue (HPA cultures, UK) of a male subject. This cell line does not contain any known p53 mutations.

The SCC-4 cell line was cultured in Dulbecco Modified Eagle's Medium (DMEM) supplemented with 10% (v/v) FBS, penicillin/streptomycin (100U/100µg) and L-glutamine (2mM). The cells were cultured as described in Section 2.2.1.

2.2.5 Culture of primary oral epithelial cells

Human tissue (mucoperiosteal tissue) was recovered at the Dublin Dental University Hospital from patients undergoing routine third molar extraction in the Department of Oral and Maxillofacial Surgery (Ethics approval- Appendix 1). The sample was immediately placed into pre-warmed collection medium [DMEM, penicillin/streptomycin (100U/100µg), amphotericin B (2.5µg/ml)] for 10min before washing the tissue three times with pre-warmed 1X PBS and placed in 0.17% trypsin overnight at 4°C. The following day the sample was washed with 1X PBS and connective tissue was removed using a scalpel. The tissue was cut into small pieces (1mm x 2mm) and the small sections placed in pre-treated T25 flasks (CELL+, Sarstedt) each with a small coating of keratinocyte growth medium (KGM) (see Table 2-1 below) on each piece. These were left to adhere to the flask for 1-2h and the flask then subsequently was flooded with KGM.

Table 2-1: Keratinocyte growth medium- 1:3 HamsF12:DMEM supplements

Supplement	Final concentration
Adenine	180mM
Insulin	0.86nM
Hydrocortisone	400ng/ml
Transferrin	5µg/ml
EGF	5ng/ml
Penicillin	1,000units
Amphotericin B	2.5µg/ml
Streptomycin	1mg

Once sufficient growth of cells from tissue was achieved (2-3 weeks), KGM was replaced with Epilife medium (Invitrogen) so epithelial cells could selectively grow. Cells were split using 0.05% trypsin and spun at 250x g for 10min at 4°C and cultured to 90% confluency and passaged.

2.2.6 Determination of cell density and viability-trypan blue exclusion

Cell density and viability were determined using the trypan blue exclusion assay. It is based on the principle that live cells have intact cell membranes and exclude certain dyes. Therefore dead cells are visible as blue under the microscope due to their permeable membrane and can be excluded from the count. A haemocytometer was cleaned with 70% (v/v) EtOH and the coverslip moistened with dH_2O and fixed. The cell suspension gently agitated through inversion to ensure homogenous suspension and a 1:1 ratio of cells to trypan blue was prepared. This solution was then pipetted into the haemocytometer.

Figure 2-1: Cell density was calculated using the following formula:

$$\frac{\text{No. of cells counted}}{\text{No. of squares counted}} \times \text{dilution factor} = \text{cells/ml}$$

2.3 Analysis of cell proliferation and cytotoxicity

AlamarBlue (Invitrogen) is a reagent used to analyse cell proliferation and cytotoxicity. The functional component of Alamar blue (resazurin) is a nontoxic, cell permeable compound that is blue in colour and virtually nonfluorescent. Upon entering cells resazurin is reduced to resorufin, which produces very bright red fluorescence. Viable cells continuously convert resazurin to resorufin, thereby generating a quantitative measure of viability and cytotoxicity.

Cells were seeded in a 96 well plate (10,000/well) and serum starved overnight (1% FBS). Cells were treated for the required time points in full serum (10% FBS) cell culture media. Six hours prior to endpoint, AlamarBlue reagent was added (10% v/v). Fluorescence was read on a SPECTRAmax PLUS Microplate spectrophotometer at 560EX nm/590EM nm.

2.4 ADH activity assay.

To assess the level of ADH activity, cells were seeded in a 96 well plate (10,000/well) and serum starved overnight (1% FBS). Cells were treated for the required time points in full serum (10% FBS) cell culture media. Culture media was removed and assay buffer (100mM sodium phosphate pH 7.5) containing 10% EtOH, nicotinamide adenine dinucleotide (NAD) (2.4mM), semicarbazide (1mM) and 1% triton was added to the cells. Kinetic absorbance was read on a SPECTRAmax PLUS Microplate spectrophotometer at 340nm for 10min to determine an initial rate.

2.5 Determination of extracellular ROS

H_2O_2 is one the most commonly found ROS in the cell and can be assayed as an indicator of ROS production. The Amplex red assay is a horseradish peroxidase (HRP)-coupled reaction. Amplex red is coupled to fluorescent resorufin when oxidised.

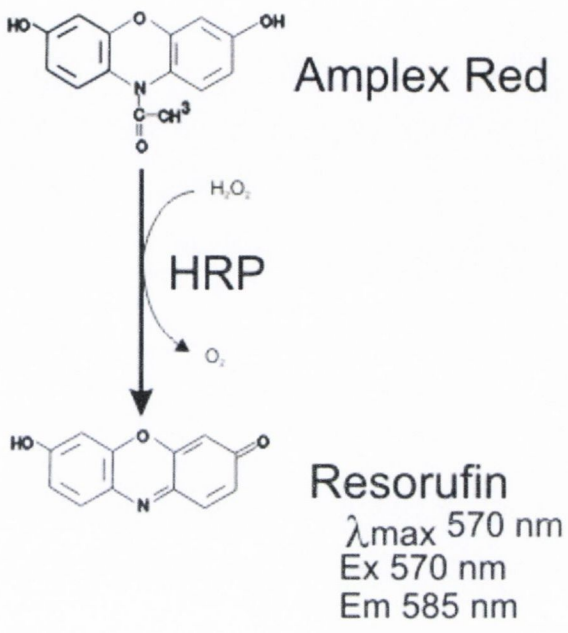


Figure 2-2: Conversion of Amplex red to resorufin in the presence of H_2O_2.

Cells were seeded (10,000/ well) and serum starved (1% FBS) overnight in a 96 well plate before treatment with varying concentrations of test sample. After the elapsed time points, cells were washed with Krebs buffer (NaCl 145mM, NaH_2PO_4 5.7mM, KCl 4.86mM, $CaCl_2$ 0.54mM, $MgSO_4$ 1.22mM, Glucose 5.5mM). Amplex red solution (50μM) and HRP (2.5U/ml) and Krebs Buffer were added to all the wells in a final volume of 200μl and the fluorescence intensity was monitored in a Spectramax Gemini XS plate reader at an excitation wavelength of 550nm and an emission wavelength of 590nm and monitored for 30 min at 37°C.

2.6 Determination of intracellular ROS

2',7'-dichlorfluorescein-diacetate (DCFH-DA) (Biosciences) is a dye, which is permitted to cross the cell membrane and can be used to determine oxidative stress (hydrogen

peroxide, peroxynitrite anion) status of a cell. DCFH-DA becomes oxidised to dichloroflourescin (DCF) in the presence of ROS and in this state is unable to leave the cell. Fluorescence intensity of DCF can be quantified by a flow cytometer and/or visualised using confocal microscopy.

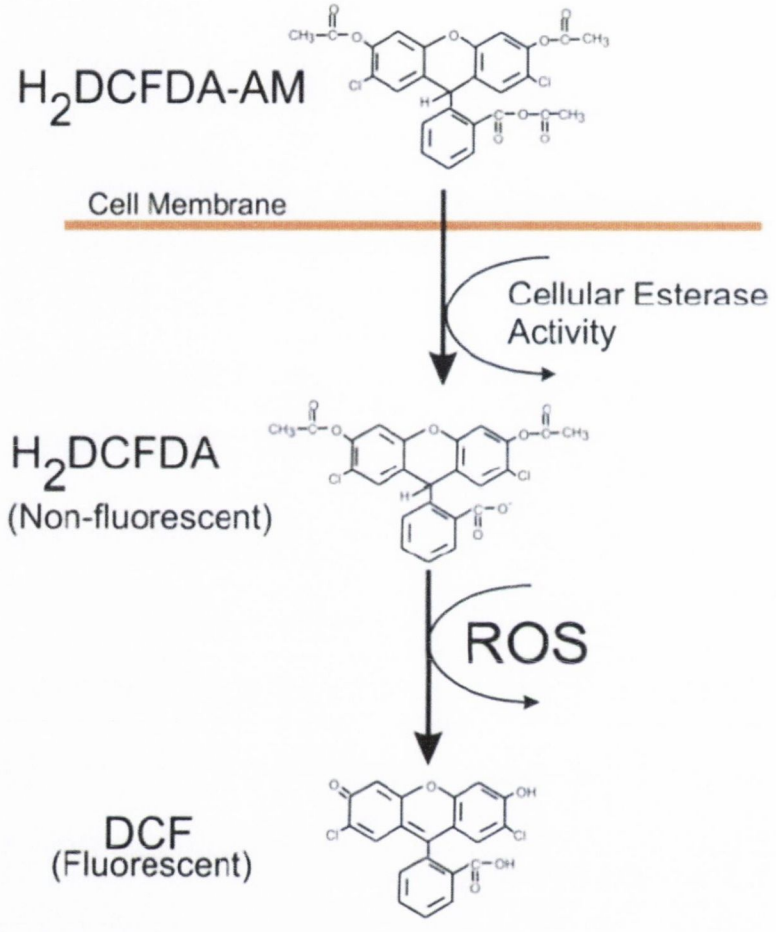


Figure 2-3 The binding of H_2DCFDA in the cell to H_2O_2.

H_2DCFDA-AM is permitted to cross the cell membrane freely. After it has crossed it is membrane it is hydrolysed by esterases to form H_2DCFDA, which is trapped within the cell. This non-fluorescent molecule is then oxidized to DCF by action of cellular oxidants.

Cells were serum starved (1% FBS) in 35 mm Wilco glass bottom confocal wells (200,000/well) overnight at 37°C and the following day treated with the test compounds in full serum media. Following treatment, cells were washed with PBS and incubated in

phenol red free media containing 10μM DCF and DAPI (nuclear stain) (1μg/ml) for 30min and for 5min in Cell Mask (membrane stain) (5μg/ml) at 37°C the presence of 5% CO_2. Cells were washed before being viewed under the microscope. Cells were viewed using an Olympus FV1000 Point scanning Confocal Microscope, using FV10-ASW Olympus Fluoview Ver.1.4a software and through a 60X oil immersion objective.

2.7 Cell Cycle Analysis

The cell cycle distribution of a whole cell population can be determined using propidium iodide (PI), a dye that intercalates with double stranded DNA. The amount of DNA in a cell is directly proportional to the fluorescence intensity of PI, which can be determined using a flow cytometer.

Following treatments, the cells were trypsinised and spun at 1200rpm for 5min to pellet the cells. Cells were washed with warm PBS (1X). The PBS was removed and the cells were resuspended in 200μl of PBS and 2mls of ice-cold EtOH (100%) and left to fix at 4 °C overnight. Samples were pelleted at 1200rpm for 5min and the EtOH was removed. The cells were resuspended in 400μl of 1X PBS containing ribonuclease A (10μg/ml) and PI (100μg/ml). The samples were incubated at 37°C in darkness for 30min. The PI was excited using a flow cytometer 488nm laser. Histograms were generated using FlowJo software (Treestar).

2.8 Transfection with p53 siRNA

The oligonucleotide sequences of small interfering RNAs (siRNAs) were designed for p53 and pooled for optimum knockdown (see Table 2-2 below). For transient transfection, the cells were seeded 2.5 $x10^4$ on a 24-well plate with serum starved medium (1% FBS). Following incubation overnight, targeting siRNA (20nm IBONI p53-siRNA pool) was transfected using RIBOXX-FECT transfection reagent (3% v/v) (MSC). Following overnight incubation, cells were treated with EtOH for the required time points.

Table 2-2: Sequences for p53 siRNA

P53 siRNA (NM_00546)	
5'-3' sequence (guide)	5'-3' sequence (passenger)
UCACAAUUGUAAUCCCAGCCCCC	GGGGGCUGGAUUACAAUUGUGA
UGUCAUCCAAAUACUCCACCCCC	GGGGGUGGAGUAUUUGGAUGACA
ACUAACCCUUAACUGCAAGCCCCC	GGGGGCUUGCAGUUAAGGGUUAGU
UUAUUUCAUUAACCCUCACCCCC	GGGGGUGAGGGUUAAUGAAAUAA

2.9 Western Blotting

2.9.1 Preparation of cell lysates

1 X 10^6 cells were seeded in T25 flasks, serum starved overnight (1% FBS) and left to adhere. The following day the cells were treated with required volume of treatment in full serum media. Following the required incubation time, cells were detached from each flask using a cell scraper. Cells and media were pelleted at 1200rpm for 5min and subsequently washed with PBS and centrifuged again. Pelleted cells were resuspended in PBS and equal amounts of 2X laemlli buffer (30mM Tris-base pH 6.2, 2% (v/v) SDS, 10% (v/v) glycerol in dH_20.) Samples were sonicated for 10s to degrade DNA. Lysates were stored at -80°C until required.

2.9.2 Determination of protein content

The protein concentrations were estimated as per the method of (Bradford, 1976), with modifications. Bovine serum albumin served as a standard and was prepared from a stock of 0.1mg/ml, as a series of dilutions ranging from 2-20µg/ml with a final volume of 500µl (in triplicate). To these and to unknown diluted samples 200µl of Protein assay Dye was added and samples were incubated for 10min at room temperature. Samples were placed in a 1ml cuvette and read on an Eppendorf Biophotometer Plus and corrected for blank (sample diluent and protein assay dye).

2.9.3 Sodium Dodecylsulphate-polyacrylamide Gel Electrophoresis

Resolving gel was prepared (% dependant on target protein size) as in Table 2-3 and left to set between the glass plates. The stacking gel was then prepared and poured into glass plates and the comb was inserted. The gel was left to set for 1h. When set, the glass plates were placed into the chamber, filled with 1X running buffer and the comb was removed to create the wells. Samples concentrations were estimated and 1X sample buffer (60mM Tris pH 6.8, 10% Glycerol, 2% SDS, 1% bromophenol blue) was added to each sample which were subsequently boiled at 90°C for 5min. Between 10- 20µg of sample protein was loaded into each well, using Spectra multicolour Broad Range Protein ladder (ThermoFisher, MA, USA) as a molecular weight marker. Gels were run at constant current (20mA/gel) for 90min in an Atto gel box using a Biorad power pack.

Table 2-3: Composition of resolving and stacking gels used in SDS-PAGE

Reagents (ml)	8% resolving gel	10% resolving gel	12% resolving gel	5% stacking gel
dH_20	4.6	4.0	3.3	3.4
Acrylamide mix	2.7	3.3	4	0.83
1.5M Tris	2.5	2.5	2.5	-
1M Tris	-	-	-	0.63
10% SDS	0.1	0.1	0.1	0.05
10% APS	0.1	0.1	0.1	0.05
TEMED	0.006	0.004	0.01	0.005

2.9.4 Western blotting

The gel was removed from the chamber and plates and soaked in 1X NuPAGE transfer buffer (500mM Bicine, 500mM Bis-Tris, 20.5mM EDTA, 1mM Chlorobutanol) along with blotting paper and immobilion PVDF membrane (previously activated in methanol). A semi-dry transfer technique was employed to transfer the samples onto Immobilion PVDF membrane (see Figure 2-4), at constant voltage (10V) for one hour in 1X transfer buffer. Non-specific binding sites were blocked in 5% milk at room temperature for 1h. The membrane was washed in TBST (50mM Tris, 150mM NaCl,

0.01% Tween 20, pH 7.6) before incubation with primary antibody at 1:1000 dilution (5% milk) overnight at 4°C. The secondary antibody was diluted 1:10,000 in 2% milk and left to incubate with the membrane for 1h at room temperature. The membrane was washed before and after secondary incubation for 45min in TBST.

For visualisation of bands the membrane was covered in 1ml of chemiluminescent reagent (Millipore) for 5min and incubated with photographic film for the necessary time, dependant on antibody signal strength. The film was developed in a dark room using a Fuji X-ray Film Processor RG II.

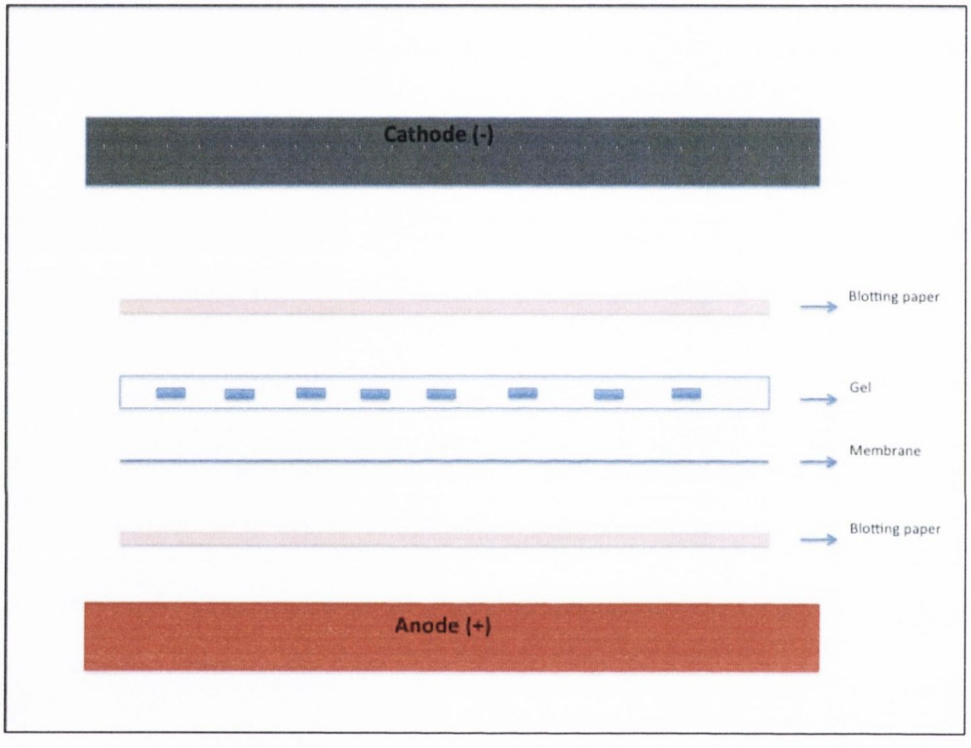


Figure 2-4: The set up of a semi dry apparatus.

2.10 RNA extraction

Cells were seeded at 700,000 cells per well in a 6 well plate and serum starved overnight before treatment for the required time-points. Cell culture media was removed and 1ml of TRI reagent was added to the wells and left to incubate for 5min at room temperature. Samples were then transferred to eppendorf tubes and stored at -80°C until required.

To extract RNA the samples were centrifuged at 12,000*g* for 10min at 4°C and the supernatants were transferred to fresh tubes. 1-Bromo-3-chloropropane (BCP)

(100µl/ml of TRI reagent) was added to each sample and mixed well before incubation for 15min at room temperature. The samples were then centrifuged at 12,000*g* for 15min at 4°C and the aqueous phase was transferred to a fresh tube.

To precipitate the RNA from the aqueous phase isopropanol was added to each sample (500µl/ml TRI-reagent) and incubated for at room temperature for 10min. To pellet the RNA the samples were spun at 12,000*g* for 8min at 4°C and the supernatant discarded. To wash the RNA, 75% EtOH was added and the samples were centrifuged for 5min at 7,500*g*. The EtOH was then removed and samples were left to air dry for 5min. The RNA was then dissolved in nuclease free H_2O and stored at -80°C.

2.11 Quantitative Reverse Transcription PCR

Quantitative Reverse Transcription PCR (qRT-PCR) enables reliable detection and measurement of products generated during each cycle of the PCR process. Cells were serum starved (1%) in six-well plate overnight, and were treated with varying concentrations of treatments. Total RNA was isolated as discussed in Section 2.10 above. Each qPCR reaction contained 50µg RNA, 200nM of each primer (see Table 2-4), and Brilliant III Sybr Green master mix one-step kit (Agilent) in 25µl reactions. The reactions were performed using a Stratagene Mx3000P/Mx3005P qPCR System. Specificity of amplification was verified by first-derivative melting curve analysis using the ABI software (SDS2.3, Applied Biosystems, Foster City, CA). Relative quantification of gene expression profile was calculated using a DDCt method (RQ manager, Applied Biosystems).

Table 2-4: Primer sequences for QPCR

Target	Forward primer	Reverse Primer
HIF-1α	TGCCACATCATCACCATATAGAG	GACTCAAAGCGACAGATAACAC
HO-1	TTGGCTGGCTTCCTTACC	GGCTCCTTCCTCCTTTCC
MnSOD	CGTGACTTTGGTTCCTTT	GCTCCCACACATCAATCC
CAT	TGAGGTTGAACAGATAGCC	CACAGGTATATGAAGATAATTGG
GPx-1	GAGAAGTGCGAGGTGAAC	AACATCGTTGCGACACAC
ADH	GGCACAAGTGTCATCGTAGG	TCCAGTCAGTAGCAGCATAGG
β-actin	AGATGACCCAGATCATGTTTGAGA	CGTCACCGGAGTCCATCAC

2.12 Raman Spectroscopy

2.12.1 Sample preparation

Calcium fluoride (CaF_2) disks were pre-coated in 2% gelatine for 6h at 4°C. To facilitate Raman spectroscopy measurements, cells were detached from the flasks using 0.025% Trypsin–EDTA at 37°C and pelleted at 250*g* for 5min at room temperature. The supernatant was removed and cells were counted and seeded at a density of 5 X 10^4 on a CaF_2 disc and maintained, as previously described (Section 2.2), until a monolayer of cells was stably growing on the CaF_2 disc. The cells were then fixed with 10% neutral buffer formaldehyde for 5 min, washed with 1X PBS and stored in 0.9% physiological saline solution prior to capture of the Raman spectrum.

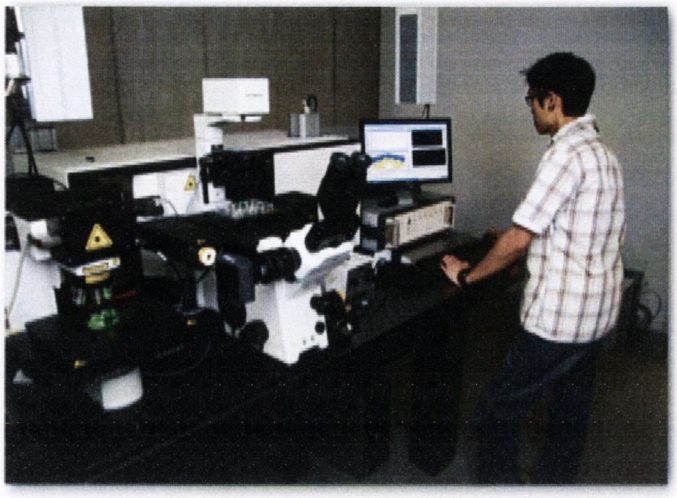
2.12.2 Raman Instrumentation

The Raman instrument used for this study was the Labram HR800 Dual microscope (Horiba Jobin Yvon) operating with a 532nm diode laser (Figure 2-5). This microscope allows for elimination of out of focus light in specimens that are thicker than the confocal plane. The laser light is focused onto the sample through a 100X water immersion microscope objective. The scattered light is collected by the objective in a backscattering, confocal geometry, and is subsequently directed to a charge coupled device (CCD) via a holographic grating.

2.12.3 Data preprocessing

Data preprocessing was performed using Matlab (Mathworks, USA) (Example of a Matlab script can be found in Appendix 2). Before statistical analysis, a Savitsky-Golat filter (5^{th} order, 7 points) was applied to smooth the spectra and the reference spectrum constituting the background signal was subtracted. The data sets have also been corrected for any baseline contributions from the substrate or scatter and (vector) normalised to remove point-to-point intensity variations and facilitate comparison of all spectra.

(a)



(b)

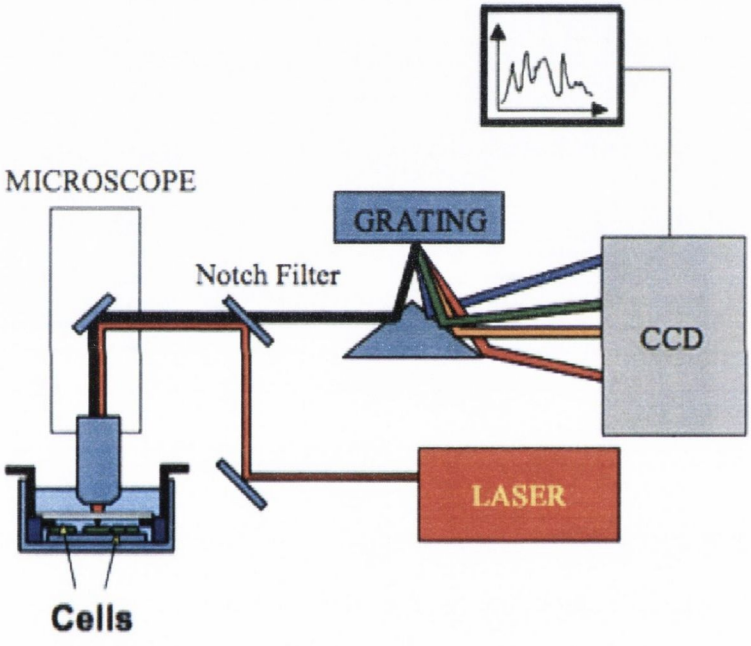


Figure 2-5 (a) Labram HR800 Raman system (b) Illustration of the set up for Raman spectroscopy measurement of cells.

2.13 Analysis of tubulin polymerisation by Western Blot

The status of tubulin polymerisation in TR146 and Ca9.22 cells was assessed using a modified version of the method employed by (Verma *et al.*, 2008). Briefly, cells treated with MTAs for 4h were harvested into microtubule (MT)-preserving buffer containing 0.1M Pipes (pH 6.9), 2M glycerol, 5mM $MgCl_2$, 5mM EGTA, 0.5% (v/v) Triton X-100, and 4μM paclitaxel. The MT buffer was supplemented with 1 complete mini protease inhibitor tablet/10ml buffer (Roche Diagnostics GmbH, Mannheim, Germany) to maintain stability of the assembled microtubules. Polymerised and unpolymerised tubulin were separated by centrifugation at 20,000g for 45min at 4°C. Supernatants, containing depolymerised tubulin, were diluted by the addition of an equal volume of 2X sample buffer [125mM Tris (pH6.8), 4% (w/v) SDS, 20% (v/v) glycerol, 0.0025% (w/v) bromophenol blue and 200mM DTT] while pellets containing sedimented polymerised tubulin were resuspended in buffer containing 62.5mM Tris (pH 6.8), 6M urea, 2% (w/v) SDS, 10% (v/v) glycerol, 0.00125% (w/v) bromophenol blue and 50mM DTT. The samples were then denatured at 65°C for 10min before separation of proteins on a polyacrylamide gel and transfer to a PVDF membrane. The PDVF membrane was probed with anti-α-tubulin antibody (1:1000 dilution) and anti-β-actin antibody (1:1000 dilution) followed by incubation with a HRP- conjugated anti-mouse antibody (1:10,000). Expression of tubulin and β-actin were visualised by enhanced chemiluminescence.

2.14 Fluorescence microscopy

2.14.1 Analysis of tubulin morphology

Cells were cultured on 13mm glass coverslips (Seeding densities were; Ca9.22: 30,000 cells and TR146: 40,000 cells per coverslip) for 24h. Cells were cultured in the presence of either PBOX-6 or PBOX-15 (100nM, 1μM, 10μM) for a further 24h. Paclitaxel (1μM) and nocozadole (10μM) were used as controls for polymerization and depolymerisation, respectively. After incubation, the cells were fixed in 4% paraformaldehyde in phosphate buffered saline (PBS) for 15min, permeabilised in 0.2% Triton in PBS for 10min, rinsed with PBS and blocked using 1% BSA in phosphate buffered saline Tween (PBST) for 30min. Cells were incubated in primary antibody mouse anti-α-tubulin (1/1000) in 1% BSA in PBST for one hour and in secondary

antibody anti-mouse 488 (Life technologies) (1/500) in 1% BSA in PBST for one hour. Coverslips were placed on 3.5µl Vectashield™ mounting medium containing the nuclear counterstain 4,6-diamidino-2-phenylindole (DAPI) (Vector Labs, CA, USA) on glass slides and stored at 4°C, in darkness, until imaging. Indirect fluorescence of the cells was examined using a standard filter set for DAPI and FITC (Blue/green), through 10X and 20X dry objectives and 60X oil objective with a Zeiss Axiovert/Axiocam CCD system and imaged with AxioVision AxioVs40 software.

2.14.2 Analysis of nucleolar morphology

Cells were cultured on 13mm glass coverslips (Seeding densities were; Ca9.22: 30,000 cells and TR146: 40,000 cells per coverslip) for 24h. Cells were cultured in the presence EtOH (1%) for a further 24h. After incubation, the cells were fixed in methanol at -20°C for 10min, washed with PBS and incubated in a 2µM of RNASelect™ green fluorescent stain (Molecular Probes) for 20min at room temperature. Coverslips were washed with PBS and placed on 3.5µl Vectashield™ mounting medium containing the nuclear counterstain 4,6-diamidino-2-phenylindole (DAPI) (Vector Labs, CA, USA) on glass slides and stored at 4°C, in darkness, until imaging. Indirect fluorescence of the cells was examined using a standard filter set for DAPI and FITC (Blue/green), through 60X oil objective with a Zeiss Axiovert/Axiocam CCD system and imaged with AxioVision AxioVs40 software.

2.15 PBOX synthesis

The pyrrolo-1,5-benzoxazepine compounds, 7-[(*N,N*-dimethylcarbamoyl)oxy]-6-(naphth-1-yl)pyrrolo[2,1-][1,5]benzoxazepine (PBOX-6) and 4-acetoxy-5-(1-(naphthyl)naphtho[2,3]pyrrolo[2,1-D][1,4]oxazepine (PBOX-15) were synthesised as previously described (Campiani *et al.*, 1996).

3 EtOH modulation of hypoxic response proteins in oral epithelial cells

3.1 Introduction

OC is the sixth most common cancer worldwide and has one of the highest death rates due to it being largely asymptomatic until the latter stages of the disease. The biggest risk factor for developing OC is smoking followed by alcohol consumption. There is a vast amount of evidence directly linking alcohol consumption to many different forms of cancer including colorectal, breast and liver however the mechanisms by which alcohol affects the oral mucosa are unclear. Many studies have stated that alcohol does not directly cause cancer of the oral cavity but indirectly facilitates carcinogenic transformation. Several methods have been envisioned for this process. Firstly, alcohol may function as a solvent, thus facilitating the passage of carcinogens through cellular membranes. Secondly, EtOH consumption leads to an enhancement in the liver drug-metabolising capability in both humans and experimental animals and may therefore, activate carcinogenic substances. Lastly, EtOH consumption may alter intracellular metabolism of the epithelial cell of the oral mucosa. Such impairment of cellular function could possibly be aggravated by the coexistence of nutritional deficiencies. The above methods have been speculated and the exact method by which alcohol causes OC is yet to be discovered.

3.1.1 Alcohol and OC

In the past OSCC was primarily found in elderly men with the risk factors being tobacco and excessive alcohol use. More recently there is a significant increase in OSCC in patients under 40 and in the female population. In Ireland in 1994 24% of new cases of OC were in women and that rose to over 32% in 2009 (NCRI). This increasing incidence of OC among the younger population is associated with increased exposure to HPV (Chaturvedi *et al.*, 2008) while the increase in women with OC is due to an increased acceptability of tobacco and alcohol use among women (Mongan D, 2007).

The association between alcohol consumption and OC has long been established. It has been estimated that over 30% of all OC cases worldwide are attributable to alcohol drinking (Boffetta *et al.*, 2006). The excessive consumption of alcohol-containing beverages is also associated with an increase risk of developing other cancers of the head and neck such as pharyngeal and laryngeal cancers. There has been no distinct differentiation on whether one type of alcoholic beverage causes a higher rate of OC

than others (Purdue *et al.*, 2009). It has been suggested that the most frequently consumed alcoholic beverage in a given culture is associated with the highest risk at equivalent levels of consumption; wine in southern Europe, beer and hard liquor in north America, Sake in Japan and cachaca in Brazil. The general consensus is the more EtOH consumed the higher the risk of developing OC. The dose response relationship between alcohol and OC risk is low (1.29 RR) for around 10g of EtOH consumption per day and significantly increasing (13.02 RR) for 125g EtOH/day (where relative risk is the ratio of the risk in the exposed divided by the risk in the unexposed) (Tramacere *et al.*, 2010).

3.1.2 EtOH

EtOH is the main constituent of alcohol containing beverages. It is produced by the fermentation of simple carbohydrates in fruit and starch in grains by yeast. Spirits like whiskey and brandy are produced by distillation of the fermented products. Fermentation is incomplete in beer and complete in wine, with resulting alcohol concentrations between 3-8% and 7-18%, respectively. Distilled products are 30% or greater alcohol by volume. EtOH is the active component in alcoholic beverages. As previously mentioned, EtOH is not thought to have a direct carcinogenic effect on the oral mucosa. However its first metabolite, acetaldehyde, is a known carcinogen and is thought to have a role in many other forms of cancer (Grewal and Viswanathen, 2012, Fedirko *et al.*, 2011, Hamajima *et al.*, 2002).

After EtOH has been consumed, it is rapidly absorbed in the stomach into the bloodstream where it is eventually metabolised by the liver. Enzymes in the liver oxidise EtOH to acetaldehyde and then to acetate, which is easily cleared by the body. The enzyme involved in the oxidation of EtOH to acetaldehyde is alcohol dehydrogenase (ADH) (E.C 1.1.1.1) and acetaldehyde is converted to acetate by acetaldehyde dehydrogenase (ALDH) (E.C 1.2.1.3). The cytochrome P450 system in the liver also functions to degrade and facilitate the removal of EtOH along with these enzymes. Several isoforms of both enzymes exist and people who have some of these isoforms are more prone to certain types of cancer (Ding *et al.*, 2008). One such isoform of ADH called ADH1B*2 metabolizes EtOH at a faster rate than the more common isoforms causing a build-up of the carcinogen acetaldehyde in the liver. A build-up of acetaldehyde can also be caused by malfunctioning isoforms of ALDH, ALDH2*1/2 and

ALDH2*2/2. These isoforms are commonly seen in Asian populations and thus these populations that are more prone to alcohol related cancers.

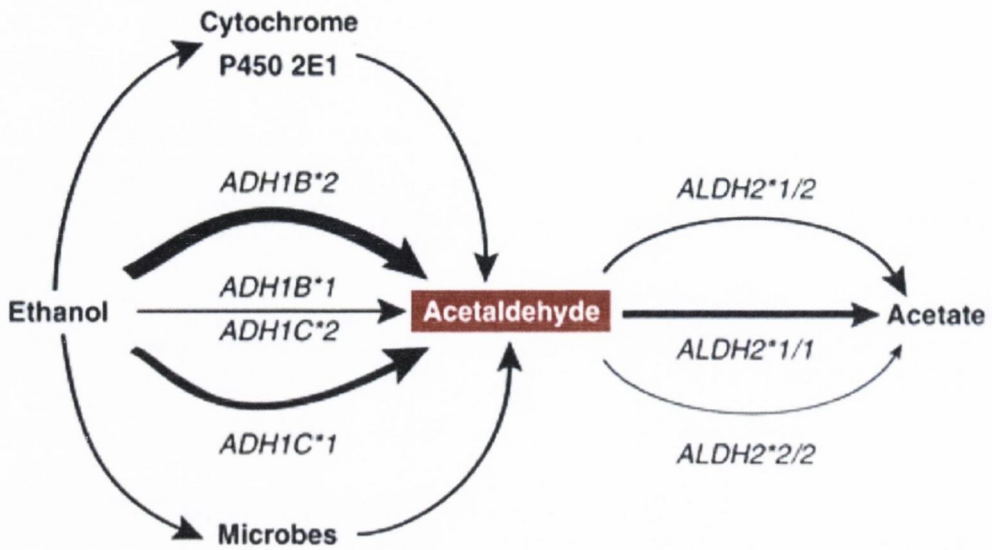


Figure 3-1 Metabolism of EtOH by liver enzymes.
EtOH is oxidised by ADH in microbes and the cytochrome P450 system in the liver to acetaldehyde. Acetaldehyde is broken down by ALDH to acetate, which is removed by the body. Abnormal isoforms of the enzymes ADH and ALDH exist which cause both EtOH and aldehyde to be broken down at different rates.

ADH enzymes are present in the cells of the oral mucosa but at very low concentrations (Dong *et al.*, 1996). Therefore the majority of the EtOH consumed is not oxidised and therefore can exert a direct effect on the oral mucosa. The effect this EtOH is having on the cells is mostly unknown and the question still remains as to whether EtOH is an oral mucosal carcinogen.

3.1.3 EtOH and oxidative stress in OC

Previous studies have demonstrated that alcohol causes an increase in epithelial proliferation and an increase in permeability to tobacco carcinogens (Valentine *et al.*, 1985, Maier *et al.*, 1994). These findings support the theory that alcohol induces direct alterations in the oral mucosa. An increase in cellular proliferation is one of the early stages in carcinogenesis and ROS are directly involved in cell cycle control and proliferation. For this reason ROS have been implicated in the pathology of many

diseases including numerous types of cancer (Waris and Ahsan, 2006). Oxidative stress is the imbalance between the production of ROS and the capacity of antioxidants to respond. These highly reactive molecules can cause adducts in DNA by binding to individual base pairs potentially leading to mutations (Ames, 1983). They have also been found to bind complex cellular structures such as lipids and proteins. This damaging aspect of ROS may potentially be one of the mechanisms associated with alcohol-induced alteration in the oral mucosa. A study in 2009 indicated that short-term exposure to alcohol induced biochemical changes and cellular proliferation in the oral mucosa of rats (Carrard *et al.*, 2009). They found that vitamin E supplementation has been shown to attenuate the cellular proliferation seen with alcohol exposure *in vivo*. This could be due to vitamin E's antioxidant properties. A more recent study in 2013 showed that the antioxidant CAT is involved in the increase in cellular proliferation seen with alcohol exposure (Carrard *et al.*, 2013).

One such ROS molecule is H_2O_2, which may have a significant role to play in EtOH mediated cell damage. H_2O_2 is a small and non-polar molecule able to diffuse across biological membranes. It is ubiquitously produced and its longer half-life than other types of ROS makes it suitable to act as a second messenger exerting prolonged effects in different signaling pathways. H_2O_2 is best known for its carcinogenic properties at higher concentrations however it has been shown to act as a cellular signalling molecule at lower concentrations (Meng *et al.*, 2002). It was not until the 1970's that H_2O_2 was discovered to have signalling properties when it was reported that exogenously added H_2O_2 could mimic the signalling activity of insulin (May and de Haen, 1979). It was later discovered that H_2O_2 could stimulate cell proliferation at low concentrations (Liu *et al.*, 2002, Sigaud *et al.*, 2005). This phenomenon may result in the increase in cell proliferation seen with alcohol exposure. H_2O_2 in certain mammalian cells has been shown to exert its affect on cellular proliferation by activating c-fos and c-jun transcription factors, both of which are involved in cell cycle control (Liu *et al.*, 2002). Similarly, H_2O_2 can activate the ERK pathway that has a modulatory role in cell mobility and metastasis (Akhiani *et al.*, 2014).

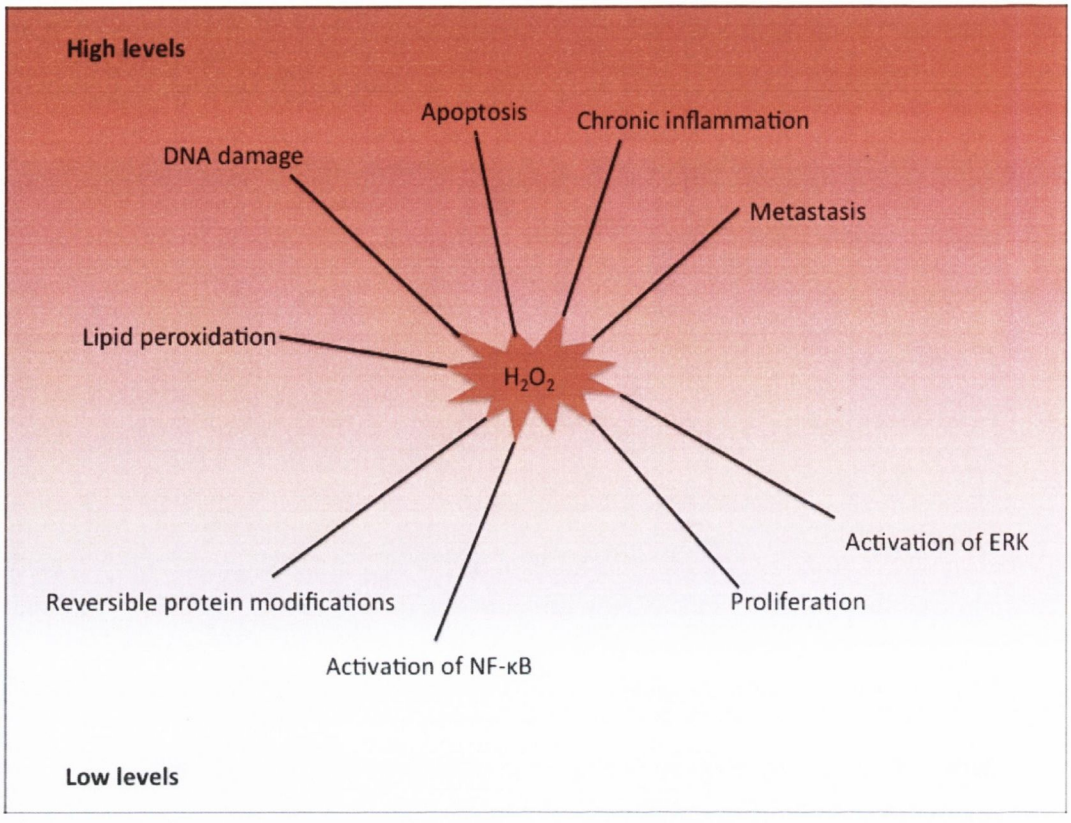


Figure 3-2 The two sides of H_2O_2

3.1.4 ROS and p53

The incidence of p53 mutations in OSCC varies from 30% to 70% however tumours with mutations of the p53 gene grow faster and have a worse prognosis with an overall reduced survival rate (Acha-Sagredo *et al.*, 2009). A mutation in the p53 gene is the most common alteration found in oral premalignant lesions and OSCC (Laimer *et al.*, 2007). The tumour suppressor protein p53 exerts its effects mainly through transcriptional induction of target genes involved in several processes including cell cycle checkpoints and apoptosis (Kastan *et al.*, 1995). p53 can also exert an antioxidant function by activation of a range of target genes (Tan *et al.*, 1999, Hussain *et al.*, 2004). Its function is dependant on its transcriptional activity and precedes the resultant induction of antioxidant and proapoptotic targets. The relationship between p53 and ROS suggests that low levels of ROS causes a p53-dependant upregulation of genes involved in antioxidant and cell cycle regulation and high levels of ROS promote transcription of proapoptotic genes. A study in 2004 found that p53 induced upregulation of the antioxidants GPx and manganese superoxide dismutase (MnSOD)

but had no involvement in control of CAT. A study in 2005 (Sablina *et al.*, 2005) showed that down regulation of p53 elevated intracellular ROS. Additionally they found that in human embryonic fibroblasts the pro and antioxidant function of p53 depended on the levels of intracellular H_2O_2 (0.2mM/1mM).

Alcohol could be exerting oncogenic changes on the oral mucosa by several different means. The question remains as to what effect alcohol is having on cells of the oral mucosa with and without p53 mutations? The rate of transformation in oral mucosal cells due to alcohol consumption could be dependant on the p53 status of the tissue.

3.2 Aims of this chapter

EtOH, although it is a major risk factor in the development of OC, it is not considered to have a direct carcinogenic effect on the oral mucosa. Previous studies have shown that EtOH affects proliferation of the cells of the mucosa, which is an early sign of carcinogenic transformation. Biochemical imbalance could be the first signal of alcohol damage. The relationship between EtOH and oxidative status of the mucosal cells is not clear however this could play a role in the development of OC in the presence of EtOH. This study was undertaken to examine the direct effects of EtOH on the redox status of OC cell lines representing several states of the carcinogenic transformation including models of carcinoma in-situ, a model displaying dysplastic characteristics and primary untransformed oral epithelial cells. Specific objectives were as follows:

1. **Determine the effects of EtOH on the key ROS generation systems in OSCC cell lines.**

   To obtain a model of the effect of EtOH on the redox status of the cell, OSCC cell lines will be treated with a range of EtOH concentrations over 48h. The levels of H_2O_2 in the cells will then be established for each cell type/line. The antioxidant status of the cells will be investigated through examination of key mediators of the ROS systems within the cell using state of the art techniques including qRT-PCR, confocal microscopy, flow cytometry and western blotting.

2. **Examine the potential effects of EtOH on ROS production in an oral dysplastic cell line.**

   Expanding on the model developed previously, an oral dysplastic cell line will be utilised and treated with a range of EtOH concentrations to determine if EtOH can drive changes in the ROS status of the cell and potentially drive carcinogenic changes.

3. **Investigate if the p53 status of oral epithelial cells can modulate the effect of EtOH on ROS production.**

   p53 function is disrupted in approximately 50 % of OC cases and normally results in a significantly poorer prognosis for the patient. Utilising the inherent genotypes of the cell lines previously examined the role of p53 in response to EtOH exposure will be examined along with implications for the ROS system. Through the use of siRNA

technology in the above model systems the influence of p53 on ROS levels and cellular survival will be determined.

4. **Determine the effect of EtOH on redox status in human primary cells.**

   Cancer results from a change of in the physiology of normal healthy cells therefore it is prudent to determine the influence EtOH has on a cohort of such cells. Isolated human primary oral epithelial cells will be exposed to a single concentration of EtOH over a 48h period and the H_2O_2 production and antioxidant status in these cells monitored.

3.3 Results

3.3.1 EtOH does not affect the viability of cell lines

The AlamarBlue viability assay was used to assess the effects of EtOH concentrations on OC cell lines, TR146 and Ca9.22. Cells were treated with a range of EtOH concentrations (0-3%) for 6h, 24h and 48h. The assay was performed on at least three occasions in triplicate. This assay was used to ascertain concentrations of EtOH that did not affect the viability of the cell. Concentrations of 5% EtOH and above caused a decrease in cell viability. Acetlyaldehyde (1nM), a known alcohol derived carcinogen, was examined to determine if breakdown of EtOH had an effect on cell viability. As shown in Figure 3-3, increasing concentrations of EtOH did not have any effect on the viability of the cells after 6h (a), 24h (b) and 48h (c) timepoints. Acetlyaldehyde (1nM) did not affect the viability of the cell lines.

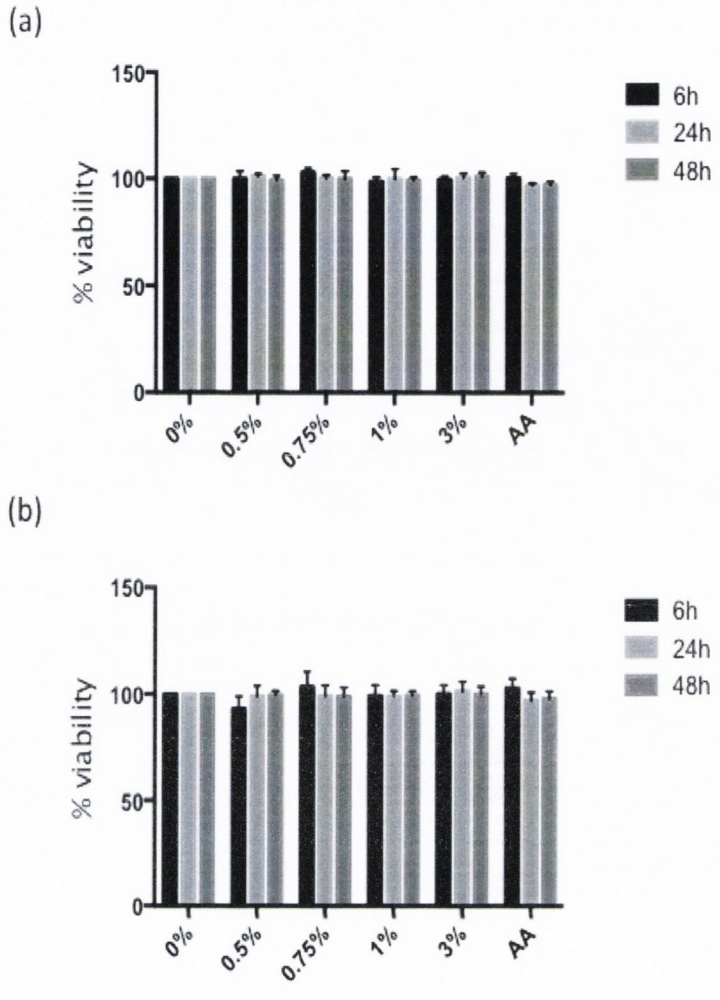


Figure 3-3 EtOH concentrations of 0-3% does not affect TR146 and Ca9.22 cell viability.

Cells were seeded (10,000/well) in a 96 well plate treated with increasing concentrations of EtOH (0-3%) and Alamar Blue reagent (10% v/v) was added 4h before being read on a SPECTRAmax PLUS Microplate spectrophotometer. All time points, 6h, 24h and 48h showed no significant difference between treatments (in comparison to control 100%). Any effect attributed to the metabolic breakdown products of EtOH was controlled for using 1nM acetaldehyde (AA). Experiments were performed in triplicate on three separate occasions (n=9) and results are expressed as mean ± SEM (error bars). Statistical analysis was performed by one-way ANOVA with post-hoc Bonferroni analysis using GraphPad Prism 6.0.

3.3.2 ADH is absent from OSCC cell lines

ADH is an enzyme that catalyses the reduction of primary alcohols into aldehydes. For this present study, it was necessary to ensure alcohol was not broken down in order to investigate and determine the direct effects of EtOH on oral cells. To ensure there was no ADH present in the OC cell lines, with and without treatment, an ADH assay was performed on lysed cell pellets, pre-treated with/without a range of EtOH concentrations for 24h.

TR146 and Ca9.22 cell lines were treated with a range of EtOH concentrations (0-3%) for 24h to investigate if ADH was present and/or upregulated in the presence of EtOH. After 24h incubation, the results show that there was no ADH present in these cells. After treatment with EtOH (0.5% -3%) there was no upregulation of ADH after 24h. As a positive control, 0.1U of ADH was added to the cells in the presence of 1% EtOH and a significant increase in activity was observed here (*** $p < 0.001$). Semi carbazide was used as a trapping agent for aldehyde so the levels of acetaldehyde could be determined.

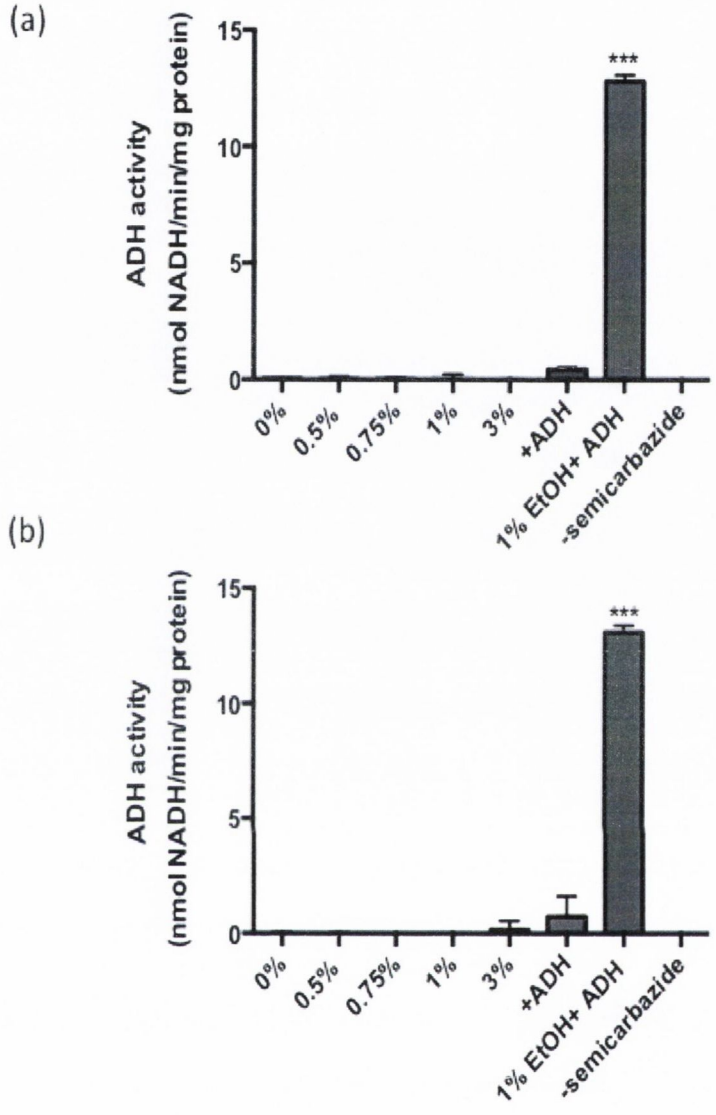


Figure 3-4 Alcohol dehydrogenase is absent from TR146 and CA9.22 cells after 24h incubation with EtOH.

TR146 (a) and Ca9.22 (b) were seeded (10,000/well) in a 96 well plate treated with increasing concentrations of EtOH for 24h. Cells were lysed (1% triton) and NAD (20mM), EtOH (10%), and sodium phosphate buffer (pH 7.5) were added to each well (FV 200µl). The kinetic assay was read at 340nm in a SPECTRAmax PLUS Microplate spectrophotometer for 30mins. Experiments were performed in triplicate on three separate occasions (n=9) and results are expressed as mean ± SEM (error bars). Statistical analysis was performed by one-way ANOVA with post-hoc Bonferroni analysis using GraphPad Prism 6.0 (*** $p<0.001$).

3.3.3 The effect of EtOH on H_2O_2 production in OSCC cell lines

EtOH is recognised to affect the production of ROS in a variety of cell lines (Xue *et al.*, 2012, Agudelo *et al.*, 2011, Heaton *et al.*, 2011) thus experiments were carried to investigate the effects of several concentrations of EtOH on H_2O_2 release from OC cell lines.

3.3.3.1 The effect of EtOH on H_2O_2 release from OSCC cell lines

H_2O_2 release from cells was monitored using a fluorescent reagent (Amplex red). Dose and time dependent studies were performed. Cells were treated for 6h, 24h, and 48h, with several concentrations of EtOH (0%-3%) before the assay was monitored using a Spectramax plate reader. The results show that in the TR146 cell line (Figure 3-5) there is a dose dependant decrease of H_2O_2 release after 6h (a), 24h (b) and 48h (c). After 6h, there is a significant decrease in H_2O_2 production with 0.75% EtOH. Interestingly post 24h treatment there is a significant decrease after 0.5% EtOH. The release of H_2O_2 significantly decreases after 0.75% after 48h treatment, which is similar to the 6h time point. This could signify that the cells have the ability to recover from the treatments at lower concentrations of EtOH. Similarly in the Ca9.22 cells (Figure 3-6) there is a dose dependant decrease after 6h (a), 24h (b), and 48h (c), however the EtOH effect on these cells in comparison to the TR146 cell line is detectable at a lower EtOH concentration of 0.5% (6h). This decrease in the presence of 0.5% EtOH is observed at both the 24h and 48h time points. The significance of the decrease at 0.5% in each case tells use that the EtOH has its peak effect after 24h and the cells begin to recover at 48h. The Ca9.22 cells are more susceptible to the EtOH effects than the TR146 cells. Both cell lines show their ability to recover at the lower concentration over 48h however the Ca9.22 cells do have a slower recovery than the TR146 cell line.

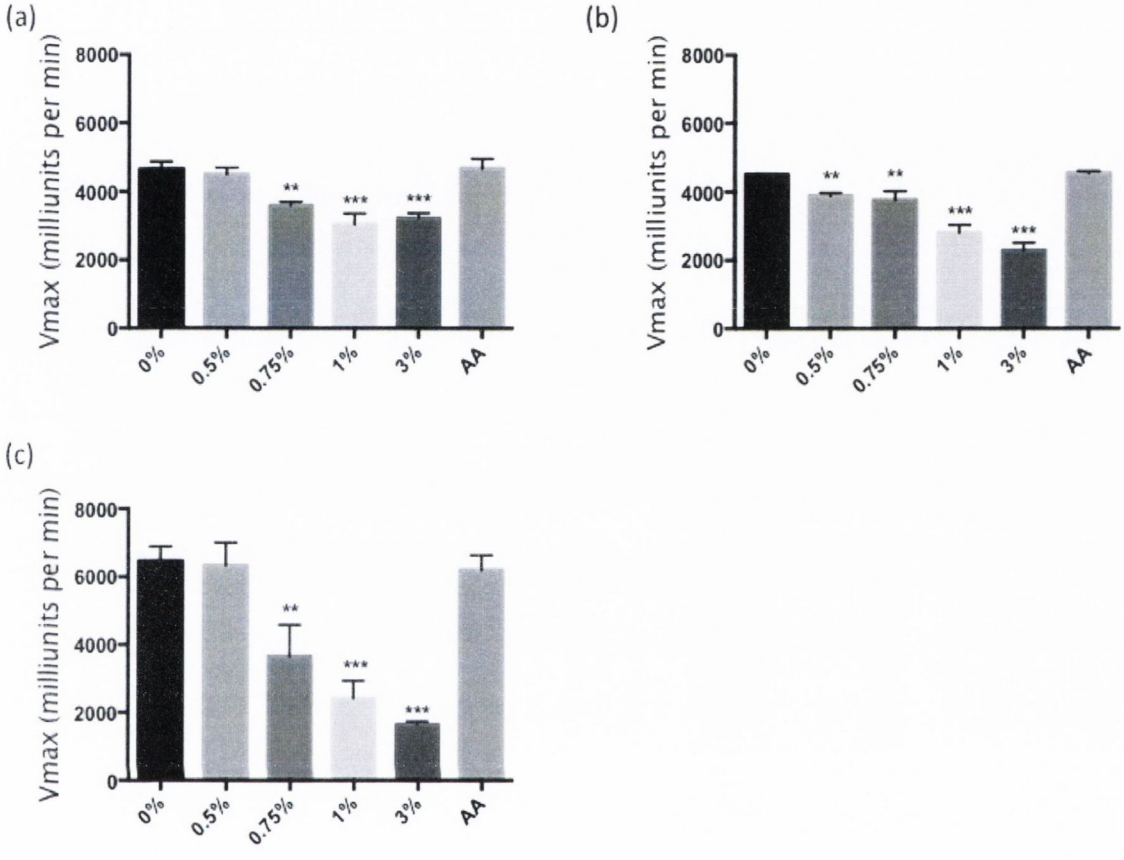


Figure 3-5 EtOH decreases the rate of H_2O_2 release after 6h, 24h, and 48h treatment in the TR146 cell line.

TR146 cells (10,000/well) were treated for 6h (a), 24h (b) and 48h (c) with a range of EtOH concentrations (0-3%). Post treatment, cells were assayed in Krebs buffer with Amplex red and HRP for 45 min at 37°C. H_2O_2 activity was monitored in a Spectramax Gemini XS plate reader with an excitation wavelength of 550nm and an emission wavelength of 580nm. Any effect attributed to the metabolic breakdown products of EtOH was controlled for using 1nM AA. Experiments were completed in triplicate on three separate occasions (n=9) and results were expressed as mean ± SEM (error bars). Statistical analysis was performed by one-way ANOVA with post-hoc Bonferroni analysis using GraphPad Prism. Samples significantly different to the control are annotated ** $p<0.01$ and *** $p<0.001$.

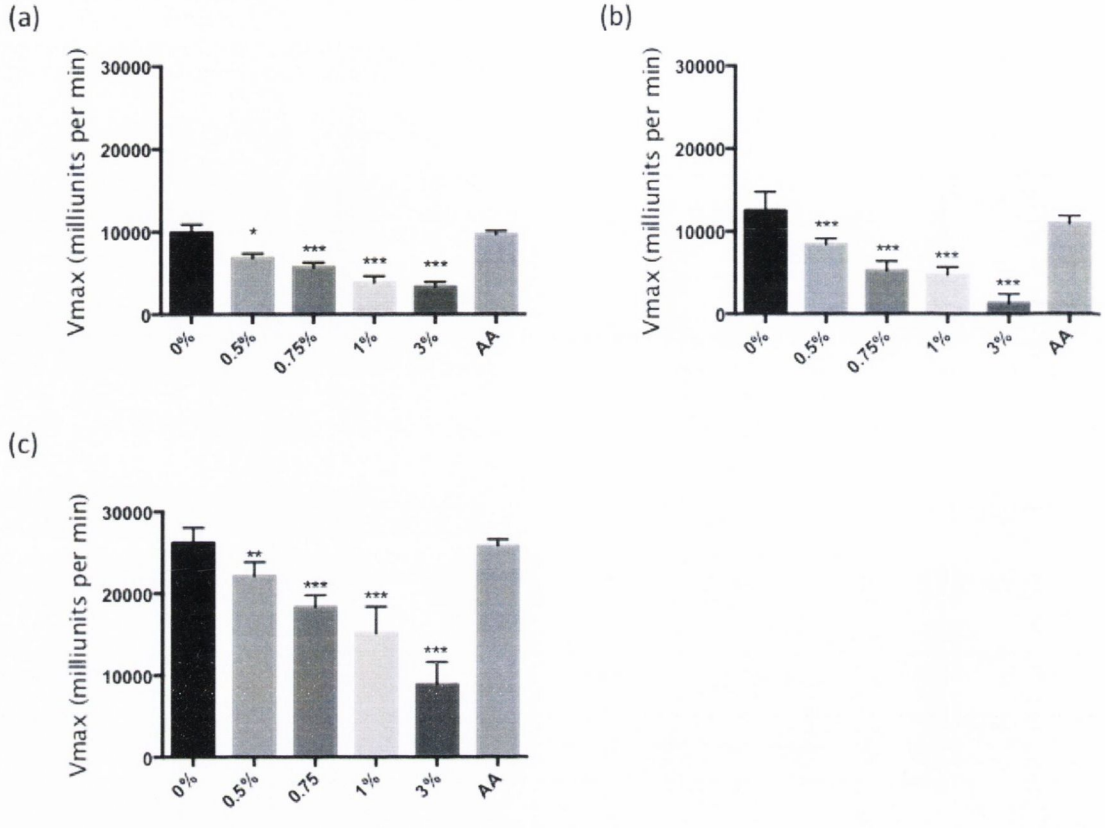


Figure 3-6 EtOH decreases the rate of H_2O_2 release after 6h, 24h, and 48h treatment in the Ca9.22 cell line.

Ca9.22 cells (10,000/well) were treated for 6h (a), 24h (b) and 48h (c) with a range of EtOH concentrations (0-3%). Post treatments, cells were assayed in Krebs buffer with Amplex red and HRP for 45 min at 37°C. H_2O_2 activity was monitored in a Spectramax Gemini XS plate reader with an excitation wavelength of 550nm and an emission wavelength of 580nm. Any effect attributed to the metabolic breakdown products of EtOH was controlled for using 1nM AA. Experiments were completed in triplicate on three individual preparations (n=9) and results were expressed as mean ± SEM (error bars). Statistical analysis was performed by one-way ANOVA with post-hoc Bonferroni analysis using GraphPad Prism. Samples significantly different to the control are annotated * $p<0.05$, ** $p<0.01$ and *** $p<0.001$.

3.3.3.2 Intracellular H_2O_2 production in OSCC cell lines in response to EtOH exposure

Results from the previous experiment indicate that EtOH affects the release of H_2O_2 from the TR146 and Ca9.22 cells. This experiment was undertaken to investigate whether internal H_2O_2 production was affected in a similar manner to its release. Cell lines were treated with EtOH (1%) for a 24h period and internal H_2O_2 was examined using a confocal microscope with 2',7'-dichlorfluorescein-diacetate (DCFH-DA). 1% EtOH was used as this was the lowest concentration that showed effect in these cells. Figure 3-7 (TR146) and Figure 3-8 (Ca9.22) below show representative fluorescent microscopy images using three different cell markers and excited at three different wavelengths. 4',6-diamidino-2-phenylindole (DAPI) a stain which binds DNA was used to visualize the nuclei, cell mask was used to visualise the plasma membrane and DCFH-DA was used to monitor the production of H_2O_2 within the cells. Images A & D of Figure 3-7 and Figure 3-8 below show a merged image of the cell mask and DAPI channels presenting a view of the general structure of the cell in the control and 1% EtOH treatment after 24h, respectively. Images B & E show the merged images of all three channels, DAPI, cell Mask and DCF in the control and treatment, respectively. This clearly shows that there is a significant decrease in the presence of H_2O_2 in both the TR146 and Ca9.22 cell lines after 24h treatment with EtOH represented by the decrease in fluorescence intensity in the green channel. Pictures C & F visualise the merged images of the DAPI & DCF channels in the control and treatment cells, respectively. These results confirm that EtOH affects both intracellular levels and release of H_2O_2 from OSCC cell lines.

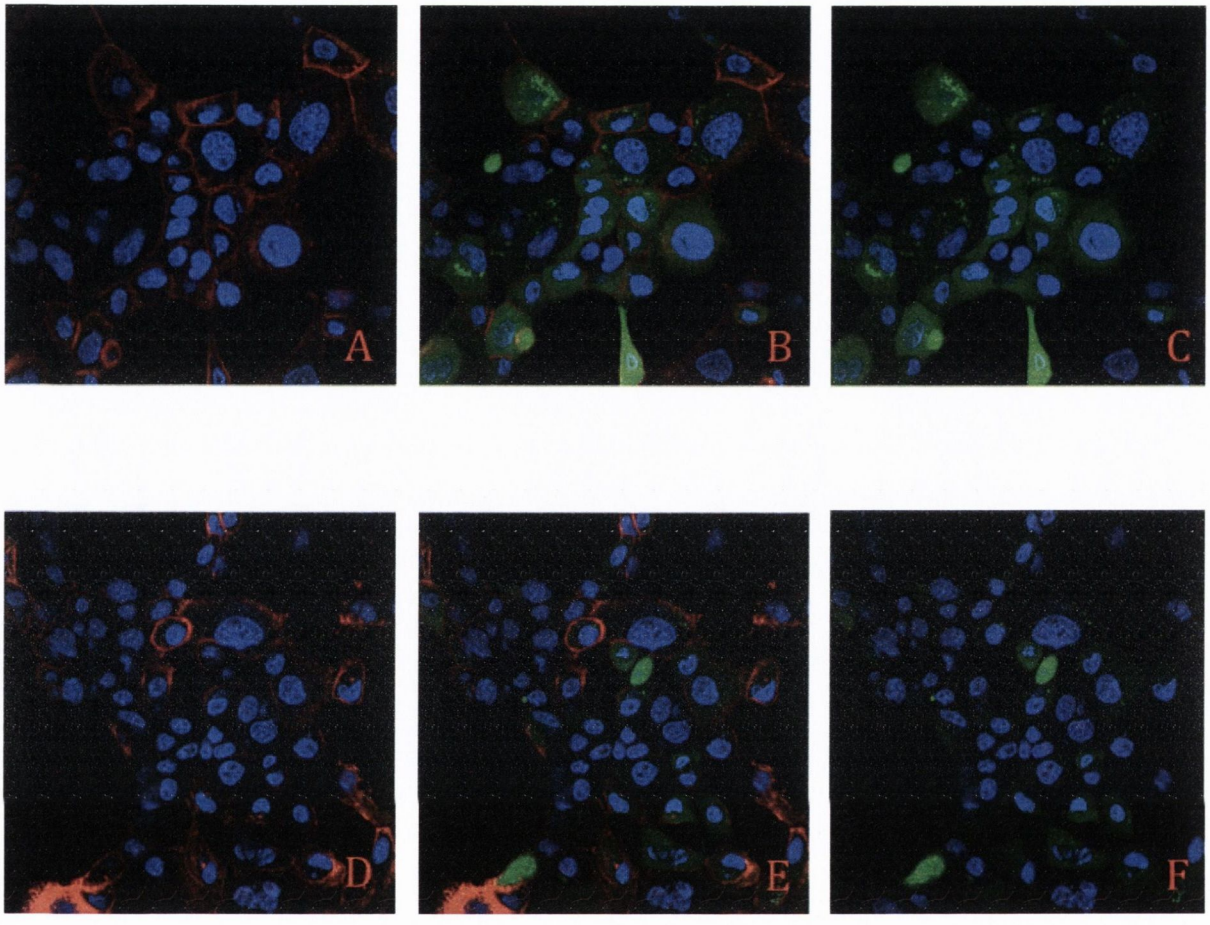


Figure 3-7 EtOH decreases intracellular H_2O_2 after 24h treatment in TR146 cells.

Confocal microscopy images of immunoflourescent staining of H_2O_2 in TR146 cells using 2',7'-dichlorodihydrofluorescein diacetate (H_2DCFDA). (A) (B) (C)- 0% EtOH (overlays of different dyes). (D) (E) (F) -24hr treatment with 1% EtOH (overlays of different dyes). (A) & (D) Cell Mask ™ plasma membrane staining (red) and DAPI nuclear stain (blue). (B) & (E) are merged images of Cell Mask™, DAPI and DCF H_2O_2 staining (green). (C) & (F) are merged images of DAPI and DCF staining. Images are representative of an experiment carried out in triplicate.

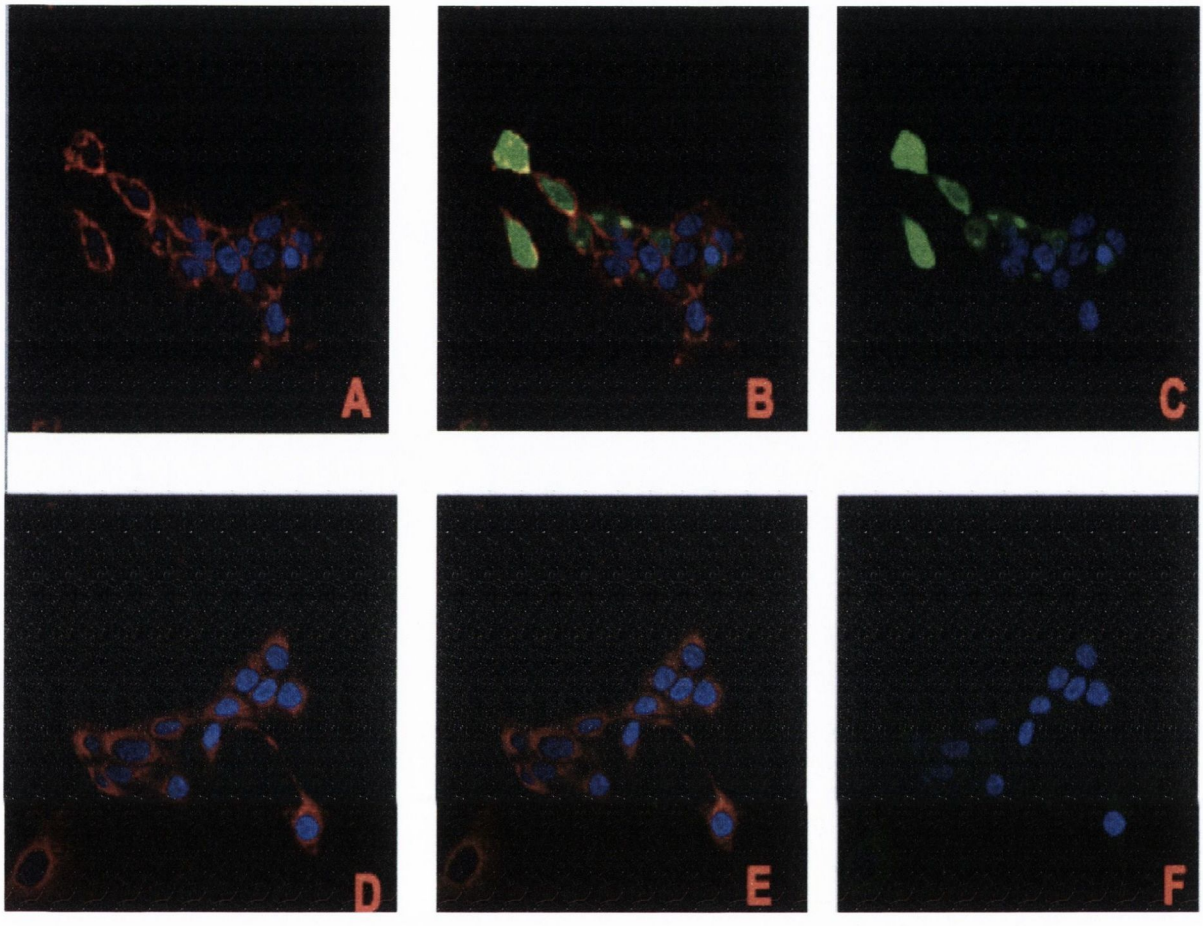


Figure 3-8 EtOH decreases intracellular H_2O_2 after 24h treatment in Ca9.22 cells.

Confocal microscopy images of immunoflourescent staining of H_2O_2 in Ca9.22 cells using 2',7'-dichlorodihydrofluorescein diacetate (H_2DCFDA). (A) (B) (C) 0% EtOH (overlays of different dyes). (D) (E) (F) 24hr treatment with 1% EtOH (overlays of different dyes). (A) & (D) Cell Mask ™ plasma membrane staining (red) and DAPI nuclear stain (blue). (B) & (E) are merged images of Cell Mask™, DAPI and DCF H_2O_2 staining (green). (C)& (F) are merged images of DAPI and DCF staining. Images are representative of an experiment carried out in triplicate.

3.3.4 The effect of EtOH on HIF1-α in OSCC cell lines.

HIF1 plays a central role in the cellular pathways by activating hundreds of genes associated with angiogenesis, ischemia, as well as energy metabolism, nutrient transport and the cell cycle (Semenza, 2004, Wang *et al.*, 1995, Goda *et al.*, 2003). It is composed of 2 subunits – α and β. HIF1-α is upregulated in an adaptive response to hypoxic conditions (Lee *et al.*, 2004). Previous results (3.3.16.1 and 3.3.3.2) showed that EtOH causes a decrease in H_2O_2 in a dose dependant manner with subsequent recovery at lower concentrations. qRT-PCR analysis of HIF1α expression was undertaken to investigate its role in the regulation of ROS during EtOH exposure.

In the TR146 cell line (Figure 3-9) there is a significant increase in HIF1-α after 6h 0.75% (a). After 24h there is a stabilisation of HIF1-α at 0.75% and 1% with a significant decrease at 3%. The 48h time point shows no significant difference at any concentration, which is consistent with the results seen in the TR146 H_2O_2 assay study. Contrastingly to the TR146 cell line, EtOH has no effect on HIF-1α expression at any time point in the Ca9.22 cell line (Figure 3-10).

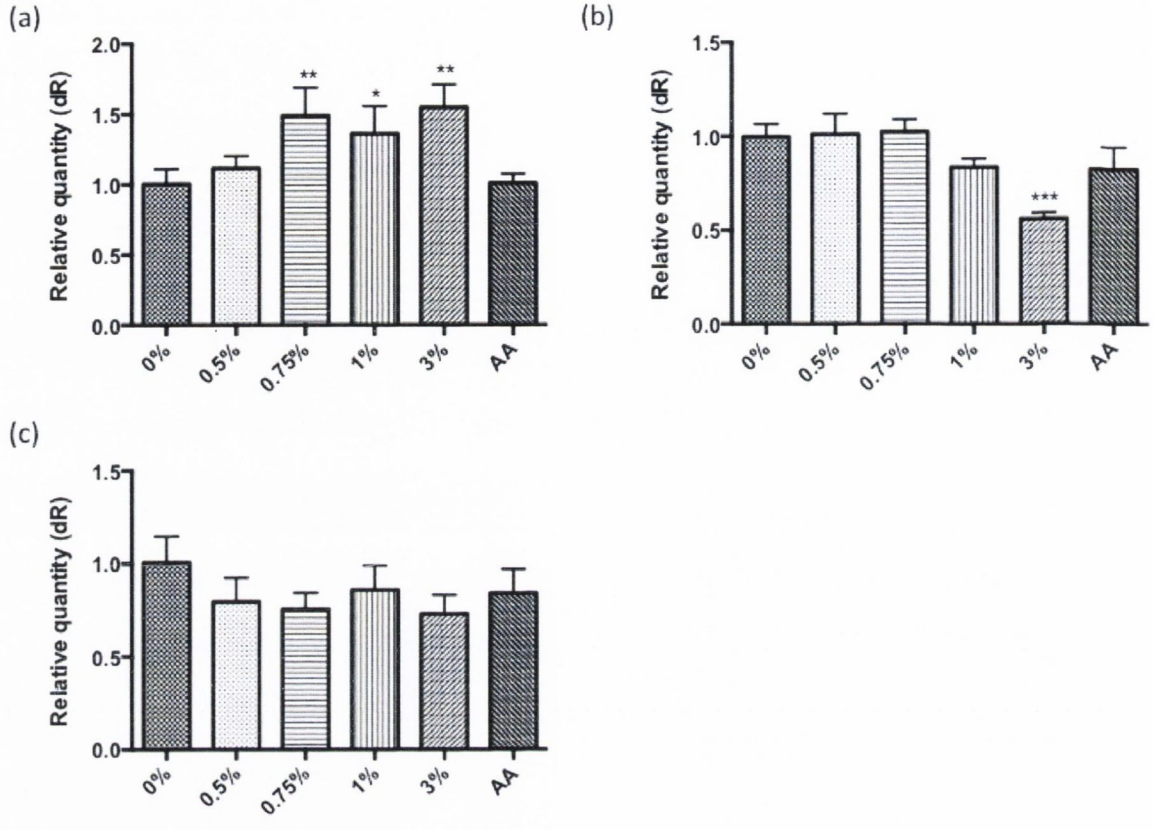


Figure 3-9 HIF1-α expression after 6h, 24h, and 48h in the presence of increasing concentrations of EtOH in TR146 cells.

TR146 cells were treated with varying concentrations of EtOH for 6h (a), 24h (b) and 48h (c). mRNA was harvested and target genes were amplified up using a Sybr green One-Step qRT-PCR with specific primers for HIF1-α. Any effect attributed to the metabolic breakdown products of EtOH was controlled for using 1nM acetaldehyde (AA). Relative quantification of gene expression profile was calculated using a DDCt method (RQ manager, Applied Biosystems). Experiments were completed in triplicate using three individual preparations (n=9) and statistical analysis was carried out using a one-way ANOVA with post-hoc Bonferroni analysis using GraphPad prism 6.0. Samples significantly different to the control are annotated * $p<0.05$, ** $p<0.01$, *** $p<0.001$.

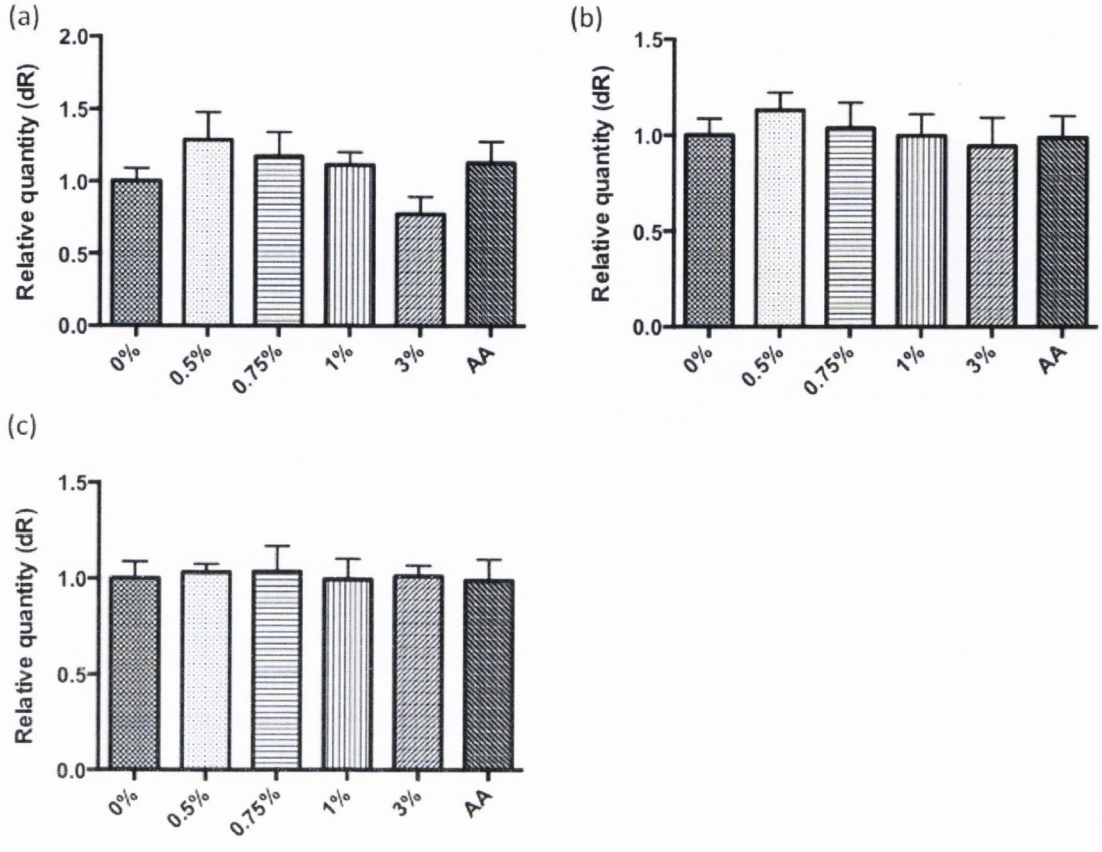


Figure 3-10 HIF1-α expression after 6h, 24h, and 48h in the presence of increasing concentrations of EtOH in Ca9.22 cells.

Ca9.22 cells were treated with varying concentrations of EtOH for 6h (a), 24h (b) and 48h (c). mRNA was harvested and target genes were amplified up using a Sybr green One-Step qRT-PCR with specific primers for HIF1-α. Any effect attributed to the metabolic breakdown products of EtOH was controlled for using 1nM acetaldehyde (AA). Relative quantification of gene expression profile was calculated using a DDCt method (RQ manager, Applied Biosystems). Experiments were completed in triplicate using three individual preparations (n=9) and statistical analysis was carried out using a one-way ANOVA with post-hoc Bonferroni analysis using GraphPad prism 6.0.

3.3.5 Modulation of antioxidant enzymes in OSCC cells in response to EtOH exposure.

ROS are produced during normal cellular function. High levels of ROS can cause damage to the cell including lipid peroxidation and oxidation of DNA and proteins. ROS need to be tightly controlled and antioxidant enzymes minimise the perturbations caused by ROS. The antioxidant system is highly complex and composed of several different enzymes. Dose dependant decreases in H_2O_2 could indicate a central role for antioxidants in this effect.

3.3.5.1 Modulation of MnSOD expression in OSCC in response to EtOH.

MnSOD is the primary antioxidant enzyme that protects cells from oxidative stress by catalysing the dismutation of O_2^- to H_2O_2. In the TR146 cell line (Figure 3-11) there is an increase in MnSOD at the mRNA level after 6h (a) at 0.75% using qRT-PCR. After 24h (b) there is still an increase in H_2O_2 at 24h however there are signs of the enzyme levels stabilising. The increase here is only seen at 1% and 3%. By 48h there is no significant difference in enzymes from the control. Western blot analysis of MnSOD protein expression was undertaken to detect if mRNA levels corresponded to protein levels in this enzyme [Figure 3-11 (d)]. Analysis of the western blot show that the protein levels of MnSOD did not noticeably change in the TR146 cell line. GAPDH was used as a loading control to ensure equal amount of protein was loaded into each lane.

Similarly to the TR146 cell line, there is an increase in MnSOD in the Ca9.22 cell line after 6h [Figure 3-12 (a)]. This increase is only significant at 3% EtOH which differs from the first cell line. Another disparity between cell lines include there is no increase in MnSOD after 24h (b) at any concentration and there is a subsequent increase after 48h 3% EtOH in the Ca9.22 cell line.

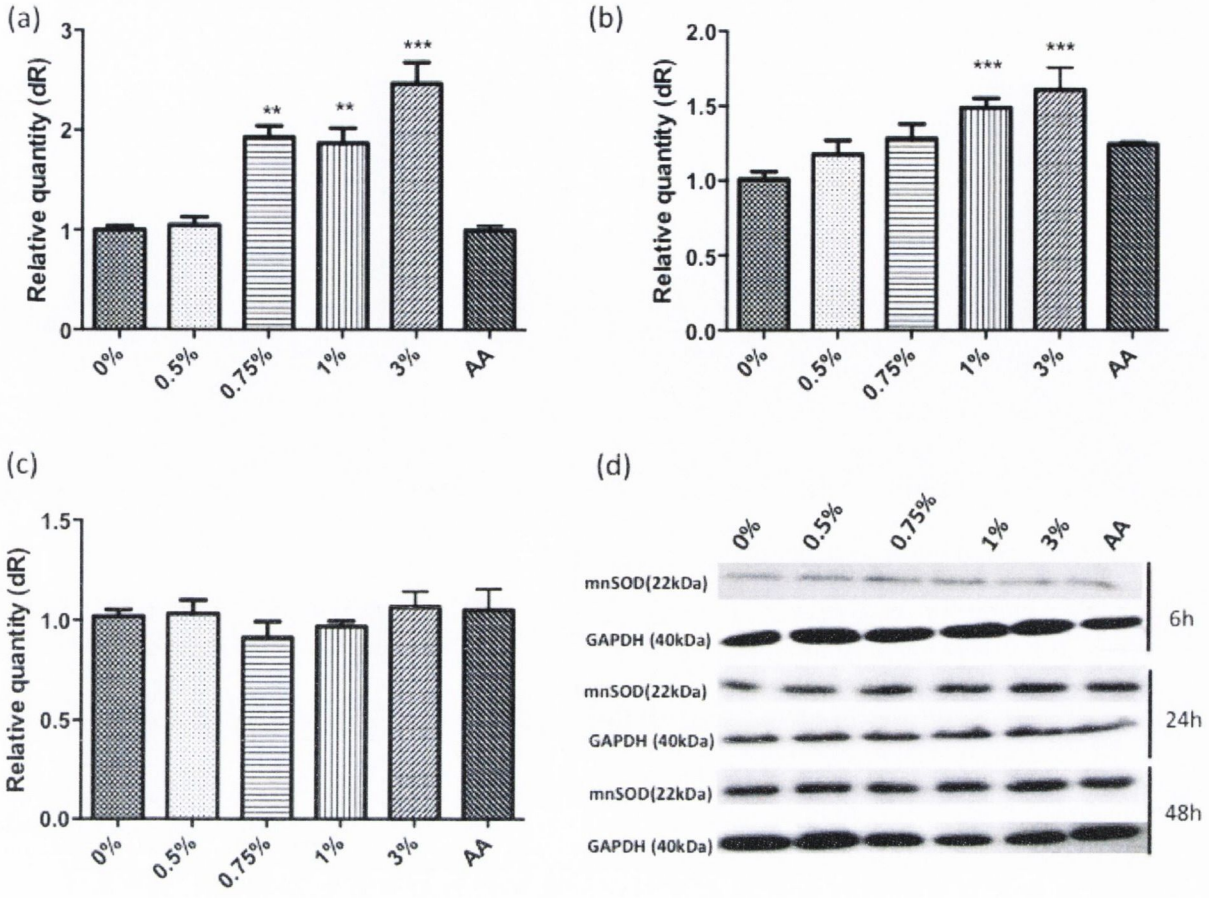


Figure 3-11 Analysis of MnSOD mRNA and protein expression in TR146 cells.

TR146 cells were seeded at a density of 3 X 10^5 in a T25 flask, left to adhere overnight and treated with varying concentrations of EtOH for 6h (a), 24h (b) and 48h (c). mRNA was harvested and target genes were amplified up using a Sybr green One-Step qRT-PCR with specific primers for MnSOD using β-actin as a normaliser. Relative quantification of gene expression profile was calculated using a DDCt method (RQ manager, Applied Biosystems). Any effect attributed to the metabolic breakdown products of EtOH was controlled for using 1nM acetaldehyde (AA). Experiments were completed in triplicate on three individual preparations (n=9) and statistical analysis was carried out using a one-way ANOVA with post-hoc Bonferroni analysis using GraphPad prism 6.0. Samples significantly different to the control are annotated ** $p<0.01$, *** $p<0.001$. (d) Cells were seeded (as in mRNA preparation), protein was harvested from treated samples and lysates were prepared for western blot analysis. 20μg of protein was separated on a 12% resolving gel with a 5% stacking gel, transferred to a PVDF membrane and probed with an anti-MnSOD antibody. Membranes were also probed for GAPDH as a loading control. Results are representative of three individuals experiments.

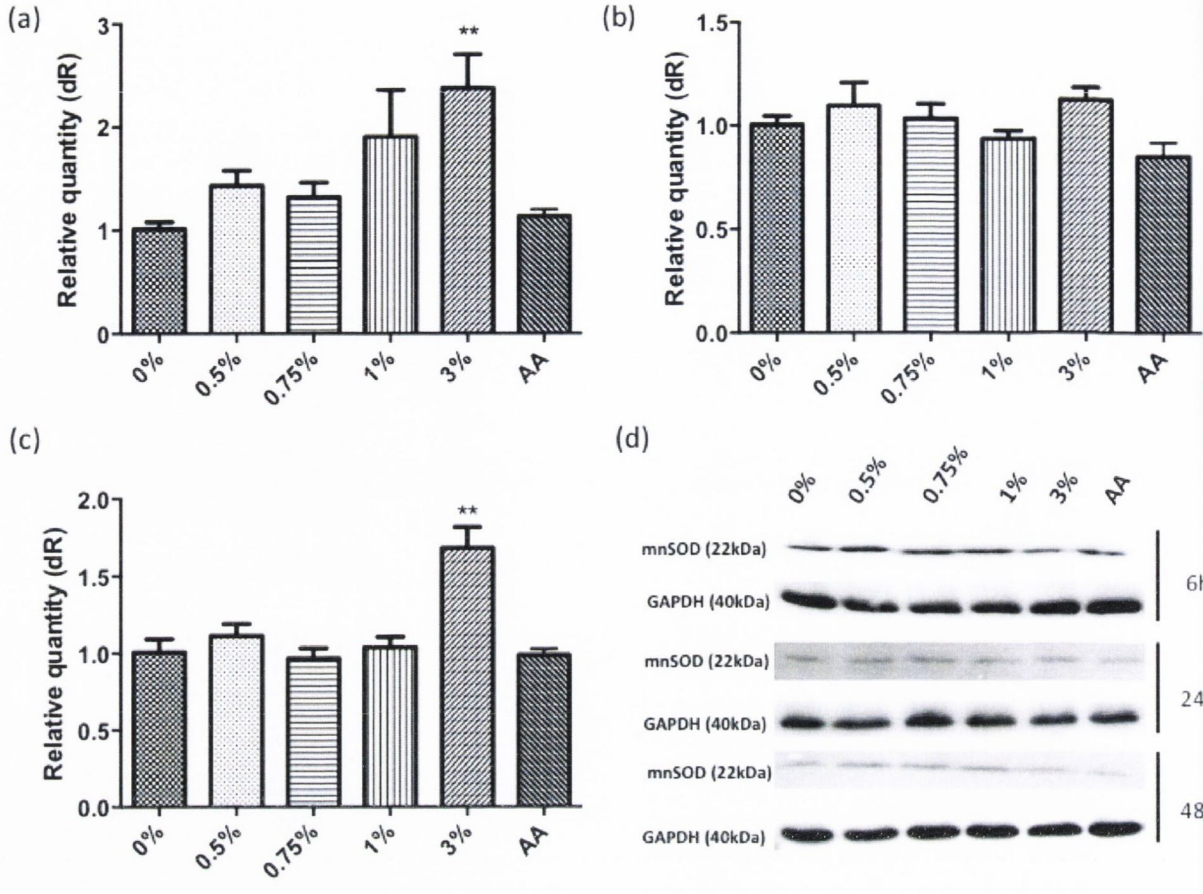


Figure 3-12 Analysis of MnSOD mRNA and protein expression in Ca9.22 cells.

Ca9.22 cells were seeded at a density of 3 X 10^5 in a T25 flask, left to adhere overnight and treated with varying concentrations of EtOH for 6h (a), 24h (b) and 48h (c). mRNA was harvested and target genes were amplified up using a Sybr green One-Step qRT-PCR with specific primers for MnSOD using β-actin as a normaliser. Relative quantification of gene expression profile was calculated using a DDCt method (RQ manager, Applied Biosystems). Any effect attributed to the metabolic breakdown products of EtOH was controlled for using 1nM acetaldehyde (AA) Experiments were completed in triplicate on three individual preparations (n=9) and statistical analysis was carried out using a one-way ANOVA with post-hoc Bonferroni analysis using GraphPad prism 6.0. Samples significantly different to the control are annotated ** $p<0.01$. (d) Cells were seeded (as in mRNA preparation), protein was harvested from treated samples and lysates were prepared for western blot analysis. 20μg of protein was separated on a 12% resolving gel with a 5% stacking gel, transferred to a PVDF membrane and probed with an anti-MnSOD antibody. Membranes were also probed for GAPDH as a loading control. Results are representative of three individuals experiments.

3.3.5.2 EtOH modulation of CAT expression in OSCC cell lines.

H_2O_2 is a toxic ROS that is tightly controlled within the cell. One of the most important enzymes in regulating H_2O_2 is CAT. As previous results demonstrated a decrease in H_2O_2 in the cell lines examined it seemed prudent to examine the role of CAT in this system. CAT catalyses the decomposition of H_2O_2 into water and O_2 and therefore may be involved in the lower levels of H_2O_2 observed.

qRT-PCR and western blot analysis of CAT was undertaken to investigate the relationship between the decrease in H_2O_2 in the presence of EtOH and CAT. In the TR146 cell line (Figure 3-13) there is no change in CAT transcription after 6h. There is a significant increase in expression after 1% in 24h time point (b) and a restoration of normal gene expression after 48h in a similar manner to MnSOD expression shown previously. Western blot analysis of protein expression shows no major alterations of CAT expression over the 48h time point in this cell line.

In comparison to the TR146 cell line, in the Ca9.22 cell line there is an increase in CAT gene expression after 6h and a highly significant subsequent decrease in expression after 24h at every EtOH treatment [Figure 3-14 (b)]. Similarly to the TR146 cell line there is no significant change in expression after 48h. Protein expression [Figure 3-14 (d)] shows no change after 6h EtOH treatment however there is a significant decrease in protein expression after 24h at 1% and 3%. This is in agreement with the gene expression profile at this time point. After 48h there is no change in protein expression of CAT.

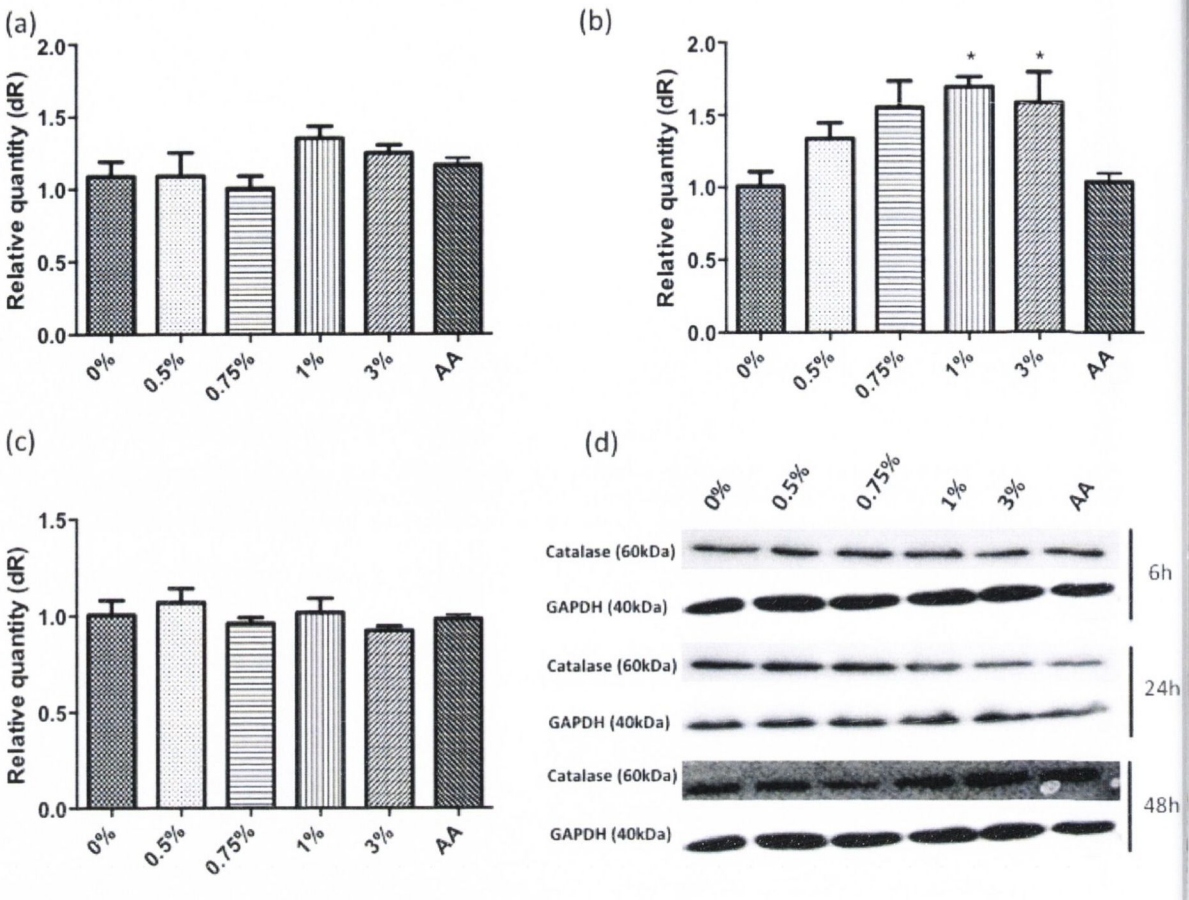


Figure 3-13 Analysis of CAT mRNA and protein expression in TR146 cells.

TR146 cells were seeded at a density of 3 X 10^5 in a T25 flask, left to adhere overnight and treated with varying concentrations of EtOH for 6h (a), 24h (b) and 48h (c). mRNA was harvested and target genes were amplified up using a Sybr green One-Step qRT-PCR with specific primers for CAT using β-actin as a normaliser. Relative quantification of gene expression profile was calculated using a DDCt method (RQ manager, Applied Biosystems). Any effect attributed to the metabolic breakdown products of EtOH was controlled for using 1nM acetaldehyde (AA) Experiments were completed in triplicate on three individual preparations (n=9) and statistical analysis was carried out using a one-way ANOVA with post-hoc Bonferroni analysis using GraphPad prism 6.0. Samples significantly different to the control are annotated * $p<0.05$. (d) Cells were seeded (as in mRNA preparation), protein was harvested from treated samples and lysates were prepared for western blot analysis. 20μg of protein was separated on a 12% resolving gel with a 5% stacking gel, transferred to a PVDF membrane and probed with an anti-CAT antibody. Membranes were also probed for GAPDH as a loading control. Results are representative of three individuals experiments.

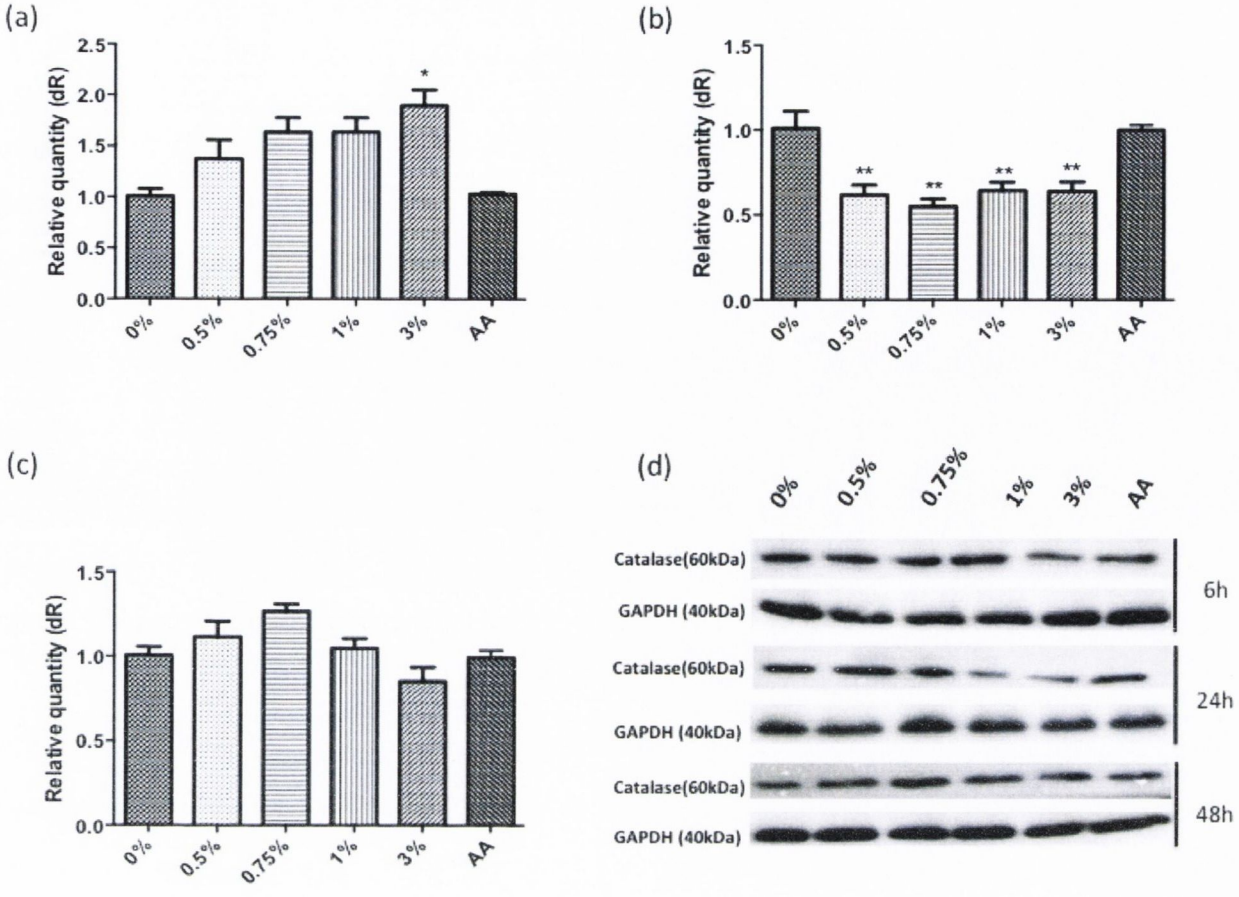


Figure 3-14 Analysis of CAT mRNA and protein expression in Ca9.22 cells.

Ca9.22 cells were seeded at a density of 3 X 10^5 in a T25 flask, left to adhere overnight and treated with varying concentrations of EtOH for 6h (a), 24h (b) and 48h (c). mRNA was harvested and target genes were amplified up using a Sybr green One-Step qRT-PCR with specific primers for CAT using β-actin as a normaliser. Relative quantification of gene expression profile was calculated using a DDCt method (RQ manager, Applied Biosystems). Any effect attributed to the metabolic breakdown products of EtOH was controlled for using 1nM acetaldehyde (AA) Experiments were completed in triplicate on three individual preparations (n=9) and statistical analysis was carried out using a one-way ANOVA with post-hoc Bonferroni analysis using GraphPad prism 6.0. Samples significantly different to the control are annotated ** $p<0.01$. (d) Cells were seeded (as in mRNA preparation), protein was harvested from treated samples and lysates were prepared for western blot analysis. 20μg of protein was separated on a 12% resolving gel with a 5% stacking gel, transferred to a PVDF membrane and probed with an anti-CAT antibody. Membranes were also probed for GAPDH as a loading control. Results are representative of three individuals experiments.

3.3.5.3 Modulation of GPx-1 expression in OSCC lines in response to EtOH.

The antioxidation system, as mentioned before, is composed of several important enzymes involved in a multistep breakdown of highly reactive molecules that react and damage important cell structures. Another powerful antioxidant in the system is GPx-1. GPx-1 functions to catalyse the conversion of H_2O_2 into water similar to the action of CAT. The expression and protein levels of GPx-1 were examined to determine if GPx-1 is modulated in response to EtOH with an influence on the levels of key ROS species within the cell.

In the TR146 cell line there is no significant difference in GPx-1 expression at any time point (Figure 3-15). In Ca9.22 cells there is no significant difference after 6h and 24h [Figure 3-16 (a) (b)] but there is a significant decrease in expression after 48h at every concentration of EtOH [Figure 3-16 (c)].

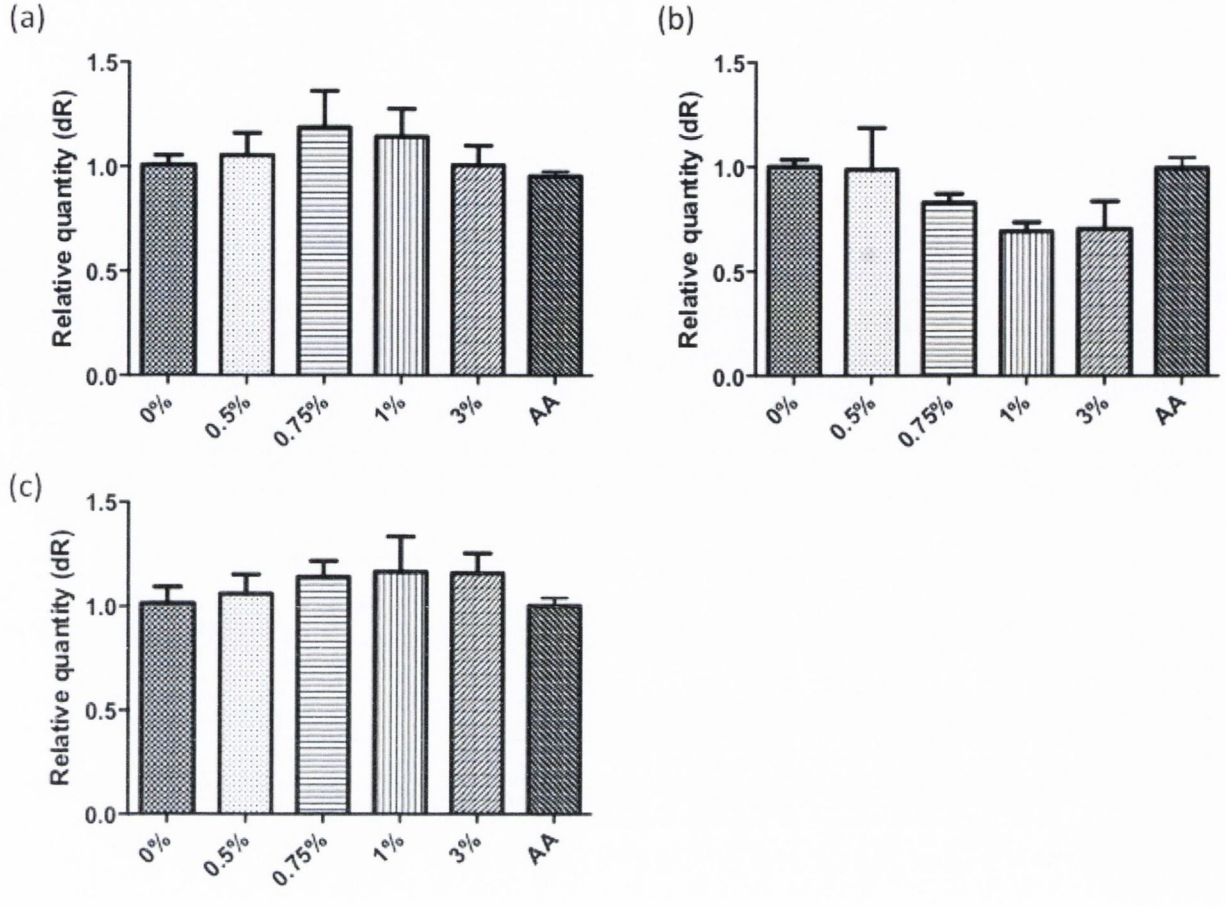


Figure 3-15 Analysis of GPx-1 mRNA expression in TR146 cells.

TR146 cells were seeded at a density of 3 X 10^5 in a T25 flask, left to adhere overnight and treated with varying concentrations of EtOH for 6h (a), 24h (b) and 48h (c). mRNA was harvested and target genes were amplified up using a Sybr green One-Step qRT-PCR with specific primers for GPx-1 using β-actin as a normaliser. Relative quantification of gene expression profile was calculated using a DDCt method (RQ manager, Applied Biosystems). Any effect attributed to the metabolic breakdown products of EtOH was controlled for using 1nM acetaldehyde (AA) Experiments were completed in triplicate on three individual preparations (n=9) and statistical analysis was carried out using a one-way ANOVA with post-hoc Bonferroni analysis using GraphPad prism 6.0.

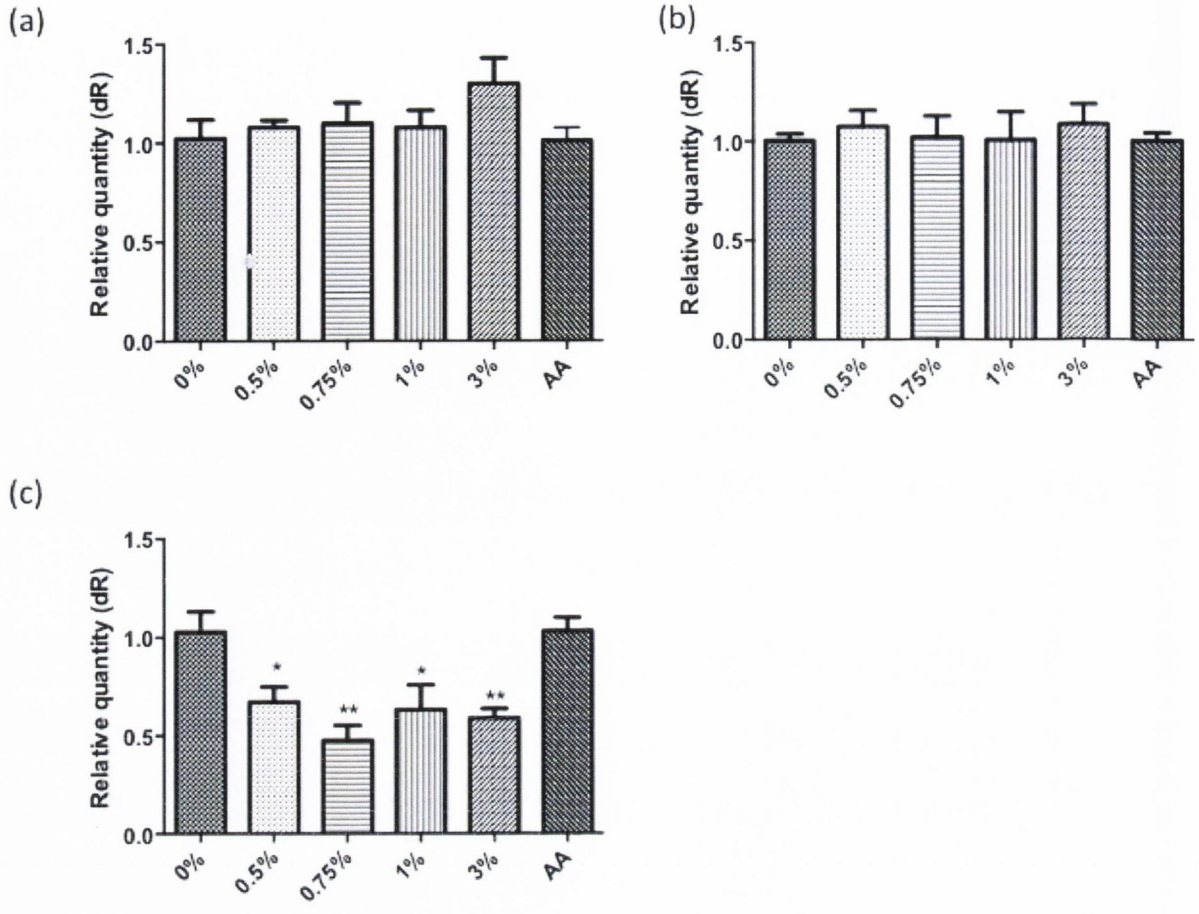


Figure 3-16 Analysis of GPx-1 mRNA expression in Ca9.22 cells.

Ca9.22 cells were seeded at a density of 3 X 10^5 in a T25 flask, left to adhere overnight and treated with varying concentrations of EtOH for 6h (a), 24h (b) and 48h (c). mRNA was harvested and target genes were amplified up using a Sybr green One-Step qRT-PCR with specific primers for GPx-1 using β-actin as a normaliser. Relative quantification of gene expression profile was calculated using a DDCt method (RQ manager, Applied Biosystems). Any effect attributed to the metabolic breakdown products of EtOH was controlled for using 1nM acetaldehyde (AA). Experiments were completed in triplicate on three individual preparations (n=9) and statistical analysis was carried out using a one-way ANOVA with post-hoc Bonferroni analysis using GraphPad prism 6.0. Samples significantly different to the control are annotated *$p<0.05$, ** $p<0.01$.

3.3.5.4 Modulation of HO-1 expression in OSCC lines in response to EtOH.

HO-1 is considered a key enzyme in the antioxidant capability of a cell however it functions differently to the previously examined antioxidants. HO-1 catabolises free heme into ferrous iron, carbon monoxide and biliverdin. Free heme can catalyse the production of toxic free radicals by catalysing the conversion of H_2O_2 into the cytotoxic hydroxyl radical $OH^{\bullet}$.

HO-1 gene expression analysis in the TR146 cell line after EtOH treatment shows a decrease in HO-1 mRNA over 48h. After 6h treatment [Figure 3-17 (a)] there is no significant change in HO-1 expression. After 24h there is a significant decrease in expression at 1% and 3% EtOH [Figure 3-17 (b)]. Interestingly after 48h there is a significant decrease in expression at every EtOH concentration in this cell line [Figure 3-17 (c)]. Contrastingly there is no change in expression at any time point in the Ca9.22 cell line (Figure 3-18). Here again it highlights the differences between the two cell lines in their antioxidant capabilities.

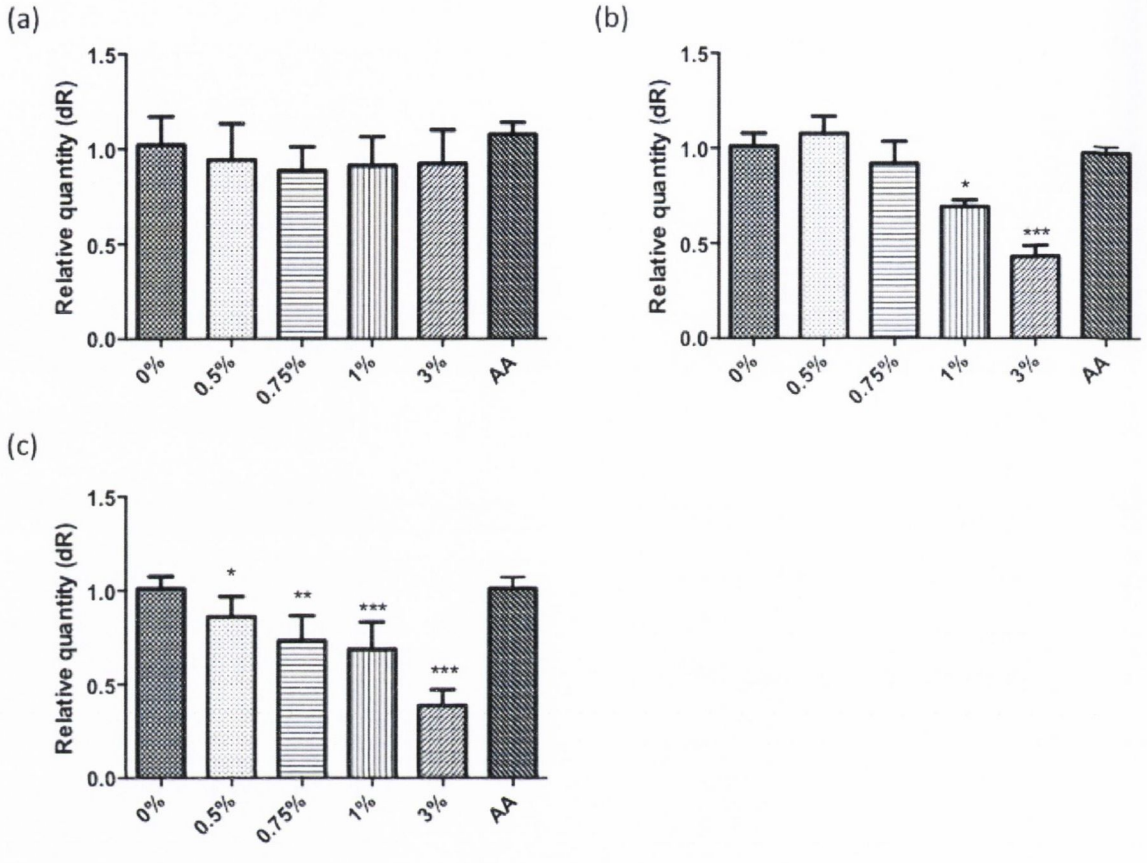


Figure 3-17 Analysis of HO-1 mRNA expression in TR146 cells.

TR146 cells were seeded at a density of 3 X 10^5 in a T25 flask, left to adhere overnight and treated with varying concentrations of EtOH for 6h (a), 24h (b) and 48h (c). mRNA was harvested and target genes were amplified up using a Sybr green One-Step qRT-PCR with specific primers for HO-1 using β-actin as a normaliser. Relative quantification of gene expression profile was calculated using a DDCt method (RQ manager, Applied Biosystems). Any effect attributed to the metabolic breakdown products of EtOH was controlled for using 1nM acetaldehyde (AA). Experiments were completed in triplicate on three individual preparations (n=9) and statistical analysis was carried out using a one-way ANOVA with post-hoc Bonferroni analysis using GraphPad prism 6.0. Samples significantly different to the control are annotated *$p<0.05$, ** $p<0.01$, ***$p<0.001$.

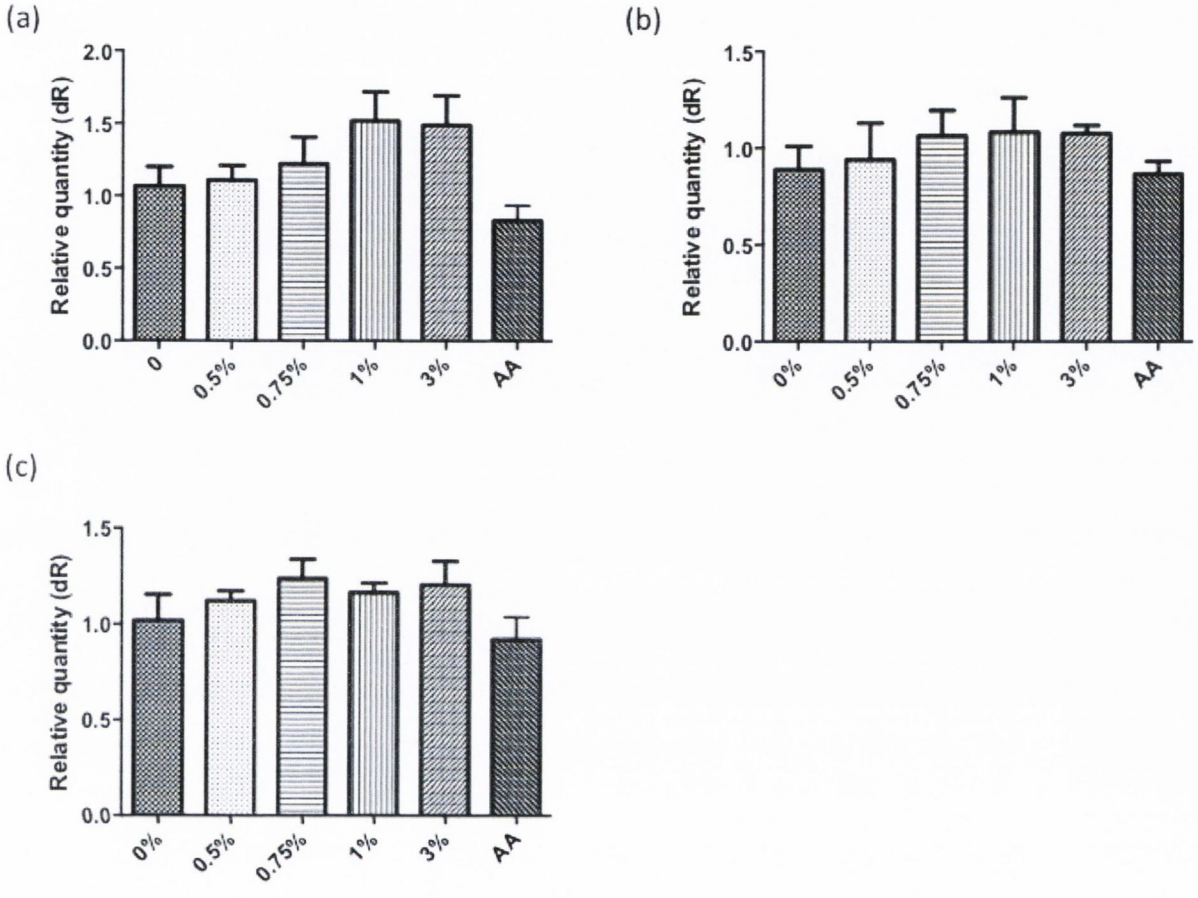


Figure 3-18 Analysis of HO-1 mRNA expression in Ca9.22 cells.

Ca9.22 cells were seeded at a density of 3 X 10^5 in a T25 flask, left to adhere overnight and treated with varying concentrations of EtOH for 6h (a), 24h (b) and 48h (c). mRNA was harvested and target genes were amplified up using a Sybr green One-Step qRT-PCR with specific primers for HO-1 using β-actin as a normaliser. Relative quantification of gene expression profile was calculated using a DDCt method (RQ manager, Applied Biosystems). Any effect attributed to the metabolic breakdown products of EtOH was controlled for using 1nM acetaldehyde (AA). Experiments were completed in triplicate on three individual preparations (n=9) and statistical analysis was carried out using a one-way ANOVA with post-hoc Bonferroni analysis using GraphPad prism 6.0. There is no significant difference between samples.

3.3.6 The influence of EtOH on the cell cycle in OSCC cell lines

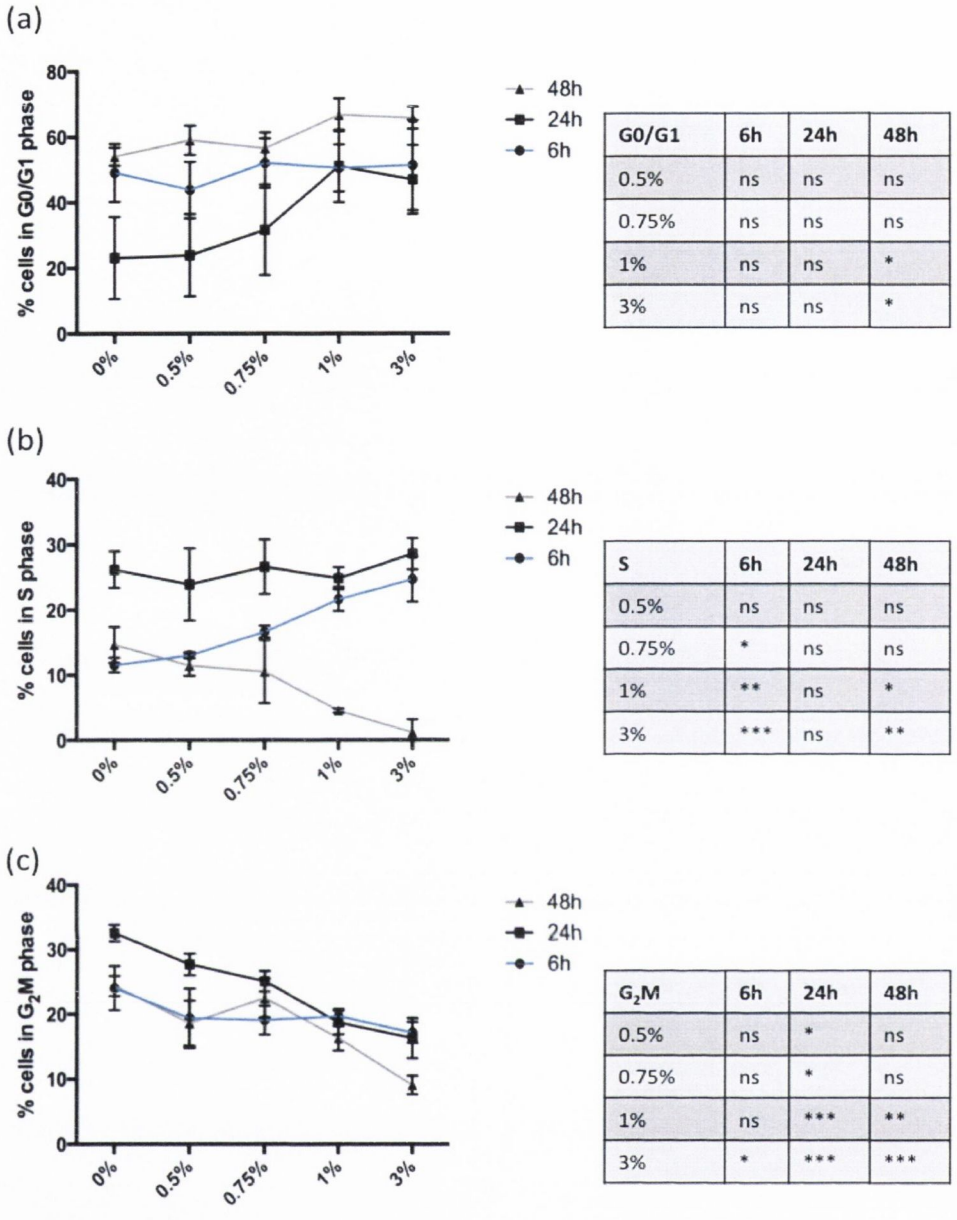
It is well known that H_2O_2 at high levels can cause extensive damage to cell structures. More recently it has become known that H_2O_2 also functions as a signalling agent and it is involved in many different aspects of cellular functions including control of the cell cycle, which can become disrupted in cancer. Previous results show lower levels of H_2O_2 in the presence of EtOH therefore experiments were undertaken to analyse the effect of EtOH on cell cycle distribution and proteins that control the cell cycle.

3.3.6.1 Cell cycle distribution in OSCC cell lines in the presence of EtOH

Flow cytometry and propidium iodide analysis of the cell cycle was used to identify changes resulting from EtOH exposure over a 48h period. In the TR146 cell line (Figure 3-19) during the G0/G1 (a) phase of the cell cycle there was no effect on cell cycle distribution within the 6h and 48h time point. After 48h treatment there was a significant increase after 1% and 3% in comparison to the untreated control. During the S phase in this cell line (b) there is a significant increase in cells during the 6h treatment with increasing concentrations of EtOH. After 24h there is an overall increase in the amount of cells in this phase however there is no significant difference between the treatments. At the later time point, 48h, there is an overall decrease in the amount of cells in the S phase and with a significant dose dependent decrease at 1%. In the G_2M phase (c), the TR146 cell line shows a significant decrease after 6h in the presence of 3% EtOH. After 24h treatment, the number of cells in the G_2M phase significantly decreases with increasing concentration of EtOH. This decrease is still observed after 48h however there is a recovery at 0.5% and 0.75% treatment with significance only been seen after 1% at this time point.

In the Ca9.22 cell line (Figure 3-20), during the G0/G1 (a) phase of the cell cycle there is no change in the percentage of cells at different concentrations of EtOH after 6h treatment. In contrast to the TR146 cell line, after 24h treatment there is a significant increase in cells during the G0/G1 phase after 1% and 3% treatment. After 48h treatment there is an increase after 1% treatment but a slight recovery in comparison to the 24h time point. During the S phase (b) in this cell line there is a significant increase in cells with increasing concentrations of EtOH after 6h treatment however no

significant changes after 24h and 48h treatment. At 48h there is a decreasing trend in the percentage of cells in the S phase without any significance observed. In the Ca9.22 cell line during the G_2M stage (c) there is a decrease in the number of cells after 3% EtOH treatment for 6h. Post 24h treatment there is a more pronounced decrease than after 6h with significance at 1% and 3% treatment. This decrease continues until 48h with significance also been noted at 1% and 3%.



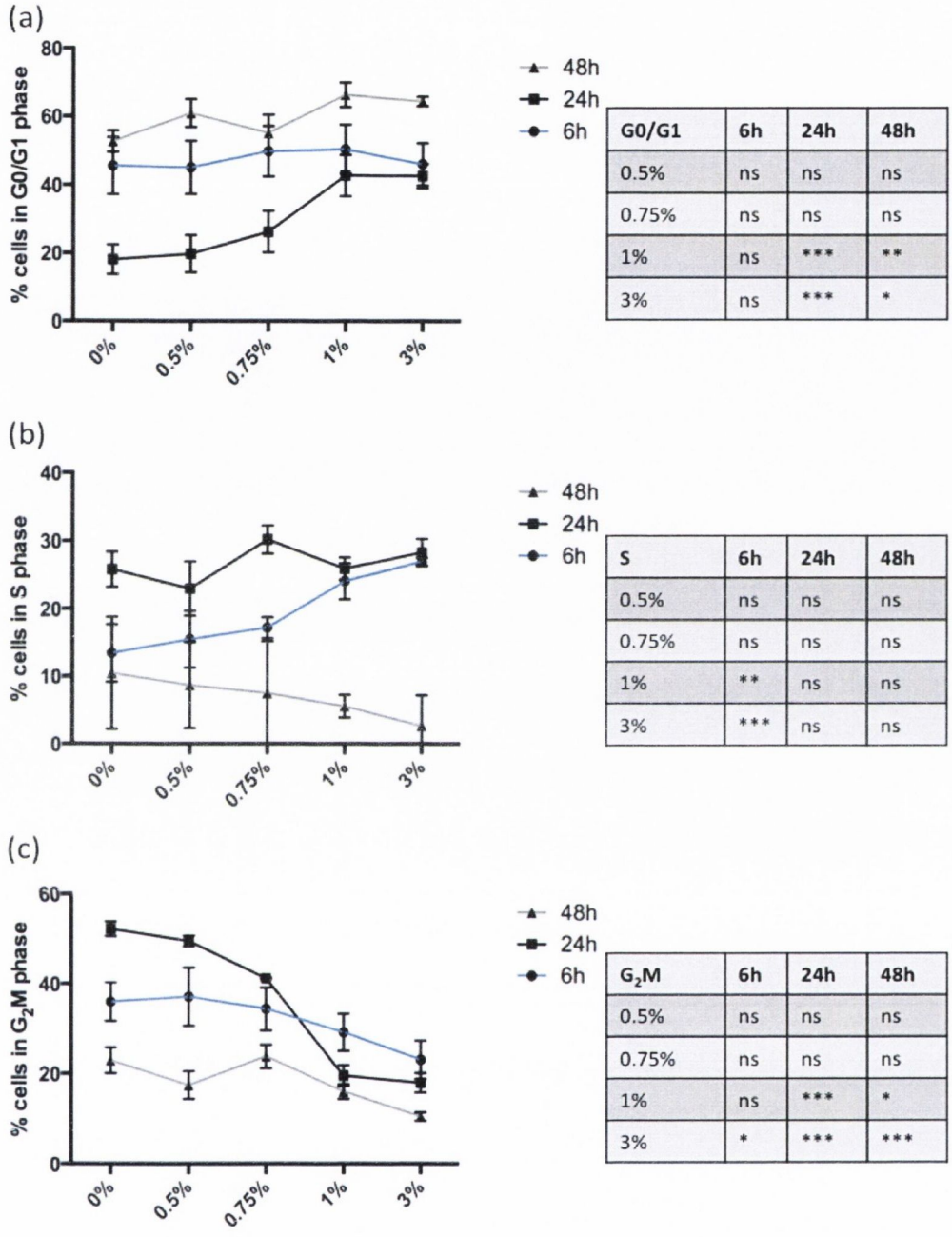
G0/G1	6h	24h	48h
0.5%	ns	ns	ns
0.75%	ns	ns	ns
1%	ns	ns	*
3%	ns	ns	*

S	6h	24h	48h
0.5%	ns	ns	ns
0.75%	*	ns	ns
1%	**	ns	*
3%	***	ns	**

G_2M	6h	24h	48h
0.5%	ns	*	ns
0.75%	ns	*	ns
1%	ns	***	**
3%	*	***	***

Figure 3-19 Analysis of cell cycle distribution in the TR146 cell line after treatment with varying concentrations of EtOH.

TR146 cells were seeded at a density of 3 X 10^5 in a T25 flask, left to adhere overnight and treated with varying concentrations of EtOH for 6h, 24h and 48h. After the required incubation time, cells were harvested, fixed in EtOH and stained with propidium iodide. Cells were analysed by flow cytometry for the percentage of cells in each stage of the cell cycle (a) G0/G1, (b) S phase and (c) G_2M phase. Values represent the mean ± SEM of three independent experiments carried out in triplicate (n=9). Samples significantly different to the control are annotated *$p<0.05$, ** $p<0.01$, ***$p<0.001$.



G0/G1	6h	24h	48h
0.5%	ns	ns	ns
0.75%	ns	ns	ns
1%	ns	***	**
3%	ns	***	*

S	6h	24h	48h
0.5%	ns	ns	ns
0.75%	ns	ns	ns
1%	**	ns	ns
3%	***	ns	ns

G_2M	6h	24h	48h
0.5%	ns	ns	ns
0.75%	ns	ns	ns
1%	ns	***	*
3%	*	***	***

Figure 3-20 Analysis of cell cycle distribution in the Ca9.22 cell line after treatment with varying concentrations of EtOH.

Ca9.22 cells were seeded at a density of 3 X 10^5 in a T25 flask, left to adhere overnight and treated with varying concentrations of EtOH for 6h, 24h and 48h. After the required incubation time, cells were harvested, fixed in EtOH and stained with propidium iodide. Cells were analysed by flow cytometry for the percentage of cells in each stage of the cell cycle (a) G0/G1, (b) S phase and (c) G_2M phase. Values represent the mean ± SEM of three independent experiments carried out in triplicate (n=9). Samples significantly different to the control are annotated *$p<0.05$, ** $p<0.01$, ***$p<0.001$.

3.3.6.2 Changes in cyclin expression after 48h exposure to EtOH in OSCC cell lines.

Cyclin proteins are a family of proteins that control progression of cells through the cell cycle. In the presence of EtOH cell cycle transition is affected as shown in the previous experiment. Western blot analysis of cyclin proteins was carried out to see if the effect of EtOH on the cell cycle is due to alterations of cyclin proteins. Cyclin B1 and D1 have both been implicated in cancer progression (Kim and Diehl, 2009, Wang *et al.*, 1997).

In the TR146 cell line (Figure 3-21), cyclin B1 expression does not alter after 6h treatment with varying concentrations of EtOH. After 24h treatment there is a significant decrease in cyclin B1 expression from 0.75% to 3% EtOH. Cyclin B1 protein levels significantly recover after 48h treatment in the TR146 cell line. Cyclin D1 expression is not altered in the TR146 cell line.

In the Ca9.22 cell line (Figure 3-22) cyclin B1 does not significantly change until the 24h time point. Here there is a decrease after 0.75% EtOH with a notable significant decrease at 3% EtOH. Interestingly at 48h there is almost no expression of cyclin B1 in the controls and significant increase in expression at 3%. Cyclin D1 expression is reduced after 3% treatment for 6h in the Ca9.22 cell line. There is no change in cyclin D1 expression after 24h and 48h in this cell line.

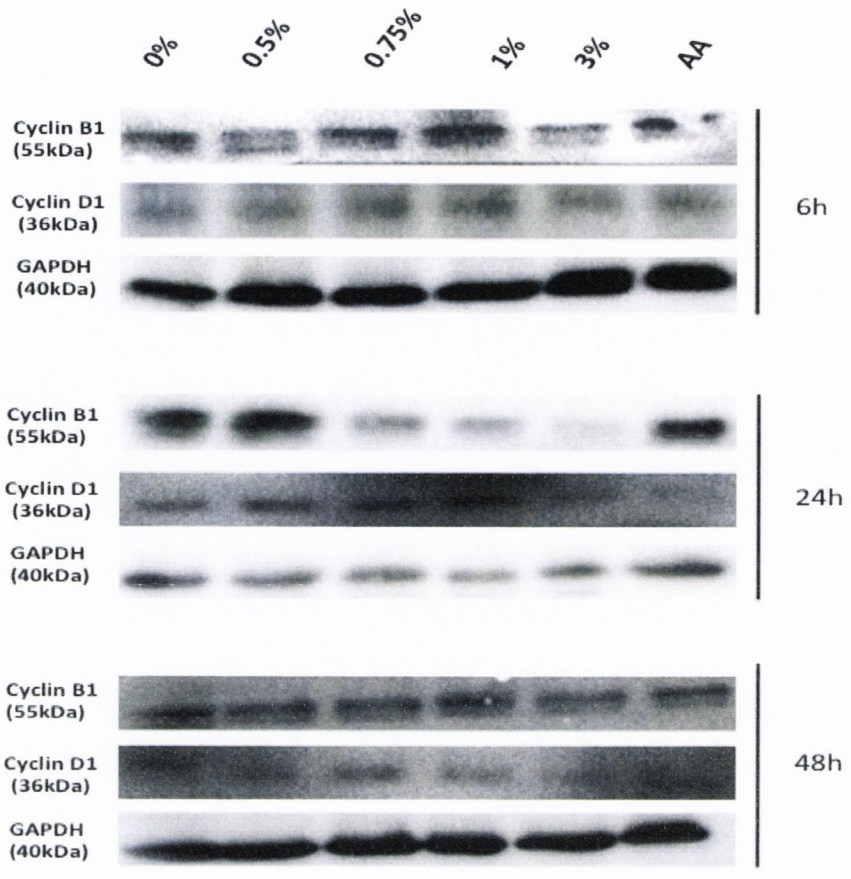


Figure 3-21 Cyclin expression in TR146 cells after 48h treatment with varying concentrations of EtOH.

TR146 cells were seeded at a density of 6 X 10^5 in a T25 flask, left to adhere overnight and treated with varying concentrations of EtOH for 6h, 24h and 48h. Post treatment, protein was harvested from treated samples and lysates were prepared for western blot analysis. 20µg of protein was separated on a 12% resolving gel with a 5% stacking gel, transferred to a PVDF membrane and probed with an anti-Cyclin B1 and anti-Cyclin D1 antibodies. Membranes were also probed for GAPDH as a loading control. Results are representative of three individuals experiments carried out in triplicate.

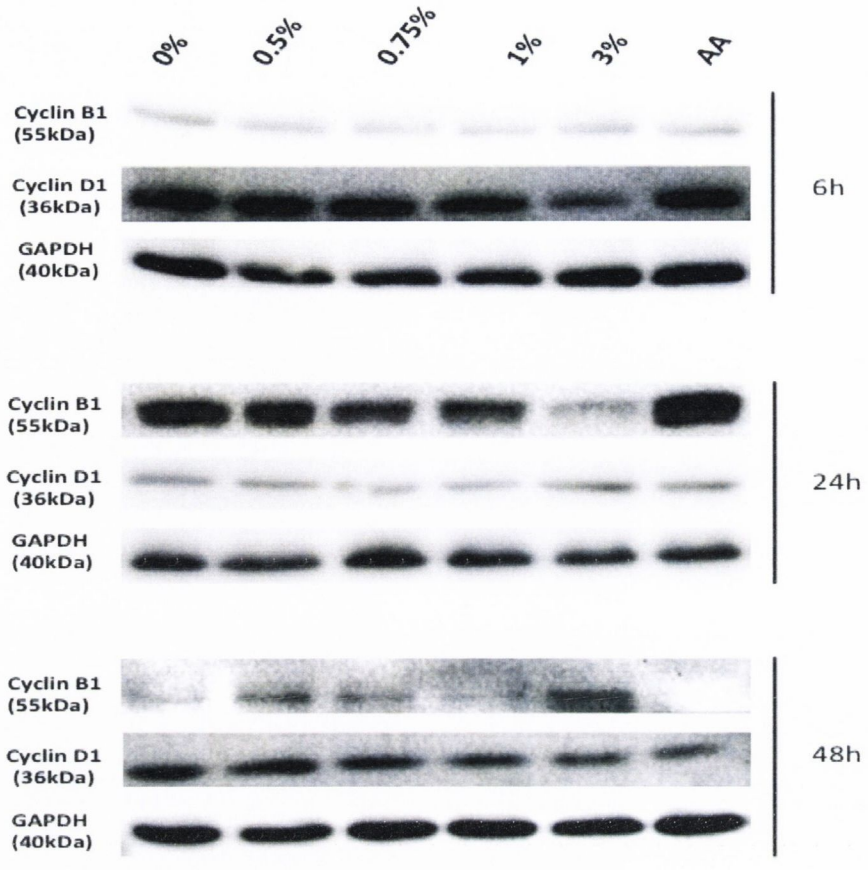


Figure 3-22 Cyclin expression in Ca9.22 cells after 48h treatment with varying concentrations of EtOH.

Ca9.22 cells were seeded at a density of 6 X 10^5 in a T25 flask, left to adhere overnight and treated with varying concentrations of EtOH for 6h, 24h and 48h. Post treatment, protein was harvested from treated samples and lysates were prepared for western blot analysis. 20μg of protein was separated on a 12% resolving gel with a 5% stacking gel, transferred to a PVDF membrane and probed with an anti-Cyclin B1 and anti-Cyclin D1 antibodies. Membranes were also probed for GAPDH as a loading control. Results are representative of three individuals experiments carried out in triplicate.

3.3.7 The effect of EtOH on dysplastic cell viability.

Previous results have shown that EtOH causes changes in the ROS production in OC cell lines. The next phase was to investigate whether EtOH causes similar changes in dysplastic cells. Using the parameters developed in the previous sections, a dysplastic cell line, DOK, was treated with several concentrations of EtOH to see whether EtOH could be aiding in transformation of these types of cells.

The AlamarBlue viability assay was used to assess the effects of EtOH concentrations on the dysplastic cell line, DOK. Cells were treated with a range of EtOH (EtOH) concentrations (0-3%) for 6h, 24h and 48h. The assay was performed on at least three occasions in triplicate. Acetlyaldehyde (1nM), a known alcohol derived carcinogen, was examined to determine if breakdown of EtOH had an effect on cell viability. As shown in Figure 3-23, increasing concentrations of EtOH did not have any effect on the viability of the cells after 6h (a), 24h (b) and 48h (c) timepoints. Acetlyaldehyde (1nM) also did not affect the viability of the cell lines.

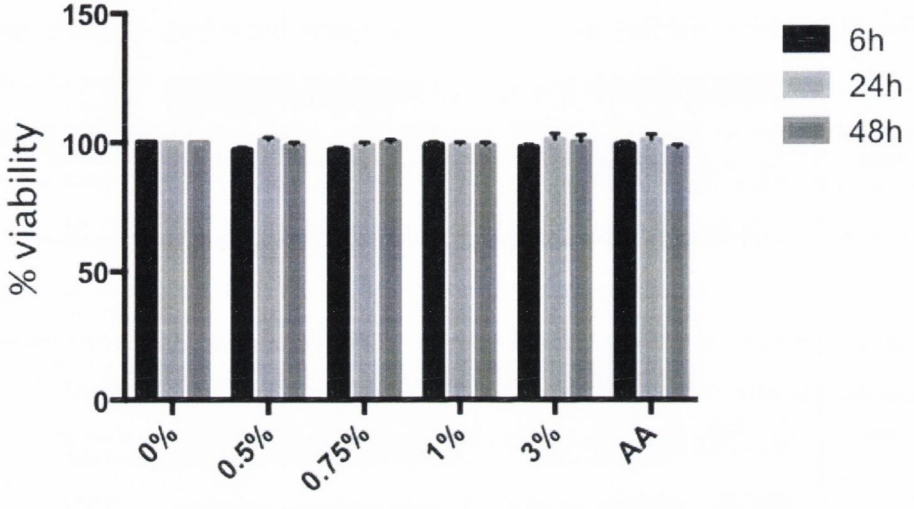


Figure 3-23 EtOH concentrations of 0-3% does not affect DOK cell viability.

DOK cells were seeded (10,000/well) in a 96 well plate treated with increasing concentrations of EtOH (0-3%) and Alamar Blue reagent (10% v/v) was added 4h before being read on a SPECTRAmax PLUS Microplate spectrophotometer. All time points, 6h, 24h and 48h showed no significant difference between treatments (in comparison to control 100%). Any effect attributed to the metabolic breakdown products of EtOH was controlled for using 1nM acetaldehyde (AA). Experiments were performed in triplicate on three separate occasions (n=9) and results are expressed as mean ± SEM (error bars). Statistical analysis was performed by one-way ANOVA with post-hoc Bonferroni analysis using GraphPad Prism 6.0.

3.3.8 ADH is absent from a dysplastic oral cell line.

ADH was shown in Section 3.3.2 to be absent in the two model OSCC cell lines. To confirm ADH is not expressed and/or upregulated to a significant level in the DOK cell line. a determination of ADH activity was performed with these cells. It is vital that no ADH is present so the effect on the cells is not due to EtOH's first metabolite.

DOK cell lines were treated with a range of EtOH concentrations (0-3%) for 24h to investigate if ADH is present and/or upregulated in the presence of EtOH. After 24h incubation there was no discernible ADH activity present in these cells. After treatment with EtOH (0.5% -3%) there is no upregulation of ADH activity after 24h. As a positive control, 0.1U of ADH was added to the cells in the presence of 1% EtOH and a significant increase in activity was observed (Figure 3-24), (*** $p<0.001$).

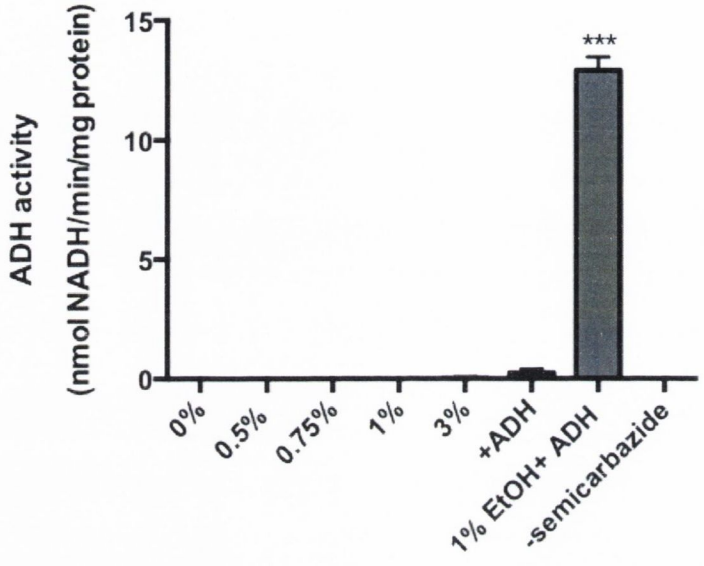


Figure 3-24 ADH is absent from DOK cells after 24h incubation with EtOH.

DOK cells were seeded (10,000/well) in a 96 well plate treated with increasing concentrations of EtOH for 24h. Cells were lysed (1% triton) and NAD (20mM), EtOH (10%), and sodium phosphate buffer (pH 7.5) were added to each well (FV 200µl). The kinetic assay was read at 340nm in a SPECTRAmax PLUS Microplate spectrophotometer for 30min. Experiments were performed in triplicate on three separate occasions and results are expressed as mean ± SEM (error bars) (n=9). Statistical analysis was performed by one-way ANOVA with post-hoc Bonferroni analysis using GraphPad Prism 6.0. Samples significantly different to the control are annotated ***$p<0.001$.

3.3.9 The effect of EtOH on H_2O_2 production in a dysplastic oral cell carcinoma cell line.

Previous results indicated a dose dependant decrease in release of H_2O_2 from OSCC cell lines. Experiments were carried out to investigate if a similar effect was present using a dysplastic cell line DOK to examine if EtOH altered H_2O_2 in a similar manner to the OSCC model.

3.3.9.1 The effect of EtOH on H_2O_2 release from dysplastic oral cell carcinoma cell line.

H_2O_2 release from DOK cells was monitored as described in Section 3.3.16.1. In the DOK cell line (Figure 3-25) there is a dose dependant decrease in the release of H_2O_2 after 6h (a) 24h (b) and 48h (c). After 6h, there is a significant decrease in H_2O_2 release at every concentration of EtOH. There is a slight recovery after 24h with there being a significant decrease only after 0.75% EtOH. Post 48h treatment with EtOH, there is a significant decrease in H_2O_2 release at 1% and 3%. The pattern of release of H_2O_2 from the cells signifies that they have the ability to recover over 48h at lower EtOH concentrations.

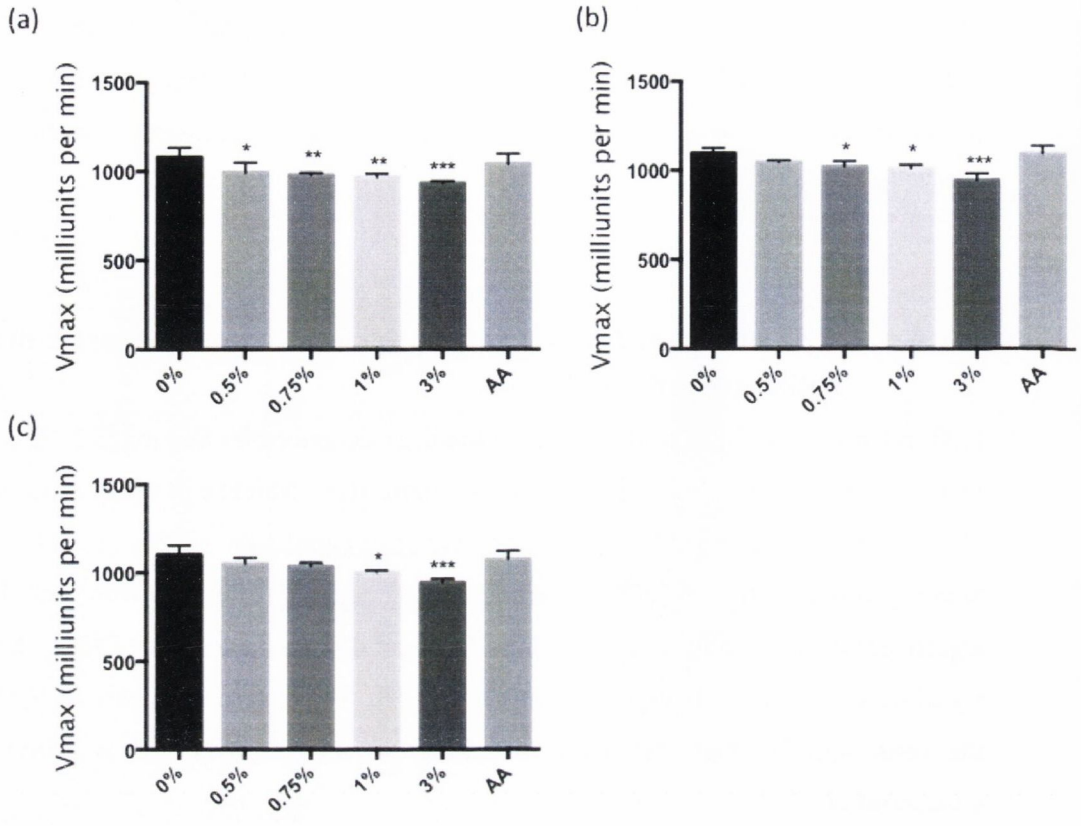


Figure 3-25 EtOH decreases the rate of H_2O_2 release after 6h, 24h, and 48h treatment in the DOK cell line.

DOK cells (10,000/well) were treated for 6h (a), 24h (b) and 48h (c) with a range of EtOH concentrations (0-3%). Post treatment, cells were assayed in Krebs buffer with Amplex red and HRP for 45 min at 37°C. H_2O_2 activity was monitored in a Spectramax Gemini XS plate reader with excitation wavelength of 550nm and emission wavelength of 580nm. Any effect attributed to the metabolic breakdown products of EtOH was controlled for using 1nM acetaldehyde (AA). Experiments were completed in triplicate on three individual preparations (n=9) and results were expressed as mean ± SEM (error bars). Statistical analysis was performed by one-way ANOVA with post-hoc Bonferroni analysis using GraphPad Prism. Samples significantly different to the control are annotated * $p<0.05$, ** $p<0.01$ and *** $p<0.001$.

3.3.10 The effect of EtOH on HIF1-α in a dysplastic oral cell line.

HIF1-α plays a central role in the hypoxic response of cells. Previous results in both OSCC cell lines and in DOK cell lines show a dose dependant decrease of H_2O_2 release in the presence of EtOH. Recovery at long time points and lower concentrations was noted. qRT-PCR analysis of HIF1-α expression was undertaken to investigate its potential role in the regulation of ROS during EtOH exposure in the DOK cells.

In the DOK cell line (Figure 3-26) there is a decreasing trend of HIF1-α expression at 24h (b) and 48h (c) but there is no significant change in HIF1-α expression over these time points.

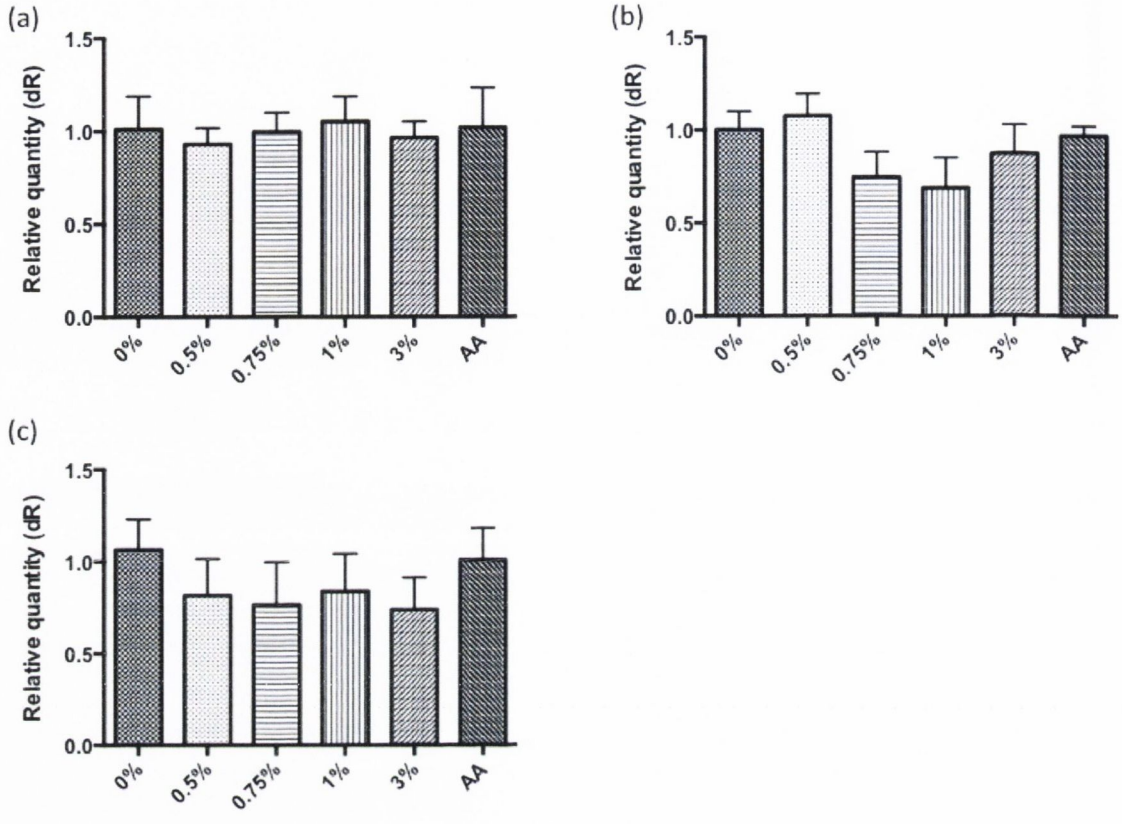


Figure 3-26 HIF1-α expression after 6h, 24h, and 48h in the presence of increasing concentrations of EtOH in DOK cells.

DOK cells were treated with varying concentrations of EtOH for 6h (a), 24h (b) and 48h (c). mRNA was harvested and targets genes were amplified up using a Sybr green One-Step qRT-PCR with specific primers for HIF1-α. Any effect attributed to the metabolic breakdown products of EtOH was controlled for using 1nM acetaldehyde (AA). Relative quantification of gene expression profile was calculated using a DDCt method (RQ manager, Applied Biosystems). Experiments were completed in triplicate using three individual preparations (n=9) and statistical analysis was carried out using a one-way ANOVA with post-hoc Bonferroni analysis using GraphPad prism 6.0. Samples significantly different to the control are annotated * $p<0.05$, ** $p<0.01$, *** $p<0.001$.

3.3.11 Modulation of antioxidant enzymes in oral dysplastic cells in response to EtOH exposure.

As shown in Section 3.3.9 ROS production is affected in DOK cells with increasing concentrations of EtOH and recovery of some levels of ROS at lower concentrations. qRT-PCR and western blot analysis of antioxidant enzymes were undertaken to determine if they have a role in controlling ROS levels in dysplastic cells.

3.3.11.1 Modulation of MnSOD expression in oral dysplastic cells in response to EtOH.

MnSOD is the primary antioxidant enzyme that protects cells from oxidative stress by catalysing dismutation of O_2^- to H_2O_2. In the DOK cell line (Figure 3-27) there is no change in MnSOD RNA expression analysed using qRT-PCR over 6h (a), 24h (b), and 48h (c). Analysis of MnSOD protein levels were performed using the western blot technique and show no change after 6h, 24h and 48h which corresponds to the RNA levels in these cells. AA also has no effect on MnSOD at either mRNA or protein level.

3.3.11.2 Modulation of CAT expression in oral dysplastic cells in response to EtOH.

CAT catalyses the decomposition of H_2O_2 to H_2O and O_2. Perturbed ROS levels in dysplastic cells could signify a change in the levels of CAT so qRT-PCR and western blot analysis was carried out to analyse any changes in the levels of this antioxidant enzyme. Results shown in Figure 3-28 indicate that there is an increasing trend in CAT expression with significance at 3% after 6h (a) treatment. After 24h (b) there is a significant increase in CAT levels at every concentration of EtOH. Recovery of enzyme expression levels is seen after 48h (c) treatment with no significant change in expression. From analysis of the western blot (d) there is no observable change in protein expression of this enzyme over 48h treatment with EtOH. AA has no effect on CAT mRNA or protein expression.

3.3.11.3 Modulation of GPx-1 expression in oral dysplastic cells in response to EtOH.

Similar in function to CAT, the enzyme GPx-1 reduces H_2O_2 to H_2O and O_2. Using qRT-PCR analysis of GPx-1 it can be seen that after 6h (a) treatment with several increasing concentrations of EtOH there is a slight increase in GPx-1 expression with significance after 3% treatment. There is no change in mRNA expression after 24h (b) treatment. After 48h (c) there is a significant decrease in expression at 3% EtOH treatment. AA has no effect on GPx-1 expression at any time point.

3.3.11.4 Modulation of HO-1 expression in oral dysplastic cells in response to EtOH.

HO-1 catabolises free heme, which is not toxic but can produce toxic free radicals in cells. HO-1 (Figure 3-30) gene expression analysis in the DOK cell line after EtOH treatment shows an increase in HO-1 mRNA over after 6h (a) treatment. At this time point there is a significant increase in HO-1 expression after 0.75% EtOH. Contrastingly after 24h (b) treatment there is a significant decrease after 0.75% EtOH. After 48h there is a recovery of mRNA expression with no significant change in HO-1.

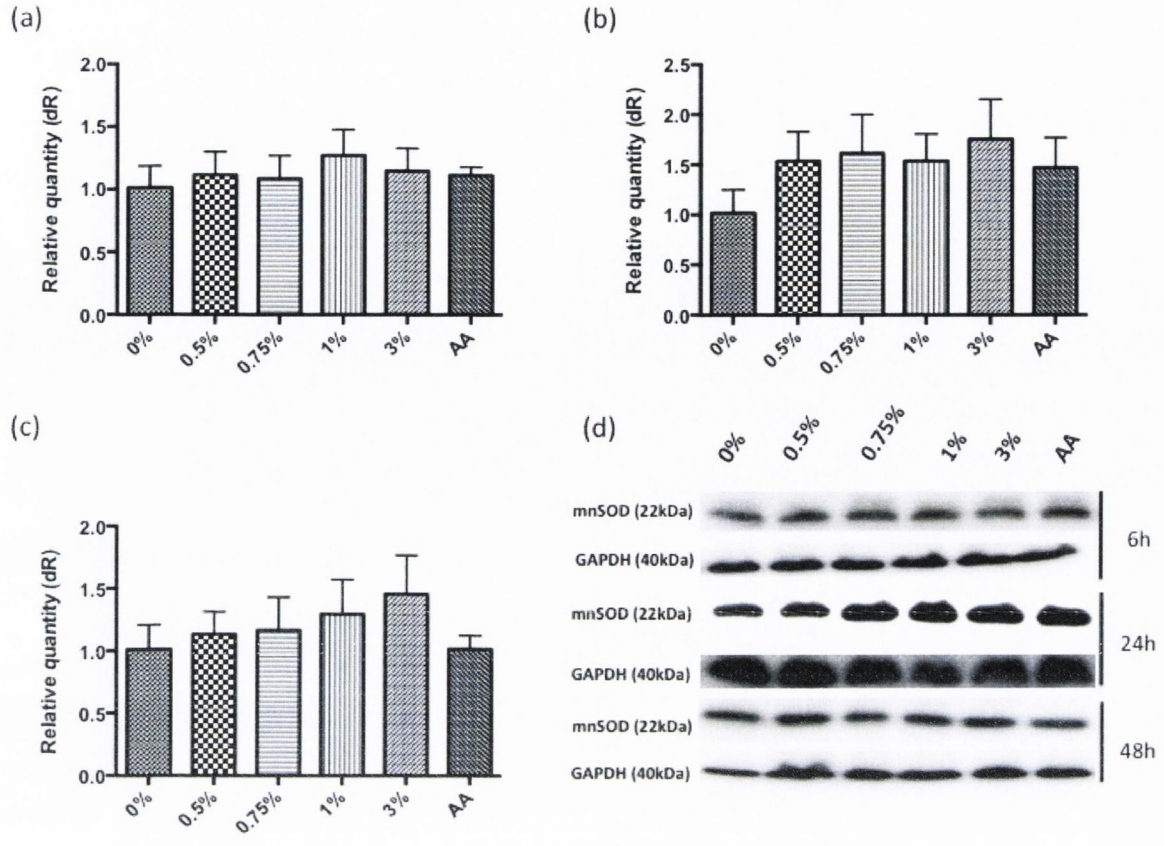


Figure 3-27 Analysis of MnSOD mRNA and protein expression in DOK cells.

DOK cells were seeded at a density of 3 X 10^5 in a T25 flask, left to adhere overnight and treated with varying concentrations of EtOH for 6h (a), 24h (b) and 48h (c). mRNA was harvested and target genes were amplified up using a Sybr green One-Step qRT-PCR with specific primers for MnSOD using β-actin as a normaliser. Relative quantification of gene expression profile was calculated using a DDCt method (RQ manager, Applied Biosystems). Any effect attributed to the metabolic breakdown products of EtOH was controlled for using 1nM acetaldehyde (AA) Experiments were completed in triplicate on three individual preparations (n=9) and statistical analysis was carried out using a one-way ANOVA with post-hoc Bonferroni analysis using GraphPad prism 6.0. (d) Cells were seeded (as in mRNA preparation), protein was harvested from treated samples and lysates were prepared for western blot analysis. 20μg of protein was separated on a 12% resolving gel with a 5% stacking gel, transferred to a PVDF membrane and probed with an anti-MnSOD antibody. Membranes were also probed for GAPDH as a loading control. Results are representative of three individuals experiments.

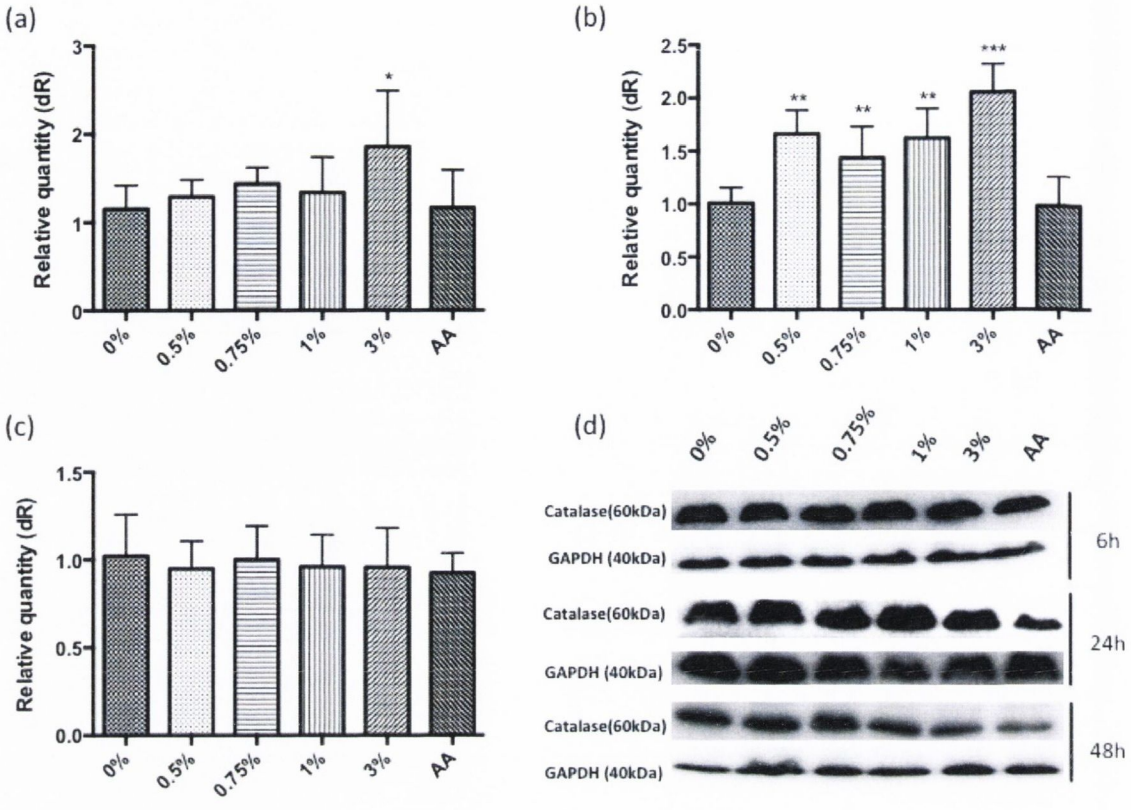


Figure 3-28 Analysis of CAT mRNA and protein expression in DOK cells.

DOK cells were seeded at a density of 3 X 10^5 in a T25 flask, left to adhere overnight and treated with varying concentrations of EtOH for 6h (a), 24h (b) and 48h (c). mRNA was harvested and target genes were amplified up using a Sybr green One-Step qRT-PCR with specific primers for CAT using β-actin as a normaliser. Relative quantification of gene expression profile was calculated using a DDCt method (RQ manager, Applied Biosystems). Any effect attributed to the metabolic breakdown products of EtOH was controlled for using 1nM acetaldehyde (AA) Experiments were completed in triplicate on three individual preparations (n=9) and statistical analysis was carried out using a one-way ANOVA with post-hoc Bonferroni analysis using GraphPad prism 6.0. Samples significantly different to the control are annotated ** $p<0.01$. (d) Cells were seeded (as in mRNA preparation), protein was harvested from treated samples and lysates were prepared for western blot analysis. 20μg of protein was separated on a 12% resolving gel with a 5% stacking gel, transferred to a PVDF membrane and probed with an anti-CAT antibody. Membranes were also probed for GAPDH as a loading control. Results are representative of three individuals experiments.

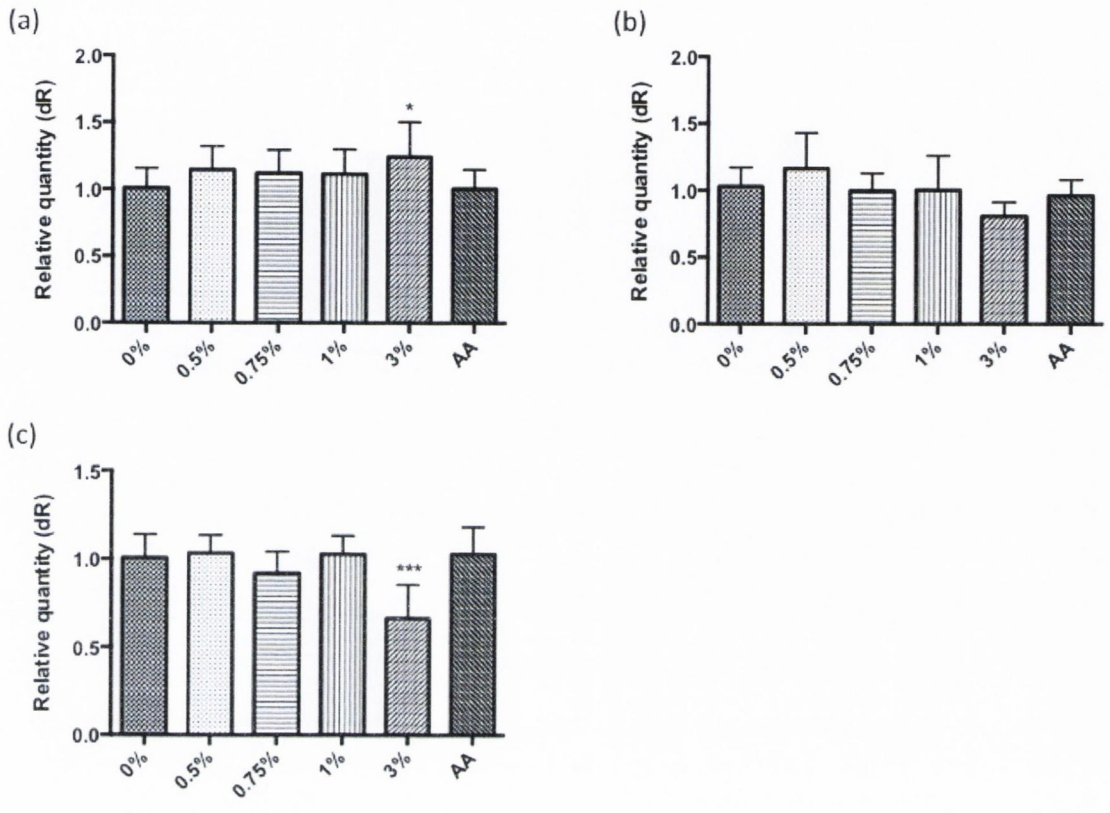


Figure 3-29 GPx-1 expression after 6h, 24h, and 48h in the presence of increasing concentrations of EtOH in DOK cells.

DOK cells were treated with varying concentrations of EtOH for 6h (a), 24h (b) and 48h (c). mRNA was harvested and target genes were amplified up using a Sybr green One-Step qRT-PCR with specific primers for GPx-1. Any effect attributed to the metabolic breakdown products of EtOH was controlled for using 1nM acetaldehyde (AA). Relative quantification of gene expression profile was calculated using a DDCt method (RQ manager, Applied Biosystems). Experiments were completed in triplicate using three individual preparations (n=9) and statistical analysis was carried out using a one-way ANOVA with post-hoc Bonferroni analysis using GraphPad prism 6.0. Samples significantly different to the control are annotated *$p<0.05$, *** $p<0.001$.

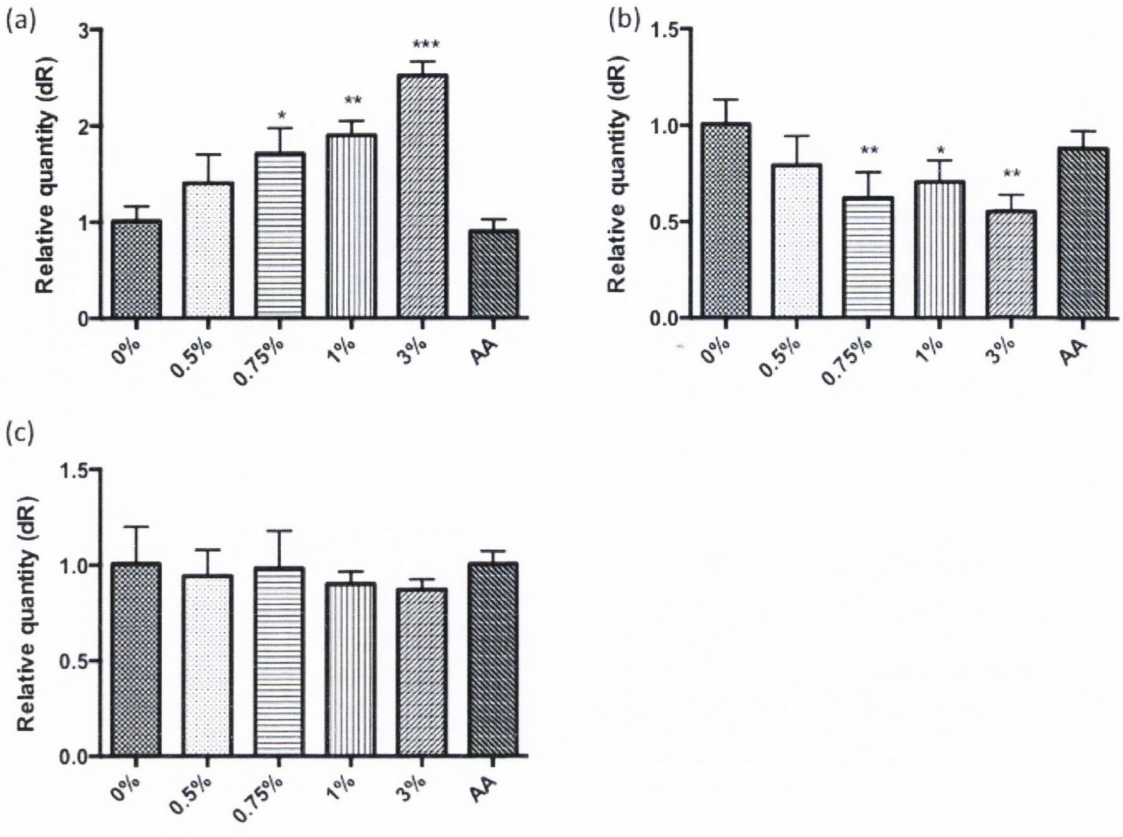


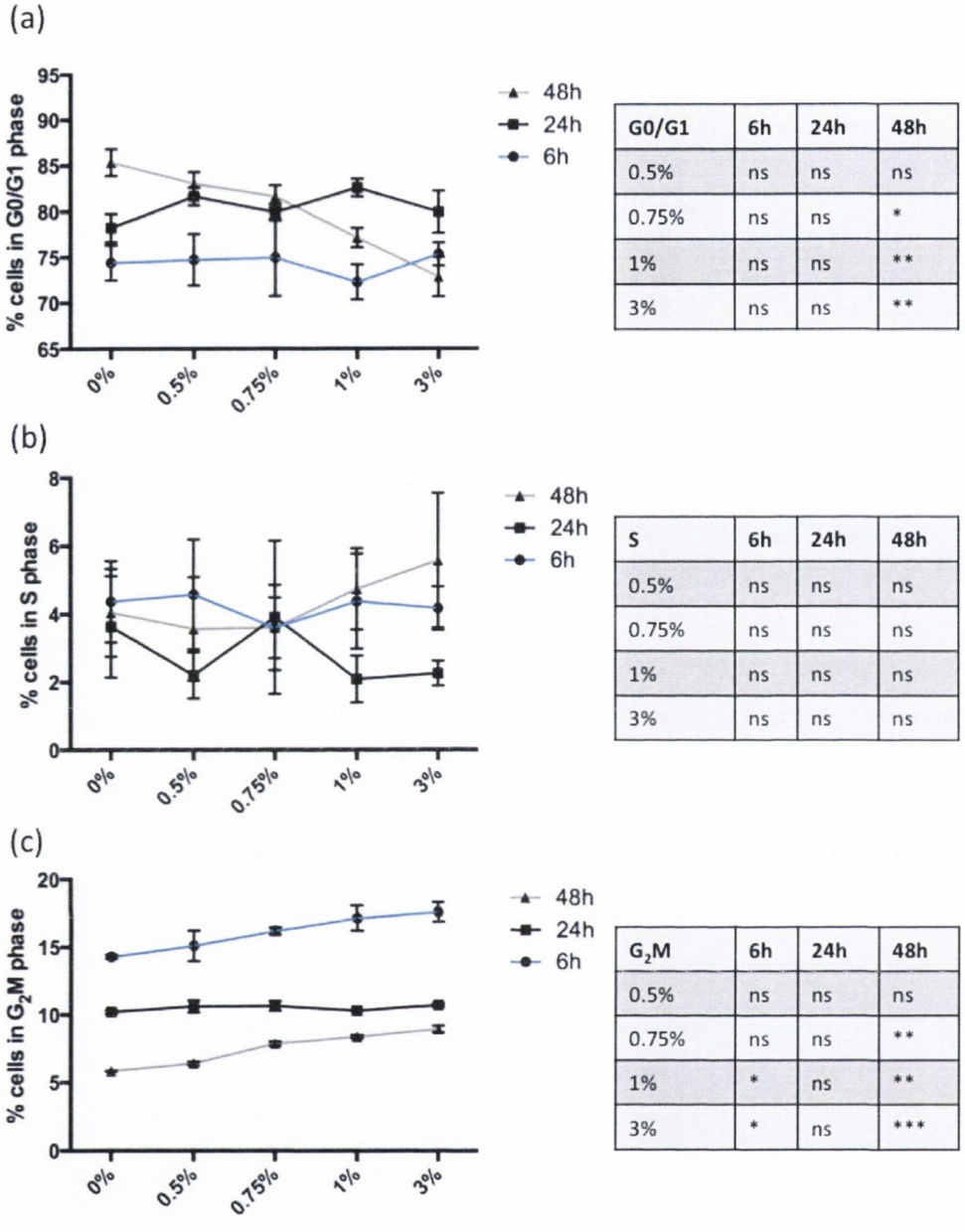
Figure 3-30 HO-1 expression after 6h, 24h, and 48h in the presence of increasing concentrations of EtOH in DOK cells.

DOK cells were treated with varying concentrations of EtOH for 6h (a), 24h (b) and 48h (c). mRNA was harvested and target genes were amplified up using a Sybr green One-Step qRT-PCR with specific primers for HO-1. Any effect attributed to the metabolic breakdown products of EtOH was controlled for using 1nM acetaldehyde (AA). Relative quantification of gene expression profile was calculated using a DDCt method (RQ manager, Applied Biosystems). Experiments were completed in triplicate using three individual preparations (n=9) and statistical analysis was carried out using a one-way ANOVA with post-hoc Bonferroni analysis using GraphPad prism 6.0. Samples significantly different to the control are annotated *$p<0.05$, ** $p<0.01$, *** $p<0.001$.

3.3.12 The influence of EtOH on the cell cycle in a dysplastic oral cell line.

Earlier experiments have shown that EtOH affects cell cycle distribution in OSCC cell lines, see Section 3.3.6. This experiment was undertaken to analyse the effects of EtOH on dysplastic cells using previously described method (Section 3.3.6.1).

Flow cytometry and propidium iodide analysis of the cell cycle was used to identify changes resulting from EtOH exposure over a 48h period. In the DOK cell line (Figure 3-31) during the G0/G1 (a) phase of the cell cycle there was no effect on cell cycle distribution over 6h, 24h and 48h. There is a decreasing trend after 6h treatment but with no significance found. There was also no change in the distribution of the cell cycle in the S phase (b) with increasing concentrations of EtOH. In the G_2M phase (c), the DOK cell line shows a significant increase after 6h in the presence of 1% and 3% EtOH. After 24h treatment, there is no significant change in the quantity of cells in the G_2M phase. After 48h in the G_2M phase there is a significant increase in the amount of cells after 0.75% EtOH -3% EtOH.



G0/G1	6h	24h	48h
0.5%	ns	ns	ns
0.75%	ns	ns	*
1%	ns	ns	**
3%	ns	ns	**

S	6h	24h	48h
0.5%	ns	ns	ns
0.75%	ns	ns	ns
1%	ns	ns	ns
3%	ns	ns	ns

G_2M	6h	24h	48h
0.5%	ns	ns	ns
0.75%	ns	ns	**
1%	*	ns	**
3%	*	ns	***

Figure 3-31 Analysis of cell cycle distribution in the DOK cell line after treatment with varying concentrations of EtOH.

DOK cells were seeded at a density of 3 X 10^5 in a T25 flask, left to adhere overnight and treated with varying concentrations of EtOH for 6h, 24h and 48h. After the required incubation time, cells were harvested, fixed in EtOH and stained with propidium iodide. Cells were analysed by flow cytometry for the percentage of cells in each stage of the cell cycle (a) G0/G1, (b) S phase and (c) G_2M phase. Values represent the mean ± SEM of three independent experiments carried out in triplicate (n=9). Samples significantly different to the control are annotated *$p<0.05$, ** $p<0.01$, ***$p<0.001$.

3.3.13 The effect of p53 on antioxidant response in the TR146 cell line.

Tumour suppressor protein p53 is a crucial multifunctional protein that controls the cell cycle and has been shown to have antioxidant capabilities. It is a protein that is mutated in a large number of cancers including approximately 50% of all OSCC. Previous results obtained show a large variability in response to EtOH effects on the cell in the two OSCC cell types used. TR146 is a buccal mucosal cell line that has a fully functional p53 whereas Ca9.22 has a p53 point mutation at codon 248. Differences between cell lines could be as a result of their p53 protein activity. Experiments were undertaken to analyse the effect of p53 on antioxidant function in the presence of EtOH.

3.3.13.1 Confirmation of p53 (transient) knockdown in TR146 cells.

p53 knockdown was confirmed by both qRT-PCR and western blot. In Figure 3-32 (a) knockdown of p53 was confirmed using qRT-PCR. After 24h incubation with p53 siRNA there is an 86% knockdown of the target RNA. The silencing increases to 94% after 48h incubation and to 96% after 72h incubation. Analysis of the western blot shows that there is almost complete knockdown after 24h at protein level and no upregulation after 6h treatment with 1% EtOH. After 48h and 72h incubation there is no p53 protein detectable at protein level and no upregulation of p53 after 24h and 48h treatment with EtOH.

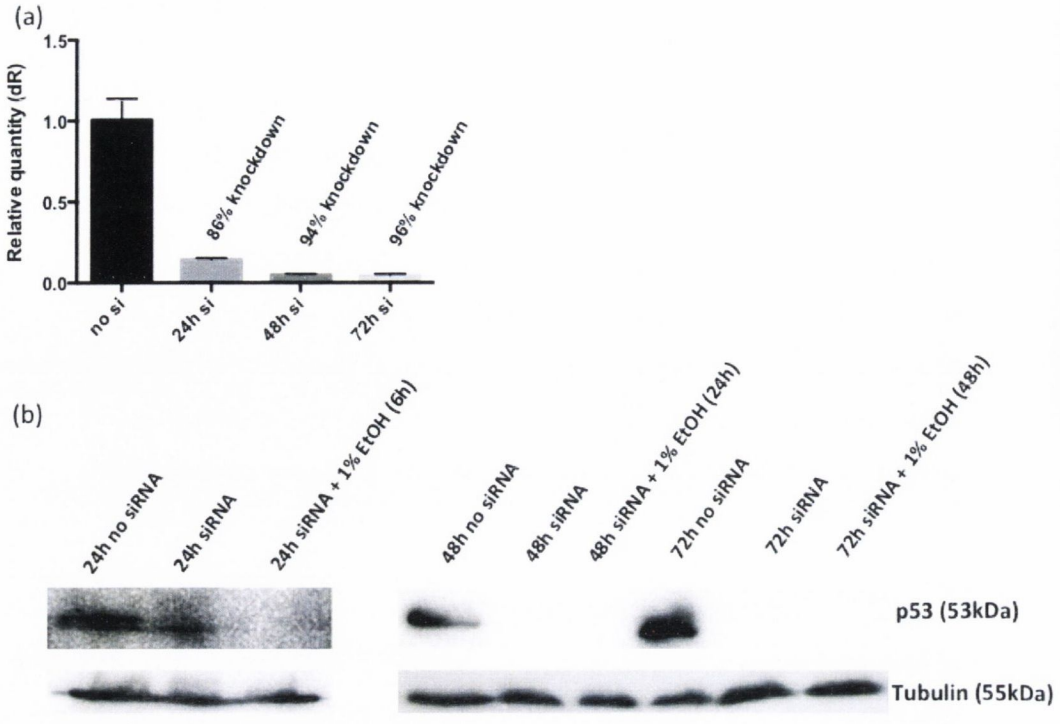


Figure 3-32 siRNA knockdown of p53 in TR146 cell line.

TR146 cells were seeded at 3 X 10^5/well in a 6 well plate, serum starved overnight and treated the following day with siRNA targeted to p53. Post knockdown (~24h) cells were treated with 1% EtOH for 6h, 24h and 48h. (a) mRNA was harvested and target genes were amplified up using a Sybr green One-Step qRT-PCR with specific primers for p53. Relative quantification of gene expression profile was calculated using a DDCt method (RQ manager, Applied Biosystems). Experiments were completed in triplicate using three individual preparations (n=9) and statistical analysis was carried out using a one-way ANOVA with post-hoc Bonferroni analysis using GraphPad prism 6.0. (b) Protein was harvested from treated samples and lysates were prepared for western blot analysis. 10μg of protein was separated on a 12% resolving gel with a 5% stacking gel, transferred to a PVDF membrane and probed with an anti-p53 antibody. Membranes were also probed for tubulin as a loading control. Results are representative of three individuals experiments carried out in triplicate.

3.3.14 The effect of p53 knockdown on HIF-1α activity in the presence and absence of EtOH in TR146 cells.

The effect of p53 on HIF-1α was monitored using qRT-PCR in the absence and presence of EtOH (1%) (Figure 3-33). Firstly HIF-1α expression was analysed after knockdown for 24h, 48h, and 72h. In comparison to the control at this time point there was a significant decrease in HIF-1α expression after 24h (a), 48h (b) and 72h (c). Next the levels of expression between the knockdowns with no treatment with EtOH were compared to knockdown with EtOH treatments for 6h (d), 24h (e) and 48h (f). After 6h, 24h and 48h EtOH treatment there was no change in expression of HIF-1α. Therefore overall there is a decrease in expression of HIF-1α with knockdown of p53 but no change in HIF-1α expression in the presence of EtOH over the series of time points.

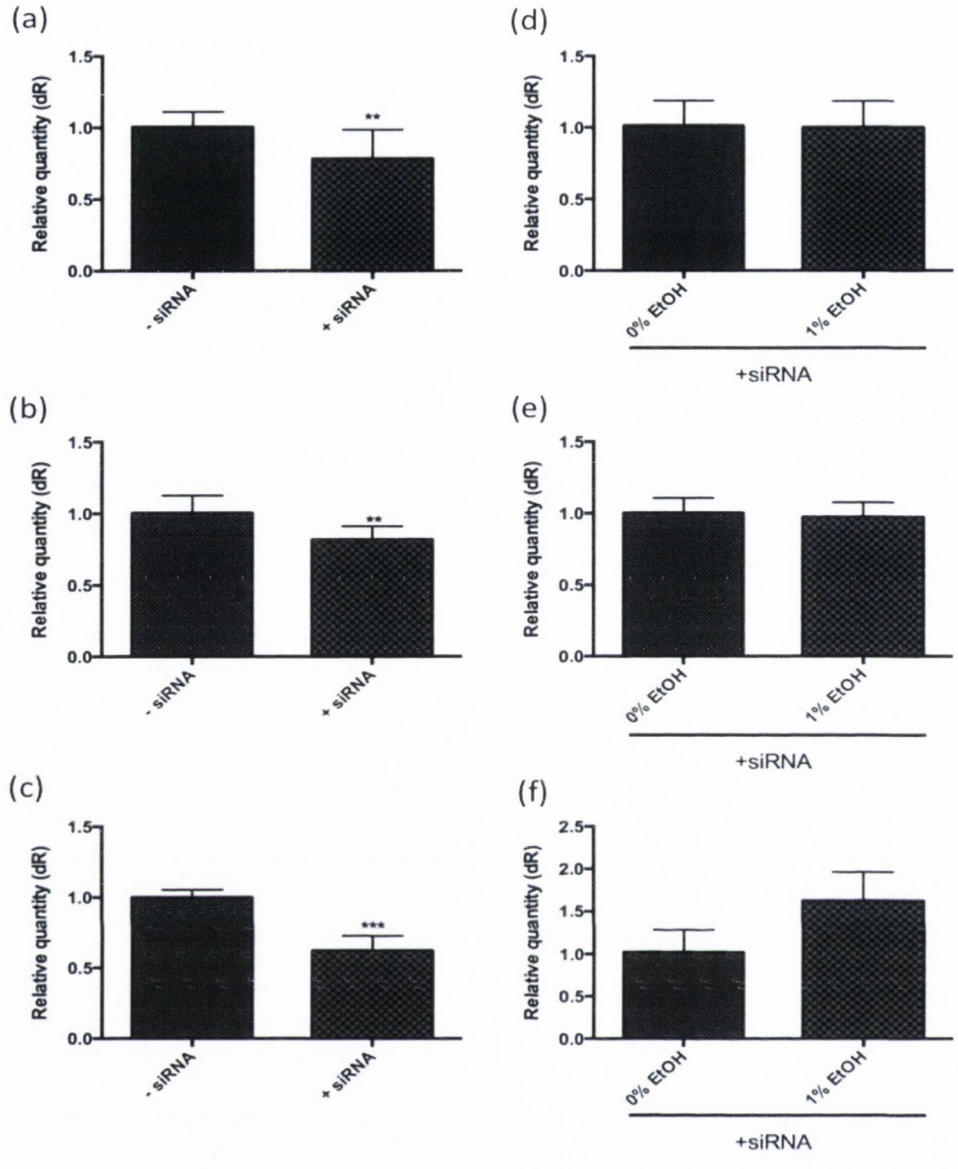


Figure 3-33 Analysis of p53 knockdown on HIF-1α expression in the presence and absence of EtOH in TR146 cells.

TR146 cells were seeded at 3 x 10^5/well in a 6 well plate, serum starved overnight and treated the following day with siRNA targeted to p53. The effect of knockdown of p53 alone on HIF1-α expression was determined after 6h (a), 24h (b) and 48h (c). The effect of EtOH and p53 knockdown on HIF1-α was determined by treating samples with 1% EtOH (~24h post knockdown) for 6h (d), 24h (e) and 48h (f). mRNA was harvested and target genes were amplified up using a Sybr green One-Step qRT-PCR with specific primers for HIF1-α. Relative quantification of gene expression profile was calculated using a DDCt method (RQ manager, Applied Biosystems). Experiments were completed in triplicate using three individual preparations (n=9) and statistical analysis was carried out using an unpaired t-test with post-hoc Bonferroni analysis using GraphPad prism 6.0. Samples significantly different to the control are annotated ** $p<0.01$, *** $p<0.001$.

3.3.15 The effect of p53 knockdown on antioxidant enzyme activity in the presence and absence of EtOH in TR146 cells

3.3.15.1 The effect of p53 knockdown on MnSOD activity in the presence and absence of EtOH in TR146 cells.

As in previous studies, the involvement of the antioxidant MnSOD was investigated in relation to EtOH effect. MnSOD mRNA expression was examined in the presence and absence of p53 siRNA using qRT-PCR (Figure 3-34). The knockdown of p53 in TR146 cells using siRNA on MnSOD had no effect on MnSOD expression levels after 24h (a), 48h (b), and 72h (c). Incubation with 1% EtOH has no effect after 6h (d) or 24h (e) but levels of MnSOD RNA were significantly decreased after 48h incubation.

3.3.15.2 The effect of p53 knockdown on CAT activity in the presence and absence of EtOH in TR146 cells.

As in section 3.3.15.1 the antioxidant CAT was analysed in the same way to MnSOD levels (Figure 3-35). The knockdown of p53 in TR146 cells shows an increase in CAT expression over 24h (a), 48h (b) and 72h (c) in comparison to the control. Incubation with EtOH (1%) shows no effect on the expression of CAT in knockdown cells after 6h incubation (d). There is a significant increase in expression after 24h (e) incubation with EtOH. After 48h (f) incubation there is no change in CAT expression.

3.3.15.3 The effect of p53 knockdown on GPx-1 activity in the presence and absence of EtOH in TR146 cells.

The effect of p53 on GPx-1 was assessed in the same manner as previous antioxidants (Figure 3-36). The expression levels of GPx-1, with an almost complete knockdown of p53, remain stable throughout a 72h period- p53 siRNA has no effect on GPx-1 levels after 24h (a), 48h (b) or 72h (c). After knockdown of p53 in the presence of EtOH shows no effect after 6h (d) and 24h (e). After 48h with 1% EtOH (f) there is a significant increase in GPx-1 expression in the TR146 cell line.

3.3.15.4 The effect of p53 knockdown on HO-1 activity in the presence and absence of EtOH in TR146 cells.

HO-1 expression was monitored as before using qRT-PCR. Cells with and without siRNA was analysed for their expression with HO-1. As shown in Figure 3-37 there is no effect of silencing of p53 on HO-1 expression after 6h and 24h. After 48h there is an increase in HO-1 expression. The effect of 1% EtOH and p53 siRNA after 6h and 24h have no effect on HO-1 expression however after 48h treatment there is a significant decrease in Ho-1 mRNA levels. Therefore, almost complete knockdown of p53 causes an upregulation of HO-1 but treatment with 1% EtOH for 48h causes a decrease in these levels.

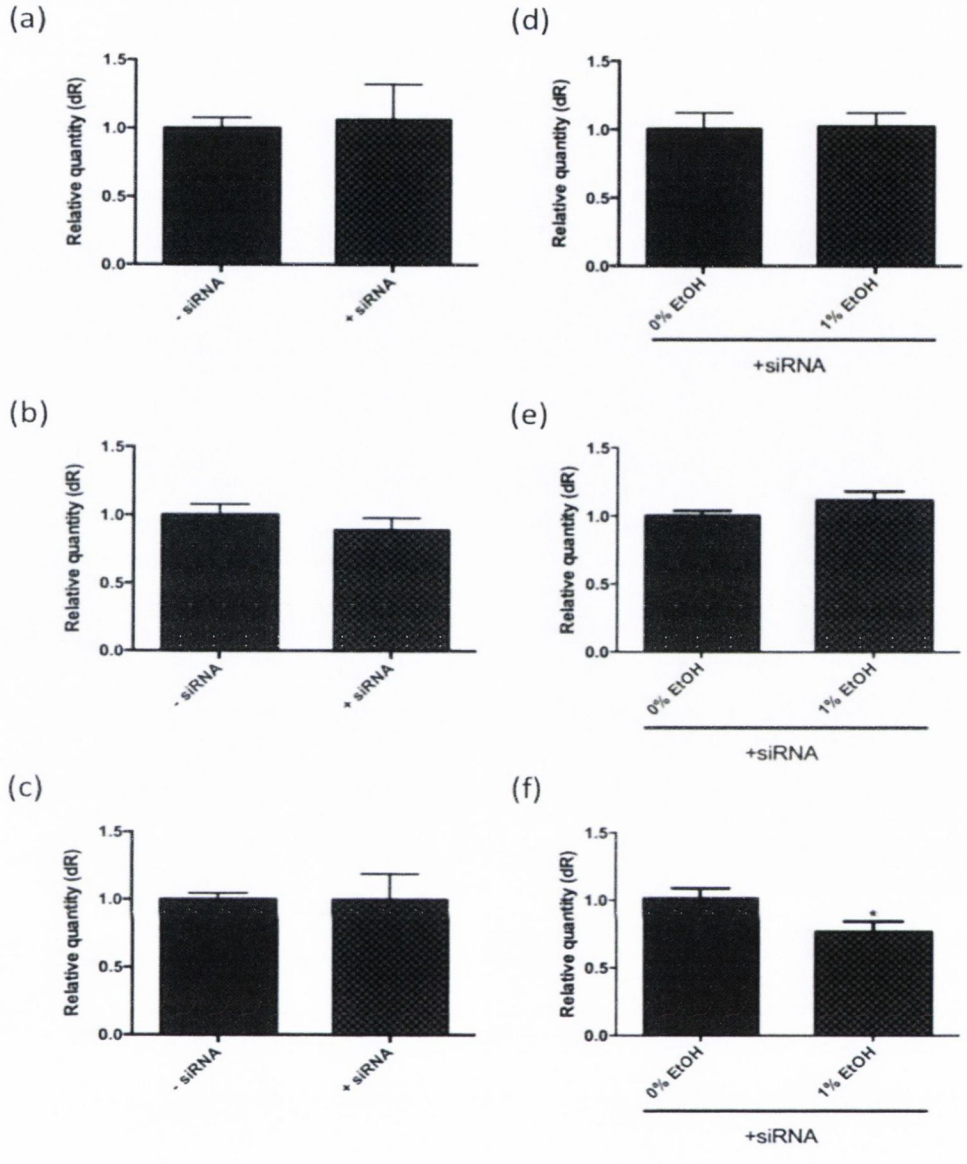


Figure 3-34 Analysis of p53 knockdown on MnSOD expression in the presence and absence of EtOH in TR146 cells.

TR146 cells were seeded at 3 x 10^5/well in a 6 well plate, serum starved overnight and treated the following day with siRNA targeted to p53. The effect of knockdown of p53 alone on MnSOD expression was determined after 6h (a), 24h (b) and 48h (c). The effect of EtOH and p53 knockdown on MnSOD was determined by treating samples with 1% EtOH (~24h post knockdown) for 6h (d), 24h (e) and 48h (f). mRNA was harvested and target genes were amplified up using a Sybr green One-Step qRT-PCR with specific primers for MnSOD. Relative quantification of gene expression profile was calculated using a DDCt method (RQ manager, Applied Biosystems). Experiments were completed in triplicate using three individual preparations (n=9) and statistical analysis was carried out using an unpaired t-test with post-hoc Bonferroni analysis using GraphPad prism 6.0. Samples significantly different to the control are annotated *$p<0.05$.

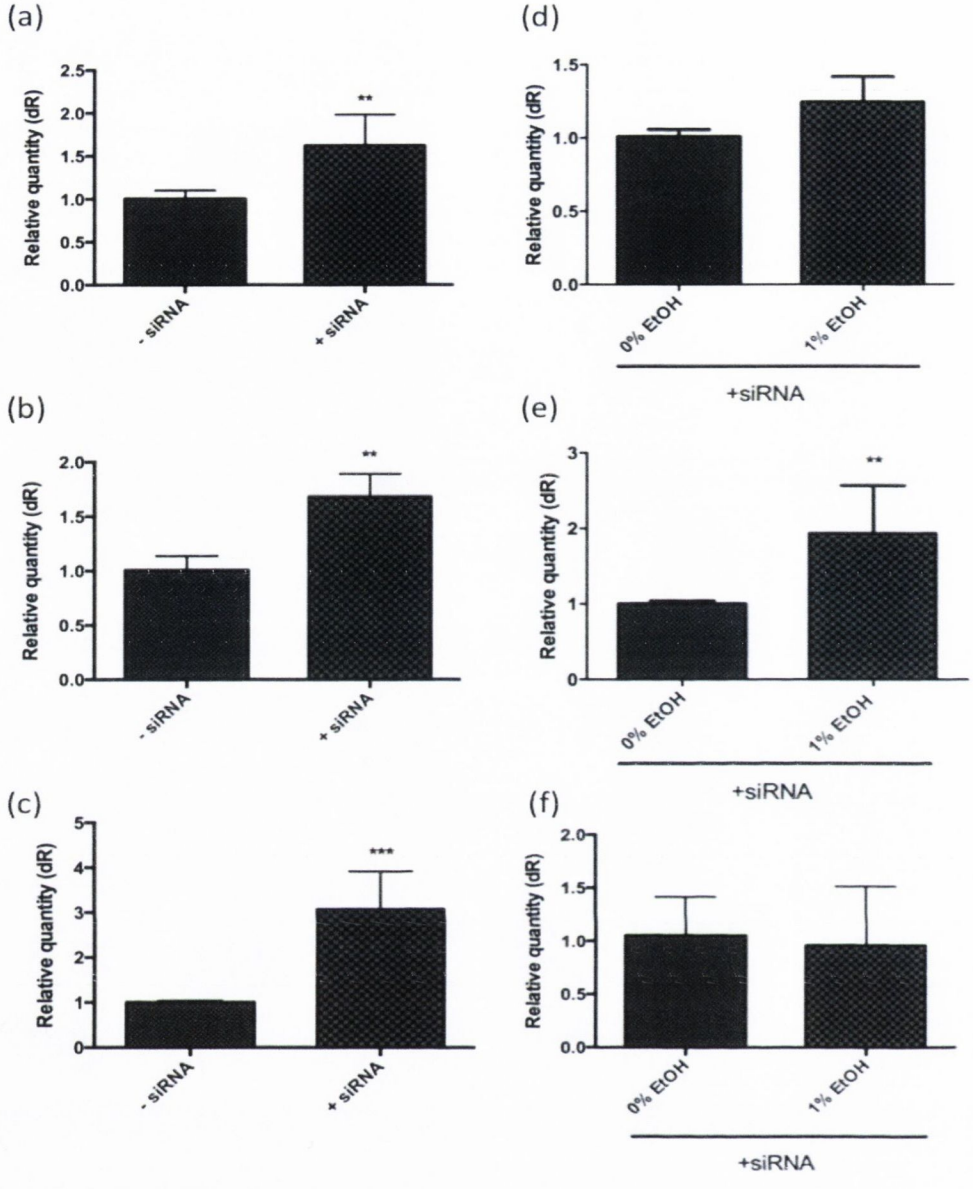


Figure 3-35 Analysis of p53 knockdown on CAT expression in the presence and absence of EtOH in TR146 cells.

TR146 cells were seeded at 3 x 10^5/well in a 6 well plate, serum starved overnight and treated the following day with siRNA targeted to p53. The effect of knockdown of p53 alone on CAT expression was determined after 6h (a), 24h (b) and 48h (c). The effect of EtOH and p53 knockdown on CAT was determined by treating samples with 1% EtOH (~24h post knockdown) for 6h (d), 24h (e) and 48h (f). mRNA was harvested and target genes were amplified up using a Sybr green One-Step qRT-PCR with specific primers for CAT. Relative quantification of gene expression profile was calculated using a DDCt method (RQ manager, Applied Biosystems). Experiments were completed in triplicate using three individual preparations (n=9) and statistical analysis was carried out using an unpaired t-test with post-hoc Bonferroni analysis using GraphPad prism 6.0. Samples significantly different to the control are annotated ** $p<0.01$, *** $p<0.001$.

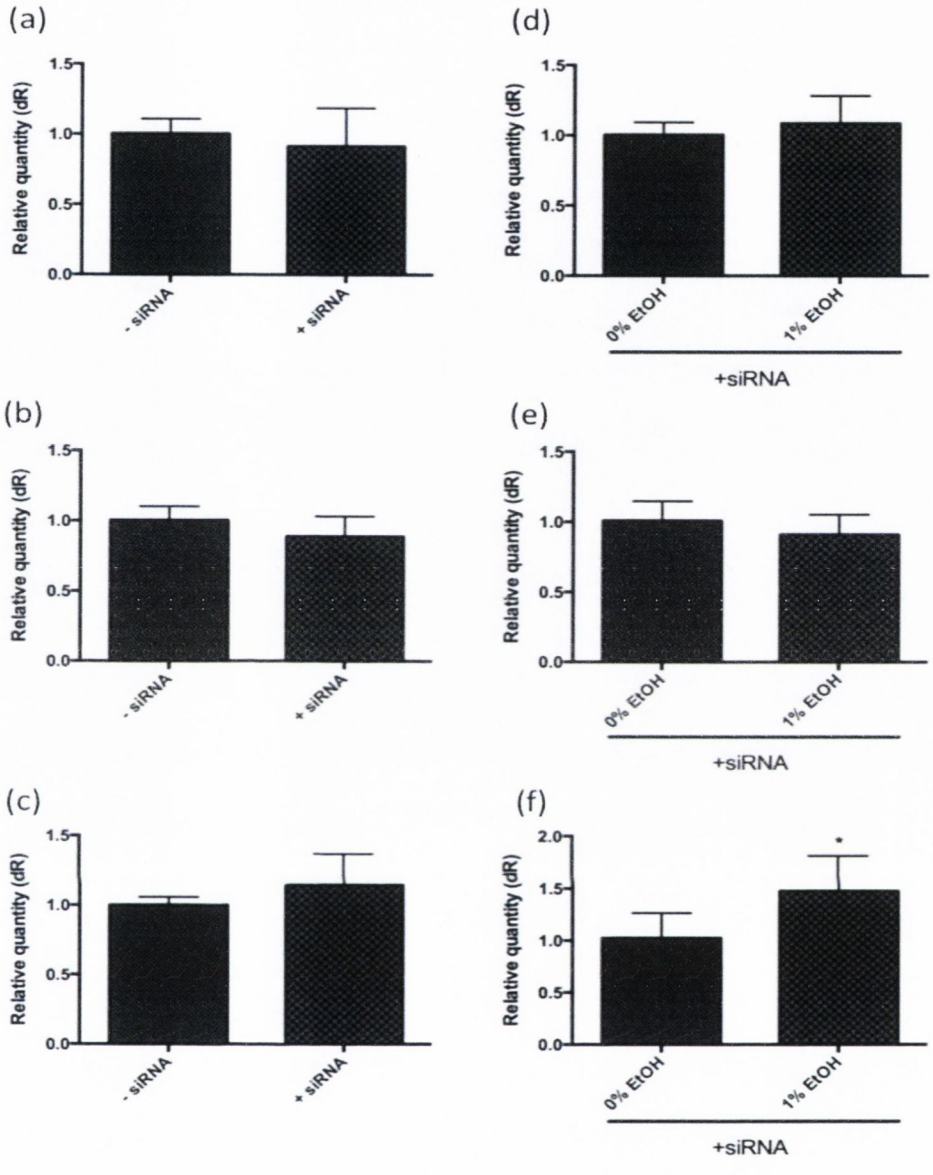


Figure 3-36 Analysis of p53 knockdown on GPx-1 expression in the presence and absence of EtOH in TR146 cells.

TR146 cells were seeded at 3 x 10^5/well in a 6 well plate, serum starved overnight and treated the following day with siRNA targeted to p53. The effect of knockdown of p53 alone on GPx-1 expression was determined after 6h (a), 24h (b) and 48h (c). The effect of EtOH and p53 knockdown on GPx-1 was determined by treating samples with 1% EtOH (~24h post knockdown) for 6h (d), 24h (e) and 48h (f). mRNA was harvested and target genes were amplified up using a Sybr green One-Step qRT-PCR with specific primers for GPx-1. Relative quantification of gene expression profile was calculated using a DDCt method (RQ manager, Applied Biosystems). Experiments were completed in triplicate using three individual preparations (n=9) and statistical analysis was carried out using an unpaired t-test with post-hoc Bonferroni analysis using GraphPad prism 6.0. Samples significantly different to the control are annotated * $p<0.05$.

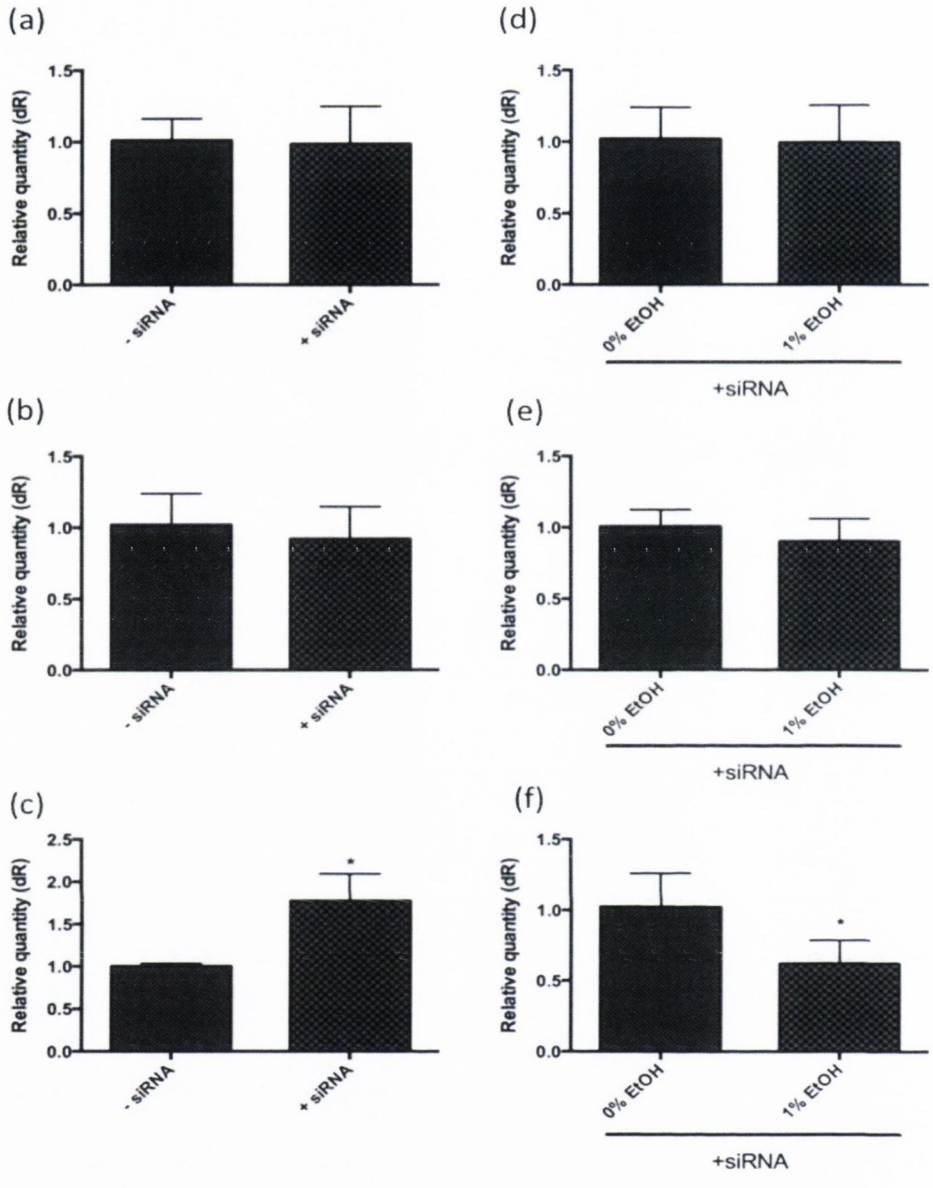


Figure 3-37 Analysis of p53 knockdown on HO-1 expression in the presence and absence of EtOH in TR146 cells.

TR146 cells were seeded at 3 x 10^5/well in a 6 well plate, serum starved overnight and treated the following day with siRNA targeted to p53. The effect of knockdown of p53 alone on HO-1 expression was determined after 6h (a), 24h (b) and 48h (c). The effect of EtOH and p53 knockdown on HO-1 was determined by treating samples with 1% EtOH (~24h post knockdown) for 6h (d), 24h (e) and 48h (f). mRNA was harvested and target genes were amplified up using a Sybr green One-Step qRT-PCR with specific primers for HO-1. Relative quantification of gene expression profile was calculated using a DDCt method (RQ manager, Applied Biosystems). Experiments were completed in triplicate using three individual preparations (n=9) and statistical analysis was carried out using an unpaired t-test with post-hoc Bonferroni analysis using GraphPad prism 6.0. Samples significantly different to the control are annotated * $p<0.05$.

3.3.16 Determining the effect of EtOH on redox status in isolated human primary oral epithelial cells

OSCC results from a change in the physiology of normal healthy epithelial cells in the oral mucosa. Previous experiments have built a model of the effect of EtOH on cells of the oral mucosa. Using this model, experiments were carried out to analyse the effects of EtOH on human primary oral cells to see if it could mediate the transformation to a potentially malignant phenotype.

3.3.16.1 The effect of EtOH on H_2O_2 release from oral cell lines

Previous results indicate that EtOH results in decreased H_2O_2 production in both an OC cell line and a dysplastic oral cell. H_2O_2 release from primary oral cells was monitored using a fluorescent reagent (Amplex red). Time dependent studies were performed in the presence of a single concentration of EtOH (1%). Cells were treated for 6h, 24h, and 48h before the assay was monitored using a Spectramax plate reader. The results (Figure 3-38) show that in the first primary cell culture (Primary 1) (a) there is a decrease of H_2O_2 release after 6h, 24h and 48h. The amount of H_2O_2 released between 6h and 24h increases however it is still significantly decreased in comparison to the control. H_2O_2 release remains stable between 24h and 48h. In the second primary cell line (Primary 2) (b) there is also a significant decrease in the release of H_2O_2 at all time points. The significance of the decrease shows a recovery between the time points. There is a significance of *** $p<0.001$ after 6h, ** $p<0.01$ after 24h and * $p<0.05$ after 48h. There is a similar trend between the two isolated cells except that Primary 2 shows a better ability to recover at a later time point.

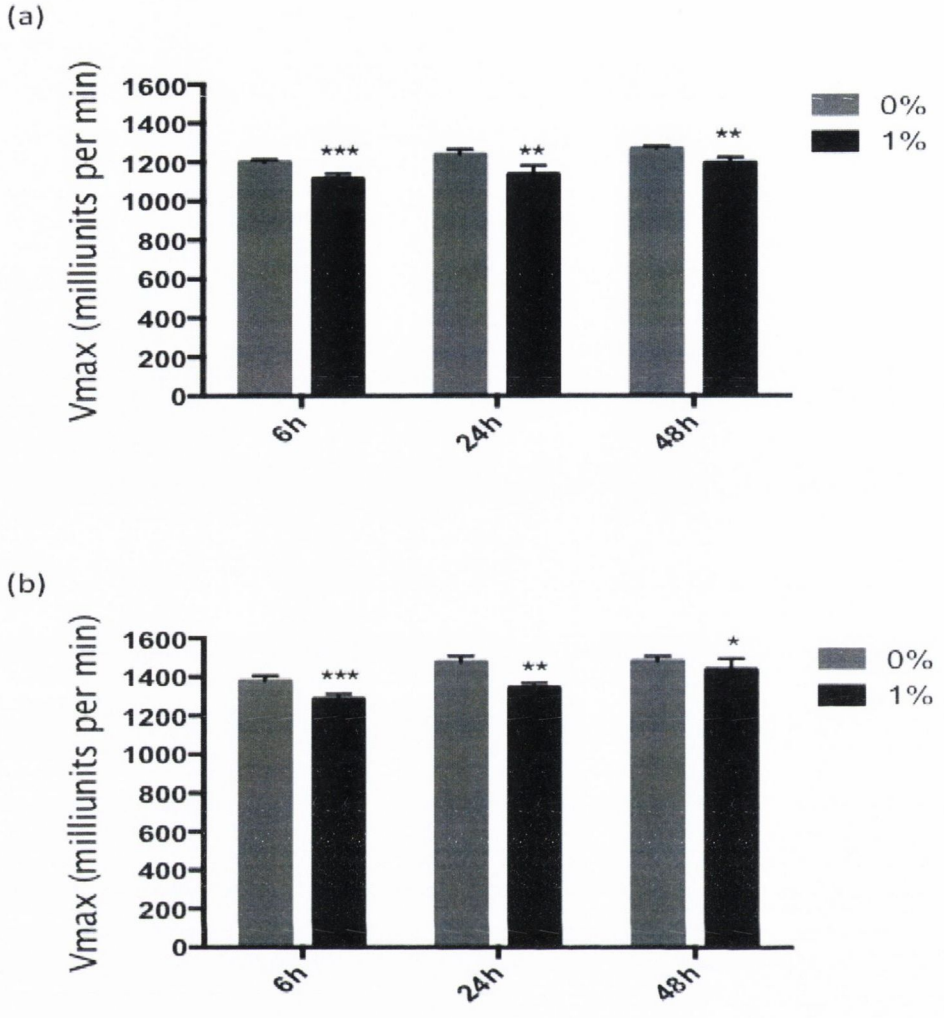


Figure 3-38 EtOH decreases the rate of H_2O_2 release after 6h, 24h, and 48h treatment in two primary oral cells.

Primary cells (10,000/well) [Primary 1 cells (a), Primary 2 cells (b)] were serum starved overnight and the following day were treated for 6h (a), 24h (b) and 48h (c) with 1% EtOH. Post treatments, cells were assayed in Krebs buffer with Amplex red and HRP for 45 min at 37°C. H_2O_2 activity was monitored in a Spectramax Gemini XS plate reader with excitation wavelength of 550nm and emission wavelength of 580nm. Experiments were completed in triplicate on three individual preparations (n=9) and results were expressed as mean ± SEM (error bars) Statistical analysis was performed using a two-tailed unpaired t-test with post-hoc Bonferroni analysis using GraphPad Prism. Samples significantly different to the control are annotated * $p<0.05$, ** $p<0.01$ and *** $p<0.001$.

3.3.17 The effect of EtOH on HIF-1α activity in isolated human primary oral epithelial cells

The effect of 1% EtOH on HIF-1α in Primary 1 and Primary 2 cells was monitored using qRT-PCR (Figure 3-39). In the Primary 1 cells there is a significant decrease in HIF-1α expression after 6h (a) but no change in expression after 24h (b) and 48h (c). There is a decreasing trend after the later time points but no significance attained. In the Primary 2 cells there is no change in HIF-1α expression after 6h (d), 24h (e) and 48h (f).

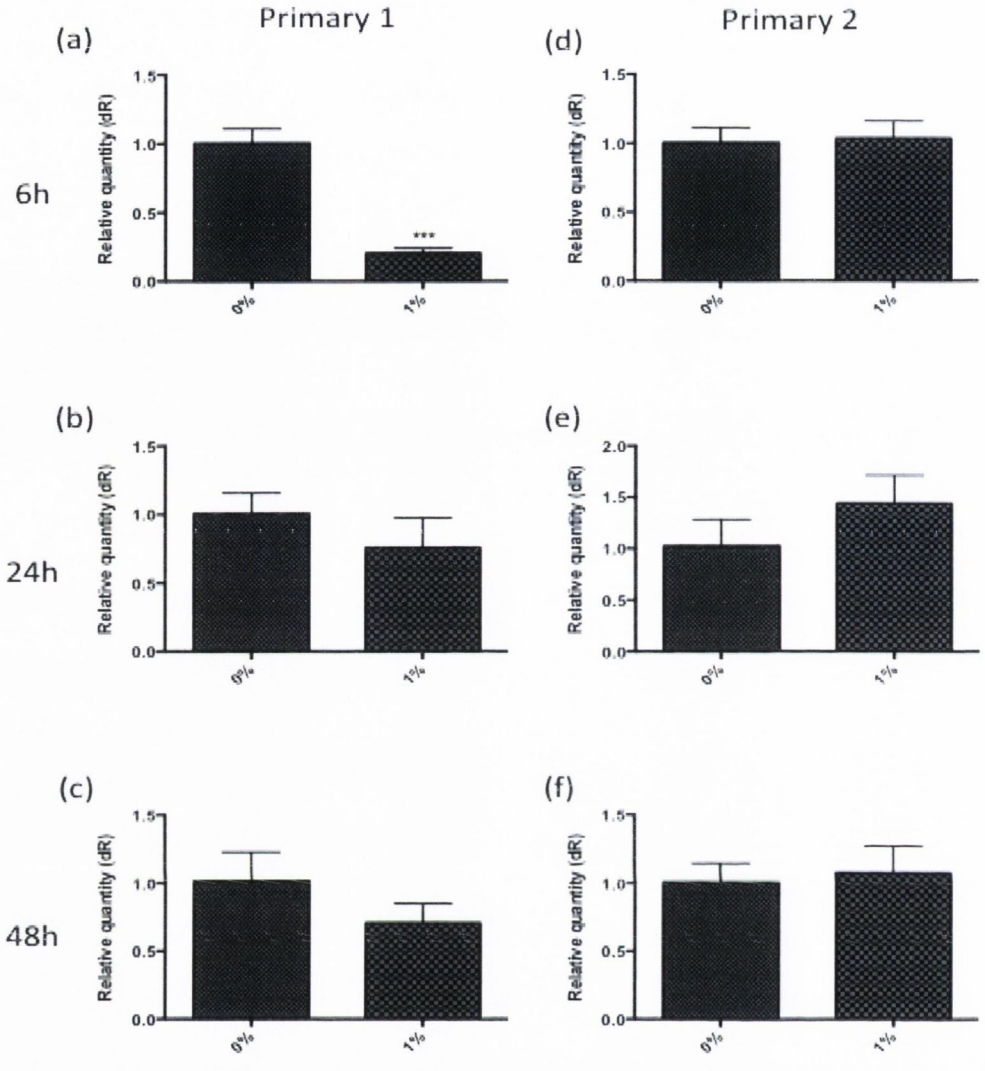


Figure 3-39 The effect of EtOH on HIF1-α expression in isolated human primary oral epithelial cells.

Primary cells (10,000/well) [Primary 1 (a) (b) (c), Primary 2 (d) (e) (f)] were serum starved overnight and the following day were treated for 6h (a) (d), 24h (b) (e) and 48h (c) (f) with 1% EtOH. mRNA was harvested and target genes were amplified up using a Sybr green One-Step qRT-PCR with specific primers for HIF1-α. Relative quantification of gene expression profile was calculated using a DDCt method (RQ manager, Applied Biosystems). Experiments were completed in triplicate using three individual preparations (n=9) and statistical analysis was carried out using an unpaired t-test with post-hoc Bonferroni analysis using GraphPad prism 6.0. Samples significantly different to the control are annotated *** $p<0.001$.

3.3.18 Analysis of antioxidant enzyme expression in human primary epithelial cells

3.3.18.1 Modulation of MnSOD expression in isolated human primary oral epithelial cells

In previous experiments, MnSOD mRNA expression was found to be altered in OSCC cell lines but not in a dysplastic cell line. qRT-PCR analysis of MnSOD expression was carried out on Primary 1 and Primary 2 cells types (Figure 3-40). After 6h (a) in the Primary 1 cells there was no change in expression of MnSOD. After 24h (b) there was a significant increase in expression of MnSOD. There was an increase in expression after 48h (c) but no significance was attained. In the Primary 2 cells there was no change in MnSOD expression over 6h (d), 24h (e) and 48h (f).

3.3.18.2 Modulation of CAT expression in isolated human primary oral epithelial cells

The antioxidant CAT was analysed by qRT-PCR in the same way to MnSOD (Figure 3-41). In the Primary 1 cells after 6h (a) 24h (b) and 48h (c) treatment with EtOH there was a significant increase in expression of CAT. In the Primary 2 cells there was also an increase in expression after 6h (d), 24h (e) and 48h (f) treatment with 1 % EtOH.

3.3.18.3 Modulation of GPx-1 expression in in isolated human primary oral epithelial cells

The effect of EtOH and p53 on GPx-1 was assessed in the same manner as previous experiments (Figure 3-42). In the Primary 1 cell line there was a decrease in expression after 6h (b) treatment with 1% EtOH but no change in expression after 24h (b) and 48h (c). In the Primary 2 cell line there was no change in expression of GPx-1 over 6h (d), 24h (e), or 48 (f).

3.3.18.4 Modulation of HO-1 expression in in isolated human primary oral epithelial cells

HO-1 expression was monitored in the primary cells as previously described using qRT-PCR. In the Primary 1 cells there was a significant decrease in expression of HO-1 after 6h (a) treatment with 1% EtOH. After 24h (b) there was a significant increase in expression of HO-1 but no change in expression after 48h (c). In the Primary 2 cell line there was an increase in expression of HO-1 after 6h (d) treatment and a decrease in expression after 24h (e) treatment. There was no change in expression after 48h (f).

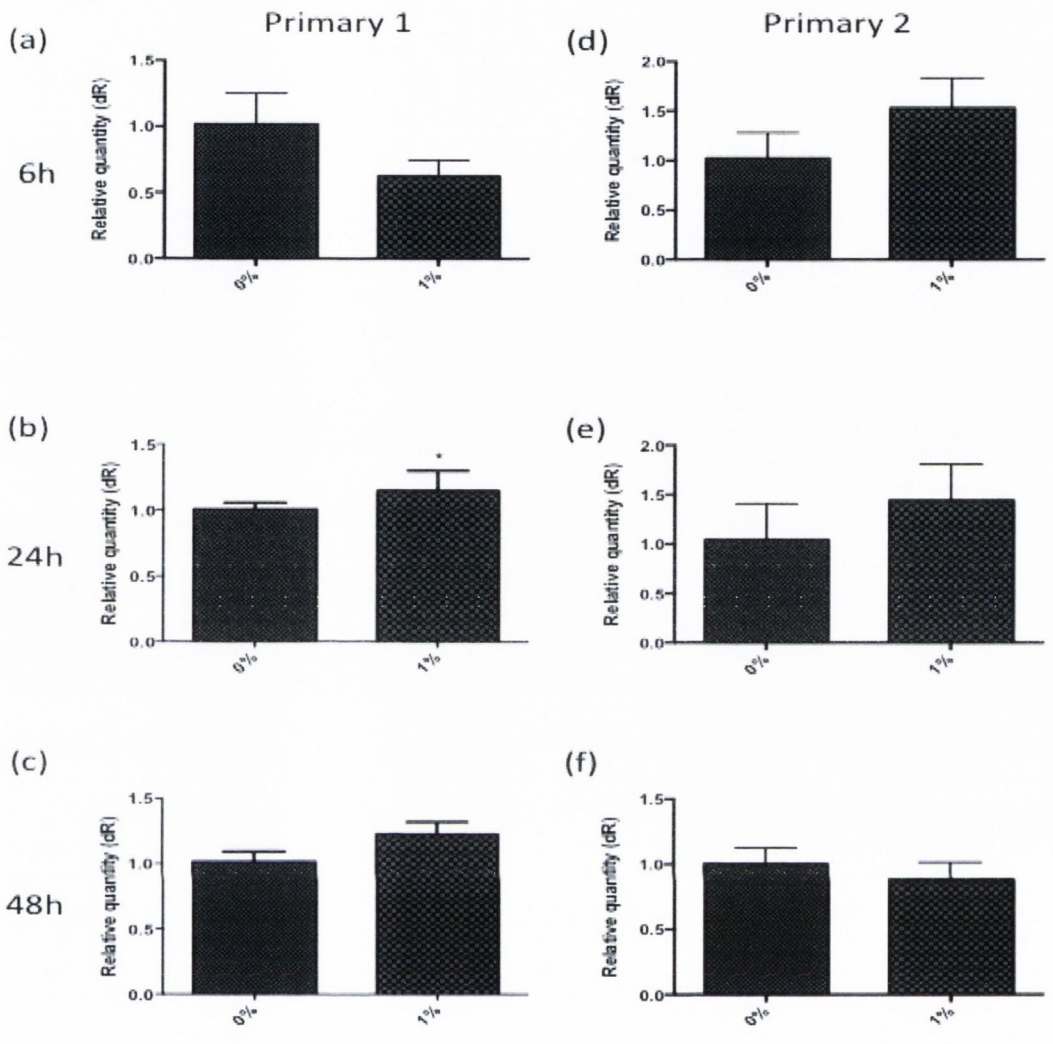


Figure 3-40 The effect of EtOH on MnSOD expression in in isolated human primary oral epithelial cells.

Primary cells (10,000/well) [Primary 1 (a) (b) (c), Primary 2 (d) (e) (f)] were serum starved overnight and the following day were treated for 6h (a) (d), 24h (b) (e) and 48h (c) (f) with 1% EtOH. mRNA was harvested and target genes were amplified up using a Sybr green One-Step qRT-PCR with specific primers for MnSOD. Relative quantification of gene expression profile was calculated using a DDCt method (RQ manager, Applied Biosystems). Experiments were completed in triplicate using three individual preparations (n=9) and statistical analysis was carried out using an unpaired t-test with post-hoc Bonferroni analysis using GraphPad prism 6.0. Samples significantly different to the control are annotated * $p<0.05$.

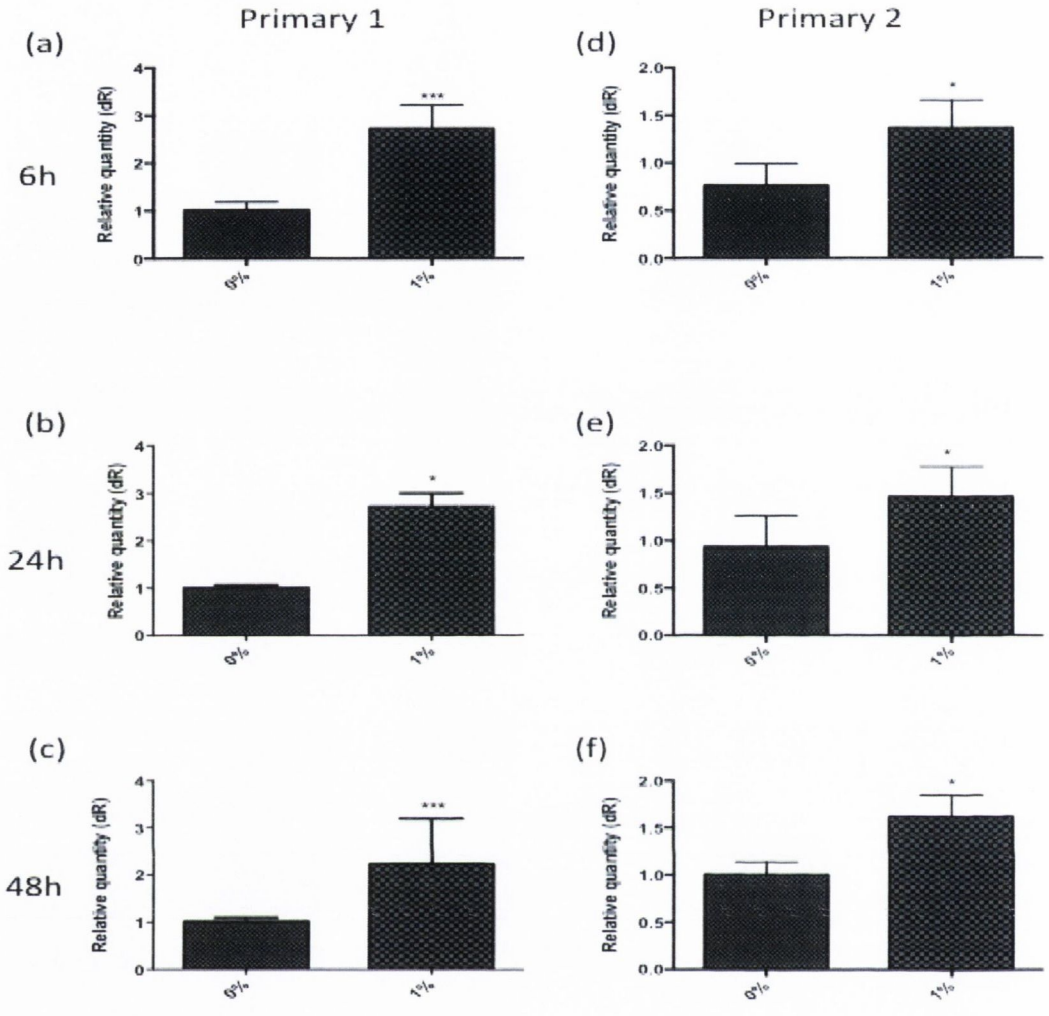


Figure 3-41 The effect of EtOH on CAT expression in isolated human primary oral epithelial cells.

Primary cells (10,000/well) [Primary 1 (a) (b) (c), Primary 2 (d) (e) (f)] were serum starved overnight and the following day were treated for 6h (a) (d), 24h (b) (e) and 48h (c) (f) with 1% EtOH. mRNA was harvested and target genes were amplified up using a Sybr green One-Step qRT-PCR with specific primers for HIF1-a. Relative quantification of gene expression profile was calculated using a DDCt method (RQ manager, Applied Biosystems). Experiments were completed in triplicate using three individual preparations (n=9) and statistical analysis was carried out using an unpaired t-test with post-hoc Bonferroni analysis using GraphPad prism 6.0. Samples significantly different to the control are annotated * $p<0.05$, *** $p<0.001$.

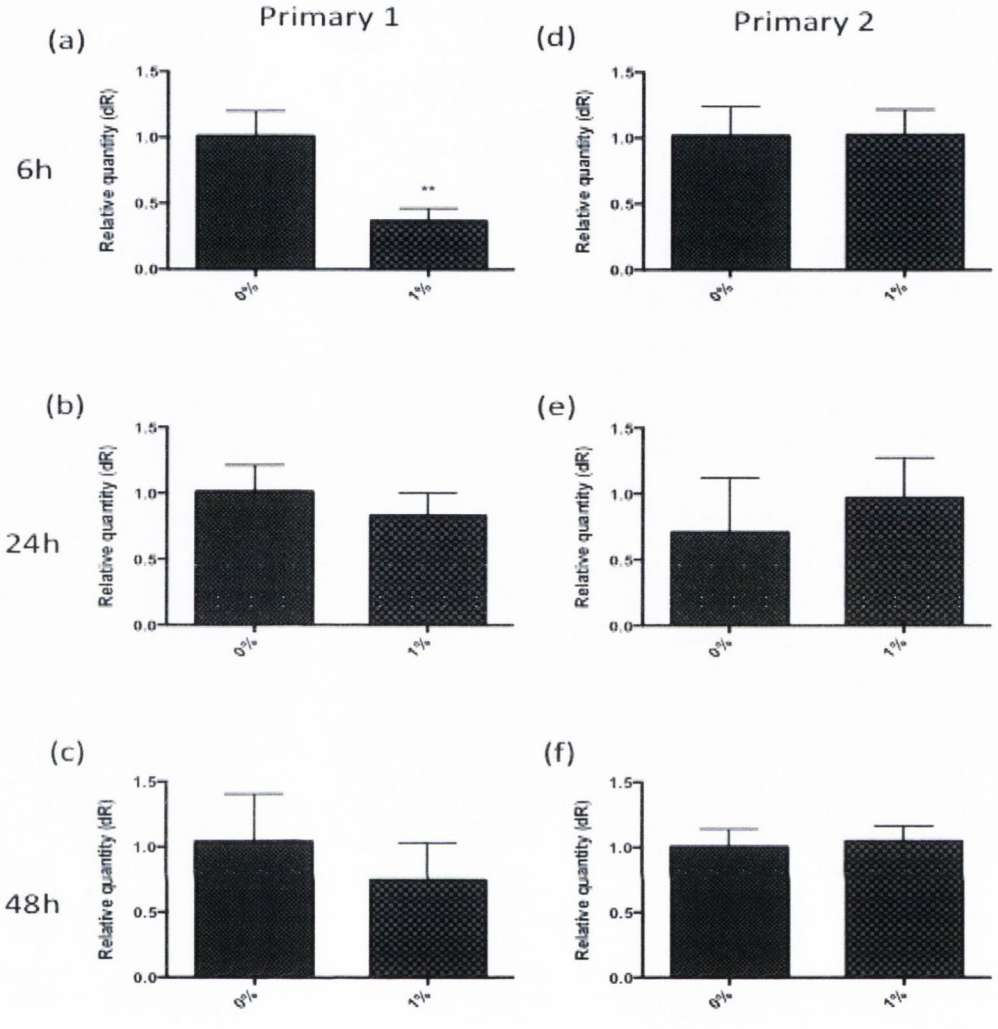


Figure 3-42 The effect of EtOH on GPx-1 expression in isolated human primary oral epithelial cells.

Primary cells (10,000/well) [Primary 1 (a) (b) (c), Primary 2 (d) (e) (f)] were serum starved overnight and the following day were treated for 6h (a) (d), 24h (b) (e) and 48h (c) (f) with 1% EtOH. mRNA was harvested and target genes were amplified up using a Sybr green One-Step qRT-PCR with specific primers for GPx-1. Relative quantification of gene expression profile was calculated using a DDCt method (RQ manager, Applied Biosystems). Experiments were completed in triplicate using three individual preparations (n=9) and statistical analysis was carried out using an unpaired t-test with post-hoc Bonferroni analysis using GraphPad prism 6.0. Samples significantly different to the control are annotated ** $p<0.01$.

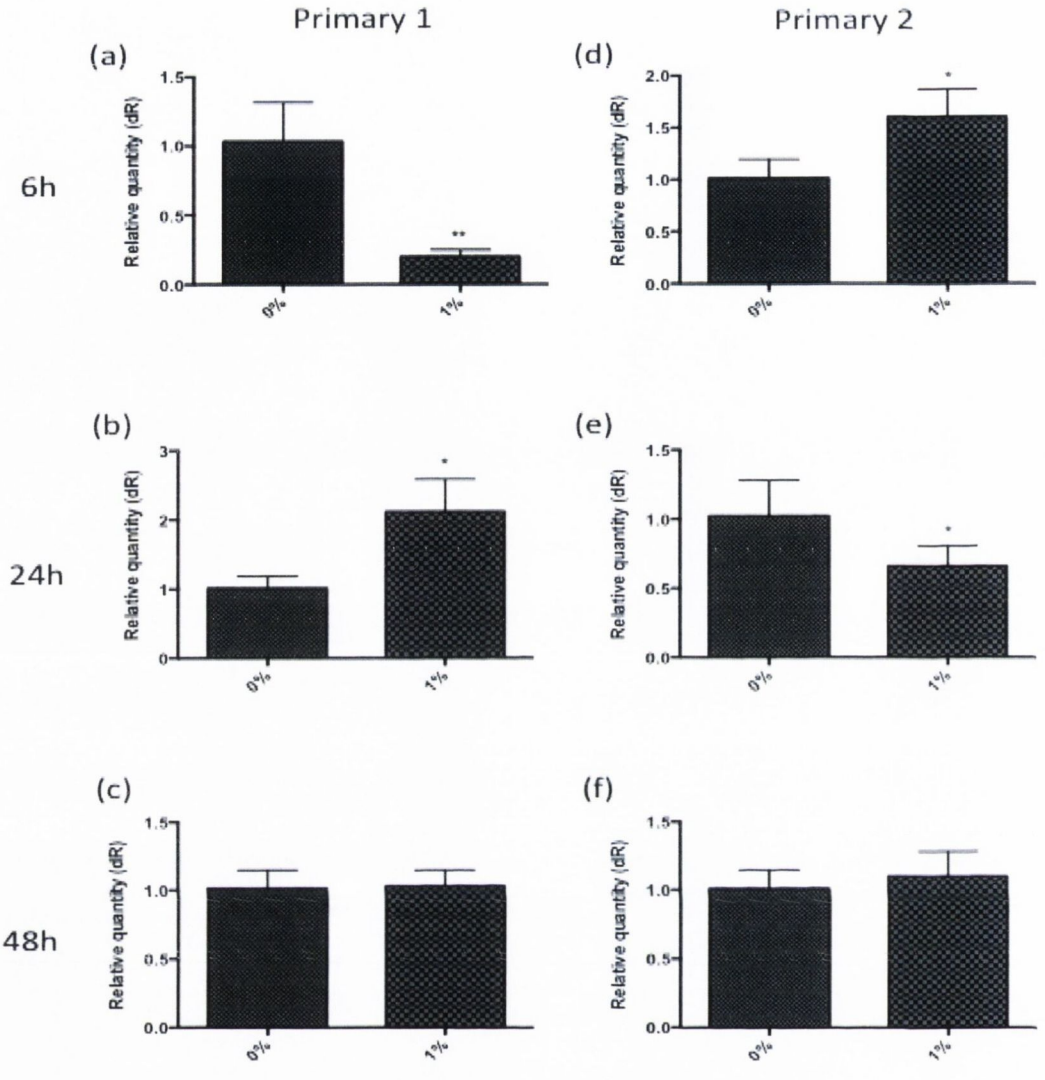


Figure 3-43 The effect of EtOH on HO-1 expression in isolated human primary oral epithelial cells.

Primary cells (10,000/well) [Primary 1 (a) (b) (c), Primary 2 (d) (e) (f)] were serum starved overnight and the following day were treated for 6h (a) (d), 24h (b) (e) and 48h (c) (f) with 1% EtOH. mRNA was harvested and target genes were amplified up using a Sybr green One-Step qRT-PCR with specific primers for HO-1. Relative quantification of gene expression profile was calculated using a DDCt method (RQ manager, Applied Biosystems). Experiments were completed in triplicate using three individual preparations (n=9) and statistical analysis was carried out using an unpaired t-test with post-hoc Bonferroni analysis using GraphPad prism 6.0. Samples significantly different to the control are annotated * $p<0.05$, ** $p<0.01$.

3.4 Discussion

Alcohol has been recognised as one of the major risk factors of OC. Despite the definite association between chronic alcohol consumption and OC, the exact role of alcohol in the pathogenesis of the disease is not fully understood. This is due in part to the concern regarding the mutagenic capabilities of downstream products such as aldehyde. This study determined the direct effect of EtOH on oral mucosal cells, dysplastic cells, and primary oral mucosal cells in relation to ROS production, control and effect on the cell cycle. The tumour suppressor protein p53 is a key regulator of cellular ROS and is found to be dysfunctional in ~50% of OC cases therefore the role of p53 tumour suppressor protein on EtOH modulation of antioxidant species was also examined.

Studies relating to the effect of EtOH on cellular function report an increase in ROS production. The majority of these studies examined report the consequence of EtOH exposure on the liver and several other cell types within the body. The nature of these studies suggest that the observed effects may be due in part to the oxidation of EtOH and is mediated through the products of this (and further oxidation) via liver enzymes. EtOH is oxidised to acetaldehyde in hepatocytes and subsequently to acetate through the action of enzymatic systems including ADH and ALDH. Therefore it is difficult to conclude that any observed effect is as a direct result of EtOH rather than one of the metabolite products. However it is interesting to note the effects of alcohol within the liver and other systems. In humans, alcohol is absorbed at a faster rate than it is oxidised, which can result in a chronic blood alcohol level. It is estimated that it can take up to 8h to complete the oxidation of a blood alcohol level of 100mg/100ml. This "lag-time" in the removal of EtOH suggests that EtOH may have a direct effect and not just the acetaldehyde metabolic product as shown by where EtOH played a role in neuroinflammation (Alfonso-Loeches *et al.*, 2010). Initial findings from this study show that there is little or no upregulation of ADH in the oral mucosal cell lines so therefore no observable breakdown of EtOH over the time course of the study. To ensure that EtOH was the primary causative agent at work in the cells, a control of 1nM acetaldehyde was used to demonstrate if any action of the primary by-product of EtOH was contributing to the observed effects. This concentration was determined from previous studies in oral mucosal cells which showed a maximum level of ADH activity of 6μM/ 24h/g protein (Dong *et al.*, 1996). By determining the amount of protein in the cell lines used along with the maximum concentration of EtOH in each experiment the

maximum amount of acetaldehyde produced during the time course of the experiments was found to be 1nM based on the previously mentioned rate.

Primary findings from this study show EtOH promotes a decrease in the ROS H_2O_2 in two OC cell lines, TR146 and Ca9.22. This decrease was observed to act in both a time and dose dependent manner and was found to reduce both intracellular and extracellular levels of H_2O_2. This is in contrast to several reports which document increases in ROS during EtOH exposure, however these studies were completed on different cell types including liver cells which have a higher level of ADH than oral cells. These studies used significantly lower doses and may involve EtOH oxidation products in some cases (Xue *et al.*, 2012, Agudelo *et al.*, 2011, Heaton *et al.*, 2011). A decreased release of H_2O_2 was determined at 6h, 24h and 48h and at the stated range of concentrations. A similar decrease in intracellular H_2O_2 was also confirmed using confocal microscopy at a single time point, 24h, with a single concentration of 1% EtOH. The use of a single time point and dose was due to the maintenance of cells in confocal dishes and duration of the experiment. The concentrations used during this study were significantly greater than a number of the previously quoted studies in an attempt to mimic contact levels observed in the oral cavity during the consumption of alcoholic beverages (100mM ~900mM in the case of 3% EtOH). These results suggest that at the low-mM range of EtOH concentrations, the initial H_2O_2 generating capacity of EtOH observed in some reports is mitigated at the mid-high mM range until a threshold level is reached approaching molar concentrations in these oral cell types. Previous studies have shown that at lower concentrations, H_2O_2 can act as a cellular signalling molecule (Meng *et al.*, 2002) so therefore lowering the amount of H_2O_2 in the cell could potentially activate pathways involved in cell growth and proliferation. Cellular proliferation has been noted in hepatoma and aveolar cells during exposure to low levels of H_2O_2 (Liu *et al.*, 2002, Sigaud *et al.*, 2005). This phenomenon may result from the decreasing levels of H_2O_2 observed with EtOH treatment in this study. Increased cellular proliferation is an early hallmark of carcinogenic transformation potentially leading to the development of OC resulting from chronic alcohol exposure. Although acute levels of EtOH does not cause an increase in proliferation as noted with the Alamar blue viability assay, chronic decreased levels of H_2O_2 could lead to increased growth in these cell types.

Upon observing that a fluctuation of the oxidative response within the cells occurred in the presence of EtOH a decision to examine the hypoxic response in these cells was taken. HIF-1α in low cellular O_2 concentrations binds to the hypoxic response elements (HREs) of antioxidant genes prompting expression and up-regulation of the cells response to hypoxia and the promotion of angiogenesis and is believed to be, in part, responsible for the metastatic events in some tumours (Semenza, 2009). With the significant decrease observed in H_2O_2 production ($p<0.001$) in both cell lines it seemed pertinent to examine the expression levels of HIF-1α. Interestingly it was observed that EtOH exposure produced a different effect on HIF-1α production in the two the cell lines. This present study revealed that EtOH caused an increase in HIF-1α in TR146 cells after 6h exposure to EtOH, a decrease at 3% after 24h exposure and no change in expression after 48h. This biphasic effect followed by a HIF-1α expression recovery may be a protective mechanism in these cells. An increased level of HIF-1α activates the hypoxic response element genes followed by a deactivation when returning to normal ROS levels observed after 48h. In the Ca9.22 cell line no effect on HIF-1α expression at any time point was observed. These findings are contrary to expectations as the cells appear to be entering a hypoxic state as demonstrated by the reduction in H_2O_2 (and therefore concurrently, O_2 levels) whereby the expression level of HIF-1α would be expected to increase in response to this stimuli in both cells lines. However it is possible that EtOH mediated modification is a hypoxic independent mechanism and that EtOH is exerting an indirect effect on the HIF-1α pathway in TR146 cells in concert with the reduction in H_2O_2 levels, due to a variation in either pheno- or genotype, in the case of the cells understudy the Ca9.22 cell line possesses a mutation in the p53 gene, a known regulator of ROS levels which suggests a potential role for this mutation in the abrogation of undesirable effects of EtOH mediated ROS disruption. A decrease in the generation of H_2O_2 may be in response to an alteration in endogenous antioxidant production, namely enzymes such as MnSOD, CAT, GPx-1 and HO-1 that are key regulators of the oxidative status of the cell. In the TR146 cell line EtOH affects several of these antioxidant enzymes. There is an increase in MnSOD after 6h and 24h at higher concentrations of EtOH, and a recovery at the 48h treatment. Since MnSOD converts O_2^- to H_2O_2 it was as expected that MnSOD expression levels would increase to make up for the decreasing levels of H_2O_2 in an attempt to try to stabilise the H_2O_2 levels. Chronic EtOH exposure then mitigates the recovery process. The change in H_2O_2 may also be driven by increased conversion of H_2O_2 to H_2O and O_2 by CAT and GPx-1. CAT levels

show an increase after 24h but no change at any other time point. The expression of GPx-1 shows no change over the time course of the experiment. CAT could be involved in some of the degradation of H_2O_2 however there was no change after 6h or 48h, which suggests that it is of minor significance in the processes at hand. Protein expression levels of MnSOD and CAT were determined to compare gene expression to functional protein under the conditions examined in these cell lines. As noted from the western blots there were no observable changes in MnSOD and CAT protein expression in the TR146 cell line. The lack of observable protein expression maybe a result of the resolution of the technique involved resulting in the changes in mRNA level not being detectable at protein level. As gene expression is controlled at many different levels including transcriptional and posttranscriptional regulation gene expression does not always correlate with protein expression. Further analysis of antioxidant enzymes continued by looking at changes in expression of HO-1. Free heme catalyses the conversion of H_2O_2 into the OH^- a more toxic radical. HO-1 expression decreased with EtOH treatment after 24h and 48h. In the TR146 cell line the decrease in H_2O_2 could be due to a decrease in HO-1 after 24h and 48h. This decrease suggests that HO-1 cannot neutralise toxic free heme allowing it to convert more H_2O_2 into OH^-. Protein expression levels of HO-1 and GPx-1 were not carried out due to a lack of suitable antibodies.

The Ca9.22 cell line showed a notable difference in the expression of the antioxidant enzymes when compared to the TR146 cell line. MnSOD was increased after 6h and 48h but no change at 24h. As expected increasing MnSOD expression is possibly making up for decreasing levels of H_2O_2. There was also no observed change in protein expression over the time points using this cell line. CAT gene expression showed a significant increase with 3% EtOH after 6h and a highly significant decrease after 24h with every concentration of EtOH suggesting that a reduction in H_2O_2 levels can modulate an abrogation of CAT expression preventing further removal of H_2O_2 thus attempting to stabilise the oxidative status of the cell. The cells recover after 48h with no change in expression. The recovery after 48h suggests that after EtOH exposure, followed by a stabilisation of the cells ROS status, CAT gene expression normalises before it has major implications on protein expression in the cells demonstrated by the absence of changes in the observed protein levels. The decrease in GPx-1 expression in the Ca9.22 cells after 48h treatment with EtOH would correlate to the decrease in H_2O_2 levels and as a minor influence in the presence of the other antioxidant enzymes it would have a

minor role in the removal of H_2O_2. In contrast to the TR146 cells, EtOH had no effect on the expression of HO-1 mRNA in Ca9.22 cells.

One of the more significant observations in this study is the increase of MnSOD expression in the TR146 and Ca9.22 cells in response to EtOH and could potentially indicate a method of transformation of these cell lines. Other studies complement these results, as an increase in MnSOD with short-term EtOH exposure has been previously noted in human hepatoma cells (Perera *et al.*, 1995) further reports showed that upregulation of an MnSOD isoform in squamous cell carcinoma patients was associated with apoptosis resistance in these cancers (Hu *et al.*, 2007). Increased MnSOD expression is also associated in metastatic gastric cancer patients (Malafa *et al.*, 2000). The change in MnSOD expression in these cell lines was likely not to be the cause of the decreasing H_2O_2 production in these cells but it could however be a driver of potential transformation by EtOH through the dysregulation of key enzymes including MnSOD. The abnormal fluctuations of CAT observed between the two cell lines reinforce the differential response of both cells to EtOH treatment. Increased production of CAT has been previously noted in OC tumour cells (Khanna *et al.*, 2005) while decreased production has been noted in other forms of cancer (Dong *et al.*, 1996). Differential expression of GPx-1 was also noted between these two cell lines. High expression levels of GPx-1 are associated with increased survival in OSCC patients (Fu *et al.*, 2011). In contrast there was no change in the TR146 cell line and a decrease in the amount of GPx-1 over 48h in response to high EtOH concentrations. In previous studies EtOH has been shown to cause an upregulation in HO-1 expression in oesophageal squamous carcinoma cells (Hu *et al.*, 2013). In EtOH fed rats the silencing of HIF-1α attenuated HO-1 upregulation (Yeligar *et al.*, 2010). Since there are no alterations in HIF-1α expression in Ca9.22 cells lines and no alteration in HO-1 expression it is possible that EtOH induced modification of HO-1 is HIF-1α dependant. With EtOH causing minor insults on antioxidant expression over a short time period, chronic EtOH consumption over a longer time course could cause more major disruptions in the antioxidant systems in these cells, which has been reported in many forms of cancer.

There are several possibilities as to why there is such different responses between the two cell lines. Gender-specific and site-specific differences could be a reason for such wide-ranging responses. The TR146 cell line originated from the buccal mucosa of a

male and the Ca9.22 cell line from the gingiva of a female however the major difference between the cell lines lies in the genotype of the Ca9.22 cell line, which contains a p53 mutation. Studies have shown that EtOH effects p53 expression (Kuhn and Miller, 1998), p53-mediated activities (Miller *et al.*, 2003) and downstream regulators of p53 (Li *et al.*, 2001). EtOH is not only driving modulations in ROS and the enzymes involved, there is also a greater influence in the p53 mutant line showing that p53 is involved in the regulation of these enzymes in response to EtOH. This could signify that mutated cells are more susceptible than a non-mutated cell line.

p53 exerts its effects through transcriptional induction of target genes including cell cycle checkpoints and apoptosis. ROS in general and H_2O_2 in particular can play a major role in apoptosis along with defined roles in the modulation of numerous other cell signalling pathways including the cell cycle (Li *et al.*, 2009). In previous studies EtOH has been shown to affect cell cycle progression by disrupting proteins involved in regulating the cell cycle checkpoints (Luo and Miller, 1997). Exposure to EtOH has also been shown to disrupt cell cycle progression by affecting growth factor signalling pathways involved in the cell cycle. In this study EtOH affected cell cycle distribution and protein levels in both cell lines. The proposed target of EtOH in the cell cycle is the G1 phase and the G1/S checkpoint (Hicks *et al.*, 2010). In the TR146 cell line there is a build-up of cells in the S phase at higher concentrations of EtOH as shown by an increase in cells in the S phase and a decrease of cells in the G2/M phase after 6h. This continues through 24h and 48h where there is a decrease in cells in both the S phase and G2/M phases and an increase in cell numbers in the G0/G1 phase. Cyclin D1, which has been implicated in the pathogenesis of many cancers, is not involved in this EtOH modulation in the TR146 cell line. Cyclin B1 however is suppressed after 24h incubation with EtOH. This suppression of cyclin B1 would limit the supply of cdk1/cyclin B1 complex required for G2/M transition. Similar results were obtained for the Ca9.22 cell line. Over 48h there was a decrease in G2/M phase cells and an increase in cells in the G1 phase. A suppression of cyclin B1 is also noted after 24h in this cell line however there is a decrease in cyclin B1 in controls at 48h and a greater expression at higher concentrations of EtOH. High cyclin B1 expression has been noted in other types of cancers including oral carcinoma (Wang *et al.*, 1997, Kushner *et al.*, 1999). Cyclin D1 is normally over expressed in cancers, which causes the cells to bypass cell cycle checkpoints and divide uncontrollably. Mutations of cyclin D1 in cancers have

been extensively recorded (Alao, 2007). In contrast with the TR146 cell line, in the Ca9.22 cell line there is a decrease in cyclin D1 expression after 6h. Altered expression of cyclin D1 has been seen with EtOH treatment of hepatocytes (Hsu *et al.*, 2006) and also in EtOH exposure during murine neurulation (Anthony *et al.*, 2008). This decrease could signify a deregulation after short-term treatment, which could cause lasting damage to cyclin D1 with long-term alcohol consumption. Alternatively the decrease in cyclin D1 could be due to the gain-of-function p53 mutation in Ca9.22 cells which has been shown to be involved in cell cycle regulation (van Oijen and Slootweg, 2000). Another explanation is that the cell line is already a transformed cell line so there could be differences in cyclin D1 expression if analysed in a normal oral mucosal cell. It would be necessary to carry out further experiments to confirm this, which was not achievable within the time permitted for project but will lead to a further interesting study.

Approximately 4-35% of all dysplastic lesions will develop into OSCC however the relationship between alcohol consumption and the transformation of dysplastic cells is unknown. Utilising the same model as previously used in the OSCC cell lines (TR146 and Ca9.22), the effect of EtOH on the DOK cells was investigated. In a manner similar to the OSCC cell lines there was a dose dependant decrease in H_2O_2 release after EtOH treatment. It is interesting to note that the amount of H_2O_2 release in the untreated cells of each cell type in comparison to one another was significantly different. It is well known that ROS levels are much higher in cancer cells than in normal cells (Trachootham *et al.*, 2006). Similar to the Ca9.22 cell line there was no change in the redox sensing protein HIF-1α expression in the DOK cell line suggesting there is no correlation with the decreasing levels of H_2O_2 observed. The decrease in H_2O_2 could be as a result of direct effects of EtOH on antioxidant enzymes however in contrast to both OSCC cell lines there was no effect on MnSOD expression. An increase in MnSOD expression is indicative of the presence of cancerous cells so therefore any EtOH associated transformation in these cells is not been driven by MnSOD alterations (Malafa *et al.*, 2000). CAT expression is acutely increased in both OSCC cell lines in the presence of EtOH and in the DOK cell line there is also a notable increase. Increased production of CAT is associated with transformed cells therefore if coupled to an observed increase in dysplastic cells there is potential to use CAT as a biomarker of transformation. GPx-1 has a similar function to CAT as it breaks down H_2O_2 as part of

the cells antioxidant system. Comparatively, the overall change in GPx-1 expression in Ca9.22 cells and DOK cells was similar. Both cells showed a decrease in expression of GPx-1 after 48h. However there was an increase in expression after 6h of this protein in the DOK cells. This biphasic effect could demonstrate that while cancer cells have no method of recovering from the effect of EtOH, DOK cells potentially contain a recovery mechanism where they can increase the amount of protein, however chronic exposure to EtOH does cause a decrease, similar to that seen with the cancerous cell lines. As with GPx-1 there was a biphasic response observed with HO-1 production. Interesting to note that in the TR146 cell line there was also a decrease in HO-1 expression after 24h and 48h however there was a recovery in the DOK cells after 48h. Over time the long term effects of EtOH could cause repeated insults to the cells antioxidant system and inhibit the cells ability to recover allowing for transformation to occur.

The cell cycle distribution in the presence of EtOH in the DOK cells was remarkably different to the OSCC cell lines. Overall in the G0/G1 phase there was no change in cell distribution over 24h but a decrease in cells after 48h. This contrasts to the OSCC cell lines where there was an increase in cells in the G0/G1 phase after 48h. This change could be in part due to the effect of EtOH on MnSOD expression in these cell lines. Previously a study (Sarsour *et al.*, 2008) found that increasing levels of MnSOD facilitated proliferating cells transition into the quiescence. Thus in the OSCC cell lines EtOH exposure induces increased levels of MnSOD and arrest in the G1 phase which can lead to uncontrolled growth of tumours (Morgan, 2006). In contrast the DOK cells arrest in the G2/M phase, which is indicative of growth inhibition and repair (Kastan and Bartek, 2004). These results indicate that alcohol consumption may worsen the prognosis for OSCC but the dysplastic DOK cells are able to undergo repair, however long term/chronic alcohol consumption affects the repair mechanisms in the cells increasing the potential of a carcinoma developing.

The DOK cell line also contains a mutation in the p53 gene. Mutations in this gene are extremely common in OC and it is this protein that may determine some of the effects on the cells. To explore the relationship between p53 and EtOH, p53 was knocked down using siRNA in TR146 cells. Using data obtained from the previous experiments a suitable exposure level to EtOH (1%) was determined.

With the knockdown of p53 there was a significant decrease in HIF-1α expression over the three time points. When treated with EtOH there was no change in HIF-1α expression. This result confirms observations from both the Ca9.22 cell line and the DOK cell line that p53 activity correlates with HIF-1α expression. This outcome reinforces the hypothesis that with a mutation in p53, HIF-1α expression is diminished and is unable to respond in the presence of EtOH. There has been much debate about the interaction and relationship between p53 and HIF-1α. It is thought that the two proteins stabilise one another in the presence of stress in the cell (An *et al.*, 1998). This interaction could prove extremely important in EtOH effect on oral mucosal cells and possibly transform to a more detrimental genotype. Additional experiments would need to be carried out to investigate this relationship further but the preliminary results are extremely interesting to observe.

Knockdown of p53 did not change the expression of MnSOD however after 48h treatment with EtOH in the knockdown there was a decrease. In the TR146^{p53wt} cells there was an increase in expression of MnSOD after 6h and 24h with 1% EtOH. Contrastingly there was no change in expression of MnSOD after these time points in the TR146$^{p53-/-}$ cells. This suggests that knockdown of p53 combined with exposure to EtOH impairs the function of MnSOD over longer time points as seen with the decrease observed over 48h. Therefore the EtOH upregulation of MnSOD in TR146 is a p53 dependant mechanism.

The down regulation of p53 does not alter the response of CAT to EtOH treatment in TR146 cells. However suppression of p53 using siRNA does alter the function of CAT. At every time point there is an upregulation of CAT expression with knockdown of p53 activity. A recent publication (Kang *et al.*, 2013) showed that p53 suppresses CAT activity in human colon carcinoma cells. Therefore down regulation of p53 causes an increase in CAT expression within the cell. As mentioned previously an increased production of CAT was noted in OC cells and could drive a more aggressive phenotype in cancer cells. Similarly to MnSOD, p53 down regulation does not alter the expression of GPx-1 in TR146 cells. However after 48h treatment with EtOH in these cells there was an increased expression of GPx-1. A link between p53 upregulation and GPx-1 induction has been shown in a lymphoblast cell line (Hussain *et al.*, 2004). The induction of GPx-1 in the TR146$^{p53-/-}$ cells was not due to p53 expression however

upregulation has been shown to be positively correlated with promoting invasion, migration, proliferation and resistance in oesophageal squamous cell carcinoma (Gan *et al.*, 2014). Down regulation of HO-1 occured the TR146 cells with and without a functional p53 in the presence of EtOH. Therefore any changes that occur to HO-1 with EtOH treatment in this cell line are not due to p53. However, in the TR146$^{p53-/-}$ cells there was an up regulation of HO-1 expression in the absence of EtOH, suggesting that p53 does have an association with HO-1. It is known that HO-1 is upregulated in many types of cancer including oesophageal carcinoma and thus the down regulation of p53 drives increased HO-1 into a more tumorigenic state (Hu *et al.*, 2013). Despite this, treatment of EtOH decreases HO-1, which could therefore be a sign that the cells are attempting to recover from EtOH insult. However if the baseline levels are increased in p53 mutants then down regulation of HO-1 might not be sufficient to enable the cells to overcome the insult.

The varying responses to EtOH by the cells containing either mutant or knockdown p53 are probably due to the nature of p53 the mutation within these cells. The Ca9.22 contains a dominant-negative (DN) R248W mutation which although the normal functions of p53 are impaired, this type of mutation is known as a gain-of-function (GOF) mutation. GOF mutations contain newly acquired activities of p53 and can contribute actively to various stages of tumour progression and increased resistance to anticancer treatments (Lotem and Sachs, 1995). DN mutants in cancer are a predictor of poor outcomes (van Oijen and Slootweg, 2000). The knockdown of p53 activity in the TR146 cells is almost 100% so therefore there is very little or no function of p53 at all and this best represents a loss-of-function mutation. The DOK cells contain a deletion in the p53 codon causing it to over express p53 which has also been shown to lose its normal function and drive mutated gain-of-function p53. A study (Blagosklonny *et al.*, 2001) has shown that mutant p53 blocks transcription of HIF-1α, which correlates to this study using Ca9.22, DOK and TR146 $^{(p53wt\ \&\ p53-/-)}$ cells. If HIF-1α is unable to mount the correct response in the presence of EtOH the prognosis for the cells/tissue involved will be significantly worse.

The inductions of dysplastic or carcinogenic changes by EtOH occur in untransformed 'normal' tissue therefore, to analyse changes that occur to normal oral cells, mucoperiosteal tissue kindly donated from patients of the Dublin Dental Hospital was

utilised and primary oral epithelial cells were obtained using a combination of enzymatic and direct explant techniques. Due to limited availability of samples and in the technical challenges involved in extracting and maintaining growth of these cells only two samples were used for this study-named Primary 1 and Primary 2. In agreement with the previous studies there was a decrease in H_2O_2 production with slight recovery over the time points. Interestingly there were several differences in response to EtOH with regards to changes in expression of analysed genes. Firstly, there was a decrease in expression of HIF-1α after 6h in the Primary 1 cells but no change in expression in the Primary 2 cells. When comparing this result to previous cells, those who had a p53 mutation did not elicit a response in the HIF-1α gene and suggests that the Primary 2 cells may contain a p53 mutation but further work would need to be carried out to analyse any genetic differences between these cell types. Next there were changes in the differences between the antioxidant enzymes response. MnSOD in the Primary 1 cells increased after 24h but recovered after 48h. In the Primary 2 cells there was no change in MnSOD expression. The differences in changes could mark the increased susceptibility of one cell type more than the other. As mentioned previously, an increase in MnSOD was observed in squamous cell carcinoma patients and was associated with apoptosis resistance in these cancers (Hu *et al.*, 2007). Following on from this another interesting response to EtOH in these two cell types was that CAT was increased at all time points in both cell lines. This was the only gene whose expression was the same in the two cell lines. As was the case with the TR146, Ca9.22 and DOK and p53 knockdown cells all primary cells showed an increase in CAT expression. As previously alluded to, an increase in CAT expression has been discovered in oral malignancies (Khanna *et al.*, 2005). Increase in CAT has been shown to increase the doubling time and delay G1 to S phase in the cell cycle. This is perhaps a defence mechanism used in the cells for protection against EtOH damage. In the primary cells, EtOH did not prompt any significant change in the expression of GPx-1 except a small increase in the Primary 1 cells after 6h. Interestingly, EtOH caused opposite responses in HO-1 in both cell types. After 6h HO-1 in the Primary 1 cells was decreased followed by an increase after 24h and contrastingly after 6h in Primary 2 cells there was an increase in HO-1 expression and a decrease after 24h. The response in the Primary 2 cells are analogous to the HO-1 expression in the DOK dysplastic cells that as previously mentioned have a mutation in the p53 gene. Once again this result supports the argument that the Primary 2 cells could possibly contain a mutation in the p53 gene. Over all the response in the

Primary cells support the hypothesis that EtOH can drive changes in the redox system that could potentially lead to dysplastic and malignant phenotypes. One limitation of this study is that the sample size is too small to be confident about distinct changes in primary oral cells but it builds a model for further analysis. Further work involving a larger sample size would be an interesting extension to this study and could confirm and provide further insight into the changes that occur in the oral mucosa due to EtOH.

Alcohol is currently not believed to cause oncogenic transformation in the oral mucosa however people who consume excessive amounts of alcohol are at a higher risk of developing OSCC in comparison to those who abstain. It is clear that acute EtOH consumption does not have the ability to drive transformation in the oral mucosa but this study shows chronic EtOH consumption over prolonged periods could be involved in transformation of these cells. This study showed that acute EtOH drives a decrease in H_2O_2 production in cell lines, dysplastic cells and primary oral human cells. This reduction in H_2O_2 along with fluctuations in cell cycle distribution and proteins could activate new pathways associated with increased proliferation as previously seen in epithelial cells. Over time this potential increase in proliferation could become uncontrolled which is a key marker of dysplasia and cancer. This study also showed that EtOH causes fluctuations in the antioxidant response in all the cell types. This response is essential for cell maintenance and alterations in these have been shown to be drivers of transformation. The antioxidant response was altered by changes in p53 activity. In particular p53 down regulation was shown to alleviate the HIF1-α response to EtOH, a key mediator in a cells defence. This study formulates novel molecular pathways that are involved in acute alcohol-induced changes in the oral mucosa that could potentially lead to oncogenic transformation with longer EtOH treatment.

4 Discrimination of OSCC cells using Raman spectroscopy

4.1 Introduction

Despite the use of combined aggressive treatments including surgery, chemotherapy and radiation therapy in OC treatment, the 5-year survival rate is low in more advanced cases of the disease. This is partly due to the fact that 60% of OCs are discovered at stages III and IV of the disease (Lingen *et al.*, 2008). Descriptive histology is currently the gold standard for the diagnosis of cancers of the oral cavity and oropharynx. There is an urgent requirement need for more accessible and less invasive methods of diagnosis in the clinic. This study examines the potential use of Raman spectroscopy as an aid in the diagnosis of OC and also its potential to elucidate more about the biochemical and carcinogenic changes that occur in OC. Raman spectroscopy is based on the principles that the biochemical composition of a cell corresponds to a fingerprint of light scattering. This light scattering can be used to obtain further information about the make up of a cell and could potentially identify biomarkers for OC. This technique has previously been shown to be successful in aiding the diagnosis of cervical cancer (Lyng *et al.*, 2007).

4.1.1 OC diagnosis

Despite the seeming ease of which OCs should be diagnosed, given their probable visibility on examination, many OCs are not identified until the latter stages of the disease. A fundamental reason for misdiagnosis is the inconsistent differentiation between pre-malignant and benign lesions of the mouth (Abbey *et al.*, 1995). Poor prognosis for OC is thought to be due to several reasons. Firstly, OC is frequently associated with multiple primary tumours, the rate of development of second primary tumours being 3-7% per year in these patients. This is higher than any other malignancy. Secondly, poor survival among cancer patients can be attributed to the advanced stage at which the disease is diagnosed, over 60% of patients presenting in stages III and IV. Such discouraging statistics seem perverse, since the disease primarily arises in the surface epithelium that is readily accessible to visual and tactile examination. This may be due to, in part, an incomplete understanding or awareness that even small asymptomatic lesions can have significant malignant potential.

Screening patients for signs of OC and precancerous lesions has relied upon conventional oral examinations. Current methods of clinic-based diagnostics include visual examination for potentially malignant lesions, including leukoplakia and erythroplakia. Depending on the size, site, shape, colour and texture of the plaque, further tests may be carried out in the clinic to investigate the risk for these pieces of tissue. These tests include toluidine blue stain, brush biopsy, exfoliative cytology, and fluorescence staining. These tests can prove useful in visualising potential malignancies. However, further analysis must always be carried out to confirm the status of the piece of tissue. This includes a surgical biopsy, which is invasive to a patient.

One approach to this problem would be to improve the ability of oral health care professionals to detect relevant potentially malignant lesions or cancerous lesions at their earliest stage with minimum invasion and discomfort to the patient. There is a need for the development and use of diagnostic aids that would more readily identify or access persistent oral lesions of uncertain biological significance. Raman spectroscopy, which is used in the diagnosis of other types of cancer, could prove a useful tool in the diagnosis of OC due to the ease of use and lack of disruption to the patient with regards to invasiveness and time.

4.1.2 Vibrational spectroscopy

Vibrational spectroscopy is a molecular characterisation technique in which normal vibrational modes specific to the molecular bonds as well as molecular fingerprints are probed. There are two main vibrational spectroscopic techniques, Fourier transform infrared spectroscopy (FTIR) spectroscopy and Raman spectroscopy. These two techniques give complementary spectral information (Chalmers, 2002).

A molecule composed of n atoms has 3n degrees of freedom. Six degrees of freedom are translations and rotations of the molecule itself. The other 3n-6, or 3n-5 for a linear molecule, is called vibrational freedom. A molecular vibration occurs when the atomic constituents of the molecule are in periodic motion, while the molecule has constant translational and rotational motion. The frequency of this periodic motion is called

vibrational frequency. Vibrational modes are often given as descriptive names, such as stretching, bending, scissoring, rocking and twisting. A schematic illustration of the main vibrational modes is shown in Figure 4-1.

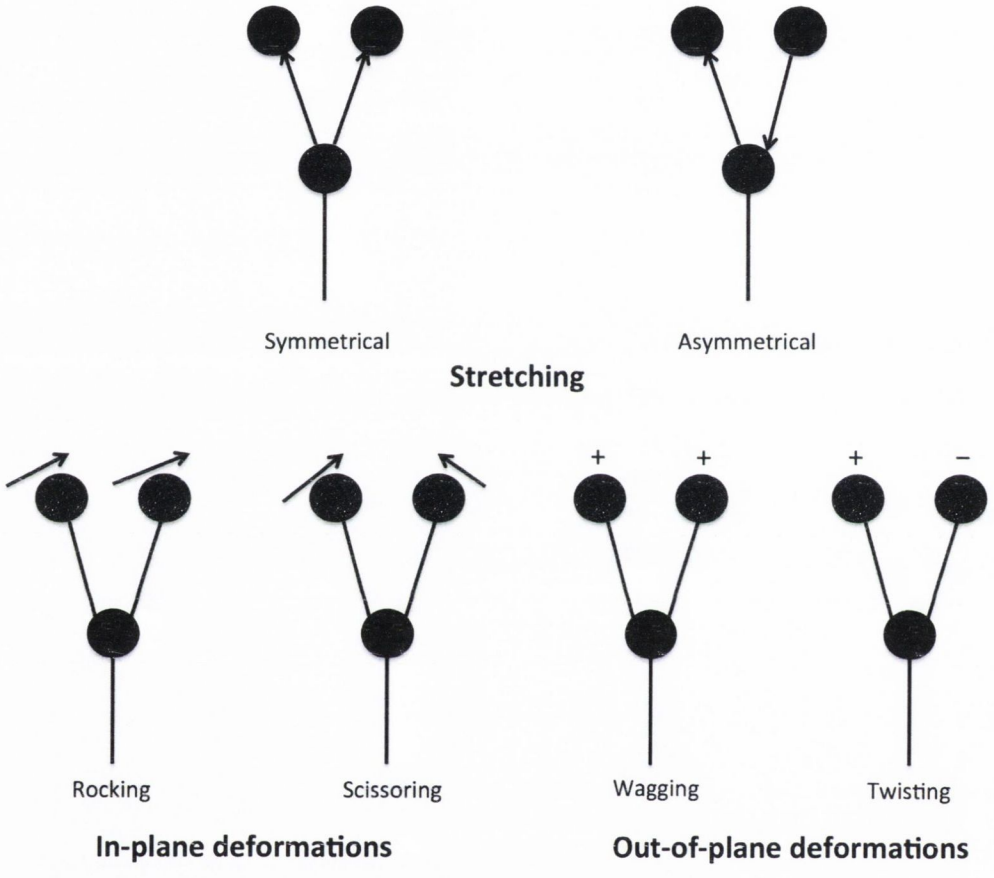


Figure 4-1 Schematic illustration of the main vibrational modes in Raman Spectroscopy.

The plus and minus signs denote movement of the atom into and out of the plane of the diagram, respectively.

4.1.3 Theoretical basis of Raman spectroscopy

Raman spectroscopy is based on the principle of the inelastic scattering of monochromatic light. It is a type of vibrational spectroscopy in which normal vibrational modes specific to molecular bonds as well as more complicated molecular fingerprints are probed. Analysis is rapid, non-invasive and delivers a fingerprint of the chemical constituents of the material analysed. Biomedical applications of Raman are rapidly developing and the techniques have been utilised in many studies for the detection of different types of cancer, including cervical (Lyng *et al.*, 2007, Schubert *et al.*, 2010), breast (Kast *et al.*, 2008, Haka *et al.*, 2005), prostate (Tollefson *et al.*, 2010), skin (Bodanese *et al.*, 2010) and lung (Magee *et al.*, 2010, Magee *et al.*, 2009).

In Raman spectroscopy measurements, incident light is scattered inelastically from a sample. The frequency of photons in the incident light changes in the process of interaction of the photons and molecules, such that the frequency of the reemitted photons is shifted up or down in comparison with the original monochromatic light. This is called the Raman effect. The exact energy required to excite a molecular vibration depends on the masses of the atoms involved in the vibration and the type of chemical bonds between these atoms and may be influenced by molecular structure, molecular interactions and the chemical microenvironment of the molecule. Therefore, the positions, relative intensities and shapes of the bands in a Raman spectrum carry detailed information about the molecular composition of the sample (Socrates, 2004).

The monochromatic laser light excites molecules and transforms them into oscillating electric dipoles. The oscillating dipoles emit light of three different frequencies. The first of these frequencies is Raleigh scattering, which is a molecule with no active Raman modes and absorbs a photon with frequency V_0. The excited molecule returns back to the same vibrational state and emits light with the same frequency as the source. Stokes shifting of the frequency occurs when the initial frequency V_0 interacts with a Raman active molecule, which at the time of interaction is in the ground vibrational state. The resulting frequency of scattered light is reduced to $V_0 - V_M$. When the Raman active molecule is in an excited vibrational state at the time of the interaction, the emitted light frequency is increased to $V_0 + V_M$. This is called the anti-Stokes frequency. Stokes

scattering results in the generation of a molecular vibration, whereas anti-Stokes results in the annihilation of a vibration. In practice, the Stokes scattered light is normally measured since, at room temperature, most molecules exist in the ground vibrational state, and thus it is easier to create a vibration than to annihilate one.

The interaction is often portrayed by an energy level diagram, as shown in Figure 4-2. The excited electronic state can be virtual, or, in the case of resonant Raman scattering, a real electronic state of the molecule.

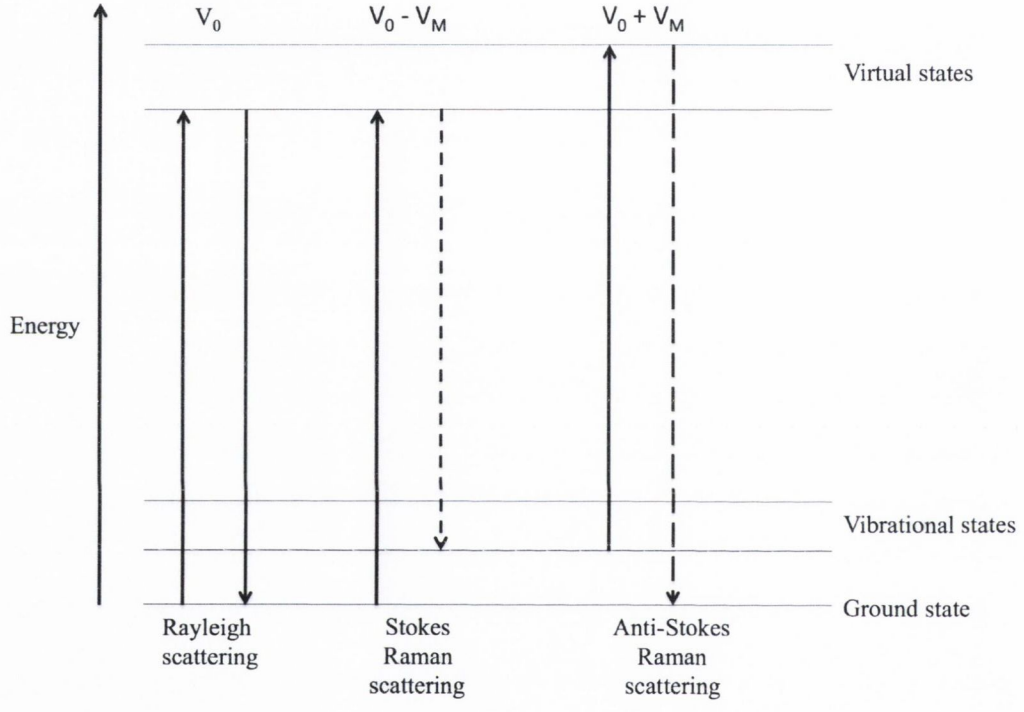


Figure 4-2 Diagrammatic representation of an energy transfer model of Rayleigh scattering, Stokes Raman and anti-Stokes Raman scattering.

4.1.4 Identification of biochemical and molecular changes using Raman Spectroscopy

Raman spectroscopy has been shown to identify and classify malignant changes in other types of cancer. As previously mentioned, the spectrum can be used to analyse different molecular components in the cell. Nucleic acids can be identified by peaks characteristic of nucleotide and sugar-phosphate backbone vibrations. The main peaks are found at 1095cm^{-1} (phosphodioxy group PO2-), 788cm^{-1} (C5'-O-P-O-C3' phosphodiester bonds in DNA) and 813cm^{-1} (C5'-O-P-O-C3' phosphodiester bonds in RNA), 782cm^{-1} (thymine, cytosine and uracil) and 1578cm^{-1} (guanine and adenine). The phosphate peaks are particularly useful to determine the structure of DNA including the common B-, right handed form of DNA and the less common A- and Z- forms. It can also differentiate between DNA and RNA (Notingher, 2007).

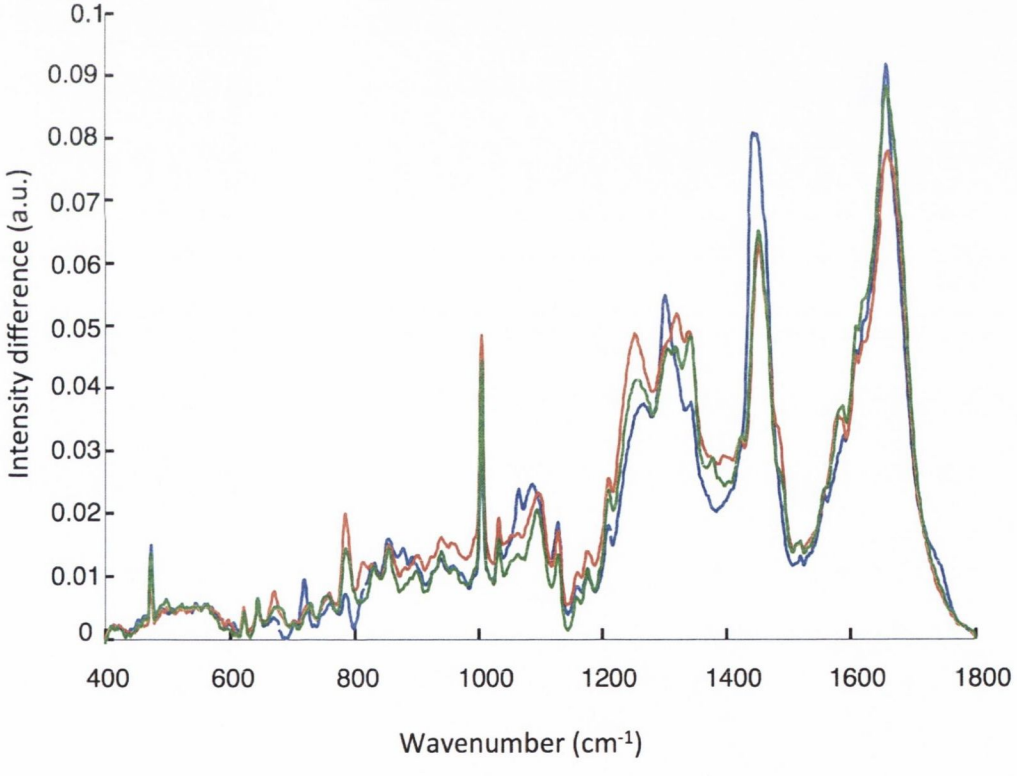


Figure 4-3 Raman spectra from the cell nucleolus (red), nucleus (green) and cytoplasm (blue) obtained with a 532nm diode laser.

The spectra of proteins are dominated by peaks corresponding to the Amide I (1660-1670cm^{-1}) and Amide III (1200-1300cm^{-1}) vibrations, which have been shown to be sensitive to the secondary structure of the proteins. There are additional Raman peaks corresponding mainly to amino acids containing phenyl groups, such as phenylalanine (1005cm^{-1}), tyrosine (854cm^{-1}) and tryptophan (760cm^{-1}) as well as C-H vibrations (1449cm^{-1}). While it is difficult to distinguish between specific types of proteins on the basis of their Raman spectra, the Amide I and Amide III peaks are sensitive to subtle changes in the secondary structure of proteins (Kinalwa *et al.*, 2010). The strongest Raman peaks of lipids are present at 1449cm^{-1}, 1301cm^{-1} (C-H vibrations) and 1660cm^{-1} (C=C stretching) and belong to vibrations of the hydrocarbon chains. Additional Raman peaks corresponding to head groups of phospholipids can also be found, such as the 719cm^{-1} peak corresponding to the C-C-N+symmetric stretching in phosphatidylcholine, a major constituent of cellular membranes. Carbohydrates can be identified and analysed reliably due to their characteristic Raman peaks of sugars, especially the C-O-C vibrations of the glycosidic bonds and sugar rings (873cm^{-1}, 1065cm^{-1}) (Stone *et al.*, 2004, Notingher, 2007, Ilin and Kraft, 2014).

Table 4-1- Main peak assignments for Raman spectra (Ilin and Kraft, 2014)

Peak cm-1	Assignment			
	Nucleic acids	**Proteins**	**Lipids**	**Carbohydrates**
622		C-C twist Phe		
645		C-C twist Tyr		
669	T, G			
719			C-C-N+	
729	A			
746	T			
754		Ring breath		
782	U,C,T			
788	C5'-O-P-O-C3'(DNA)			
813	C5'-O-P-O-C3'(RNA)			

832		CCH deformation aliphatic		
853		Ring br Tyr		
873			C-C-N+ sym str	C-O-C ring
937		C-C BK str. A-helix		
980		C-C BK str. β-sheet		
1004		Sym. Ring br Phe		
1034		C-H in-plane Phe		
1065		C-N str		C-O, C-C str
1095	PO_2			
1124		C-N str		
1214		C-C6H5. Phe, Trp		
1240		C-C/C-N str		
1301			C-H vibrations	
1449			C-H vibrations	
1578	G,A			
1600			C=C stretching	
1660-1670		Amide I		

4.1.5 Raman spectroscopy in cervical cancer

In a novel study by Lyng *et al.*, in 2007, the potential use of Raman spectroscopy in the diagnosis of cervical cancer was assessed. In their study, they obtained 40 human samples, 20 normal and 20 diagnosed with invasive carcinoma. Of the 20 diagnosed with cervical cancer, 10 had regions of cervical intraepithelial neoplasia (CIN). It was discovered that the glycogen contributions from the normal samples are absent in the carcinoma samples. This is due to the fact that cervical cells have an abnormally high level of glycogen and with the loss of differentiation during neoplasia this level of

glycogen drops and it can be visualised using Raman spectroscopy. The main peaks that contribute to the glycogen are at $482cm^{-1}$, $849cm^{-1}$ and $938cm^{-1}$ and are due to glycogen skeletal deformation, CCH aromatic deformation and CCH deformation respectively. It was also noted that the invasive carcinoma shows characteristic nucleic acids bands and some of these were identified in the CIN samples. Using the spectral features identified with invasive carcinoma, the sensitivity and specificity values were calculated as 99.5% and 100% for normal tissue, 99% and 99.2% respectively for CIN and 98.5% and 99% respectively for invasive carcinoma. Similar methods have been also used to classify bladder, prostate, breast and basal cell carcinoma (Crow *et al.*, 2005, Haka *et al.*, 2005, Nijssen *et al.*, 2002).

4.1.6 Principal components analysis

The analysis of Raman spectra is often a complicated process involving several detailed steps. In order to extract useful information from the spectra in an objective manner, multivariate statistical techniques can be employed. Principal components analysis (PCA), one of these techniques, was developed at the beginning of the twentieth century (Pearson, 1901) and is a statistical method widely used in the exploratory analysis and establishing predictive models.

PCA consists of several mathematical steps which begins with mean data centering, a process by which the mean or average across each dimension is subtracted from the data for each data dimension. The covariance matrix is then calculated for the data set, which is a measure of the linear relationships between the variables (Figure 4-4). The eigenvectors, which are perpendicular to each other in the data set, are then calculated and each eigenvector has a corresponding eigenvalue. The eigenvector with the highest eigenvalue explains the most variance in the data set and is called the first principal component. The second principal component contains information about the remaining variances and so on for the subsequent principle components. Eigenvectors are organised according to their eigenvalues, from highest to lowest, to give the components in order of significance.

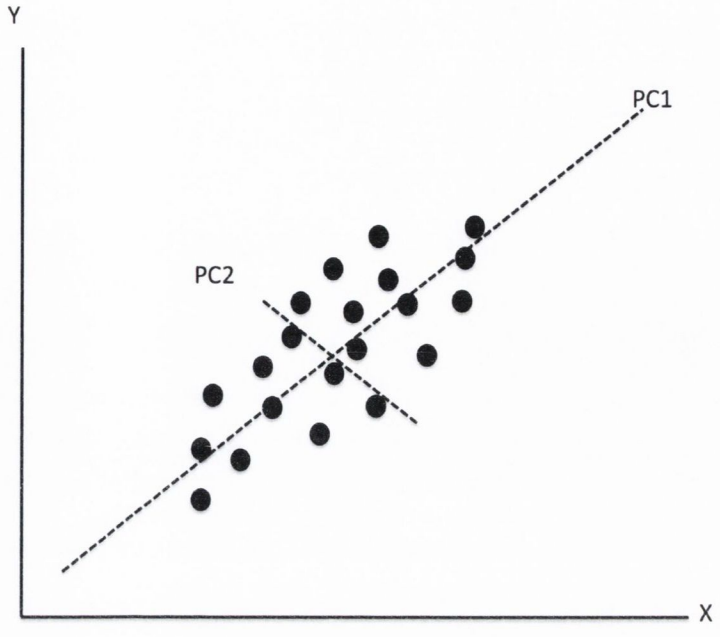


Figure 4-4 Graphical representation of a PCA transformation in only two dimensions.

Rotated coordinate axes (PC1, PC2) capturing the maximum variance of the data set, where X and Y represent variables.

PCA is a very common statistical method used in vibrational biospectroscopy data analysis. The wide range of applications includes diagnostic classification of normal and cancerous cells (Bodanese *et al.*, 2010, Oliveira *et al.*, 2006, Teh *et al.*, 2008). This multivariate statistical technique was also applied in the study of classification of cells under variable influencing factors such as fixation (Meade *et al.*, 2010), drugs (Krishna *et al.*, 2006), viruses (Ostrowska *et al.*, 2010) or photosensitisers (Chio-Srichan *et al.*, 2008). In the present work, PCA was used to investigate the diversity in the spectrum between normal oral cells, dysplastic cell lines and OC cell lines.

4.2 Aims of the chapter

Early diagnosis of OC is of the utmost importance as the 5-year survival rate is extremely low. This is due to the disease being asymptomatic until the latter stages and difficulty in diagnosing the disease at the incipient stage. As mentioned above, Raman spectroscopy has been successfully used to differentiate between other cancer types from normal tissue. It is a non-invasive and rapid technique so it could have the potential to be superior to current diagnostic methods. The aim of this study is to examine if Raman can differentiate between the biochemical signature of cancer, pre-cancerous cell lines and normal cell lines. Specific objectives were as follows;

1. Identify if Raman spectroscopy and PCA can differentiate the biochemical signature from sub-cellular regions (nucleolus, nucleus and cytoplasm) of oral cell lines.

2. Determine if Raman spectroscopy and PCA can discriminate between OC cell lines and isolated normal human primary cells.

3. Investigate if Raman spectroscopy and PCA can differentiate between an OC cell line, a dysplastic cell line and isolated human primary cells.

4.3 Results

4.3.1 Raman analysis of the subcellular regions within human primary oral epithelial cells.

There is an increasing number of studies involving the use of Raman spectroscopy as an optical biopsy method, as the technique is based on optical microscopy, it can also be extended to the analysis of cytological samples at a cellular and subcellular level. The aim of this study was to assess the potential of Raman spectroscopy to differentiate and analyse the biochemical signature from the sub-cellular regions of oral epithelial cells (cytoplasm, nucleus and nucleolus) in a label free manner.

Figure 4-5 shows the differentiation of the subcellular components of a cell captured by Raman spectroscopy. Spectra were captured from the nucleolus, nucleus and cytoplasm from 20 individual cells within each sample preparation. In Figure 4-6 (a, b), the spectra for each sub component before and after the 20 spectra are averaged. Figure 4-6 (d, e, f) shows the individual spectrum for each subcellular component of the cell, each with a degree of similarity but differing in their biochemical make up. Using Raman spectroscopy and PCA analysis it was possible to discriminate between the molecular components of the subcellular regions.

PCA analysis was applied to distinguish all the recognised spectral signals of the subcellular components. The variances captured for the first three principal components (PCs) were as follows- 76.67%, 6.11%, and 2.92%. The results of PCA are demonstrated in Figure 4-7 and show a very good separation of the groups of Raman spectra. The scatterplot includes 60 data points, 20 for each subcellular component. PC1 shows good separation of the nucleus and nucleolus from the cytoplasm. No separation of the nuclear components by the first component would be expected, as they are both very similar in their molecular structure. PC2 shows good separation of the nucleus from the nucleolus, however. PC3 does not show any separation of the subcellular regions.

Differences in loading, with assignments of the main peaks, contribute to discriminate between the data (Figure 4-8). The scatterplots show that PC1 separates the cytoplasm from the nuclear structures. The positive peaks represent the nuclear components and the negative peaks are the cytoplasmic components. The nuclear components show an increase in nucleic acid and proteins. This is shown by the band at 788cm^{-1}, related to O-P-O stretching of DNA and nucleic acids in general, the band at 1033cm^{-1}, related to C-H in phenylalanine vibrational modes and can be found in proteins in general, the band at 1220cm^{-1}, related to A (adenine), G (guanine) vibrational modes of nucleic acids and C-H stretching from protein, the bands at 1480/1578cm^{-1}, related to adenine guanine and C-H deformation from nucleic acids vibrational modes and the band at 1680cm^{-1}, related to Amide I vibrational modes of proteins. The cytoplasmic components show a decrease in lipids and carbohydrates. This includes the band at 717cm^{-1}, related to $CN^{+}(CH_3)_3$ stretching of lipids vibrational modes, the band at 1301cm^{-1}, related to CH_2 twists of lipids vibrational modes, the band at 1420cm^{-1}, related to CH_2 deformation from lipids and carbohydrates, the band at 1655cm^{-1}, related to C=C stretching of lipids vibrational modes and the band at 1736cm^{-1}, related to C=O ester lipids vibrational modes.

The PC2 scatterplot shows discrimination between the nucleus and nucleolus. The positive peaks represent the increase in nucleolar components and the negative peaks represent the decrease in nuclear components. An increase in the contributions of nucleic acids, carbohydrates and lipids is seen in the nucleolus. This is shown by the band at 788cm^{-1} which represents an increase in the O-P-O stretching in DNA, the band at 1301cm^{-1} which represents an increase in the CH_2 twist in lipids and the band at 1420cm^{-1} which is a CH deformation in carbohydrates and lipids. There is only a single decreasing peak in the nucleus which is at1680cm^{-1}, which represents a decrease in Amide I proteins [represented by the C=O stretching vibrations (70-85%) and by the C-N groups (10-20%].

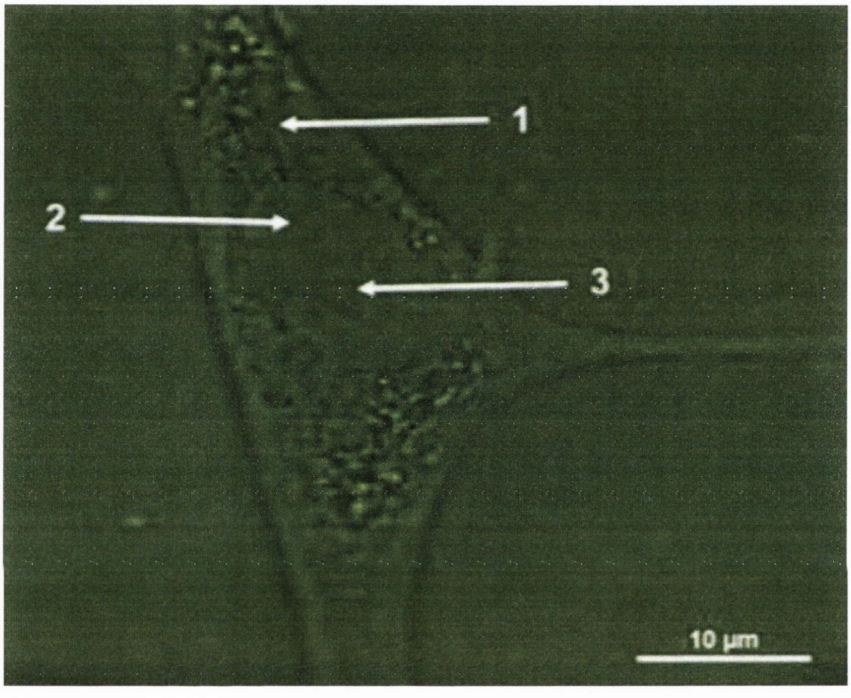


Figure 4-5 Image of a human primary cell captured by the Raman microscope video system. (1) Cytoplasm, (2) Nucleus, and (3) Nucleolus.

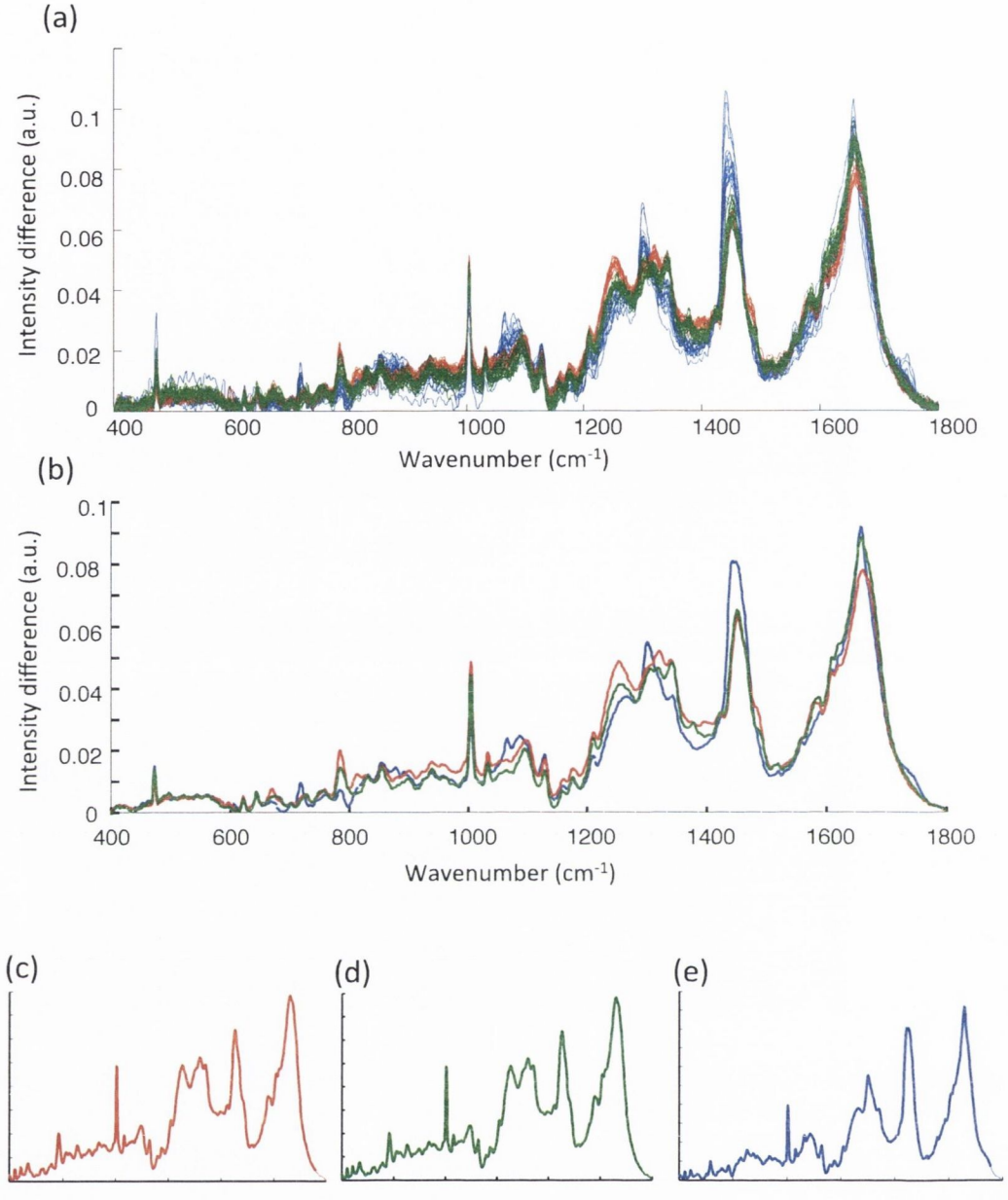


Figure 4-6 Capturing the Raman spectra of the nucleolus, nucleus and cytoplasm of OSCC cells.

(a)-Twenty different spectra were obtained from each sub cellular component, nucleolus (c) (red), nucleus (d) (green), and cytoplasm (e) (blue). (b) The mean of each spectrum was calculated using Matlab software. Each sub cellular component spectra differentiates relative to the molecular components within that part of the cell. The differences were analysed in detail using in house DIT Matlab scripts.

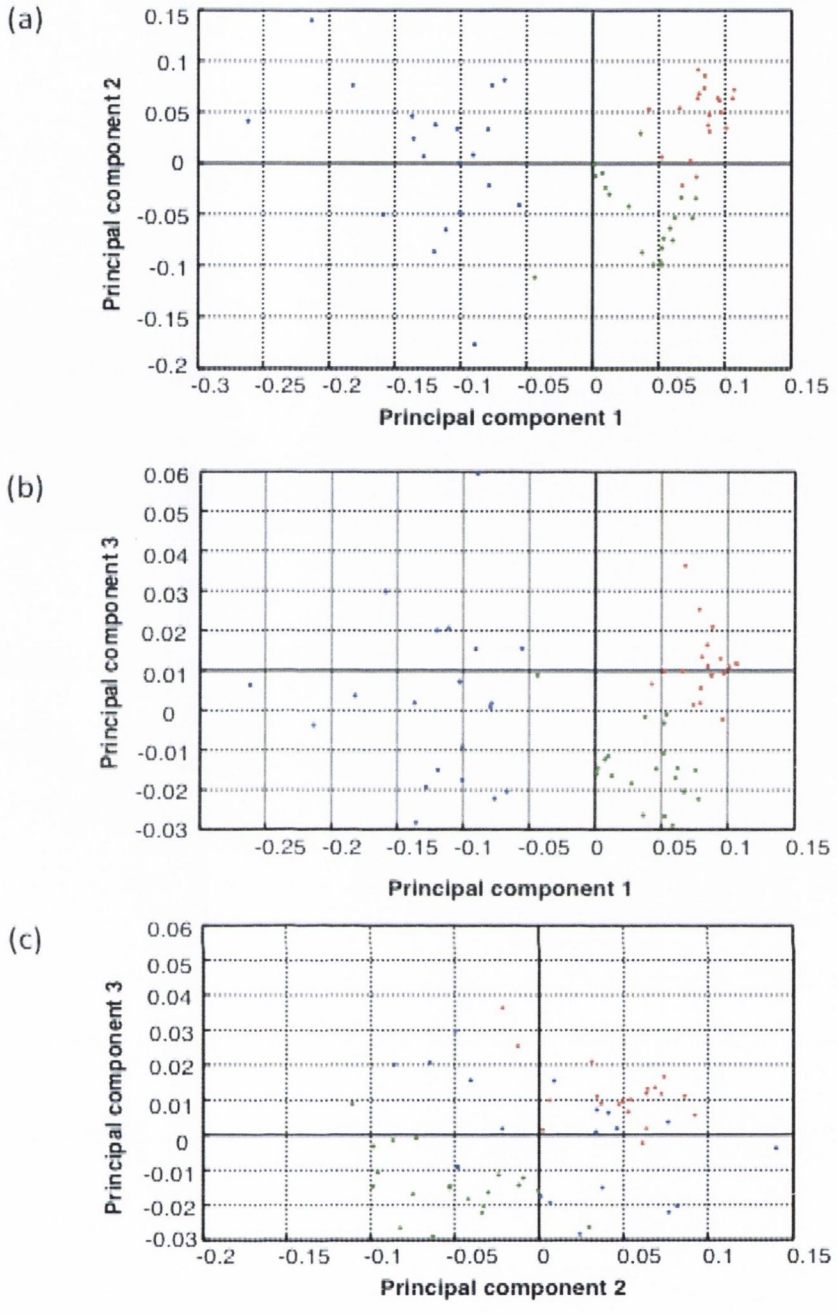


Figure 4-7 Comparisons of the subcellular regions using Principal Component Analysis scatterplots.

The nucleolus (red) and the nucleus (green) can be separated from the cytoplasm (blue) using PC1 (a). PC2 (c) shows a good separation of the nucleus from the nucleolus.

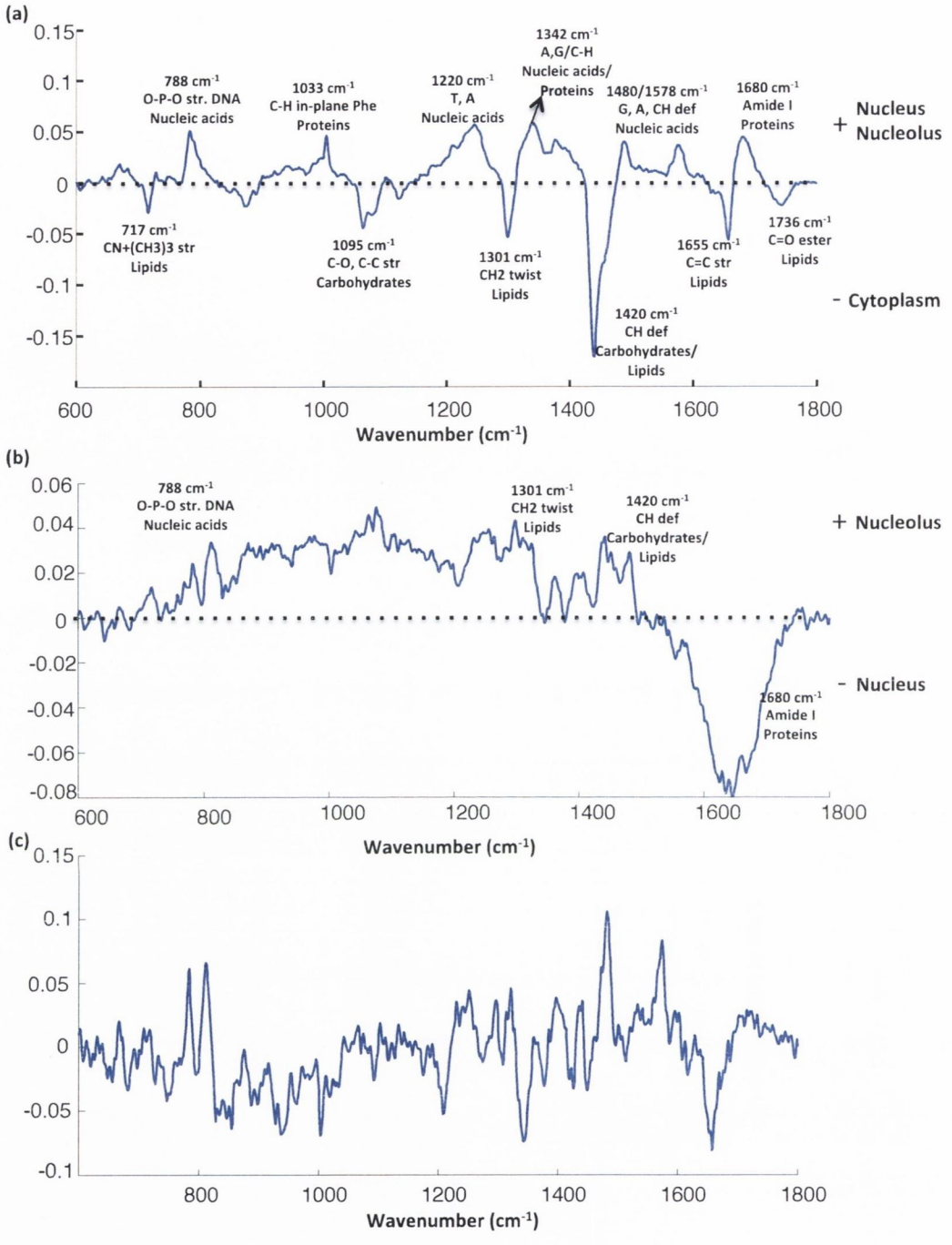


Figure 4-8 Principal component loadings demonstrating the main peaks contributing to discrimination between the subcellular regions.

Loading plots of PC1 (a), PC2 (b), and PC3 (c). PC1 show the differences between the nuclear components and the cytoplasm as confirmed using the scatterplots in Figure 4-7. PC2 displays the loading changes between the nucleolus (positive) and the nucleus (negative).

4.3.2 Determination and analysis of the variation between Raman spectra of human OC cell lines and human primary oral mucosal cells.

The previous section shows that Raman spectroscopy can be used to differentiate between sub cellular components within a single cell. To further expand the potential for the use of Raman in OC, investigations were undertaken to determine whether Raman spectroscopy can differentiate between sub cellular components of OC cells and normal healthy cells. Raman spectra were obtained from 20 individual cell samples in one culture dish from the nucleolus, nucleus and cytoplasm of Ca9.22, TR146 and human primary oral cells. Data was processed using Matlab scripts and protocols developed in-house at Dublin Institute of Technology (Appendix 2). Pre-processing of each Raman spectra was carried out prior to statistical analysis. This included baseline correction and averaging each cell lines total spectra for further analysis. After pre-processing the spectra, PCA was applied to the data set. PC1 was not included in this study it was found to show solely water contributions from the cells (Figure 4-9). The variances captured for the first four PCs are listed in Table 4-2.

%	Nucleolus	Nucleus	Cytoplasm
PC1	84.87	62.52	67.76
PC2	4.19	11.18	17.78
PC3	2.47	4.44	3.96
PC4	1.60	2.88	2.69

Table 4-2: Variances for principal component analysis for the respective cellular regions in TR146, Ca9.22 and human oral primary cells.

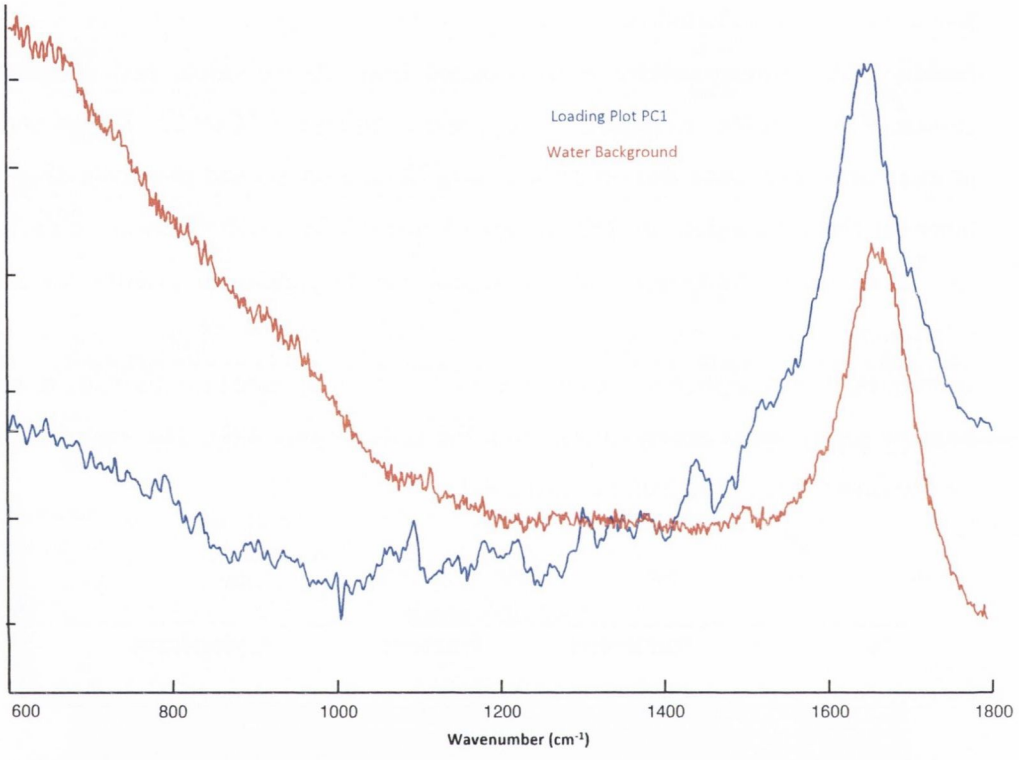


Figure 4-9 PC 1 shows major contributions from the water background.

For this reason PC1 was excluded from further analysis.

4.3.2.1 Nucleolus

Raman spectra from the nucleolus were pre-processed prior to PCA (Figure 4-10). PCA analysis was applied to distinguish all the recognised spectral signals of the nucleolus in TR146, Ca9.22 and primary cell lines. PCA analysis (Figure 4-11) shows a very good separation of the cell types of Raman spectra. The scatterplot includes 60 data points, 20 for each cell type. PC2 shows good separation of TR146 and Ca9.22 from primary cells. PC3 shows no separation of any of the cell types. The 3D scatterplot clearly defines the boundaries of the cancer and non-cancer cell types. Loadings, with assignments of the main peaks contribution to discrimination between the data sets, are presented in Figure 4-12. From the scatterplots, it can be shown that PC2 discriminates the cancer cell types from the normal cells. The positive peaks represent the cancer components and the negative peaks are the normal cell components. The molecular changes associated with the cancer cells are nucleic acids and proteins. The cancer components show an increase in nucleic acids and proteins. This is shown with the band at 813cm^{-1}, related to O-P-O stretching of RNA and nucleic acids in general, the band at 1004cm^{-1}, related to phenylalanine vibrational modes and can be found in proteins in general, the band at 1342cm^{-1}, related to A (adenine), G (guanine) vibrational modes of nucleic acids and C-H stretching from protein, the band at 1480cm^{-1}, related to adenine guanine vibrational modes and the band at 1680cm^{-1}, related to Amide I vibrational modes of proteins. The normal cell components show a decrease in lipids and proteins. This includes the band at 717cm^{-1}, related to $CN^{+}(CH_3)_3$ stretching of lipids vibrational modes, the band at 1301cm^{-1}, related to CH_2 twists of lipids vibrational modes, bands between 1510-1580cm^{-1}, related to Amide II vibrational modes, and the band at 1736cm^{-1}, related to C=O ester lipids vibrational modes.

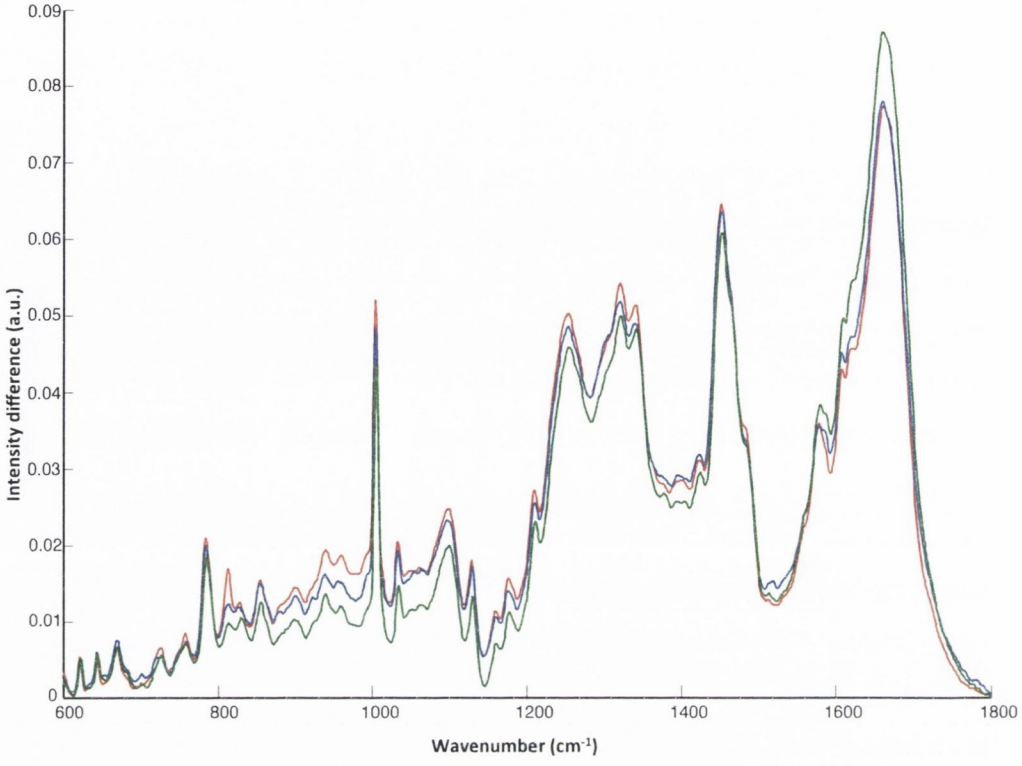


Figure 4-10- Baseline correction of Raman spectrum of nucleoli of TR146, Ca9.22 and primary oral epithelial cells.

Total average spectra from 20 nucleoli from each cell type. Baseline correction was applied as in Section 4.3.1 and the mean was calculated prior to further analysis. TR146 cells (red), Ca9.22 cells (green) and primary cells (blue).

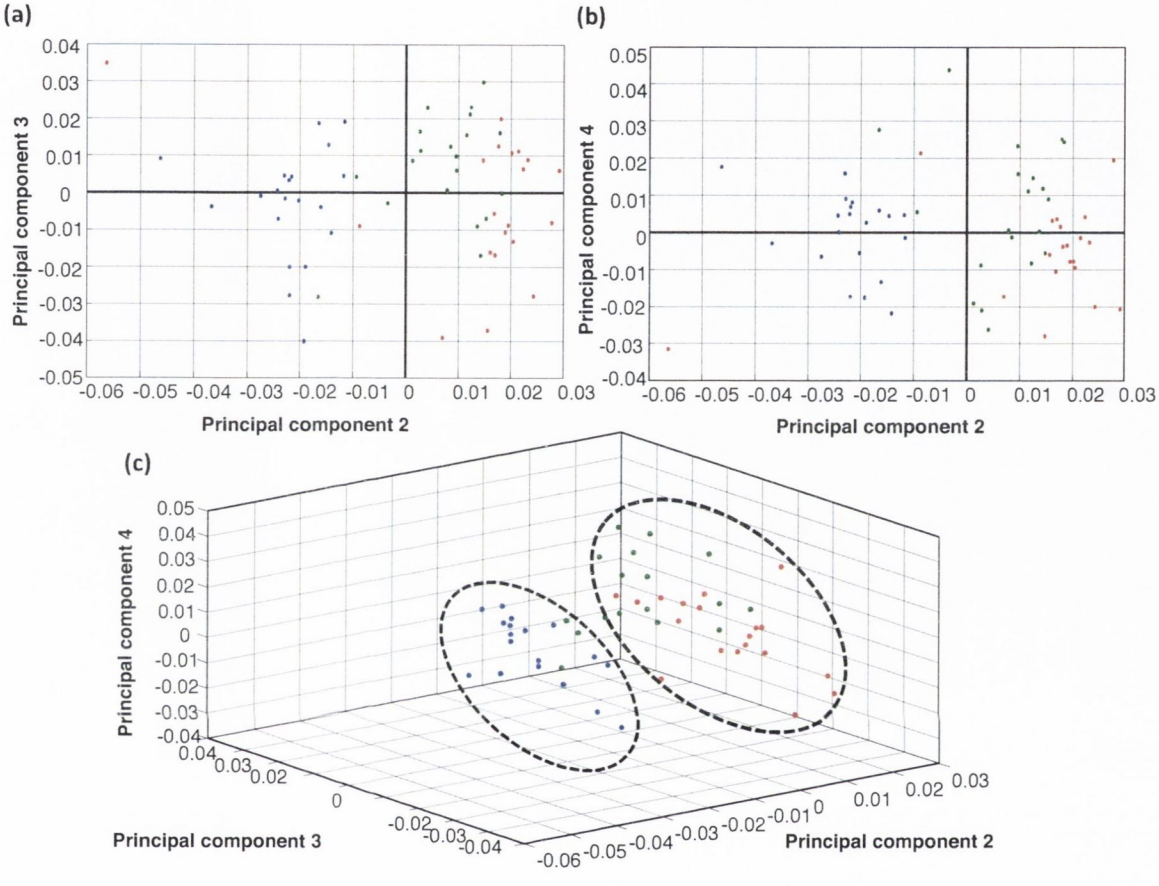


Figure 4-11 Principal component scatterplots of nucleoli of TR146, Ca9.22 and primary oral epithelial cells.

TR146 cells (red) and the Ca9.22 cells (green) can be distinguished from the primary cells (blue) using PC2 (a). PC3 (a) and PC4 (b) do not separate the cell types, although the 3D scatterplot (c) using PC2, PC3, and PC4 shows the separation of the primary cells from the cancer cells lines.

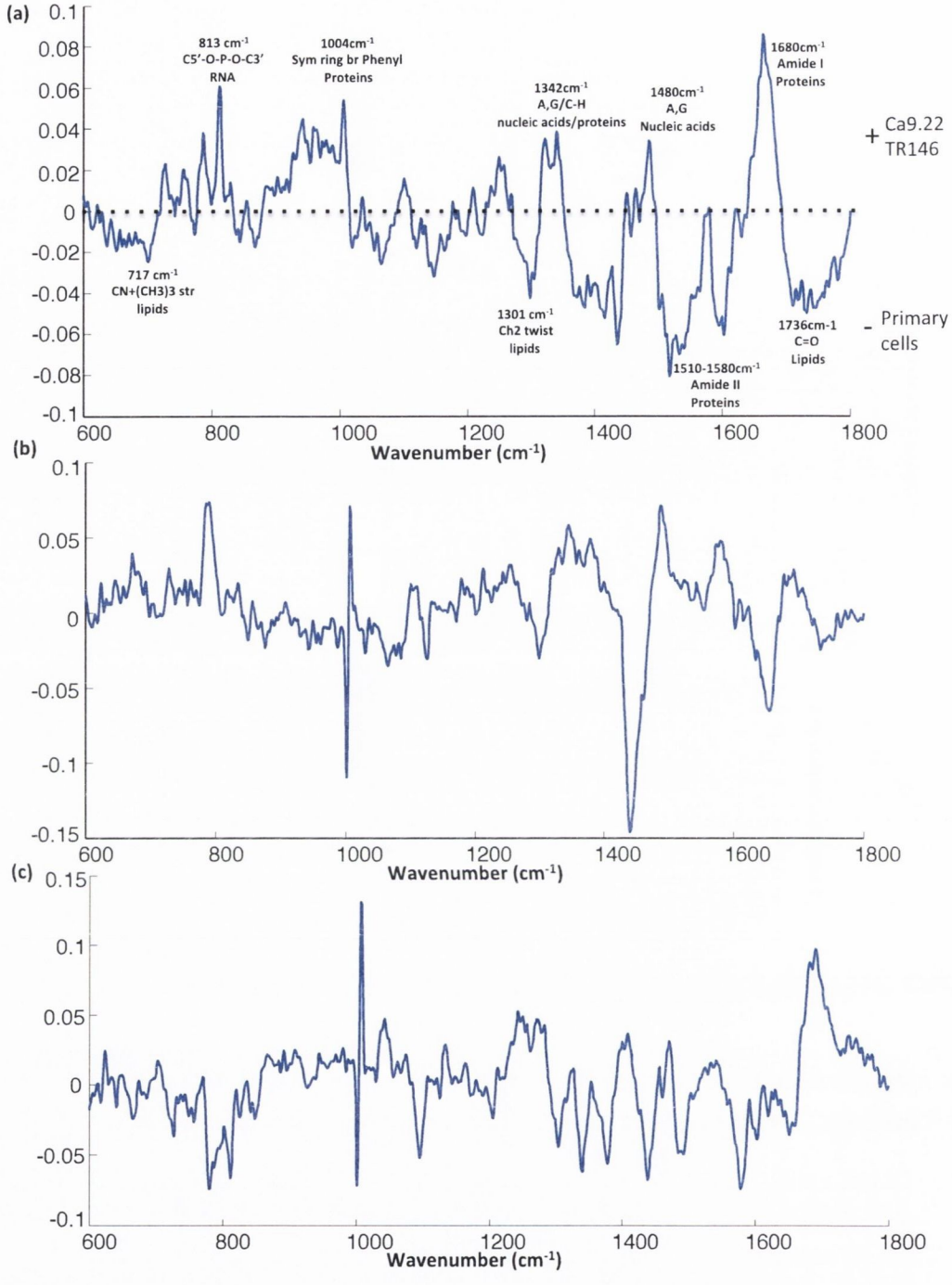


Figure 4-12 Principal component loading controls of nucleoli of TR146, Ca9.22 and primary oral epithelial cells.

Loading plots of PC2 (a), PC3 (b) and PC4 (c). PC2 shows the changes between the TR146/Ca9.22 cells and the primary cells. PC3 and PC4x show no loading variations between the samples.

4.3.2.2 Nucleus

Raman spectra from the nucleus were pre-processed prior to PCA (Figure 4-13). PCA analysis was applied to distinguish all the recognised spectral signals of the nucleus in TR146, Ca9.22 and primary cell lines. PCA of the nucleus is shown in (Figure 4-14) and shows a good separation of the Raman spectra for each cell type. The scatterplot includes 60 data points, 20 for each cell type. PC2 and PC3 both show good separation of TR146 and primary cells from Ca9.22 cells. PC4 does not show good separation of the cell types however inclusion of PC4 in the 3D scatterplot clearly defines the boundaries of the nuclear components of the Ca9.22 from the TR146 and primary cell type. Loading with assignments of the main peaks contribution to discrimination between the data sets are presented in Figure 4-15. The scatterplots separate the TR146 and normal cells from the Ca9.22 cells using PC2 and PC3. The positive peaks represent the TR146 and normal cell components and the negative peaks are the Ca9.22 components. The changes observed in the TR146 and primary cells relate to lipids and nucleic acids. This is observed with the peak at 850cm^{-1}, that represents an increase in tyrosine ring breathing, the peak at 1095cm^{-1} representing an increase in the phosphodioxy group in nucleic acids, the band at 1301cm^{-1}, showing an increase in the CH_2 twist in lipids and the band at 1480cm^{-1} which is an increase in adenine and guanine in nucleic acids. The changes observed in the Ca9.22 cells relate to nucleic acids and proteins. This is shown by the band at 813cm^{-1}, related to O-P-O stretching of RNA and nucleic acids in general, the band at 1004cm^{-1}, related to phenylalanine vibrational modes and can be found in proteins in general, band 1342cm^{-1}, related to A (adenine), G (guanine) vibrational modes of nucleic acids and C-H stretching from protein, the band at 1480cm^{-1}, related to adenine guanine vibrational modes and the band at 1680cm^{-1}, related to Amide I vibrational modes of proteins.

PC3 was also able to separate the Ca9.22 cell line from the TR146 cell line and the primary cells. In this case, the positive peaks represent the Ca9.22 cell line and the negative peaks are the TR146 and primary cell line. As with PC2, the Ca9.22 cells differ from the other cell types in relation to RNA, proteins and nucleic acids. This is shown by the peak at 813cm^{-1}, representing the O-P-O stretching in RNA, the peak at 1004cm^{-1}, representing the symmetric ring-breathing mode of phenylalanine, the peak at 1480cm^{-1}, showing an increase in adenine and guanine in nucleic acids and the peak at 1680cm^{-1},

showing an increase in Amide I proteins. The negative peaks of the TR146/primary cells show changes in nucleic acids, proteins, and lipids. This is shown by O-P-O stretching of nucleic acids at 788cm^{-1}, the deformation and asymmetric deformation of CH_2 and CH_3 respectively, in proteins and lipids at 1398cm^{-1}, and the change in Amide I proteins at 1680cm^{-1}.

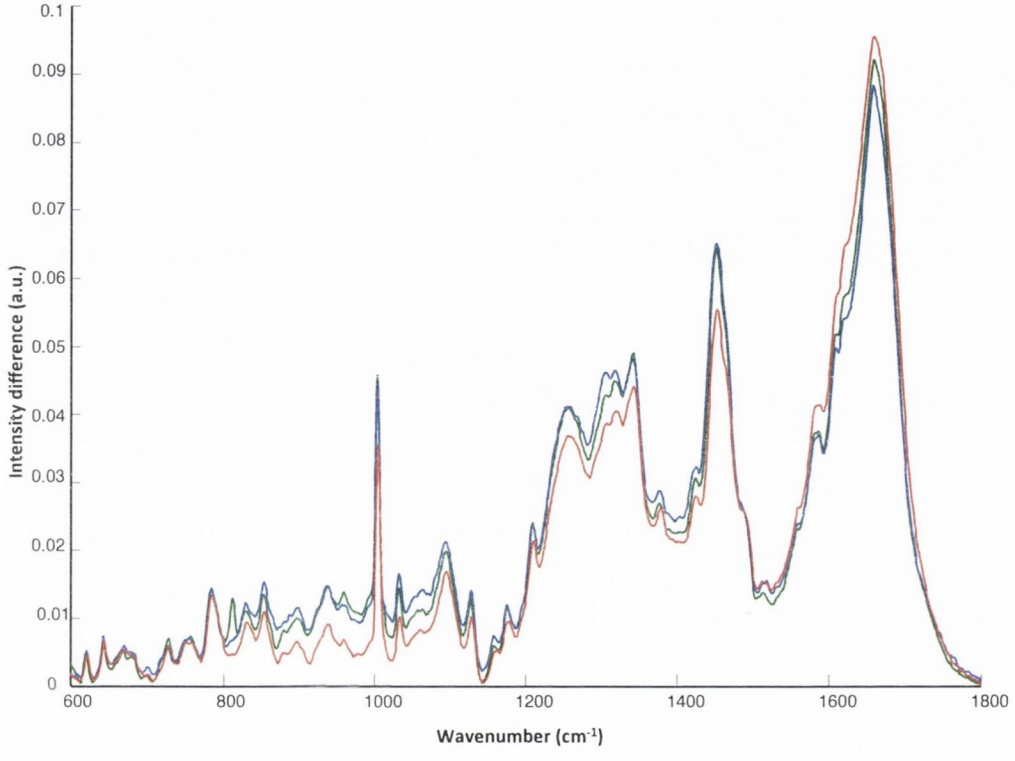


Figure 4-13 Advanced preprocessing of Raman spectrum of nuclei of TR146, Ca9.22 and primary oral epithelial cells.

Total average spectra from 20 nuclei from each cell type- TR146 (red), Ca9.22 (green) and primary cells (blue). Baseline correction was applied as in Section 4.3.1 and the mean was calculated prior to further analysis.

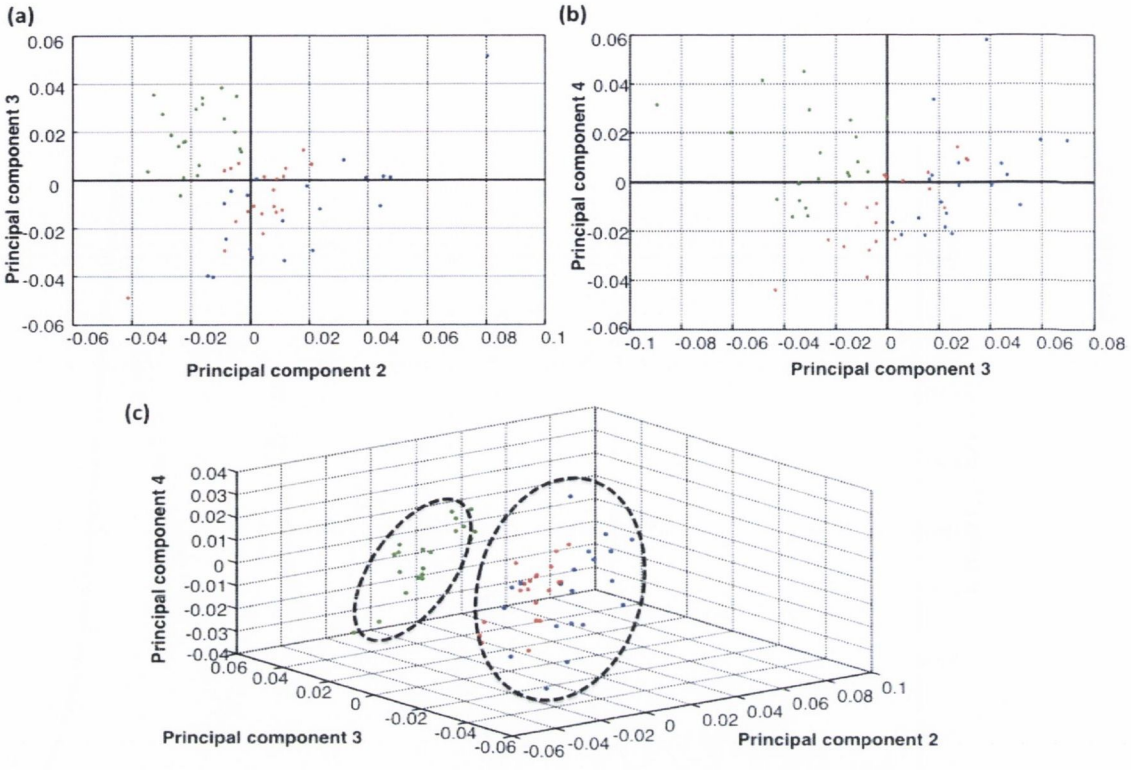


Figure 4-14 Principal component scatterplots of nuclei of TR146, Ca9.22 and primary oral epithelial cells.

Ca9.22 cells (green) can be distinguished from the TR146 cells (red) and the primary cells (blue) using PC2 (a) and PC3 (a). PC4 (b) does not separate the cell types, although the 3D scatterplot (c) using PC2, PC3, and PC4 shows the separation of the Ca9.22 cells from the TR146 and primary cells.

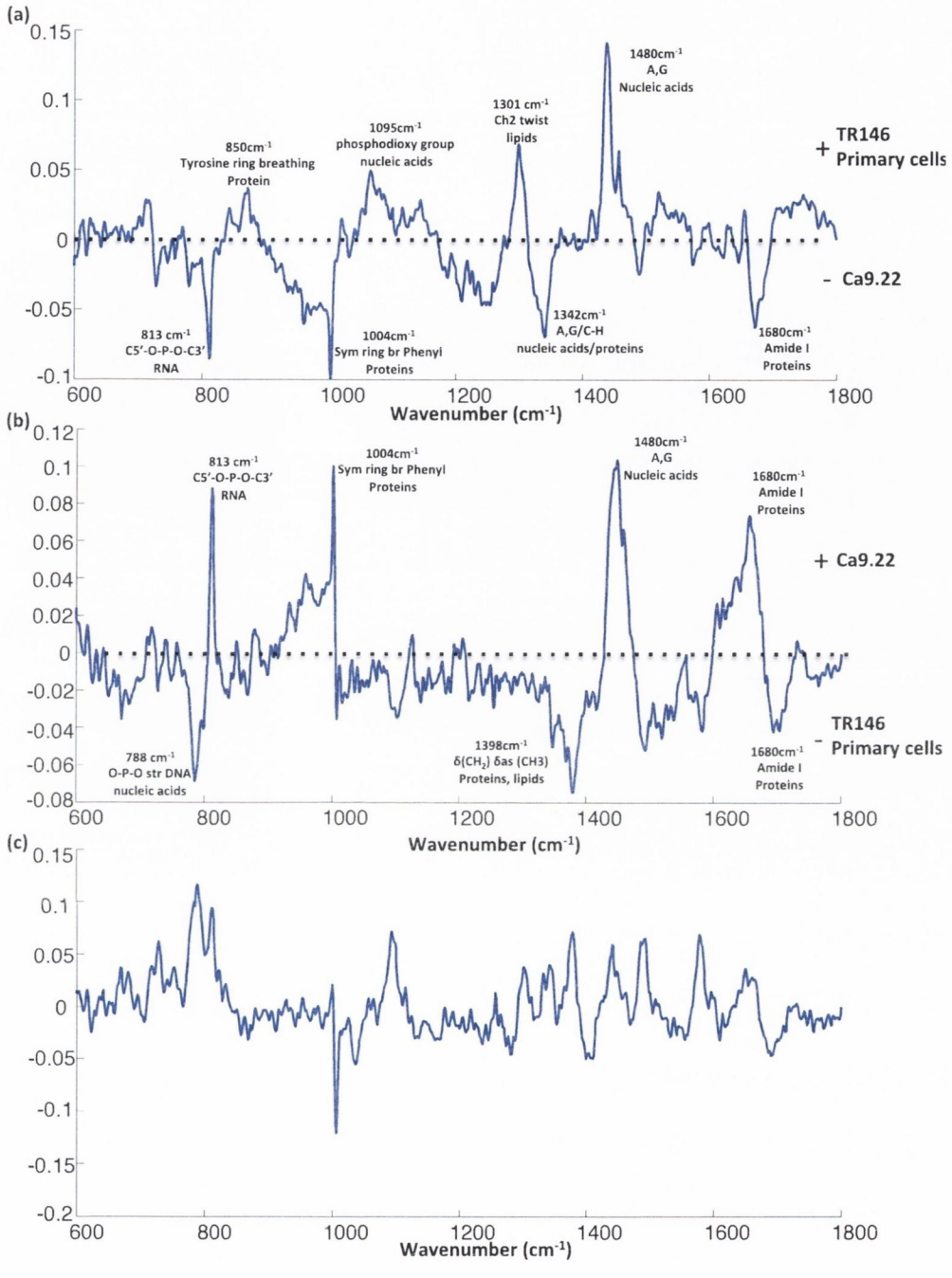


Figure 4-15 Principal component loading plots of nuclei of TR146, Ca9.22 and primary oral epithelial cells.

Loading plots of PC2, PC3 and PC4. PC2 (a) show the differences between the TR146/primary cells (positive) and the Ca9.22 cells (negative). PC3 (b) shows the differences between the Ca9.22 cells (positive) and the TR146/primary cells (negative). PC4 (c) show no changes in loading between the cell types.

4.3.2.3 Cytoplasm

Raman spectra from the cytoplasm were pre-processed prior to PCA (Figure 4-13). PCA analysis was applied to distinguish all the recognised spectral signals of the cytoplasm in TR146, Ca9.22 and primary cell line. The results of PCA are presented in Figure 4-16 and do not show a clear separation of the points. The scatterplot includes 60 data points, 20 for each cell type. The cell types cannot be separated using PC2, PC3 or PC4, although it is clear from the plots that the groups of cells all have different biochemical makeups in their cytoplasm. All cell type boundaries are clearly defined as shown in Figure 4-17. PCs loading plots are shown in Figure 4-18 and, using the data obtained, the scatterplots showed no significant changes in the samples

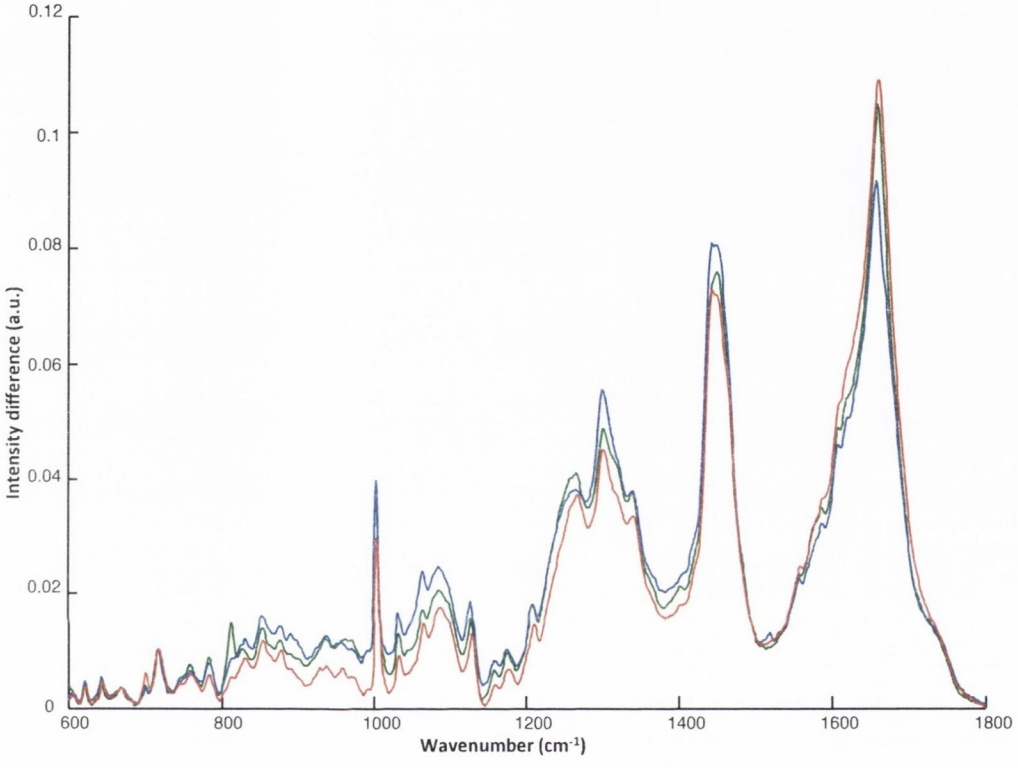


Figure 4-16 Advanced preprocessing of Raman spectrum of cytoplasm of TR146, Ca9.22 and primary oral epithelial cells.

Total average spectra from the cytoplasmic region of 20 cells of each type- TR146 (red), Ca9.22 (green), and primary cells (blue). Baseline correction was applied as in Section 4.3.1 and the mean was calculated prior to further analysis.

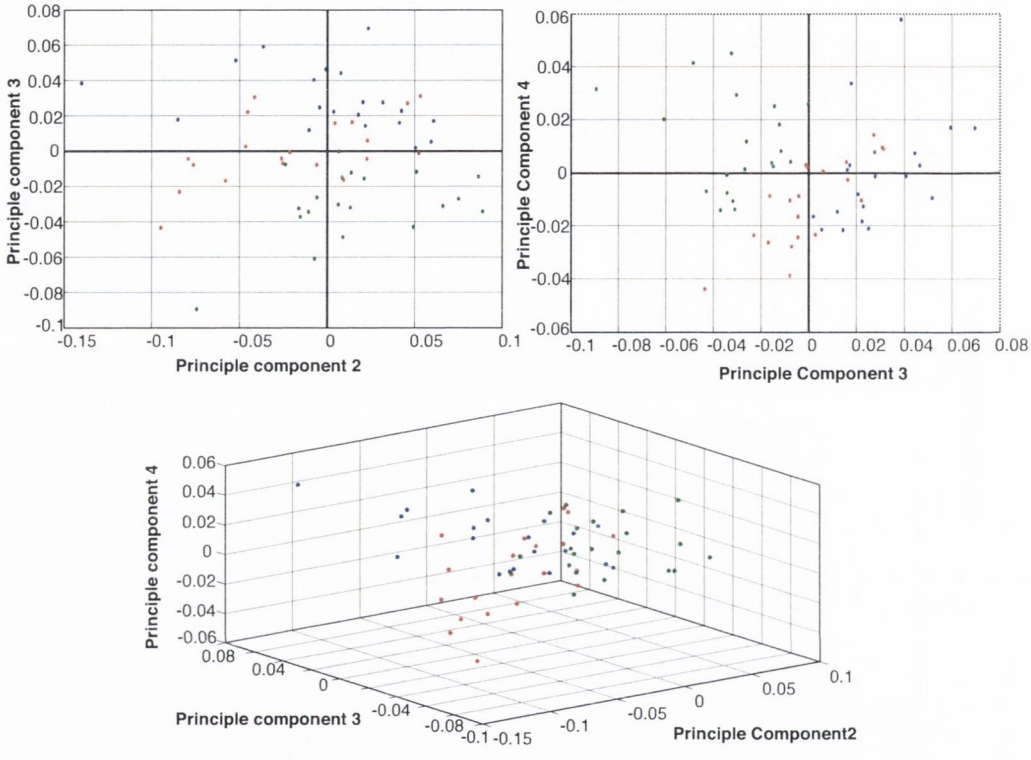


Figure 4-17 Principal component scatterplots of cytoplasm of TR146, Ca9.22 and primary oral epithelial cells.

TR146 cells (red), Ca9.22 (green) and primary cells (blue) have no significant changes in their cytoplasmic make up according to the PC2/PC3 (a), PC2/PC4 (b), and the 3D loading plot (c).

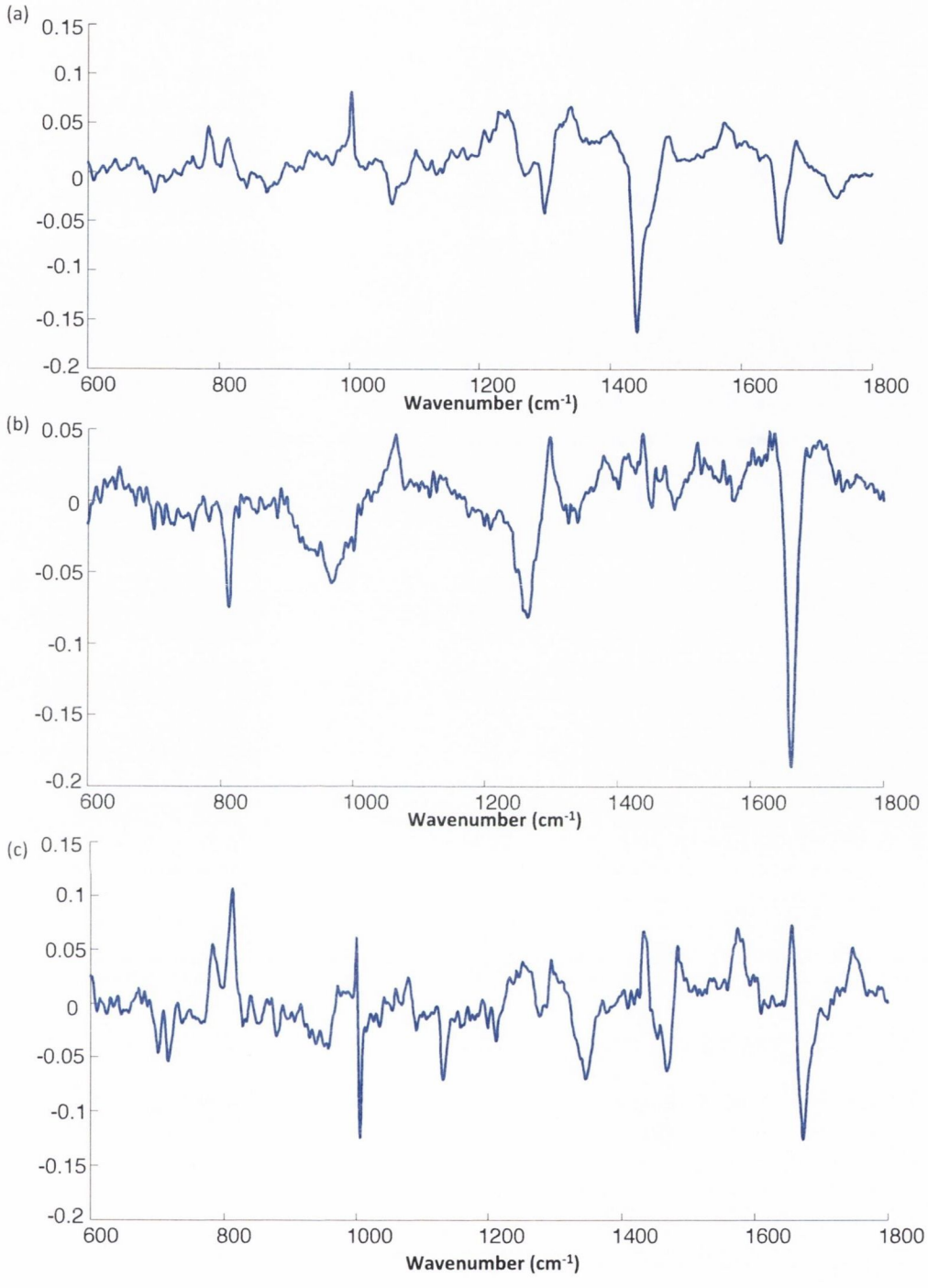


Figure 4-18 Principal component loading plots of cytoplasm of TR146, Ca9.22 and primary oral epithelial cells.

Loading plots of PC1, PC2 and PC3. PC1 (a), PC2 (b) and PC3 (c) show no changes in loading between the cell types.

4.3.3 Raman spectroscopy has potential in differentiation of dysplastic lesions from OSCC

These studies demonstrate that Raman spectroscopy can be used to differentiate between sub cellular components of normal oral epithelial cells and those of OSCC cell lines in relation to both the nucleus and nucleolus. A follow up hypothesis was to determine whether Raman spectroscopy could be used to differentiate dysplastic cells from normal cells and also from OSCC. The dysplastic cell line DOK, is a cell line established from human dysplastic oral mucosa of the tongue which was compared to an OSCC cell type, SCC-4, a cell line also derived from the tongue. The SCC-4 cell line was used as it originated from the same site (tongue) as the dysplastic cell line DOK and so this eliminated any potential site-specific differences from the study. Raman spectra were obtained from 20 individual cells in culture from the nucleolus, nucleus and cytoplasm of DOK, SCC-4 and human primary oral cells. The data was processed using the same in-house protocol as described in Section 4.3.1. As was previously observed PC1 was dominated by the water background, and was thus excluded from the analysis (Figure 4-9). The variances captured for the first four PCs are listed in Table 4.3.

%	Nucleolus	Nucleus	Cytoplasm
PC1	76.08	76.69	63.42
PC2	5.42	6.30	17.72
PC3	4.05	4.05	6.34
PC4	1.65	1.23	2.01

Table 4-3: Variances for principal component analysis for the respective cellular regions in SCC-4, DOK and human oral primary cells.

4.3.3.1 Nucleolus

Raman spectra from the nucleolus of SCC-4, DOK and primary cells were pre-processed and averaged prior to PCA (Figure 4-19). PCA analysis was applied to distinguish all the recognised spectral signals of the nucleolus in these cell lines. The results of PCA are shown in Figure 4-20 and show good separation of the Raman spectra. As before, the

scatterplot includes 60 data points, 20 for each cell type. PCA 2 shows a good separation of the dysplastic DOK cells and SCC-4 tongue carcinoma cells from the normal cells. PC-3 and PC-4 show no significant differences between the cell types. However, the 3D scatterplot including all three PC's clearly defines the boundaries of the nucleolar components with 100% separation between the DOK/SCC-4 and the normal cells (Figure 4-20c) Loadings with assignments of the main peaks contribution to discrimination between the data sets are presented in Figure 4-21. From the scatterplots, it can be seen that PC2 differentiates between the dysplastic and cancer cells from the normal cells. The positive peaks represent the dysplastic/cancer cells and the negative peaks are the normal cell components. The changes in relation to the DOK/SCC-4 are nucleic acids and proteins. The SCC-4 and DOK cells show an increase in the DNA bases adenine and guanine at $1480cm^{-1}$ and an increase in the Amide I proteins at $1680cm^{-1}$. The normal cells show an increase in C-C_6H_5 stretching mode of tyrosine, phenylalanine and tryptophan in proteins as shown by the peak at $1214cm^{-1}$ and also a decrease in the Amide II proteins between $1510\text{-}1580cm^{-1}$.

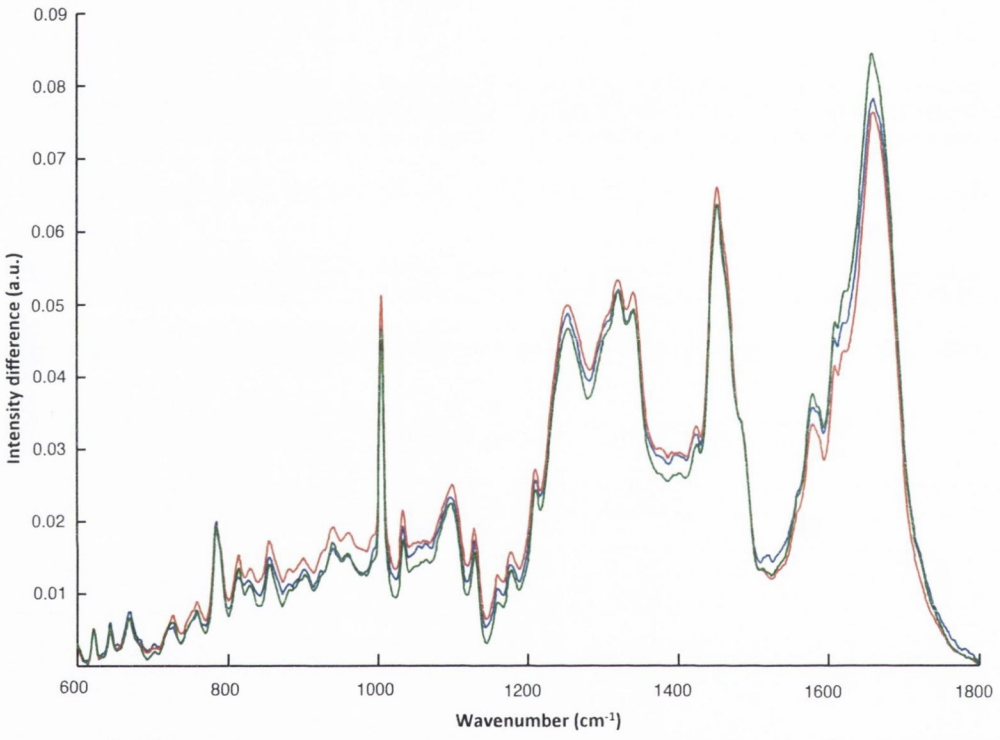


Figure 4-19 Advanced preprocessing of Raman spectrum of nucleolus of SCC-4, DOK and primary oral epithelial cells.

Average of 20 spectra from the nucleolus of each cell type- SCC-4 (red), DOK (green) and primary cells (blue). Baseline correction was applied as in Section 4.3.1 and the mean was calculated prior to further analysis.

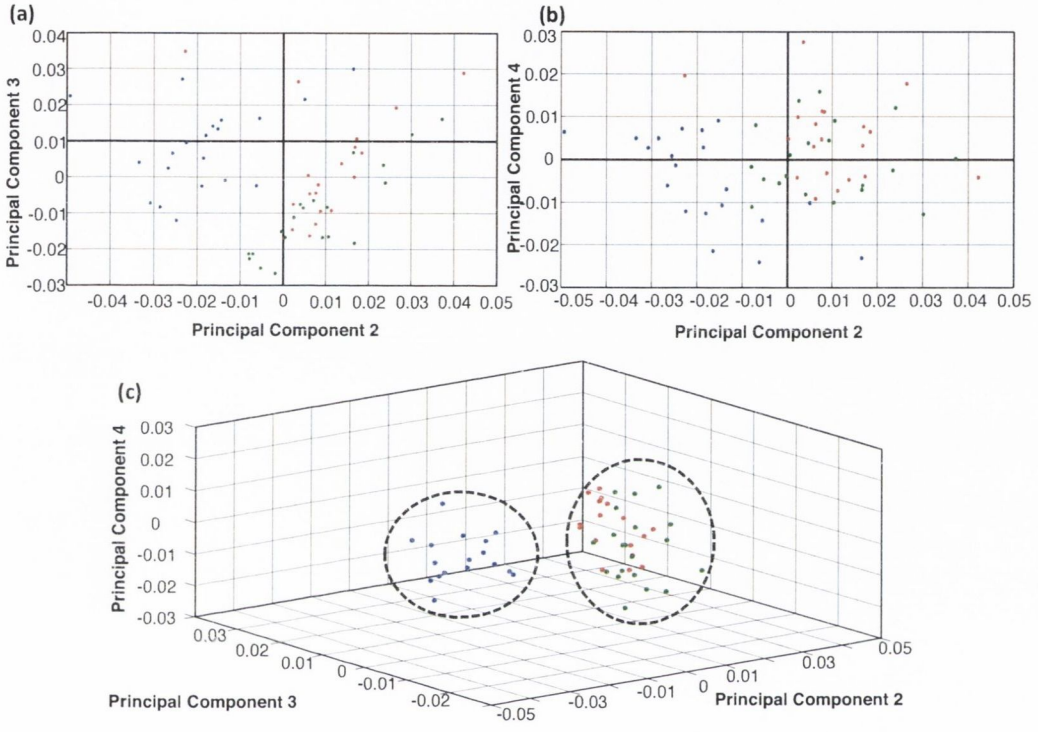


Figure 4-20 Principal component scatterplots of nucleolus of SCC-4, DOK and primary oral epithelial cells.

SCC-4 cells (red) and the DOK cells (green) can be separated from the primary cells (blue) using PC2. PC2 and PC4 do not separate the cell types however the 3D scatterplot using PC2, PC3, and PC4 shows 100% separation of the primary cells from the cancer/dysplastic cells lines.

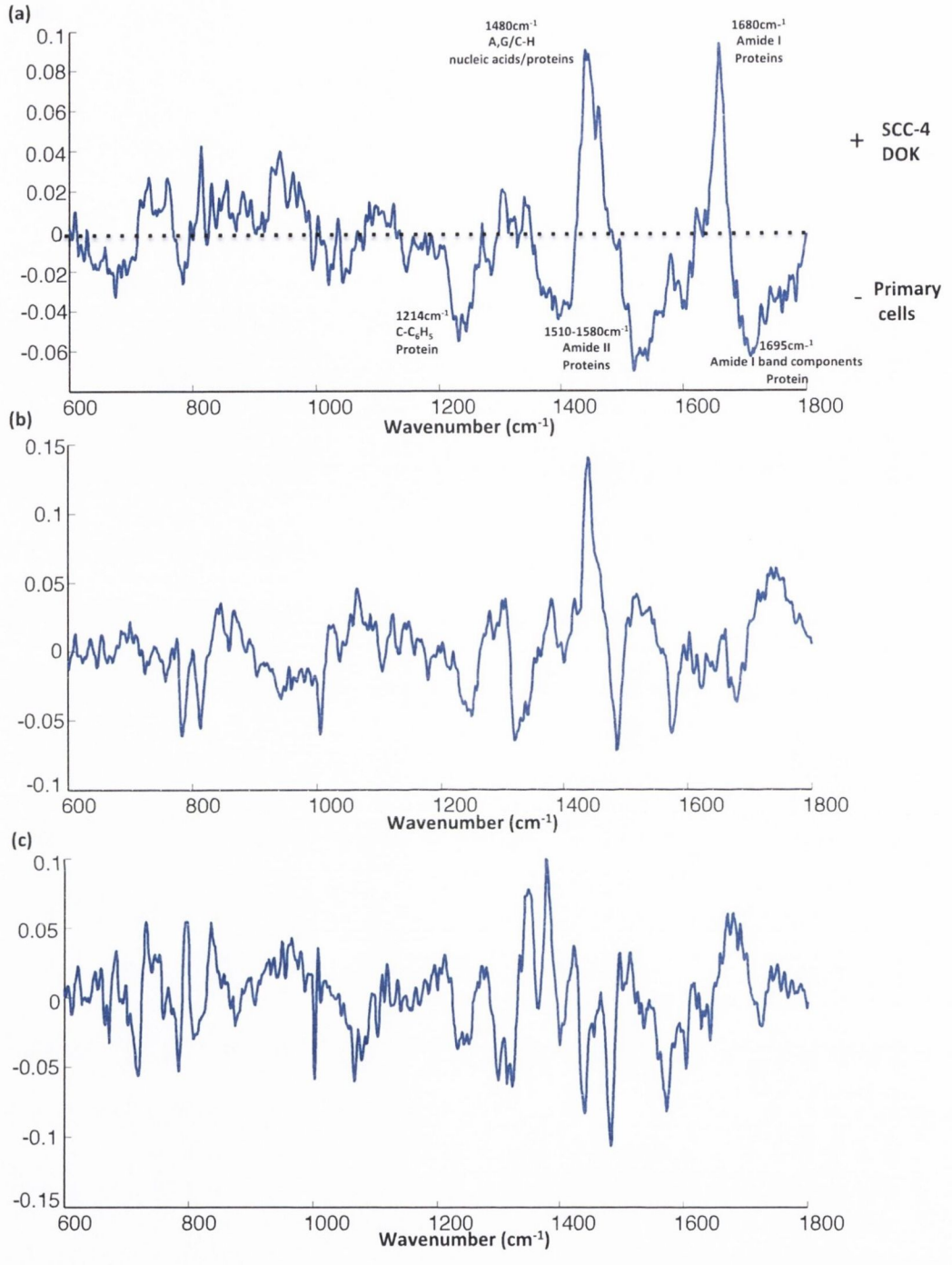


Figure 4-21 Principal component loading plots of nucleolus of SCC-4, DOK and primary oral epithelial cells.

Loading plots of PC1, PC2 and PC3. PC1 shows the changes between the SCC-4/DOK cells and the primary cells. PC2 and PC3 show no loading variations between the samples.

4.3.3.2 Nucleus

Raman spectra from the nucleus of SCC-4, DOK and primary cells were pre-processed and averaged prior to PCA (Figure 4-22). PCA analysis was applied to distinguish all the recognised spectral signals of the nucleus in SCC-4, DOK and primary cells. The results of PCA are demonstrated in Figure 4-23 and show a good separation of the groups of Raman spectra. Each scatterplot includes 60 data points, 20 for each cell type. PC2 and PC4 do not show good separation of the cell types. PC3 shows good separation of the normal cells from the SCC-4 and DOK cell lines. Loadings with assignments of the main peaks contribution to discrimination between the data sets are presented in Figure 4-24. The positive peaks in PC3 represent the DOK/SCC-4 components and the negative peaks are the normal cell components. DOK/SCC-4 cells show a change in protein levels. This is shown with the band at 937cm^{-1}, related to C-C backbone stretch in the α-helix of proteins, the band at 1004cm^{-1}, related to phenylalanine vibrational modes and can be found in proteins in general and the band at 1680cm^{-1}, related to Amide I vibrational modes of proteins. The normal cell components show a decrease in lipids and nucleic acids. This includes the band at 788cm^{-1}, related to O-P-O stretching of DNA, the band at 1095cm^{-1}, related to the phosphodioxy group of nucleic acids, bands at 1301cm^{-1}, related to CH_2 twist of lipids and 1438cm^{-1}, related to the deformation and asymmetric deformation of lipids vibrational modes.

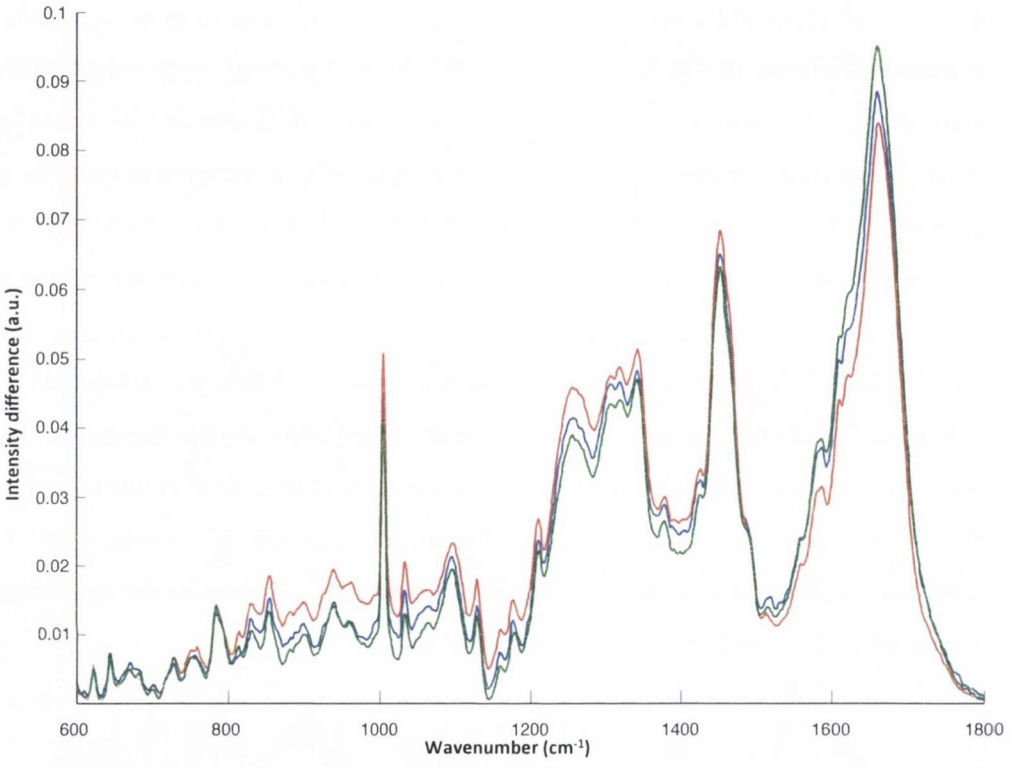


Figure 4-22 Advanced preprocessing of Raman spectrum of nucleus of SCC-4, DOK and primary oral epithelial cells.

Average of 20 spectra from the nucleus of each cell type. Baseline correction was applied as in Section 4.3.1 and the mean was calculated prior to further analysis.

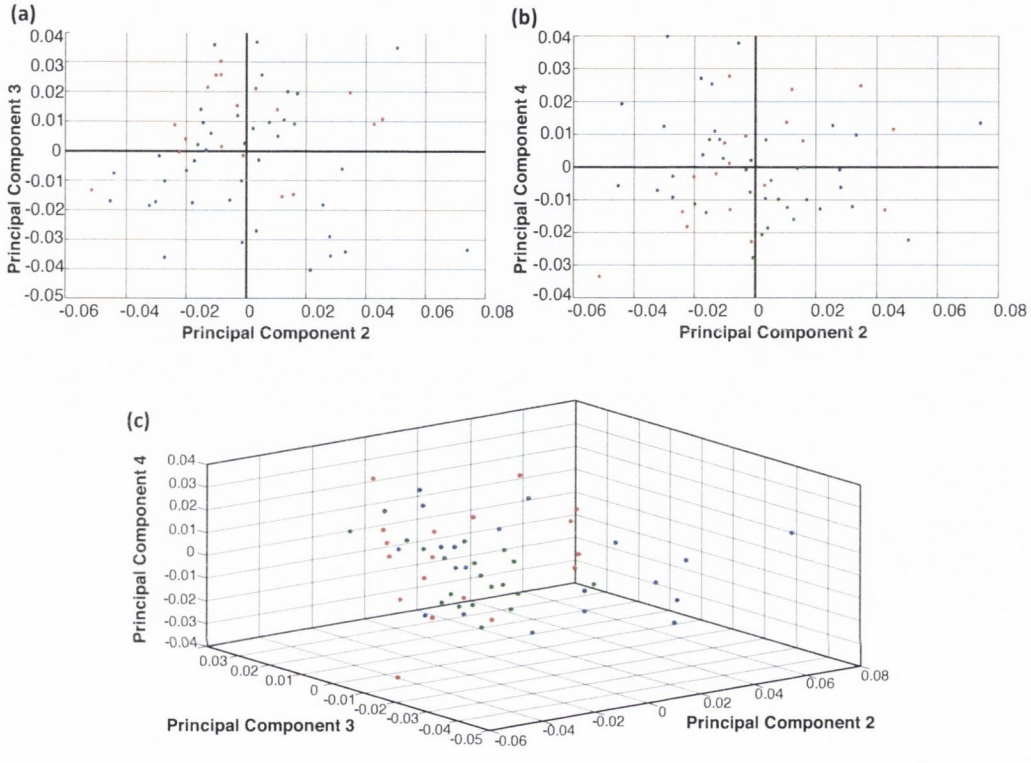


Figure 4-23 Principal component scatterplots of nucleus of SCC-4, DOK and primary oral epithelial cells.

SCC-4 (red) and the DOK (green) cells can be separated from the primary cells (blue) using PC3. PC3 and PC4 do not separate the cell types.

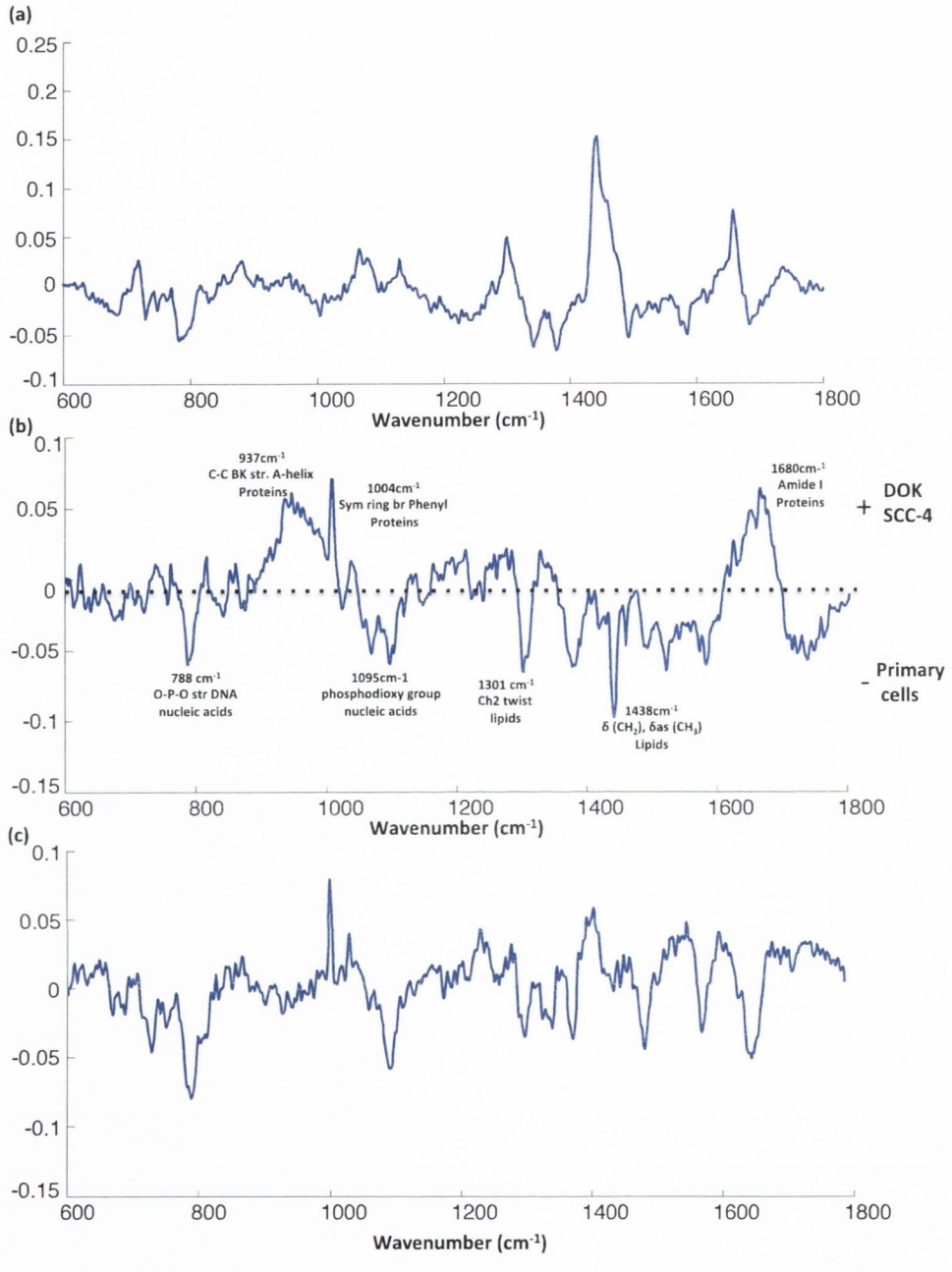


Figure 4-24 Principal component loading plots of nuclei of SCC-4, DOK and primary oral epithelial cells.

Loading plots of PC2, PC3 and PC4. PC2 shows the changes between the SCC-4/DOK cells and the primary cells. PC2 and PC4 show no loading variations between the samples.

4.3.3.3 Cytoplasm

Raman spectra from the cytoplasm were pre-processed prior to PCA as before (Figure 4-25). PCA analysis was applied to distinguish all the recognised spectral signals of the cytoplasm in SCC-4, DOK and primary cells. The results of PCA are demonstrated in Figure 4-26 and show a good separation of the groups of Raman spectra. Each scatterplot includes 60 data points, 20 for each cell type. PC2 shows good separation of the SCC-4 cells from the DOK cells and PC3 shows good separation of the normal cells from the DOK/ SCC-4 cells. Loadings with assignments of the main peaks contribution to discrimination between the data sets are presented in Figure 4-27. The positive peaks in PC2 represent the SCC-4 components and the negative peaks are the DOK cell components. SCC-4 cells show a change in protein levels. This is shown with the band 1004cm^{-1}, related to symmetric ring breathing mode of phenylalanine and can be found in proteins in general, bands between 1258-1262cm^{-1} and 1334-1341cm^{-1}, related to Amide III vibrational modes of proteins. The DOK cell components show a decrease in lipids and nucleic acids. This includes the band at 1301cm^{-1}, related to CH_2 twist of lipids, the band at 1438cm^{-1}, related to deformation and asymmetric deformation of lipids, and bands between 1650-1652cm^{-1} related to cytidine and thymidine of RNA/DNA vibrational modes.

The scatterplots were also able to differentiate between normal and DOK cells through PC3. The positive peaks represent the normal cells and the negative peaks represent the DOK cells. The normal cells do not show any increase in biochemical components in relation to the DOK cells but the DOK cells show a decrease in proteins, lipids and nucleic acids in comparison to the normal cells. This is demonstrated by peaks at 959cm^{-1}, which represent a change in the CH_2 rocking of proteins and at 1270cm^{-1}, which indicates a change in the C-N stretching and N-H deformation of α-helix, collagen and tryptophan. It also represents a change in the C=CH_2 deformation of lipids. A decrease in cytidine and thymidine in DNA/RNA is also seen in the DOK cells.

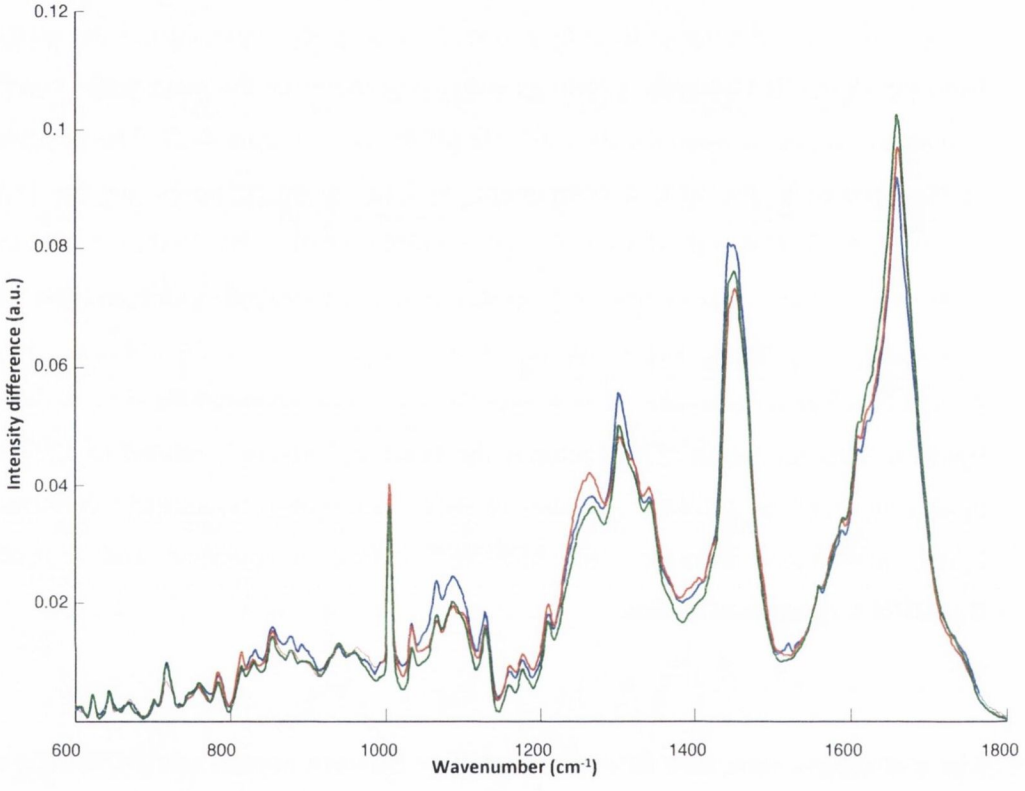


Figure 4-25 Advanced preprocessing of Raman spectrum of cytoplasm of SCC-4, DOK and primary oral epithelial cells.

Total average spectra from the cytoplasmic region of 20 cells of each type. Baseline correction was applied as in section 4.3.1 and the mean was calculated prior to further analysis.

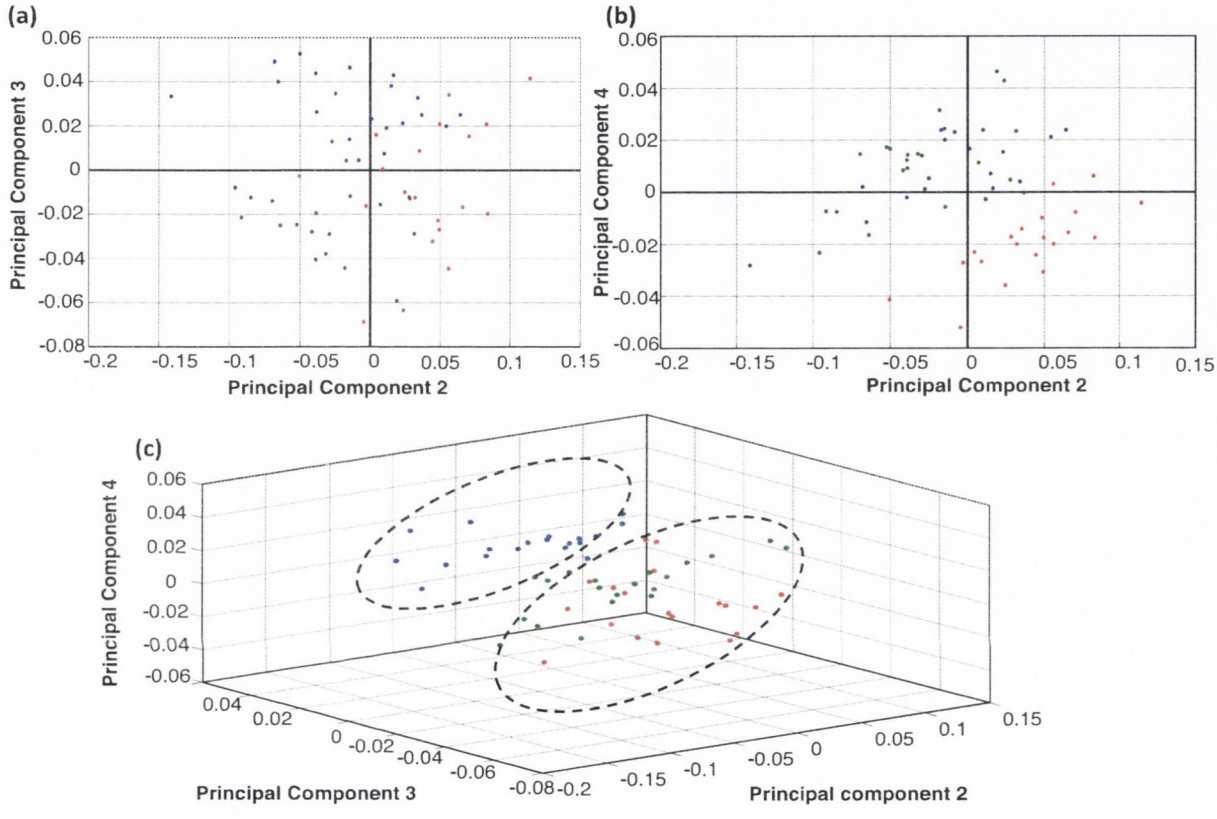


Figure 4-26 Principal component scatterplots of cytoplasm of SCC-4, DOK and primary oral epithelial cells.

SCC-4 (red) and the DOK (green) cells can be separated from each other using PC2. PC3 separates the primary cells (blue) from the DOK cells. PC4 does not separate the cell types however the 3D scatterplot separates the SCC-4/DOK cells from the primary cells.

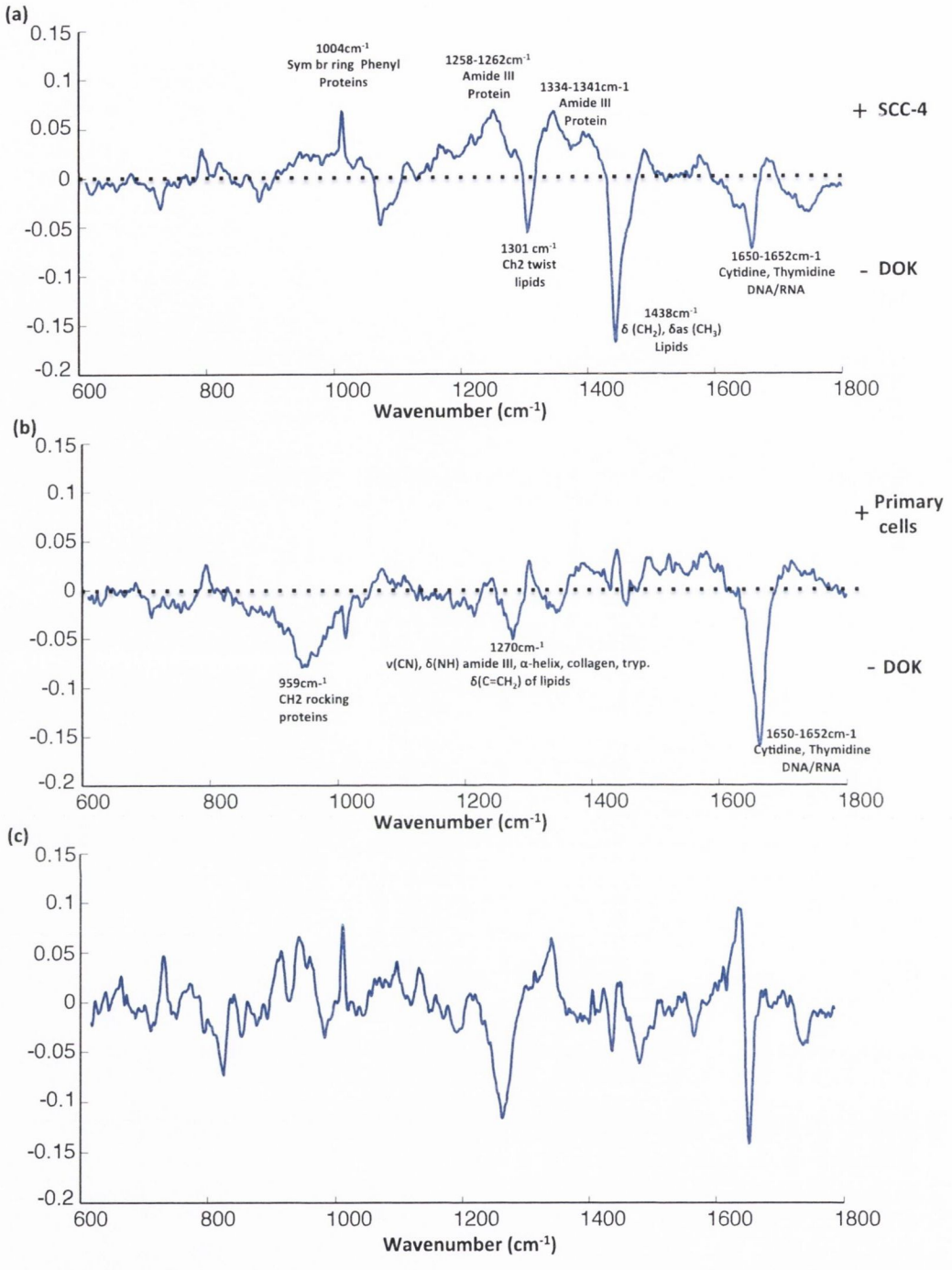


Figure 4-27 Principal component loading plots of the cytoplasm regions of SCC-4, DOK and primary oral epithelial cells.

Loading plots of PC2, PC3 and PC4. PC2 (a) shows the changes between the SCC-4 (positive) and DOK cells (negative). PC3 (b) shows the changes between the primary cells (positive) and the DOK cells (negative). PC4 (c) does not separate the cell types.

4.4 Discussion

There is a substantial amount of evidence indicating that early diagnosis is correlated with increased survival in OC patients (Baykul *et al.*, 2010). Despite the apparent ease with which OCs should be diagnosed, given their probable visibility on examination, many OCs are not identified until the latter stages of the disease resulting in poor prognosis for the patient. Many factors influence the speed at which cancer is diagnosed including a lack of profound clinical presentation. Studies have also shown that there are inconsistent interpretations of what constitutes a precancerous lesion among clinicians (Abbey *et al.*, 1995). The principal methods of OC detection take time and can be quite invasive. Despite a variety of advanced clinical diagnostic techniques, some can prove unreliable and occasionally a small percentage of false positive and negative tests are reported which can be distressing for patients.

Previous studies have indicated the use of Raman spectroscopy as an aid in the diagnosis and treatment of various types of cancer (Crow *et al.*, 2005, Haka *et al.*, 2005, Kast *et al.*, 2008, Lyng *et al.*, 2007). Studies examining the diagnosis of cervical cancer using Raman spectroscopy are in the initial stages, but are looking promising. Studies by Lyng *et al.*, have demonstrated that Raman spectroscopy can be successfully used to classify cervical cancer and pre-cancer with high specificity and high sensitivity, 99% and 99.2% respectively for invasive carcinoma (Lyng *et al.*, 2007). This study set out to build on the premise that this technology is an aid to the quick and accurate diagnosis in cases of OC. The initial findings of this study demonstrate the potential for Raman spectroscopy in the diagnosis, monitoring and treatment of OC in a similar manner to the cervical cancer studies. This study demonstrated that not only could Raman spectroscopy differentiate between different populations of cells in OC; it can also be used to differentiate between different regions within a single cell.

Initial investigations showed that Raman spectroscopy was able to differentiate between the nucleolus, nucleus and cytoplasm of a single oral epithelial cell from a tumour cell line. The nucleus and nucleolus were distinguished from the cytoplasm due to the presence of nucleic acid peaks in the nucleus/nucleolus whereas lipids and carbohydrates dominate the cytoplasm, as shown in Figure 4-8. As expected, the nucleus and

nucleolus contain higher amounts of DNA and RNA than the cytoplasm and the cytoplasm contains higher levels of lipids and carbohydrates. The Raman spectra show up several specific peaks in relation to both nucleic acids and carbohydrates.

This data shows the potential of Raman spectroscopy in analysing specific cellular changes within specific regions in a cell and also relative changes through monitoring fluctuations between defined areas within a cell. Monitoring changes in the cytoplasmic composition of cells potentially undergoing transformation could aid in diagnosing, monitoring and predicating outcomes for patients with OC or dysplastic lesions. Based on this research, a suggested targeted approach to study neoplastic changes in OC cells using Raman spectroscopy would be to monitor specific fluctuations in carbohydrates associated with neoplastic transformations in the cytoplasm. Glucose and lactate have been extensively studied due to the shift in metabolism observed in most cancer cells (Hirschhaeuser *et al.*, 2011). Cancer cells predominately produce their cellular energy ATP by a high rate of glycolysis followed by lactic acid fermentation, in an anaerobic manner known as the Warburg effect (Warburg, 1956). The Warburg effect results in a high level of glucose uptake by the cell and a proportionate level of lactate production. Previous studies using Raman spectroscopy have followed glucose uptake and lactate production to aid the diagnosis of diabetes (Ren and Arnold, 2007). This study reports that the distinguishing bands for glucose in the Raman spectra are centred at $1072cm^{-1}$ and $1128cm^{-1}$, which correspond to C-O stretching and C-O-H bending, respectively. The main peaks for lactate are centred at $845cm^{-1}$ and $1455cm^{-1}$, which correspond to C-$COOO^{-}$ stretching and CH_3 deformation, respectively. Using data from such studies along with the work presented herein may make it possible to detect/analyse small changes in glucose and lactate a goal of predicting potential early pre cancerous changes within a cell.

The two nuclear elements of the cell, the nucleus and nucleolus, can be separated through examination of specific peaks relating to DNA and RNA. The nucleolus contains an increased number of nucleic acids, lipids and carbohydrates (Figure 4-8). These results are in line with expectations, as the laser light must travel through the nucleus when aimed at the nucleolus. This results in an overlap in some components within these structures with the nucleolus spectra containing additional peaks

corresponding to nucleic acids. Given that one of the major neoplastic processes in cancer cells results in an increased nuclear volume, resulting from increased nucleic acid production (Zink *et al.*, 2004), Raman spectroscopy could potentially be used to monitor increases in DNA quantity in pre malignant lesions, thereby predicting a progression towards the uncontrolled growth associated with cancer cells. Not only could Raman spectroscopy be used to monitor increases of nucleic acids, it could also be used to monitor specific changes to the nucleic acids. Previous studies revealed that, using Raman microscopy, it is possible to analyse epigenetic changes that occur in the DNA of the cell (Barhoumi and Halas, 2011). Epigenetic changes occur when there is an alteration of gene expression without modifications in the genetic code. This process is very important in controlling gene expression. However, it has also been shown to strongly correlate with some forms of cancer in humans (Yu *et al.*, 2014). Hypomethylation of DNA in human tumours, hypermethlyation of tumour-suppressor genes and the inactivation of microRNA by DNA methylation are all strong evidentiary factors in the development and progression of human cancers (Ehrlich, 2002). Raman spectroscopy can discriminate between these different chemically modified DNA bases (Barhoumi and Halas, 2011) making it possible (noting the results from this study) to monitor and detect changes in the post translational modifications of DNA in OC to develop a procedure to predict the outcome and survival in patients.

In the next phase of the study, an investigation was undertaken to determine whether Raman spectroscopy could differentiate between subcellular components of cancer cells and normal cells. As mentioned above, Raman spectroscopy has already been shown to identify neoplastic cells in other types of cancer to a high specificity and selectivity and therefore the potential use of Raman spectroscopy in a clinical setting is promising. This study has shown that normal oral cells can be differentiated from two cancer cell lines, the TR146 cell line and the Ca9.22 cell line based on several different parameters. Since the normal cells are easily distinguishable from the cancer cells, the potential for this therapy in an oral medicine setting is high. The sole use of Raman spectroscopy in the future, as a diagnostic technique, is conceivable. However, until then its use in combination with current diagnostic tools is a more realistic approach. Until more detailed development work is carried out confirming the potential of this technique in a clinical setting, samples would still be required to undergo analysis in the laboratory, but future studies could eliminate the need for further examination. The development of an

in-house clinical Raman spectroscopy system could facilitate the diagnosis of OC for the patient.

The main focus of the separation between the two cancer cell lines and the primary cells is within the nucleolus. There is an increase in the amount of RNA, proteins, lipids and nucleic acids within the nucleolus. While it is difficult to determine what exact biochemical components are augmented, is it interesting to note the significant changes between the different types of cells. For several decades the primary function of the nucleolus was thought to be ribosomal transcription. More recently, it has been noted that the nucleolus has a diverse range of functions including controlling cellular functions and it has also been implemented in controlling certain tumour suppressor proteins. Under certain conditions, the nucleolus regulates murine double minute 2 (MDM2), the E3 ubiquitin ligase that negatively regulates p53, a critical tumour suppressor protein (Weber *et al.*, 1999). In doing so, it has a central role in regulating cell cycle progression, senescence and apoptosis. Several studies in recent times have investigated the central role the nucleolus may have to play in malignant transformation and results suggest that several proteins are increased in the nucleolus in cancer cells. The earliest link between the nucleolus and malignant transformation stemmed from the recognition by pathologists that enlarged and/or an increased number of nucleoli were a marker of an aggressive tumour. More recently it has been determined that this increase in nucleoli is due to hyper activated rDNA transcriptions (Ruggero and Pandolfi, 2003). The results presented here support this theory, as the proteins identified in the TR146 and Ca9.22 cells are unregulated in the nucleoli. Further evidence for this observed increase in nucleolar proteins could be due to the fact that the nucleolus has been implicated in controlling several cellular functions including regulation of the cell cycle, DNA replication and repair, stress signalling and induction of apoptosis. Perhaps the most important of the pathways mentioned here is the nucleolar stress pathway, also known as the ribosomal surveillance pathway, in which insults to the nucleolus or ribosomal biogenesis lead to the accumulation of p53. The current proposed mechanism suggests that, under normal physiological conditions, the p53/MDM2 complex is co-exported with ribosomal components to the cytoplasm triggering proteosomal degradation of p53. During times of nucleolar stress, p53 accumulates due to impaired export of the ribosomal proteins. This could explain the observed increase in nucleolar proteins seen in the cancer cells. The p53 protein is mutated in a large majority of all

cancers and between 30-70% of OCs (Acha-Sagredo *et al.*, 2009). The Ca9.22 cell line used for this study contains a mutation in p53. This mutation (R248W) is known as a gain-of-function mutation, as the protein possesses new molecular functions due to the point mutation in the p53 gene. This mutation could affect the nucleolar translocation of the protein causing a build up of the ribosomal proteins.

A further recently discovered function of the nucleolus is the timely retention of proteins in a process known as the nucleolar detention pathway (NoDP) (Audas *et al.*, 2012). In this pathway, the nucleolus affects post-translational modifications by immobilising essential cellular proteins so they are concealed from their targets until the precise time they are required. This is known to occur in the presence of diverse stimuli such as acidosis, heat shock and transcriptional stress (Audas *et al.*, 2012). A novel class of inducible long non coding RNA expressed in distinct loci within the ribosomal intergenic spacer (IGS RNA) have been shown to capture and immobilise molecules within the nucleolus rendering them functionally inert. A possible reason for the increase in the amount of protein within cancer cell nucleoli is due to more proteins being immobilised to interrupt biochemical pathways that control cell division and apoptosis. This increase in protein retention could signify the transformation of normal cells towards a more oncogenic cell type. Therefore, Raman spectroscopy could be used to analyse specific nucleolar changes to deduce deviations that could indicate carcinogenic transformation.

Within the nucleolus of the primary oral cells, there is a decrease in lipids in comparison to the two cancer cell lines. The nucleolus itself has not been found to contain any lipids, nor does it have a lipid membrane. A possible reason for this decrease in lipids could be due in part to the fact that the Raman laser penetrates the nucleus prior to the nucleolus so the lipid peak contribution could be due to the increase in size of the nucleus in cancer cells so therefore more lipid interaction from its lipid membrane.

The separation between the nucleus of cancer cells and the primary cells is not as evidently defined as the spectrum between the nucleoli. Using both principal component 2 and 3, there is a trend in the division between the Ca9.22 and the TR146 and primary

cells. However, using the 3D scatterplot, a clear separation is noted between the two groups of cells (Figure 4-14). This result is interesting to note, in that the TR146 Raman spectroscopy nucleus spectrum is similar to the primary cells but not the other cancer cell line, Ca9.22. There is a broad range of changes in comparison between the cells with regards to nucleic acids, lipids and proteins. The differences between the cells could stem from the fact that the Ca9.22 cells contain a p53 mutation, which, as mentioned before, has a wide range of targets and functions within the nucleus of the cell. This could cause an increase and decrease in the transcription of certain types of proteins, since the p53 protein is a well-known transcription factor. This could be the cause of the variation seen between the cell types.

To further examine the potential for Raman spectroscopy as an early diagnostic tool it is imperative to determine the sensitivity of the system and how early in cellular transformation can the changes described be detected. To achieve this, an examination of dysplastic oral cells was undertaken. Dysplasia is a term used to describe cells that contain abnormalities and is often indicative of early neoplastic changes. Dysplastic lesions are frequent in the oral cavity and it is apparent that as many as 50% of OSCC arise from dysplastic lesions of the oral mucosa (Shafer and Waldron, 1961, Pindborg *et al.*, 1963). There is currently no method of predicting which lesions will progress to OSCC. Raman analysis was utilised in this study to determine if the components of a dysplastic oral cell line (DOK cell line), originating from the tongue could be distinguished from both oral primary cells and an OC cell line (SCC-4).

When comparing the Raman spectra of nucleolar and nucleus components of the DOK, SCC-4 and primary cells, there was significant separation between the primary cells and the DOK/SCC-4 cells when analysing the 3D scatterplot of the nucleolar components and PC3 of the nuclear components of the PCA. Compared to previous results (section 4.3.2), there was a complete separation between the primary cells and the cancer cells. However, it is interesting to note that the dysplastic cell line could not be separated from the OC cell line. While morphological and clinical differences between dysplastic and cancer cells are hard to detect, this suggests that Raman spectroscopy could be used to differentiate more harmful pre cancerous lesions that will go on to develop into OSCC. Further studies with a broad range of mild, moderate and severe dysplasia would be

interesting to determine whether slight changes between the spectra of these cells could be used to predict the outcome for a patient. In contrast, the cytoplasmic spectra from the cell lines differentiate both the SCC-4 from the DOK cells based on PC2 and the primary cells from the DOK cells based on PC3. Although both separations are weak, it is interesting to note the trend. The SCC-4 cells contain higher levels of proteins in the cytoplasm and the DOK cells contain fewer lipids. With regards to the PC3 separation, the DOK cells contain fewer proteins, lipids and nucleic acids in comparison to the primary cells. The broad range of differences between the cytoplasmic components is probably due to fluctuating and variable components within each cell including differences in cell division and growth patterns. The cytoplasm contains a large number of different organelles that could cause a vast number of changes between the cell types.

To conclude, these results show the ability of Raman spectroscopy to detect OC and it could prove useful as a viable diagnostic strategy. Raman spectroscopy can also discriminate between different components of oral cells and detect specific changes within those components. This might lead to insights into the transitions which drive the transformation of the cell into a carcinogenic state and facilitate the examination of the underlying cellular function. Significant clinical interest will no doubt lie in the potential prognostic capability of this technology. To date, there is no method of accurately determining the prognostic significance of an individual lesion in the oral mucosa i.e. will a given lesion resolve to a normal state or continue to transform resulting in tumour formation. Data from this study illustrates that Raman spectroscopy has the potential to distinguish malignant dysplastic cells and possible tumour margins in some cases of OC with the caveat that further examination of clinical samples is required to confirm this finding. The development of clinical Raman instrumentation could decrease the cost of surgical procedures and improve the clinical outcome for the patient. There are technical challenges to be overcome, such as development of easy-to-use software interfaces for clinicians, before Raman spectroscopy can become a standardised clinical tool but the current research looks promising. The presented study has clearly demonstrated that Raman spectroscopy offers potential as a novel technology to assist pathologists and dental professionals with OC screening and diagnosis.

5 Analysis of EtOH induced changes in the biochemical profile of oral epithelial cells using Raman Spectroscopy.

5.1 Introduction

Chapter 3 demonstrated that EtOH produced alterations in ROS levels, antioxidant enzyme expression and perturbations in the cell cycle in OSCC, dysplastic and human primary epithelial cells, which all have the potential to drive oncogenic changes in these cell types. In Chapter 4 Raman spectroscopy was used to differentiate between sub cellular components and it was demonstrated that the technology could differentiate between cells with a cancerous phenotype and wild type normal primary cells based on specific molecular components in these cells. This chapter examines the potential of Raman spectroscopy as tool for following EtOH induced changes in oral epithelial cells.

Recently there has been a lot of interest in using Raman spectroscopy as a diagnostic tool as illustrated in Chapter 4. The Raman spectroscopy fingerprint provides a detailed spectrum of the molecular components of the cells imparting a number of useful functions, many of which are currently underused. The potential of Raman spectroscopy for the analysis of external agents (anti-cancer drugs and nanoparticles) on the cell has been demonstrated (Lin, 2012, Huang, 2012). Recently it has been studied as a tool for monitoring the progress of chemotherapy treatment in leukaemia (Gonzalez-Solis *et al.*, 2014). It can also successfully monitor drug distribution and metabolism in colon cancer cells (El-Mashtoly *et al.*, 2014).

Raman spectroscopy has been shown to monitor detailed changes in the carbohydrates glucose and lactate (Ren and Arnold, 2007). Increased glucose uptake and accumulation of lactate are key signs of cancer metabolism due to a process known as the Warburg effect. The ability to monitor specific changes in cellular metabolites such as glucose and lactate has the potential to aid in the early detection of carcinogenic changes in the cell. Additionally analysing changes to DNA levels and post translational modifications may aid in finding specific biomarkers in OC (Barhoumi and Halas, 2011). Monitoring the changes in OC cell lines, dysplastic cells and primary cells in response to a potential carcinogenic insult, such as EtOH, using Raman spectroscopy has not previously been reported. Raman spectroscopy and principal component analysis could identify potential cellular targets and early cellular changes in response to EtOH within the nucleolus,

nucleus and cytoplasm leading to a better understanding of the processes involved coupled to early diagnosis and improved prognosis for patients.

5.2 Aims of the chapter

Previous work for this thesis has shown that EtOH has significant effects on a number of cellular processes in various oral cell types and that Raman Spectroscopy can discriminate between the subcellular structures in oral cells based on their biochemical makeup. As biochemical variations in the cells were detectable using Raman spectroscopy technology the potential to monitor in-situ changes within a cell using Raman spectroscopy was examined using EtOH as a protagonist given that it has demonstrated potential to exert changes within these cells. This novel study allows for further examination of the effect of EtOH on the oral cell types and to gain a wider understanding of the processes involved and potentially find targets affected by EtOH in the cells. Specific objectives were as follows;

1. Identify changes in the biochemical fingerprint of OSCC cell lines, TR146 and Ca9.22 in response to EtOH exposure using Raman spectroscopy and Principal Component Analysis.

2. Identify changes in the biochemical fingerprint of the dysplastic cell line DOK in response to EtOH exposure using Raman spectroscopy and Principal Component Analysis.

3. Identify changes in the biochemical fingerprint of primary oral epithelial cells in response to EtOH exposure using Raman spectroscopy and Principal Component Analysis.

4. Confirmation of the effect of EtOH on the nucleoli using Raman spectra of TR146 and Ca9.22 cells using fluorescent microscopy.

5.3 Results

5.3.1 Raman analysis of OSCC cellular components after exposure to EtOH

While there are an increasing number of studies analysing the use of Raman as an optical biopsy method in cancer diagnosis it can also be used to monitor and examine biochemical changes that occur within the cell. The aim of this study was to assess the potential of Raman spectroscopy in analysing the effects of EtOH (1% for 24h) on OSCC, TR146 and Ca9.22, to see determine if there is a change in the biochemical signature in sub-cellular regions (nucleolus, nucleus and cytoplasm).

Raman spectra were obtained from 20 individual cell samples in one culture dish from the nucleolus, nucleus and cytoplasm of TR146, Ca9.22 untreated and treated with 1% EtOH. Data was processed using Matlab scripts and protocols developed in-house at Dublin Institute of Technology. Pre-processing of each Raman spectra was carried out prior to statistical analysis. This included baseline correction and averaging each cell lines total spectra for further analysis. After pre-processing the spectra PCA was applied to the data set. PC1 was not included in this study as it was found show solely water contributions from the cells as previously described in Chapter 4. The variances captured for the first four PCs are stated in Table 5-1 (TR146) and Table 5-2 (Ca9.22) below.

%	Nucleolus	Nucleus	Cytoplasm
PC1	84.87	62.52	67.76
PC2	4.19	11.18	17.78
PC3	2.47	4.44	3.96
PC4	1.60	2.88	2.69

Table 5-1 Variances for principal component analysis for the respective cellular regions in TR146 cells treated with and without EtOH.

%	Nucleolus	Nucleus	Cytoplasm
PC1	84.31	61.99	61.40
PC2	4.82	20	17.64
PC3	2.75	3.32	6.09
PC4	1.44	2.63	3.80

Table 5-2 Variances for principal component analysis for the respective cellular regions in Ca9.22 cells treated with and without EtOH.

5.3.1.1 Raman spectroscopy and principal component analysis of TR146 cells after exposure to EtOH

5.3.1.1.1 Nucleolus

Raman spectra from the nucleolus were pre-processed prior to PCA (Figure 5-1). PCA analysis was applied to distinguish all the recognised spectral signals of the nucleolus in TR146 treated with and without EtOH (1% 24h). The results of PCA are presented in (Figure 5-2) and do not show a clear separation of the points. The scatterplot included 60 data points, 20 for each cell type. The cell types cannot be separated using either PC2, PC3 or PC4. Principle loading plots are shown in Figure 5-3 and confirmed using the scatterplots there was no separation between the data sets.

5.3.1.1.2 Nucleus

Raman spectra from the nucleus of the TR146 data sets were pre-processed prior to PCA (Figure 5-4). PCA analysis was applied to distinguish all the recognised spectral signals of the nucleolus in TR146 treated with and without EtOH (1% 24h). The results of PCA are presented in (Figure 5-5) and did not show a clear separation of the points. The scatterplot included 60 data points, 20 for each cell type. The cell types cannot be separated using with PC2, PC3 or PC4. Principle loading plots are shown in Figure 5-6 and as confirmed using the scatterplots there is no separation between the data sets.

5.3.1.1.3 Cytoplasm

Raman spectra from the cytoplasm were pre-processed prior to PCA (Figure 5-7). PCA analysis was applied to distinguish all the recognised spectral signals of the cytoplasm in TR146 treated with and without EtOH (1% 24h). PCA analysis (Figure 5-8) showed a very good separation of the cell types of Raman spectra. The scatterplot included 60 data points, 20 for each cell type. PC4 showed good separation of TR146 data. PC2 and PC3 showed no separation of any of the cell types. The 3D scatterplot clearly defines the boundaries of the treated and untreated cell types (Figure 5-8 (c)). Loading with assignments of the main peaks contribution to discrimination between the data sets are presented in Figure 5-9. From the scatterplots it can be shown that PC4 discriminated the treated cells from the untreated cells. The positive peaks represent the control cells and the negative peaks are the treated cells. The molecular changes associated with the control cells were proteins while the treated cells showed a decrease in nucleic acids and lipids. The increase in molecular components in controls cells is shown by the band 1004cm^{-1} related to phenylalanine vibrational modes and can be found in proteins in general and band 1214cm^{-1} related to phenylalanine and tryptophan. The decrease shown with the treated cells included band 669cm^{-1} related to thymine and guanine in nucleic acids, band 813cm^{-1} related to the C5'-O-P-O-C3' phosphodiester bonds in RNA and band 1449cm^{-1} related to the C-H vibrations in lipids.

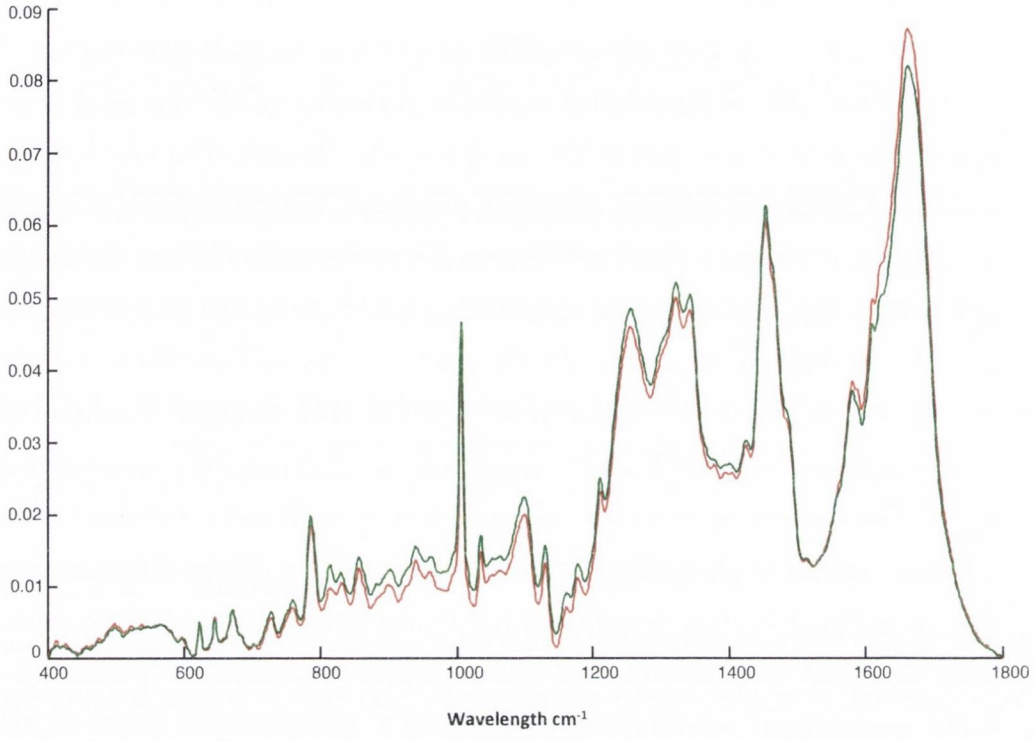


Figure 5-1 Advanced preprocessing of Raman spectrum of the nucleoli of untreated and treated TR146 cells.

Total average spectra from 20 nucleoli from each cell type. Baseline correction was applied as described in Chapter 4 and the mean was calculated prior to further analysis.

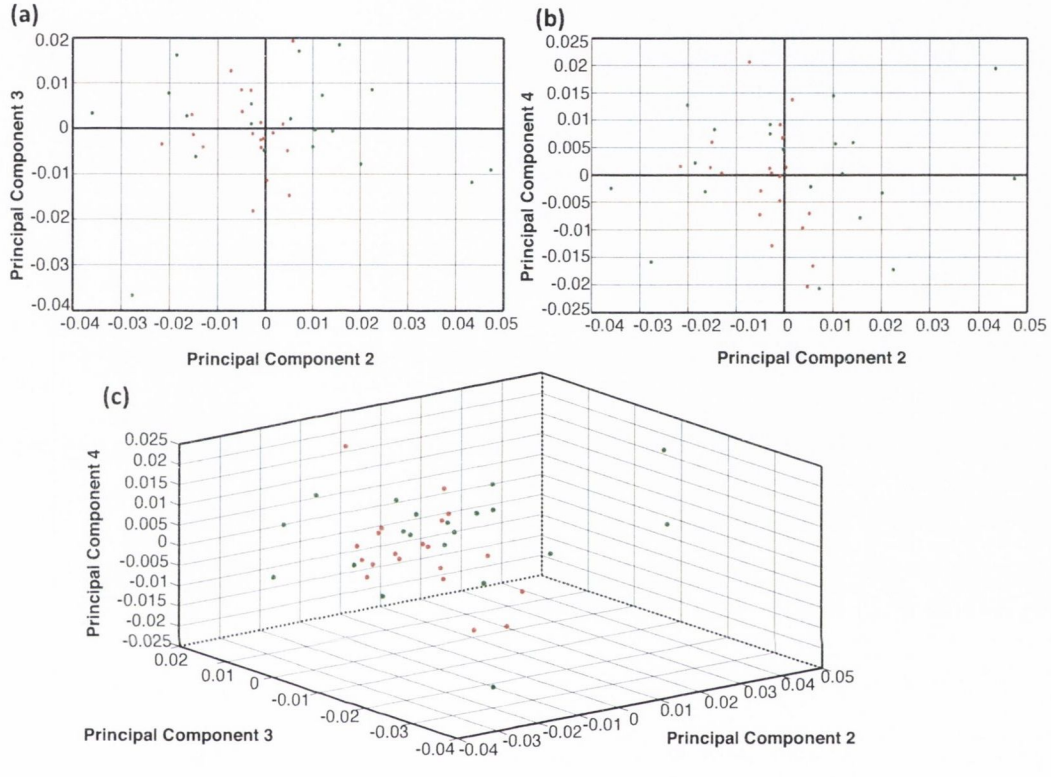


Figure 5-2 Principal component scatterplots of the nucleoli in untreated and treated TR146 cells.

PCA scatter plot showing the nucleoli Raman Spectra spread of points between the untreated cells (green) and the treated cells (red). There is no difference between the groups of points which means EtOH has no effect on the nucleoli after 24h treatment with PC2, PC3, or PC4.

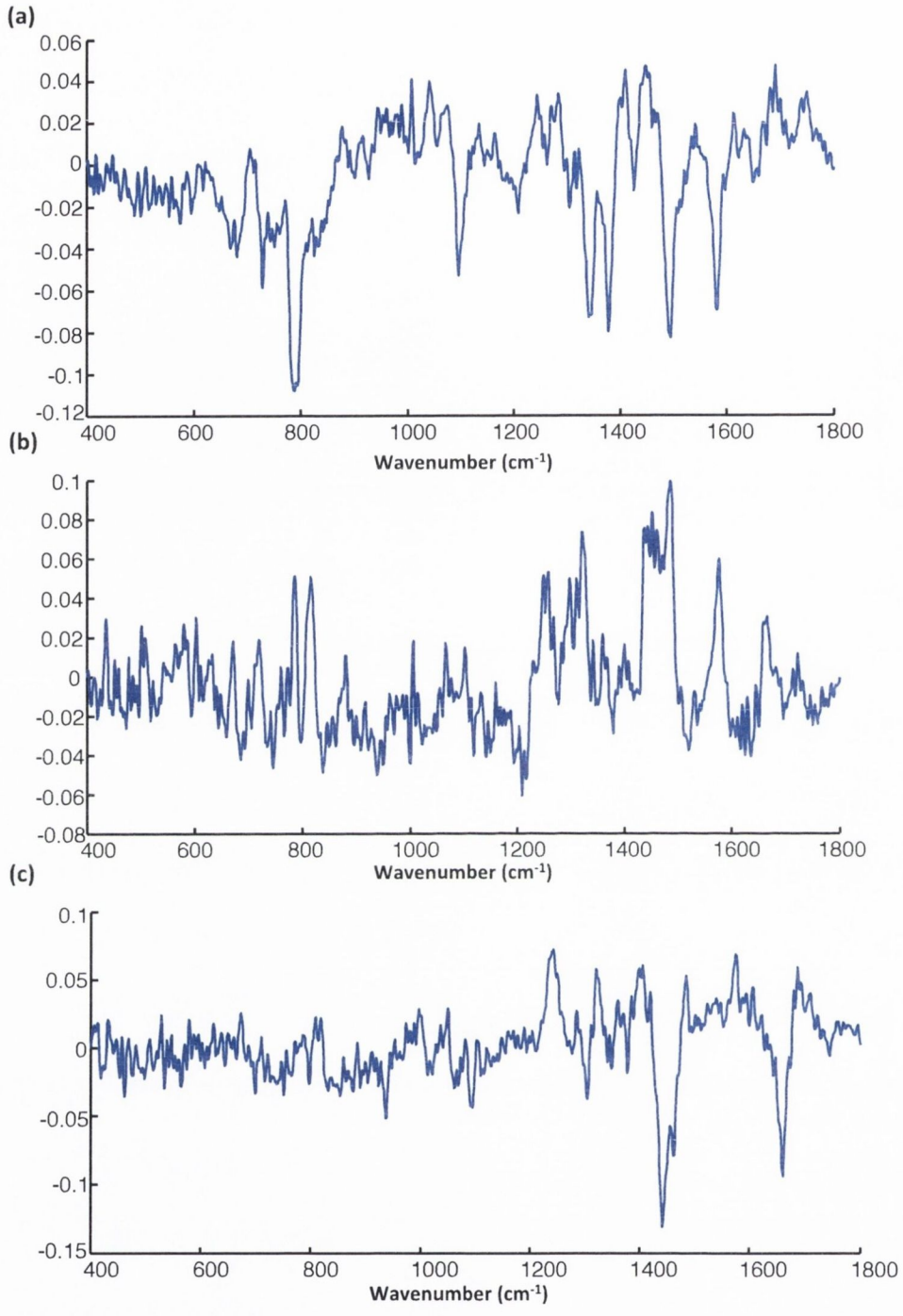


Figure 5-3 Principal component loading plots of untreated and treated nucleoli of TR146.

Loading plots of PC2 (a), PC3 (b) and PC4 (c). As shown in the PCA scatter plots there is no changes between the TR146 cells and treatment.

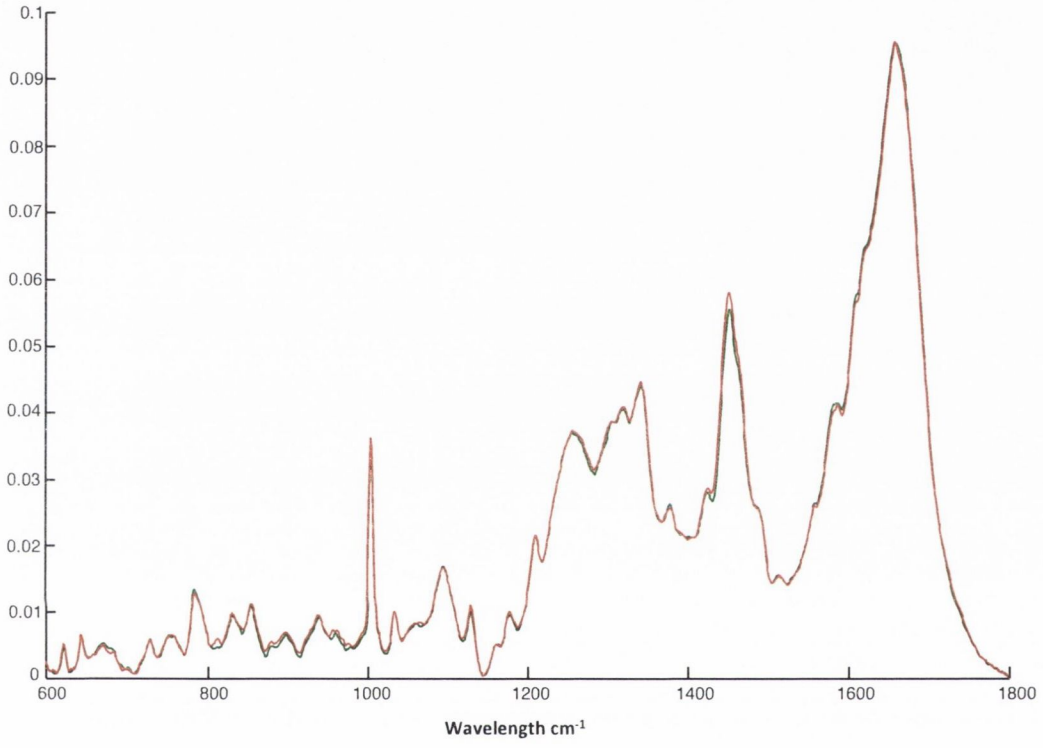


Figure 5-4 Advanced preprocessing of Raman spectrum of the nuclei of TR146 cells.

Total average spectra from 20 nuclei from each cell type. Baseline correction was applied as described in Chapter 4 and the mean was calculated prior to further analysis.

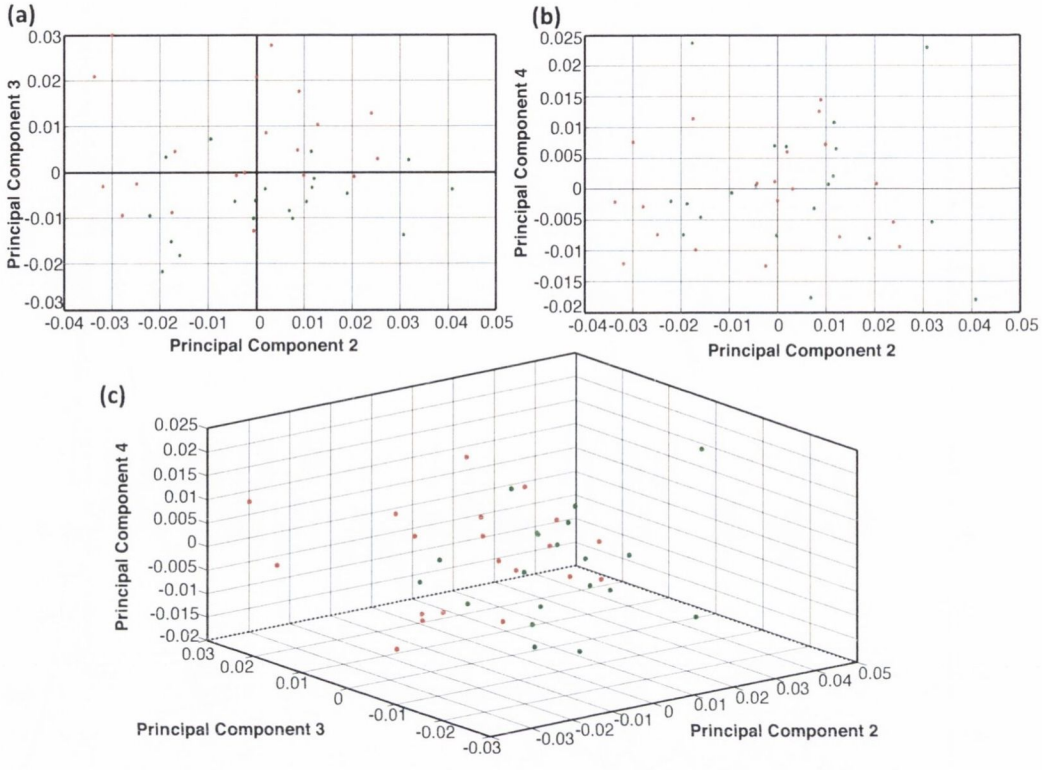


Figure 5-5 Principal component scatterplots of the nuclei of TR146 cells.

PCA scatter plot showing the nuclei Raman Spectra spread of points between the untreated cells (green) and the treated cells (red). There is no difference between the groups of points which means EtOH has no effect on the nuclei after 24h treatment with PC2, PC3, or PC4.

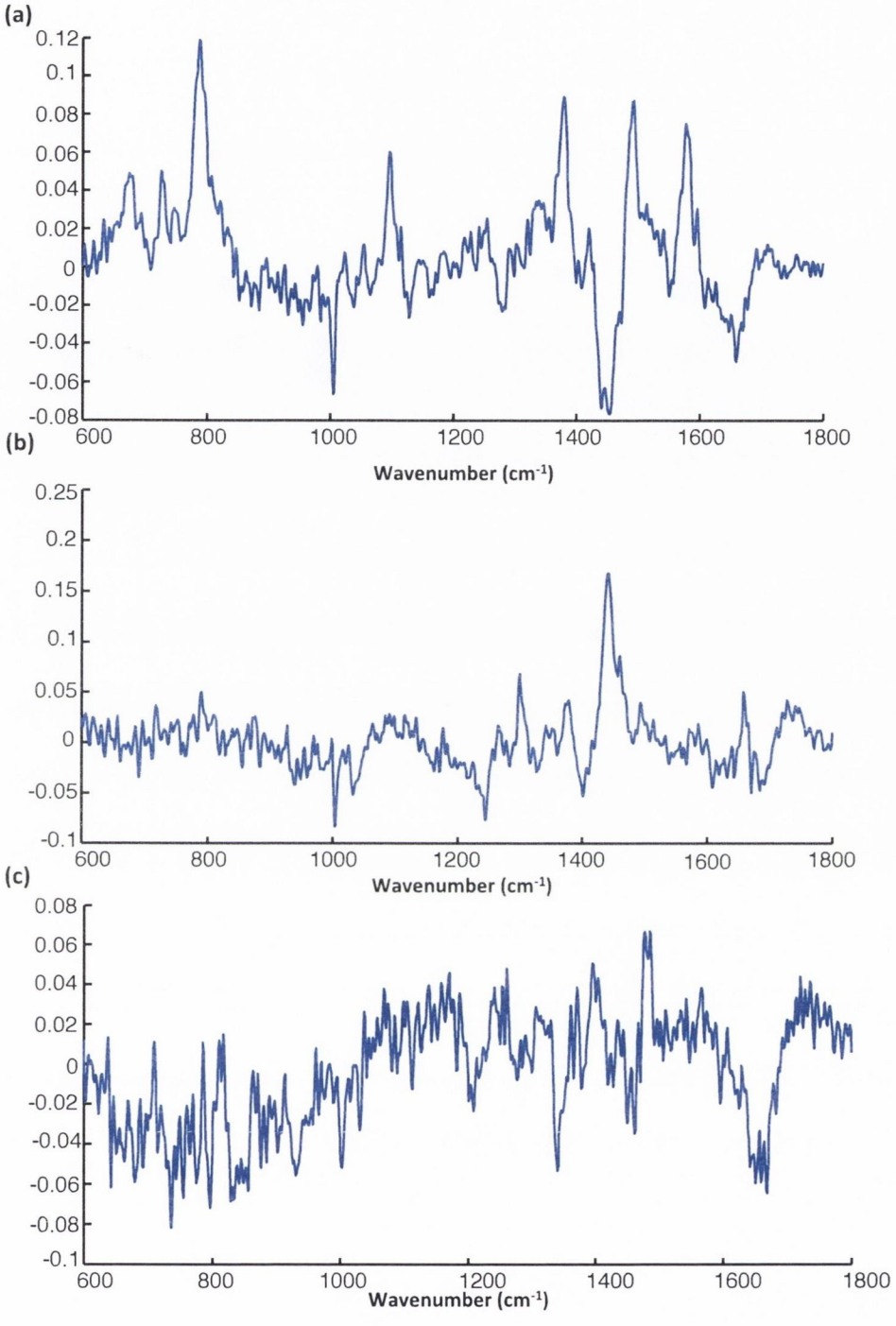


Figure 5-6 Principal component loading plots of the nuclei of TR146 cells.

Loading plots of PC2 (a), PC3 (b) and PC4 (c). As shown in the PCA scatter plots there is no changes between the TR146 cells and treatment.

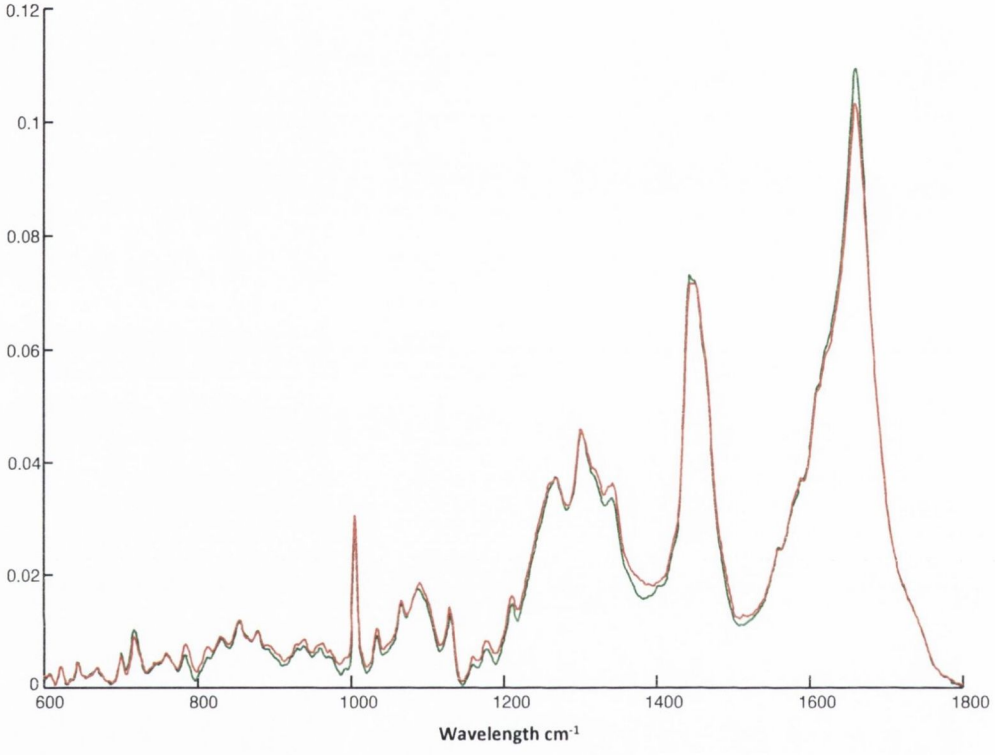


Figure 5-7 Advanced preprocessing of Raman spectrum of cytoplasm TR146 cells.

Total average spectra from the cytoplasmic region of 20 cells of each type. Baseline correction was applied as described in Chapter 4 and the mean was calculated prior to further analysis.

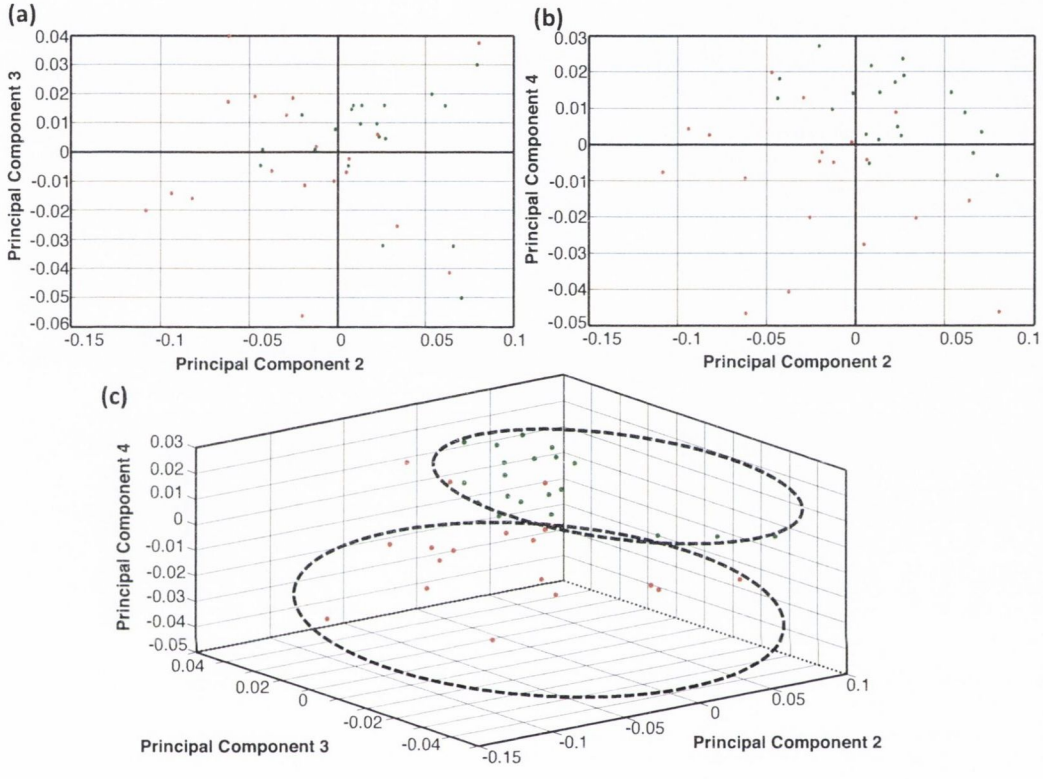


Figure 5-8 Principal component scatterplots of cytoplasm of TR146 cells.

Untreated (green) and treated cells (red) can be separated from each other using PC4.This separation is clear on the 3D scatterplot in figure (c).

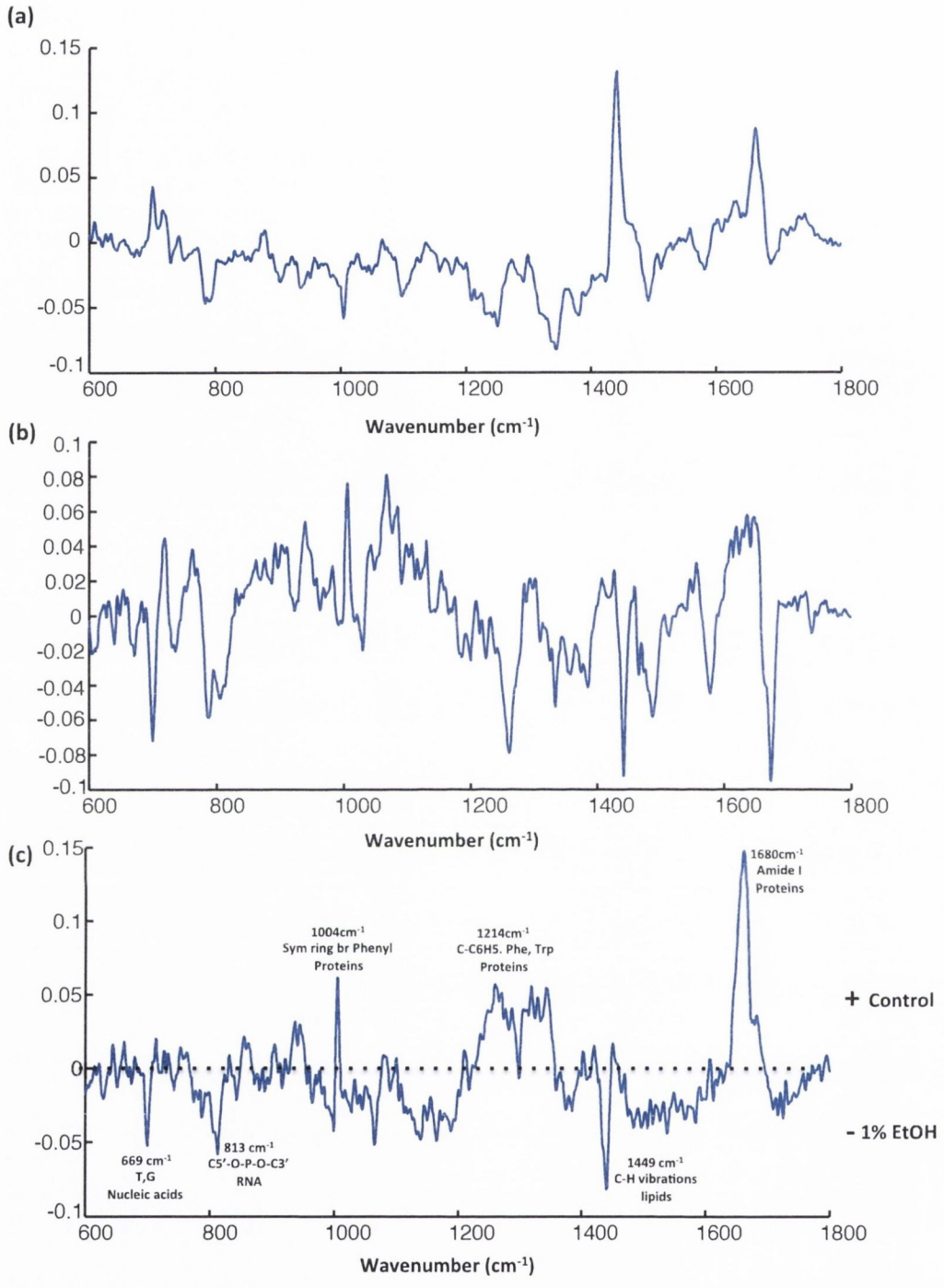


Figure 5-9 Principal component loading plots of the cytoplasm regions of untreated and treated TR146 cells.

Loading plots of PC2 (a), PC3 (b) and PC4 (c). As shown in the PCA scatter plots PC4 separates the control cells (+ve) and the treated cells (-ve).

5.3.1.2 Raman spectroscopy and principal component analysis of Ca9.22 cells after exposure to EtOH

5.3.1.2.1 Nucleolus

Raman spectra from the treated and untreated nucleolus of Ca9.22 were pre-processed prior to PCA (Figure 5-10). PCA analysis was applied to distinguish all the recognised spectral signals of the nucleolus in Ca9.22 treated with and without EtOH (1% 24h). The results of PCA are presented in (Figure 5-11) and do not show a clear separation of the points. The scatterplot includes 60 data points, 20 for each cell type. The cell types cannot be separated using with PC2, PC3 or PC4. Principle loading plots are shown in Figure 5-12 and as confirmed using the scatterplots there was no separation between the data sets.

5.3.1.2.2 Nucleus

Raman spectra from the nucleus of the Ca9.22 data sets were pre-processed prior to PCA (Figure 5-13). PCA analysis was applied to distinguish all the recognised spectral signals of the nucleolus in Ca9.22 treated with and without EtOH (1% 24h). The results of PCA are presented in (Figure 5-14) and do not show a clear separation of the points. The scatterplot includes 60 data points, 20 for each cell type. The cell types cannot be separated using with PC2, PC3 or PC4. Principle loading plots are shown in Figure 5-15 and as confirmed using the scatterplots there is no separation between the data sets.

5.3.1.2.3 Cytoplasm

Raman spectra from the cytoplasm were pre-processed prior to PCA (Figure 5-16). PCA analysis was applied to distinguish all the recognised spectral signals of the cytoplasm in Ca9.22 treated with and without EtOH (1% 24h). PCA analysis (Figure 5-17) shows a very good separation of the cell types of Raman spectra. The scatterplot includes 60 data points, 20 for each cell type. Similarly to the TR146 cells, PC4 shows good separation of Ca9.22 data sets. PC2 and PC3 show no separation of any of the cell types. The 3D scatterplot clearly defines the boundaries of the untreated and treated Ca9.22 cells [Figure 5-17 (c)]. Loading with assignments of the main peaks contribution to

discrimination between the data sets are presented in Figure 5-18. From the scatterplots it can be shown that PC4 discriminates the untreated from the treated Ca9.22 cells. The negative peaks represent the control cells and the positive peaks are the treated cells. The molecular changes associated with the control cells are proteins and nucleic acids while the treated cells showed an increase in proteins. The decrease in molecular components in controls cells was shown by the band 813cm^{-1} related to the C5'-O-P-O-C3' phosphodiester bonds in RNA, band 1004cm^{-1} related to phenylalanine vibrational modes and can be found in proteins in general and band 1480cm^{-1} related to adenine guanine vibrational modes. The increase shown with the treated cells includes band 1240cm^{-1} related to C-C stretch in protein vibrational modes and band 1680cm^{-1} related to the Amide I vibrational modes of proteins.

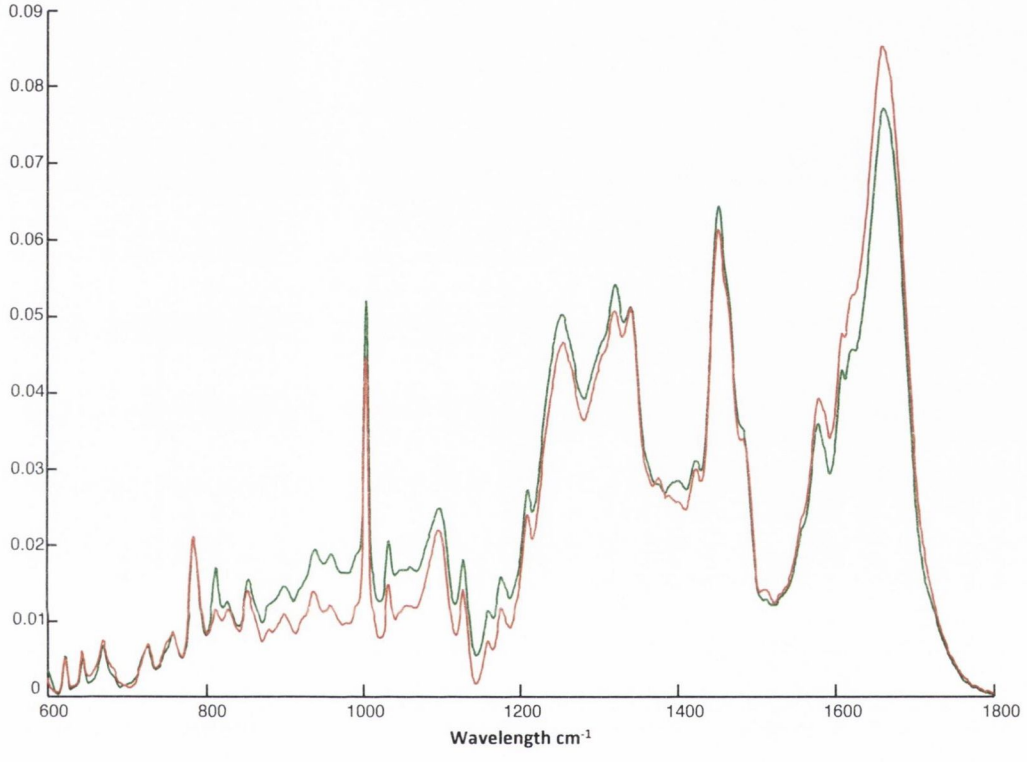


Figure 5-10 Advanced preprocessing of Raman spectrum of nucleoli of untreated and treated Ca9.22 cells.

Total average spectra from 20 nucleoli from each cell type. Baseline correction was applied as described in Chapter 4 and the mean was calculated prior to further analysis.

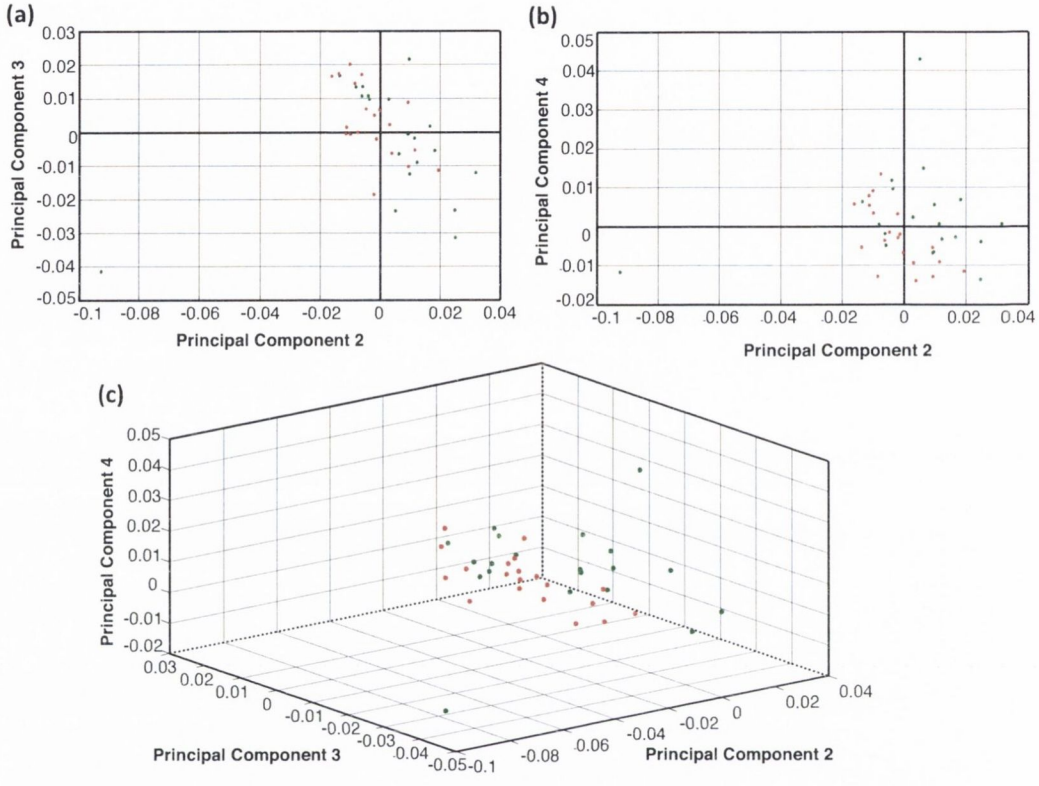


Figure 5-11 Principal component scatterplots of the nucleoli of untreated and treated Ca9.22 cells.

PCA scatter plot showing the nucleoli Raman Spectra spread of points between the untreated cells (green) and the treated cells (red). There is no difference between the groups of points which means EtOH has no effect on the nucleoli after 24h treatment with PC2, PC3, or PC4.

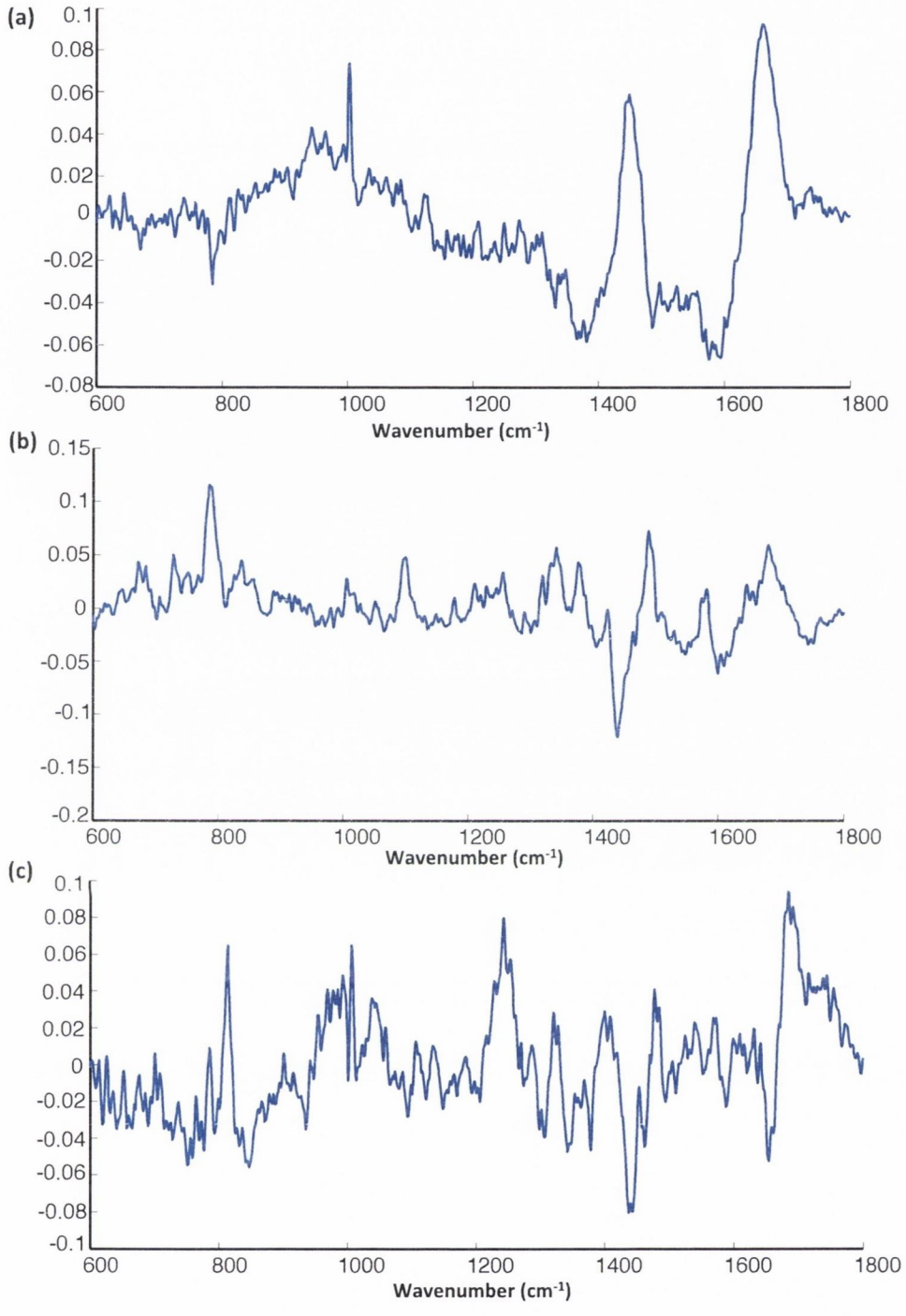


Figure 5-12 Principal component loading plots of the nucleoli of untreated and treated Ca9.22 cells.

Loading plots of PC2 (a), PC3 (b) and PC4 (c). As shown in the PCA scatter plots there is no changes between the Ca9.22 cells and treatment.

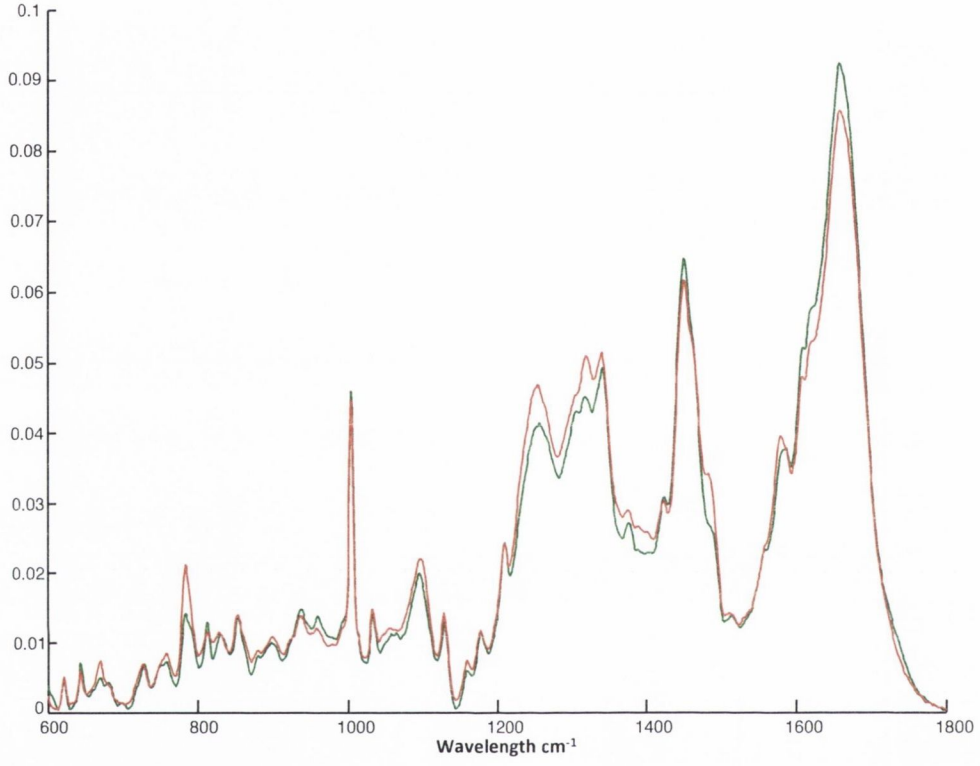


Figure 5-13 Advanced preprocessing of Raman spectrum of the nuclei of untreated and treated Ca9.22 cells.

Total average spectra from the nuclei of 20 cells of each type. Baseline correction was applied as described in Chapter 4 and the mean was calculated prior to further analysis.

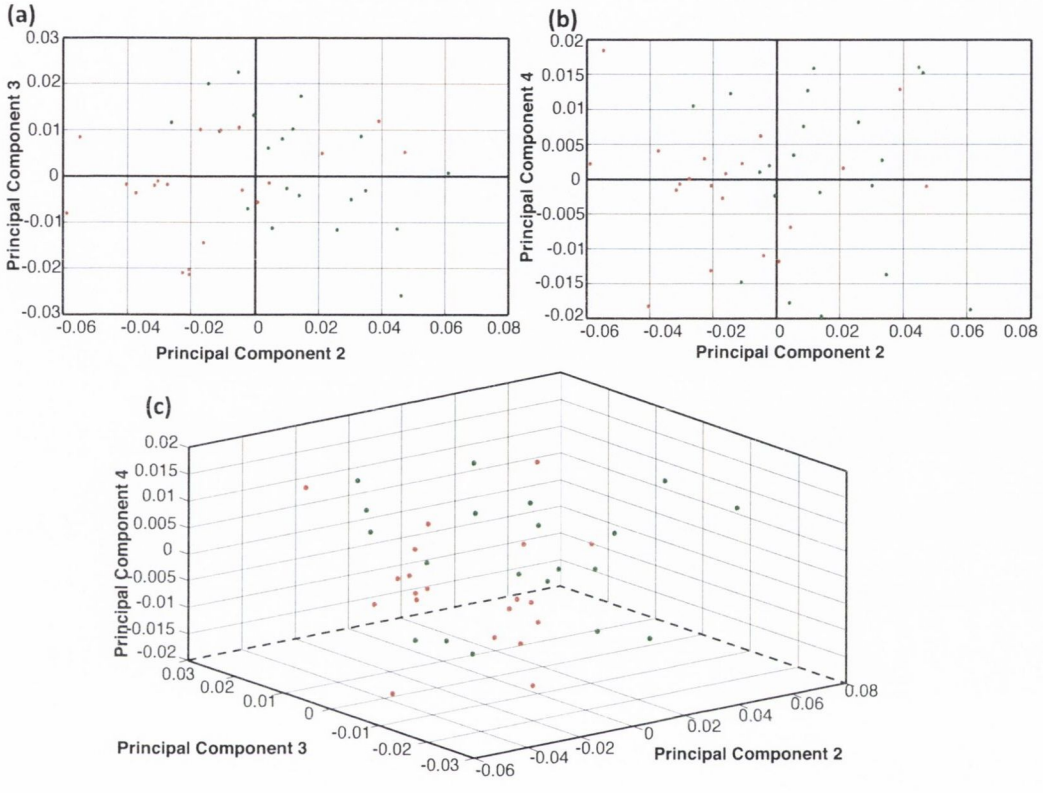


Figure 5-14 Principal component scatterplots of the nuclei of untreated and treated Ca9.22 cells.

There is no difference between the groups of points which means EtOH has no effect on the nuclei after 24h treatment with PC2, PC3, or PC4.

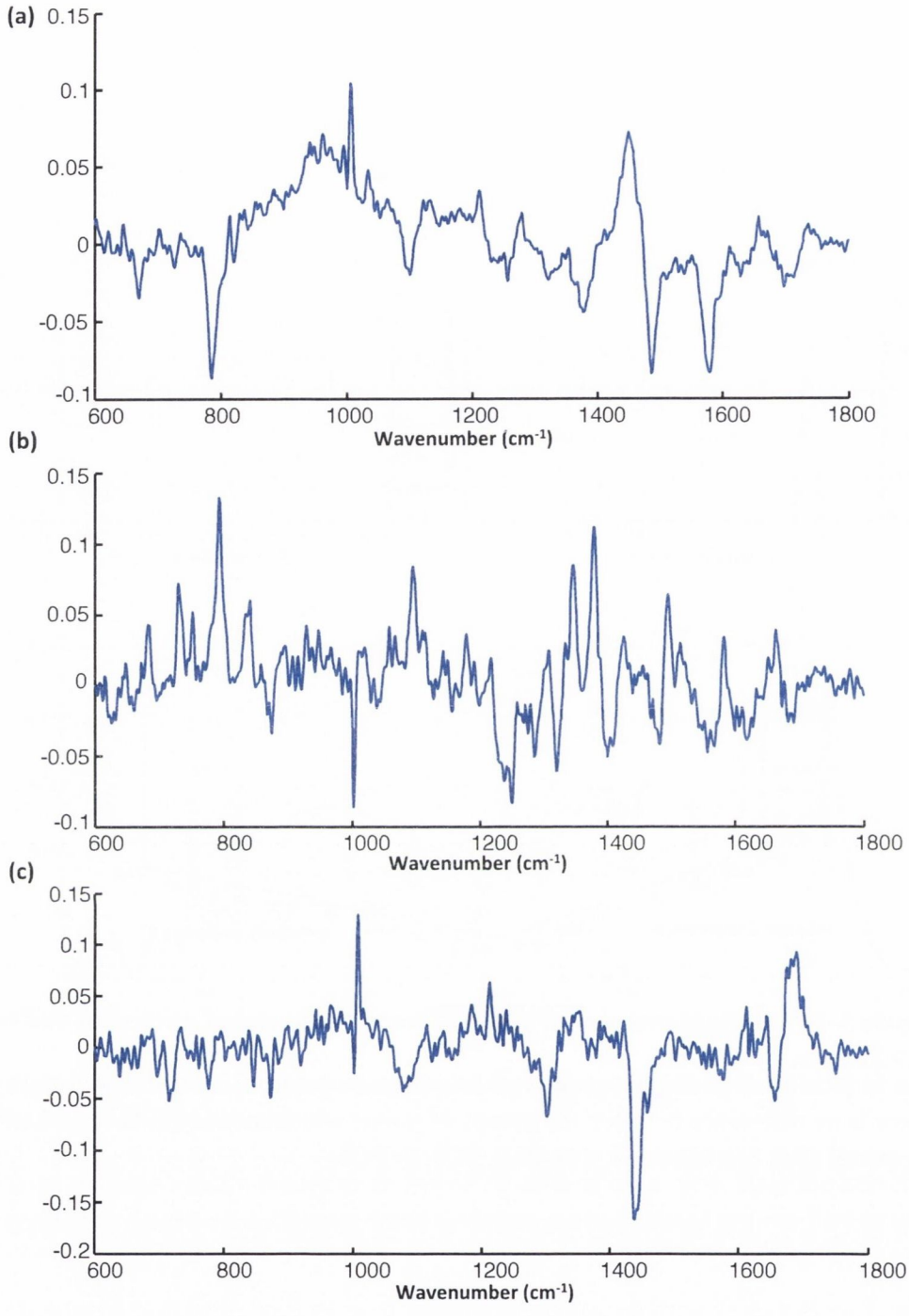


Figure 5-15 Principal component loading plots of the nuclei of untreated and treated Ca9.22 cells.

Loading plots of PC2 (a), PC3 (b) and PC4 (c). As shown in the PCA scatter plots there is no changes between the Ca9.22 cells and treatment.

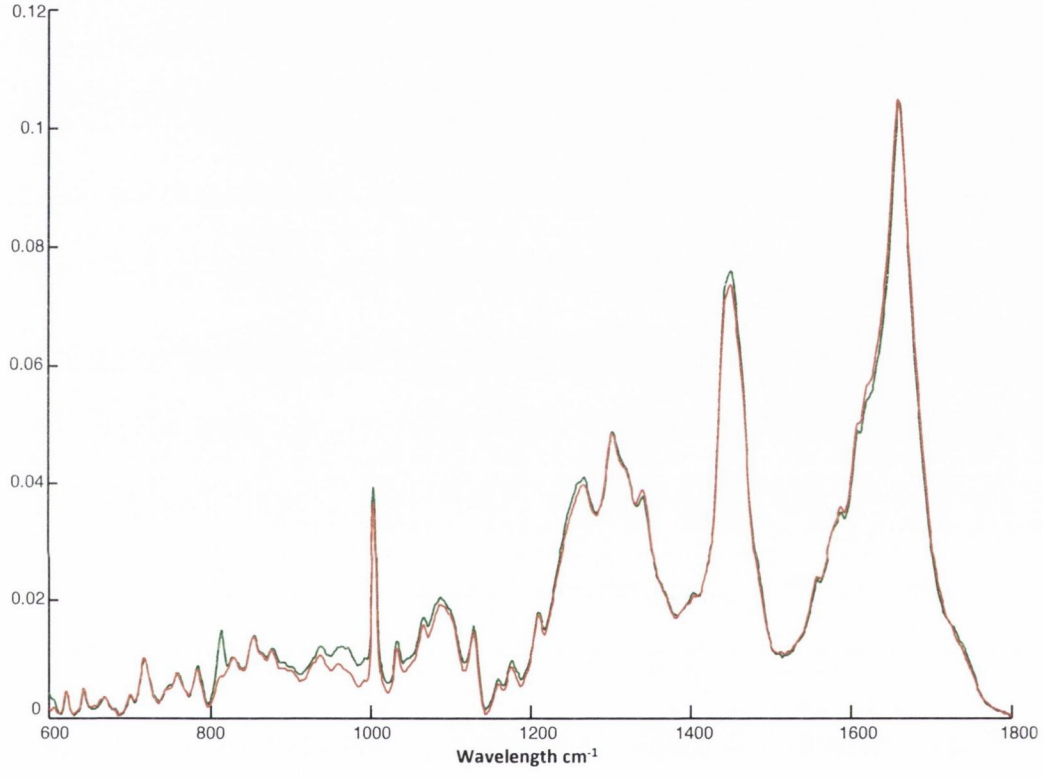


Figure 5-16 Advanced preprocessing of Raman spectrum of cytoplasm of untreated and treated Ca9.22 cells.

Total average spectra from the cytoplasmic region of 20 cells of each type. Baseline correction was applied as described in Chapter 4 and the mean was calculated prior to further analysis.

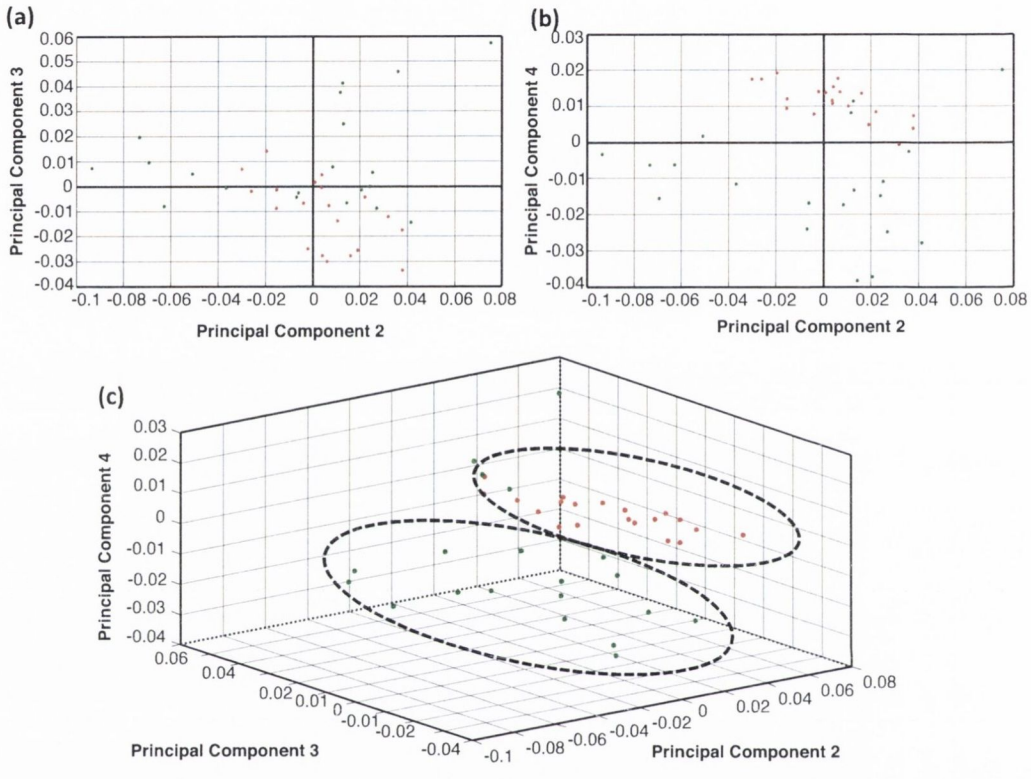


Figure 5-17 Principal component scatterplots of cytoplasm of untreated and treated Ca9.22 cells.

There is a clear separation using PC4 (b) between the untreated cells (green) and the treated cells (red). The separation is clear using the 3D scatterplot in part (c).

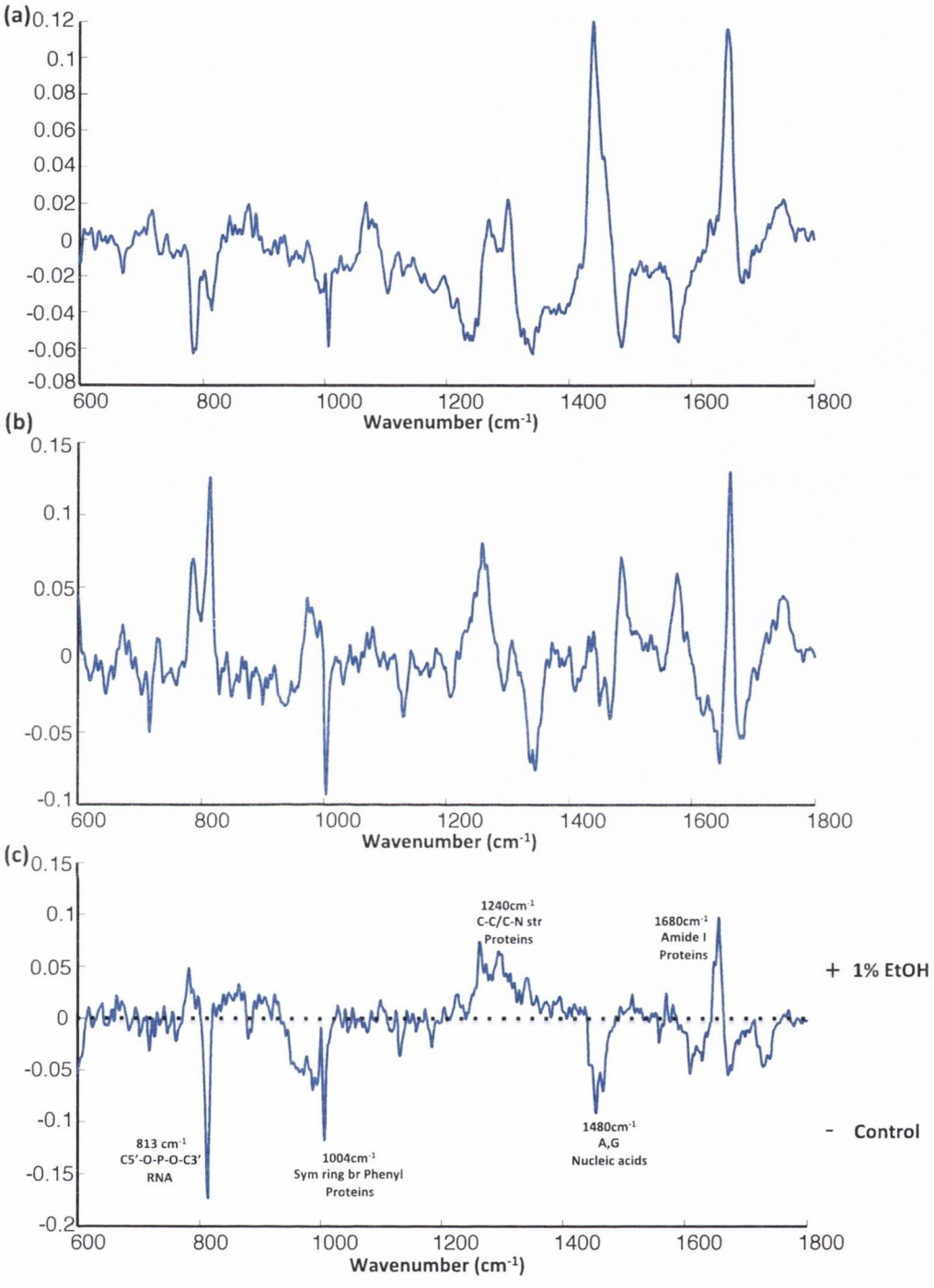


Figure 5-18 Principal component loading plots of the cytoplasm regions of untreated and treated Ca9.22 cells.

Loading plots of PC2 (a), PC3 (b) and PC4 (c). As shown in the PCA scatter plots there is a separation between the untreated cells (-ve) and the treated cells (+ve) using PC4 (c).

5.3.2 Analysing the effect of EtOH on the DOK dysplastic cell line using Raman spectroscopy and principal component analysis

Results from previous chapters indicated that EtOH has a different effect on dysplastic cells when compared to changes observed in OSCC cell lines. The next phase was to investigate if EtOH affects subcellular components in the dysplastic cell line. Using the same parameters as previously described DOK cells were treated with 1% EtOH for 24h to investigate if Raman spectroscopy could detect EtOH induced modifications to this cell line. The variances captured for the first four PCs in DOK cells were as stated in Table 5-3 below.

%	Nucleolus	Nucleus	Cytoplasm
PC1	82.07	65.23	71.30
PC2	5.26	10.62	14.40
PC3	2.67	5.39	3.64
PC4	2.16	3.42	2.36

Table 5-3 Variances for principal component analysis for the respective cellular regions in DOK cells treated with and without EtOH.

5.3.2.1 Nucleolus

Raman spectra from the treated and untreated nucleolus of DOK cells were pre-processed prior to PCA (Figure 5-19). PCA analysis was applied to distinguish all the recognised spectral signals of the nucleolus in DOK treated with and without EtOH (1% 24h). PCA analysis (Figure 5-20) shows a weak separation of the cell types of Raman spectra. The scatterplot includes 60 data points, 20 for each cell type. PC2 shows faint separation of DOK data sets. PC3 and PC4 show no separation of any of the cell types. Loading with assignments of the main peaks contribution to discrimination between the data sets are presented in Figure 5-21. From the scatterplots it can be shown that PC2 discriminates the untreated from the treated DOK cells. The negative peaks represent the control cells and the positive peaks are the treated cells. The molecular changes

associated with the control cells are proteins and nucleic acids while the treated cells show an increase in proteins and lipids. The decrease in molecular components in controls cells is shown by the band 813cm^{-1} related to the C5'-O-P-O-C3' phosphodiester bonds in RNA, band 1004cm^{-1} related to phenylalanine vibrational modes and can be found in proteins in general and band 1480cm-1 related to adenine guanine vibrational modes. The increase shown with the treated cells includes bands 1301cm^{-1} and band 1449cm^{-1} related to CH2 twist and C-H vibrations in lipids vibrational modes, respectively, and band 1680cm^{-1} related to the Amide I vibrational modes of proteins.

5.3.2.2 Nucleus

Raman spectra from the nucleus of the DOK data sets were pre-processed prior to PCA (Figure 5-22). PCA analysis was applied to distinguish all the recognised spectral signals of the nucleus in DOK treated with and without EtOH (1% 24h). PCA analysis (Figure 5-23) shows separation of the cell types of Raman spectra although the separation is weak as it is defined using PC4, which shows only slight variations between cell types. The scatterplot includes 60 data points, 20 for each cell type. PC4 shows good separation of DOK data sets. PC2 and PC3 show no separation of any of the cell types. Loading with assignments of the main peaks contribution to discrimination between the data sets are presented in Figure 5-24. From the scatterplots it can be shown that PC4 discriminates the untreated from the treated DOK cells. The positive peaks represent the control cells and the negative peaks are the treated cells. The molecular changes associated with the control cells include proteins, nucleic acids and lipids while the treated cells show a decrease in both proteins and lipids. The increase in molecular components in the controls cells is shown by the band 813cm^{-1} related to the C5'-O-P-O-C3' phosphodiester bonds in RNA, band 1342cm^{-1} related to related to A (adenine), G (guanine) vibrational modes of nucleic acids and band 1449cm-1 related C-H vibrations in lipids. The decrease shown with the treated cells includes band 1004cm^{-1} related to phenylalanine vibrational modes and can be found in proteins in general and band 1600cm^{-1} related to the C-H vibrations in lipids.

5.3.2.3 Cytoplasm

Raman spectra from the cytoplasm were pre-processed prior to PCA (Figure 5-25). PCA analysis was applied to distinguish all the recognised spectral signals of the cytoplasm in DOK cells treated with and without EtOH (1% 24h). PCA analysis (Figure 5-26) shows a separation of the cell types of Raman spectra. The scatterplot includes 60 data points, 20 for each cell type. PC3 shows good separation of DOK data sets. PC2 and PC4 show no separation of any of the cell types. Loading with assignments of the main peaks contribution to discrimination between the data sets are presented in Figure 5-27. From the scatterplots it can be shown that PC4 discriminates the untreated from the treated DOK cells. The positive peaks represent the control cells and the negative peaks are the treated cells. The molecular changes associated with the control cells are proteins and nucleic acids while the treated cells show a decrease in lipids. The increase in molecular components in controls cells is shown by the band 1004cm^{-1} related to phenylalanine vibrational modes and can be found in proteins in general, band 1480cm-1 related to adenine and guanine vibrational modes and band 1680cm^{-1} related to the Amide I vibrational modes of proteins. The decrease shown with the treated cells includes band 1449cm^{-1} and band 1600cm^{-1} both related C-H vibrations in lipids.

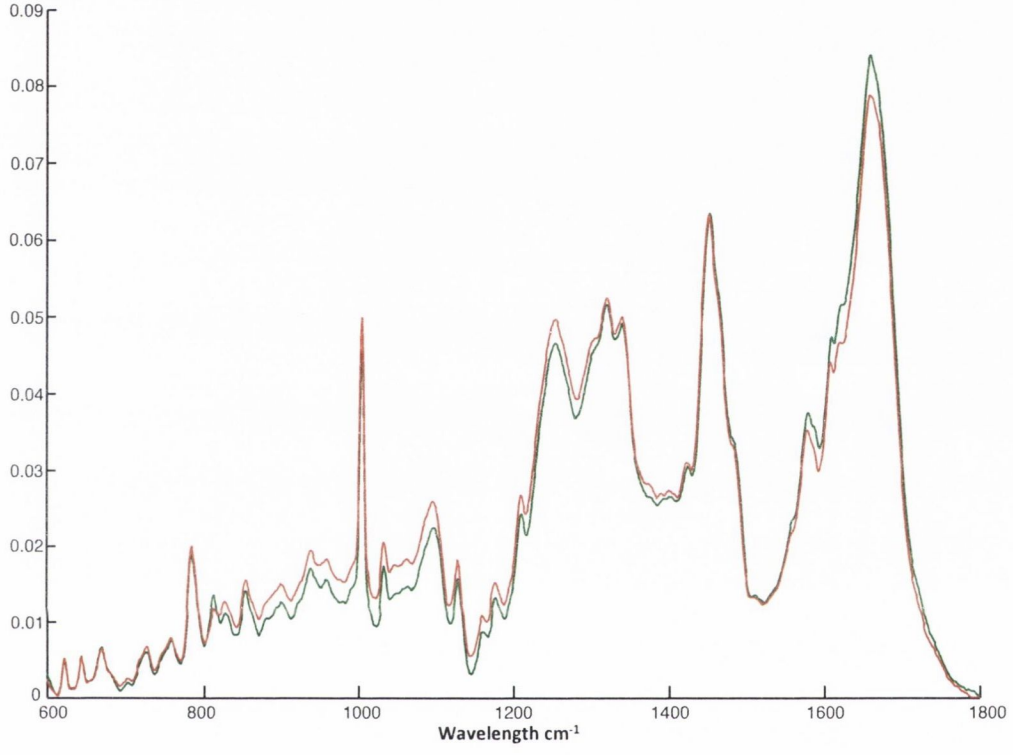


Figure 5-19 Advanced preprocessing of Raman spectrum of the nucleoli of untreated and treated DOK cells.

Total average spectra from 20 nucleoli from each cell type. Baseline correction was applied as described in Chapter 4 and the mean was calculated prior to further analysis.

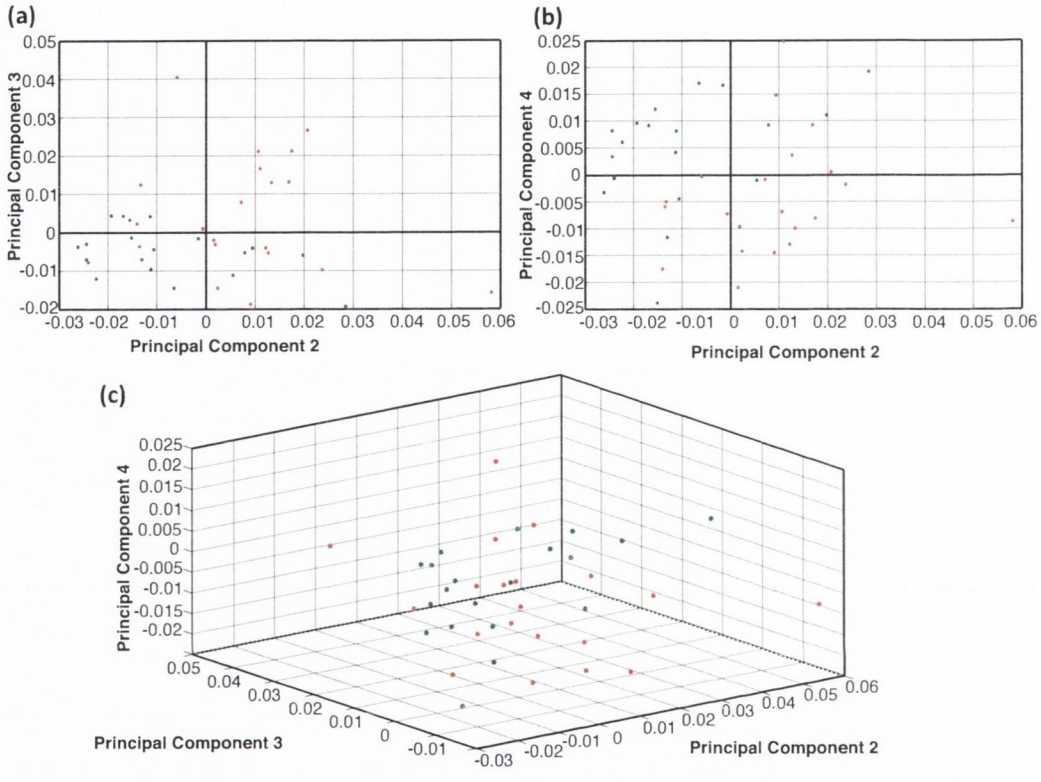


Figure 5-20 Principal component scatterplots of the nucleoli of untreated and treated DOK cells.

PCA scatter plot showing the nucleoli Raman Spectra spread of points between the untreated cells (green) and the treated cells (red). PC2 shows separation of the control cells from the treated cells.

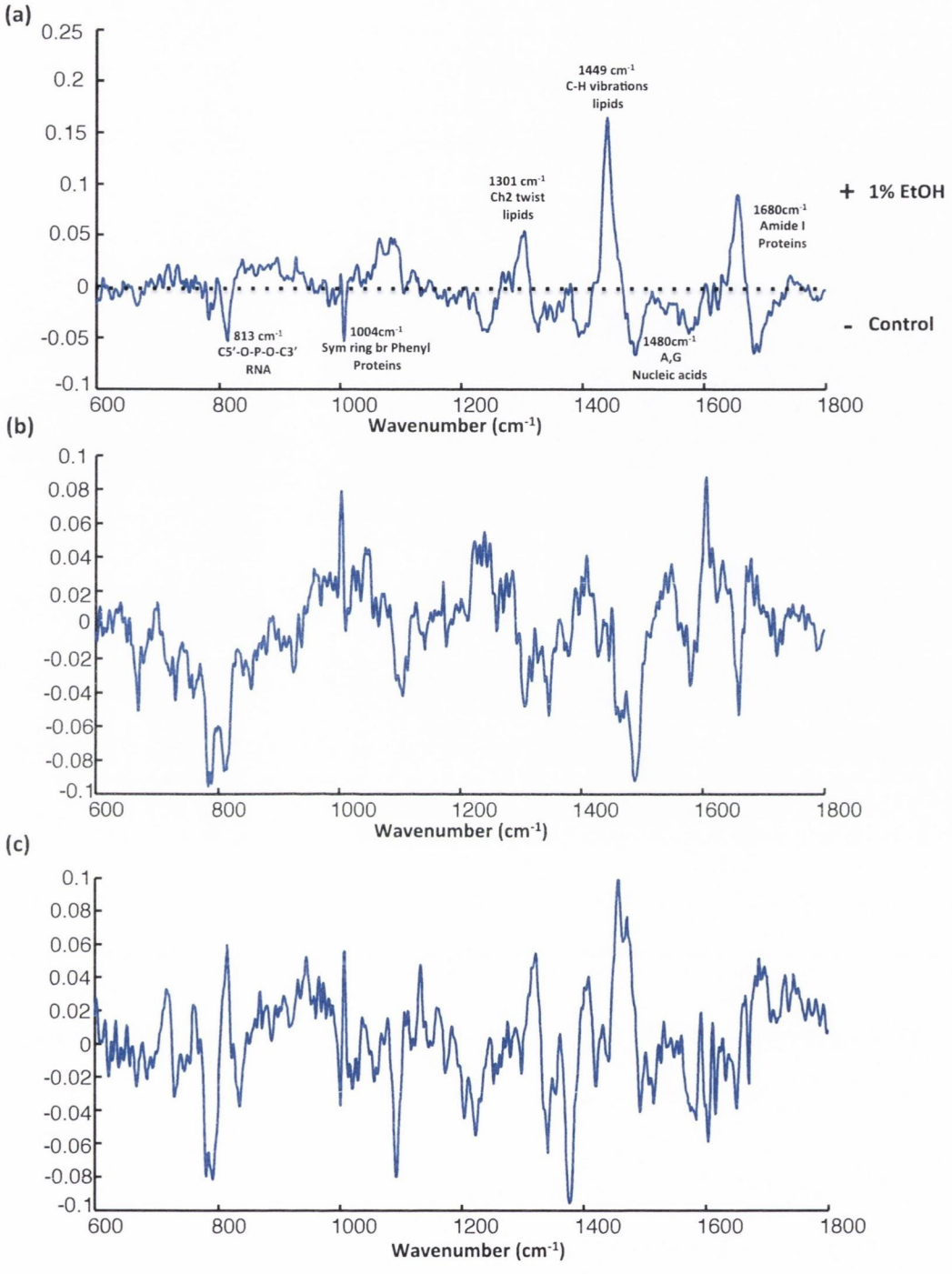


Figure 5-21 Principal component loading plots of the nucleoli of untreated and treated DOK cells.

Loading plots of PC2 (a), PC3 (b) and PC4 (c). As shown in the PCA scatter plots PC2 separates the control cell from the treated cells.

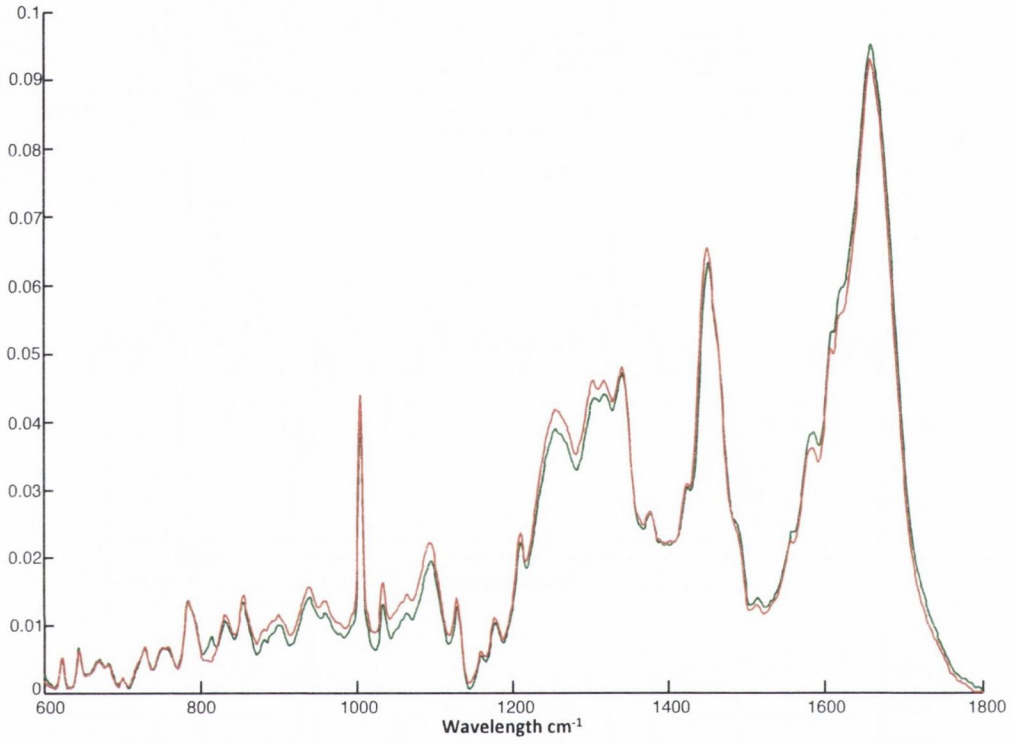


Figure 5-22 Advanced preprocessing of Raman spectrum of the nuclei of untreated and treated DOK cells.

Total average spectra from 20 nuclei from each cell type. Baseline correction was applied as described in Chapter 4 and the mean was calculated prior to further analysis.

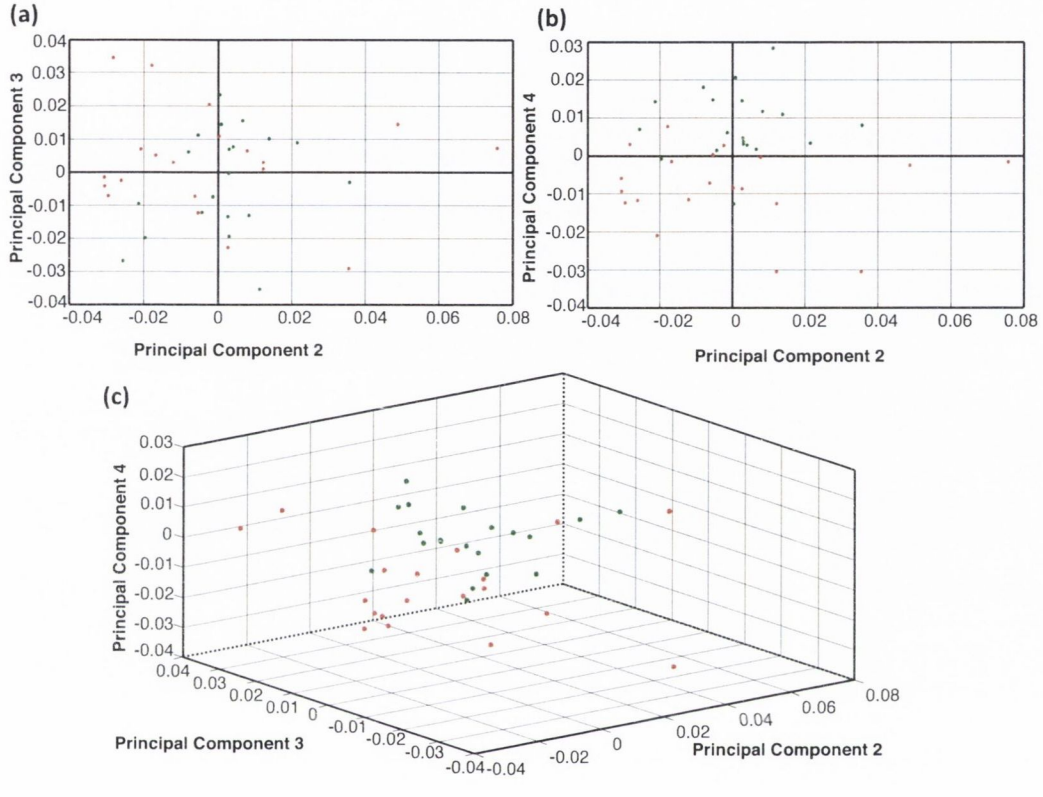


Figure 5-23 Principal component scatterplots of the nuclei of untreated and treated DOK cells.

PCA scatter plot showing the nuclei Raman Spectra spread of points between the untreated cells (green) and the treated cells (red). PC4 shows separation of the control cells from the treated cells.

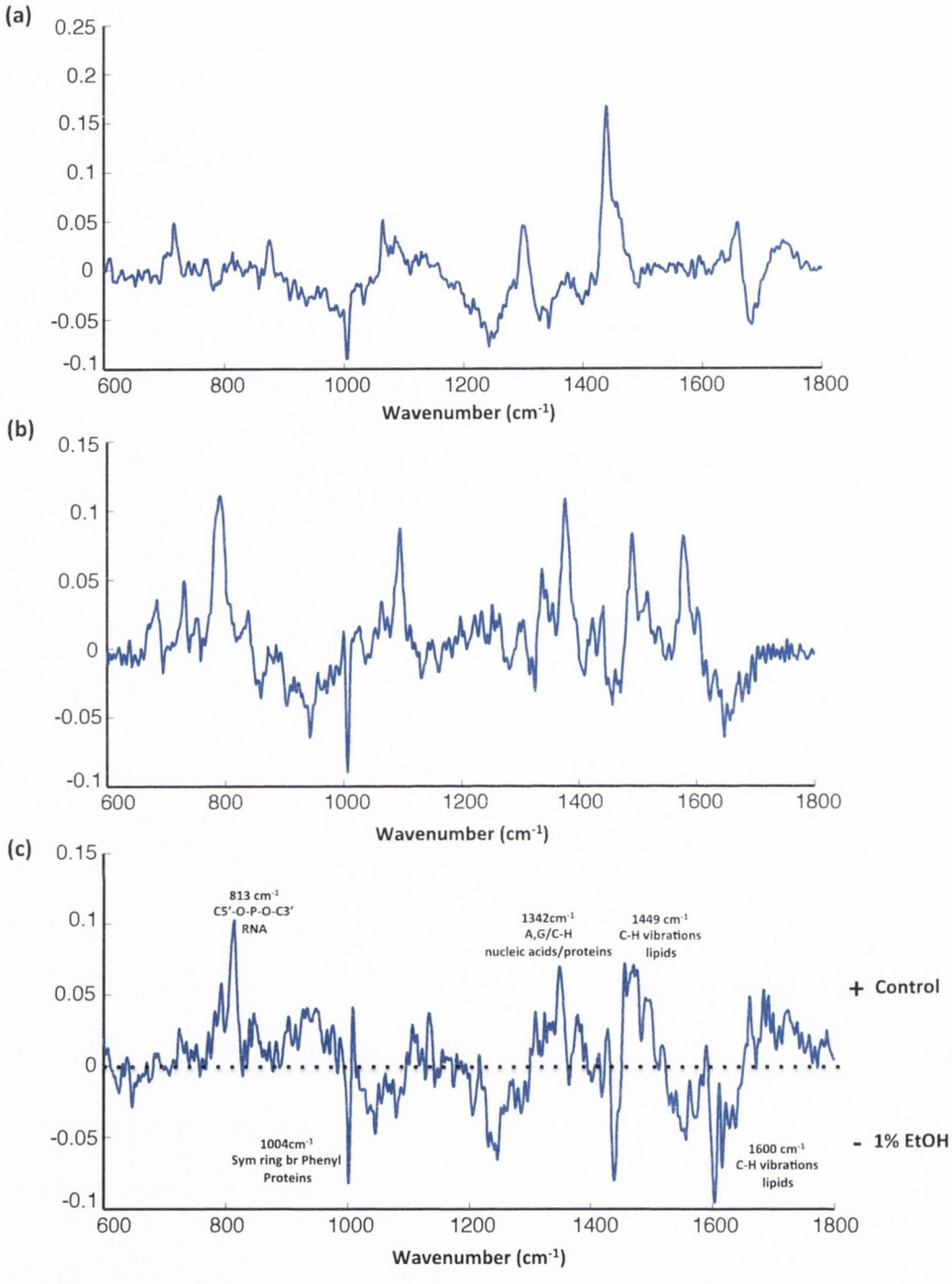


Figure 5-24 Principal component loading plots of the nuclei of untreated and treated DOK cells.

Loading plots of PC2 (a), PC3 (b) and PC4 (c). PC4 separates the control cells from the treated cells.

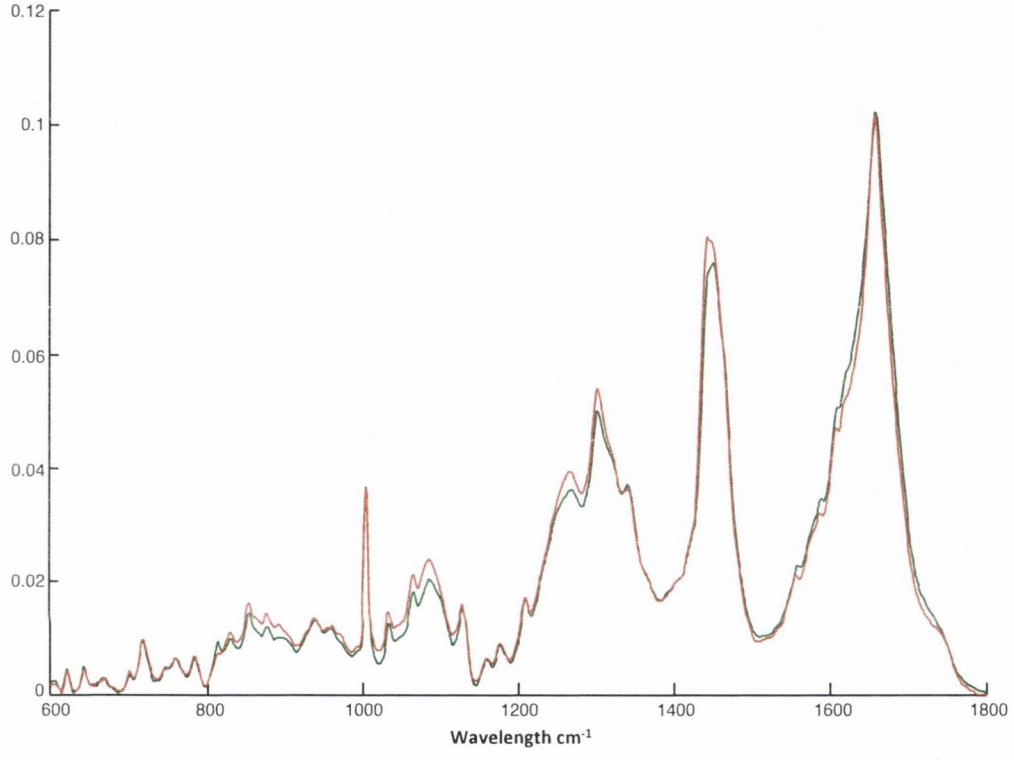


Figure 5-25 Advanced preprocessing of Raman spectrum of cytoplasm untreated and treated DOK cells

Total average spectra from the cytoplasmic region of 20 cells of each type. Baseline correction was applied as described in Chapter 4 and the mean was calculated prior to further analysis.

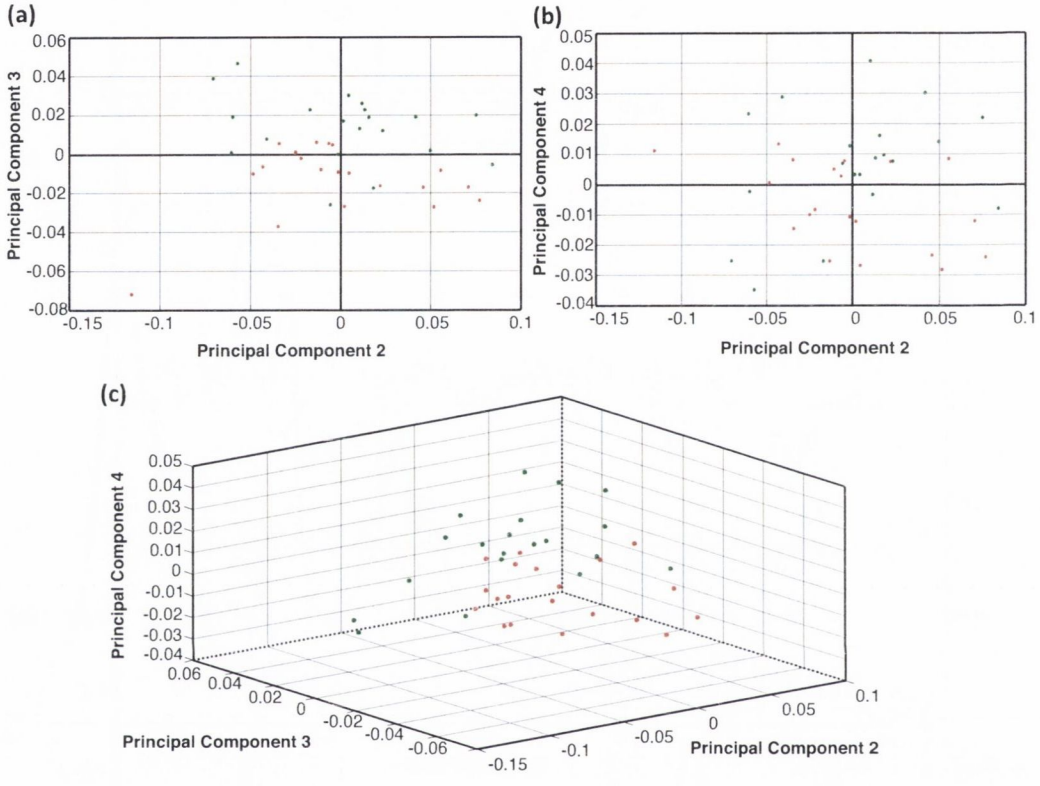


Figure 5-26 Principal component scatterplots of cytoplasm of DOK cells.

PCA scatter plot showing the cytoplasmic regions Raman spectra spread of points between the untreated cells (green) and the treated cells (red). PC3 shows separation of the control cells from the treated cells.

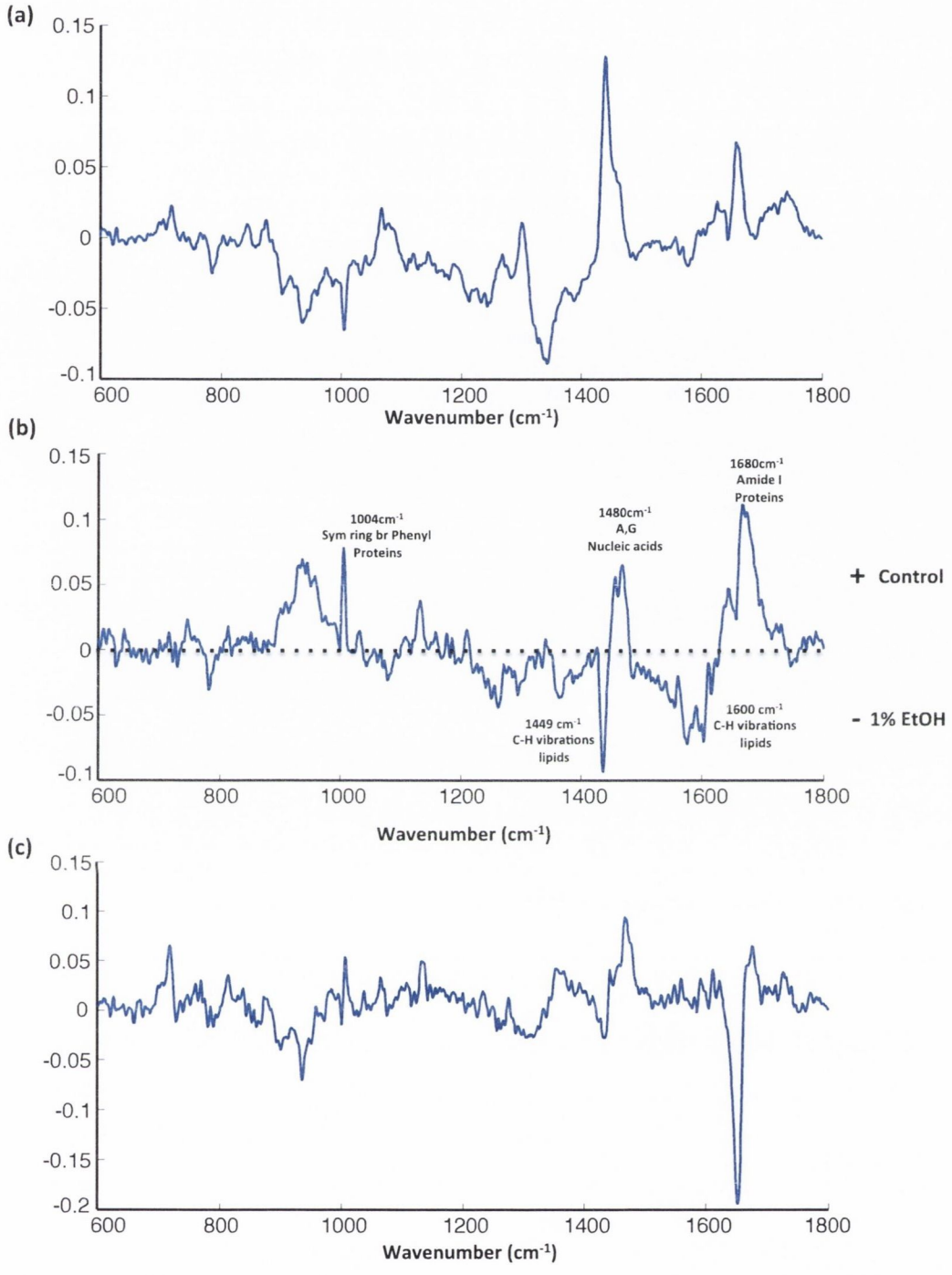


Figure 5-27 Principal component loading plots of the cytoplasm regions of untreated and treated DOK cells.

Loading plots of PC2 (a), PC3 (b) and PC4 (c). As shown in the PCA scatter plots PC3 shows separation of the control cells from the treated cells.

5.3.3 Raman spectroscopy and principal component analysis of isolated human primary cells after exposure to EtOH

As mentioned previously OSCC occurs from a transformation of the normal oral mucosa, therefore the optimum model for examining changes due to EtOH are primary oral epithelial cells. Based on the models above, Raman spectra were captured for oral primary cells untreated and treated with 1% EtOH for 24h. The variances captured for the first four PCs in primary cells were as stated in Table 5-4 below.

%	Nucleolus	Nucleus	Cytoplasm
PC1	76.67	63.30	72.27
PC2	6.11	12.57	14.57
PC3	2.92	4.75	3.79
PC4	2.11	2.98	1.35

Table 5-4 Variances for PCA for the respective cellular regions in primary cells treated with and without EtOH.

5.3.3.1 Nucleolus

Raman spectra from the treated and untreated nucleolus of primary epithelial cells were pre-processed prior to PCA (Figure 5-28). PCA analysis was applied to distinguish all the recognised spectral signals of the nucleolus in primary epithelial cells treated with and without EtOH (1% 24h). PCA analysis (Figure 5-29) shows a very good separation of the cell types of Raman spectra using PC2. The scatterplot includes 60 data points, 20 for each cell type. PC3 and PC4 show no separation of any of the cell types. Loading with assignments of the main peaks contribution to discrimination between the data sets are presented in Figure 5-30. From the scatterplots it can be shown that PC2 discriminates the untreated from the treated primary epithelial cells. The negative peaks represent the control cells and the positive peaks are the treated cells. The molecular changes associated with the control cells are proteins and lipids while the treated cells show an increase in proteins and nucleic acids. The decrease in molecular components in

controls cells is shown by the band 850cm^{-1} related to the tyrosine ring breathing in proteins, band 1301cm^{-1} related to CH2 twist in lipids and band 1449cm-1 related to C-H vibrations in lipids. The increase shown with the treated cells includes band 788cm^{-1} related to O-P-O stretch in DNA, band 1004cm^{-1} related to phenylalanine vibrational modes and can be found in proteins in general, band 1214cm^{-1} related phenylalanine and tryptophan and band 1680cm^{-1} related to the Amide I vibrational modes of proteins.

5.3.3.2 Nucleus

Raman spectra from the nucleus of the primary epithelial cells data sets were pre-processed prior to PCA (Figure 5-31). PCA analysis was applied to distinguish all the recognised spectral signals of the nucleus in primary epithelial cells treated with and without EtOH (1% 24h). The results of PCA are presented in (Figure 5-32) and do not show a clear separation of the points. The scatterplot includes 60 data points, 20 for each cell type. The cell types cannot be separated using with PC2, PC3 or PC4. Principle loading plots are shown in Figure 5-33 and as confirmed using the scatterplots there is no separation between the data sets.

5.3.3.3 Cytoplasm

Raman spectra from the cytoplasm were pre-processed prior to PCA (Figure 5-34). PCA analysis was applied to distinguish all the recognised spectral signals of the cytoplasm in primary epithelial cells treated with and without EtOH (1% 24h). PCA analysis (Figure 5-35) shows a very good separation of the cell types of Raman spectra. The scatterplot includes 60 data points, 20 for each cell type. PC3 and PC4 show no separation of any of the cell types. Loading with assignments of the main peaks contribution to discrimination between the data sets are presented in Figure 5-36. From the scatterplots it can be shown that PC2 weakly discriminates the untreated from the treated primary epithelial cells. The positive peaks represent the control cells and the negative peaks are the treated cells. The molecular changes associated with the control cells are proteins and nucleic acids while the treated cells show a decrease in lipids. The increase in molecular components in controls cells is shown by the band 1004cm^{-1} related to phenylalanine vibrational modes and can be found in proteins in general, band 1342cm^{-1} related to related to A (adenine), G (guanine) vibrational modes of nucleic acids and

band 1680cm^{-1} related to the Amide I vibrational modes of proteins. The decrease shown with the treated cells includes band 1301cm^{-1}, band 1449cm^{-1} and band 1600cm^{-1} related to CH2 twist and C-H vibrations in lipids.

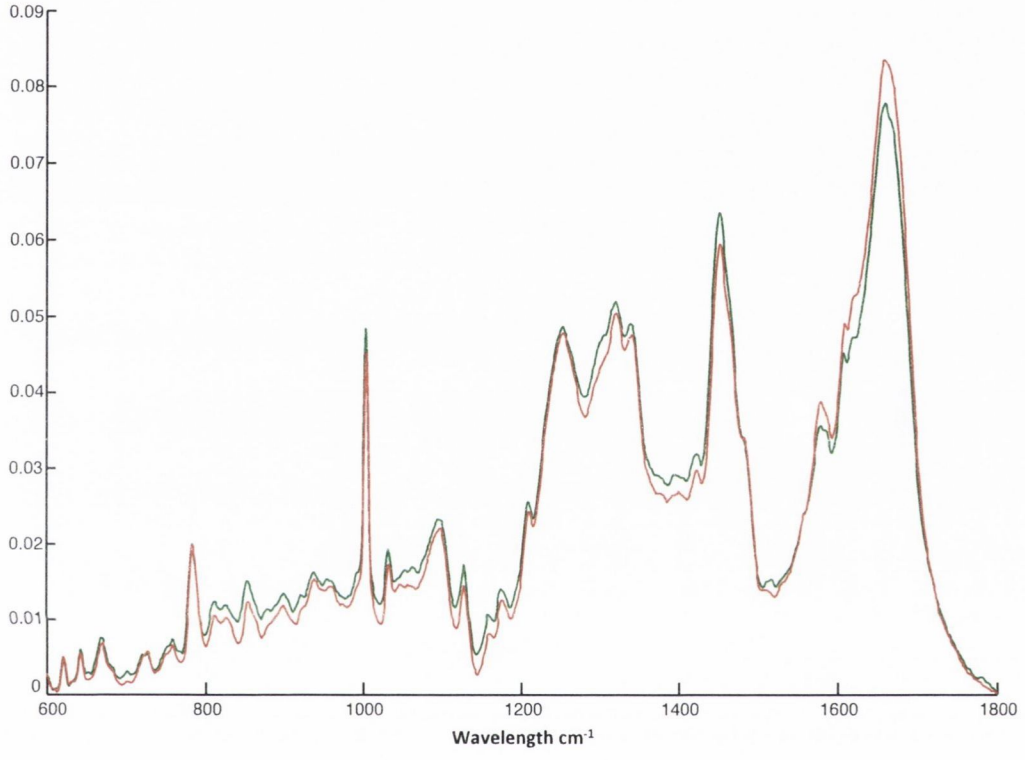


Figure 5-28 Advanced preprocessing of Raman spectrum of the nucleoli of untreated and treated primary oral epithelial cells.

Total average spectra from 20 nucleoli from each cell type. Baseline correction was applied as described in Chapter 4 and the mean was calculated prior to further analysis.

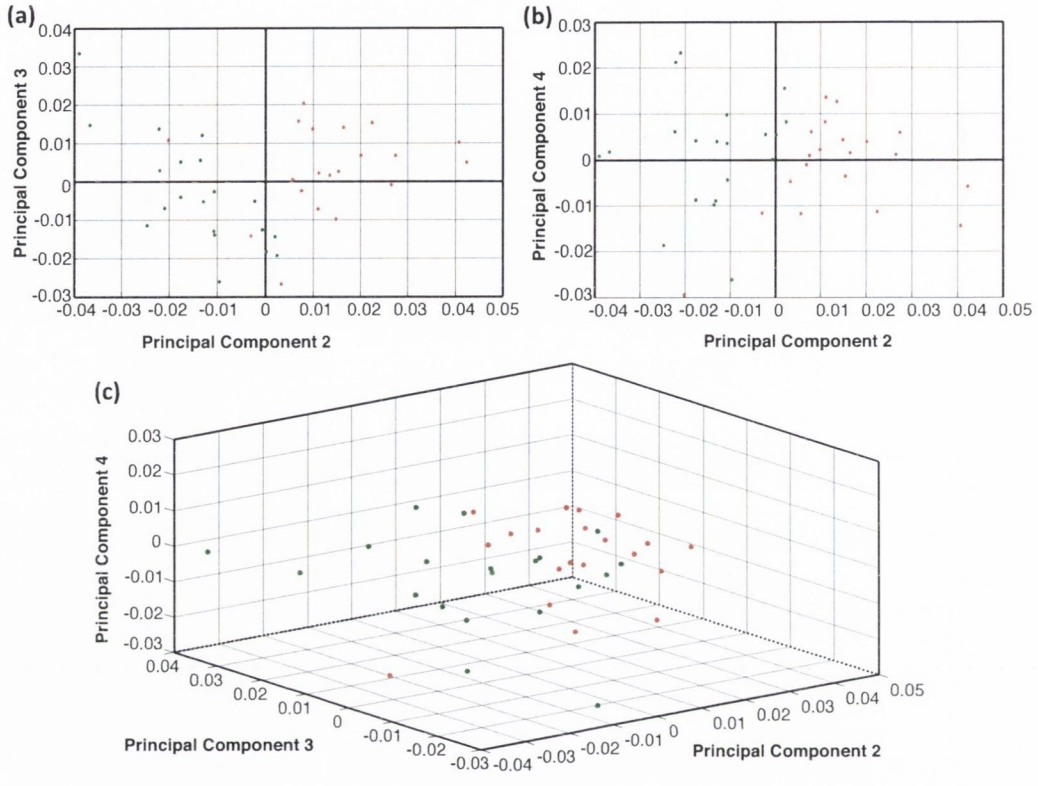


Figure 5-29 Principal component scatterplots of nucleolus of untreated and treated primary oral epithelial cells.

Untreated cells (green) and the treated cells (red) can be separated from each other using PC2. PC3 and PC4 do not show any separation of the cell types.

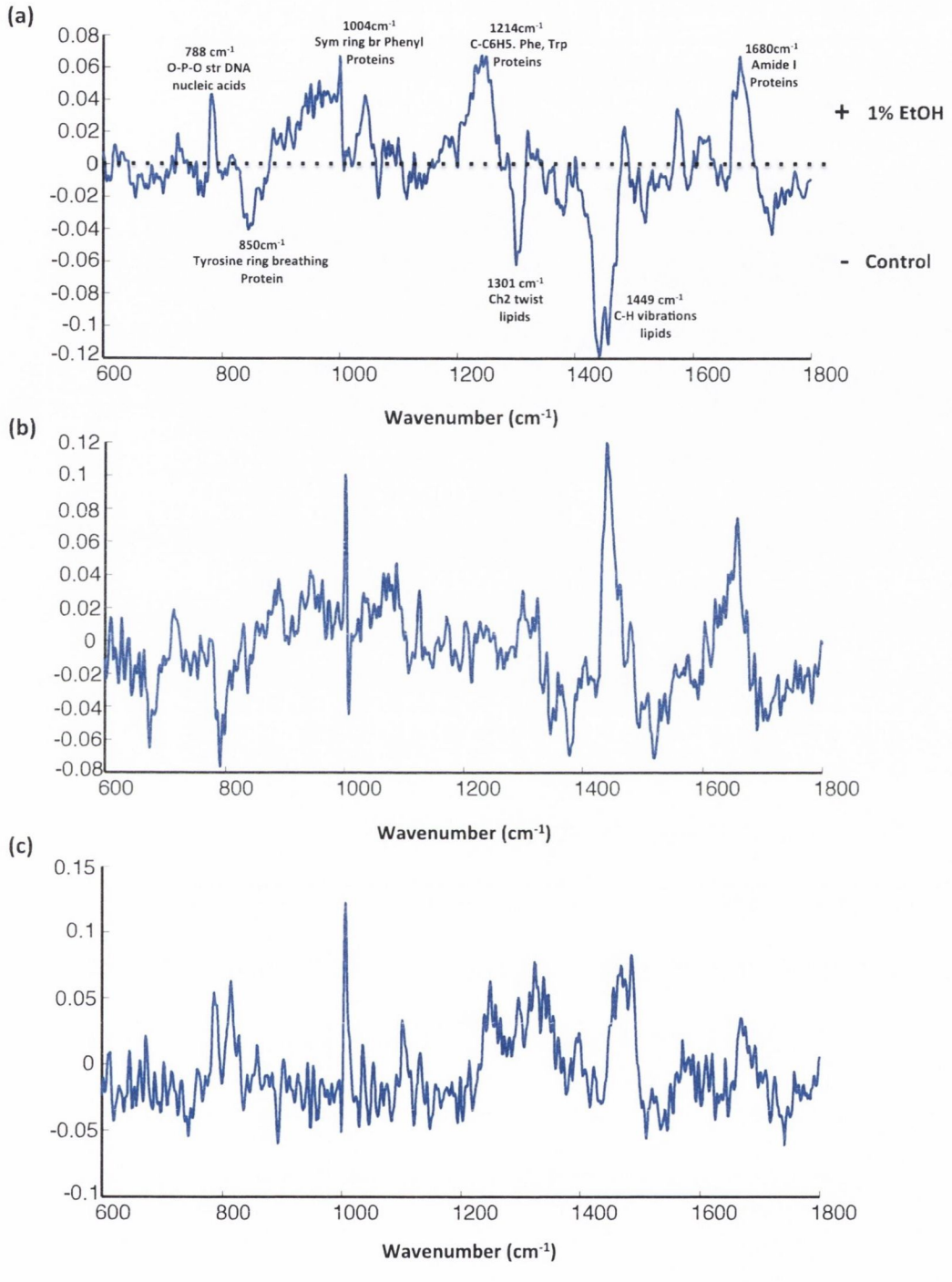


Figure 5-30 Principal component loading plots of nucleolus of untreated and treated primary oral epithelial cells.

Loading plots of PC2 (a), PC3 (b) and PC4 (c). As shown in the PCA scatter plots PC2 discriminates the untreated from the treated cells.

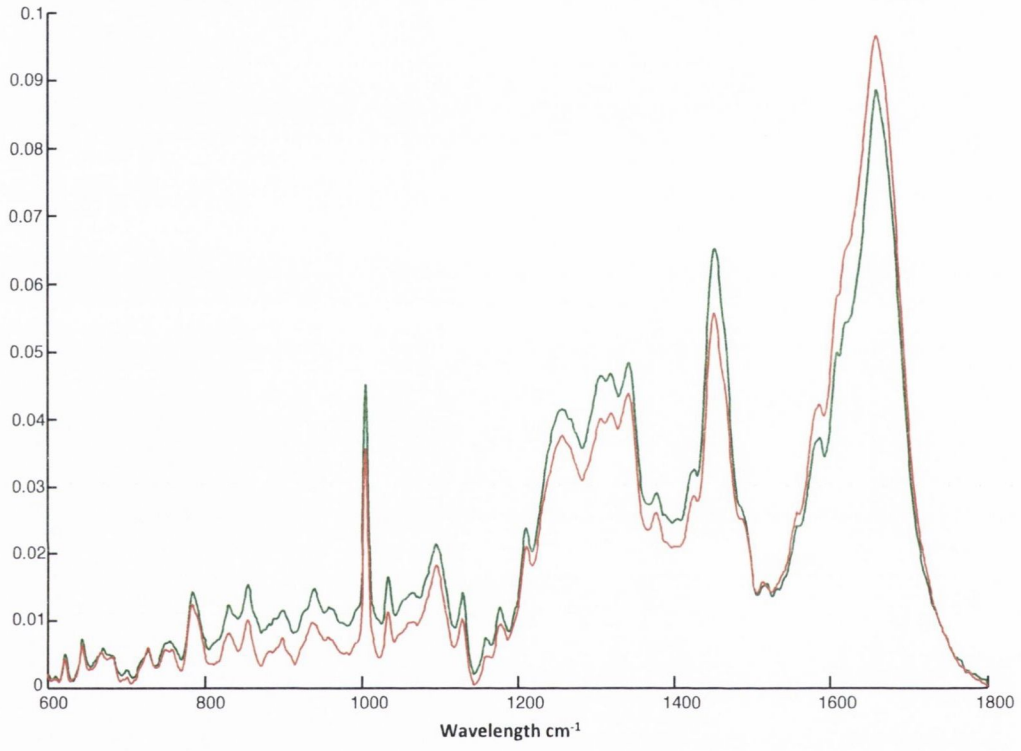


Figure 5-31 Advanced preprocessing of Raman spectrum of the nucleus of treated and untreated primary oral epithelial cells.

Total average spectra from 20 nuclei from each cell type. Baseline correction was applied as described in Chapter 4 and the mean was calculated prior to further analysis.

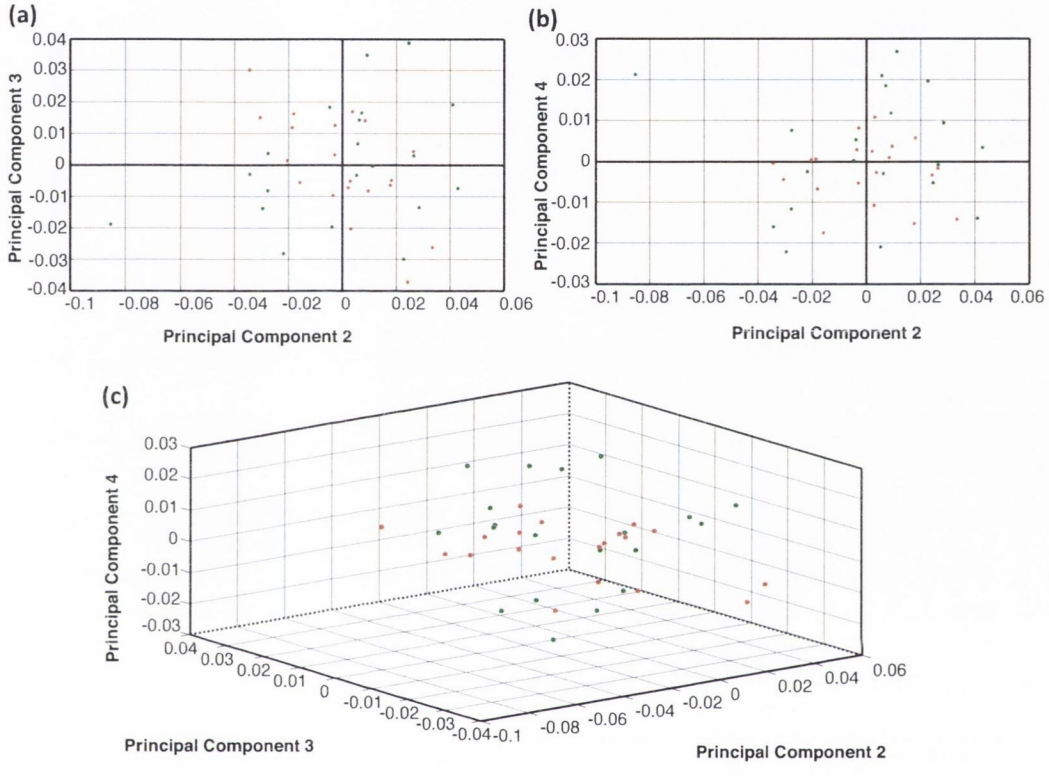


Figure 5-32 Principal component scatterplots of nucleus of untreated and treated primary oral epithelial cells.

PCA scatter plot showing the nuclei Raman Spectra spread of points between the untreated cells (green) and the treated cells (red). There is no difference between the groups of points which means EtOH has no effect on the nuclei after 24h treatment with PC2, PC3, or PC4.

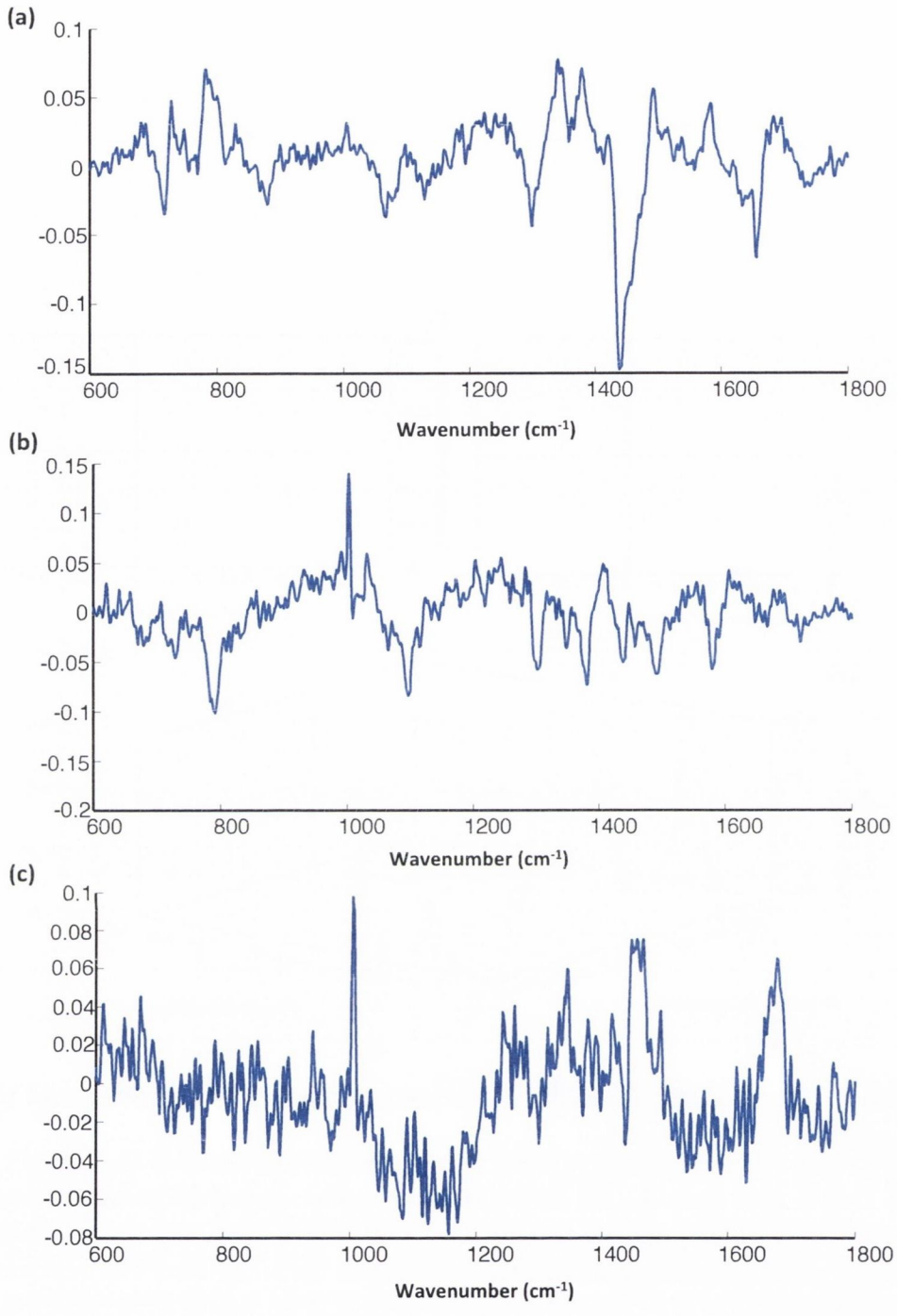


Figure 5-33 Principal component loading plots of nuclei of untreated and treated primary oral epithelial cells.

Loading plots of PC2 (a), PC3 (b) and PC4 (c). As shown in the PCA scatter plots there are no changes between the primary cells and treatment.

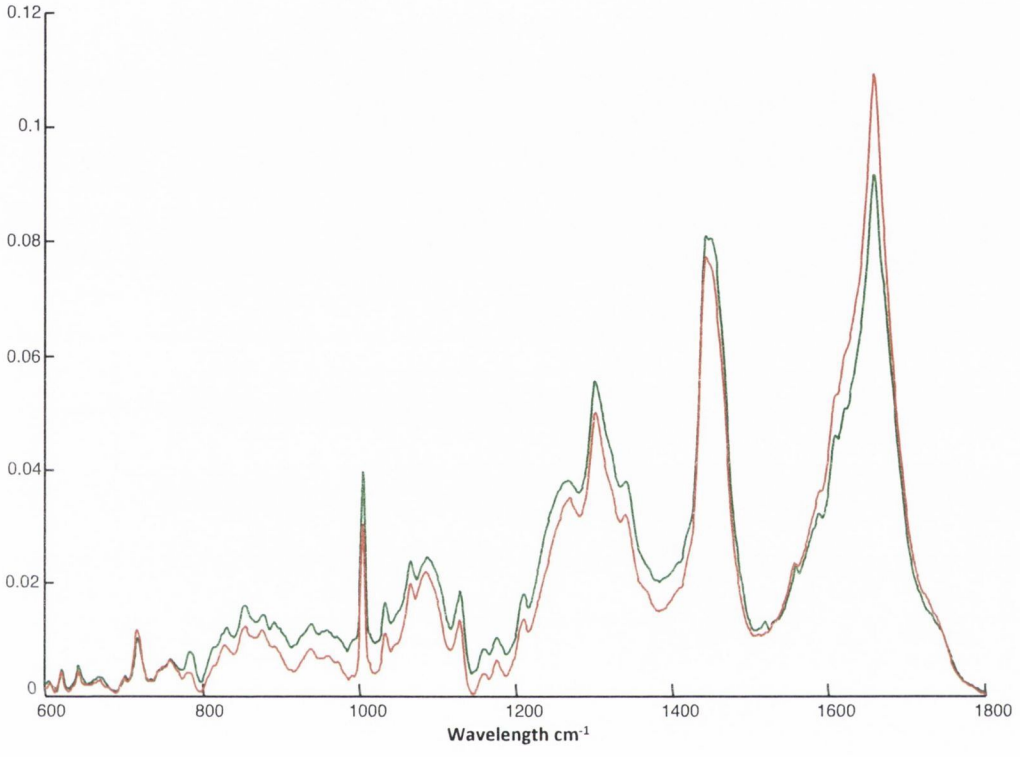


Figure 5-34 Advanced preprocessing of Raman spectrum of cytoplasm of treated and untreated primary oral epithelial cells.

Total average spectra from the cytoplasmic region of 20 cells of each type. Baseline correction was applied as in Section 4 and the mean was calculated prior to further analysis.

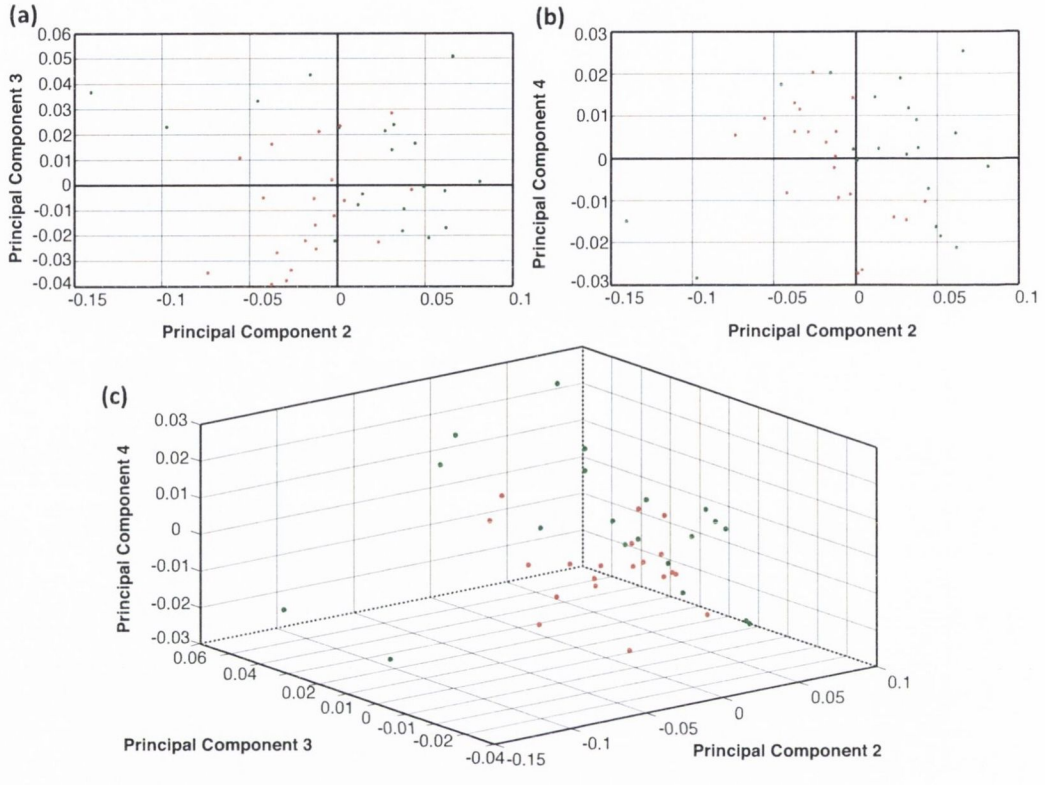


Figure 5-35 Principal component scatterplots of cytoplasm of untreated and treated primary oral epithelial cells.

Untreated cells (green) and the treated cells (red) can be separated from each other using PC2. PC3 and PC4 do not show any separation of the cell types.

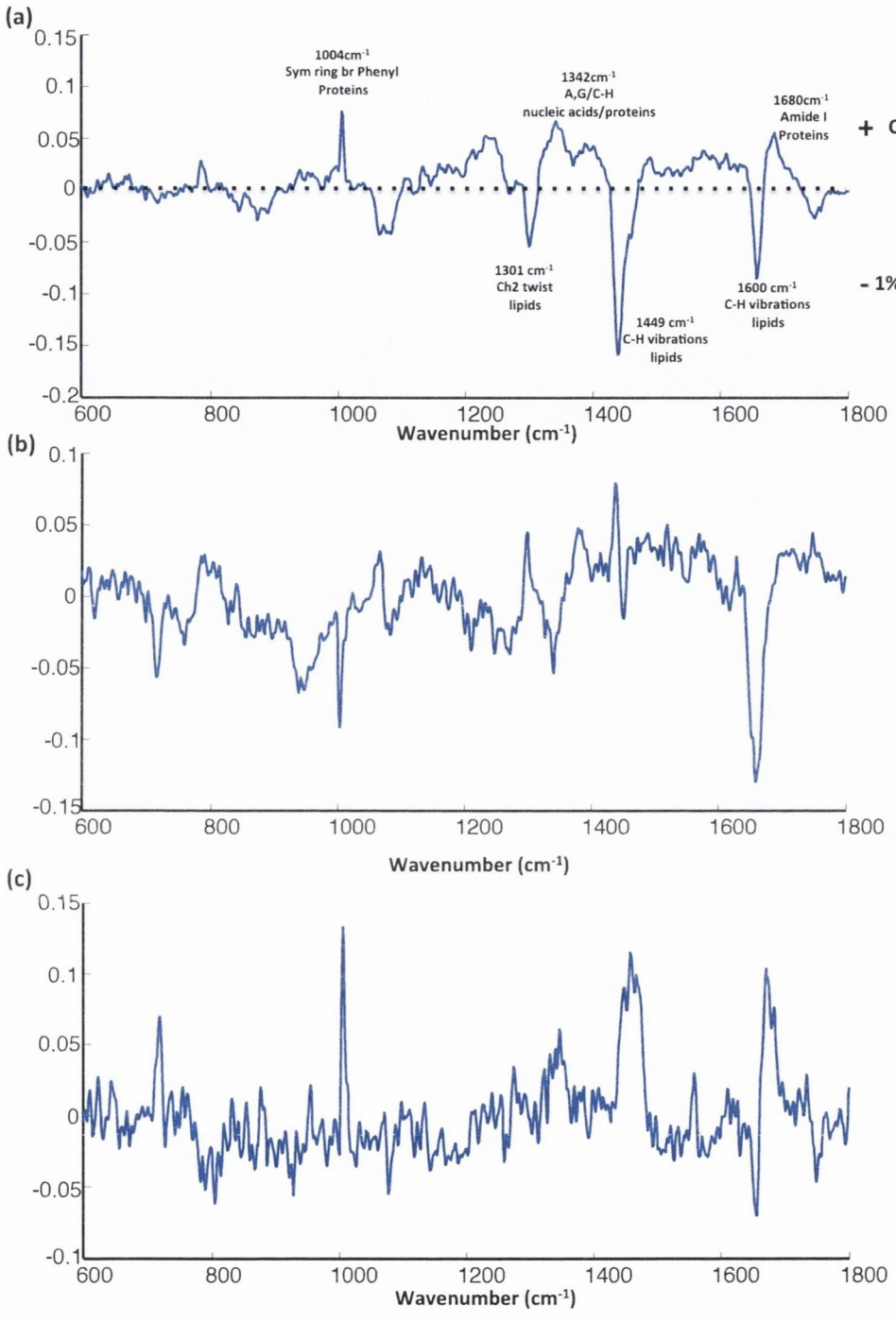


Figure 5-36 Principal component loading plots of the cytoplasm regions untreated and treated primary oral epithelial cells.

Loading plots of PC2 (a), PC3 (b) and PC4 (c). As shown in the PCA scatter plots PC2 (a) separates the control cells (+ve) from the treated cells (-ve).

5.4 Confirmation of the effect of EtOH on the nucleoli Raman spectra of TR146 and Ca9.22 cells using fluorescent microscopy

It was noted during the study that post 24h EtOH treatment that using a 100X water immersion objective lens that it was difficult to visualise the nucleolus hence capturing the Raman spectra was impossible. It was therefore decided, using fluorescence microscopy, to visualise the nucleolus after 6h, 24h and 48h treatment with 1% EtOH using RNA specific stain to monitor any changes in the nucleolar structure.

Figure 5-37 (a) and Figure 5-38 (a) and shows the 6h time point from both cell lines. The top line of images in represent the control cells and the bottom line represent the cells treated with 1% EtOH. The left-stacked images show the nucleolar dye alone, the right-stacked images show the nuclear dye alone and the central images show both of these stains merged. This is the same lay out of images in both the 24h (b) and 48h (c) for both the TR146 and Ca9.22 cell lines. After 6h treatment with EtOH there is no change in the structure of the nucleoli in either the TR146 or Ca9.22 cell line as shown by no change in fluorescence intensity or distribution of RNAselect™ stain in the green channel. After 24h (b) in both cell lines there is a visible decrease in nucleolar fluorescence intensity after treatment in comparison to the control. 48h treatment (c) with EtOH shows a marked decrease in punctuate green intensity forming in the nucleolus of both cell lines. In the TR146 is it impossible to make out any specific nucleoli however the staining intensity throughout the nucleus has increased in comparison to the control. In the Ca9.22 cell line the nucleolus is still visible however there is also an increase in intensity of staining throughout the nucleus and a decrease in the boundaries of the nucleolus in comparison to the control.

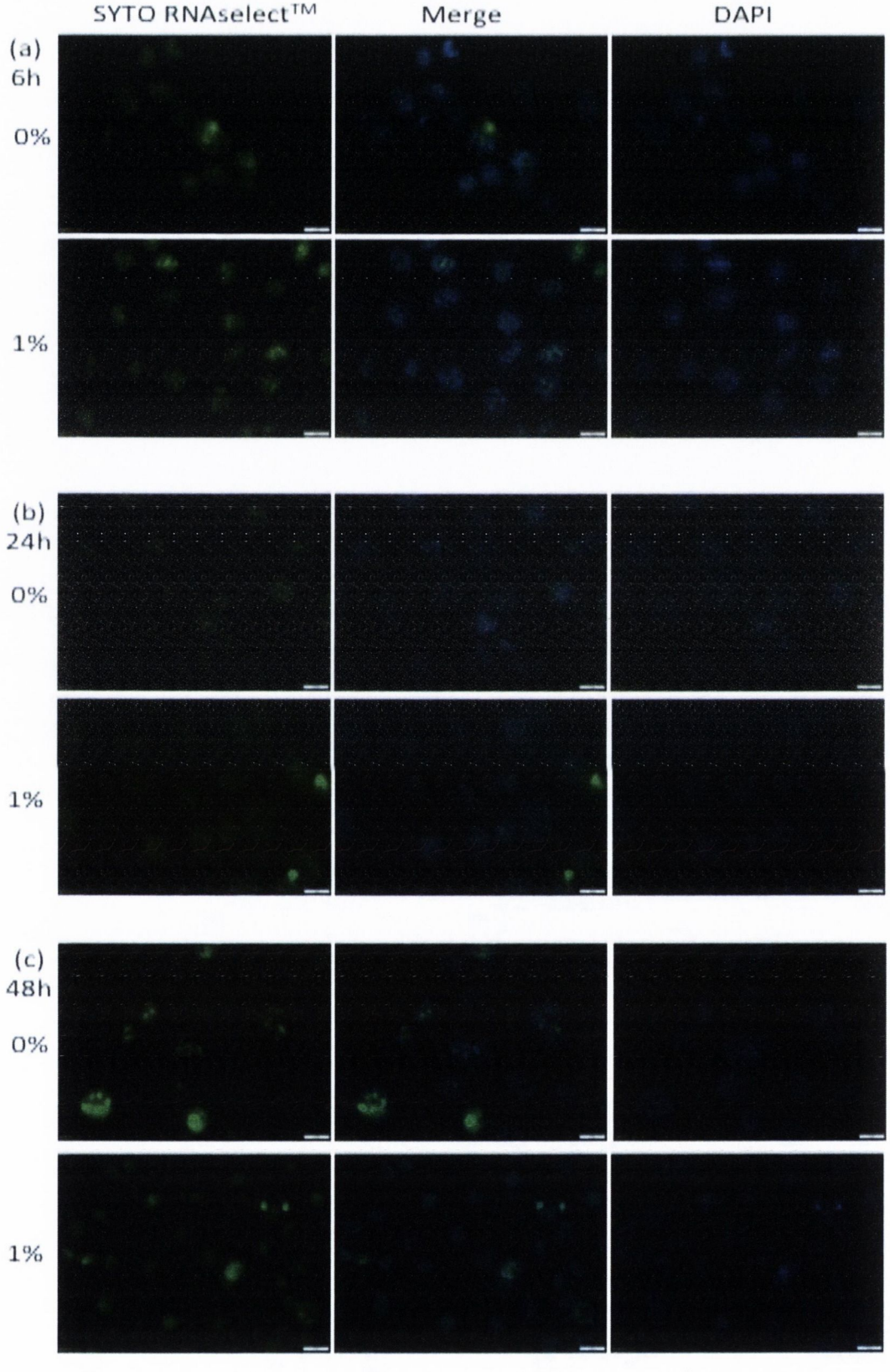

SYTO RNAselect™
Merge
DAPI
(a)
6h
0%
1%
(b)
24h
0%
1%
(c)
48h
0%
1%

Figure 5-37 Changes in nucleolar structure after treatment with EtOH in TR146 cell line.

Fluorescent microscopy images of immunofluorescent stain of nucleoli using RNAselect™ in TR146 cells. (a) 6h (b) 24h and (c) 48h are images of controls and treatment groups using 1% EtOH. Left-hand images are nucleolar staining in the green channel, right-hand images are DAPI in the blue channel and central images are merged DAPI and RNAselect™ staining. Images are representative of an individual experiment carried out in triplicate.

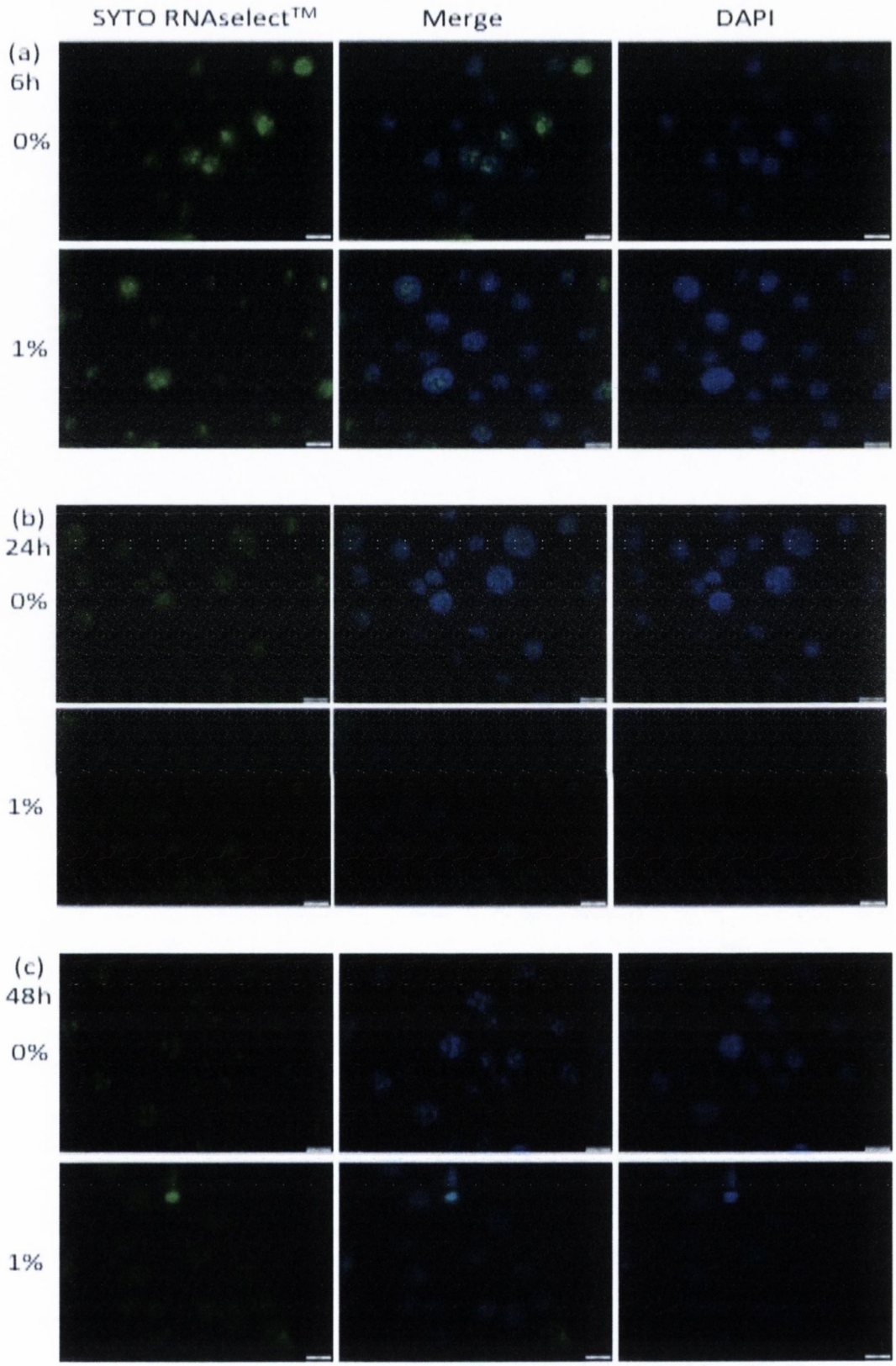

SYTO RNAselect™
Merge
DAPI
(a)
6h
0%
1%
(b)
24h
0%
1%
(c)
48h
0%
1%

Figure 5-38 Changes in nucleolar structure after treatment with EtOH in Ca9.22 cell line.

Fluorescent microscopy images of immunofluorescent stain of nucleoli using RNAselect™ in Ca9.22 cells. (a) 6h (b) 24h and (c) 48h are images of controls and treatment groups using 1% EtOH. Left-hand images are nucleolar staining in the green channel, right-hand images are DAPI in the blue channel and central images are merged DAPI and RNAselect™ staining. Images are representative of an individual experiment carried out in triplicate.

5.5 Discussion

Studies have shown that Raman spectroscopy can successfully distinguish cancer cell lines from normal cell lines using a spectrum of the cells molecular fingerprint (Chapter 4). This chapter focused on the use of Raman in monitoring changes in the cell caused by a potentially carcinogenic insult, EtOH. Previous chapters have shown that EtOH can induce changes to the antioxidant system in OC cell lines, dysplastic cells and normal primary cells, which could possibly lead to carcinogenic transformations. Using Raman analysis directly after the exposure period, changes to proteins, carbohydrates, lipids and nucleic acids can be distinguished to attempt to determine cellular targets that may possess potential biomarkers that could indicate alteration in these cells. All cell types were treated with 1% EtOH for 24h as longer time points were not possible as the nucleolus could not be visually distinguished.

Firstly, there was no observable effect on the nucleolus or nucleus in the TR146 or Ca9.22 cell line. The major effect of EtOH had in these cell lines was directed towards the cytoplasm and its components. Raman spectroscopy was able to differentiate changes within the cytoplasm between the untreated and treated cells based on PC4 in both cell lines. In the control for the TR146 cell line there was an increase in proteins. The TR146 treated cells showed a decrease in nucleic acids, RNA, lipids and proteins. Previous studies support these observations as EtOH is known to cause a decrease in protein synthesis *in vitro* and *in vivo* (Hong-Brown *et al.*, 2001, Rawat, 1985). A possible mechanism for this decrease in protein levels is via EtOH regulation of the mammalian target of rapamycin (mTOR) pathway. EtOH causes stabilisation of regulatory-associated protein of mTOR (RAPTOR), which inhibits the activity of mTOR kinase (Hagner *et al.*, 2009). This pathway has been known to be involved in regulation of cell growth, proliferation, survival, protein synthesis and transcription. Additionally in Chapter 3 it was noted that there were fluctuations in antioxidant response proteins in the cells whose main site of action is in the cytoplasm. Although it is not possible to specifically identify proteins that are changing with Raman spectroscopy, changes noted in the spectra could be partly due to the changing antioxidant response in these cells. Previously EtOH has also been shown to alter the lipids in biological membranes thus it could react with lipids within the cell itself (Gurtovenko and Anwar, 2009). Lipids have unique and important functions in cells including cell signalling, cellular structure, and

energy storage (Glatz *et al.*, 1995, Frauenfelder, 2010). In the Ca9.22 cell line, treated cells show an increase in RNA, proteins and nucleic acids in comparison to untreated cells. This is in contrast to what was observed in the other cell line. As mentioned in previous chapters, differences between TR146 cell line and the Ca9.22 could be site or gender specific however the major disparity between the cell lines lies in the genotype of the Ca9.22 cell line, which contains a p53 mutation. The differences shown here between the cells could be due to p53 regulation of EtOH targets. Activation of p53 has been shown to control mTOR in a variety of cells (Feng *et al.*, 2005). It is therefore possible that in the Ca9.22 cells, the effect of EtOH on mTOR is not as potent or efficient due to the p53 mutant thereby reducing protein synthesis.

In contrast to the cell lines, EtOH exposure altered the Raman spectroscopy molecular fingerprint of DOK cells in the nucleolus, nucleus and cytoplasm. In the treated cells there was more RNA and nucleic acids in the nucleoli and a decrease in the nucleus in comparison to the untreated cells. Therefore EtOH is causing an accumulation of RNA and nucleic acids in nucleolus, which possibly originated from the nucleus. As mentioned previously the nucleolus has a diverse range of functions within the cell. It is implicated in controlling several cellular functions including regulation of the cell cycle, DNA replication and repair, stress signalling and induction of apoptosis. This study found that not only is there an increase in nucleic acids in the nucleoli there is also an increase in lipids and proteins due to EtOH treatment and a decrease in the nucleus in comparison to the untreated cells. Protein accumulation has previously been noted in the nucleolus of cancer cells (Ruggero and Pandolfi, 2003). It was not until recently that the role of lipids in the nucleus had been established. Lipids within the nucleus are involved in cell cycle regulation as they have been found in interphase chromatin and metaphase chromosomes (Alessenko, 1990). Decrease in regulation of lipid dispersion in the nucleus may interfere with correct cell cycle function in cells treated with EtOH.

Not only does EtOH affect the nuclei and nucleoli of DOK cells it also affects the cytoplasm, in contrast to the TR146 and Ca9.22 cells. In line with the results noted in the nuclear components of the treated DOK cells there is also a decrease in protein, nucleic acids and lipids in the treated cells cytoplasm in comparison to the control. This decrease in molecules in the cytoplasm may be due to the dysregulation of proteins and lipids in

the nucleus so therefore transport of specific components from the nucleus to the cytoplasm would be affected. The impact of EtOH on the nucleolus might be partly responsible for the alterations in mRNA expression in antioxidant enzymes noted in Chapter 3. Lipids and proteins are involved in transportation of molecules from the nucleus to the cytoplasm (Lev, 2010). Therefore if nucleic acid production is decreased then protein and lipid function would be disrupted within in the nucleus and transport of molecules to the cytoplasm will be reduced, as the cell will focus on repair or initiating apoptosis resulting in the decreased levels of molecules in the cytoplasm as observed here. This concurs with results noted in Chapter 3 as the cells arrest in the G2/M phase of the cell cycle, a distinguishing feature of growth inhibition and repair (Kastan and Bartek, 2004). The decrease in protein levels may also be a result of effect of EtOH on mTOR as previously mentioned in the OSCC cell lines. EtOH can cause the stabilisation of molecules that can inhibit the activity of mTOR kinase in its cell regulation activities, an action that has been implicated in oncogenic transformation (Guertin and Sabatini, 2007). Additionally decreasing levels of certain antioxidants were noted in Chapter 3 in the DOK cells, in particular GPx-1 and HO-1, therefore decreasing levels of these enzymes could be causing some of the reduction noted in the cells cytoplasm, their main place of action.

Utilising Raman to follow the effect of EtOH exposure on primary epithelial cells yielded results comparable to those observed on DOK cells. There was an accumulation of proteins and lipids in the nucleolus of the primary cells after treatment with EtOH. However there was no change observed in the component content of the nucleus. This discrepancy between cells maybe phenotypic in nature and a result of the dysplastic nature of the DOK cells. Differential lipid composition between the primary and dysplastic cells is likely due to the membrane lipid composition, a factor that is known to change in oncogenic cells (Leach, 1996, Negendank, 1992). The accumulation of proteins in the nucleoli of primary cells is perhaps due to the nucleolar retention pathway, as stated previously, that causes an accumulation of protein to regulate cell function. There was also a decrease in lipids and proteins in the cytoplasm of primary cells, which was similar to the DOK cells and could be due to the direct effects of EtOH on the components in the cells. Similarly to DOK cells there was a decrease in HO-1 noted in the primary cells in Chapter 3 which could cause some of the reduction noted in components in the cytoplasm. It must be also taken into account that the cytoplasm

contains a large number of organelles that may vary in size and integrity between the cell types, which may influence to overall cellular content of lipids and proteins. The changes within the nuclear components are perhaps the more influential irregularities that could cause greater damage within the cell.

After 48h treatment with EtOH there was no visible nucleoli in the cells when examined with the microscope attached to the Raman spectrometer. Analysing the Raman fingerprint there was a significant changes in the nucleoli when treated with EtOH for 24h in the dysplastic and primary cells. The separations were made using PC2 which demonstrates that the changes were greater than any other changes in other cellular components. Using a fluorescent stain to highlight the nucleoli in the TR146 and Ca9.22 cells showed that after 24h treatment there were significant changes in nucleoli structure. In the controls there is a distinct boundary between the nucleus and nucleoli however in the treated cells the boundary becomes diffuse after 24h possibly due to the increased accumulation of proteins and lipids in the nucleoli. Increased retention of proteins and lipids will cause dispersion of the RNA, which is the target of the stain, therefore decreasing the intensity of the fluorescence. After 48h in the TR146 cell there were no visible nucleoli and very faint nucleoli in the Ca9.22 cells. Although there was no direct effect of EtOH on the nucleoli Raman spectra after 24h in the cell lines it is possible that as the cells are already a cancer phenotype they are somewhat more resistant to EtOH disruption but after 48h the threshold is reached and EtOH causes accumulation of cellular components in the nucleolus. Such irregularities in nucleoli function are markers of oncogenic changes in cells as stated previously and appear to be the result of the presence of EtOH in the models used during these experiments. EtOH induced nucleoli damage is a potential early event in the transformation of cells. With recurrent excessive consumption of alcoholic beverages patients are causing repeated insults in this region of the cell and can potentially give rise to a malignant species should intracellular mechanism of control fail to supress these changes.

This novel study found that EtOH affects lipids, protein and nucleic acids levels and distribution in all cell types analysed and that these changes can be successfully identified using Raman spectroscopy. Specifically of interest, in the transformed cells there is a direct effect on the nucleoli spectra. The cancer cell lines may be able to

protect the nucleoli for a longer time period perhaps because cancer cells have larger nucleoli. However the nucleoli in all cell types were not visible after 48h treatment as determined by Raman spectroscopy and confirmed by fluorescent microscopy demonstrating that EtOH is responsible for alterations in the nucleolar structure. The nucleolus is widely implicated in cancer as it controls the functions of many tumour suppressor proteins. In conclusion, EtOH mediated transformation of these cell types is predominately focused on damaging the nucleoli and hence causing disruption to the pathways under nucleoli control and potentially can cause dysregulation in untransformed oral cell types resulting in the initiation of carcinogenesis.

6 Induction of apoptosis in OSCC cell lines by pyrrolo-1,5-benzoxazepines

6.1 Introduction

The treatment of OC usually has a multi- disciplinary approach and the elements involved depend on the size, stage and location of the cancer. Surgery is typically the main treatment of OCs with the use radiation and chemotherapy drugs adjunctively. After surgical removal of the cancerous tissues there is typically a requirement for plastic and reconstructive surgery to rebuild bones and tissues in the mouth. This is highly invasive and debilitating to the patient. The use of chemotherapy drugs alone without surgical intervention has not been shown to improve survival rates among patients. There is a need for a new treatment options that are less invasive and more effective than those on the current market. This study investigates the use of a novel microtubule-targeting agent in the treatment of OSCC.

6.1.1 Microtubules

Microtubules are filamentous cell structures that comprise the cytoskeleton, the protein network that gives the structure to the eukaryotic cell and allows for various types of movements within the cell including cell division and organelle movement. α-tubulin and β-tubulin are the primary components of microtubules. α and β-tubulin form dimers that polymerise into protofilaments by joining end to end. The microtubule is formed when 13 linear protofilaments assemble around a hollow core. In each protofilament, α-tubulin is exposed at one end and β-tubulin at the other. Microtubules are polar structures with a positive and negative end and this polarity determines the direction of movement. Both α and β-tubulin can bind GTP. Unlike α-tubulin, β-tubulin can hydrolyse this bound GTP to GDP and Pi. Likewise it can release the Pi and exchange the GDP for GTP (Lowe *et al.*, 2001).

Microtubules are dynamic structures that carry out their functions in the cell by assembly and disassembly through polymerisation and depolymerisation. During polymerisation GTP bound to β-tubulin is hydrolysed. This weakens β-tubulins affinity for adjacent molecules resulting in depolymerisation. Tubulin with bound GDP are repetitively lost from the minus end and replaced at the plus end with GDP bound tubulin. The microtubule will continue to grow as long as there is an excess of GTP bound tubulin. If the rate of GTP hydrolysis becomes faster than the rate of addition, the

GDP bound tubulin at the end will dissociate and disassembly occurs. The switch between phases of growth and shrinkage is referred to as dynamic instability (Horio and Murata, 2014).

During mitosis, the key function of microtubules is attachment and alignment of the sister chromatids. The microtubule organising centre (MTOC) is the anchoring point near the centre of the cell from which the microtubules extend out. During interphase the MTOC is at the centrosome. Throughout cell division the microtubules disassemble from the MTOC and reassemble to form the mitotic spindle (de Forges *et al.*, 2012). The spindle tubulin ensures correct attachment to the kinetochores on the chromatids. In metaphase, microtubules align the chromosomes along the metaphase plate. Later, during anaphase and telophase the microtubules aid the movement of chromosomes to opposite poles to ensure they are in the proper position when the cell divides into daughter cells.

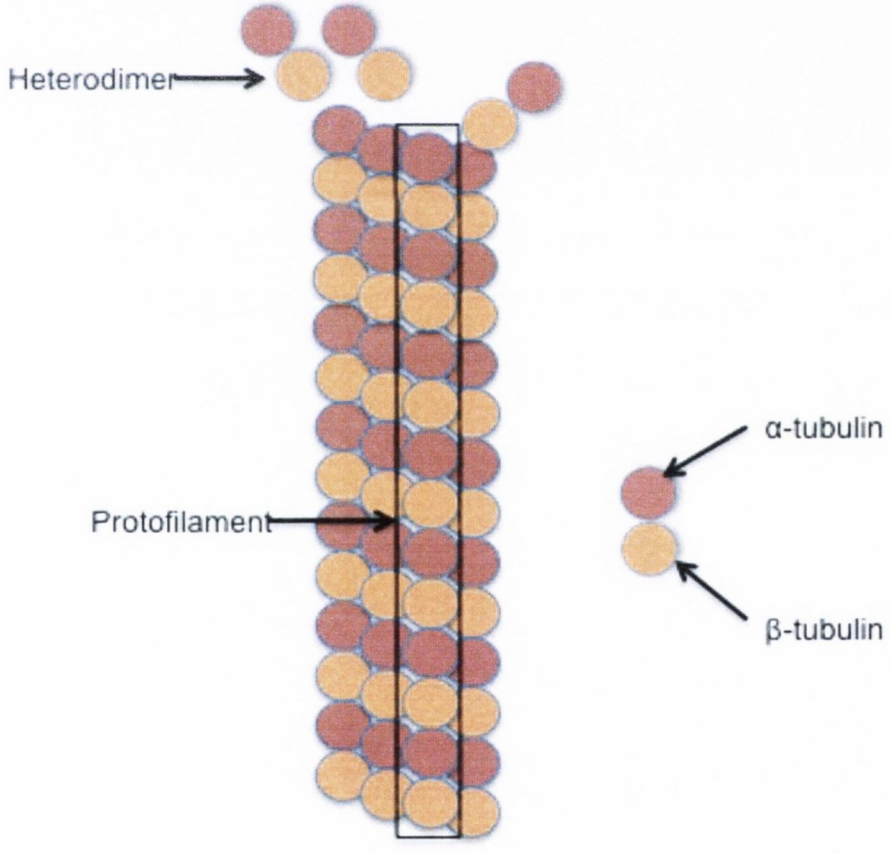


Figure 6-1 the structure of a tubulin polymer.

6.1.2 Microtubule targeting agents

The cell cycle has a number of checkpoints, which become faulty in cancerous cells allowing for uncontrolled proliferation. Therefore one approach to combatting these defective cells is to use drugs that target certain processes or proteins that impinge on the cell cycle machinery. As previously discussed above microtubules play a critical role in cell division therefore making them an attractive candidate for cancer therapy. Microtubule targeting agents (MTAs) inhibit cell division by binding to microtubules (see Figure 6-3 and Figure 6-4) and inhibiting microtubule dynamics during mitosis. The binding site for PBOX compounds on tubulin is currently unknown but studies of the binding sites of other MTAs might aid in hypothesising the potential binding sites (Figure 6-4). During mitosis, microtubules that form the spindle become 4-100 times more dynamic than interphase microtubules. MTAs inhibit cell division by interfering with the spindle microtubule dynamics.

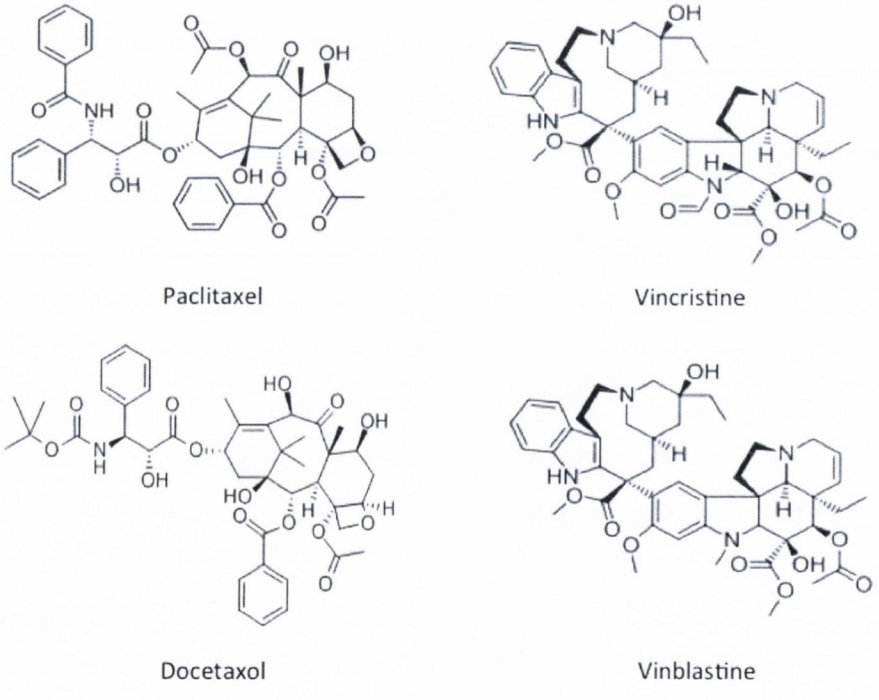


Figure 6-2 Chemical structures of common MTAs.

Two classes of MTAs exist; those which stabilise microtubules and those which destabilise. Destabilisers inhibit polymerisation e.g vinca alkaloids, colchicine and combretastations. Stabilisers increase polymerisation e.g paxlitaxel and epothilones. Vinca alkaloids were first isolated from the leaves of the periwinkle plant *Catharanthus roseu.* Since the 17th century the leaves of this plant have been known for its medicinal properties. Two groups discovered the anti-cancer potential of the drug in the late 1950's (Johnson *et al.*, 1959) (Noble *et al.*, 1958). The mechanism of action for this group of compounds is to induce apoptosis through binding tubulin causing depolymerisation and formation of large crystalline structures composed of drug and tubulin (Malawista *et al.*, 1968) (Lengsfeld *et al.*, 1981) (Bensch and Malawista, 1968). This tubulin disruption causes metaphase arrest in dividing cells (Howard *et al.*, 1980). Each heterodimer of α-β tubulin possesses a single vinca-specific site of high affinity located at the plus end of the tubulin heterodimer.

Paclitaxel (Taxol), from the Taxane group of compounds, was first isolated in 1971 from the bark of a western yew tree, *Taxus Brevifolia nut*, and was found to promote tubulin assembly. This in turn shifts the equilibrium in a cell towards polymerisation of tubulin molecules. Unlike other anti neoplastic drugs, tubulin is the only confirmed target of paclitaxel. The polymerisation of tubulin in the presence of paclitaxel causes tubulin to have the inability to carry out many functions within the cell. Tubulin, as mentioned above, is very dynamic and polymerisation/depolymerisation allows it to move organelles and other cell structures for normal cellular processes. Inhibition of these processes will render the cell unable to divide and it will drive its machinery into the apoptotic cell death pathway.

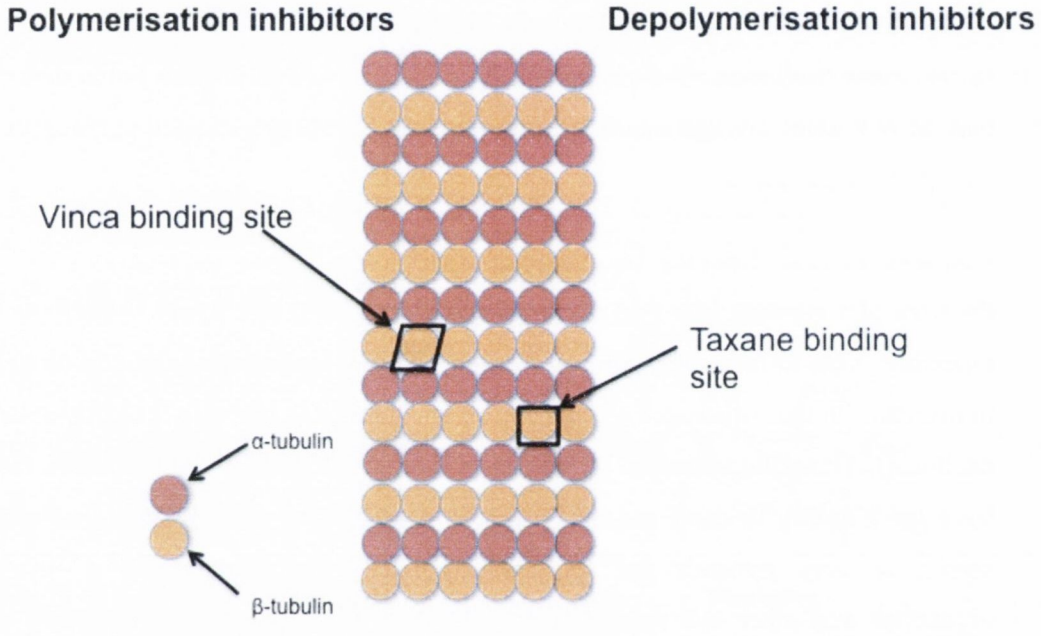


Figure 6-3 The binding sites for microtubule targeting drugs on tubulin.

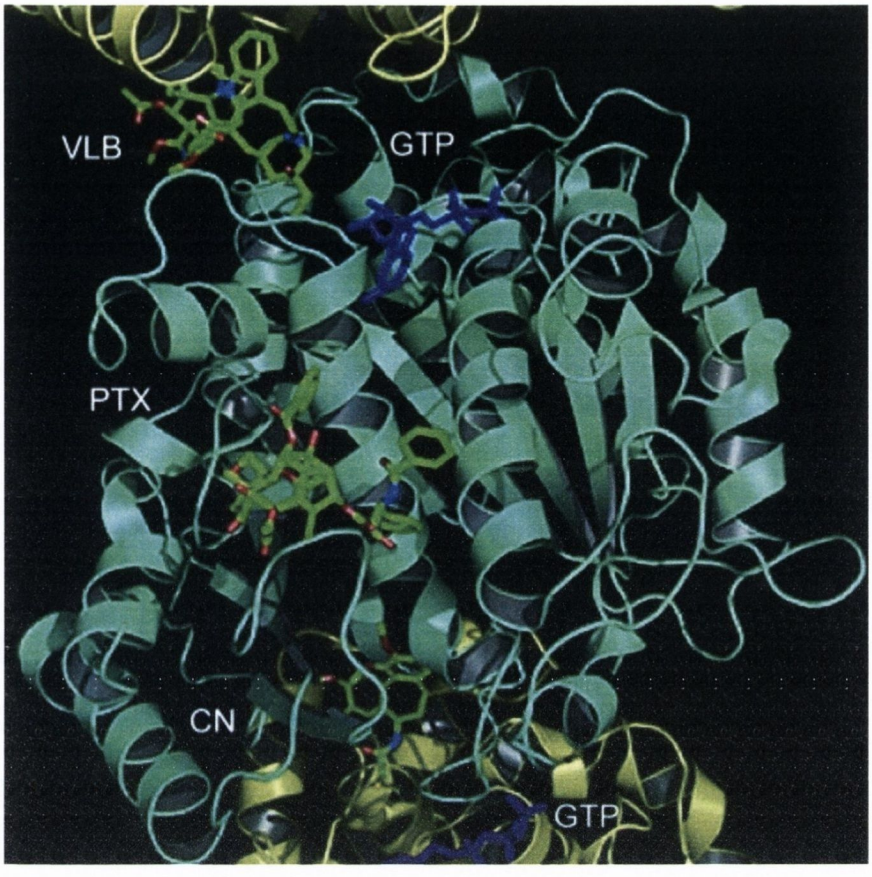


Figure 6-4 Computer generated 3D image of common tubulin binding sites for microtubule targeting agents.

Image of the α/β tubulin protafilament with binding sites of paclitaxel (PTX), colchicine (CN) and vinblastine (VLB) shown. A single α/β-tubulin heterodimer comprises the β-tubulin monomer (green) in the center of the image and two α-tubulin monomers (yellow) at the top and bottom of the frame. The GTP at the non-exchangeable and GDP at the exchangeable site are colored purple. PDB (Protein Data Bank)

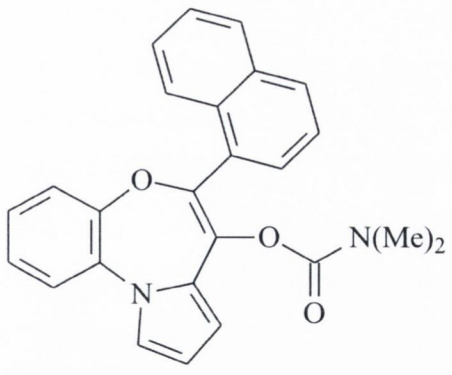
6.1.3 Pyrrolo-1,5-Benzoxazepine (PBOX)

PBOXs are a group of novel compounds designed and synthesised by a group in Siena, Italy originally designed as high affinity ligands for the peripheral benzodiazepine receptor (PBR), which is expressed in multiple locations throughout the body. The exact role of the PBR receptor is yet to be elucidated however it has been observed that PBR ligands have a role in apoptosis. Over the past decade it has was noted that PBOX compounds have anti proliferative effects in a range of cancerous cell lines, in *ex vivo* patient samples and *in-vivo* models (Bright *et al.*, 2010).

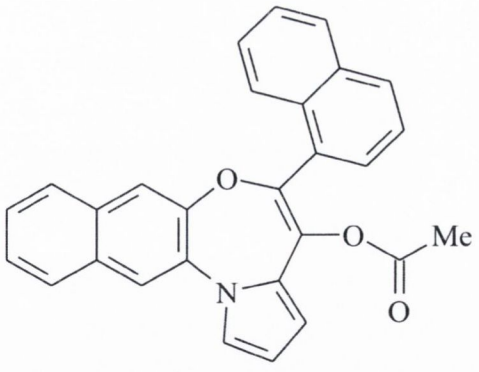
The PBOX compounds can be divided into two classes, those that arrest cells in the G1 phase such as PBOX-21 and those which induce apoptotic cell death, for example

PBOX-6. Two of the more potent members of the latter class, PBOX-6 and PBOX-15 (Figure 6-5) have been shown to induce cell death in a number of cell lines including, MCF-7 breast cancer cells (Mulligan *et al.*, 2006, Greene *et al.*, 2005), A2780 ovarian cancer cells (Nathwani *et al.*, 2010a), Jurkat and HUT-78 T-lymphoma cells (Zisterer *et al.*, 2000). Importantly these drugs have been shown to induce apoptosis in a number of multi drug resistant cells lines, for example the highly drug-resistant chronic myeloid leukaemia, K562 cell line (Zisterer *et al.*, 2001). The PBOX compounds are not only potent against neoplastic cells they also show minimal toxicity towards normal peripheral bone marrow cells, normal B-cells and bone marrow progenitor cells (Mc Gee *et al.*, 2004, McElligott *et al.*, 2009). Therefore these compounds target cancer cells specifically without damaging surrounding normal cells unlike many common chemotherapy drugs. Both PBOX-6 and PBOX-15 have been shown to cause apoptosis by depolymerisation of the microtubule network in a similar manner to MTAs previously mentioned (Mulligan *et al.*, 2006). Although tubulin has been identified as the molecular target, the binding site on the tubulin heterodimer is yet to be identified.

Previously members of the PBOX family have been shown to work in combination with other non-MTA drugs in several malignant cell types such as CML cell lines, K562 and LAMA84 (Mc Gee *et al.*, 2004, Nathwani *et al.*, 2010b, Bright *et al.*, 2009). CML is caused by a constitutively active tyrosine kinase, breakpoint cluster region-Abelson (Bcr-Abl). This tyrosine kinase phosphorylates proteins involved in growth factor signalling or cell adhesion. It is the result of the reciprocal translocation between chromosome 9 and 22, t(9;22), more commonly known as the Philadelphia chromosome (Deininger *et al.*, 2000). The current first line treatment of CML is Imatinib (STI-571) however cells can become resistant to this tyrosine kinase inhibitor. PBOX-6 has been shown to synergistically enhance the effects of Imatinib and more importantly it has been shown to induce apoptosis with co –treatment with Imatinib in Imatinib-resistant cell lines. Co-treatment with flavopiridol, a cyclin-dependant kinase inhibitor, also induced apoptosis in CML cells. More recently PBOX-6 has been shown to induce apoptosis and improve the efficacy of carboplatin in drug sensitive and MDR neuroblastoma cells (Lennon *et al.*, 2014). PBOX-15 has been shown to improve efficacy of oxalipatin, a platinum-based antineoplastic agent, in colorectal cancer cell lines (Gangemi *et al.*, 2013). Interestingly PBOX-15 increases radiosensitivity in several cancer cell lines (Forde *et al.*, 2011).



PBOX-6



PBOX-15

Figure 6-5 Chemical structure of the microtubule targeting agents PBOX-6 and PBOX-15.

Treatment of OC is usually determined by the stage, size and location of the cancer. The use of anti neoplastic agents is common but they are usually used in combination with another form of treatment i.e. neoadjuvant and adjuvant therapy. The most commonly used chemotherapy drug is cisplatin, which is a platinum containing drug (Bhide and Nutting, 2010). Carboplatin, another platinum containing compound is used in the treatment of OC. As mentioned above, PBOX compounds have been shown to increase efficacy of some common non-MTA drugs in different types of cancer. Recently, carboplatin has been shown to work in combination with PBOX-6 in neuroblastoma cells (Lennon *et al.*, 2014).

6.2 Aims of the chapter

Given the prevalence of chemoresistance now occurring in cases of OSCC, this study focused on the potential of PBOX compounds as novel agents in the treatment of OC. Numerous studies have investigated the effects of PBOX compounds on several carcinoma cell lines, *ex vivo* models and *in vivo* studies. In these studies the PBOX compounds have been shown to induce apoptosis by the irreversible binding of tubulin and its depolymerisation. This study is the first to examine the potential of PBOX compounds for use in OC and in particular OSCC. This study focuses on the effects of PBOX-6 and PBOX-15 on TR146, a buccal mucosa cell line, and Ca9.22, a gingiva cell line. Specific objectives were as follows:

1. Examine the potential anti proliferative effects of PBOX-6 and PBOX-15 on two OSCC cell lines.

Cell lines were treated with a range of concentrations of PBOX to determine effective doses over a 72h period of treatment. This allows determination of the optimum concentration of drug needed for maximal response.

2. Determine the cellular processes through which PBOX compounds induce apoptosis in these cell lines.

Using fluorescent microscopy, the structure of tubulin was assessed after treatment with PBOX compounds. Polymerisation assays were completed to investigate if PBOX compounds are promoting the depolymerising of tubulin.

3. Investigate the effect of PBOX compounds on the cell cycle.

The cell cycle was examined using flow cytometry after exposure with each compound to assess whether observed effects of tubulin could be correlated with any changes in the cell cycle.

4. Investigate the process by which PBOX compounds are inducing death.

Investigating the mechanisms involved in cell death by the PBOX compounds. Apoptotic cell markers were analysed by western blot.

6.3 Results

6.3.1 PBOX compounds reduced OC cell proliferation

OSCC cell lines were treated for 24-72h with a range of concentrations of PBOX-6 or PBOX-15. Cell proliferation was measured using an AlamarBlue viability assay. PBOX-6 and PBOX-15 reduced proliferation of both Ca.922 and TR146 cell lines in a dose dependant manner (Figure 6-6). PBOX-15 was found to be the more potent of the two analogues. IC-50 values (concentration of drug resulting in 50% reduction in cell viability) were 35 ±2.7μM and 470 ±86nM for PBOX-6 (a) and PBOX 15 (b) at 72h, respectively in TR146 cells and 2.6 ±1μM and 83 ±32nM for PBOX-6 (c) and PBOX-15 (d) at 72h, respectively in the Ca9.22 cell line (Table 6-1). Therefore the Ca9.22 cells were more sensitive to PBOX compounds due to the lower IC-50 values. Time-dependant inhibition was observed in the TR146 cell line with treatment of PBOX-15 (b).

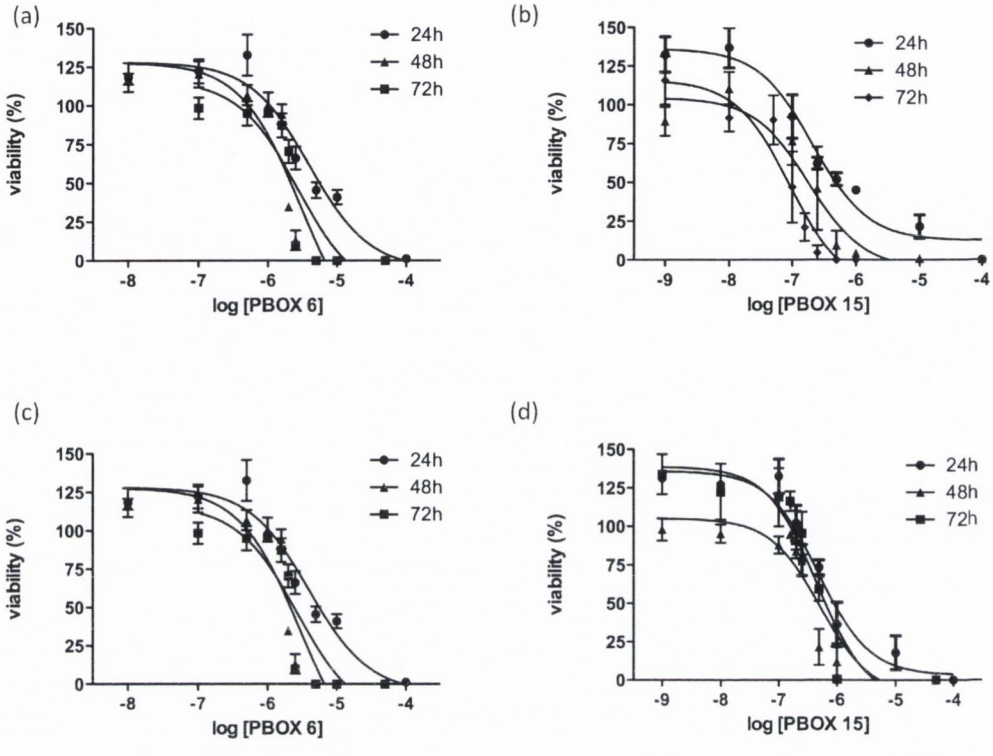


Figure 6-6 PBOX-6 and PBOX-15 reduce viability of TR146 and Ca9.22 cell lines.

OSCC cell lines TR146 (a) (b) and Ca9.22 (c) (d) were seeded at 1 x10^4 cells/well in a clear 96 well plate. Cells were then treated with a range of PBOX -6 (a) (c) and PBOX-15 (b) (d). After 20h, 44h and 68h AlamarBlue was added to the wells for 4h. Fluorescence levels were determined using a Spectramax Gemini Plate reader at excitation and emission wavelengths of 544nm and 590nm respectively. Values represent the mean ± S.E.M of three independent experiments.

IC-50 TR146			
	24h	**48h**	**72h**
PBOX-6	9.2± 2.3μM	8.1± 0.3μM	35± 2.7μM
PBOX-15	480± 92nM	530± 52nM	470± 86nM
IC-50 Ca9.22			
	24h	**48h**	**72h**
PBOX-6	4.5± 1.5μM	2.9± 0.7μM	2.6± 1μM
PBOX-15	210± 28nM	170± 81nM	83± 32nM

Table 6-1 IC-50 values of PBOX-6 and PBOX-15 in Ca9.22 and TR146 cell lines.

6.3.2 PBOX compounds destabilised the microtubule network in OC cells

Ca9.22 and TR146 cells were treated with PBOX-6 or PBOX-15 for 24h. As a positive control, cells were also treated with the known tubulin polymeriser paclitaxel and the tubulin depolymeriser nocozadole. Immunofluorescent staining was used to detect morphological changes in the microtubule network, such as, alterations in organisation and arrangement (Figure 6-7 and Figure 6-8). In untreated TR146 and Ca9.22 cells, the microtubule network is organised as cytoplasmic tubulin filaments radiating from a central point to the periphery. Cells treated with vehicle alone (1% EtOH) displayed this typical tubulin morphology. Exposure of cells to the tubulin polymerising agent paclitaxel resulted in highly concentrated accumulation of filaments into dense peripheral bundles indicative of microtubule stabilisation. The tubulin depolymerising agent nocozadole resulted in diffuse tubule staining with no defined structure caused by microtubule disassembly. While no change in microtubule structure was evident following treatment with low dose (100nM) PBOX-6 and PBOX-15, higher concentrations of 10μM PBOX-6 and 1μM PBOX-15 resulted in a clear observable change in tubulin morphology resembling that of the drug nocozadole. This demonstrates that PBOX compounds can destabilise the microtubule network in a similar manner to a recognised depolymerising agent in both TR146 and Ca9.22 cell lines.

Confirmation that the disruption observed using fluorescent microscopy is depolymerisation of the tubulin network, tubulin polymerisation assays were completed using differential centrifugation followed by detection using immunoblotting. After a 4h

exposure, tubulin is completely depolymerised (Figure 6-9) with 10μM PBOX-6 and 1μM PBOX-15 in both cell lines. After 4h exposure with paclitaxel the tubulin is polymerised and with nocozadole it is unpolymerised. In the presence of the vehicle (1% EtOH) there is no effect on the tubulin network and equal levels of polymerised to unpolymerised tubulin are present. This confirms that the disruption observed using fluorescent microscopy is depolymerisation of the tubulin network as a result of exposure to PBOX compounds.

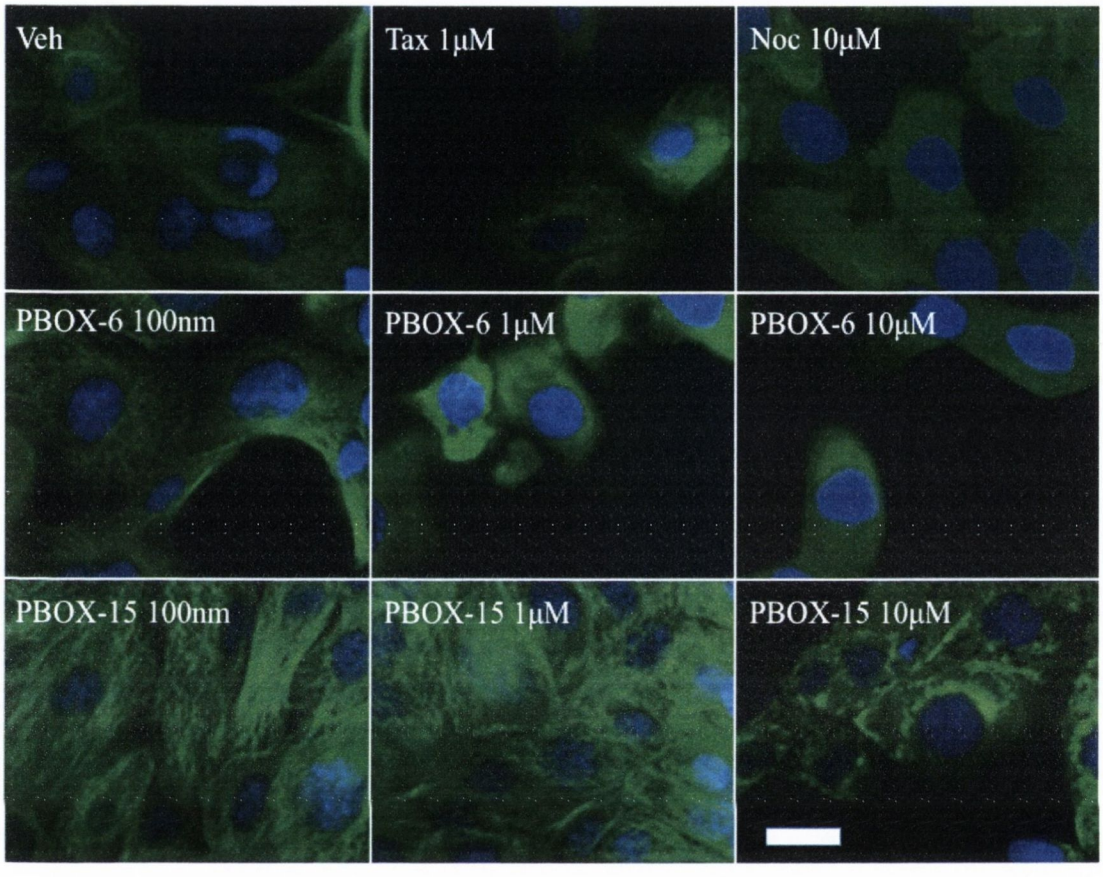


Figure 6-7 PBOX compounds cause disruption of microtubule network in TR146 cells.

TR146 cells were treated with either only media 1μM paclitaxel (tax) 10μM nocodazole (noc), 100nM, 1μM, 10μM PBOX-6 and 100nM, 1μM, 10μM PBOX-15 for 24h. After this time, the medium was carefully removed and the cells were washed and fixed in 4% paraformaldehyde. Cells were incubated with monoclonal anti-α-tubulin antibody (1:2000) for 1h at room temperature followed by incubation with anti-mouse secondary antibody (1:500) for a further hour at room temperature. The organization of the microtubule network (green) and the cellular DNA (blue) was visualized by a Zeiss Axiovert/ Axiocam CCD system through a 60X oil objective. Scale bar= 20μM. These images are representiative of an experiment completed three times.

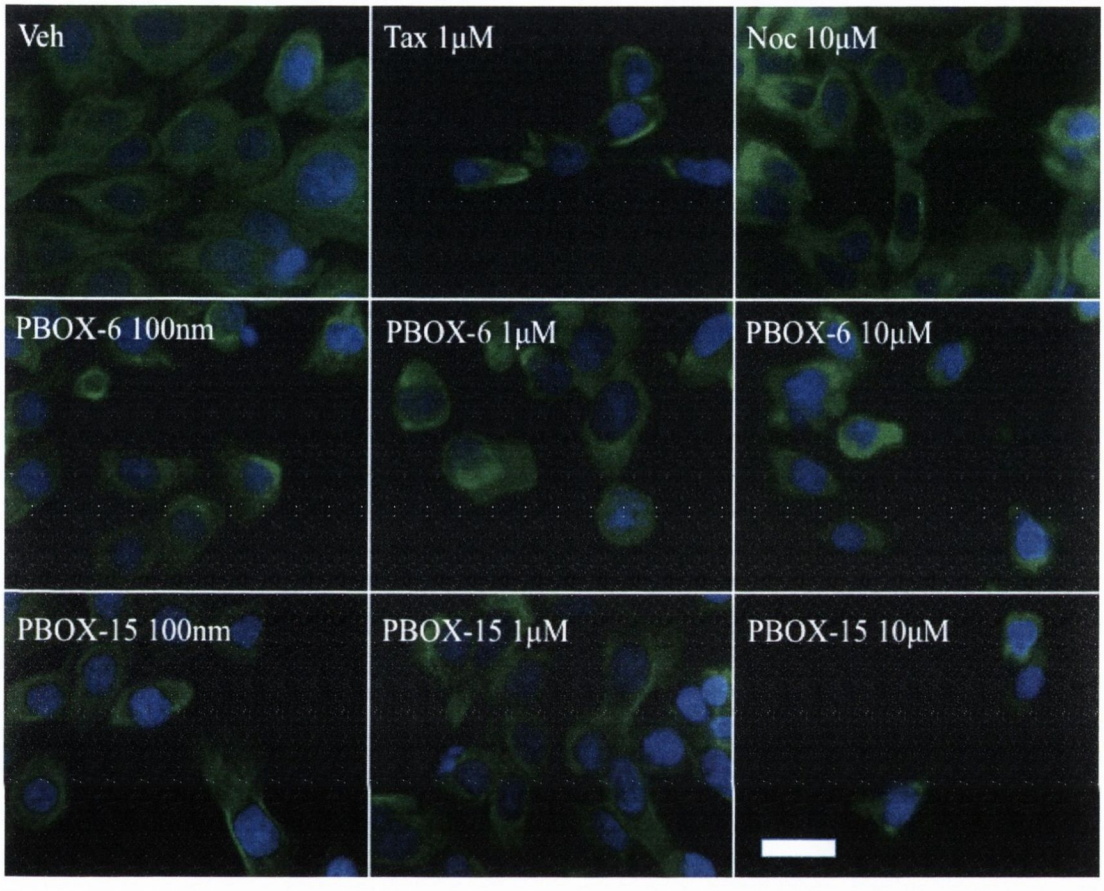


Figure 6-8 PBOX compounds cause disruption of microtubule network in Ca9.22 cells.

Ca9.22 cells were treated with either only media 1μM paclitaxel (tax) 10μM nocodazole (noc), 100nM, 1μM, 10μM PBOX-6 and 100nM, 1μM, 10μM PBOX-15 for 24h. After this time, the medium was carefully removed and the cells were washed and fixed in 4% paraformaldehyde. Cells were incubated with monoclonal anti-α-tubulin antibody (1:2000) for 1h at room temperature followed by incubation with anti-mouse secondary antibody (1:500) for a further hour at room temperature. The organization of the microtubule network (green) and the cellular DNA (blue) was visualized by a Zeiss Axiovert/ Axiocam CCD system through a 60X oil objective. Scale bar= 20μM. These images are representiative of an experiment completed three times.

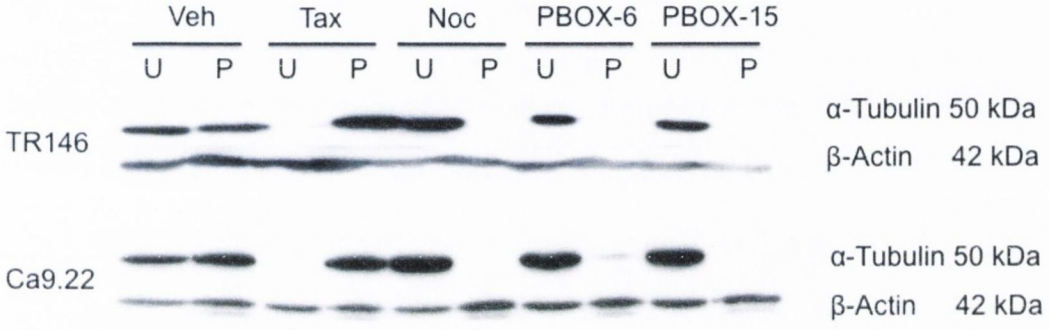


Figure 6-9 PBOX treatment resulted in tubulin depolymerisation in the TR146 and Ca9.22 cell lines.

PBOX-6 and PBOX-15 exposure resulted in tubulin depolymerisation in the TR146 and Ca9.22 cells and disruption of the organisation of the microtubule network. Cells were treated for 4h with either vehicle (1% (v/v) EtOH) PBOX-6 (10μM), PBOX-15 (1μM), paclitaxel (1μM) or nocozadole (10μM). Polymerised (P) or unpolymerised (U) tubulin was then separated by centrifugation in a microtubule-preserving buffer. The quantity of polymerised compared to unpolymerised was tubulin was assessed by Western Blot using monoclonal antibodies directed against tubulin and loading control β-actin followed by incubation with a HRP-conjugated anti-mouse antibody. These blots are representative of an experiment completed three times.

6.3.3 PBOX compounds induce G2/M arrest and apoptosis in OC cell lines

Flow cytometric analysis of propidium iodide stained cells allowed determination of DNA content of TR146 and Ca9.22 cells and thus any induction of cell cycle arrest or the onset of apoptosis was observed (Figure 6-10). There are significant increases in the amount of apoptotic cells with levels of apoptosis rising from 4.4±1.210% for control cells to 57.6±8.1% for 10μM PBOX-6 (***P<0.001) and to 39.1±6.6% for 1μM PBOX-15 (***p<0.001) after 48h in the TR146 cell line (a). Similarly in the Ca9.22 cell line (b) there was an increase in cells in the sub-G0/G1 peak from 2.120 ±0.8% in control cells to 40.84± 0.8% (***p<0.001) for PBOX -6 and to 30.45±1.56% (***p<0.001) for PBOX-15 after 72h. This increase in the levels of sub-G0/G1 cells corresponded with a decrease in cells in the G2/M phase of the cell cycle seen from 8h in both cell lines with PBOX-6 (10 μM) and PBOX-15 (1μM) treatment. Statistically significant decreases of the levels of G2/M arrest reduced at later time points to 15.4±1.07% (**p<0.01) and 12.6±1.87% (*p<0.05) for PBOX-6 and -15, respectively after 48h in TR146 cells (c). There was also a significant decrease of 22.23±0.95% (*p<0.05) and 16.6±1.25% (**p<0.01) in Ca9.22 cells (d) over 48h with PBOX-6 and PBOX-15 respectively. Treatments were compared to the vehicle control and statistical analysis was carried out using a one-way ANOVA with post-hoc Bonferroni analysis using GraphPad prism 6.0.

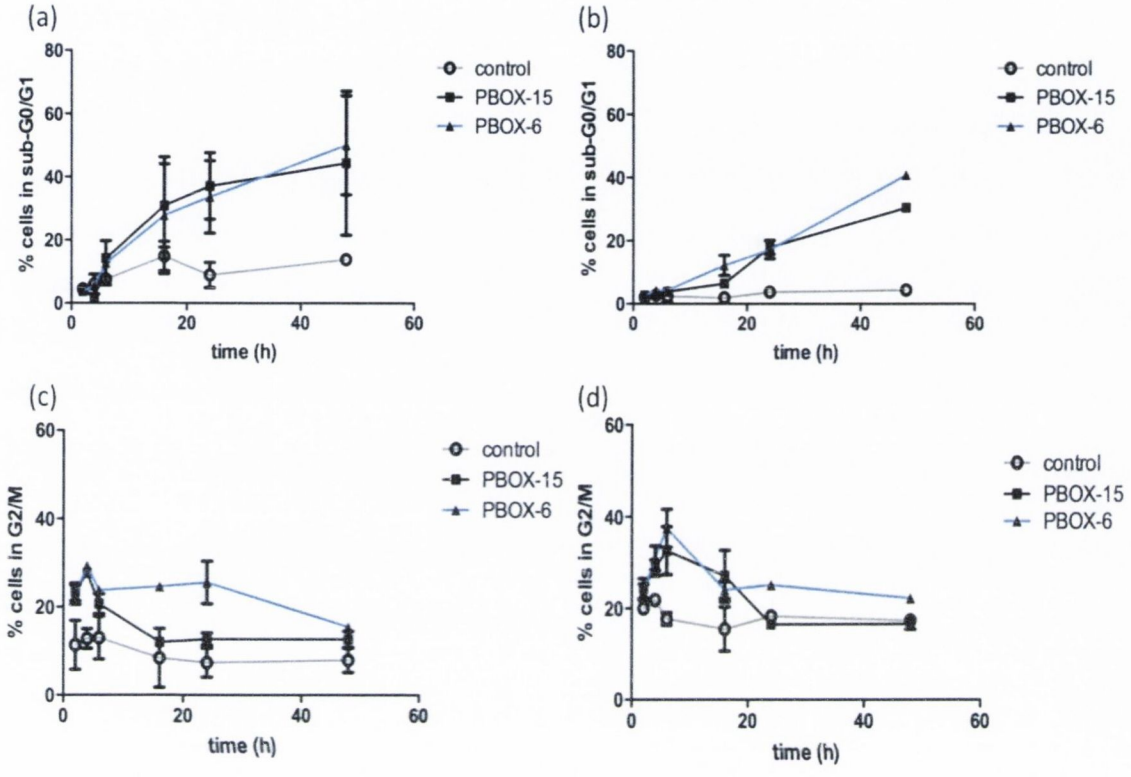


Figure 6-10 PBOX compounds increase cells in sub G0/G1 phase of cell cycle and induce G2/M arrest.

TR146 (a) (c) and Ca9.22 (b) (d) cells were seeded onto 6 well plates and treated with 10μM PBOX 6 and 1μM PBOX 15 for stated time points up to 72h. The cells were then fixed overnight in ice-cold EtOH before being resuspended in PBS and propidium iodide. The cells were then analysed using a BD canto flow cytometer, DNA content was detected using a 630/22 nm band pass filter. Values represent mean + SEM for three independent experiments. Cells in the sub G0/G1 peak with <2N DNA were considered to be apoptotic (a) (b) while cells with 4N quantities of DNA were considered to be in the G2/M phase of the cell cycle (c) (d).

6.3.4 PBOX compounds induce degradation of PARP in OC cell lines

To confirm that the cell death observed from flow cytometric analysis was due to induction of apoptosis, the degradation of PARP was assessed. PARP cleavage is a hallmark associated with this controlled cell death pathway. Using western blot techniques Figure 6-11 (a) it was found that both PBOX-6 (10μM) and PBOX-15 (1μM) induced a decrease in expression of full length PARP in Ca9.22 and TR146 cells over 72h. Treatment with vehicle (1% (v/v) EtOH) alone showed no effect on PARP expression in either cell line (Figure 6-11). In the TR146 cell line there is degradation of PARP after 24h with 1μM PBOX-15 when compared to the vehicle control. The reduction of PARP is clearly seen in the TR146 cell line after 48h with both PBOX compounds. Degradation of PARP is noted after 48h with treatment of both PBOX compounds in the Ca9.22 cell line. β-Actin was used as a loading control in all experiments. PARP blots were further analysed using Image J and normalised to the housekeeping protein. In the TR146 cell line (b) there is a significant decrease in PARP protein after 48h and 72h with both PBOX compounds. In comparison, after 48h in the Ca9.22 cell line (c) there is no significant decrease in PARP protein with treatment of PBOX-6. There is a significant decrease after 48h using PBOX-15 and significant decreases after 72h using both PBOX compounds in the Ca9.22 cell line.

These results confirm that the PBOX compounds induce the apoptotic cell death pathway via tubulin disassembly in OC cell lines.

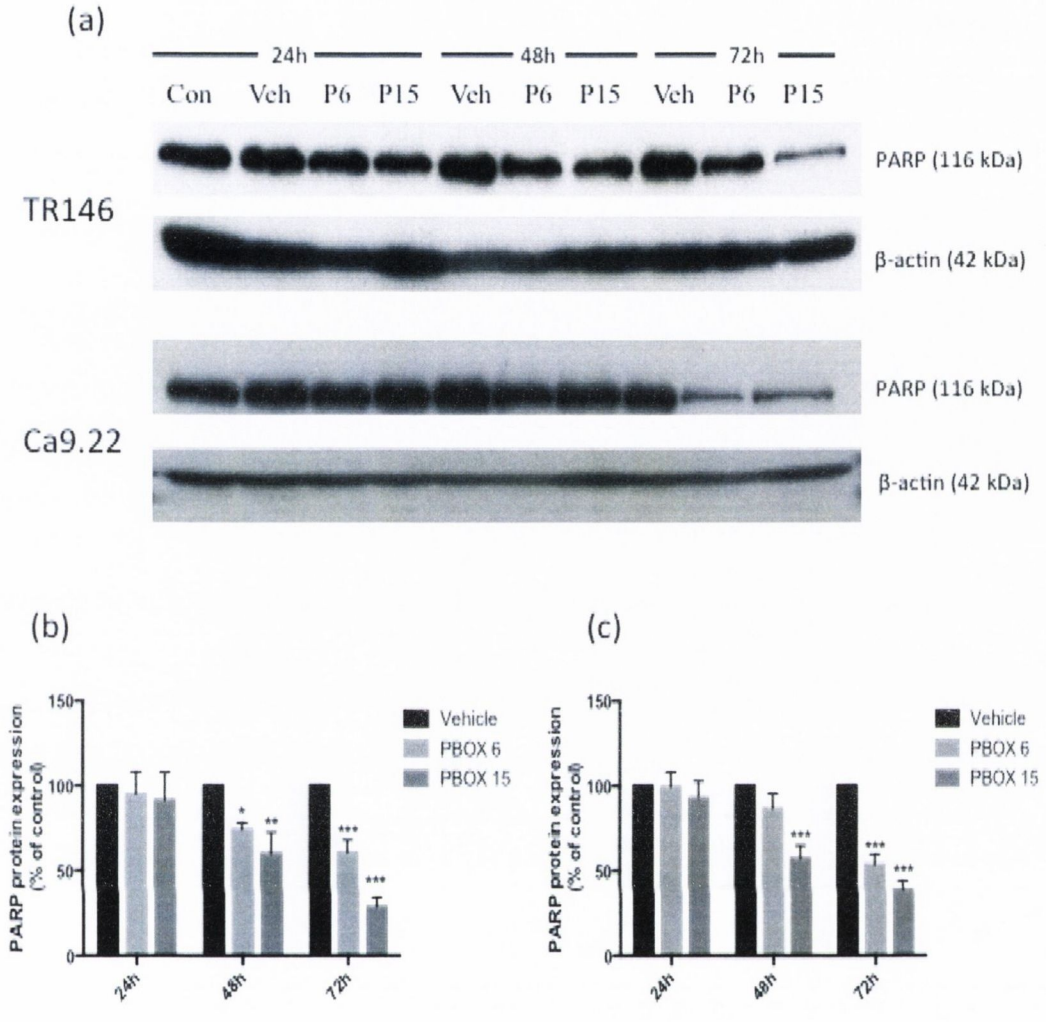


Figure 6-11 PBOX compounds cause a reduction in PARP protein.

PBOX-6 and PBOX-15 induced a reduction in full length PARP in Ca9.22 and TR146 cells. Both cell lines were treated with vehicle (1% (v/v) EtOH), 10μM PBOX-6 or 1μM PBOX-15 for the indicated times. (a) Degradation of PARP was assessed by Western blot analysis using monoclonal antibodies generated against PARP or loading control β-actin, followed by HRP-conjugated anti-mouse secondary antibodies. Blots are representative of an experiment completed three times. Using Image J software, TR146 (b) and Ca9.22 (c) western blot bands were quantified and normalised to the housekeeping protein β-actin. Treatments were compared to the vehicle control (100%) and statistical analysis was carried out using an unpaired t-test with post-hoc Bonferroni analysis using GraphPad prism 6.0. Samples significantly different to the control are annotated * $p<0.05$ ** $p<0.01$, *** $p<0.001$.

6.3.5 The effect of p53 knockdown on the viability of TR146 cells in the presence of PBOX compounds

In Chapter 3 it was discovered that cells respond differently to treatments of EtOH if they contain a p53 mutation or knockdown. In Section 6.3.1 it was shown that the Ca9.22 cell line was more sensitive to PBOX treatment and this could be due to the fact it contains a mutation in the p53 gene. Experiments were carried out to examine the effect of p53 on the efficacy of PBOX compounds in the TR146 cell line.

Using a p53 siRNA, p53 was knocked down using the same method as in Chapter 3. Results shown in Figure 6-12 indicate the IC-50 from the TR146 knockdown cells using both PBOX-6 (a) and PBOX-15 (b). The IC-50 from the PBOX 6 cells is 3.3±1.4μM and the IC-50 after using PBOX-15 in the knockdown cells is 520±1.08nM. Comparing these results to the IC-50 values after 24h in TR146 cells (Table 6-1) without knockdown we can see that there is no significant difference after PBOX-15 treatment. However after PBOX-6 treatment in the knockdown cells there is a significant decrease in the IC-50 value in comparison to the normal TR146 cells at the same time point [carried out using a t-test between the means of the IC-50 values (**$p<0.01$)]. This indicates that less drug is needed to kill the same amount of cells- i.e. the cells are more susceptible to PBOX treatment with a mutation in the p53 gene.

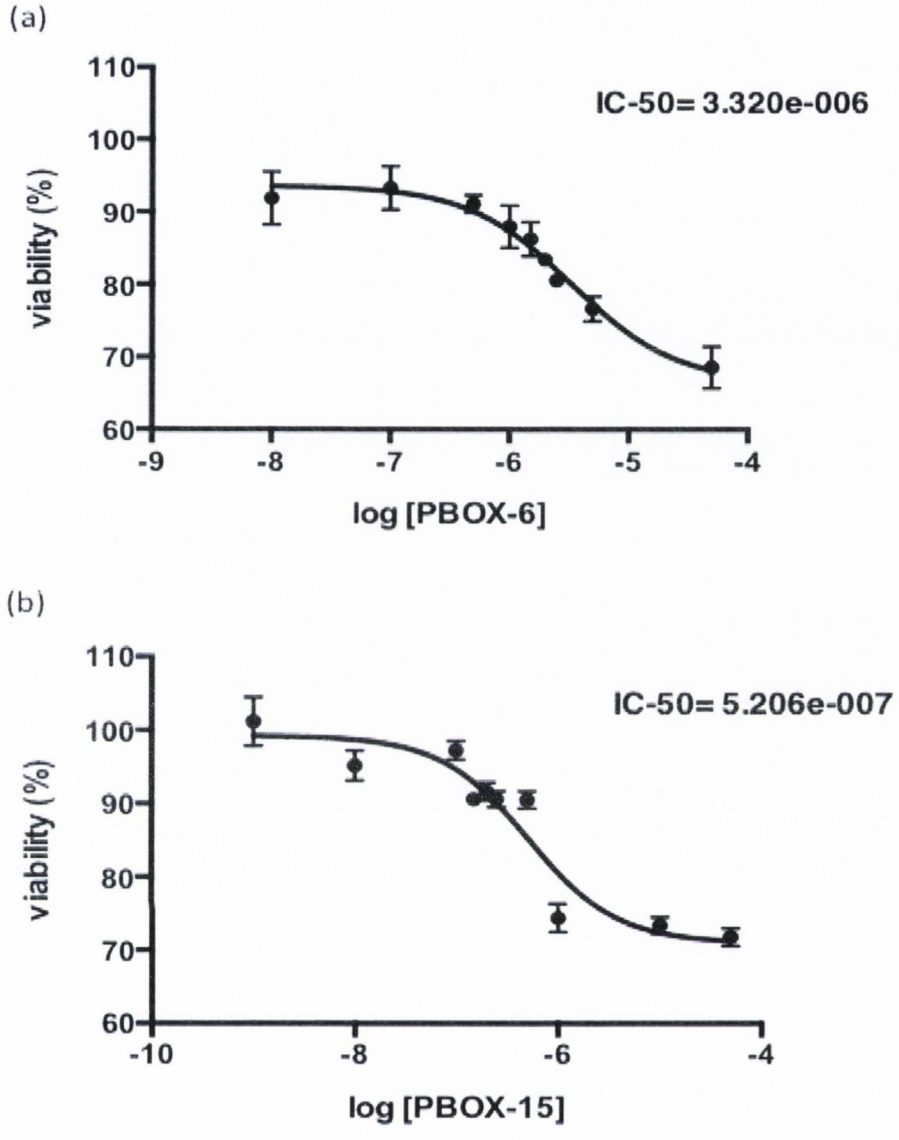


Figure 6-12 The effect of PBOX compounds on TR146 viability with p53 knockdown.

TR146 cells were seeded at 3 x 10^5 cells/well in a 6 well plate, serum starved overnight and treated the following day with siRNA targeted to p53. Cells were then treated with a range of PBOX -6 (a) and PBOX- 15 (b) concentrations. After 24h, Alamar blue was added to the wells for 4h. Fluorescence was measured using a Spectramax Gemini Plate reader at excitation and emission wavelengths of 544nm and 590nm respectively. Values represent mean ± S.E.M of three independent experiments.

6.4 Discussion

Multidrug resistance, the principal mechanism by which many cancers develop resistance to chemotherapy drugs, is a major factor in the failure of many forms of chemotherapy. It affects many types of cancer including OSCC. There is a need for the development of novel agents that have the ability to kill chemotherapy-resistant cells. In this chapter a novel set of compounds have been assessed in relation to their potential therapeutic value in OC. PBOX-15 and PBOX-6 are potent pro-apoptotic members of the PBOX series of compounds which have previously been shown to induce apoptosis in several human tumour cell lines and to have anticancer proprieties in various cell culture systems, animal models and clinical samples (Greene *et al.*, 2005). In addition to inducing apoptosis in a variety of cancerous cell types, they possess the added benefit of inducing cytotoxicity in multidrug resistant cancer cells (Nathwani *et al.*, 2010d).

Herein we report that PBOX compounds are capable of reducing the proliferation of the OC cell lines TR146 and Ca9.22 with IC-50 values of 35μM and 2.6μM for PBOX-6 and 470nM and 69nM for PBOX-15, respectively. These values are within a range previously observed in other cancer cell lines exposed to PBOX compounds including CACO-2 human colorectal carcinoma cell (PBOX-6 11.16μM, PBOX-15 0.63μM) neuroblastoma cells SHSY5Y (PBOX-6 1.73μM, PBOX-15 0.06μM) and PC3 prostate cancer cells (PBOX-6 5.8μM, PBOX-15 0.37μM) (Greene *et al.*, 2013, Lennon *et al.*, 2014, Nathwani *et al.*, 2010c). PBOX-15, as previously noted, is the more potent of the two compounds, which is confirmed here in both cell lines as shown by an order of magnitude difference in the calculated IC-50 values. It is interesting to note that the IC-50 values in the nM range for the PBOX-15 is lower than some common chemotherapeutic agents, for example, Taxol and Cisplatin both of which IC-50 values are in the μM range (Huang *et al.*, 2004). The lower the IC-50 value in comparison to common chemotherapeutic agents could reduce side effects commonly seen with these drugs. Although PBOX-6 has a higher IC-50 value to the PBOX-15 compound it is still within the range of other chemotherapeutic agents. Significant variation in the sensitivity of each cell type was also observed, the Ca9.22, the gingiva cell line, was sensitive to both compounds and had significantly lower IC-50 values when compared to the TR146 cells. The variations in efficacy of PBOXs observed between the two analysed cell lines suggest a phenotypic or genotypic factor may be involved.

The disruption of the microtubule network in other cancer cell lines following treatment with PBOX-6 and PBOX-15 suggested that they act as microtubule depolymerizing agents (Mulligan *et al.*, 2006). To examine this hypothesis in OSCC cell lines, cells were treated with several concentrations of PBOX-6 and PBOX-15. We found our results to be in agreement with previous results in other studies -both PBOX compounds caused disruption of tubulin after 24h *in vitro* (Mulligan *et al.*, 2006). As expected, the control compounds, nocodazole depolymerised tubulin and paclitaxel resulted in tubulin aggregation through polymerisation confirmed by the polymerisation assay (Figure 6-9). PBOX-15 the more potent of the two compounds was effective at disrupting tubulin at 1μM in both cell lines whereas PBOX-6 mediated depolymerisation was observed at concentrations of 10μM. Confirmation that the tubulin disruption by PBOX compounds is a depolymerisation effect was demonstrated as shown after 4h both compounds fully depolymerised the tubulin *in vitro* (Figure 6-9). This depolymerisation and destabilisation of the tubulin network was in a manner similar to nocozadole, a MTA depolymeriser.

This inhibition of tubulin assembly is likely to be the cause of cell death by the PBOX compounds (Mulligan *et al.*, 2006). Tubulin is a key protein in spindle formation during the cell cycle. A mechanism known as the spindle assembly checkpoint (SAC) is activated during metaphase in the cell cycle (Rudner and Murray, 1996). If there is a breakdown of tubulin and a loss of spindle tension then the cell will not be able to continue into anaphase. To elucidate part of the mechanism involved in the response of OSCC cells to PBOX treatment their effect on the cell cycle was examined. The PBOXs caused a time dependent accumulation of cells in G2/M as early as 4h in TR146 cells and 8h in Ca9.22. This was followed by an increase of cells in sub G0/G1 indicative of apoptosis and a concomitant decrease in the percentage of cells in G2/M. To confirm the mode of cell death, degradation of the DNA repair enzyme PARP that is indicative of apoptosis was examined. The decrease in expression of the full-length 116kDa PARP over 72h is evident in both cell lines with both compounds. The decrease in full length of PARP in the Ca9.22 cell line is more prominent than in the TR146 cell line which is comparable to the IC-50 values for both compounds.

In OSCC approximately 50% of cases present with a mutation in the p53 gene with subsequent phenotypic manifestations and impaired p53 function and as such the Ca9.22 cells have a known p53 gain-of-function (R248W) mutation (Kaneda *et al.*, 2006, Liu *et al.*, 2010a) whereas the TR146 cells have no known reported p53 mutation. Previous

studies have reported the influence of p53 in modifying drug efficiency and function in cancer cells (Bunz *et al.*, 1999) and it may be a potential contributor to the variation in sensitivity seen in this study. As previously mentioned, there is significant variation in IC-50 values for both compounds between the two cell lines. Experiments were carried out to determine if p53 plays a role in the efficacy of PBOX compounds. It was found that PBOX-6 IC-50 was significantly altered between the TR146 cells and the TR146 cells with a p53 knockdown. The p53 knockdown decreases the IC-50 value, which means the cells are more sensitive to PBOX-6 induced apoptosis. This sensitivity is also noted in the Ca9.22 cells, which contain a p53 mutation and are also more sensitive to PBOX-6. There was no significant change in IC-50 value with treatment of PBOX-15 in the p53 knockdown cells. This finding, that PBOX-6 compound is more potent in p53-mutated cells, could be used to personalise treatment for patients with certain types of OSCC.

These results indicate that PBOX-6 and its more potent analogue PBOX-15 could prove effective in the treatment of OSCC. This study has shown that the compounds depolymerise their molecular target, tubulin, resulting in cell death through apoptosis in OSCC cell lines. Given the accessibility afforded in a large number of OSCC cases the use of PBOX compounds, as a topical agent could be a potential therapeutic strategy for this disease with a conceivable use as a personalised treatment based on the p53 status of the patient. PBOX compounds used alone or in combination with the other antineoplastic agents could prove useful in the treatment of OSCC.

7 General Discussion

7.1 General discussion

Mechanisms underlying the pathogenesis of OSCC are yet to be fully elucidated. It is a cancer with an extremely low 5-year survival rate as risk factors are not fully understood and it can be difficult to diagnose at early stages and thus treatment options are limited. Research in the last decade has focused on the association of smoking in the pathogenesis of OC with alcohol merely seen as a synergistic enhancer and not a sole contributor (Ide *et al.*, 2008, Zygogianni *et al.*, 2011). However meta-analysis studies have shown that individuals who consume alcohol but do not smoke are at an increased risk of cancer of the oral cavity (Tramacere *et al.*, 2010). Studies pertaining to the direct effect of alcohol and OC mechanism are currently lacking. Furthermore diagnosis and treatment of OC can prove to be challenging which seems extraordinary since the site of cancer is so easily accessible. The research within this thesis not only demonstrates that alcohol induces direct changes in primary epithelial cells which may directly increase cellular transformation, it also examines novel diagnostic tools and therapeutics aimed at earlier intervention in OC.

While a sizeable amount of studies have attempted to deduce the secondary effects of alcohol induced oral carcinogenesis, very few have looked into direct results of EtOH on the biochemical changes in the oral mucosa. One cellular system in particular has emerged as a therapeutic target in recent times and is referred to as the antioxidant enzyme system (Glasauer and Chandel, 2014). This system is of great importance in the cell as it controls the levels of ROS. This study showed that in the presence of acute alcohol that levels of ROS were perturbed in addition to the levels of key antioxidant enzymes. While it may be safe to assume that the antioxidant enzymes are not the sole cause of the deregulation of H_2O_2 homeostasis, the impact of EtOH on this cell system could have a profound long-term effect on the cells. The decreasing levels of H_2O_2 are of particular interest. H_2O_2 has been put under the spotlight as a possible cancer-causing molecule when the levels are uncontrollably high. It can bind and damage cellular structures including DNA leading to carcinogenesis (Waris and Ahsan, 2006). The effect of diminished levels of H_2O_2 in the presence of EtOH has not been recognised before. In more recent times H_2O_2 has been shown at lower levels to be involved in normal cellular regulation including cell cycle and proliferation (Gough and Cotter, 2011, Burdon, 1995). Therefore a certain threshold of H_2O_2 is necessary for normal cell function. By

depleting levels of H_2O_2 could this perturb normal cellular systems and lead to transformation? This unwarranted side effect of EtOH may open up new approaches for therapeutics in alcohol-induced carcinogenesis in the oral mucosa by targeting restoration of the normal levels of ROS. Following on from these findings, efforts were made to elucidate the changes to H_2O_2 by analysing antioxidant enzyme levels. While various changes to several enzymes occurred in response to EtOH exposure the most intriguing was the change observed in CAT expression. This enzyme was increased in response to EtOH, a modification observed in other types of OC (Khanna *et al.*, 2005) and could be a driver of permanent damage to cellular function. This finding could render new therapeutic targets when treating alcohol induced OC.

With the influence of genotype prevalent in cancer Chapter 3, we examined the effects of p53 (commonly mutated in OC) status on alcohol-induced changes in oral mucosal cells by employing a siRNA transient knockdown molecule. Inhibition of p53 impacted upon the HIF1-α response to EtOH treatment most severely in oral epithelial cells. Personalised medicine is a recent model developed and aims to treat individuals based on specific genetic abnormalities related to their disease. Using the information gathered in this study, personalised medicine regarding individuals with p53 mutations could be an interesting approach for treatment. Those with p53 mutations may potentially benefit from treatment with targeted inducers of HIF1-α or in more severe cases targeted gene therapy for p53, an approach currently undergoing clinical tests for use in metastatic colon cancer patients and to date has provided promising results (Speetjens *et al.*, 2009, Speetjens *et al.*, 2011).

Mechanisms underlying OC pathogenesis are not the only limitations that arise when it comes to analysis and diagnosis of this disease. Confirmation of disease status can prove unreliable and can be clinically subjective particularly in the mild to severe dysplastic stages of oral transformation. To address this situation Chapter 4 examined the potential role of Raman spectroscopy in diagnosis of OC with emphasis on dysplastic classification. This relatively new technique has so far proved useful in the diagnosis of cervical cancer but it is still in infantile stages (Lyng *et al.*, 2007). This study established that Raman spectroscopy can successfully and reproducibly differentiate between cancerous and primary cells of the oral mucosa based on sub cellular regions, with the

molecular content revealing spectral fingerprints for each region. The possibilities for this technique in OC are immense. Raman spectroscopy offers the potential for performing an 'optical biopsy' with important clinical benefits. Excisional tissue biopsies carry risks and can be intrusive to the patient and require a period of recovery. Raman spectroscopy would alleviate the need for invasive procedures by either using brush biopsy approach or with the development of hand held Raman instruments allowing direct *in vivo* analysis of tissue. Raman spectroscopy could also have significant economic benefits through decreasing the time and associated costs of OC diagnosis. With in-clinic Raman spectroscopy tools the need for further analysis using laboratory techniques would be redundant. Immediate results showing specific molecular profiles would be available directly to the clinician enabling immediate review and potentially diagnosis. In addition, long term monitoring of suspicious lesions using Raman spectroscopy in parallel with visual examination could reduce the length of diagnostic periods through employing similar techniques as described in Chapter 5 of this study. There are many difficulties in distinguishing normal tissue from abnormal or potentially cancerous tissue without using standard invasive biopsy techniques. These areas of abnormality can also be identified using wide field methods such as fluorescence, which as mentioned has various limitations. Identifying and grading dysplastic lesions and early tumours are troublesome. It is within this setting that Raman spectroscopy has a potential clinical role. Most asymptomatic dysplastic lesions of the oral cavity are monitored visually over a prolonged period of time, even up to a year to watch for signs of transformation. Although this study could not show differences between a dysplastic and OC cell lines, with a greater cohort of normal, dysplastic and *in situ* carcinoma patient samples, novel differences within the spectra would potentially be distinguished.

Combining the findings from Chapter 3 and 4, Chapter 5 took the application of Raman in OC one step further and adopted the technology for use in analysing the mechanisms underlying alcohol induced oral carcinogenesis. Alcohol affected components of the cytoplasm in all cell types. This corroborated a number of observations presented in Chapter 3 since antioxidant enzymes are for the most part mainly confined to the cytoplasm therefore the changes in the Raman spectra may represent changes in the status of these proteins or their transcripts post expression. Furthermore this chapter exposed novel effects of EtOH on nucleoli, which in recent times have been linked to

control of critical cellular functions and have been linked to cancer. In the presence of EtOH there is an increase in protein levels within the nucleolus, which may be an early sign of dysregulation and may drive early carcinogenic changes. For this reason it has become an emerging target for cancer therapy. Common OC chemotherapeutics, like 5-Fluorouracil and Mitomycin C, impact on ribosomal biogenesis and cause nucleolar disintegration, respectively (Burger *et al.*, 2010). Accelerated ribosome generation and rRNA synthesis is essential for tumour maintenance so targeting therapies to interfere with nucleolar function could decrease the rate of ribosome generation thus limiting critical cellular necessities (Hein *et al.*, 2013).

Many individuals taking chemotherapeutics for OC develop chemoresistance via several proposed mechanisms (Wang *et al.*, 2012, Gatti and Zunino, 2005) and in particular this is a cause for concern in patients with reoccurring cancers. Novel PBOX compounds, PBOX-6 and PBOX-15, examined in Chapter 6 have been previously studied as potential agents in several different forms of cancer (Bright *et al.*, 2010, Gangemi *et al.*, 2013, Greene *et al.*, 2005, Lennon *et al.*, 2014). This is the first study to look at the potential of these compounds as therapeutic agents in OC. They are potentially an exciting breakthrough in the realm of cancer therapeutics as they can induce apoptosis in multidrug resistant cells (Lennon *et al.*, 2014, Nathwani *et al.*, 2010a). The potency of these compounds at low concentrations, especially PBOX-15, is one of the beneficial aspects of these compounds as they may induce less systemic side effects than many other common chemotherapeutic agents. While this study was limited and examined just two members of the PBOX family, albeit the two most potent members currently available, many others are being modeled and synthesised which opens the way for the development and availability of enhanced PBOX derivatives with greater potency and specificity. Use of such compounds may also lend themselves to alternative treatment regimes. Due to the accessibility of OC sites, the use of PBOX compounds as a topical agent could be conceivable and would show far less adverse reactions, shorter duration in hospital receiving chemotherapy and less discomfort for patients, as an intravenous route would no longer be necessary. Treatment of skin cancers with topical treatments has shown promise (Gross *et al.*, 2007). With further studies, not only could cancerous lesions be treated topically, pre cancerous or dysplastic lesions could be treated as a preventative measure.

7.2 Future Work

7.2.1 Examination of the role of alcohol in OC development

There are many aspects of OC that await further investigation and further studies into alcohol-induced carcinogenesis will broaden the knowledge and understanding of the mechanisms shown within this thesis. One question that dominates the study regarding alcohol and oral mucosal interaction is what lasting effects are going to occur with longer EtOH exposure, particularly in the case of the isolated primary cells, since this transformation would mimic what occurs in normal cells. This could not be achieved in this study due to the paucity of suitable patient samples and the technical challenges involved in maintaining stable primary cells. A larger cohort of samples would not only provide a greater understanding into the effects shown in the study with acute treatment but also facilitate an understanding of the lasting effects of EtOH through longer treatment durations and repeated exposure to mimic chronic alcoholism. This is especially pertinent in the case of diminished levels of H_2O_2 in the cells with EtOH treatment. Studies in recent times have shown that H_2O_2 (at low levels) has significant functions within the cell involved in the control and regulation normal cellular processes (Gough and Cotter, 2011), therefore further studies should target the effect of a sudden decline will have over an extended period on cellular regulation? This issue clearly warrants further investigation particularly as H_2O_2 is known to play a role in proliferation, migration, survival and autophagy all key pathways in a normal functional cell.

Further studies examining the antioxidant enzymes, would have to focus on the consequences of altered enzyme function. Long-term irregularities in these enzymes could permanently damage the cells as abnormalities observed with this class of protein are repeatedly seen in malignancies. The enzyme CAT is of particular importance as it has unique expression patterns in cancer and EtOH induced a modification of this enzymes behaviour across all cell types analysed. This suggests fragility in this enzyme, which could manifest into greater weaknesses in the cells defences not only in the presence of EtOH but also in the presence of other carcinogens in tandem. A recent study has also noted that the levels of cellular oxidative stress can affect the response to chemotherapeutic agents, therefore analysis of individual patients alcohol intake may be

a valuable source of clinical information and aid in appropriate treatment regimes (Filippova *et al.*, 2014).

The impact of p53 mutations on the antioxidant response in the cell lines presented interesting and intriguing results, which require further investigation to terminally define a role for p53 in OC related ROS modulation. The expression levels of HIF-1α in particular were noteworthy as this gene is extremely important in cell regulation in response to hypoxic changes in the cell (Goda *et al.*, 2003). Therefore it would be interesting to assess the response to treatment in primary cells with p53-targeted siRNA to develop a greater understanding of p53-alcohol interaction. A further investigation would be a comprehensive examination of the effects the different forms of p53 mutations play in the ROS modulation, e.g. are gain of function mutations more or less severe in terms of ROS manipulation. Also determining the minimum level of p53 function which can still act as a regulator in this context. Double knockout studies may yield interesting results and give further insight into the mechanisms described this thesis, in particular knockouts of the main antioxidant enzymes coupled to a complete knockout of p53 may lead to alternate mechanisms of ROS control within the cell in response to EtOH stimuli.

7.2.2 Investigation of the use of Raman spectroscopy as a diagnostic aid in OC

Numerous lines of investigation are open regarding studies involving Raman spectroscopy. The highest priority would be further investigation into its use as a clinical diagnostic tool to replace more invasive methods currently used and to identify biochemical changes in tissue where morphological changes are not yet prominent. To achieve a step closer to this goal, analysis of patients samples of both normal and carcinogenic samples in a similar study to those done by (Lyng *et al.*, 2007) on cervical samples. Further to this, carrying out studies involving monitoring of leukoplakia, erythroplakia and dysplastic lesions to uncover molecular fingerprints related to transformation could lead to more efficacious treatment. Raman also lends itself to potentially become a diagnostic technology that can be utilised within a clinical setting and possibly become a chair side diagnostic tool. This would have significant benefits

for both patient and clinician as suspicious lesions can be monitored on the spot without the need for lengthy laboratory diagnosis, the system would be no more invasive than a curing gun commonly used in the dental setting although initially a brush biopsy protocol may be a first step.

Improvements on the resolution of Raman would be of great benefit. Currently Raman can determine classes of molecules e.g. protein, nucleic acids, lipids and so on but should the technology become enhanced with the ability to discriminate between nucleic acids e.g. DNA and mRNA confirmation of changes in expression level, perhaps identification of phosphorylation events on proteins determining activation. This information would prove invaluable particularly as currently the technology permits a discrimination of regions within the cell.

7.2.3 Explore the therapeutic efficacy of PBOX compounds in OC treatment

The results obtained using PBOX compounds for treatment of OSCC are promising. Developing drugs for human use can take years, as there is a strict process to ensure safety of a drug. The next stage to assess the efficacy of the PBOX compounds in OC is to characterise out their toxicity, pharmacokinetics and metabolism *in vivo*. In a recent study (Bright *et al.*, 2010), PBOX compounds were examined in a mouse model for chronic myeloid leukaemia (CML) with promising results. Design of a representative animal model of oral dysplasia and/or OC would confirm the efficacy of PBOXs in a preclinical setting and would also facilitate the trial of topical application. Given the on-going development of new novel PBOX compounds further screening may elucidate more potent and specific compounds.

7.3 Conclusions of the thesis

Together the results of this study broaden the understanding of the complex mechanisms underlying OC development. New possible pathways of alcohol-induced carcinogenesis have been established and the use of Raman spectroscopy for OC diagnosis in the near future looks promising, based on the results herein. This study has also demonstrated that PBOX compounds have the ability to induce apoptosis in OSCC cell lines indicating they could be a promising therapeutic alternative to common chemotherapeutic agents.

8 References

Abbey, L. M., Kaugars, G. E., Gunsolley, J. C., Burns, J. C., Page, D. G., Svirsky, J. A., Eisenberg, E., Krutchkoff, D. J. & Cushing, M. 1995. Intraexaminer and interexaminer reliability in the diagnosis of oral epithelial dysplasia. *Oral surgery, oral medicine, oral pathology, oral radiology, and endodontics,* 80, 188-191.

Acha-Sagredo, A., Ruesga, M. T., Rodriguez, C., Aguirregaviria, J. I., De Pancorbo, M. M., Califano, J. A. & Aguirre, J. M. 2009. p53 mutation is rare in oral mucosa brushings from patients previously treated for a head and neck squamous cell carcinoma. *Oral oncology,* 45, 661-664.

Agudelo, M., Gandhi, N., Saiyed, Z., Pichili, V., Thangavel, S., Khatavkar, P., Yndart-Arias, A. & Nair, M. 2011. Effects of alcohol on histone deacetylase 2 (HDAC2) and the neuroprotective role of trichostatin A (TSA). *Alcoholism, clinical and experimental research,* 35, 1550-1556.

Ahluwalia, K., Ro, M., Erwin, K. & Treadwell, H. 2005. Racial disparities in oral cancer risk and outcomes. *Journal of cancer education : the official journal of the American Association for Cancer Education,* 20, 70-71.

Akhiani, A. A., Werlenius, O., Aurelius, J., Movitz, C., Martner, A., Hellstrand, K. & Thoren, F. B. 2014. Role of the ERK pathway for oxidant-induced parthanatos in human lymphocytes. *PloS one,* 9, e89646.

Alao, J. P. 2007. The regulation of cyclin D1 degradation: roles in cancer development and the potential for therapeutic invention. *Molecular cancer,* 6, 24.

Alessenko 1990. Role of Lipids in Functional Activity of Cell Nucleus. *Nuclear Structure and Function.*

Alfonso-Loeches, S., Pascual-Lucas, M., Blanco, A. M., Sanchez-Vera, I. & Guerri, C. 2010. Pivotal role of TLR4 receptors in alcohol-induced neuroinflammation and brain damage. *The Journal of neuroscience : the official journal of the Society for Neuroscience,* 30, 8285-8295.

Alqawi, O., Wang, H. P., Espiritu, M. & Singh, G. 2007. Chronic hypoxia promotes an aggressive phenotype in rat prostate cancer cells. *Free radical research,* 41, 788-797.

Ames, B. N. 1983. Dietary carcinogens and anticarcinogens. Oxygen radicals and degenerative diseases. *Science,* 221, 1256-1264.

An, W. G., Kanekal, M., Simon, M. C., Maltepe, E., Blagosklonny, M. V. & Neckers, L. M. 1998. Stabilization of wild-type p53 by hypoxia-inducible factor 1alpha. *Nature,* 392, 405-408.

Anand, A. K., Jain, J., Negi, P. S., Chaudhoory, A. R., Sinha, S. N., Choudhury, P. S., Kumar, R. & Munjal, R. K. 2006. Can dose reduction to one parotid gland prevent xerostomia?--A feasibility study for locally advanced head and neck cancer patients treated with intensity-modulated radiotherapy. *Clinical oncology,* 18, 497-504.

Anthony, B., Zhou, F. C., Ogawa, T., Goodlett, C. R. & Ruiz, J. 2008. Alcohol exposure alters cell cycle and apoptotic events during early neurulation. *Alcohol and alcoholism,* 43, 261-273.

Arosarena, O. A., Madsen, M. & Haug, R. 2006. Special considerations with floor of mouth and tongue cancer. *Oral and maxillofacial surgery clinics of North America,* 18, 521-531.

Audas, T. E., Jacob, M. D. & Lee, S. 2012. The nucleolar detention pathway: A cellular strategy for regulating molecular networks. *Cell cycle,* 11, 2059-2062.

Bacac, M. & Stamenkovic, I. 2008. Metastatic cancer cell. *Annual review of pathology,* 3, 221-247.

Bae, Y. S., Kang, S. W., Seo, M. S., Baines, I. C., Tekle, E., Chock, P. B. & Rhee, S. G. 1997. Epidermal growth factor (EGF)-induced generation of hydrogen peroxide. Role in EGF receptor-mediated tyrosine phosphorylation. *The Journal of biological chemistry,* 272, 217-221.

Banoczy, J. & Csiba, A. 1976. Occurrence of epithelial dysplasia in oral leukoplakia. Analysis and follow-up study of 12 cases. *Oral surgery, oral medicine, and oral pathology,* 42, 766-774.

Barhoumi, A. & Halas, N. J. 2011. Detecting Chemically Modified DNA Bases Using Surface Enhanced Raman Spectroscopy. *The journal of physical chemistry letters,* 2, 3118-3123.

Baykul, T., Yilmaz, H. H., Aydin, U., Aydin, M. A., Aksoy, M. & Yildirim, D. 2010. Early diagnosis of oral cancer. *The Journal of international medical research,* 38, 737-749.

Bensch, K. G. & Malawista, S. E. 1968. Microtubule crystals: a new biophysical phenomenon induced by Vinca alkaloids. *Nature,* 218, 1176-1177.

Bertoli, C., Skotheim, J. M. & De Bruin, R. A. 2013. Control of cell cycle transcription during G1 and S phases. *Nature reviews. Molecular cell biology,* 14, 518-528.

Bhide, S. A. & Nutting, C. M. 2010. Advances in chemotherapy for head and neck cancer. *Oral oncology,* 46, 436-438.

Blagosklonny, M. V., Giannakakou, P., Romanova, L. Y., Ryan, K. M., Vousden, K. H. & Fojo, T. 2001. Inhibition of HIF-1- and wild-type p53-stimulated transcription by codon Arg175 p53 mutants with selective loss of functions. *Carcinogenesis,* 22, 861-867.

Blot, W. J. 1992. Alcohol and cancer. *Cancer research,* 52, 2119s-2123s.

Blot, W. J., Mclaughlin, J. K., Winn, D. M., Austin, D. F., Greenberg, R. S., Preston-Martin, S., Bernstein, L., Schoenberg, J. B., Stemhagen, A. & Fraumeni, J. F., Jr. 1988. Smoking and drinking in relation to oral and pharyngeal cancer. *Cancer research,* 48, 3282-3287.

Bodanese, B., Silveira, L., Jr., Albertini, R., Zangaro, R. A. & Pacheco, M. T. 2010. Differentiating normal and basal cell carcinoma human skin tissues in vitro using dispersive Raman spectroscopy: a comparison between principal components analysis and simplified biochemical models. *Photomedicine and laser surgery,* 28 Suppl 1, S119-127.

Boffetta, P., Hashibe, M., La Vecchia, C., Zatonski, W. & Rehm, J. 2006. The burden of cancer attributable to alcohol drinking. *International journal of cancer. Journal international du cancer,* 119, 884-887.

Boulaamane, L., Boutayeb, S. & Errihani, H. 2012. Bevacizumab based chemotherapy in first line treatment of HER2 negative metastatic breast cancer: results of a Moroccan observational institutional study. *BMC research notes,* 5, 162.

Bouquot, J. E. & Gorlin, R. J. 1986. Leukoplakia, lichen planus, and other oral keratoses in 23,616 white Americans over the age of 35 years. *Oral surgery, oral medicine, and oral pathology,* 61, 373-381.

Bradford, M. M. 1976. A rapid and sensitive method for the quantitation of microgram quantities of protein utilizing the principle of protein-dye binding. *Analytical biochemistry,* 72, 248-254.

Bright, S. A., Greene, L. M., Greene, T. F., Campiani, G., Butini, S., Brindisi, M., Lawler, M., Meegan, M. J., Williams, D. C. & Zisterer, D. M. 2009. The novel pyrrolo-1,5-benzoxazepine, PBOX-21, potentiates the apoptotic efficacy of STI571 (imatinib mesylate) in human chronic myeloid leukaemia cells. *Biochem Pharmacol,* 77, 310-321.

Bright, S. A., Mcelligott, A. M., O'connell, J. W., O'connor, L., Carroll, P., Campiani, G., Deininger, M. W., Conneally, E., Lawler, M., Williams, D. C. & Zisterer, D. M. 2010. Novel pyrrolo-1,5-benzoxazepine compounds display significant activity against resistant chronic myeloid leukaemia cells in vitro, in ex vivo patient samples and in vivo. *British journal of cancer,* 102, 1474-1482.

Bristow, R. G. & Hill, R. P. 2008. Hypoxia and metabolism. Hypoxia, DNA repair and genetic instability. *Nature reviews. Cancer,* 8, 180-192.

Bunz, F., Hwang, P. M., Torrance, C., Waldman, T., Zhang, Y., Dillehay, L., Williams, J., Lengauer, C., Kinzler, K. W. & Vogelstein, B. 1999. Disruption of p53 in human cancer cells alters the responses to therapeutic agents. *The Journal of clinical investigation,* 104, 263-269.

Burdon, R. H. 1995. Superoxide and hydrogen peroxide in relation to mammalian cell proliferation. *Free radical biology & medicine,* 18, 775-794.

Burger, K., Muhl, B., Harasim, T., Rohrmoser, M., Malamoussi, A., Orban, M., Kellner, M., Gruber-Eber, A., Kremmer, E., Holzel, M. & Eick, D. 2010. Chemotherapeutic drugs inhibit ribosome biogenesis at various levels. *The Journal of biological chemistry,* 285, 12416-12425.

Burri, R. J. & Lee, N. Y. 2009. Concurrent chemotherapy and radiotherapy for head and neck cancer. *Expert review of anticancer therapy,* 9, 293-302.

Campiani, G., Nacci, V., Fiorini, I., De Filippis, M. P., Garofalo, A., Ciani, S. M., Greco, G., Novellino, E., Williams, D. C., Zisterer, D. M., Woods, M. J., Mihai, C., Manzoni, C. & Mennini, T. 1996. Synthesis, biological activity, and SARs of pyrrolobenzoxazepine derivatives, a new class of specific "peripheral-type" benzodiazepine receptor ligands. *Journal of medicinal chemistry,* 39, 3435-3450.

Carrard, V. C., Pires, A. S., Mendez, M., Mattos, F., Moreira, J. C. & Sant'ana Filho, M. 2009. Effects of acute alcohol consumption and vitamin E co-treatment on oxidative stress parameters in rats tongue. *Food and chemical toxicology : an international journal published for the British Industrial Biological Research Association,* 47, 1058-1063.

Carrard, V. C., Pires, A. S., Mendez, M., Pasquali, M. A., Badauy, C. M., Lauxen, I. S., Moreira, J. C. & Sant'ana Filho, M. 2013. Exploring the mechanisms of alcohol-related damage in oral mucosa - is oxidative stress associated with the increase in cell proliferation in rat tongue epithelium? *Pharmaceutical biology,* 51, 160-169.

Cavallaro, U. & Christofori, G. 2004. Cell adhesion and signalling by cadherins and Ig-CAMs in cancer. *Nature reviews. Cancer,* 4, 118-132.

Chalmers, M. 2002. Handbook of vibrational spectroscopy. 1.

Chaturvedi, A. K., Engels, E. A., Anderson, W. F. & Gillison, M. L. 2008. Incidence trends for human papillomavirus-related and -unrelated oral squamous cell carcinomas in the United States. *Journal of clinical oncology : official journal of the American Society of Clinical Oncology,* 26, 612-619.

Chio-Srichan, S., Refregiers, M., Jamme, F., Kascakova, S., Rouam, V. & Dumas, P. 2008. Photosensitizer effects on cancerous cells: a combined study using synchrotron infrared and fluorescence microscopies. *Biochimica et biophysica acta,* 1780, 854-860.

Cockman, M. E., Masson, N., Mole, D. R., Jaakkola, P., Chang, G. W., Clifford, S. C., Maher, E. R., Pugh, C. W., Ratcliffe, P. J. & Maxwell, P. H. 2000. Hypoxia inducible factor-alpha binding and ubiquitylation by the von Hippel-Lindau tumor suppressor protein. *The Journal of biological chemistry,* 275, 25733-25741.

Commission, T. E. 2009. Annex XVII. *Reach regulation.*

Conley, J. J. 1954. Surgical treatment of cancer of the tongue, floor of the mouth and alveolus. *Acta - Unio Internationalis Contra Cancrum,* 10, 233-245.

Crow, P., Barrass, B., Kendall, C., Hart-Prieto, M., Wright, M., Persad, R. & Stone, N. 2005. The use of Raman spectroscopy to differentiate between different prostatic adenocarcinoma cell lines. *British journal of cancer,* 92, 2166-2170.

Czech, M. P., Lawrence, J. C., Jr. & Lynn, W. S. 1974. Evidence for the involvement of sulfhydryl oxidation in the regulation of fat cell hexose transport by insulin. *Proceedings of the National Academy of Sciences of the United States of America,* 71, 4173-4177.

D'souza, G. & Dempsey, A. 2011. The role of HPV in head and neck cancer and review of the HPV vaccine. *Preventive medicine,* 53 Suppl 1, S5-S11.

De Forges, H., Bouissou, A. & Perez, F. 2012. Interplay between microtubule dynamics and intracellular organization. *The international journal of biochemistry & cell biology,* 44, 266-274.

Dearfield, K. L., Abernathy, C. O., Ottley, M. S., Brantner, J. H. & Hayes, P. F. 1988. Acrylamide: its metabolism, developmental and reproductive effects, genotoxicity, and carcinogenicity. *Mutation research,* 195, 45-77.

Deininger, M. W., Vieira, S., Mendiola, R., Schultheis, B., Goldman, J. M. & Melo, J. V. 2000. BCR-ABL tyrosine kinase activity regulates the expression of multiple genes implicated in the pathogenesis of chronic myeloid leukemia. *Cancer research,* 60, 2049-2055.

Devaney, J., Glennon, M., Farrell, G., Ruttledge, M., Smith, T., Houghton, J. A. & Maher, M. 2003. Cystic fibrosis mutation frequencies in an Irish population. *Clinical genetics,* 63, 121-125.

Ding, J., Li, S., Wu, J., Gao, C., Zhou, J., Cao, H., Su, P. S., Liu, Y., Zhou, X. & Chang, J. 2008. Alcohol dehydrogenase-2 and aldehyde dehydrogenase-2 genotypes, alcohol drinking and the risk of primary hepatocellular carcinoma in a Chinese population. *Asian Pacific journal of cancer prevention : APJCP,* 9, 31-35.

Donehower, R. C., Myers, C. E. & Chabner, B. A. 1979. New developments on the mechanisms of action of antineoplastic drugs. *Life sciences,* 25, 1-14.

Dong, Y. J., Peng, T. K. & Yin, S. J. 1996. Expression and activities of class IV alcohol dehydrogenase and class III aldehyde dehydrogenase in human mouth. *Alcohol,* 13, 257-262.

Ehrlich, M. 2002. DNA methylation in cancer: too much, but also too little. *Oncogene,* 21, 5400-5413.

El-Mashtoly, S. F., Petersen, D., Yosef, H. K., Mosig, A., Reinacher-Schick, A., Kotting, C. & Gerwert, K. 2014. Label-free imaging of drug distribution and metabolism in colon cancer cells by Raman microscopy. *The Analyst,* 139, 1155-1161.

Elango, K. J., Suresh, A., Erode, E. M., Subhadradevi, L., Ravindran, H. K., Iyer, S. K. & Kuriakose, M. A. 2011. Role of human papilloma virus in oral tongue squamous cell carcinoma. *Asian Pacific journal of cancer prevention : APJCP,* 12, 889-896.

Elmore, S. 2007. Apoptosis: a review of programmed cell death. *Toxicologic pathology,* 35, 495-516.

Epstein, J. B., Oakley, C., Millner, A., Emerton, S., Van Der Meij, E. & Le, N. 1997. The utility of toluidine blue application as a diagnostic aid in patients previously treated for upper oropharyngeal carcinoma. *Oral surgery, oral medicine, oral pathology, oral radiology, and endodontics,* 83, 537-547.

Evans, T., Rosenthal, E. T., Youngblom, J., Distel, D. & Hunt, T. 1983. Cyclin: a protein specified by maternal mRNA in sea urchin eggs that is destroyed at each cleavage division. *Cell,* 33, 389-396.

Fedirko, V., Tramacere, I., Bagnardi, V., Rota, M., Scotti, L., Islami, F., Negri, E., Straif, K., Romieu, I., La Vecchia, C., Boffetta, P. & Jenab, M. 2011. Alcohol drinking and colorectal cancer risk: an overall and dose-response meta-analysis of published studies. *Annals of oncology : official journal of the European Society for Medical Oncology / ESMO,* 22, 1958-1972.

Feller, L., Altini, M. & Slabbert, H. 1991. Pre-malignant lesions of the oral mucosa in a South African sample--a clinicopathological study. *The Journal of the Dental Association of South Africa = Die Tydskrif van die Tandheelkundige Vereniging van Suid-Afrika,* 46, 261-265.

Feng, Z., Zhang, H., Levine, A. J. & Jin, S. 2005. The coordinate regulation of the p53 and mTOR pathways in cells. *Proceedings of the National Academy of Sciences of the United States of America,* 102, 8204-8209.

Filippova, M., Filippov, V., Williams, V. M., Zhang, K., Kokoza, A., Bashkirova, S. & Duerksen-Hughes, P. 2014. Cellular levels of oxidative stress affect the response of cervical cancer cells to chemotherapeutic agents. *BioMed research international,* 2014, 574659.

Flemming, W. 1878. *"Flemming, W. Zur Kenntniss der Zelle und ihrer Theilungs-Erscheinungen. In: Schriften des Naturwissenschaftlichen Vereins für Schleswig-Holstein 3 (1878), 23–27."* [Online].

Forde, J. C., Maginn, E. N., Mcnamara, G., Martin, L. M., Campiani, G., Williams, D. C., Zisterer, D., Mcelligott, A. M., Lawler, M., Lynch, T. H., Hollywood, D. & Marignol, L. 2011. Microtubule-targeting-compound PBOX-15 radiosensitizes cancer cells in vitro. *Cancer biology & therapy,* 11, 421-428.

Franceschi, S., Levi, F., Dal Maso, L., Talamini, R., Conti, E., Negri, E. & La Vecchia, C. 2000. Cessation of alcohol drinking and risk of cancer of the oral cavity and pharynx. *International journal of cancer. Journal international du cancer,* 85, 787-790.

Frauenfelder, H. 2010. The Physics of Proteins. 53-58.

Frazier, M. W., He, X., Wang, J., Gu, Z., Cleveland, J. L. & Zambetti, G. P. 1998. Activation of c-myc gene expression by tumor-derived p53 mutants requires a discrete C-terminal domain. *Molecular and cellular biology,* 18, 3735-3743.

Friedberg, W., Siede 1995. *DNA repair and mutagenesis.*

Fu, T. Y., Hou, Y. Y., Chu, S. T., Liu, C. F., Huang, C. H., Chen, H. C., Hsiao, M., Lu, P. J., Wang, J. S. & Ger, L. P. 2011. Manganese superoxide dismutase and glutathione peroxidase as prognostic markers in patients with buccal mucosal squamous cell carcinomas. *Head & neck,* 33, 1606-1615.

Furuse, J. 2008. Sorafenib for the treatment of unresectable hepatocellular carcinoma. *Biologics : targets & therapy,* 2, 779-788.

Gadhia, K., Mcdonald, S., Arkutu, N. & Malik, K. 2012. Amelogenesis imperfecta: an introduction. *British dental journal,* 212, 377-379.

Gan, X., Chen, B., Shen, Z., Liu, Y., Li, H., Xie, X., Xu, X., Li, H., Huang, Z. & Chen, J. 2014. High GPX1 expression promotes esophageal squamous cell carcinoma invasion, migration, proliferation and cisplatin-resistance but can be reduced by vitamin D. *International journal of clinical and experimental medicine,* 7, 2530-2540.

Gangemi, G., Gazzerro, P., Fiore, D., Proto, M. C., Butini, S., Gemma, S., Casagni, A., Laezza, C., Vitale, M., Ligresti, A., Di Marzo, V., Zisterer, D. M., Nathwani, S., Clive Williams, D., Campiani, G. & Bifulco, M. 2013. PBOX-15 induces

apoptosis and improves the efficacy of oxaliplatin in human colorectal cancer cell lines. *European journal of pharmacology,* 714, 379-387.
Gatti, L. & Zunino, F. 2005. Overview of tumor cell chemoresistance mechanisms. *Methods in molecular medicine,* 111, 127-148.
Genden, E. M., Ferlito, A., Shaha, A. R. & Rinaldo, A. 2003. Management of cancer of the retromolar trigone. *Oral oncology,* 39, 633-637.
Glasauer, A. & Chandel, N. S. 2014. Targeting antioxidants for cancer therapy. *Biochem Pharmacol,* 92, 90-101.
Glatz, J. F., Borchers, T., Spener, F. & Van Der Vusse, G. J. 1995. Fatty acids in cell signalling: modulation by lipid binding proteins. *Prostaglandins, leukotrienes, and essential fatty acids,* 52, 121-127.
Goda, N., Dozier, S. J. & Johnson, R. S. 2003. HIF-1 in cell cycle regulation, apoptosis, and tumor progression. *Antioxidants & redox signaling,* 5, 467-473.
Gonzalez-Solis, J. L., Martinez-Espinosa, J. C., Salgado-Roman, J. M. & Palomares-Anda, P. 2014. Monitoring of chemotherapy leukemia treatment using Raman spectroscopy and principal component analysis. *Lasers in medical science,* 29, 1241-1249.
Goswami, E., Craven, V., Dahlstrom, D. L., Alexander, D. & Mowat, F. 2013. Domestic asbestos exposure: a review of epidemiologic and exposure data. *International journal of environmental research and public health,* 10, 5629-5670.
Gough, D. R. & Cotter, T. G. 2011. Hydrogen peroxide: a Jekyll and Hyde signalling molecule. *Cell death & disease,* 2, e213.
Green, D. R. & Kroemer, G. 2009. Cytoplasmic functions of the tumour suppressor p53. *Nature,* 458, 1127-1130.
Greene, L. M., Fleeton, M., Mulligan, J., Gowda, C., Sheahan, B. J., Atkins, G. J., Campiani, G., Nacci, V., Lawler, M., Williams, D. C. & Zisterer, D. M. 2005. The pyrrolo-1,5-benzoxazepine, PBOX-6, inhibits the growth of breast cancer cells in vitro independent of estrogen receptor status and inhibits breast tumour growth in vivo. *Oncology reports,* 14, 1357-1363.
Greene, L. M., Nolan, D. P., Regan-Komito, D., Campiani, G., Williams, D. C. & Zisterer, D. M. 2013. Inhibition of late-stage autophagy synergistically enhances pyrrolo-1,5-benzoxazepine-6-induced apoptotic cell death in human colon cancer cells. *International journal of oncology,* 43, 927-935.
Grewal, P. & Viswanathen, V. A. 2012. Liver cancer and alcohol. *Clinics in liver disease,* 16, 839-850.
Gross, K., Kircik, L. & Kricorian, G. 2007. 5% 5-Fluorouracil cream for the treatment of small superficial Basal cell carcinoma: efficacy, tolerability, cosmetic outcome, and patient satisfaction. *Dermatologic surgery : official publication for American Society for Dermatologic Surgery [et al.],* 33, 433-439; discussion 440.
Grubbe, E. H. 1902. X-rays in the treatment of cancer and other malignant diseases. *Medical record (W.Wood),* 62, 692-695.
Gu, J., Zhu, S., Li, X., Wu, H., Li, Y. & Hua, F. 2014. Effect of amifostine in head and neck cancer patients treated with radiotherapy: a systematic review and meta-analysis based on randomized controlled trials. *PloS one,* 9, e95968.
Guertin, D. A. & Sabatini, D. M. 2007. Defining the role of mTOR in cancer. *Cancer cell,* 12, 9-22.
Gurtovenko, A. A. & Anwar, J. 2009. Interaction of ethanol with biological membranes: the formation of non-bilayer structures within the membrane interior and their significance. *The journal of physical chemistry. B,* 113, 1983-1992.

Hagner, P. R., Mazan-Mamczarz, K., Dai, B., Corl, S., Zhao, X. F. & Gartenhaus, R. B. 2009. Alcohol consumption and decreased risk of non-Hodgkin lymphoma: role of mTOR dysfunction. *Blood,* 113, 5526-5535.

Haka, A. S., Shafer-Peltier, K. E., Fitzmaurice, M., Crowe, J., Dasari, R. R. & Feld, M. S. 2005. Diagnosing breast cancer by using Raman spectroscopy. *Proceedings of the National Academy of Sciences of the United States of America,* 102, 12371-12376.

Hamajima, N., Hirose, K., Tajima, K., Rohan, T., Calle, E. E., Heath, C. W., Jr., Coates, R. J., Liff, J. M., Talamini, R., Chantarakul, N., Koetsawang, S., Rachawat, D., Morabia, A., Schuman, L., Stewart, W., Szklo, M., Bain, C., Schofield, F., Siskind, V., Band, P., Coldman, A. J., Gallagher, R. P., Hislop, T. G., Yang, P., Kolonel, L. M., Nomura, A. M., Hu, J., Johnson, K. C., Mao, Y., De Sanjose, S., Lee, N., Marchbanks, P., Ory, H. W., Peterson, H. B., Wilson, H. G., Wingo, P. A., Ebeling, K., Kunde, D., Nishan, P., Hopper, J. L., Colditz, G., Gajalanski, V., Martin, N., Pardthaisong, T., Silpisornkosol, S., Theetranont, C., Boosiri, B., Chutivongse, S., Jimakorn, P., Virutamasen, P., Wongsrichanalai, C., Ewertz, M., Adami, H. O., Bergkvist, L., Magnusson, C., Persson, I., Chang-Claude, J., Paul, C., Skegg, D. C., Spears, G. F., Boyle, P., Evstifeeva, T., Daling, J. R., Hutchinson, W. B., Malone, K., Noonan, E. A., Stanford, J. L., Thomas, D. B., Weiss, N. S., White, E., Andrieu, N., Bremond, A., Clavel, F., Gairard, B., Lansac, J., Piana, L., Renaud, R., Izquierdo, A., Viladiu, P., Cuevas, H. R., Ontiveros, P., Palet, A., Salazar, S. B., Aristizabel, N., Cuadros, A., Tryggvadottir, L., Tulinius, H., Bachelot, A., Le, M. G., Peto, J., Franceschi, S., Lubin, F., Modan, B., Ron, E., Wax, Y., Friedman, G. D., Hiatt, R. A., Levi, F., Bishop, T., Kosmelj, K., Primic-Zakelj, M., Ravnihar, B., Stare, J., Beeson, W. L., Fraser, G., Bullbrook, R. D., Cuzick, J., Duffy, S. W., Fentiman, I. S., Hayward, J. L., Wang, D. Y., Mcmichael, A. J., Mcpherson, K., Hanson, R. L., Leske, M. C., Mahoney, M. C., Nasca, P. C., Varma, A. O., Weinstein, A. L., Moller, T. R., Olsson, H., Ranstam, J., Goldbohm, R. A., Van Den Brandt, P. A., Apelo, R. A., Baens, J., De La Cruz, J. R., Javier, B., Lacaya, L. B., Ngelangel, C. A., La Vecchia, C., Negri, E., Marubini, E., Ferraroni, M., Gerber, M., Richardson, S., Segala, C., Gatei, D., Kenya, P., Kungu, A., Mati, J. G., Brinton, L. A., Hoover, R., Schairer, C., Spirtas, R., Lee, H. P., Rookus, M. A., Van Leeuwen, F. E., Schoenberg, J. A., Mccredie, M., Gammon, M. D., Clarke, E. A., Jones, L., Neil, A., Vessey, M., Yeates, D., Appleby, P., Banks, E., Beral, V., Bull, D., Crossley, B., Goodill, A., Green, J., Hermon, C., Key, T., Langston, N., Lewis, C., Reeves, G., Collins, R., Doll, R., Peto, R., Mabuchi, K., Preston, D., Hannaford, P., Kay, C., Rosero-Bixby, L., Gao, Y. T., Jin, F., Yuan, J. M., Wei, H. Y., Yun, T., Zhiheng, C., Berry, G., Cooper Booth, J., Jelihovsky, T., Maclennan, R., Shearman, R., Wang, Q. S., Baines, C. J., Miller, A. B., Wall, C., Lund, E., Stalsberg, H., Shu, X. O., Zheng, W., Katsouyanni, K., Trichopoulou, A., Trichopoulos, D., Dabancens, A., Martinez, L., Molina, R., Salas, O., Alexander, F. E., Anderson, K., Folsom, A. R., Hulka, B. S., Bernstein, L., Enger, S., Haile, R. W., Paganini-Hill, A., Pike, M. C., Ross, R. K., Ursin, G., Yu, M. C., Longnecker, M. P., Newcomb, P., Bergkvist, L., Kalache, A., Farley, T. M., Holck, S., Meirik, O. & Collaborative Group on Hormonal Factors in Breast, C. 2002. Alcohol, tobacco and breast cancer--collaborative reanalysis of individual data from 53 epidemiological studies, including 58,515 women with breast cancer and 95,067 women without the disease. *British journal of cancer,* 87, 1234-1245.

Hanahan, D. & Weinberg, R. A. 2011. Hallmarks of cancer: the next generation. *Cell,* 144, 646-674.

Harris, A. L. 2002. Hypoxia--a key regulatory factor in tumour growth. *Nature reviews. Cancer,* 2, 38-47.

Heaton, M. B., Paiva, M. & Siler-Marsiglio, K. 2011. Ethanol influences on Bax translocation, mitochondrial membrane potential, and reactive oxygen species generation are modulated by vitamin E and brain-derived neurotrophic factor. *Alcoholism, clinical and experimental research,* 35, 1122-1133.

Hecht, S. S. 1999. Tobacco smoke carcinogens and lung cancer. *Journal of the National Cancer Institute,* 91, 1194-1210.

Hein, N., Hannan, K. M., George, A. J., Sanij, E. & Hannan, R. D. 2013. The nucleolus: an emerging target for cancer therapy. *Trends in molecular medicine,* 19, 643-654.

Helmlinger, G., Yuan, F., Dellian, M. & Jain, R. K. 1997. Interstitial pH and pO2 gradients in solid tumors in vivo: high-resolution measurements reveal a lack of correlation. *Nature medicine,* 3, 177-182.

Hicks, S. D., Middleton, F. A. & Miller, M. W. 2010. Ethanol-induced methylation of cell cycle genes in neural stem cells. *Journal of neurochemistry,* 114, 1767-1780.

Hirschhaeuser, F., Sattler, U. G. & Mueller-Klieser, W. 2011. Lactate: a metabolic key player in cancer. *Cancer research,* 71, 6921-6925.

Hochegger, H., Takeda, S. & Hunt, T. 2008. Cyclin-dependent kinases and cell-cycle transitions: does one fit all? *Nature reviews. Molecular cell biology,* 9, 910-916.

Hong-Brown, L. Q., Frost, R. A. & Lang, C. H. 2001. Alcohol impairs protein synthesis and degradation in cultured skeletal muscle cells. *Alcoholism, clinical and experimental research,* 25, 1373-1382.

Horio, T. & Murata, T. 2014. The role of dynamic instability in microtubule organization. *Frontiers in plant science,* 5, 511.

Howard, S. M., Theologides, A. & Sheppard, J. R. 1980. Comparative effects of vindesine, vinblastine, and vincristine on mitotic arrest and hormonal response of L1210 leukemia cells. *Cancer research,* 40, 2695-2700.

Hsu, M. K., Qiao, L., Ho, V., Zhang, B. H., Zhang, H., Teoh, N., Dent, P. & Farrell, G. C. 2006. Ethanol reduces p38 kinase activation and cyclin D1 protein expression after partial hepatectomy in rats. *Journal of hepatology,* 44, 375-382.

Hu, H., Luo, M. L., Du, X. L., Feng, Y. B., Zhang, Y., Shen, X. M., Xu, X., Cai, Y., Han, Y. L. & Wang, M. R. 2007. Up-regulated manganese superoxide dismutase expression increases apoptosis resistance in human esophageal squamous cell carcinomas. *Chinese medical journal,* 120, 2092-2098.

Hu, J. L., Xiao, L., Li, Z. Y., Wang, Q., Chang, Y. & Jin, Y. 2013. Upregulation of HO-1 is accompanied by activation of p38MAPK and mTOR in human oesophageal squamous carcinoma cells. *Cell biology international,* 37, 584-592.

Huang, G. C., Liu, S. Y., Lin, M. H., Kuo, Y. Y. & Liu, Y. C. 2004. The synergistic cytotoxicity of cisplatin and taxol in killing oral squamous cell carcinoma. *Japanese journal of clinical oncology,* 34, 499-504.

Huang, H. S., S. Feng, W. Chen, Y. Yu, D. Lin, and R. Chen 2012. Confocal Raman spectroscopic analysis of the cytotoxic response to cisplatin in nasopharyngeal carcinoma cells. *Analysis Methods,* 5, 260-266.

Hussain, S. P., Amstad, P., He, P., Robles, A., Lupold, S., Kaneko, I., Ichimiya, M., Sengupta, S., Mechanic, L., Okamura, S., Hofseth, L. J., Moake, M., Nagashima, M., Forrester, K. S. & Harris, C. C. 2004. p53-induced up-regulation of MnSOD and GPx but not catalase increases oxidative stress and apoptosis. *Cancer research,* 64, 2350-2356.

Ide, R., Mizoue, T., Fujino, Y., Hoshiyama, Y., Sakata, K., Tamakoshi, A., Yoshimura, T. & Group, J. S. 2008. Cigarette smoking, alcohol drinking, and oral and pharyngeal cancer mortality in Japan. *Oral diseases,* 14, 314-319.

Ilin, Y. & Kraft, M. L. 2014. Identifying the lineages of individual cells in cocultures by multivariate analysis of Raman spectra. *The Analyst,* 139, 2177-2185.

Inoue, S. & Sato, H. 1967. Cell motility by labile association of molecules. The nature of mitotic spindle fibers and their role in chromosome movement. *The Journal of general physiology,* 50, Suppl:259-292.

Ivan, M., Kondo, K., Yang, H., Kim, W., Valiando, J., Ohh, M., Salic, A., Asara, J. M., Lane, W. S. & Kaelin, W. G., Jr. 2001. HIFalpha targeted for VHL-mediated destruction by proline hydroxylation: implications for O2 sensing. *Science,* 292, 464-468.

Iype, E. M., Pandey, M., Mathew, A., Thomas, G. & Nair, M. K. 2004. Squamous cell cancer of the buccal mucosa in young adults. *The British journal of oral & maxillofacial surgery,* 42, 185-189.

Jaakkola, P., Mole, D. R., Tian, Y. M., Wilson, M. I., Gielbert, J., Gaskell, S. J., Kriegsheim, A., Hebestreit, H. F., Mukherji, M., Schofield, C. J., Maxwell, P. H., Pugh, C. W. & Ratcliffe, P. J. 2001. Targeting of HIF-alpha to the von Hippel-Lindau ubiquitylation complex by O2-regulated prolyl hydroxylation. *Science,* 292, 468-472.

Jayaprakash, V., Reid, M., Hatton, E., Merzianu, M., Rigual, N., Marshall, J., Gill, S., Frustino, J., Wilding, G., Loree, T., Popat, S. & Sullivan, M. 2011. Human papillomavirus types 16 and 18 in epithelial dysplasia of oral cavity and oropharynx: a meta-analysis, 1985-2010. *Oral oncology,* 47, 1048-1054.

Johnson, I. S., Wright, H. F. & Svoboda, G. H. 1959. Experimental Basis for Clinical Evaluation of Anti Tumor Principles Derived from Vinca-Rosea Linn. *J Lab Clin Med,* 54, 830-830.

Jones, R. G. & Thompson, C. B. 2009. Tumor suppressors and cell metabolism: a recipe for cancer growth. *Genes & development,* 23, 537-548.

Kanduc, D., Mittelman, A., Serpico, R., Sinigaglia, E., Sinha, A. A., Natale, C., Santacroce, R., Di Corcia, M. G., Lucchese, A., Dini, L., Pani, P., Santacroce, S., Simone, S., Bucci, R. & Farber, E. 2002. Cell death: apoptosis versus necrosis (review). *International journal of oncology,* 21, 165-170.

Kaneda, Y., Shimamoto, H., Matsumura, K., Arvind, R., Zhang, S., Sakai, E., Omura, K. & Tsuchida, N. 2006. Role of caspase 8 as a determinant in chemosensitivity of p53-mutated head and neck squamous cell carcinoma cell lines. *Journal of medical and dental sciences,* 53, 57-66.

Kang, M. Y., Kim, H. B., Piao, C., Lee, K. H., Hyun, J. W., Chang, I. Y. & You, H. J. 2013. The critical role of catalase in prooxidant and antioxidant function of p53. *Cell death and differentiation,* 20, 117-129.

Kast, R. E., Serhatkulu, G. K., Cao, A., Pandya, A. K., Dai, H., Thakur, J. S., Naik, V. M., Naik, R., Klein, M. D., Auner, G. W. & Rabah, R. 2008. Raman spectroscopy can differentiate malignant tumors from normal breast tissue and detect early neoplastic changes in a mouse model. *Biopolymers,* 89, 235-241.

Kastan, M. B. & Bartek, J. 2004. Cell-cycle checkpoints and cancer. *Nature,* 432, 316-323.

Kastan, M. B., Canman, C. E. & Leonard, C. J. 1995. P53, cell cycle control and apoptosis: implications for cancer. *Cancer metastasis reviews,* 14, 3-15.

Khanna, R., Thapa, P. B., Khanna, H. D., Khanna, S., Khanna, A. K. & Shukla, H. S. 2005. Lipid peroxidation and antioxidant enzyme status in oral carcinoma patients. *Kathmandu University medical journal,* 3, 334-339.

Kikuchi, T. 2006. Genetically modified dendritic cells for therapeutic immunity. *The Tohoku journal of experimental medicine,* 208, 1-8.
Kim, J. K. & Diehl, J. A. 2009. Nuclear cyclin D1: an oncogenic driver in human cancer. *Journal of cellular physiology,* 220, 292-296.
Kinalwa, M. N., Blanch, E. W. & Doig, A. J. 2010. Accurate determination of protein secondary structure content from Raman and Raman optical activity spectra. *Analytical chemistry,* 82, 6347-6349.
King, R. J. B. 2000. Cancer Biology. 120-133.
Kowalczyk, D. W., Wysocki, P. J. & Mackiewicz, A. 2003. Cancer immunotherapy using cells modified with cytokine genes. *Acta biochimica Polonica,* 50, 613-624.
Krishna, C. M., Kegelaer, G., Adt, I., Rubin, S., Kartha, V. B., Manfait, M. & Sockalingum, G. D. 2006. Combined Fourier transform infrared and Raman spectroscopic approach for identification of multidrug resistance phenotype in cancer cell lines. *Biopolymers,* 82, 462-470.
Krokan, H. E. & Bjoras, M. 2013. Base excision repair. *Cold Spring Harbor perspectives in biology,* 5, a012583.
Kuhn, P. E. & Miller, M. W. 1998. Expression of p53 and ALZ-50 immunoreactivity in rat cortex: effect of prenatal exposure to ethanol. *Experimental neurology,* 154, 418-429.
Kushner, J., Bradley, G., Young, B. & Jordan, R. C. 1999. Aberrant expression of cyclin A and cyclin B1 proteins in oral carcinoma. *Journal of oral pathology & medicine : official publication of the International Association of Oral Pathologists and the American Academy of Oral Pathology,* 28, 77-81.
Laimer, K., Spizzo, G., Gastl, G., Obrist, P., Brunhuber, T., Fong, D., Barbieri, V., Jank, S., Doppler, W., Rasse, M. & Norer, B. 2007. High EGFR expression predicts poor prognosis in patients with squamous cell carcinoma of the oral cavity and oropharynx: a TMA-based immunohistochemical analysis. *Oral oncology,* 43, 193-198.
Leach, M. O. 1996. Introduction to in vivo MRS of cancer: new perspectives and open problems. *Anticancer research,* 16, 1503-1514.
Lee, J. W., Bae, S. H., Jeong, J. W., Kim, S. H. & Kim, K. W. 2004. Hypoxia-inducible factor (HIF-1)alpha: its protein stability and biological functions. *Experimental & molecular medicine,* 36, 1-12.
Lengsfeld, A. M., Schultze, B. & Maurer, W. 1981. Time-lapse studies on the effect of vincristine on HeLa cells. *European journal of cancer,* 17, 307-319.
Lennon, J. C., Bright, S. A., Carroll, E., Butini, S., Campiani, G., O'meara, A., Williams, D. C. & Zisterer, D. M. 2014. The novel pyrrolo-1,5-benzoxazepine, PBOX-6, synergistically enhances the apoptotic effects of carboplatin in drug sensitive and multidrug resistant neuroblastoma cells. *Biochem Pharmacol,* 87, 611-624.
Lev, S. 2010. Non-vesicular lipid transport by lipid-transfer proteins and beyond. *Nature reviews. Molecular cell biology,* 11, 739-750.
Li, M., Zhao, L., Liu, J., Liu, A. L., Zeng, W. S., Luo, S. Q. & Bai, X. C. 2009. Hydrogen peroxide induces G2 cell cycle arrest and inhibits cell proliferation in osteoblasts. *Anatomical record,* 292, 1107-1113.
Li, Z., Lin, H., Zhu, Y., Wang, M. & Luo, J. 2001. Disruption of cell cycle kinetics and cyclin-dependent kinase system by ethanol in cultured cerebellar granule progenitors. *Brain research. Developmental brain research,* 132, 47-58.
Licitra, L. & Vermorken, J. B. 2004. Is there still a role for neoadjuvant chemotherapy in head and neck cancer? *Annals of oncology : official journal of the European Society for Medical Oncology / ESMO,* 15, 7-11.

Lin, J., Yu, Y., Li, B., Huang, H., Lin, S., Li, C., Su, Y., Feng, S., Chen, G., Li, Y., Huang, Z., Zeng, H. And Chen, R. 2012. Electrical pulse – mediated enhanced delivery of silver nanoparticles into living suspension cells for surface enhanced Raman spectroscopy. *Laser Physics Letters,* 9, 240-246.

Lingen, M. W., Kalmar, J. R., Karrison, T. & Speight, P. M. 2008. Critical evaluation of diagnostic aids for the detection of oral cancer. *Oral oncology,* 44, 10-22.

Liu, D. P., Song, H. & Xu, Y. 2010a. A common gain of function of p53 cancer mutants in inducing genetic instability. *Oncogene,* 29, 949-956.

Liu, G., Beri, R., Mueller, A. & Kamp, D. W. 2010b. Molecular mechanisms of asbestos-induced lung epithelial cell apoptosis. *Chemico-biological interactions,* 188, 309-318.

Liu, S. L., Lin, X., Shi, D. Y., Cheng, J., Wu, C. Q. & Zhang, Y. D. 2002. Reactive oxygen species stimulated human hepatoma cell proliferation via cross-talk between PI3-K/PKB and JNK signaling pathways. *Archives of biochemistry and biophysics,* 406, 173-182.

Liu, S. W., Guitart, J. G., Kuzel, T. M., Gandhi, M. & Lacouture, M. 2009. Effect of sunitinib on renal cell carcinoma cutaneous metastasis. *International journal of dermatology,* 48, 1269-1270.

Lotem, J. & Sachs, L. 1995. A mutant p53 antagonizes the deregulated c-myc-mediated enhancement of apoptosis and decrease in leukemogenicity. *Proceedings of the National Academy of Sciences of the United States of America,* 92, 9672-9676.

Lowary, P. T. & Widom, J. 1997. Nucleosome packaging and nucleosome positioning of genomic DNA. *Proceedings of the National Academy of Sciences of the United States of America,* 94, 1183-1188.

Lowe, J., Li, H., Downing, K. H. & Nogales, E. 2001. Refined structure of alpha beta-tubulin at 3.5 A resolution. *Journal of molecular biology,* 313, 1045-1057.

Lundberg, A. S. & Weinberg, R. A. 1999. Control of the cell cycle and apoptosis. *European journal of cancer,* 35, 1886-1894.

Luo, J. & Miller, M. W. 1997. Basic fibroblast growth factor- and platelet-derived growth factor-mediated cell proliferation in B104 neuroblastoma cells: effect of ethanol on cell cycle kinetics. *Brain research,* 770, 139-150.

Lyng, F. M., Faolain, E. O., Conroy, J., Meade, A. D., Knief, P., Duffy, B., Hunter, M B., Byrne, J. M., Kelehan, P. & Byrne, H. J. 2007. Vibrational spectroscopy for cervical cancer pathology, from biochemical analysis to diagnostic tool. *Experimental and molecular pathology,* 82, 121-129.

Madkan, V. K., Cook-Norris, R. H., Steadman, M. C., Arora, A., Mendoza, N. & Tyring, S. K. 2007. The oncogenic potential of human papillomaviruses: a review on the role of host genetics and environmental cofactors. *The British journal of dermatology,* 157, 228-241.

Magee, N. D., Beattie, J. R., Carland, C., Davis, R., Mcmanus, K., Bradbury, I., Fennell, D. A., Hamilton, P. W., Ennis, M., Mcgarvey, J. J. & Elborn, J. S. 2010. Raman microscopy in the diagnosis and prognosis of surgically resected nonsmall cell lung cancer. *Journal of biomedical optics,* 15, 026015.

Magee, N. D., Villaumie, J. S., Marple, E. T., Ennis, M., Elborn, J. S. & Mcgarvey, J. J. 2009. Ex vivo diagnosis of lung cancer using a Raman miniprobe. *The journal of physical chemistry. B,* 113, 8137-8141.

Maier, H., Weidauer, H., Zoller, J., Seitz, H. K., Flentje, M., Mall, G. & Born, I. A. 1994. Effect of chronic alcohol consumption on the morphology of the oral mucosa. *Alcoholism, clinical and experimental research,* 18, 387-391.

Malafa, M., Margenthaler, J., Webb, B., Neitzel, L. & Christophersen, M. 2000. MnSOD expression is increased in metastatic gastric cancer. *The Journal of surgical research,* 88, 130-134.

Malawista, S. E., Sato, H. & Bensch, K. G. 1968. Vinblastine and griseofulvin reversibly disrupt the living mitotic spindle. *Science,* 160, 770-772.

Marteijn, J. A., Lans, H., Vermeulen, W. & Hoeijmakers, J. H. 2014. Understanding nucleotide excision repair and its roles in cancer and ageing. *Nature reviews. Molecular cell biology,* 15, 465-481.

May, J. M. & De Haen, C. 1979. Insulin-stimulated intracellular hydrogen peroxide production in rat epididymal fat cells. *The Journal of biological chemistry,* 254, 2214-2220.

Mc Gee, M. M., Greene, L. M., Ledwidge, S., Campiani, G., Nacci, V., Lawler, M., Williams, D. C. & Zisterer, D. M. 2004. Selective induction of apoptosis by the pyrrolo-1,5-benzoxazepine 7-[[dimethylcarbamoyl]oxy]-6-(2-naphthyl)pyrrolo-[2,1-d] (1,5)-benzoxazepine (PBOX-6) in Leukemia cells occurs via the c-Jun NH2-terminal kinase-dependent phosphorylation and inactivation of Bcl-2 and Bcl-XL. *The Journal of pharmacology and experimental therapeutics,* 310, 1084-1095.

Mcelligott, A. M., Maginn, E. N., Greene, L. M., Mcguckin, S., Hayat, A., Browne, P. V., Butini, S., Campiani, G., Catherwood, M. A., Vandenberghe, E., Williams, D. C., Zisterer, D. M. & Lawler, M. 2009. The novel tubulin-targeting agent pyrrolo-1,5-benzoxazepine-15 induces apoptosis in poor prognostic subgroups of chronic lymphocytic leukemia. *Cancer research,* 69, 8366-8375.

Mcilwain, D. R., Berger, T. & Mak, T. W. 2013. Caspase functions in cell death and disease. *Cold Spring Harbor perspectives in biology,* 5, a008656.

Meade, A. D., Clarke, C., Draux, F., Sockalingum, G. D., Manfait, M., Lyng, F. M. & Byrne, H. J. 2010. Studies of chemical fixation effects in human cell lines using Raman microspectroscopy. *Analytical and bioanalytical chemistry,* 396, 1781-1791.

Meng, T. C., Fukada, T. & Tonks, N. K. 2002. Reversible oxidation and inactivation of protein tyrosine phosphatases in vivo. *Molecular cell,* 9, 387-399.

Miller, M. W., Peter, A., Wharton, S. B. & Wyllie, A. H. 2003. Proliferation and death of conditionally immortalized neural cells from murine neocortex: p53 alters the ability of neuron-like cells to re-enter the cell cycle. *Brain research,* 965, 57-66.

Mladenov, E. & Iliakis, G. 2011. Induction and repair of DNA double strand breaks: the increasing spectrum of non-homologous end joining pathways. *Mutation research,* 711, 61-72.

Modest, D. P., Reinacher-Schick, A., Stintzing, S., Giessen, C., Tannapfel, A., Laubender, R. P., Brodowicz, T., Knittelfelder, R., Vrbanec, D., Schmiegel, W., Heinemann, V. & Zielinski, C. C. 2012. Cetuximab-based or bevacizumab-based first-line treatment in patients with KRAS p.G13D-mutated metastatic colorectal cancer: a pooled analysis. *Anti-cancer drugs.*

Mongan D, R. S., Fanagan S and Long J 2007. Health-related consequences of problem d alcohol use. *Health Research Board,* 6.

Moretti, A., Vitullo, F., Augurio, A., Pacella, A. & Croce, A. 2011. Surgical management of lip cancer. *Acta otorhinolaryngologica Italica : organo ufficiale della Societa italiana di otorinolaringologia e chirurgia cervico-facciale,* 31, 5-10.

Morgan, D. 2006. Cell Cycle: Principles of Control. *Yale Journal of Biology and Medicine,* 28-54.

Morotti, M., Valenzano Menada, M., Venturini, P. L. & Ferrero, S. 2012. Bevacizumab in endometrial cancer treatment. *Expert opinion on biological therapy.*

Moynahan, M. E. & Jasin, M. 2010. Mitotic homologous recombination maintains genomic stability and suppresses tumorigenesis. *Nature reviews. Molecular cell biology,* 11, 196-207.

Mulligan, J. M., Greene, L. M., Cloonan, S., Mc Gee, M. M., Onnis, V., Campiani, G., Fattorusso, C., Lawler, M., Williams, D. C. & Zisterer, D. M. 2006. Identification of tubulin as the molecular target of proapoptotic pyrrolo-1,5-benzoxazepines. *Molecular pharmacology,* 70, 60-70.

Nathwani, S. M., Butler, S., Fayne, D., Mcgovern, N. N., Sarkadi, B., Meegan, M. J., Lloyd, D. G., Campiani, G., Lawler, M., Williams, D. C. & Zisterer, D. M. 2010a. Novel microtubule-targeting agents, pyrrolo-1,5-benzoxazepines, induce apoptosis in multi-drug-resistant cancer cells. *Cancer chemotherapy and pharmacology,* 66, 585-596.

Nathwani, S. M., Butler, S., Meegan, M. J., Campiani, G., Lawler, M., Williams, D. C. & Zisterer, D. M. 2010b. Dual targeting of tumour cells and host endothelial cells by novel microtubule-targeting agents, pyrrolo-1,5-benzoxazepines. *Cancer chemotherapy and pharmacology,* 65, 289-300.

Nathwani, S. M., Cloonan, S. M., Stronach, M., Campiani, G., Lawler, M., Williams, D. C. & Zisterer, D. M. 2010c. Novel microtubule-targeting agents, pyrrolo-1,5-benzoxazepines, induce cell cycle arrest and apoptosis in prostate cancer cells. *Oncology reports,* 24, 1499-1507.

Nathwani, S. M., Cloonan, S. M., Stronach, M., Campiani, G., Lawler, M., Williams, D. C. & Zisterer, D. M. 2010d. Novel microtubule-targeting agents, pyrrolo-1,5-benzoxazepines, induce cell cycle arrest and apoptosis in prostate cancer cells. *Oncology reports,* 24, 1499-1507.

Nawrocki, S., Wysocki, P. J. & Mackiewicz, A. 2001. Genetically modified tumour vaccines: an obstacle race to break host tolerance to cancer. *Expert opinion on biological therapy,* 1, 193-204.

Negendank, W. 1992. Studies of human tumors by MRS: a review. *NMR in biomedicine,* 5, 303-324.

Nelson, D. M., Ye, X., Hall, C., Santos, H., Ma, T., Kao, G. D., Yen, T. J., Harper, J. W. & Adams, P. D. 2002. Coupling of DNA synthesis and histone synthesis in S phase independent of cyclin/cdk2 activity. *Molecular and cellular biology,* 22, 7459-7472.

Nijssen, A., Bakker Schut, T. C., Heule, F., Caspers, P. J., Hayes, D. P., Neumann, M. H. & Puppels, G. J. 2002. Discriminating basal cell carcinoma from its surrounding tissue by Raman spectroscopy. *The Journal of investigative dermatology,* 119, 64-69.

Noble, R. L., Beer, C. T. & Cutts, J. H. 1958. Further Biological Activities of Vincaleukoblastine - an Alkaloid Isolated from Vinca-Rosea-(L). *Biochem Pharmacol,* 1, 347-348.

Notingher, I. 2007. Raman Spectroscopy Cell-Based Biosensors. *Sensors,* 7, 1343-1358.

Oliveira, A. P., Bitar, R. A., Silveira, L., Zangaro, R. A. & Martin, A. A. 2006. Near-infrared Raman spectroscopy for oral carcinoma diagnosis. *Photomedicine and laser surgery,* 24, 348-353.

Ostrowska, K. M., Malkin, A., Meade, A., O'leary, J., Martin, C., Spillane, C., Byrne, H. J. & Lyng, F. M. 2010. Investigation of the influence of high-risk human papillomavirus on the biochemical composition of cervical cancer cells using vibrational spectroscopy. *The Analyst,* 135, 3087-3093.

Pal, S. K. & Mittal, B. 2004. Improving cancer care in India: prospects and challenges. *Asian Pacific journal of cancer prevention : APJCP,* 5, 226-228.

Pan, H. N., Sun, R., Jaruga, B., Hong, F., Kim, W. H. & Gao, B. 2006. Chronic ethanol consumption inhibits hepatic natural killer cell activity and accelerates murine cytomegalovirus-induced hepatitis. *Alcoholism, clinical and experimental research,* 30, 1615-1623.

Parkin, D. M., Bray, F., Ferlay, J. & Pisani, P. 2005. Global cancer statistics, 2002. *CA: a cancer journal for clinicians,* 55, 74-108.

Paul, A. & Paul, S. 2014. The breast cancer susceptibility genes (BRCA) in breast and ovarian cancers. *Frontiers in bioscience,* 19, 605-618.

Paweletz, N. 2001. Walther Flemming: pioneer of mitosis research. *Nature reviews. Molecular cell biology,* 2, 72-75.

Pearson, R. A. 1901. Section I, Social and Economic Science. *Science,* 14, 912-926.

Perera, C. S., St Clair, D. K. & Mcclain, C. J. 1995. Differential regulation of manganese superoxide dismutase activity by alcohol and TNF in human hepatoma cells. *Archives of biochemistry and biophysics,* 323, 471-476.

Pindborg, J. J., Renstrup, G., Poulsen, H. E. & Silverman, S., Jr. 1963. Studies in Oral Leukoplakias. V. Clinical and Histologic Signs of Malignancy. *Acta odontologica Scandinavica,* 21, 407-414.

Poschl, G. & Seitz, H. K. 2004. Alcohol and cancer. *Alcohol and alcoholism,* 39, 155-165.

Purdue, M. P., Hashibe, M., Berthiller, J., La Vecchia, C., Dal Maso, L., Herrero, R., Franceschi, S., Castellsague, X., Wei, Q., Sturgis, E. M., Morgenstern, H., Zhang, Z. F., Levi, F., Talamini, R., Smith, E., Muscat, J., Lazarus, P., Schwartz, S. M., Chen, C., Neto, J. E., Wunsch-Filho, V., Zaridze, D., Koifman, S., Curado, M. P., Benhamou, S., Matos, E., Szeszenia-Dabrowska, N., Olshan, A. F., Lence, J., Menezes, A., Daudt, A. W., Mates, I. N., Pilarska, A., Fabianova, E., Rudnai, P., Winn, D., Ferro, G., Brennan, P., Boffetta, P. & Hayes, R. B. 2009. Type of alcoholic beverage and risk of head and neck cancer--a pooled analysis within the INHANCE Consortium. *American journal of epidemiology,* 169, 132-142.

Raman, C. V. 1928. A new type of secondary radiation. *Nature,* 121, 501-502.

Rawat, A. K. 1985. Nucleic acid and protein synthesis inhibition in developing brain by ethanol in the absence of hypothermia. *Neurobehavioral toxicology and teratology,* 7, 161-166.

Reddy, C. R., Prahlad, D. & Ramulu, C. 1975. Incidence of oral cancer with particular reference to hard palate cancer in 1 million population in the District of Visakhapatnam. *Indian journal of cancer,* 12, 72-76.

Ren, M. & Arnold, M. A. 2007. Comparison of multivariate calibration models for glucose, urea, and lactate from near-infrared and Raman spectra. *Analytical and bioanalytical chemistry,* 387, 879-888.

Riley, T., Sontag, E., Chen, P. & Levine, A. 2008. Transcriptional control of human p53-regulated genes. *Nature reviews. Molecular cell biology,* 9, 402-412.

Rudner, A. D. & Murray, A. W. 1996. The spindle assembly checkpoint. *Current opinion in cell biology,* 8, 773-780.

Ruggero, D. & Pandolfi, P. P. 2003. Does the ribosome translate cancer? *Nature reviews. Cancer,* 3, 179-192.

Sablina, A. A., Budanov, A. V., Ilyinskaya, G. V., Agapova, L. S., Kravchenko, J. E. & Chumakov, P. M. 2005. The antioxidant function of the p53 tumor suppressor. *Nature medicine,* 11, 1306-1313.

Sancar, A., Lindsey-Boltz, L. A., Unsal-Kacmaz, K. & Linn, S. 2004. Molecular mechanisms of mammalian DNA repair and the DNA damage checkpoints. *Annual review of biochemistry,* 73, 39-85.

Sarsour, E. H., Venkataraman, S., Kalen, A. L., Oberley, L. W. & Goswami, P. C. 2008. Manganese superoxide dismutase activity regulates transitions between quiescent and proliferative growth. *Aging cell,* 7, 405-417.

Schubert, J. M., Bird, B., Papamarkakis, K., Miljkovic, M., Bedrossian, K., Laver, N. & Diem, M. 2010. Spectral cytopathology of cervical samples: detecting cellular abnormalities in cytologically normal cells. *Laboratory investigation; a journd of technical methods and pathology,* 90, 1068-1077.

Sciubba, J. J. 1999. Improving detection of precancerous and cancerous oral lesions. Computer-assisted analysis of the oral brush biopsy. U.S. Collaborative OralCDx Study Group. *Journal of the American Dental Association,* 130, 1445-1457.

Semenza, G. L. 2004. Hydroxylation of HIF-1: oxygen sensing at the molecular level. *Physiology,* 19, 176-182.

Semenza, G. L. 2009. Regulation of cancer cell metabolism by hypoxia-inducible factor 1. *Seminars in cancer biology,* 19, 12-16.

Semenza, G. L. 2010. Defining the role of hypoxia-inducible factor 1 in cancer biology and therapeutics. *Oncogene,* 29, 625-634.

Serrano, M., Hannon, G. J. & Beach, D. 1993. A new regulatory motif in cell-cycle control causing specific inhibition of cyclin D/CDK4. *Nature,* 366, 704-707.

Shafer, W. G. & Waldron, C. A. 1961. A clinical and histopathologic study of oral leukoplakia. *Surgery, gynecology & obstetrics,* 112, 411-420.

Shah, J. P. & Gil, Z. 2009. Current concepts in management of oral cancer--surgery. *Oral oncology,* 45, 394-401.

Sigaud, S., Evelson, P. & Gonzalez-Flecha, B. 2005. H2O2-induced proliferation of primary alveolar epithelial cells is mediated by MAP kinases. *Antioxidants & redox signaling,* 7, 6-13.

Society, A. C. 2011. Annual Report. *CA: A Cancer Journal for Clinicians*, 321-322.

Socrates, G. 2004. Infrared and Raman Characteristic Group Frequences: Tables and Charts- 3rd edition. *John Wiley & Sons*, 328-335.

Speetjens, F. M., Kuppen, P. J., Welters, M. J., Essahsah, F., Voet Van Den Brink, A. M., Lantrua, M. G., Valentijn, A. R., Oostendorp, J., Fathers, L. M., Nijman, H. W., Drijfhout, J. W., Van De Velde, C. J., Melief, C. J. & Van Der Burg, S. H. 2009. Induction of p53-specific immunity by a p53 synthetic long peptide vaccine in patients treated for metastatic colorectal cancer. *Clinical cancer research : an official journal of the American Association for Cancer Research,* 15, 1086-1095.

Speetjens, F. M., Zeestraten, E. C., Kuppen, P. J., Melief, C. J. & Van Der Burg, S. H. 2011. Colorectal cancer vaccines in clinical trials. *Expert review of vaccines,* 10, 899-921.

Srivastava, S. P. & Sharma, S. C. 1968. Gingival cancer. *Indian journal of cancer,* 5, 89-97.

Stone, N., Kendall, C., Smith, J., Crow, P. & Barr, H. 2004. Raman spectroscopy for identification of epithelial cancers. *Faraday discussions,* 126, 141-157; discussion 169-183.

Sundaresan, M., Yu, Z. X., Ferrans, V. J., Irani, K. & Finkel, T. 1995. Requirement for generation of H2O2 for platelet-derived growth factor signal transduction. *Science,* 270, 296-299.

Tan, M., Li, S., Swaroop, M., Guan, K., Oberley, L. W. & Sun, Y. 1999. Transcriptional activation of the human glutathione peroxidase promoter by p53. *The Journal of biological chemistry,* 274, 12061-12066.

Tanimoto, K., Makino, Y., Pereira, T. & Poellinger, L. 2000. Mechanism of regulation of the hypoxia-inducible factor-1 alpha by the von Hippel-Lindau tumor suppressor protein. *The EMBO journal,* 19, 4298-4309.

Teh, S. K., Zheng, W., Ho, K. Y., Teh, M., Yeoh, K. G. & Huang, Z. 2008. Diagnostic potential of near-infrared Raman spectroscopy in the stomach: differentiating dysplasia from normal tissue. *British journal of cancer,* 98, 457-465.

Thomlinson, R. H. & Gray, L. H. 1955. The histological structure of some human lung cancers and the possible implications for radiotherapy. *British journal of cancer,* 9, 539-549.

Tollefson, M., Magera, J., Sebo, T., Cohen, J., Drauch, A., Maier, J. & Frank, I. 2010. Raman spectral imaging of prostate cancer: can Raman molecular imaging be used to augment standard histopathology? *BJU international,* 106, 484-488.

Trachootham, D., Zhou, Y., Zhang, H., Demizu, Y., Chen, Z., Pelicano, H., Chiao, P. J., Achanta, G., Arlinghaus, R. B., Liu, J. & Huang, P. 2006. Selective killing of oncogenically transformed cells through a ROS-mediated mechanism by beta-phenylethyl isothiocyanate. *Cancer cell,* 10, 241-252.

Tramacere, I., Negri, E., Bagnardi, V., Garavello, W., Rota, M., Scotti, L., Islami, F., Corrao, G., Boffetta, P. & La Vecchia, C. 2010. A meta-analysis of alcohol drinking and oral and pharyngeal cancers. Part 1: overall results and dose-risk relation. *Oral oncology,* 46, 497-503.

Turrens, J. F. 2003. Mitochondrial formation of reactive oxygen species. *The Journal of physiology,* 552, 335-344.

Valentine, J. A., Scott, J., West, C. R. & St Hill, C. A. 1985. A histological analysis of the early effects of alcohol and tobacco usage on human lingual epithelium. *Journal of oral pathology,* 14, 654-665.

Van Oijen, M. G. & Slootweg, P. J. 2000. Gain-of-function mutations in the tumor suppressor gene p53. *Clinical cancer research : an official journal of the American Association for Cancer Research,* 6, 2138-2145.

Vashisht, N., Ravikiran, A., Samatha, Y., Rao, P. C., Naik, R. & Vashisht, D. 2014. Chemiluminescence and Toluidine Blue as Diagnostic Tools for Detecting Early Stages of Oral Cancer: An *in vivo* Study. *Journal of clinical and diagnostic research : JCDR,* 8, ZC35-38.

Vaupel, P. & Mayer, A. 2007. Hypoxia in cancer: significance and impact on clinical outcome. *Cancer metastasis reviews,* 26, 225-239.

Verma, N. K., Dempsey, E., Conroy, J., Olwell, P., Mcelligott, A. M., Davies, A. M., Kelleher, D., Butini, S., Campiani, G., Williams, D. C., Zisterer, D. M., Lawler, M. & Volkov, Y. 2008. A new microtubule-targeting compound PBOX-15 inhibits T-cell migration via post-translational modifications of tubulin. *Journal of molecular medicine,* 86, 457-469.

Waldron, C. A. & Shafer, W. G. 1975. Leukoplakia revisited. A clinicopathologic study 3256 oral leukoplakias. *Cancer,* 36, 1386-1392.

Wang, A., Yoshimi, N., Ino, N., Tanaka, T. & Mori, H. 1997. Overexpression of cyclin B1 in human colorectal cancers. *Journal of cancer research and clinical oncology,* 123, 124-127.

Wang, G. L., Jiang, B. H., Rue, E. A. & Semenza, G. L. 1995. Hypoxia-inducible factor 1 is a basic-helix-loop-helix-PAS heterodimer regulated by cellular O2 tension. *Proceedings of the National Academy of Sciences of the United States of America,* 92, 5510-5514.

Wang, L., Mosel, A. J., Oakley, G. G. & Peng, A. 2012. Deficient DNA damage signaling leads to chemoresistance to cisplatin in oral cancer. *Molecular cancer therapeutics,* 11, 2401-2409.

Warburg, O. 1956. On the origin of cancer cells. *Science,* 123, 309-314.

Waris, G. & Ahsan, H. 2006. Reactive oxygen species: role in the development of cancer and various chronic conditions. *Journal of carcinogenesis,* 5, 14.

Weber, J. D., Taylor, L. J., Roussel, M. F., Sherr, C. J. & Bar-Sagi, D. 1999. Nucleolar Arf sequesters Mdm2 and activates p53. *Nature cell biology,* 1, 20-26.

Wheeler, R. 2006. Zephyris. Richardwheeler.net.

White, R. A., Neiman, J. M., Reddi, A., Han, G., Birlea, S., Mitra, D., Dionne, L., Fernandez, P., Murao, K., Bian, L., Keysar, S. B., Goldstein, N. B., Song, N., Bornstein, S., Han, Z., Lu, X., Wisell, J., Li, F., Song, J., Lu, S. L., Jimeno, A., Roop, D. R. & Wang, X. J. 2013. Epithelial stem cell mutations that promote squamous cell carcinoma metastasis. *The Journal of clinical investigation,* 123, 4390-4404.

Xue, L., Xu, F., Meng, L., Wei, S., Wang, J., Hao, P., Bian, Y., Zhang, Y. & Chen, Y. 2012. Acetylation-dependent regulation of mitochondrial ALDH2 activation by SIRT3 mediates acute ethanol-induced eNOS activation. *FEBS letters,* 586, 137-142.

Yang, M. H., Wu, M. Z., Chiou, S. H., Chen, P. M., Chang, S. Y., Liu, C. J., Teng, S. C. & Wu, K. J. 2008. Direct regulation of TWIST by HIF-1alpha promotes metastasis. *Nature cell biology,* 10, 295-305.

Yee, K. S. & Vousden, K. H. 2005. Complicating the complexity of p53. *Carcinogenesis,* 26, 1317-1322.

Yeligar, S. M., Machida, K. & Kalra, V. K. 2010. Ethanol-induced HO-1 and NQO1 are differentially regulated by HIF-1alpha and Nrf2 to attenuate inflammatory cytokine expression. *The Journal of biological chemistry,* 285, 35359-35373.

Yu, D. H., Waterland, R. A., Zhang, P., Schady, D., Chen, M. H., Guan, Y., Gadkari, M. & Shen, L. 2014. Targeted p16(Ink4a) epimutation causes tumorigenesis and reduces survival in mice. *The Journal of clinical investigation,* 124, 3708-3712.

Zhai, Y., Kronebusch, P. J., Simon, P. M. & Borisy, G. G. 1996. Microtubule dynamics at the G2/M transition: abrupt breakdown of cytoplasmic microtubules at nuclear envelope breakdown and implications for spindle morphogenesis. *The Journal of cell biology,* 135, 201-214.

Zhang, L., Zhou, X., Yao, X., Wu, Y. & Zhang, Q. 2012. Oral tongue cancer patients show a better overall survival than base of tongue cancer patients. *Journal of cancer research and clinical oncology,* 138, 341-346.

Zhou, J., Schmid, T., Schnitzer, S. & Brune, B. 2006. Tumor hypoxia and cancer progression. *Cancer letters,* 237, 10-21.

Zhou, L. L., Zhou, L. Y., Luo, K. Q. & Chang, D. C. 2005. Smac/DIABLO and cytochrome c are released from mitochondria through a similar mechanism during UV-induced apoptosis. *Apoptosis : an international journal on programmed cell death,* 10, 289-299.

Zink, D., Fischer, A. H. & Nickerson, J. A. 2004. Nuclear structure in cancer cells. *Nature reviews. Cancer,* 4, 677-687.

Zisterer, D. M., Campiani, G., Nacci, V. & Williams, D. C. 2000. Pyrrolo-1,5-benzoxazepines induce apoptosis in HL-60, Jurkat, and Hut-78 cells: a new class of apoptotic agents. *The Journal of pharmacology and experimental therapeutics,* 293, 48-59.

Zisterer, D. M., Mcgee, M. M., Campiani, G., Ramunno, A., Fattorusso, C., Nacci, V., Lawler, M. & Williams, D. C. 2001. Pyrrolo-1,5-benzoxazepines: a new class of apoptotic agents. *Biochemical Society transactions,* 29**,** 704-706.

Zygogianni, A. G., Kyrgias, G., Karakitsos, P., Psyrri, A., Kouvaris, J., Kelekis, N. & Kouloulias, V. 2011. Oral squamous cell cancer: early detection and the role of alcohol and smoking. *Head & neck oncology,* 3**,** 2.

9 Publications

Induction of apoptosis in oral squamous carcinoma cells by pyrrolo-1,5-benzoxazepines

KATE O'CALLAGHAN[1], ELEONORA PALAGANO[2], STEFANIA BUTINI[3], GIUSEPPE CAMPIANI[3], D. CLIVE WILLIAMS[2], DANIELA M ZISTERER[2], and JEFF O'SULLIVAN[1].

[1]School of Dental Science; [2]School of Biochemistry and Immunology, Trinity Biomedical Sciences Institute, Trinity College Dublin, Dublin 2, Ireland; [3]Dipartimento Farmaco Chimico Tecnologico, Universita di Siena; [4]European Research Centre for Drug Discovery and Development (NatSynDrugs), 53100 Siena, Italy.

DOI: 10.3892/mmr_xxxxxxxx

Abstract. Oral cancer (OC) is a largely asymptomatic disease, resulting in one of the highest mortality rates of any cancer. OC is currently ranked as the sixth most common cancer in the world, according to a recent World Health Organization analysis, and its prevalence is increasing, both in western and developing regions. Depending on the stage of OC, treatment strategies include surgery, radiation therapy and chemotherapy, or a combination thereof. As with numerous other types of cancer, resistance to conventional chemotherapeutic drugs is increasing in oral squamous cell carcinoma (OSCC). The present study aimed to investigate the use of a novel group of compounds, the pyrrolo-1,5-benzoxazepines (PBOXs), as a therapeutic alternative for the treatment of OC. PBOXs are microtubule-targeting agents that are able to induce apoptosis in numerous cancer cell types, thereby preventing tumour cell proliferation. Ca9.22 gingival and TR146 buccal cell lines were used as models for OSSC. Cell viability and proliferation in the presence of two PBOXs: PBOX-6 and PBOX-15, was monitored using an AlamarBlue™ assay. Flow cytometric analysis of propidium iodide-stained cells was used to determine the DNA content, and therefore the percentage of cells in each phase of the cell cycle. Microtubule disruption was determined by indirect immunofluorescence staining. Changes in protein expression and degradation were determined by western blotting. The results of the present study indicated that both PBOX-6 and -15 were able to induce apoptotic cell death by disrupting the microtubule network in both cell lines. The EC_{50} values were subsequently calculated for both PBOX-6 and -15, and PBOX-15 was shown to possess a higher potency. Both compounds displayed anti-proliferative effects mediated through sustained G_2/M arrest accompanied by tubulin disruption, and a decrease in DNA repair protein poly (ADP ribose) polymerase expression. These findings suggest that PBOXs may prove useful, either alone or in combination with other agents, in the treatment of chemotherapeutic resistant OSCC.

Correspondence to: Ms. Kate O'Callaghan, School of Dental Science, Trinity College Dublin, College Green, Dublin 2, Ireland
E-mail: ocallaka@tcd.ie

Key words: pyrrolo-1,5-benzoxazepines, microtubule-targeting agents, oral cancer

Introduction

Oral cancer (OC) is the sixth most common cancer worldwide and has one of the highest mortality rates, due to it being largely asymptomatic until the latter stages of the disease. Cancers of the oral cavity include cancers that occur in the tongue, floor of the mouth, buccal mucosa, alveolus, retromolar trigone, gingival, hard palate, and lips (1,2). A total of 90% of OCs are squamous cell carcinomas (SCC). SCC is caused by the presence of malignant cells in the epithelium. Oral SCC (OSCC) accounts for 2-3% of all malignancies, the prevalence of which ranges between 1-10 cases per 100,000 people in the majority of countries (3).

OSCC prognosis is poor, with a 5-year survival rate of ~50%, according to the National Cancer Research Institute. Treatments for OSCC are usually limited to a combination of chemotherapy and radiation, in order to reduce tumour size prior to the surgical removal of the tumour margins. Two of the most common chemotherapeutic agents used in the treatment of OSCC are cisplatin and 5-fluorouracil (4), and recurrent tumours are usually treated with one of these two chemotherapy drugs. However, resistance to these drugs may develop following treatment, as is the case in numerous types of cancer (5,6).

Pyrrolo-1,5-benzoxazepines (PBOXs) are a novel family of compounds that have been shown to induce cell cycle arrest and apoptosis in numerous cancer cell lines, including chemotherapy-resistant cell lines (7,8). In addition, PBOXs have been shown to induce cell apoptosis in *ex vivo* patient samples and in *in vivo* animal models of breast cancer and chronic myeloid leukaemia (8,9). Notably, PBOXs display minimal toxicity towards normal blood and bone marrow cells (10). A recently improved understanding regarding the molecular mechanisms underlying the apoptotic effects of PBOX compounds has allowed their development as antineoplastic therapeutic agents. Within the PBOX family, two members exhibit markedly elevated activity, PBOX-6 and PBOX-15 (Fig. 1) (8).

Mulligan *et al* (13) previously demonstrated that PBOX-induced apoptosis in cancer cells is preceded by a marked G_2/M phase cell cycle arrest, and that the cells displayed morphological features that suggested an inhibition of mitosis, notably in pro-metaphase. The effects of PBOXs on cell morphology are similar to those induced by two microtubule-targeting drugs, paclitaxel and nocodazole, which are polymerising and depolymerising agents, respectively. These results are concordant with previous studies that also demonstrated that anti-microtubule agents arrest the cell cycle in pro-metaphase (11,12).

Previous studies have suggested that PBOXs possess anti-microtubule activity. Through indirect immunofluorescence analysis, Mulligan *et al* (13) demonstrated that pro-apoptotic PBOX compounds result in depolymerisation of the microtubule network, and an inhibition of the assembly of purified tubulin *in vitro*. Tubulin has therefore been identified as the molecular target of the pro-apoptotic PBOX compounds (13).

In the present study the pro-apoptotic capabilities of two representative members of the PBOX family: PBOX-6 and PBOX-15, were examined in the following two OC cell lines: TR146 (buccal mucosa) and Ca9.22 (gingival carcinoma). The results of the present study demonstrated that these compounds were capable of inhibiting the proliferation of OSCC cells. This response was manifested by an initial G_2/M phase cell cycle arrest, followed by cellular apoptosis. These events coincided with a disruption of the microtubular network. Together, these results indicate that PBOX compounds may prove to be useful agents in the treatment of OSCC, and therefore merit further investigation, either alone, or in combination with other agents as potential treatments for OC.

Materials and Methods

Reagents. All reagents were obtained from Sigma-Aldrich (Arklow, Ireland) unless otherwise stated. The PBOX compounds, 7-[(N,N-dimethycarbomoyl) oxy]-6-(naphth-1-yl) pyrrolo[2,1-d][1,5]benzoxazepine (PBOX-6), and 4-acetoxy-5-(naphth-1-yl)naphtho[2,3-b] pyrrolo[2,1-d][1,4]oxazepine (PBOX-15), were synthesized as previously described (16). The PBOX compounds were subsequently dissolved in ethanol, and stored at -20°C. The antibodies used in the present study were as follows: Mouse anti-α-tubulin (EMD Millipore, Billerica, MA, USA); mouse anti-poly (ADP ribose) polymerase (PARP) (Merck Biosciences Ltd., Nottingham, UK); and mouse anti-β-actin (EMD Millipore).

Cell culture. Both cell lines were maintained in a 95% humidified atmosphere containing 5% CO_2 at 37°C, and all cell culture experiments were carried out under sterile conditions in a laminar flow hood. Cell growth and viability were visually monitored using a light microscope with 10 and 20x dry objectives. The TR146 cell line was initially derived from the neck node of a 67 year-old female (the primary tumour was located in the buccal mucosa) and was obtained from the Health Protection Agency Culture Collection (UK). The TR146 cells were maintained in Dulbecco's Modified Eagle's medium, supplemented with 10% v/v foetal bovine serum (FBS), 10 U/ml penicillin, 0.1 mg/ml streptomycin, and 2 mM glutamine. The Ca9.22 cell line was obtained from the Japanese Collection of Research Bioresources Cell Bank (Japan). The Ca9.22 cells were maintained in Minimum Essential medium, supplemented with 10% v/v FBS, 10 U penicillin, 0.1 mg/ml streptomycin, and 2 mM glutamine.

Cell proliferation. Cell proliferation was determined using AlamarBlue™ dye (Life Technologies, Grand Island, NY, USA), which allowed the visualisation of changes in compound fluorescence that occur as a consequence of the reduced number of viable, proliferating cells. The cells were seeded in 96-well plates for each of the time points with specified concentrations of PBOX-6 or PBOX-15, and were incubated at 37°C in 5% CO_2. A final concentration of 10% (v/v) AlamarBlue™ was added to the cells 4 h prior to the end of each time point. Fluorescence was measured at an excitation wavelength of 544 nm and at an emission wavelength of 590 nm, using a SpectraMax Gemini spectrofluorometric plate reader (Molecular Devices (UK) Ltd, Wokingham, UK). Cell viability was determined as a percentage of the vehicle-only cells. The experimental results were displayed as dose-response curves and half maximal effective concentration (EC_{50}) values, as determined using Prism GraphPad 5 (GraphPad Software, Inc., La Jolla, CA, USA).

Immunofluorescence. The cells were cultured for 24 h on 13 mm glass coverslips with the following seed densities: Ca9.22, $3x10^4$ cells/coverslip; and TR146, $4x10^4$ cells/coverslip. The cells were subsequently cultured in the presence of either PBOX-6 or PBOX-15 for a further 24 h. Following incubation, the cells were fixed with 4% paraformaldehyde in phosphate-buffered saline (PBS) for 15 min, permeabilised with 0.2% Triton in PBS for 10 min, rinsed with PBS, and blocked using 1% bovine serum albumin (BSA) in PBS containing Tween® 20 (PBST) for 30 min. The cells were then incubated with the following primary antibodies: Mouse anti-α-tubulin (1:1,000) in 1% BSA and PBST for 1 h, prior to incubation with secondary anti-mouse antibody 488 (Life Technologies) (1:500) in 1% BSA and PBST for 1 h. The coverslips were then placed on glass slides with 3.5 µl Vectashield™ mounting medium (Vector Labs, Burlingame, CA, USA) containing the nuclear counterstain 4,6-diamidino-2-phenylindole (DAPI), and stored in the dark at 4°C until imaging. The indirect fluorescence of the cells was examined using a standard filter set for DAPI and fluorescein isothiocyanate (blue/green), through 10 and 20x dry objectives, and a 60x oil objective using a Zeiss Axiovert/Axiocam CCD system, and imaged using AxioVision AxioVs40 software (Carl Zeiss Ltd., Cambridge, UK).

DNA content. The cellular DNA content was determined using of propidium iodide (PI), intercalated with fluorescent dye. The fluorescence intensity is proportional to the quantity of DNA present in the cell. Both cell lines were cultured in the presence of PBOX-6 or PBOX-15 at the desired concentrations and time points. The cells were then harvested by trypsinisation, prior to being centrifuged at 220 x g for 5 min, washed with PBS, and centrifuged once more. The supernatant was decanted and the cell pellets were resuspended in 200 µl PBS, prior to the addition of 2 ml ice-cold 70% ethanol in order to fix the cells. Following overnight fixation at 4°C, the cells were

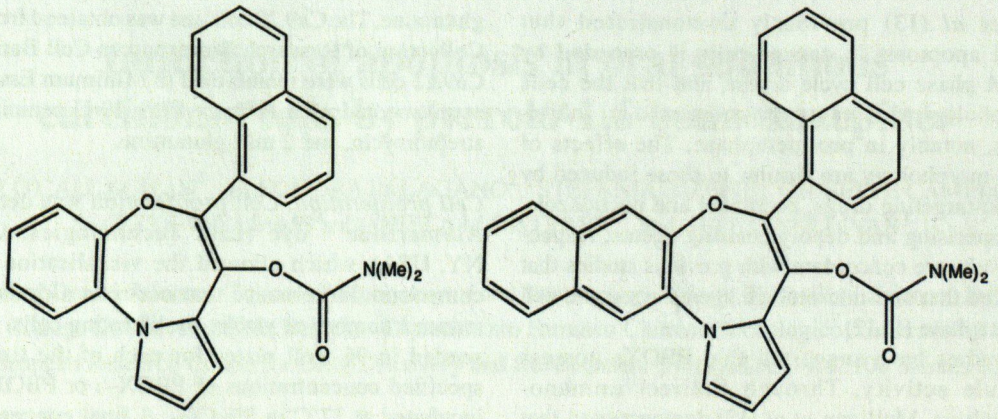


Figure 1. Chemical structures of pyrrolo-1,5-benzoxazepine (PBOX)-analogues PBOX-6 and PBOX-15.

centrifuged at 200 x g for 5 min in order to remove the ethanol, and the pellet was resuspended in 400 μl PBS, followed by 25 μl RNase A, and 75 μl PI. The cells were incubated in the dark at 37°C for 30 min. The samples were subsequently transferred to appropriately labeled fluorescence activated cell sorting (FACS) tubes, and were analysed using a FACSCalibur flow cytometer (BD Biosciences, Oxford, UK). The fluorescent signal was detected using a 630-22 nm band pass filter (FL2). The cell lines were gated in order to prevent cell debris and doublets from being counted. A total of >10,000 cells were counted and analysed using Treestar Flow Jo.

Analysis of protein expression by western blotting. The cells cultured in the presence of PBOX-6 or PBOX-15 for 24, 48, and 72 h, were harvested and centrifuged at 220 x g for 5 min, following which the supernatants were discarded and the cell pellets were resuspended in 2 ml ice-cold PBS. Following further centrifugation at 220 x g for 5 min, the supernatant was removed and the pellets were resuspended in 80 μl ice-cold lysis buffer (150 mM sodium chloride, 1.0% Triton X-100, 50 mM Tris; pH 8.0) containing Complete Protease Inhibitor Cocktail (Roche Diagnostics Ltd., Burgess Hill, UK). The samples were maintained under constant agitation at 1,000 rpm for 30 min at 4°C, prior to being centrifuged at 13,000 x g for 20 min at 4°C. The supernatants were aspirated and placed in an eppendorf tube on ice until further experimentation. The protein concentrations were determined using a bicinchoninic acid assay. The protein samples were separated by SDS-PAGE with an 8% resolving gel. The proteins were then transferred to a polyvinylidene difluoride (PVDF) membrane using a semi-dry blotter for 1 h. The PVDF membranes were subsequently blocked with 5% non-fat milk, and probed with the appropriate primary antibodies prior to being incubated with horseradish peroxidase-conjugated secondary antibodies. Protein expression was visualised through chemiluminescence.

Results

PBOX compounds reduce OC cell proliferation. The OSCC cell lines were treated for 72 h with PBOX-6 or PBOX-15 at various concentrations. Cell proliferation was subsequently measured using AlamarBlue™ assay. The results of the assay indicated that PBOX-6 and PBOX-15 reduced proliferation of both the Ca.922 and the TR146 cell lines in a dose-dependent manner (Fig. 2). PBOX-15 was the more potent of the two analogues. After 72 h, the EC_{50} values of PBOX-6 and PBOX-15 were 35±2.7 μM and 470±86 nM for the TR146 cells, and 2.6±1 μM and 83±32 nM for the Ca9.22 cells, respectively (Table I). The drug concentrations used for the remaining experiments were chosen according to the results of this cell proliferation assay.

PBOX compounds destabilise and depolymerise the microtubule network in OC cells. The Ca9.22 and TR146 cells were treated with either PBOX-6 or PBOX-15 for 24 h. In addition, the cells were also treated with the known tubulin polymeriser paclitaxel, and tubulin depolymeriser nocodazole, which served as positive controls. Immunofluorescent staining was used to detect morphological changes in the microtubule network, such as alterations in microtubule organisation and arrangement (Fig. 3). In the untreated TR146 (Fig. 3A) and Ca9.22 (Fig. 3B) cells, the microtubule network was organised as cytoplasmic tubulin filaments radiating from a central point to the periphery. The cells treated with vehicle alone (1% EtOH) also displayed this typical tubulin morphology. Exposure of the cells to the tubulin polymerising agent paclitaxel resulted in a highly concentrated accumulation of filaments in dense peripheral bundles, indicative of microtubule stabilisation. Conversely, exposure to the tubulin depolymerising agent nocodazole resulted in diffuse tubule staining with no definition of structure caused by microtubule disassembly. No alterations in microtubule structure were evident following treatment with a low dose of 100 nM PBOX-6 and PBOX-15, whereas higher doses of 10 μM PBOX-6 and 1 μM PBOX-15 resulted in a change in tubulin morphology resembling that induced by nocodazole. These results indicate that PBOX compounds destabilise the microtubule network in a similar manner to a depolymerising agent, in both TR146 and Ca9.22 cell lines.

In order to confirm the results of previous studies, namely that the disruption observed using a confocal microscope is

Table I. Half maximal effective concentration (EC_{50}) values obtained for each pyrrolo-1,5-benzoxazepine (PBOX) compound in the TR146 and Ca9.22 oral squamous cell carcinoma cell lines.

	EC_{50}		
Cell line	24 h	48 h	72 h
TR146			
PBOX-6	9.2±2.3 μM	8.1±0.3 μM	35±2.7μM
PBOX-15	480±92 nM	530±52 nM	470±86 nM
Ca9.22			
PBOX-6	4.5±1.5 μM	2.9±0.7 μM	2.6±1 μM
PBOX-15	210±28 nM	170±81 nM	83±32 nM

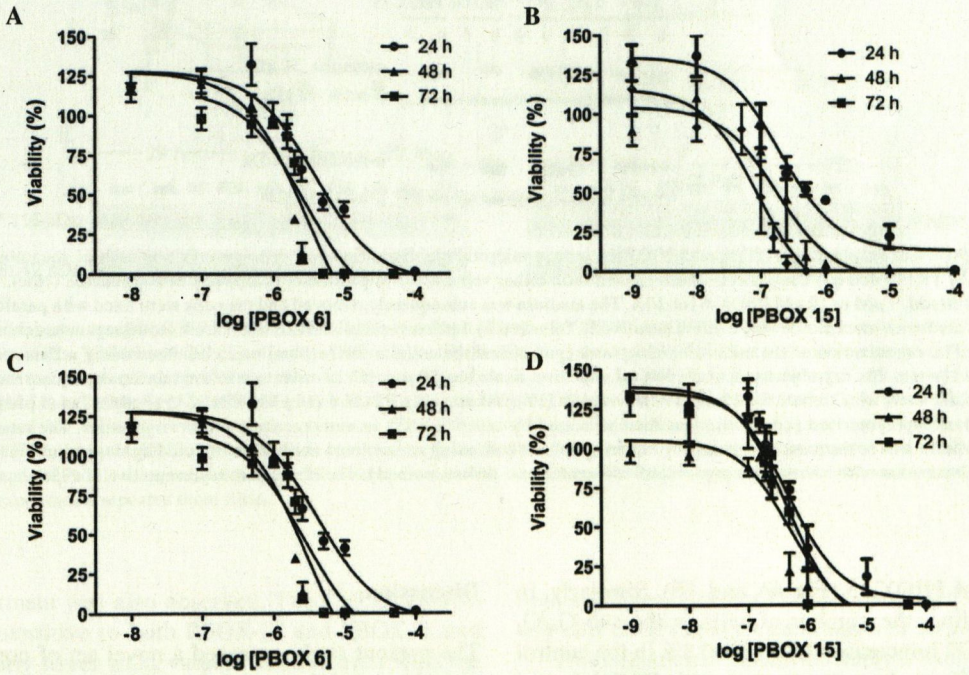


Figure 2. Pyrrolo-1,5-benzoxazepines (PBOX)-6 and PBOX-15 reduce the viability of oral squamous cell carcinoma (OSCC) cell lines. OSCC cell lines (A and B) TR146 and (C and D) Ca9.22 were treated with a range of (A and C) PBOX-6 and (B and D) PBOX-15 for 24, 48, and 72 h. AlamarBlue™ was added 4 h prior to endpoint reading. Fluorescence was measured using a Spectramax Gemini Plate reader at excitation and emission wavelengths of 544 nm and 590 nm, respectively. The values are presented as the mean ± standar error of the mean for three independent experiments.

the result of depolymerisation of the tubulin network, tubulin polymerisation assays were performed using western blotting (Fig. 3C). Following 4 h treatment with 10 μM PBOX-6 or 1 μM PBOX-15, tubulin was shown to be completely depolymerised in both cell lines. Following 4 h treatment with paclitaxel, tubulin was polymerised, whereas treatment with nocozadole resulted in unpolymerised tubulin. Treatment with the vehicle (1% EtOH) resulted in equal amounts of polymerised to unpolymerised tubulin. These results indicate that the disruption observed by confocal microscopy was indeed depolymerisation of the tubulin network.

PBOX compounds induce G_2/M arrest and apoptosis in OC cells. The DNA content of the PI-stained TR146 and Ca9.22 cells was measured using flow cytometric analysis, thus allowing the successful identification of cell cycle arrest or apoptosis. A decrease in the number of cells in the G_2/M phase of the cell cycle was observed in both cell lines following 8h treatment with PBOX-6 (10 μM) and PBOX-15 (1 μM) (Fig. 4C and 4D). A marked decrease was observed in the number of TR146 cells arrested in G_2/M phase following 72 h treatment, 15.4±1.07% and 12.6±1.87% for PBOX-6 and -15, respectively. A significant decrease also occurred in the number of Ca9.22 cells arrested in the G_2/M phase following 72 h of treatment, 22.23±0.95% and 16.6±1.25% for PBOX-6 and PBOX-15, respectively. This decline in the levels of G_2/M phase cells correlated with a marked increase in the number of apoptotic TR146 cells, with the levels of apoptosis rising to 4.4±1.210% in the control cells, 57.6±8.1% in the cells treated with 10 μM PBOX-6, and 39.1±6.6% in the cells

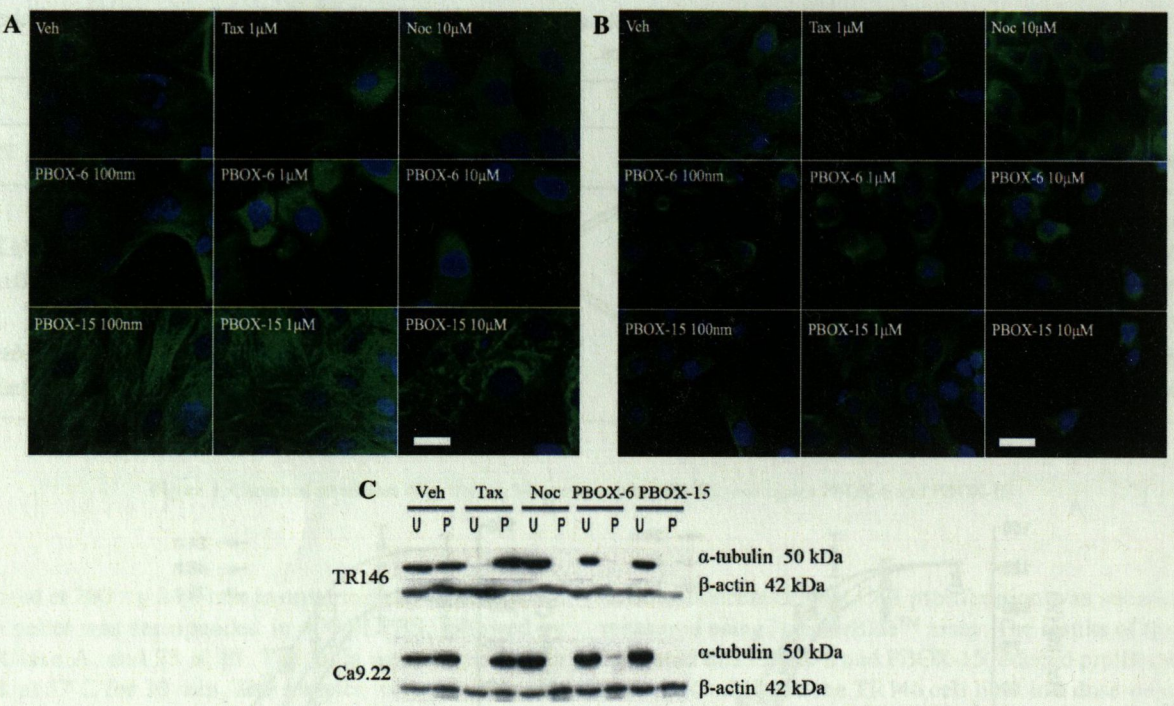


Figure 3. Pyrrolo-1,5-benzoxazepines (PBOX)-6 and PBOX-15 induce microtubule disruption and depolymerisation of oral squamous cell carcinoma (OSCC) cell lines. (A) TR146 and (B) Ca9.22 cells were treated with either vehicle, 1 μM paclitaxel (Tax), 10 μM nocodazole (Noc), 100 nM, 1 μM or 10 μM PBOX-15, or 100 nM, 1 μM or 10 μM PBOX-6 for 24 h. The medium was subsequently removed and the cells were fixed with paraformaldehyde. The cells were then incubated with monoclonal anti-α-tubulin antibody, followed by further incubation with fluorescein isothiocyanate-conjugated anti-mouse secondary antibody. The organization of the microtubule network (green) and the cellular DNA (blue) was visualized using a Zeiss Axiovert/Axiocam CCD system through 10x and 20x dry objectives, and a 60x oil objective. Scale bar, 20 μm. (C) In order to confirm tubulin depolymerisation in the TR146 and Ca9.22 cell lines, the cells were treated for 4 h with either vehicle (1% (v/v) ethanol), PBOX-6 (10 μM), PBOX-15 (1 μM), Tax (1 μM), or Noc (10 μM). The polymerised (P) or unpolymerised (U) tubulin was then separated by centrifugation in a microtubule-preserving buffer. The ratio of polymerised, vs. unpolymerised tubulin was subsequently assessed by western blot analysis using monoclonal antibodies directed against tubulin and loading control β-actin, followed by incubation with horseradish peroxidase-conjugated anti-mouse antibody. The images are representative of experiments repeated three times.

treated with 1μM PBOX-15 (Fig 4A and 4B). Similarly, in the Ca9.22 cell line, the number of cells in the sub-G_0/G_1 phase following 72 h increased to 2.120±0.8% in the control cells, 40.84±0.8% in the cells treated with PBOX-6, and 30.45±1.56% in the cells treated with PBOX-15.

PBOX compounds induce degradation of PARP in OC cell lines. In order to confirm that the cell death observed during flow cytometric analysis was indeed cellular apoptosis, PARP degradation, which is associated with controlled cell death, was assessed. Concordant with the DNA content analysis results, both PBOX-6 (10 μM) and PBOX-15 (1 μM) induced a decrease in the expression levels of full length PARP in Ca9.22 and TR146 cells following 72 h treatment (Fig. 4E and 4F). Treatment with the vehicle (1% (v/v) EtOH) did not affect PARP expression in either cell line. In the TR146 cell line, PARP degradation was observed following 24 h treatment with 1 μM PBOX-15, as compared with the vehicle control. PARP degradation was clearly observed in the TR146 cell line following 48 h treatment with both PBOX compounds. In addition, PARP degradation was also observed in the Ca9.22 cell line following 48 h treatment with both PBOX compounds. β-actin was used as a loading control in all experiments. These results indicate that the PBOX compounds induce apoptosis via tubulin disassembly.

Discussion

The present study assessed a novel set of compounds with regards to their potential therapeutic value in OC. PBOX-15 and PBOX-6 are potent pro-apoptotic members of the PBOX family, and have previously been shown to induce apoptosis in numerous human tumour cell lines, and to have anti-cancer properties in various cell culture systems, animal models, and clinical samples (9,14). In addition to inducing apoptosis in various cancer cell types, PBOX-6 and -15 possess the added benefit of inducing cytotoxicity in multi drug-resistant cancer cells (15).

The present study demonstrated that PBOX compounds were capable of reducing the proliferation of OC cell lines TR146 and Ca9.22, with EC_{50} values of 35±2.7 μM and 2.6±1 μM for PBOX-6, and 470±86 nM and 83±32 nM for PBOX-15. These values are within a range previously observed in other cancer cell lines exposed to PBOX compounds, including K562 chronic myeloid leukemia cells, A2780 ovarian carcinoma cells, and various cancerous mammary cells (7,14,16). PBOX-15, as previously reported, is the more potent of the two compounds, a result that was confirmed in the present study in both cell lines tested, as demonstrated by the order of magnitude of difference in the calculated EC_{50} values. Significant variation in the sensitivity of each cell type

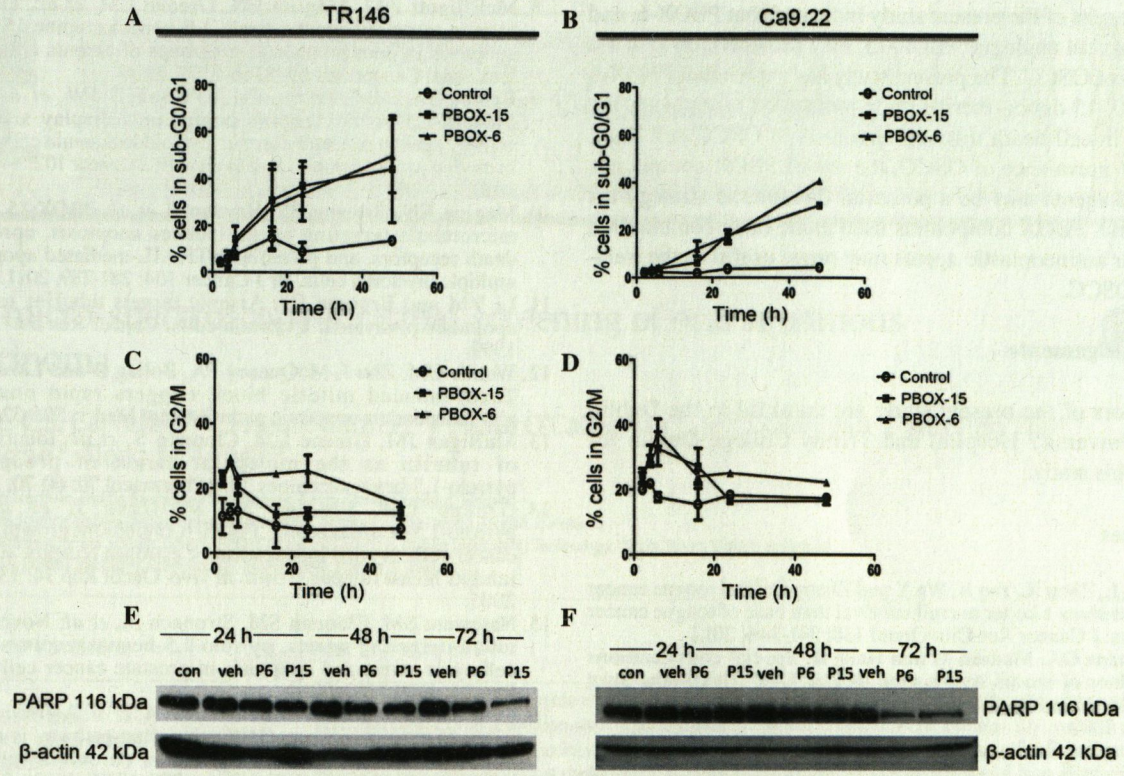


Figure 4. Pyrrolo-1,5-benzoxazepines (PBOX)-6 and PBOX-15 reduced proliferation of TR146 and Ca9.22 cells through induction of G_2/M cell cycle arrest and cellular apoptosis. The TR146 and Ca9.22 cells were treated with 10 μM PBOX-6, and 1 μM PBOX-15 at various time points for up to 72 h. The values are presented as the mean ± standard error of the mean for three independent experiments. (A and B) Cells in the sub-G_0/G_1 phase with <2N quantities of DNA were considered to be apoptotic, (C and D) whereas cells with 4N quantities of DNA were considered to be in the G_2/M phase of the cell cycle. PBOX-6 and PBOX-15 reduced full length poly (ADP ribose) polymerase (PARP) in Ca9.22 and TR146 cells. Both cell lines were treated with either vehicle (1% (v/v) EtOH), 10 μM PBOX-6, or 1 μM PBOX-15 for the indicated times. (E and F) PARP degradation was assessed by western blot analysis using monoclonal antibodies targeting PARP, or loading control β-actin, followed by horseradish peroxidase (HRP)-conjugated anti-mouse secondary antibodies. The blots are representative of experiments repeated three times.

to PBOX treatment was also observed. The Ca9.22 gingiva cell line was sensitive to both PBOX-15 and PBOX-6, and had significantly lower EC_{50} values, as compared with the TR146 buccal cell line. The observed variation in efficacy of the PBOXs in the two experimental cell lines suggests a phenotypic or genotypic factor may be involved. In OSCC, ~50% of cases are associated with a mutation in the p53 gene, which results in deleterious phenotypic manifestations and impaired p53 function. The Ca9.22 cells have a known p53 mutation (17), whereas the TR146 cells have no known p53 mutation. Previous studies have reported the influence of p53 in modifying drug efficacy and function in cancer cells (18).

The disassembly of the microtubule network in other cancer cell lines following treatment with PBOX-6 and PBOX-15 suggested that the compounds act as microtubule depolymerizing agents (13). To examine this hypothesis in OSCC, the Ca9.22 and TR146 cells were treated with various concentrations of PBOX-6 and PBOX-15. The results of the present study were concordant with previous studies, demonstrating that both PBOX compounds caused disassembly of tubulin following 24 h treatment *in vitro* (13). In the case of the control compounds, nocodazole depolymerised tubulin, whereas treatment with paclitaxel resulted in tubulin aggregation through polymerisation. PBOX-15, the more potent of the two compounds, was effective at disrupting tubulin at 1 μM in both cell lines, whereas PBOX-6-mediated depolymerisation was only observed at concentrations of 10 μM.

This inhibition of tubulin assembly is likely to be the cause of cell death following treatment with the PBOX compounds (13). Tubulin is a key protein in spindle formation during the cell cycle. A mechanism known as the spindle assembly checkpoint is activated during metaphase in the cell cycle (19). In the presence of tubulin breakdown and loss of spindle tension, the cell will not be able to continue into anaphase. In order to determine part of the mechanism underlying the response of OSCC cells to PBOX treatment, the effects of PBOX-6 and PBOX-15 on the cell cycle were examined. The PBOXs caused a time-dependent accumulation of cells in G_2/M phase, as early as 4 h in TR146 cells, and 8 h in Ca9.22 cells. This was followed by an increase in the number of cells in sub-G_0/G_1 phase, indicative of apoptosis and a concomitant decrease in the percentage of cells in G_2/M. To confirm the mechanism of cell death, degradation of the DNA repair enzyme PARP, which is indicative of apoptosis, was examined. A decrease in the expression levels of the full-length 116 kDa PARP was evident in both cell lines following treatment with both compounds after 72 h, suggesting PARP had been cleaved. The decrease in full-length PARP in the Ca9.22 cell line was more prominent than in the TR146 cell line, a result that was also confirmed by the EC_{50} values for both compounds.

The results of the present study indicated that PBOX-6, and its more potent analogue PBOX-15, may prove effective in the treatment of OSCC. The present study has shown that PBOX-6 and PBOX-15 depolymerise their molecular target, tubulin, resulting in cell death through apoptosis in OSCC cell lines. Given the prevalence of OSCC, the use of PBOX compounds as topical agents may be a potential therapeutic strategy for this disease. PBOX compounds used alone or in combination with other antineoplastic agents may prove useful in the treatment of OSCC.

Acknowledgements

The authors of the present study are thankful to the Dublin Dental University Hospital and Trinity College Dublin for funding this study.

References

1. Zhang L, Zhou X, Yao X, Wu Y and Zhang Q: Oral tongue cancer patients show a better overall survival than base of tongue cancer patients. J Cancer Res Clin Oncol 138: 341-346, 2012.
2. Arosarena OA, Madsen M and Haug R: Special considerations with floor of mouth and tongue cancer. Oral Maxillofac Surg Clin North Am 18: 521-531, 2006.
3. WHO: 2008.
4. Andreadis C, Vahtsevanos K, Sidiras T, Thomaidis I, Antoniadis K and Mouratidou D: 5-Fluorouracil and cisplatin in the treatment of advanced oral cancer. Oral Oncol 39: 380-385, 2003.
5. Galluzzi L, Senovilla L, Vitale I, *et al*: Molecular mechanisms of cisplatin resistance. Oncogene 31: 1869-1883, 2012.
6. Zhang N, Yin Y, Xu SJ and Chen WS: 5-Fluorouracil: Mechanisms of resistance and reversal strategies. Molecules 13: 1551-1569, 2008.
7. Nathwani SM, Butler S, Fayne D, *et al*: Novel microtubule-targeting agents, pyrrolo-1,5-benzoxazepines, induce apoptosis in multi-drug-resistant cancer cells. Cancer Chemother Pharmacol 66: 585-596, 2010.
8. McElligott AM, Maginn EN, Greene LM, *et al*: The novel tubulin-targeting agent pyrrolo-1,5-benzoxazepine-15 induces apoptosis in poor prognostic subgroups of chronic lymphocytic leukemia. Cancer Res 69: 8366-8375, 2009.
9. Bright SA, McElligott AM, O'Connell JW, *et al*: Novel pyrrolo-1,5-benzoxazepine compounds display significant activity against resistant chronic myeloid leukaemia cells *in vitro*, in *ex vivo* patient samples and *in vivo*. Br J Cancer 102: 1474-1482, 2010.
10. Maginn EN, Browne PV, Hayden P, *et al*: PBOX-15, a novel microtubule targeting agent, induces apoptosis, upregulates death receptors, and potentiates TRAIL-mediated apoptosis in multiple myeloma cells. Br J Cancer 104: 281-289, 2011.
11. Li YM and Broome JD: Arsenic targets tubulins to induce apoptosis in myeloid leukemia cells. Cancer Res 59: 776-780, 1999.
12. Woods CM, Zhu J, McQueney PA, Bollag D and Lazarides E: Taxol-induced mitotic block triggers rapid onset of a p53-independent apoptotic pathway. Mol Med 1: 506-526, 1995.
13. Mulligan JM, Greene LM, Cloonan S, *et al*: Identification of tubulin as the molecular target of proapoptotic pyrrolo-1,5-benzoxazepines. Mol Pharmacol 70: 60-70, 2006.
14. Greene LM, Fleeton M, Mulligan J, *et al*: The pyrrolo-1,5-benzoxazepine, PBOX-6, inhibits the growth of breast cancer cells *in vitro* independent of estrogen receptor status and inhibits breast tumour growth *in vivo*. Oncol Rep 14: 1357-1363, 2005.
15. Nathwani SM, Cloonan SM, Stronach M, *et al*: Novel microtubule-targeting agents, pyrrolo-1,5-benzoxazepines, induce cell cycle arrest and apoptosis in prostate cancer cells. Oncol Rep 24: 1499-1507, 2010.
16. Mc Gee MM, Campiani G, Ramunno A, *et al*: Activation of the c-Jun N-terminal kinase (JNK) signaling pathway is essential during PBOX-6-induced apoptosis in chronic myelogenous leukemia (CML) cells. J Biol Chem 277: 18383-18389, 2002.
17. Kaneda Y, Shimamoto H, Matsumura K, *et al*: Role of caspase 8 as a determinant in chemosensitivity of p53-mutated head and neck squamous cell carcinoma cell lines. J Med Dent Sci 53: 57-66, 2006.
18. Bunz F, Hwang PM, Torrance C, *et al*: Disruption of p53 in human cancer cells alters the responses to therapeutic agents. J Clin Invest 104: 263-269, 1999.
19. Rudner AD and Murray AW: The spindle assembly checkpoint. Curr Opin Cell Biol 8: 773-780, 1996.

Experimental and Molecular Pathology 98 (2015) 502–509

Contents lists available at ScienceDirect

Experimental and Molecular Pathology

journal homepage: www.elsevier.com/locate/yexmp

Raman micro-spectroscopy for rapid screening of oral squamous cell carcinoma

Luis Felipe C.S. Carvalho [a,*], Franck Bonnier [a,1], Kate O'Callaghan [b], Jeff O'Sullivan [b], Stephen Flint [b], Hugh J. Byrne [a], Fiona M. Lyng [c,d]

[a] FOCAS Research Institute, Dublin Institute of Technology, Kevin Street, Dublin 8, Ireland
[b] School of Dental Science, Dublin Dental University Hospital, Trinity College Dublin, Dublin 2, Ireland
[c] Radiation and Environmental Science Centre, FOCAS Research Institute, Dublin Institute of Technology, Kevin Street, Dublin 8, Ireland
[d] School of Physics, Dublin Institute of Technology, Kevin Street, Dublin 8, Ireland

ARTICLE INFO

Article history:
Received 8 December 2014
and in revised form 12 March 2015
Accepted 18 March 2015
Available online 21 March 2015

Keywords:
Raman micro-spectroscopy
Oral cancer
Oral dysplasia
Optical biopsy
Oral cell lines
Principal component analysis

ABSTRACT

Raman spectroscopy can provide a molecular-level fingerprint of the biochemical composition and structure of cells with excellent spatial resolution and could be useful to monitor changes in composition for dysplasia and early, non-invasive cancer diagnosis (carcinoma in situ), both ex-vivo and in vivo. In this study, we demonstrate this potential by collecting Raman spectra of the nucleoli, nuclei and cytoplasm from oral epithelial cancer (SCC-4) and dysplastic (pre-cancerous, DOK) cell lines and from normal oral epithelial primary cell cultures, in vitro, which were then analysed by principal component analysis (PCA) as a multivariate statistical method to discriminate the spectra. Results show significant discrimination between cancer and normal cell lines. Furthermore, the dysplastic and cancer cell lines could be discriminated based on the spectral profiles of the cytoplasmic regions. The principal component loading plot, which elucidates the biochemical features responsible for the discrimination, showed significant contributions of nucleic acid and proteins for nucleolar and nuclear sites and variation in features of lipids for the cytoplasmic area. This technique may provide a rapid screening method and have potential use in the diagnosis of dysplasia and early, non-invasive oral cancer, the treatment of which involves much less extensive and complex surgery and a reduction in associated co-morbidity for the patient.

© 2015 Elsevier Inc. All rights reserved.

1. Introduction

Oral cancer is one of the more common cancers worldwide, and in non-developed countries is next in prevalence to skin and breast cancers. Tumours are primarily located around the tongue, floor of the mouth, gingiva and buccal mucosa (Cabral et al., 2010; Kelly et al., 2014). Although clinical diagnosis of late stage, invasive oral cancer is relatively straightforward, the clinical challenge remains to detect early cancerous lesions, which are significantly harder to identify. Surgical treatment of early oral squamous cell carcinoma involves much less extensive and complex surgery and leads to a significant reduction in co-morbidity. Currently, the gold standard for diagnosis is histological analysis of tissue biopsies. However, numerous studies are being conducted in order to improve histopathological techniques with the ultimate goal to obtain a non-invasive, high throughput detection method for screening suspect cancer cells (Peer, 2014).

In this context, optically-based spectroscopic techniques are prominent among potential candidate non-invasive and rapid diagnostic methods. These methods are widely used as a tool for analysis of many biological tissues and the technique has been referred to as an "optical biopsy" (Carvalho et al., 2010; Evers et al., 2012; Kallaway et al., 2013; Nawaz et al., 2011) or "spectral cytopathology" (Schubert et al., 2010) because of its capacity to show features of underlying pathological tissues when compared with normal samples. Raman spectroscopy is one of the most popular techniques with demonstrated potential in studies examining different types of cancer, including lung cancer (Wang et al., 2014), neural cancer (Tanahashi et al., 2014), breast cancer (Damayanti et al., 2013; Marro et al., 2014) cervical cancer (Lyng et al., 2007), gastric cancer (Luo et al., 2013), skin cancer (Mittal et al., 2013) and head and neck cancer (Singh et al., 2012).

The power of the method is primarily related to the molecular and biochemical signature it provides of the biological sample when the fingerprint region is analysed. The Raman effect is a result of inelastic scattering of monochromatic electromagnetic radiation due to interaction with molecular vibrations, such that the frequency of the scattered radiation is different from the incident radiation (Raman and Krishnan,

* Corresponding author at: Laboratory of Biomedical Vibrational Spectroscopy, Institute of Research and Development, Universidade do Vale do Paraíba (UNIVAP), São José dos Campos, SP, Brazil.
E-mail address: luisfelipecarvalho@hotmail.com (L.F.C.S. Carvalho).
[1] Present address: Université François-Rabelais de Tours, Faculty of Pharmacy, EA 6295 Nanomédicaments et Nanosondes, 31 Avenue Monge, 37200 Tours, France.

http://dx.doi.org/10.1016/j.yexmp.2015.03.027
0014-4800/© 2015 Elsevier Inc. All rights reserved.

1928). The Raman spectrum of a given molecule consists of a series of peaks or bands, each corresponding to a characteristic vibrational mode of that molecule. Each molecule exhibits a characteristic spectrum, and thus the Raman spectrum can provide a "fingerprint" of a substance from which the molecular composition can be determined (Lyng et al., 2007; Nawaz et al., 2011). Changes in molecular composition due to the presence of disease are often subtle, requiring the use of multivariate statistical analysis (Byrne et al., 2014). In this way, Raman spectroscopy has been demonstrated to elucidate biochemical signatures not only from cancer studies but from other different pathological conditions in tissues and cells. Carvalho et al. (2010), using Raman spectroscopy to discriminate buccal inflammatory processes and normal tissues, revealed that the discrimination is possible using Soft Independent Modelling of Class Analogy (SIMCA) methods of analysis.

Although there are increased numbers of studies involving Raman spectroscopy as an optical biopsy method, as the technique is based on optical microscopy, it can also be extended to the analysis of cytological samples at a cellular and subcellular level (Bonnier et al., 2010b). Thus, interactions of, for example, anticancer agents and nanoparticles can be explored at a subcellular level (Dorney et al., 2012; Nawaz et al., 2011). Of clinical relevance, Raman spectroscopy has been explored for routine cytological screening for cervical cancer (Bonnier et al., 2014; Vargis et al., 2012). However, only a few studies have been published on oral squamous cell carcinoma and Raman microspectroscopy (Guze et al., 2011; Lasalvia et al., 2015; Su et al., 2012). The present study demonstrates the potential of Raman spectroscopy to provide and differentiate the biochemical signature from subcellular regions of oral cell lines, such as the cytoplasm, nucleus and nucleolus, in a label free manner. Also, we illustrate the potential of the technique to discriminate between cancer, pre-cancerous dysplastic cells and normal oral cell lines.

2. Materials and methods

2.1. Oral cell lines

To determine the efficacy of Raman spectroscopy in distinguishing between the cellular states observed during carcinogenic transformation, three different types of oral cell lines namely SCC-4 (malignant cell line), DOK (dysplastic cell line) and primary cells (normal oral epithelial cell line) were utilised. It is important to note that both pathological cell lines were originally from tongue, one of the sites of highest incidence of oral squamous cell carcinoma.

2.1.1. SCC-4 and DOK cell cultures

The SCC-4 and DOK (HPA cultures, UK) cell lines were cultured in Dulbecco Modified Eagle's Medium (DMEM) supplemented with 10% (v/v) FBS, penicillin/streptomycin (100 U/100 μg) and L-glutamine (2 mM). For the DOK cell line, hydrocortisone (5 μg/ml) was also added. The medium was pre-warmed at 37 °C before incubation of the cells. Cells were cultured until 90% confluency in a humidified environment at 5% CO_2, before being passaged. When confluent, the cells were washed in pre-warmed phosphate buffered saline (PBS) (0.01 M phosphate buffer, 0.154 M sodium chloride) and incubated with trypsin–EDTA (0.5% trypsin, 0.02% EDTA) for 5 min at 37 °C. Fresh, pre-warmed medium was added to deactivate trypsin, and the suspended cells were centrifuged at 250 *g* for 5 min. The supernatant was discarded and the cell pellet was resuspended in a sufficient volume of fresh pre-warmed medium, counted and passaged at a ratio of 1:3.

2.1.2. Primary cell culture

Human oral mucosa was recovered at the Dublin Dental University Hospital from patients undergoing routine third molar extraction in the Department of Oral and Maxillofacial Surgery. The sample was immediately placed into pre-warmed collection medium [DMEM, penicillin/streptomycin (100 U/100 μg), amphotericin B (2.5 μg/ml)] for 10 min before washing the tissue three times with pre-warmed 1× PBS and placing it in 0.17% trypsin overnight at 4 °C. The following day, the sample was washed with 1× PBS and the connective tissue was removed using a scalpel. The tissue was cut into small pieces (1 mm × 2 mm) and the small sections were placed in pre-treated T25 flasks (CELL+, Sarstedt), each with a small coating of keratinocyte growth medium (KGM). These were left to adhere to the flask for 1–2 h and the flask was subsequently flooded with KGM. Once sufficient growth of cells from tissue was achieved (2–3 weeks), KGM was replaced with Epilife medium (Invitrogen) to select for epithelial cell growth. Cells were passaged using 0.05% trypsin and spun at 250 *g* for 10 min at 4 °C and cultured to 90% confluency.

2.1.3. Sample preparation

To facilitate Raman spectroscopy measurements, cells were detached from the flasks using 0.025% trypsin–EDTA at 37 °C and pelleted at 250 *g* for 5 min at room temperature. The supernatant was removed and cells were counted and seeded at a density of 5×10^4 cells/calcium fluoride (CaF_2) disc in a multiwell plate and maintained, as previously described, until a monolayer of cells was stably growing on the disc. The cells were then fixed with 10% neutral buffered formaldehyde for 5 min, washed with 1× PBS and stored in 0.9% physiological saline solution prior to capture of the Raman spectrum.

2.2. Raman spectroscopy measurements

The study was conducted with a Horiba Jobin-Yvon LabRam HR800 instrument using a 532 nm laser as the source in a backscattering geometry, and a 300 lines/mm grating, providing a dispersion of ~1.5 cm^{-1} per pixel. The laser power was approximately 35 mW at the sample. Spectra were taken in the range from 600 cm^{-1} to 1800 cm^{-1} with a confocal hole diameter of 100 μm. A 100× water immersion objective (LUMPlanF1, Olympus, N.A.: 1.0) was used to focus the laser on the sample, immersed in distilled water, providing a spatial resolution of ~1 μm (Bonnier et al., 2010a, 2010b; Bonnier et al., 2012; Fullwood et al., 2014). Water immersion has been demonstrated to reduce any photothermal damage to the cells during measurement, and the signals were observed to be stable and reproducible (Bonnier et al., 2012). For each cell line, 20 cells were analysed. For each cell, three different subcellular regions were analysed, resulting in one spectrum for each subcellular region of each cell. Thus, for each cell line, 20 nucleolar, 20 nuclear and 20 cytoplasmic spectra were recorded, each for a period of 2 × 20 s.

2.3. Data preprocessing

Data preprocessing was performed using Matlab (Mathworks, USA). Before statistical analysis, a Savitsky–Golay filter (5th order, 7 points) was applied to smooth the spectra. As it has been demonstrated that, in water immersion, the background to the Raman spectrum is simply the spectrum of the overlying water (Bonnier et al., 2010a), and no background was subtracted. All spectra were (vector) normalized to remove point to point intensity variations and facilitate comparison of all spectra.

2.4. Data analysis

Principal component analysis (PCA) is a method of multivariate analysis broadly used with datasets of multiple dimensions (Varmuza, 2009; Laurikkala and Juhola, 2007; German et al., 2006). It allows the reduction of the number of variables in a multidimensional dataset, although it retains most of the variation within the dataset. The order of the principal components (PCs) denotes their importance to the dataset. PC1 describes the highest amount of variation, PC2 the second highest, and so on (Kelly et al., 2011; Martin et al., 2007). A PCA scatter plot groups similar datasets (spectra) according to the loadings of the PCs

and can be used to distinguish different datasets (samples). The loadings represent the variance for each variable (wavenumber) for a given PC. Analysing the loadings of a PC can give information about the source of the variability inside a dataset, in the case of spectroscopy, derived from variations in the molecular components contributing to the spectra.

PCA was employed in this study to highlight the variability existing in the spectral data set recorded for the different subcellular regions, and to differentiate the spectroscopic signatures of different cell lines.

3. Results and discussion

3.1. Single cell analysis (normal primary cell culture)

Analysis of the subcellular regions, nucleolus, nucleus and cytoplasm, from the primary cell culture (Fig. 1A), was completed and the different subcellular regions were compared using PCA analysis. Fig. 1B, C, D shows the average spectra for each subcellular region, the standard deviation being illustrated by the shaded region. Visually, it is possible to note the similarities, but few differences, between the average spectra of the nucleolus and nucleus. That of the cytoplasm is, however, clearly different. Notable differences, highlighted by the boxes in Fig. 1B, C and D, include the peak at ~700 cm^{-1} observed in the cytoplasm, the single peak around ~800 cm^{-1} observed in the nucleolus and nucleus, and also the profiles of the spectra between 1200 cm^{-1} and 1400 cm^{-1}. These features can be associated with specific chemical moieties, as indicated in Table 1, and their differing relative strengths are an indication of differing chemical composition of the subcellular region analysed. For example, the peak at ~720 cm^{-1} can be associated with lipidic components, which are relatively strong in the cytoplasm, while the peak at ~790 cm^{-1} is associated with nucleic acids, predictably relatively strong in the nucleus and nucleolus. The changes in the spectral region from 1200 to 1400 cm^{-1} are more complex and subtle, illustrating the need for more sophisticated multivariate data analysis techniques such as PCA (Bonnier and Byrne, 2012; Yasser et al., 2014).

Using PCA clustering, the nucleolus, nucleus and cytoplasm were clearly differentiated and spatially located. In confocal operation, the focal depth is ~1–2 μm, and thus it can be expected that while sampling the nucleus or nucleolus, the overlying plasmatic membrane and cytoplasm may contribute to the observed signal. Nevertheless, good discrimination of the respective subcellular regions is achievable. The nuclear (nucleolus and nucleus) regions and cytoplasm are effectively separated according to PC1 as shown in Fig. 2A. Similarly, it can be seen that the nucleolus and nucleus are differentiated according to PC3, although no significant differences in the average spectra are immediately obvious in Fig. 1B, C. No significant differentiation is observed according to PC2, and the loadings plot of this component is dominated by spectral features of water. A detailed analysis of the peaks of the

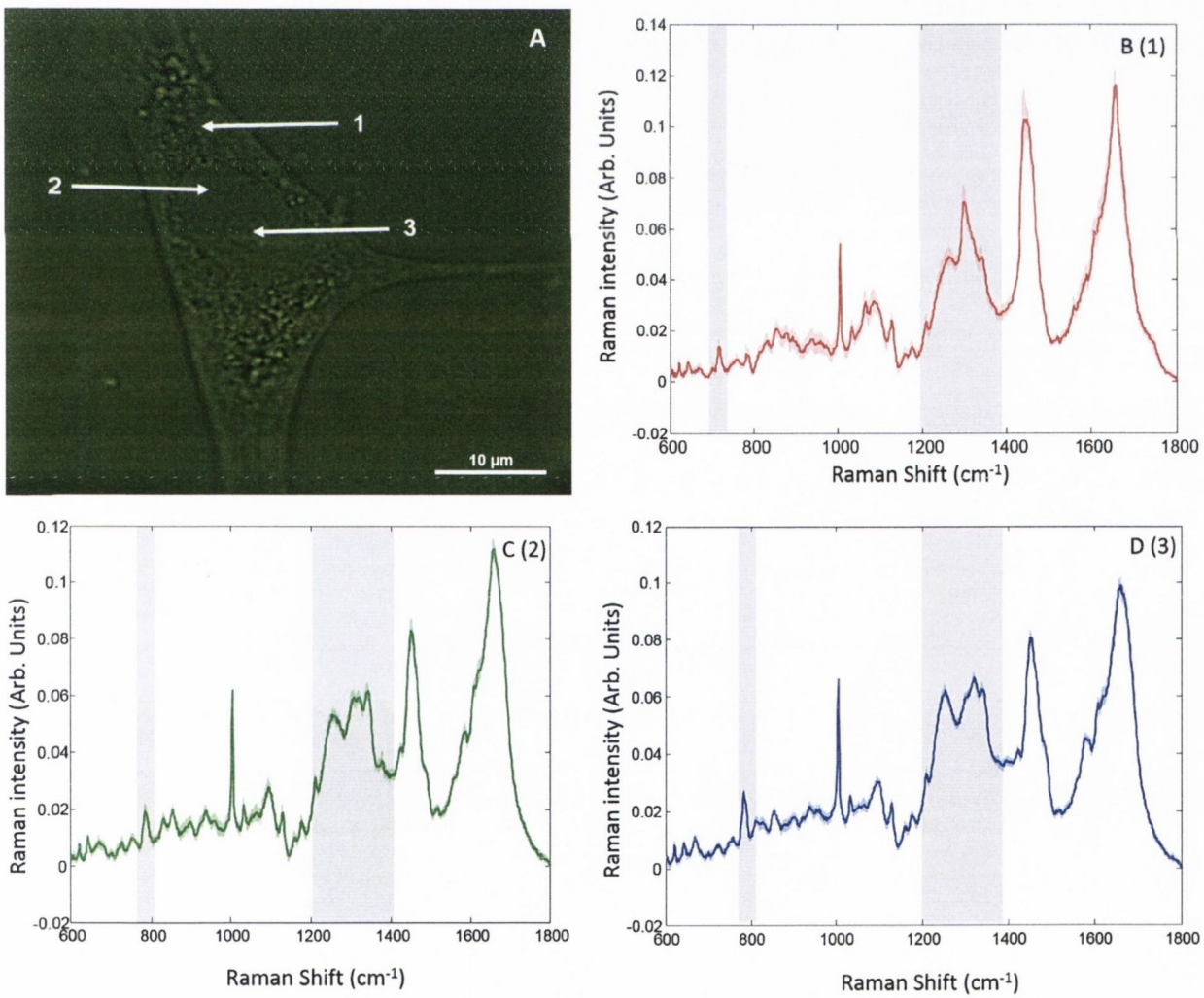


Fig. 1. A – Optical Micrograph of a primary cell cultured from human mucoperiosteal tissue. Mean Raman spectra from (B) Cytoplasm (C) Nucleus (D) Nucleolus of primary cell line with the standard deviation denoted by the shaded region.

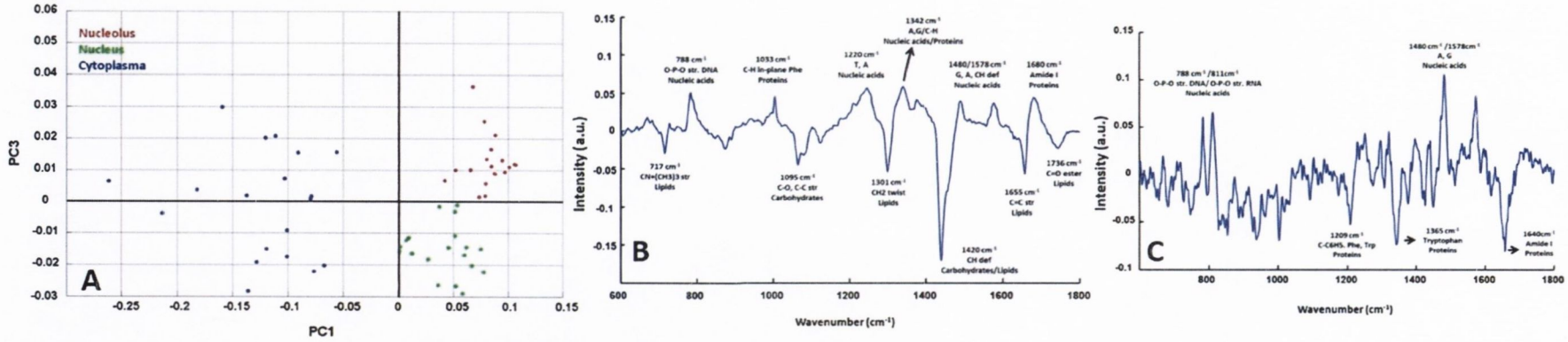


Fig. 2. A – PCA scatter plot of Raman spectra of primary cell line: nucleolus (red), nucleus (green) and cytoplasm (blue). B – Spectral loading of PC1, differentiating cytoplasm (negative) from the nucleus/nucleolus (positive) of primary cell line. C – Spectral loading of PC3, differentiating nucleus (negative) from the nucleolus (positive) of primary cell line. (For interpretation of the references to color in this figure legend, the reader is referred to the web version of this article.)

loadings of PC1 and PC3 shows that it was possible to separate the subcellular regions from each other based on their biochemical content, even though the nucleolus and nucleus are molecularly quite similar (Bonnier and Byrne, 2012).

The spectral loadings from PC1 and PC3 are respectively illustrated in Fig. 2B and C. With respect to PC1, the spectra from the nucleolus and nucleus are clustered on the right (positive values) and the spectra from the cytoplasm clustered on the left (negative values) of Fig. 2B. Thus, positive peaks in the loading of PC1 correspond to chemical species which are more abundant in the nucleolus and nucleus, and negative to species which are relatively more abundant in the cytoplasm (Notingher, 2007). Clearly, the main features associated with the nucleolus and nucleus are related to nucleic acids, and protein structural components, whereas the features associated with the cytoplasm are derived from lipids and carbohydrate components, which could be related to organelle membrane content.

With respect to PC3, the spectra from the nucleolus are clustered on the top right quadrant (positive values) and the spectra from the nucleus are clustered on the bottom right (negative values) of Fig. 2A. Thus, positive peaks in the loading of PC3 shown in Fig. 2C correspond to species which are more abundant in the nucleolus, and negative to species which are relatively more abundant in the nucleus (Notingher, 2007). Thus, the main features associated with the nucleolus are related to nucleic acids, whereas the features associated with the nucleus are related to protein structural components, indicating a higher density of these components in the respective subcellular regions (Table 1).

3.2. Squamous cell carcinoma vs dysplastic cells vs normal cells

In individual cell lines, Raman spectroscopy, coupled with multivariate statistical analysis, has thus been demonstrated to be a powerful tool to discriminate different subcellular regions based on their biochemical content. The technique can also be extended to differentiate between different cell lines, representing different oral pathologies.

A similar spectral screening was conducted for the three cell lines, SCC-4, DOK and primary mucosal epithelial cells and PCA was used for statistical analysis of the Raman spectroscopic data from the respective subcellular regions for each cell line. In all cases, PC1 was discarded, as it was dominated by water contributions and the analysis was therefore based on PC2, PC3 and PC4 in order to discriminate the cell lines according to each subcellular region. The variances explained by each PC for the respective cellular regions are tabulated in Table 2.

The peak at ~720 cm^{-1} can be associated with lipidic components, which are relatively strong in the cytoplasm, while the peak at ~790 cm^{-1} is associated with nucleic acids, predictably relatively strong in the nucleus and nucleolus. The changes in the spectral region from 1200 to 1400 cm^{-1} are more complex and subtle, illustrating the need for more sophisticated multivariate data analysis techniques such as PCA (Bonnier and Byrne, 2012; Yasser et al., 2014).

Table 2
Variances explained by each PC for the respective cellular regions.

PC/region	Nucleolus%	Nucleus%	Cytoplasm%
PC1 (water)	76.08	76.69	63.42
PC2	5.42	6.30	17.72
PC3	4.05	4.05	6.34

3.2.1. Nucleolus

The scatter plot of Fig. 3A shows the PCA of the Raman spectral data of the nucleolar regions of the three cell lines, comparing PC2 and PC3. Normal cells (blue) score predominantly negative with respect to PC2, while abnormal cells (SCC-4 (red) and DOK (green)), both score predominantly positive, giving a 90% discrimination according to PC2, calculated as the ratio of the number of spectra which are "correctly" clustered negatively, to those which are "incorrectly" clustered positively. The loading plot for this PC (Fig. 3B), therefore shows positive peaks corresponding to species which are more prominent in the spectra of nucleoli of abnormal cells, while the negative peaks are related to spectra of normal cells. As detailed below, the nucleolar region contains the main percentage of nucleic acids (Chen et al., 2014) compared to the other subcellular regions, so we can argue that, from a spectroscopic point of view, every peak related to vibrational modes of nucleic acids could be important as a biomarker for discrimination of the cell lines in the nucleolus region.

Positive features include bands at 788/811 cm^{-1}, related to O–P–O stretching of DNA and nucleic acids in general, 1420 cm^{-1} related to CH_2 deformation from lipids and carbohydrates, and 1680 cm^{-1}, related to amide I vibrational modes of proteins. Negative peaks include 1220 cm^{-1}, related to A (adenine), and T (thymine) vibrational modes from nucleic acids (Notingher, 2007).

3.2.2. Nucleus

Fig. 4A shows the PCA scatter plot for the Raman spectral data from the nuclear region of the three cell lines. In this case, there is little or no differentiation of the data according to PC2, but there is some degree of differentiation between the cell lines according to PC3, the normal cell lines being predominantly distributed on the negative axis, while the diseased SCC-4 and DOK data points are primarily distributed on the positive side, giving an 82.5% differentiation. The loading plot for this PC (Fig. 4B) shows positive peaks corresponding to biochemical species which are more abundant in the nucleus of abnormal cell lines, whereas the negative peaks were related to spectra from the normal primary cells. The subcellular region of the nucleus contains a large percentage of nucleic acids compared to the cytoplasm, although some changes to lipid content are observed. Thus, a combination of nucleic acid/lipid content has spectroscopic significance as a biomarker to discriminate the

Table 1
Band assignments of Raman peaks (Notingher, 2007).

Band (cm^{-1})/subcellular region	Nucleolus Vibrational mode/structural component	Nucleus Vibrational mode/structural component	Cytoplasm Vibrational mode/structural component
717			CN + $(CH_3)_3$ str. – lipids
729	A – nucleic acids		
760	Ring breath Try – proteins		
811–14	O–P–O str. RNA – nucleic acids		
937			C–C Bk str. α-helix – proteins
			C–O–C glycos. – carbohydrates
1065	PO_2^- str. – nucleic acids	PO_2^- str. – nucleic acids	Chain C–C str. – lipids
1301		CH_2 twist – lipids	CH_2 twist – lipids
1320–4	G–N ac./C–H – proteins		
1342		A, G–N ac./C–H – proteins	C–H def. – carbohydrates
1441	G, A, CH def – nucleic acids	G, A, CH def – nucleic acids	C–H def. – carbohydrates/lipids
1487			C–H def. – carbohydrates/lipids
1658		Amide I – proteins	

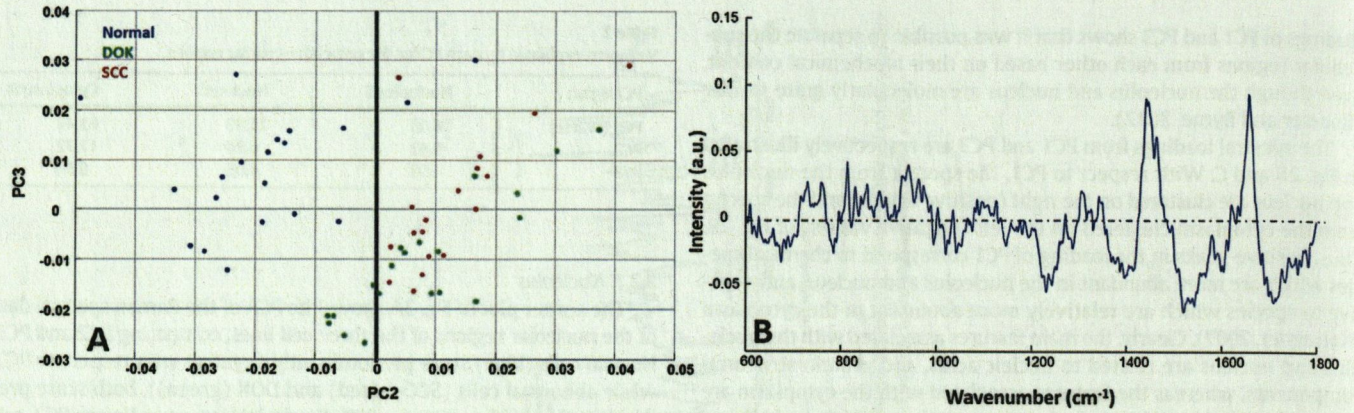


Fig. 3. A – PCA scatter plot differentiating the Raman spectra of the nucleoli of the primary (normal) cell line (blue), from those of the abnormal cell lines (SCC-4 (red) and DOK (green)). B – Spectral loading of PC2, differentiating the Raman spectra of the nucleoli of the primary (normal) cell line (negative), from those of the abnormal cell lines (positive). (For interpretation of the references to color in this figure legend, the reader is referred to the web version of this article.)

normal and abnormal cell lines in the nuclear region. In this case, little or no differentiation is observed between the two abnormal cell lines, however.

Positive features include mostly bands at 1065 cm^{-1}, related to PO_2^- of nucleic acids, and 1680 cm^{-1}, related to the Amide I vibrational modes from proteins (Chen et al., 2014). Negative peaks mostly include 788/811 cm^{-1}, related to O–P–O stretching of DNA and nucleic acids in general, 1301 cm^{-1} related to CH_2 twist of lipids and 1420 cm^{-1} related to CH_2 deformation from lipids and carbohydrates (Notingher, 2007).

3.2.3. Cytoplasm

The scatter plot of Fig. 5A shows PCA of the cytoplasmic regions of the three cell lines. Some degree of differentiation between the normal and abnormal cell lines according to PC3 is apparent giving 90% of discrimination. Similarly, PC2 differentiates between the spectra of the dysplastic and cancer cell lines giving 77.5% of discrimination (Fig. 5A).

Analysing PC3, the main features include positive bands at 788/811 cm^{-1}, related to O–P–O stretching of DNA, 1301 cm^{-1} related to CH_2 twist of lipids and 1420 cm^{-1} related to CH_2 deformation from lipids and carbohydrates. Negative peaks include 937 cm^{-1}, related to the C–C backbone stretch of the α-helix of proteins and the C–O–C vibrations of carbohydrates, and 1658 cm^{-1}, related to Amide I-proteins (Fig. 5B) (Notingher, 2007). The spectral profile of the cytoplasm subcellular region is dominated by vibrational modes from lipids and carbohydrates, which could be related to any physiologic subcellular transport and organelle membranes and both constituents could be important as biomarkers for discrimination of the cell lines in the cytoplasm region. Notably, the cytoplasm was the only subcellular region in which some discrimination between dysplastic and cancer cells was observed according to the loading plot of PC2 (Fig. 5B).

The analysis demonstrates that the technique may not only be utilised to differentiate normal and abnormal cells, but also dysplastic and cancer cells, based on cytoplasmic biomarkers. It is notable that the dysplastic and cancer cells are discriminated only based on cytoplasmic, rather than on nucleolar or nuclear biomarkers, suggesting that the cells are relatively similar in biochemical content in these regions and the pathological differences are largely manifest in the cytoplasmic regions. Further analysis is required to explore this further, however.

Notably, the cytoplasm was the only subcellular region in which some discrimination between dysplastic and cancer cells was observed according to the loading plot of PC2 (Fig. 5B). Positive features include mostly bands at 788 cm^{-1}, related to O–P–O stretching of DNA and nucleic acids in general, 1301 cm^{-1} related to CH_2 twist of lipids and 1420 cm^{-1} related to CH_2 deformation from lipids and carbohydrates. Negative peaks mostly include 937 cm^{-1}, related to C–C backbone stretching in α-helical proteins and C–O–C vibrations in glycosylated carbohydrates, 1220–1284 cm^{-1} related to =CH bend of lipids and 1640 cm^{-1} related to the Amide I band of proteins (Notingher, 2007).

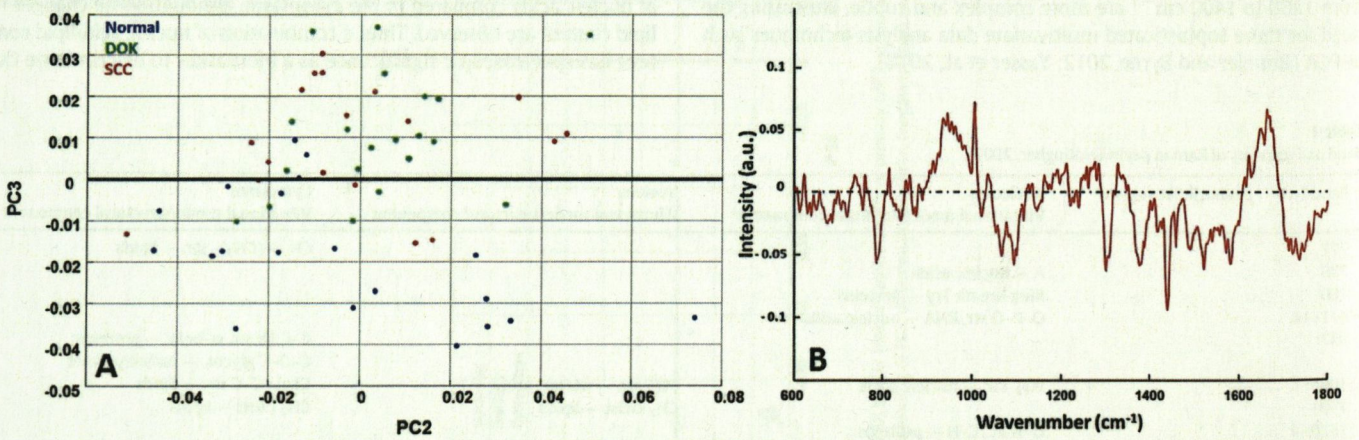


Fig. 4. A – PCA scatter plot differentiating the Raman spectra of the nuclei of the primary (normal) cell line (blue), from those of the abnormal cell lines (SCC-4 (red) and DOK (green)). B – Spectral loading of PC3, differentiating the Raman spectra of the nuclei of the primary (normal) cell line (negative), from those of the abnormal cell lines (positive). (For interpretation of the references to color in this figure legend, the reader is referred to the web version of this article.)

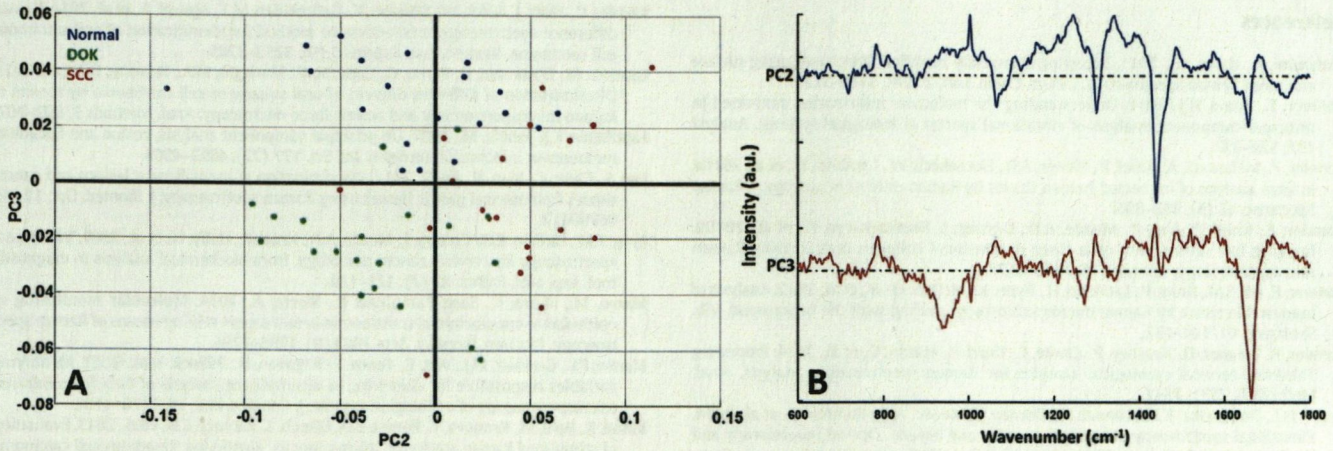


Fig. 5. A — PCA scatter plot differentiating the Raman spectra of the cytoplasm of the primary (normal) cell line (blue), from those of the abnormal cell lines (SCC-4 (red) and DOK (green)). B — Spectral loading of PC2 and PC3, differentiating the Raman spectra of the nuclei of the primary (normal) cell line (negative), from those of the abnormal cell lines (positive). (For interpretation of the references to color in this figure legend, the reader is referred to the web version of this article.)

Variations between the samples as reported here have a number of possible origins, both intrinsic and due to measurement conditions. As the measurements were performed in immersion geometry, and no explicit removal of it was carried out, the water spectrum emerges as one of the most significant principal components, in all measurements. In the case of the normal cells, the water contribution to the variance of the difference between the nucleus, nucleolus and cytoplasm, described by PC2, as the differences between the subcellular regions are dominantly those associated with the biochemical makeup and described by PC1 (~70% variance). In the case of the comparison of the same subcellular regions of different cells, slight variations in size and shape contribute significant variations in the contributions of the overlying water, represented by PC1 (~70% variances). This variance is larger than the more subtle differences in the biochemical makeup of the respective subcellular regions between the cell types. Cancer cells are continually undergoing transformation to enable survival, replication and metastasis and potentially changes observed in the Raman spectra may be a direct observation of some of these changes. These changes are driven through a number of cellular mechanisms and can manifest as posttranslational modification (chemical processes resulting in the cleavage or modification of proteins) e.g., glycosylation, phosphorylation, or epigenetic changes (heritable changes not due to changes in the DNA sequence) e.g., histone modification and DNA methylation. The sensitivity of the analysis used in this study is unlikely to identify such specific changes in cells, but both posttranslational modification and epigenetic changes have been observed utilising surface-enhanced Raman spectroscopy (Barhoumi and Halas, 2011; Sundararajan et al., 2006) and variation between the cell types used is potentially the result of an accumulation of these cellular changes (>75%). Notably, however, more sophisticated multivariate classification techniques can be applied to achieve higher degrees of sensitivity and specificity for real clinical applications (Knipfer et al., 2014; Lasalvia et al., 2015; Lyng et al., 2007).

4. Conclusion

It has been demonstrated that Raman micro-spectroscopy can differentiate each subcellular region (nucleolus, nucleus and cytoplasm), based on biomolecular content, revealing specific spectral biomarkers for each region. Although the spectral differences are subtle, the use of an unsupervised multivariate analytical method, PCA, allows a detailed, high content analysis of the spectral markers associated with the biochemical differences. The technique is completely label free, requires little sample preparation and is nondestructive.

Importantly, it was also possible to discriminate the pathological cell lines from the normal primary cells based on differences in the spectral profiles of either the nuclear (>90%) or nucleolar (>80%) regions of the respective cell lines. Interestingly, the dysplastic and cancer cells were only discriminated in the analysis of the cytoplasmic regions.

Although the study presented is a proof of concept, and more elaborate analysis of normal and dysplasia/cancer cytological samples from the same patients will be required to explore intra and inter patient variabilities, the model cells used in this study are well established oral cancer models and are representative of the stage of the disease described and are indicative of clinical samples. The inclusion of isolated primary cells which are of a normal phenotype is an acceptable comparator in this study. Further such studies of a range of clinical samples are planned.

Notably, as an optically-based microscopic technique, the Raman spectroscopic analysis is readily adaptable to clinical applications. The development of fibre optic Raman probes ultimately offers the promise of in vivo, optically-directed biopsy in extensive areas of leukoplakia and intraoperative applications in determining tumour resection margins. In the short term, existing microscope based Raman technologies might also be adopted for chair-side diagnosis based on exfoliated cytological samples which could yield a rapid outcome and a significant reduction in the number of false negatives/positives along with early cancer detection, as evidenced by the observed changes in established cancer and dysplastic lesions.

Conflict of interest statement

The authors declare that there are no conflicts of interest.

Acknowledgements

Luis Felipe CS Carvalho was funded by the Conselho Nacional de Desenvolvimento Científico e Tecnológico (CNPq — Brazil) for post doctoral research under Science Without Borders (237749/2012-2).

This research was supported in part by the Science Foundation Ireland (12/IP/1494) and the National Biophotonics and Imaging Platform (NBIP) Ireland funded under the Higher Education Authority PRTLI (Programme for Research in Third Level Institutions) Cycle 4, co-funded by the Irish Government and the European Union Structural Fund.

References

Barhoumi, A., Halas, N.J., 2011. Detecting chemically modified DNA bases using surface enhanced Raman spectroscopy. J. Phys. Chem. Lett. 2 (24), 3118–3123.

Bonnier, F., Byrne, H.J., 2012. Understanding the molecular information contained in principal component analysis of vibrational spectra of biological systems. Analyst 137, 322–332.

Bonnier, F., Mehmood, A., Knief, P., Meade, A.D., Hornebeck, W., Lambkin, H., et al., 2010a. In vitro analysis of immersed human tissues by Raman microspectroscopy. J. Raman Spectrosc. 42 (5), 888–896.

Bonnier, F., Knief, P., Lim, B., Meade, A.D., Dorney, J., Bhattacharya, K., et al., 2010b. Imaging live cells grown on a three dimensional collagen matrix using Raman microspectroscopy. Analyst 135, 3169–3177.

Bonnier, F., Ali, S.M., Knief, P., Lambkin, H., Flynn, K., McDonagh, V., et al., 2012. Analysis of human skin tissue by Raman microspectroscopy: dealing with the background. Vib. Spectrosc. 61, 124–132.

Bonnier, F., Traynor, D., Kearney, P., Clarke, C., Knief, P., Martin, C., et al., 2014. Processing ThinPrep cervical cytological samples for Raman spectroscopic analysis. Anal. Methods 6, 7831–7841.

Byrne, H.J., Ostrowska, K.M., Nawaz, H., Dorney, J., Meade, A.D., Bonnier, F., et al., 2014. Vibrational spectroscopy: disease diagnostics and beyond. Optical Spectroscopy and Computational Methods in Biology and Medicine. Challenges and Advances in Computational Chemistry and Physics 14, pp. 355–399.

Cabral, L., de Carvalho, L.F., Salgado, J., Brandão, A.A., Almeida, J.D., 2010. Gingival squamous cell carcinoma: a case report. J Oral Maxillofac. Res. 1 (3), e6 (1).

Carvalho, L.F., Bitar, R.A., Arisawa, E.A., Brandão, A.A., Honório, K.M., Cabral, L.A., et al., 2010. Spectral region optimization for Raman-based optical biopsy of inflammatory lesions. Photomed. Laser Surg. 28 (Suppl. 1), S111–S117.

Chen, Y., Dai, J., Zhou, X., Liu, Y., Zhang, W., Peng, G., 2014. Raman spectroscopy analysis of the biochemical characteristics of molecules associated with the malignant transformation of gastric mucosa. PLoS One 9 (4), e93906 (7).

Damayanti, N.P., Fang, Y., Parikh, M.R., Craig, A.P., Kirshner, J., Irudayaraj, J., 2013. Differentiation of cancer cells in two-dimensional and three-dimensional breast cancer models by Raman spectroscopy. J. Biomed. Opt. 18 (11), 117008.

Dorney, J., Bonnier, F., Garcia, A., Casey, A., Chambers, G., Byrne, H.J., 2012. Identifying and localizing intracellular nanoparticles using Raman spectroscopy. Analyst 137, 1111–1119.

Evers, D., Hendriks, B., Lucassen, G., Ruers, T., 2012. Optical spectroscopy: current advances and future applications in cancer diagnostics and therapy. Future Oncol. 8 (3), 307–320.

Fullwood, L.M., Griffiths, D., Ashton, K., Dawson, T., Lea, R.W., Davis, C., et al., 2014. Effect of substrate choice and tissue type on tissue preparation for spectral histopathology by Raman microspectroscopy. Analyst 139 (2), 446–454.

German, M.J., Hammiche, A., Ragavan, N., Tobin, M.J., Cooper, L.J., Matanhelia, S.S., et al., 2006. Infrared spectroscopy with multivariate analysis potentially facilitates the segregation of different types of prostate cell. Biophys. J. 90 (10), 3783–3795.

Guze, K., Short, M., Zeng, H., Lerman, M., Sonis, S., 2011. Comparison of molecular images as defined by Raman spectra between normal mucosa and squamous cell carcinoma in the oral cavity. J. Raman Spectrosc. 42 (6), 1232–1239.

Kallaway, C., Almond, L.M., Barr, H., Wood, J., Hutchings, J., Kendall, C., et al., 2013. Advances in the clinical application of Raman spectroscopy for cancer diagnostics. Photodiagnosis Photodyn. Ther. 10 (3), 207–219.

Kelly, J.G., Trevisan, J., Scott, A.D., Carmichael, P.L., Pollock, H.M., Martin-Hirsch, P.L., et al., 2011. Biospectroscopy to metabolically profile biomolecular structure: a multistage approach linking computational analysis with biomarkers. J. Proteome Res. 10 (4), 1437–1448.

Kelly, K., Johnson-Obaseki, S., Lumingu, J., Corsten, M., 2014. Oncologic, functional and surgical outcomes of primary transoral robotic surgery for early squamous cell cancer of the oropharynx: a systematic review. Oral Oncol. 50 (8), 696–703.

Knipfer, C., Motz, J., Adler, W., Brunner, K., Gebrekidan, M.T., Agaimi, A., et al., 2014. Raman difference spectroscopy: a non-invasive method for identification of oral squamous cell carcinoma. Biomed. Opt. Express 5 (9), 3252–3265.

Lasalvia, M., D'Antonio, P., Perna, G., Capozzi, V., Mariggiò, M.A., Perrone, D., et al., 2015. Discrimination of different degrees of oral squamous cell carcinoma by means of Raman microspectroscopy and atomic force microscopy. Anal. Methods 7, 699–707.

Laurikkala, K.J., Juhola, M., 2007. On principal component analysis, cosine and Euclidean measures in information retrieval. Inf. Sci. 177 (22), 4893–4905.

Luo, S., Chen, C., Mao, H., Jin, S., 2013. Discrimination of premalignant lesions and cancer tissues from normal gastric tissues using Raman spectroscopy. J. Biomed. Opt. 18 (6), 06700412.

Lyng, F.M., Faoláin, E.O., Conroy, J., Meade, A.D., Knief, P., Duffy, B., et al., 2007. Vibrational spectroscopy for cervical cancer pathology, from biochemical analysis to diagnostic tool. Exp. Mol. Pathol. 82 (2), 121–129.

Marro, M., Nieva, C., Sanz-Pamplona, R., Sierra, A., 2014. Molecular monitoring of epithelial-to-mesenchymal transition in breast cancer cells by means of Raman spectroscopy. Biochim. Biophys. Acta 1843 (9), 1785–1795.

Martin, F.L., German, M.J., Wit, E., Fearn, T., Ragavan, N., Pollock, H.M., 2007. Identifying variables responsible for clustering in discriminant analysis of data from infrared microspectroscopy of a biological sample. J. Comput. Biol. 14, 1176–1184.

Mittal, R., Balu, M., Krasieva, T., Potma, E.O., Elkeeb, L., Zachary, C.B., et al., 2013. Evaluation of stimulated Raman scattering microscopy for identifying squamous cell carcinoma in human skin. Lasers Surg. Med. 45 (8), 496–502.

Nawaz, H., Bonnier, F., Meade, A.D., Lyng, F.M., Byrne, H.J., 2011. Comparison of subcellular responses for the evaluation and prediction of the chemotherapeutic response to cisplatin in lung adenocarcinoma using Raman spectroscopy. Analyst 136 (12), 2450–2463.

Notingher, I., 2007. Raman biospectroscopy cell based biosensors. Sensors 7, 1343–1358.

Peer, D., 2014. Precision medicine – delivering the goods? Cancer Lett. 352 (1), 2–3.

Raman, C.V., Krishnan, K.S., 1928. A new type of secondary radiation. Nature 121, 501–502.

Schubert, J.A., Bird, B., Papamarkakis, K., Miljković, M., Bedrossian, K., Laver, N., et al., 2010. Spectral cytopathology of cervical samples: detecting cellular abnormalities in cytologically normal cells. Lab. Investig. 90 (7), 1068–1077.

Singh, S.P., Deshmukh, A., Chaturvedi, P., Krishna, C.M., 2012. Raman spectroscopy in head and neck cancers: toward oncological applications. J. Cancer Res. Ther. 8 (6), 126–132.

Su, L., Sun, Y.F., Chen, Y., Chen, P., Shen, A.G., Wang, X.H., et al., 2012. Raman spectral properties of squamous cell carcinoma of oral tissues and cells. Laser Phys. 22 (1), 311–316.

Sundararajan, N., Mao, D., Chan, S., Koo, T.W., Su, X., Sun, L., et al., 2006. Ultrasensitive detection and characterization of posttranslational modifications using surface-enhanced Raman spectroscopy. Anal. Chem. 78 (11), 3543–3550.

Tanahashi, K., Natsume, A., Ohka, F., Momota, H., Kato, A., Motomura, K., et al., 2014. Assessment of tumor cells in a mouse model of diffuse infiltrative glioma by Raman spectroscopy. BioMed Res. Int. 860241.

Vargis, E., Tang, Y.W., Khabele, D., Mahadevan-Jansen, A., 2012. Near-infrared Raman microspectroscopy detects high-risk human papillomaviruses. Transl. Oncol. 5 (3), 172–179.

Varmuza, K., 2009. In: Taylor & Francis Group (Ed.), Introduction to Multivariate Statistical Analysis in Chemometrics. CRC Press, New York, pp. 59–102.

Wang, L., Zhang, Z., Huang, L., Li, W., Lu, Q., Wen, M., et al., 2014. Evaluation of Raman spectroscopy for diagnosing EGFR mutation status in lung adenocarcinoma. Analyst 139 (2), 455–463.

Yasser, M., Shaikh, R., Chilakapati, M.K., Teni, T., 2014. Raman spectroscopic study of radioresistant oral cancer sublines established by fractionated ionizing radiation. PLoS One 9 (5), e97777 (19).

10 Appendix 1

10.1 Ethics approval

THE UNIVERSITY OF DUBLIN

TRINITY COLLEGE **FACULTY OF HEALTH SCIENCES**

Trinity College, Dublin 2, Ireland

Chair Faculty Research Ethics Committee
Professor Orla Sheils MA (Dub)
MA Med Law and Ethics (Lond)
PhD FAMLS FRCPath FTCD

Tel: +353 1 896 2893
Fax: +353 1 671 3956
Email: doylej12@tcd.ie

Secretary to Faculty Research Ethics Committee
Ms Janet Doyle

Mr. Jeffrey O'Sullivan
School of Dental Science,
Dublin Dental University Hospital,
TCD
Dublin 2

19th September, 2011

Study: A role for Ethanol in oral Carcinogensis

Dear Applicant (s),

Further to a meeting of the Faculty of Health Sciences Ethics Committee held in June 2011, we are pleased to inform you that the above project has been approved without further audit.

Yours sincerely

_____

Prof. Orla Sheils
Chairperson
Faculty Research Ethics Committee

Other Applicants:

Prof. Stephen Flint
Ms Kate O'Callaghan
Dr Mary Clarke
Ms Rose Glacken
Dr. Gavin Davey

10.2 Patient Consent Form

Project Title: "A role for ethanol in oral carcinogensis"

Principal Investigators:

Dr Jeff O'Sullivan
Prof. Stephen Flint
Dr Mary Clarke

BACKGROUND: This project will investigate the relationship between the consumption of alcohol and damage to the oral mucosal tissues. This will aid in our understanding of the effects of alcohol in oral conditions such as leukoplakia and the development of oral cancer. To facilitate this study we ask permission to recover a piece of tissue, which maybe removed during your extraction and would be normally discarded. Cells will be isolated from a small piece of the recovered tissue, these cells will be grown in the presence of alcohol and changes in the levels of inflammatory proteins will be monitored to establish if the alcohol has any effect on normal cell growth. The benefit of the study will be better understanding of the nature of the disease and possible improvement of the treatment approaches to this disease, with an aim of cancer prevention.

Your data will be anonymised, confidential and securely stored.

DECLARATION:
I have read, or had read to me, this consent form. I have had the opportunity to ask questions and all my questions have been answered to my satisfaction. I freely and voluntarily agree to be part of this research study, though without prejudice to my legal and ethical rights. I understand I may withdraw from the study at any time. I have received a copy of this agreement.

Patient's Name

Contact Details

Participant's Signature: **Date:**

The Researcher:

I have explained the nature and purpose of this research study, the procedures to be undertaken and any risks that may be involved. I have offered to answer any questions and fully answered such questions. I believe that the participant understands my explanation and has freely given informed consent.

Investigator's Signature: **Date:**

10.3 Patient Information Sheet

Names of researchers:
Dr Jeff O'Sullivan
Prof. Stephen Flint
Dr Mary Clarke

Working title of study:
"A role for ethanol in oral carcinogensis"

Introduction
Leukoplakia is a white lesion of the mouth with the potential to turn cancerous. The diagnosis of leukoplakia is made by taking a biopsy (sample) of the tissue and looking at it under a microscope. We cannot predict with any certainty which leukoplakias will become cancers. However, we do know that some leukoplakias present with substantial inflammation. Common alcohol can cause a temporary inflammatory response in tissues, which are exposed to it. What is also not obvious is whether the present of alcohol can causes the progression of leukoplakia and if it is responsible for the observed inflammation.

Description of study
• Aims and objectives of study
1) Determine the normal pattern of oral tissue growth/inflammation and respiration
2) We then propose to grow normal healthy cells derived from your tissue sample to determine the interaction between alcohol and normal (tissue) cells by culturing both together and monitoring the production of inflammatory proteins.
3) We also propose to investigate if several potential compounds can alleviate the onset of inflammation and/or carcinogenesis.

Contribution required from participant
The study involves recovering a piece of tissue, which maybe routinely removed (as part of your extraction) and would be normally discarded after treatment. We are asking your permission to use a small piece of the recovered specimen for our investigations outlined in 1), 2) and 3) above.

Possible benefits of the study.
The possible benefits of the study will be better understanding of the nature of the effect alcohol consumption can have on the rate of oral cancer development, with an aim of cancer prevention or early detection.

Possible risks to participants and after effects
There are no more risks than if you were **not** in the study, since this tissue is routinely removed and discarded as part of your procedure. You are at no more risk of the normal side effects or complications of any extraction, namely: post-operative bleeding, swelling, pain and infection. We aim to prevent these through postoperative instructions, ensuring an atraumatic technique, pain killers and post-operative antiseptic mouthrinses.

Location of research.
Dublin Dental University Hospital

What will happen to the results of the study
This project is part of PhD degree and the results of the study will be published in a scientific journal, with due consideration of confidentiality.

Confidentiality of information
Your identity will remain entirely confidential. Your name will not be published and will not be disclosed to anyone outside the study group. Your data and sample will be coded and anonymised.
The data will be stored securely at Dublin Dental School & Hospital in the data information system and protected by the use of security software. The DDSH has its own server, security and secure access systems. The anonymised samples will be kept for five years and then destroyed

Voluntary participation
You are **NOT obliged** to take part.

Permission
Ethical approval from Faculty Research Ethics Group - Faculty of Health Sciences, TCD.

Further information and how to take part
The procedures will be explained to you and an informed consent form must be signed by you if you agree to take part in this study. The research will be conducted in Dublin Dental School & Hospital.

Contact details of researchers
Dr. Jeff O'Sullivan
Prof. Stephen Flint
Dr. Mary Clarke
Dublin Dental University Hospital
Lincoln Place, Dublin 2
Tel: 01 6127200. Email: jeff.osullivan@dental.tcd.ie.
This study is covered by standard institutional indemnity insurance.
Nothing in this document restricts or curtails your rights

11 Appendix 2

11.1 DIT Matlab script

SCCx DOKx NC nucleolus

Figures are generated at several steps along the script ('figure') producing the loading plots and scatterplots observed in Chapters 4 and 5. Colours are given to the specific plots. 'r' =red, 'g'=green.

```
%%%%%loading of the files%%%%

readfiles_pk

Nucleolus_SCC_FA = ans(:,2:end)

readfiles_pk

Nucleolus_DOK_FA = ans(:,2:end)

readfiles_pk

Nucleolus_NC_FA = ans(:,2:end)


wavenumbers = ans(:,1)

figure
hold on
plot(wavenumbers,Nucleolus_SCC_FA,'r')
plot(wavenumbers,Nucleolus_DOK_FA,'g')


k=5;
w=13;


Nucleolus_SCC_FA_S = sgolayfilt(Nucleolus_SCC_FA(:,:),k,w);
Nucleolus_DOK_FA_S = sgolayfilt(Nucleolus_DOK_FA(:,:),k,w);


figure
hold on
plot(wavenumbers,Nucleolus_DOK_FA_S,'r')
plot(wavenumbers,Nucleolus_SCC_FA_S,'g')



mean_Nucleolus_NC_FA_S = mean(Nucleolus_NC_FA_S(:,:),2)
mean_Nucleolus_SCC_FA_S = mean(Nucleolus_SCC_FA_S(:,:),2)
mean_Nucleolus_DOK_FA_S = mean(Nucleolus_DOK_FA_S(:,:),2)

figure
hold on
plot(wavenumbers,mean_Nucleolus_SCC_FA_S,'r')
plot(wavenumbers,mean_Nucleolus_DOK_FA_S,'g')




%%%%%%%%%%% baseline correction %%%%%%%%%%%%%
```

```
Nucleolus_SCC_FA_B1 =  mrubberbandp_pk(wavenumbers,Nucleolus_SCC_FA_S',0);
Nucleolus_SCC_FA_B2 = flipdim(Nucleolus_SCC_FA_B1,2)
Nucleolus_SCC_FA_BN = normaliz(Nucleolus_SCC_FA_B2)

Nucleolus_DOK_FA_B1 =  mrubberbandp_pk(wavenumbers,Nucleolus_DOK_FA_S',0);
Nucleolus_DOK_FA_B2 = flipdim(Nucleolus_DOK_FA_B1,2)
Nucleolus_DOK_FA_BN = normaliz(Nucleolus_DOK_FA_B2)

figure
hold on
plot(wavenumbers,Nucleolus_SCC_FA_BN,'r')
plot(wavenumbers,Nucleolus_DOK_FA_BN,'g')


mean_Nucleolus_NC_FA_BN = mean(Nucleolus_NC_FA_BN(:,:),1)
figure
plot(wavenumbers,mean_Nucleolus_NC_FA_BN)

mean_Nucleolus_SCC_FA_BN = mean(Nucleolus_SCC_FA_BN(:,:),1)
figure
plot(wavenumbers,mean_Nucleolus_SCC_FA_BN)

mean_Nucleolus_DOK_FA_BN = mean(Nucleolus_DOK_FA_BN(:,:),1)
figure
plot(wavenumbers,mean_Nucleolus_SCC_FA_BN)


figure
hold on
plot(wavenumbers,mean_Nucleolus_SCC_FA_BN,'r')
plot(wavenumbers,mean_Nucleolus_DOK_FA_BN,'g')



figure
hold on
plot(Nucleolus_SCC_FA_BN','g')


clear end_spectrum;

axes = wavenumbers

j  = 1;

k = 1;

for i = 1:size(Nucleolus_SCC_FA_BN)

clear new_values;

current_spectrum = Nucleolus_SCC_FA_BN(i,:);
```

```
[max_int,max_ind] = max(current_spectrum(600:615));
y_correct = 599+max_ind;


%right shifted spectrum
if axes(y_correct) <  1005
diff_pos= axes(y_correct) -  1005 ;
%remove y number of elements from end of spectrum and add y elements with same value as↙
first element element
corrected_spectrum = current_spectrum;
first_value  = current_spectrum(1);
corrected_spectrum(end-abs(diff_pos)+1:end) = [];
new_values(1:abs(diff_pos)) = first_value;
corrected_spectrum = single(corrected_spectrum)
end_spectrum(j,:) = [new_values corrected_spectrum];
j = j +1;

end



%left shifted spectrum
if axes(y_correct) >  1005
    diff_pos= axes(y_correct) -  1005 ;
    %remove y number of elements from start of spectrum and add y elements with same↙
value as first element element
    corrected_spectrum = current_spectrum;
    last_value  = current_spectrum(end);
    corrected_spectrum(1:diff_pos) = [];
    new_values(1:abs(diff_pos)) = last_value;
    corrected_spectrum = single(corrected_spectrum)
        end_spectrum(j,:) = [corrected_spectrum new_values];
    j = j +1;
end

if axes(y_correct) == 1005
  end_spectrum(j,:) = current_spectrum;
      j = j +1;
end
end


Nucleolus_SCC_FA_BN_R = end_spectrum


figure
hold on
plot(wavenumbers,Nucleolus_SCC_FA_BN_R,'r')
plot(wavenumbers,Nucleolus_DOK_FA_BN_R_2,'g')

mean_Nucleolus_SCC_FA_BN_R = mean(Nucleolus_SCC_FA_BN_R(:,:),1)
mean_Nucleolus_DOK_FA_BN_R = mean(Nucleolus_DOK_FA_BN_R(:,:),1)

figure
hold on
plot(wavenumbers_cut,mean_Nucleolus_SCC_FA_BN_R,'g')
plot(wavenumbers_cut,mean_Nucleolus_DOK_FA_BN_R,'r')
```

```
ind_end= find(wavenumbers==1800);

ind_start=find(wavenumbers==600);

wavenumbers_cut=wavenumbers(ind_start:ind_end);

% wavenumbers_cut=flipdim(wavenumbers_cut,2);

Nucleolus_SCC_FA_S_R = Nucleolus_SCC_FA_BN_R(:,ind_start:ind_end);
Nucleolus_DOK_FA_S_R_2 = Nucleolus_DOK_FA_BN_R_2(:,ind_start:ind_end);

figure
hold on
plot(wavenumbers_cut,Nucleolus_SCC_FA_S_R,'g')
plot(wavenumbers_cut,Nucleolus_DOK_FA_S_R_2,'r')



mean_Nucleolus_SCC_FA_S_R = mean(Nucleolus_SCC_FA_S_R(:,:),1)
figure
plot(wavenumbers_cut,mean_Nucleolus_SCC_FA_S_R,'r')

mean_Nucleolus_DOK_FA_S_R_2 = mean(Nucleolus_DOK_FA_S_R_2(:,:),1)

figure
hold on
plot(wavenumbers_cut,mean_Nucleolus_SCC_FA_S_R,'g')
plot(wavenumbers_cut,mean_Nucleolus_DOK_FA_S_R_2,'r')



spectraPCA = [Nucleolus_SCC_FA_S_R; Nucleolus_DOK_FA_S_R_2]


[x y]=size(Nucleolus_SCC_FA_S_R);ind_Nucleolus_SCC_FA_S_R=x;
[x y]=size(Nucleolus_DOK_FA_S_R_2);ind_Nucleolus_DOK_FA_S_R_2=x;


group=zeros(1,ind_Nucleolus_SCC_FA_S_R+ind_Nucleolus_DOK_FA_S_R_2);

ind1=1:ind_Nucleolus_SCC_FA_S_R;
ind2=ind_Nucleolus_SCC_FA_S_R+1:ind_Nucleolus_SCC_FA_S_R+ind_Nucleolus_DOK_FA_S_R_2;


group(ind1)=1;
group(ind2)=2;


[coeff1, scores1, latent1] = princomp(spectraPCA);


figure



scatter3(scores1(ind1,2),scores1(ind1,3),scores1(ind1,4),'go','filled');hold on
scatter3(scores1(ind2,2),scores1(ind2,3),scores1(ind2,4),'ro','filled');hold on

% scatter3(scores1(ind4,1),scores1(ind4,2),scores1(ind4,3),'rs','filled');hold on
% scatter3(scores(ind5,1),scores(ind5,2),scores(ind5,3),'yo','filled');hold on
xlabel('PC2');
ylabel('PC3');
zlabel('PC4');
```

```
percent_explained = 100*latent1/sum(latent1);
figure;
hold on
plot(percent_explained(1:10,1))




figure;
hold on
plot(wavenumbers_cut,coeff1(:,4),'b')
% plot(wavenumber_2,coeff4(:,2),'r')
% set(gca,'XDir','reverse')


figure;
hold on
plot(wavenumbers_cut,coeff1(:,3),'b')
```